LIQUID HYDROGEN TURBOPUMP
RAPID START PROGRAM

Prepared By

G. S. Wong
Principal Engineer
Manager, Advanced Turbomachinery

ROCKETDYNE
A DIVISION OF NORTH AMERICAN ROCKWELL CORPORATION

Prepared For

NATIONAL AERONAUTICS AND SPACE ADMINISTRATION
George C. Marshall Space Flight Center
Huntsville, Alabama

(NASA-CR-120209) LIQUID HYDROGEN TURBOPUMP RAPID START PROGRAM Final Report, 30 Jun. 1971 - 27 Apr. 1973 (Rocketdyne) 325 p HC $19.25 CSCL 13K

N74-21067

Unclas
G3/15 15997

R-9273

LIQUID HYDROGEN TURBOPUMP
RAPID START PROGRAM

October, 1973

NAS8-27608

Prepared For

National Aeronautics and Space Administration
Technical Management
Marshall Space Flight Center
Huntsville, Alabama

T. W. Winstead

Prepared By

G. S. Wong
Principal Engineer
Manager, Advanced Turbomachinery

Rocketdyne Division
Rockwell International
6633 Canoga Avenue
Canoga Park, California 91304

FOREWORD

This final report documents studies conducted by Rocketdyne Division, Rockwell International, for Marshall Space Flight Center of the National Aeronautics and Space Administration under contract NAS 8-27608. The NASA Technical Project Manager was Mr. T. W. Winstead. The studies were conducted during the period of 30 June 1971 through 27 April 1973.

ABSTRACT

The purpose of this program was to analyze, test, and evaluate methods of achieving rapid-start of a liquid hydrogen feed system (inlet duct and turbopump) using a minimum of thermal preconditioning time and propellant. The program was divided into four tasks.

Task I includes analytical sutdies of the testing conducted in the other three tasks. Task II describes the results from laboratory testing of coating samples and the successful adherence of a KX-635 coating to the internal surfaces of the feed system tested in Task IV. Task III presents results of testing an uncoated feed system. Tank pressure was varied to determine the effect of flowrate on preconditioning. The discharge volume and the discharge pressure which initiates opening of the discharge valve were varied to determine the effect on deadhead (no through-flow) start transients. Task IV describes results of testing a similar, internally coated feed system and illustrates the savings in preconditioning time and propellant resulting from the coatings.

ACKNOWLEDGMENT

Acknowledgment is made to the following Rocketdyne personnel for their contributions to the program: W. R. Wagner and R. E. Rankel for heat transfer analyses; R. E. Mowers and J. T. Lee for coated-material studies; W. R. Bissell and N. C. Gulbrandsen for turbopump analyses and tests; and W. M. Stanley for feed system startup evaluation. Acknowledgment is also made to the following Convair Aerospace personnel: K. E. Leonhard, R. C. Day, and A. Gay for heat transfer analyses of the coated inlet line to the feed system. The Rocketdyne Program Manager was H. G. Diem.

SYNOPSIS

This program was undertaken to demonstrate the feasibility of using coatings applied to the wetted surfaces of a liquid hydrogen feed system (inlet line and pump) as a method of reducing the time and propellant required to thermally condition the pump before rotation. Extensive analytical studies preceded both testing of material samples in the laboratory and testing of the full-scale uncoated and coated feed systems in appropriate test facilities. The purpose of these studies was to generate parametric data as a means of establishing the influence of parameter variations to guide subsequent testing.

The chilldown characteristics of several coatings were experimentally determined using small samples. These samples used titanium, CRES, and aluminum as the base material; each with several different types and thicknesses of coatings. Tests included chilldown from ambient conditions by immersing solid cylinders in liquid nitrogen and hydrogen and flowing liquid hydrogen through cylindrical tubes. The coatings, when judiciously used, caused the heat energy stored in the base material to be removed by the coolant either faster or slower than for an uncoated metal, depending on the coating material and thickness, and the mass flow velocity. For low mass velocities, thin coatings can be used to increase heat transfer rates and reduce required chill time, such as on a pump impeller, and thick coatings can be used to obtain a rapid surface chill, while insulating or reducing the heat transfer rates of the base material, such as on larger components like pump housings and propellant lines.

For high mass velocities, the trends are the same as just described, but the thin coatings result in little, if any, reduction in chill time from the value for an uncoated metal.

Based on these heat transfer tests and adherence characteristics as determined by stressing coated samples, a KX-635 coating was selected for the feed system to be tested. A thin, 0.005-inch coating was selected for the rotating pump parts to provide rapid thermal conditioning of the metal and preclude abnormal blade stress conditions during rotation after minimal chill. A thicker, 0.020-inch

insulative coating was selected for the stationary pump parts and inlet line to minimize the heat transfer rate and its effect on the propellant conditions.

The procedure for selecting the appropriate coating thickness for liquid hydrogen applications is shown schematically in Fig. i. First, it is necessary to establish the desired effect of the coating, i.e., enhancement or insulation. This decision is influenced by the mass of the base metal and stress considerations. For massive components, the objective of reducing the heat flux to a low level in a short time period is not practical with an enhancement coating. Also, if rotating components such as inducers and impellers are stress-designed at low temperatures and design limits would be exceeded during rotation at higher metal temperatures, use of insulating coatings is precluded.

For a desired chill factor, the coating Biot number (N_{Bi}) is selected from Fig. ii. The range of values corresponds to the experimental data obtained under the Rapid Start Program. The chill factor (ψ) should be selected as low as practical for enhancement and relatively high for insulation. Knowing the coating thermal conductivity (k) and the film coefficient (h) for the uncoated surface, the coating thickness (t) can be selected from Fig. iii for the selected Biot number. The procedure then becomes iterative depending on the suitability of the selected coating thickness. This decision is based on the compatibility of the thickness with application techniques and adherance qualities. Unless limiting Biot numbers for the desired effect (enhancement or insulation) have been reached, the desired chill factor must be altered and a new Biot number selected. If limits have been reached, it is necessary to change the desired effect.

Thermal conditioning and turbopump start tests were conducted with both uncoated and coated feed systems consisting of inlet lines designed for the Centaur stage and RL-10 "hydrogen turbopumps" (turbopumps with the oxygen pumps removed). Start tests were conducted with the uncoated system to determine deadhead (no through-flow) start characteristics. The system's start transient was found to be insensitive to the value of discharge pressure used to initiate opening of the discharge valve, but was dependent on the discharge volume. Deadhead starts were successfully achieved only with very large discharge volumes.

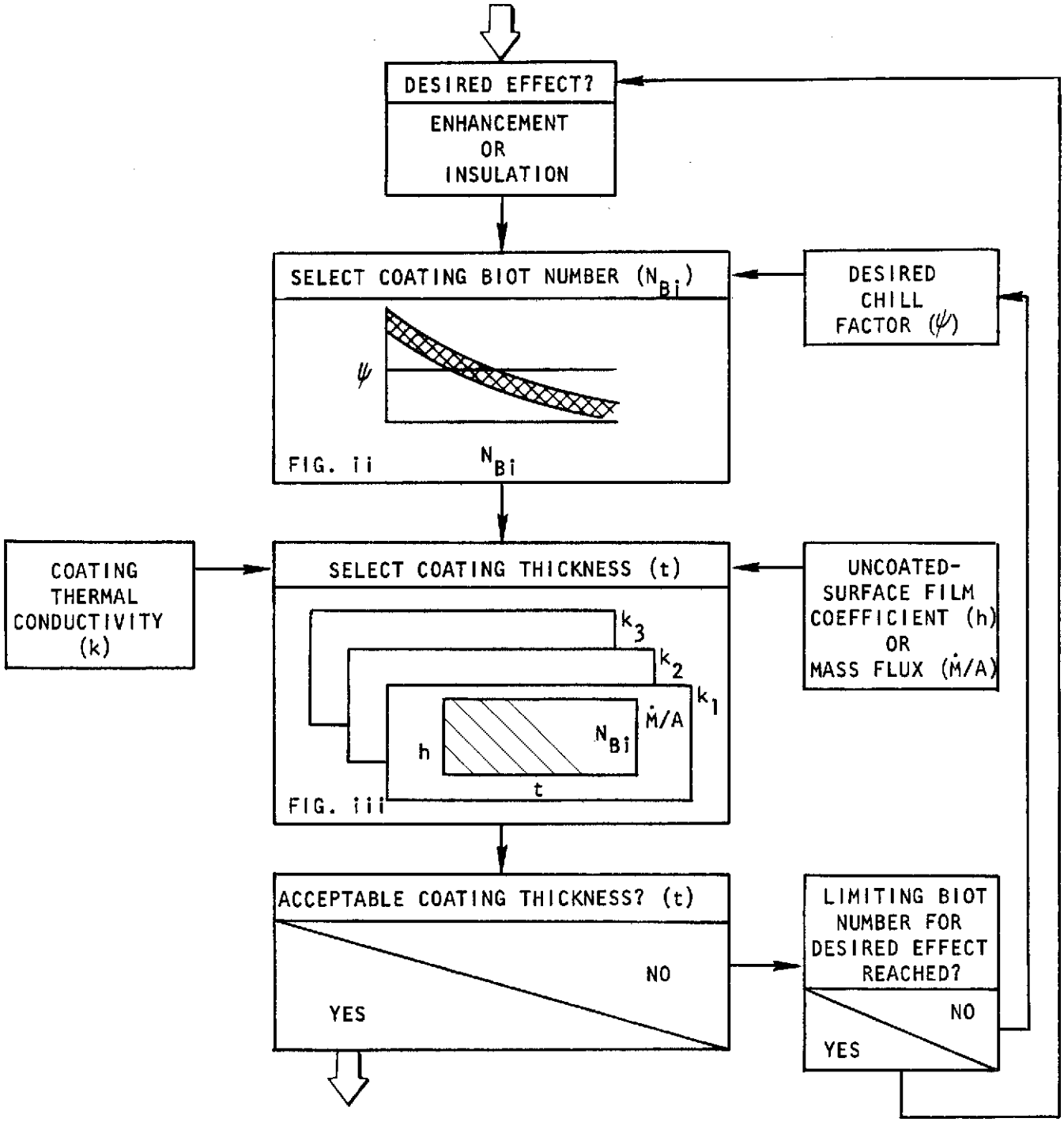

Figure i. Procedure for Selecting Coating Thickness

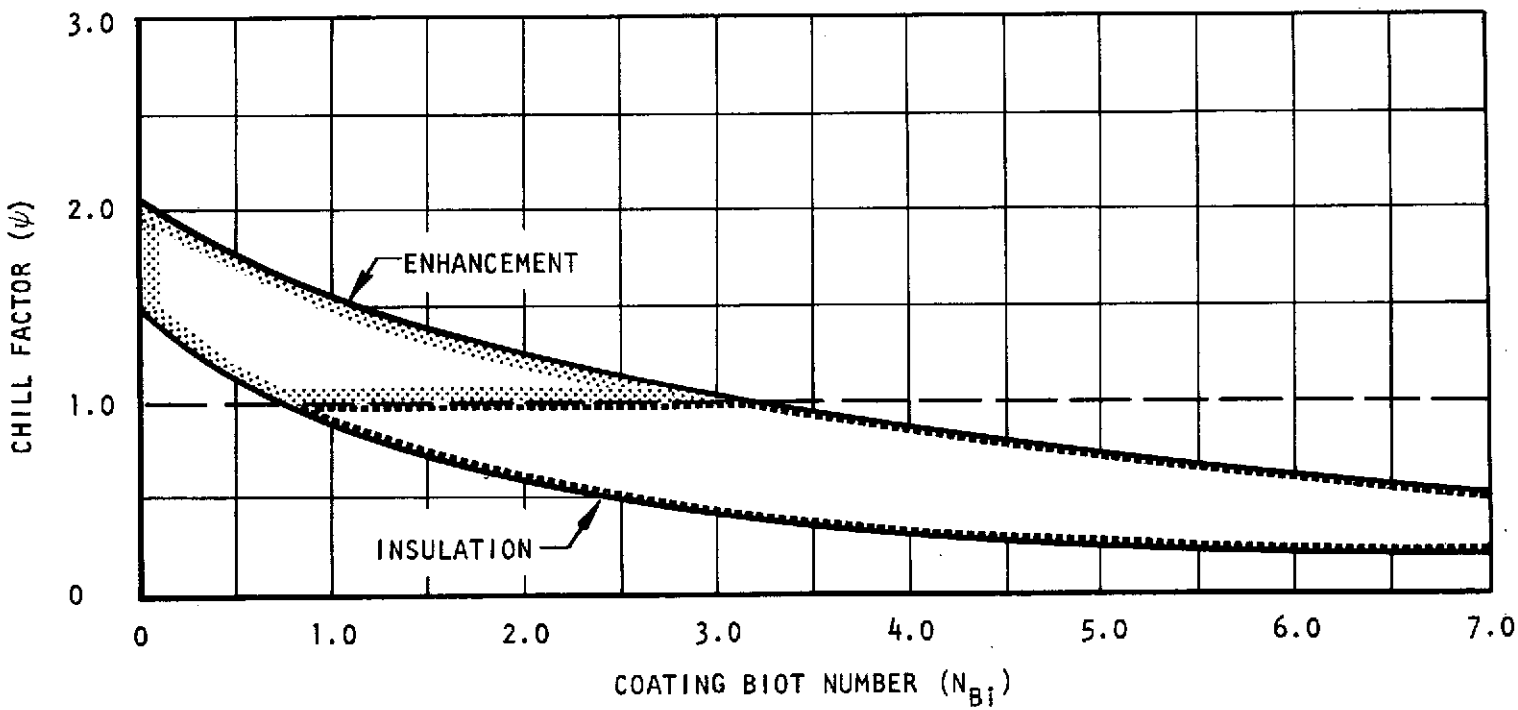

Figure ii. Coating Biot Number Selection

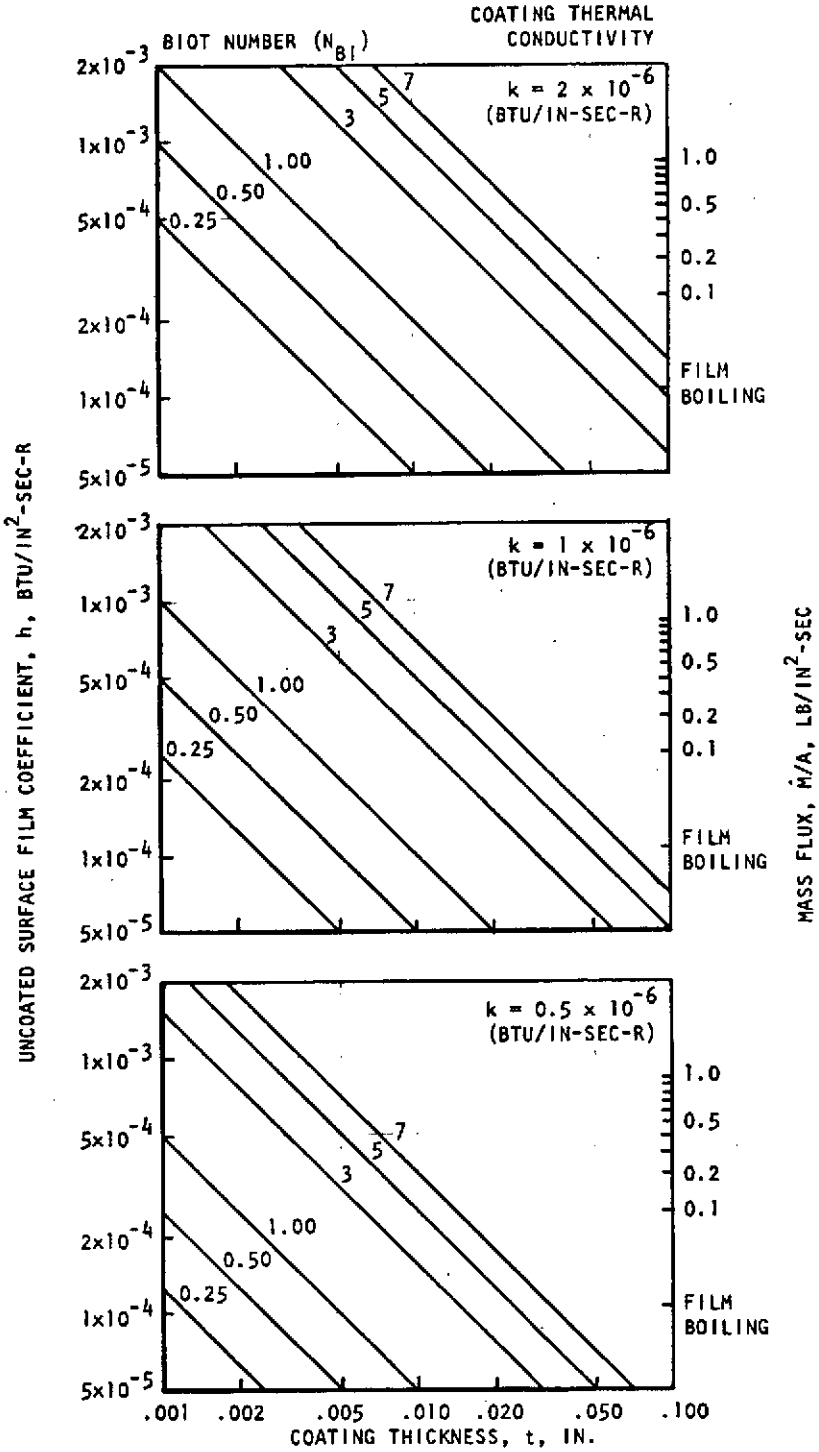

Figure iii. Selection of Coating Thickness

Comparative thermal conditioning tests demonstrated the advantages that can be realized by coating the wetted surfaces. The time and propellant weight required to achieve saturated liquid at the pump exit with the coated system were 20 seconds and 20.6 pounds, as compared to 29 seconds and 35 pounds for the uncoated system with a similar supply pressure and under similar initial conditions.

In order to determine the minimum chilldown required to achieve a successful start, a series of three tests was conducted with different degrees of preconditioning. Although not actually demonstrated, the results support the conclusion that the system could be started from ambient initial conditions after 10 seconds of chilldown for test conditions used, which were different from those used in the chill tests mentioned above. The two least chilled cases were unsuccessful, but this was most probably due to sequencing peculiar to the test facility.

During testing of the coated feed system, a total of 11 tests were run for over 680 seconds, of which 10 tests and 450 seconds were with the pump operating. Post-test inspection revealed excellent adhesion qualities of the selected coating.

CONTENTS

ILLUSTRATIONS

TABLES

INTRODUCTION

The purpose of this program was to analyze, prepare, and test a liquid hydrogen feed system (inlet duct and turbopump) that can achieve rapid starts with minimum thermal preconditioning. The results can be applied to increase the payload potential and mission flexibility of the Space Shuttle vehicle. These feed systems would be particularly attractive in a cryogenic auxiliary propulsion system (APS), where minimum start times after various coast periods are required and also for Space Tug propulsion systems.

Propellant feed system chilldown time and expended propellants can be reduced through the use of internal coatings. Previous contracted efforts (NAS8-20167 and NAS8-20324) have demonstrated this improved chilldown efficiency, as well as material compatibility and application techniques. Rapid pump starts, particularly in an APS application, suggest turbomachinery designs and controls that provide a "deadhead" (no through-flow) start capability. The objective of this program was to develop data on a typical auxiliary propulsion hydrogen feed system to determine the interrelationship between feed system coatings, chilldown time, deadhead starting, minimum start times, feed system geometry, and control functions.

As a demonstration of the benefits to be derived from using coatings on future cryogenic space propulsion systems, an analysis was made for an assumed Space Tug synchronous equatorial deployment mission. This mission includes eight separate burns over a twenty-eight hour period. Test data indicates that a reduction of 25 percent on the total chill propellant can be achieved by using coatings on low thermal conductivity materials such as titanium and CRES in advanced engine hydrogen turbomachinery. Savings of 50 percent for similar oxygen turbopumps are projected based on liquid nitrogen test data (liquid nitrogen and liquid oxygen have similar heat transfer properties).

A summary comparison of propellant chill requirements for coated and uncoated pumps is presented in Table 1. Coatings reduce the required propellant weight by 213 pounds when used in an overboard dump chilldown mode (no propulsive thrust) which corresponds to approximately 190 pounds of payload (3% of nominal), 60 pounds of inert weight (15% of engine weight), or 1.9 seconds of specific impulse. Lesser advantages are realized if the propellants are utilized in some other manner such as engine idle-mode operation.

TABLE 1. TOTAL MISSION CHILL REQUIREMENTS

	COATED PUMPS	UNCOATED PUMPS
Oxygen, lb	191	382
Hydrogen, lb	87	109
Total, lb	278	491
Savings, lb	213	Reference

SUMMARY AND CONCLUSIONS

The objectives of the work conducted under this contract were to analyze, test, and evaluate internal coatings as a method of achieving a rapid-start of a liquid hydrogen feed system (inlet line and turbopump). The advantages to be realized from a rapid-start are reduced thermal conditioning time and propellant use. The program was divided into four tasks; each will be summarized separately.

TASK I: ANALYTICAL STUDIES

The first task included analytical investigations titled Thermal Analysis, Turbomachinery Analysis, System Evaluation, and General Dynamics Inlet Line Analysis. The Thermal Analysis studies consisted of an investigation and prediction of the chilldown characteristics of the coated laboratory samples tested during the second task. These samples used titanium, CRES, and aluminum as the base material and several different types and thicknesses of coatings. Three types of tests were simulated, including immersion of solid cylinders in liquid nitrogen and hydrogen, and liquid hydrogen flow through cylindrical tubes. For the simulated immersion tests, the heat transfer rates were significantly increased when relatively thin coatings were applied. The time required for the coated metal cylinders to reach equilibrium temperatures was reduced by factors of up to 3.7 and 2.35 in the nitrogen and hydrogen baths, respectively, when compared to the uncoated cylinder data. These results agreed well with subsequent testing in the second task. In both the nitrogen and hydrogen immersion simulations, coating thicknesses of less than approximately 7.62×10^{-4} m (0.030 inch.) did enhance the heat transfer rate rather than retard it.

Evaluation of liquid hydrogen flow through cylindrical tubes showed that chilldown of the base material can either be enhanced or retarded depending on the hydrogen flowrate and the coating thickness. These trends were substantiated during testing in the second task. As an illustration of these trends, analysis of an aluminum cylinder spray-coated with KX-635 indicated that a coating thickness of 1.78×10^{-4} m (0.007 in.) reduced the time required to achieve a specified fluid temperature by a factor of 1.35, and a thickness of 4.32×10^{-4} m (0.017 in.) increased

the chill-time by a factor of 2.66 for a flowrate of 1.89×10^{-3} m^3/s (30 gpm). As indicated, the function of the coating reverses from that of enhancing the heat transfer rate to that of acting as an insulator as the thickness is increased. The effect of increasing the flowrate is to reduce the chill-time, e.g., for the coating thickness of 1.78×10^{-4} m (0.007 in.) just mentioned, the chill-time is reduced by a factor of 2.05 as the flowrate is increased from 1.89×10^{-3} m^3/s (30 gpm) to 1.26×10^{-2} m^3/s (200 gpm).

The turbomachinery Analysis study consisted of using a simplified model to estimate start characteristics of the RL-10 turbopump under deadhead (no through-flow) conditions. During a deadhead-start, accumulative heating of the trapped fluid due to pump inefficiency significantly affects the developed discharge pressure. During this study the discharge pressure transient was predicted assuming a fully-chilled pump, a fixed mass of trapped fluid, and a uniform fluid density equal to the value at the discharge. Results show that the discharge pressure peaks at a value of 4.55×10^6 N/m^2 (660 psia) when the rotational speed is 85 percent of the design value. As the speed continues to increase, accumulative heating reduces the fluid density enough to cause the discharge pressure to decrease. Consequently, it would be necessary to allow through-flow to be initiated during the transient prior to reaching a discharge pressure of approximately 4.55×10^6 N/m^2 (660 psia).

The System Evaluation study consisted of using a more detailed analytical model of the hydrogen feed systems, tested in the third and fourth task, to specify experimental parameter values, establish a start sequence, and predict the experimental results. The heat-transfer from the duct and pump, the discharge volume, and the discharge pressure which initiates opening of the discharge valve were varied parametrically to determine their effects on deadhead-start. The effect of the size of the discharge volume is to shift the start-transient with respect to the pump performance map. Small volumes result in low flows and flow reversals very early in the transient, while large volumes result in high flowrates and a breakdown in developed-head because of cavitation. For an intermediate size discharge volume of 6.17×10^{-2} m^3 (2.18 cu ft^3), backflow occurs if the discharge valve is scheduled to open at a pressure greater than approximately 4.14×10^6 N/m^2 (600

psia). The pump does not recover from backflow because the pressure of the high energy reverse flow is reduced and the fluid is vaporized as it flows to the inlet duct. Since a very detailed heat transfer model was used in the Thermal Analysis studies, the start transient model contained a simplified approach consisting of a specification of the heat transfer rate at the design flowrate and variations programmed proportional to the square root of the flowrate. The maximum allowable total heat-transfer during the start-transient for an initially warm feed system corresponded to a specification of approximately 1.64×10^5 joules/second (155 Btu/second) at the design flowrate. This amount of heat-transfer shifted the pump transient performance to the threshold of breakdown in the developed-head due to cavitation. With this schedule of heat-transfer and a discharge volume of 6.17×10^{-2} m^3 (2.18 ft^3), backflow through the pump occurred if the discharge valve was scheduled to open at a pressure greater than 4.83×10^6 N/m^2 (700 psia). The shift to the right of the transient performance on the pump map and the resulting higher efficiency accounts for the warm pump being able to operate with higher back pressures than the preconditioned one. For the range of parameters considered, propellant heating due to pump inefficiency is at least as important as the chill-down heat-transfer in affecting the deadhead start transient.

The General Dynamics Inlet Line Analysis was conducted by their Convair Aerospace Division. A literature survey acquired current data relative to chilldown with cryogenic fluids and the application of internal coatings to reduce chilldown requirements. The thermal analyzer program developed by the Knolls Atomic Power Laboratory was modified and used to determine the effects on line chilldown of (1) line material, (2) line diameter, (3) coating material, (4) coating thickness, (5) line pressure drop, and (6) fluid flowrate. Thermodynamic models of both the uncoated and coated lines tested in the third and fourth tasks were developed and used to determine the effect of variations in major parameters. These studies confirmed the results of the Thermal Analysis studies and laboratory testing of sample cylindrical tubes in the second task.

TASK II: LABORATORY SAMPLE TESTS

The purpose of the second task was to test the analytically derived results obtained in the Thermal Analysis studies conducted during the first task and to select the optimum coating and method of application for use on the inlet duct and pump that was tested in the fourth task. A KX-635 coating was selected on the basis of: (1) its heat transfer characteristics as determined by immersion of coated solid metal cylinders in liquid nitrogen and hydrogen, and by liquid hydrogen flow tests in internally coated cylindrical tubes; (2) its adherence to metals as determined by stressing coated samples; and (3) its corrosion resistance quality based on the hydrogen flow tests. The recommended inlet time and pump coating thicknesses were 1.27×10^{-4} m (0.005 in.) for rotating parts and 5.08×10^{-4} m (0.020 in.) for stationary parts. Both spray and fill-and-drain applications were recommended depending on the accesibility of specific areas to be coated. Examination of the coated experimental feed system at the completion of testing in the fourth task revealed excellent adhesion qualities after more than 7-1/2 minutes of turbopump operation.

TASK III: UNCOATED FEED SYSTEM TESTS

During the third task, a test stand was constructed and instrumented for testing both the uncoated and coated hydrogen feed systems. The feed systems consisted of an inlet line, manufactured by Convair Aerospace Division of General Dynamics for the Centaur stage, and an RL-10 hydrogen turbopump (turbopump with oxygen pump removed), which were supplied by NASA. Twenty-three tests were conducted with an uncoated feed system to check out the facility and obtain data on thermal conditioning and deadhead turbopump starts. During the pressure-fed chill tests, the hardware was at ambient initial conditions. The inlet pressure was varied between 1.93×10^5 and 5.17×10^5 N/m^2 gage (28 and 75 psig) and the time required to achieve saturated liquid at the pump exit varied from 59 to 29 seconds, respectively. Saturated liquid was evidenced at the interface between the inlet duct and pump in 43 seconds for a pressure of 1.93×10^5 N/m^2 gage (28 psig) and 20 seconds for a pressure of 5.17×10^5 N/m^2 gage (75 psig). Although flowrate was

a function of the inlet pressure, the total weight of hydrogen required to chill the feed system was approximately 1.5 kilograms (33 pounds) and virtually independent of pressure and flowrate.

The turbopump start transient tests were conducted with the discharge valve closed, i.e., under deadhead conditions. The start transients were insensitive to the value of pump discharge used to initiate opening of the discharge valve. There was no effect that could be attributed to trigger pressures between 3.55×10^6 and 2.17×10^6 N/m^2 (515 and 315 psia) for the three unsuccessful starts with the intermediate sized downstream volume, or to pressures between 4.24×10^6 and 2.17×10^6 N/m^2 (615 and 315 psia) for the three successful starts with the largest volume. The turbopump deadhead start was dependent on the volume between the pump discharge and the discharge valve. Successful deadhead-starts could not be accomplines with volumes of 0.0014 and 0.024 m^3 (0.05 and 0.85 ft^3), but they were successful with a volume of 0.098 m^3 (3.45 ft^3).

TASK IV: COATED FEED SYSTEM TESTS

During the fourth task, 11 tests were conducted with the coated feed system to determine thermal conditioning characteristics and steady-state pump performance for comparison with the uncoated feed system data, and also to obtain data on starting the pump when only partially chilled. Both the chill-time and total propellant weight were reduced by coating the wetted surfaces of the inlet duct and pump. For an inlet pressure of 5.03×10^5 N/m^2 gage (73 psig), the time and propellant weight required to achieve saturated liquid at the pump exit with the coated feed system was 20 seconds and 9.3 kilograms (20.6 pounds), as compared to 29 seconds and 15.9 kilograms (35 pounds) for the uncoated system with an inlet pressure of 5.17×10^5 N/m^2 gage (75 psig). The values for achieving saturated liquid at the pump inlet were 14.5 seconds and 6.4 kilograms (14 pounds) for the coated system, and 20 second and 10.9 kilograms (24 pounds) for the uncoated system.

Coated feed system tests were conducted to obtain data on steady-state performance. The steady-state developed head of the coated pump was approximately 20-percent

less than that of the uncoated pump for a given flow and rotational speed. No investigation to determine the cause of this performance loss was made, but it is possible that the coatings reduced the flow areas within the pump, especially the discharge flow area, and therefore, altered the fluid velocity vectors in the pump stages.

Turbopump start tests were conducted with an inlet pressure of 4.48 $x10^5$ N/m^2 gage (65 psig) and three different degrees of preconditioning. Only the most chilled condition resulted in a successful start. However, a thorough analysis of the test results indicated that the other tests were probably unsuccessful because of pump inlet propellant conditions resulting from manual sequencing of a discharge valve, rather than being due to a lesser degree of prechill. This sequencing occurred approximately 1.5 seconds before turbopump rotation and resulted in a lower chill flow and higher fluid temperature at the pump inlet when rotation was initiated. It is significant that propellant conditions after sequencing the valve for the successful start were nearly identical to the conditions that existed before sequencing the valve for an unsuccessful start with 10 seconds of preconditioning. Although not demonstrated, it is therefore reasonable to expect that the coated feed system could be started from ambient initial conditions after 10 seconds of preconditioning.

TASK 1
ANALYTICAL STUDIES

TASK I: ANALYTICAL STUDIES

This task is divided into four subtasks: Thermal Analysis, Turbomachinery Analysis, System Evaluation, and General Dynamics Inlet Line Analysis. The thermal analysis study was an in-depth evaluation of chilldown times for a variety of base materials and surface coatings. Both analytical and experimental data were obtained for samples of titanium, CRES, and aluminum. The turbomachinery analysis investigated startup of the RL-10 turbopump under deadhead (no flow) conditions. During deadhead starts, propellant heating may become a problem because the heat input is rejected only to the trapped propellant within the pump, and therefore causes a large heat input per unit mass of propellant.

Under the system evaluation subtask, an analytical model of the experimental feed system was developed. This model was used to determine the effects of chilldown heat transfer on turbopump deadhead start. The heat transferred into the hydrogen from the inlet duct and pump, and the discharge pressure required to initiate opening of the discharge valve were varied parametrically. Both a preconditioned and warm feed system with various downstream duct volumes were analyzed. The inlet line analysis, which was conducted by Convair Aerospace Division of General Dynamics, used the modified thermal analyzer program. This analysis included the following effects on line chilldown: (1) line material, (2) line diameter, (3) coatings, (4) coating thickness, (5) line pressure drops, and (6) fluid flowrates. These four subtasks are discussed in detail in the following sections.

THERMAL ANALYSIS

The pump thermal analysis study consisted of the evaluation and prediction of chilldown of the samples tested during Task II: Laboratory Sample Tests. In addition, a computer analysis model of the RL-10 hydrogen pump was formulated for prediction of the chilldown results acquired during Task III: Uncoated Feed System Tests, and Task IV: Coated Feed System Tests. The work on the liquid nitrogen (LN_2) immersion cylinder chill analyses, the liquid hydrogen (LH_2) immersion cylinder chill analyses, the tubular collar LH_2 flow chill analyses, and the RL-10 turbopump chill analysis approach are discussed below.

Thermal Analysis of LN_2 Immersion Chilldown of Coated and Uncoated Metal Cylinders

Figures 1 through 8 show the immersion testing chilldown data for aluminum, CRES, and titanium. The instrumented cylinder samples tested in LN_2 are described in Task II: Laboratory Sample Tests. The results are presented at this time for comparison with the analytical studies.

Computer Chilldown Model. The DEAP-1 program (Ref. 1), with 32 and 22 nodes, was used for predicting the chilldown characteristics of bare and coated metal cylinders (heat transfer rods) in LN_2 and LH_2, tested by immersion in Task II. The nodal sketches for insulated (coated) and noninsulated metal cylinders are shown in Fig. 9 and 10. The analytically predicted data were found to compare well to experimental data. Typical analytical results obtained for coated and bare cyclinders, with and without external cork insulation, are described below.

LN_2 Chilldown of Bare Titanium Cylinder. Figure 11 illustrates the computer model chilldown of the titanium cylinder based on equal film coefficients on all three surfaces of the cylinder throughout the film and nucleate boiling range. The titanium cylinder is shown to enter the LN_2 nucleate boiling range at about 50 seconds, with only some thermal gradient through the cylinder; with chilldown complete at about 65 seconds.

LN_2 Chilldown of Bare CRES Cylinder. Figure 12 illustrates the analytical chilldown of the bare CRES cylinder in the LN_2 bath. The break point between film and nucleate boiling is shown at 80 seconds, with the chilldown nearly complete at 90 seconds. A lesser differential temperature throughout the cylinder is noted as compared to titanium as a result of a higher thermal conductivity.

LN_2 Chilldown of Bare Aluminum Cylinder. Chilldown analysis simulation of the aluminum cylinder is shown in Fig. 13. The nucleate boiling onset is shown at 50 seconds, with chilldown essentially complete at 60 seconds.

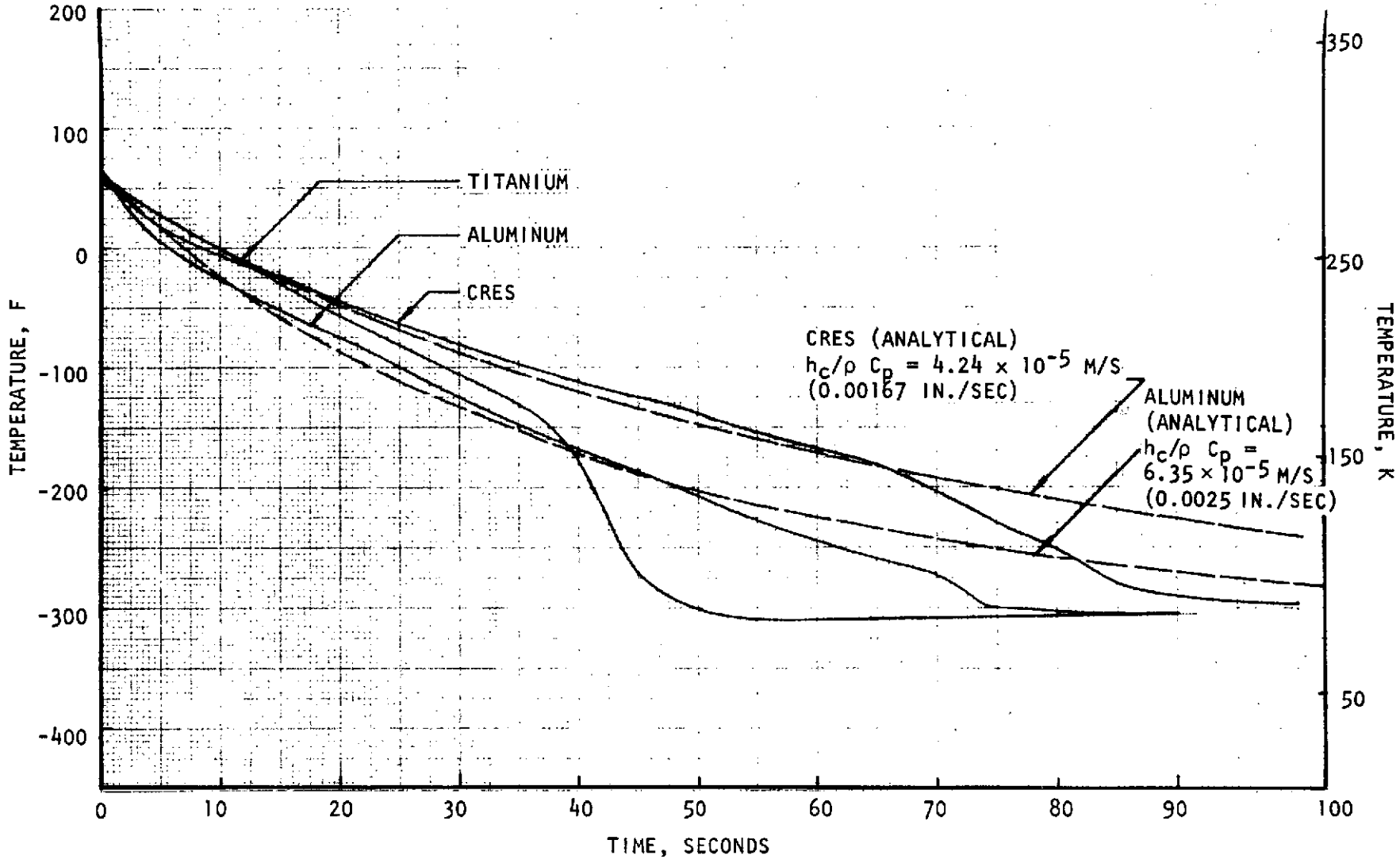

Figure 1. LN_2 Bath Chilldown of Bare Cylinders With No Insulator

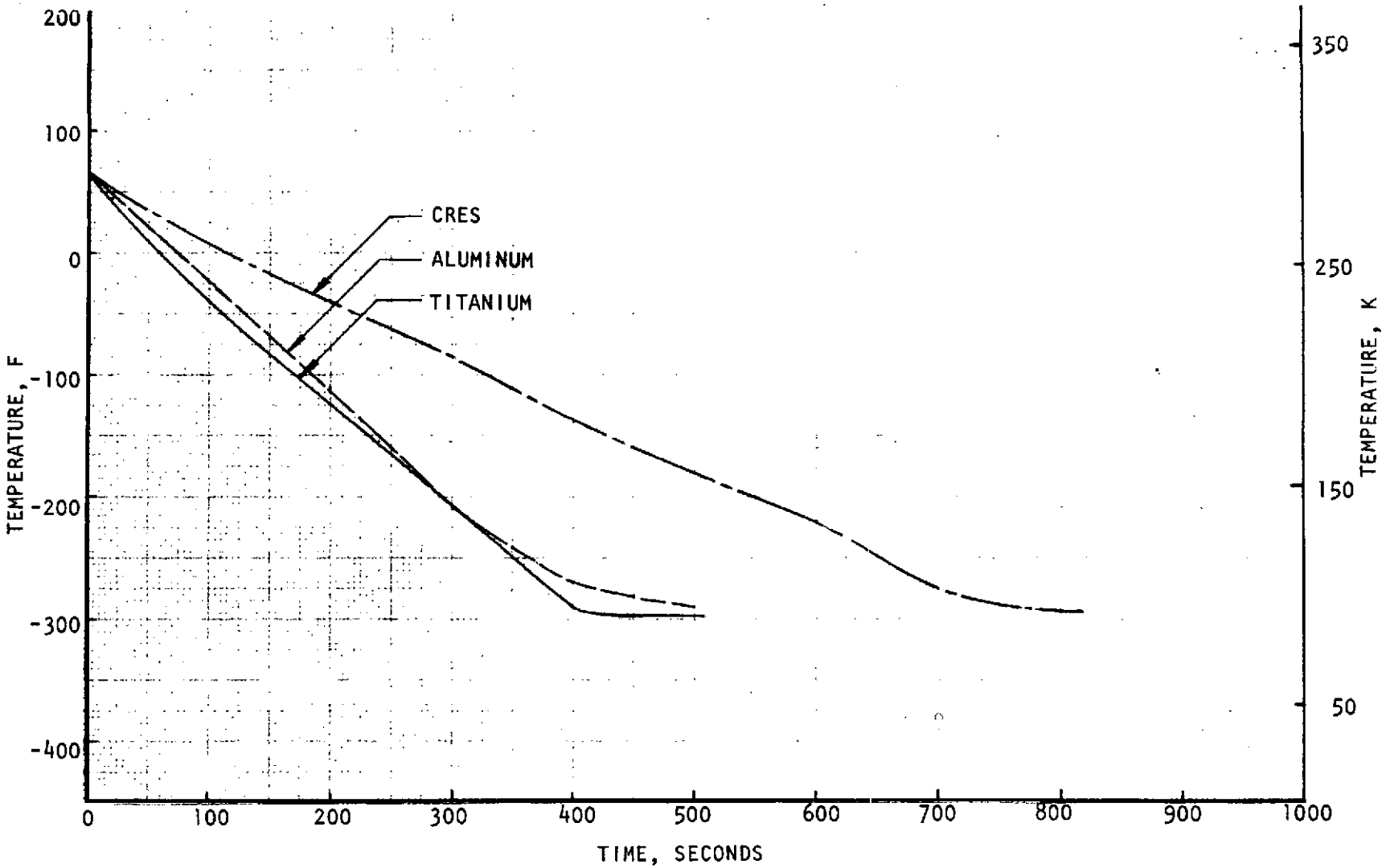

Figure 2. LN_2 Bath Chilldown of Bare Cylinders With Cork Insulators

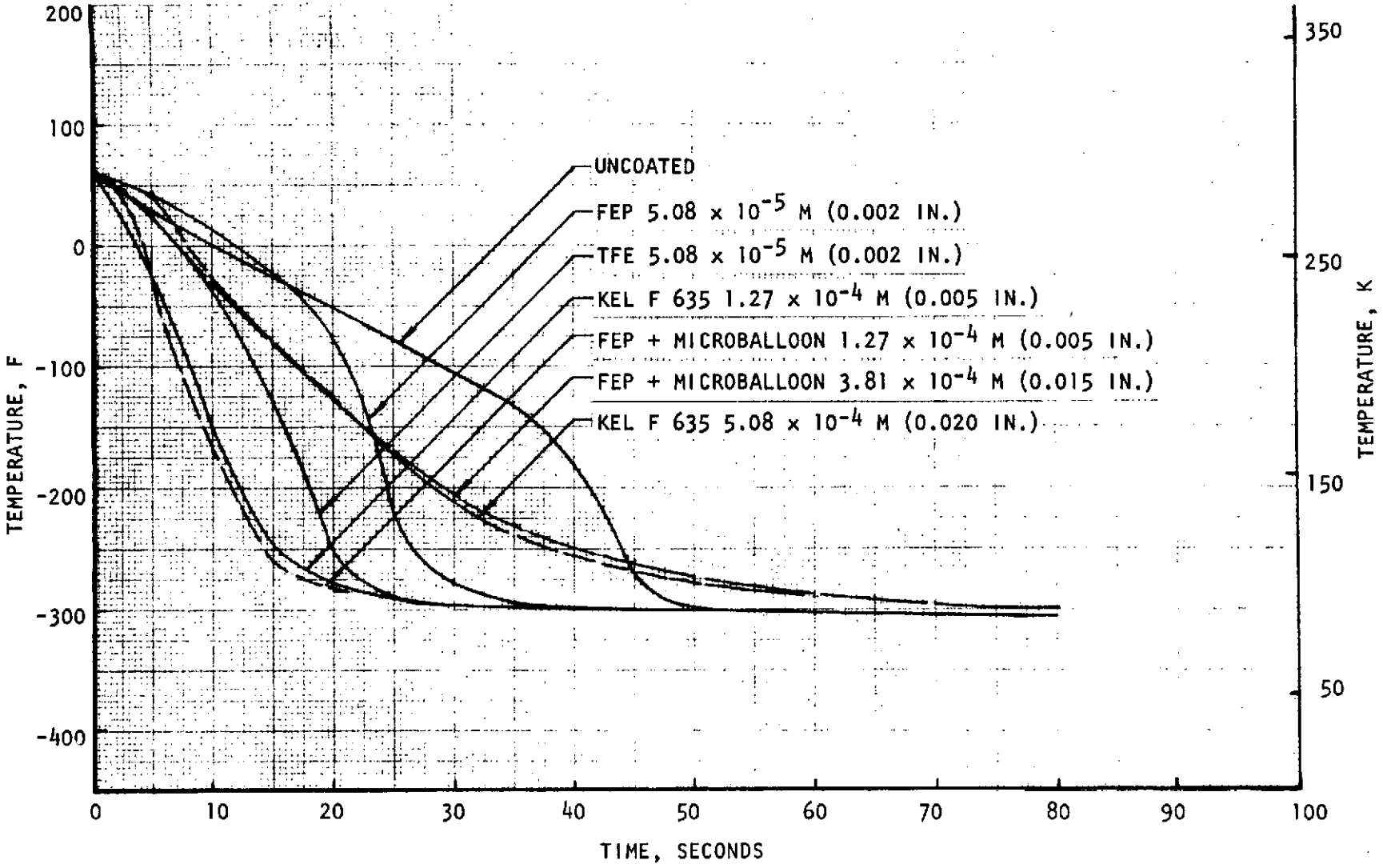

Figure 3. LN_2 Bath Chilldown of Coated Titanium Cylinders With No Cork Insulator

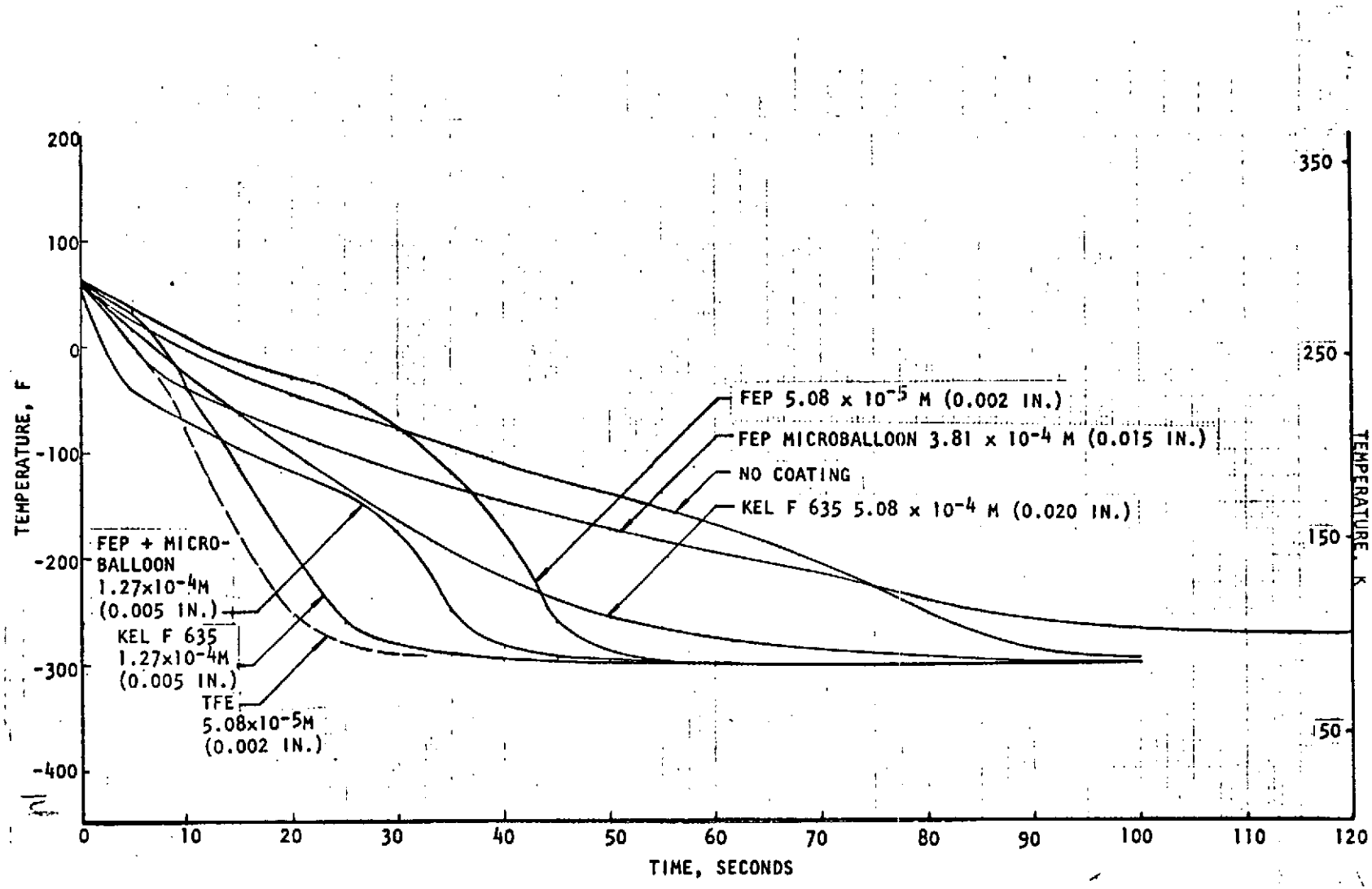

Figure 4. LN_2 Bath Chilldown of Coated CRES Cylinders With No Cork Insulator

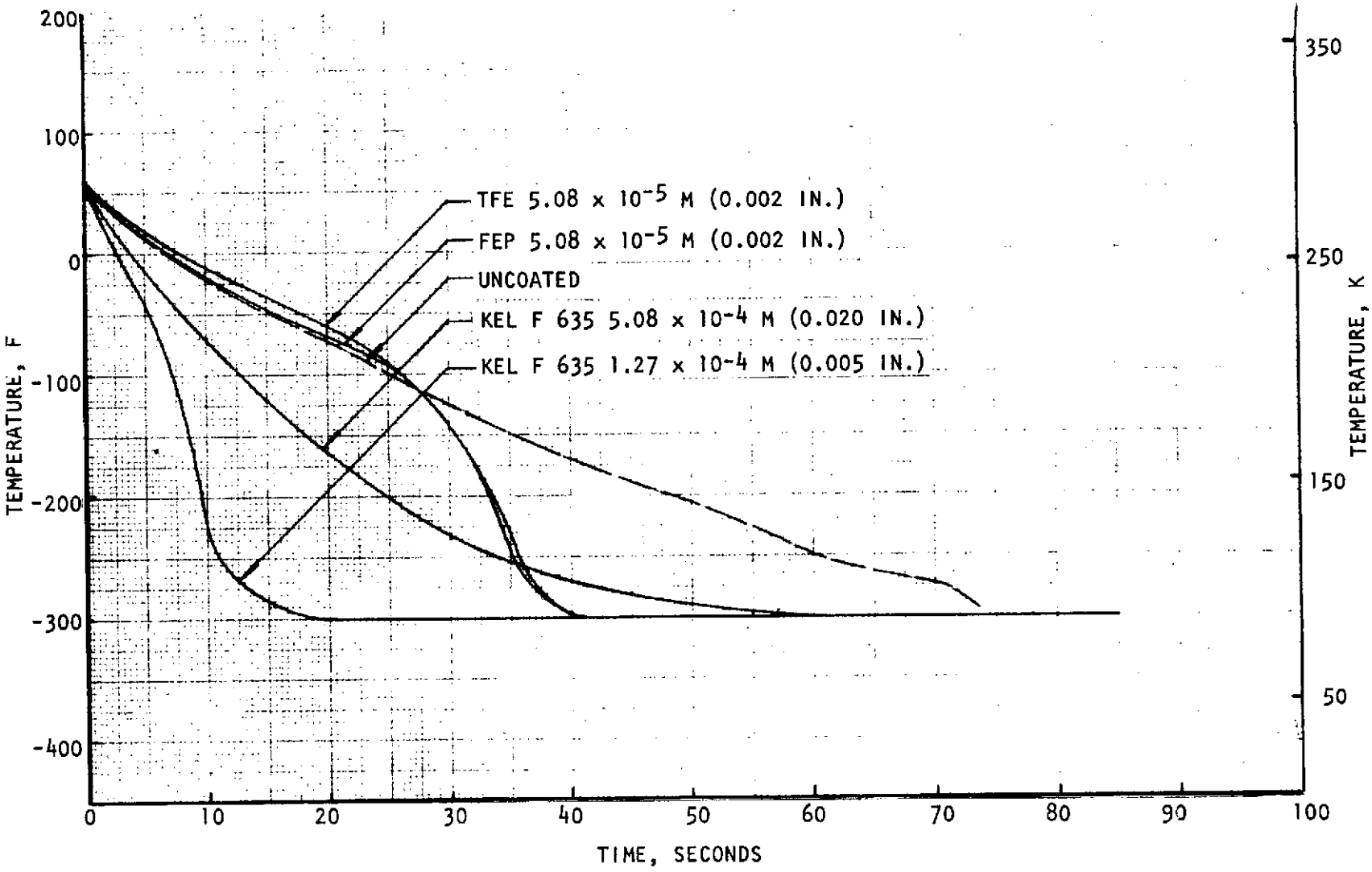

Figure 5. LN_2 Bath Chilldown of Coated Aluminum With No Cork Insulator

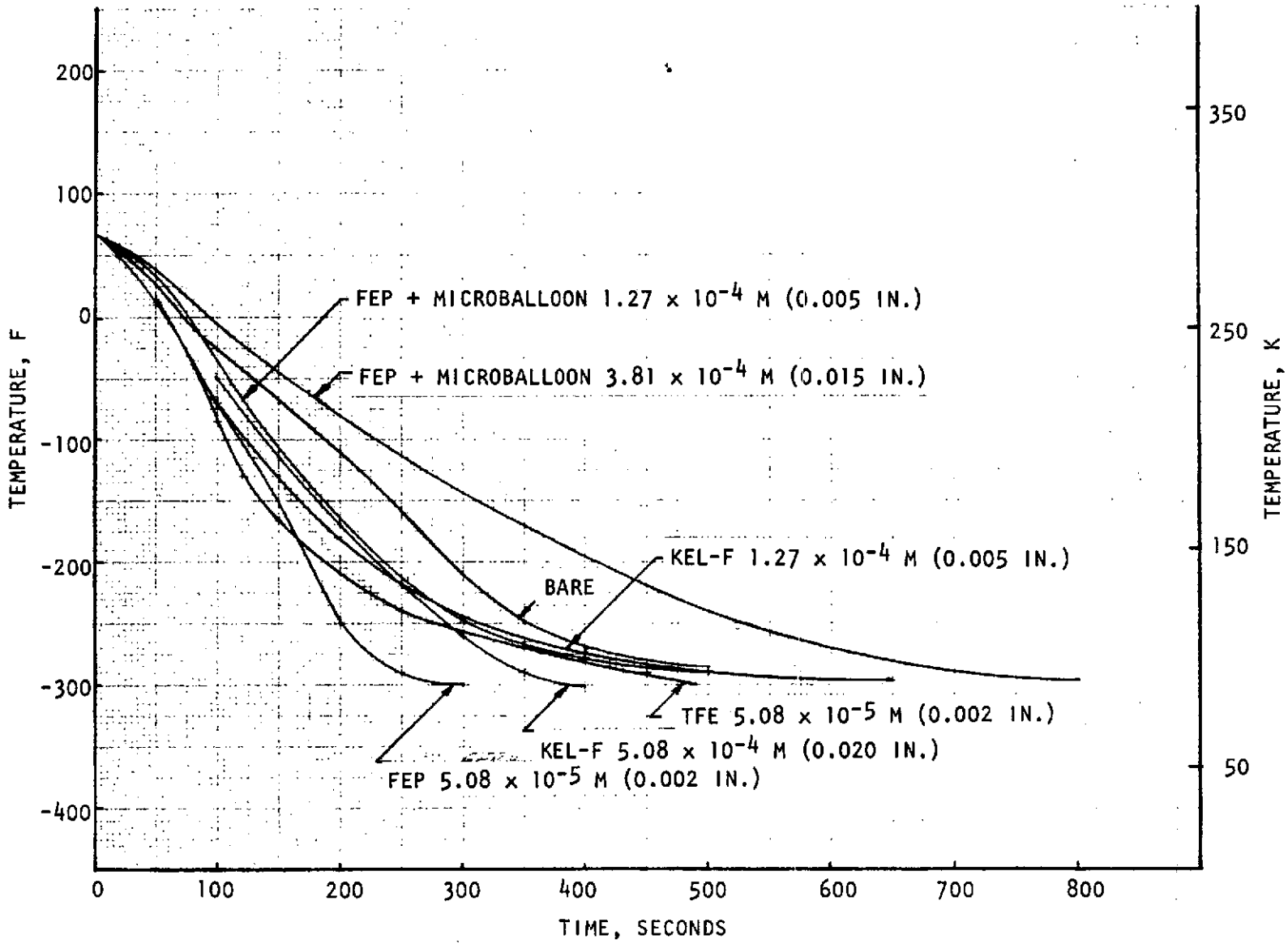

Figure 6. LN_2 Bath Chilldown of Coated Titanium With Cork Insulator

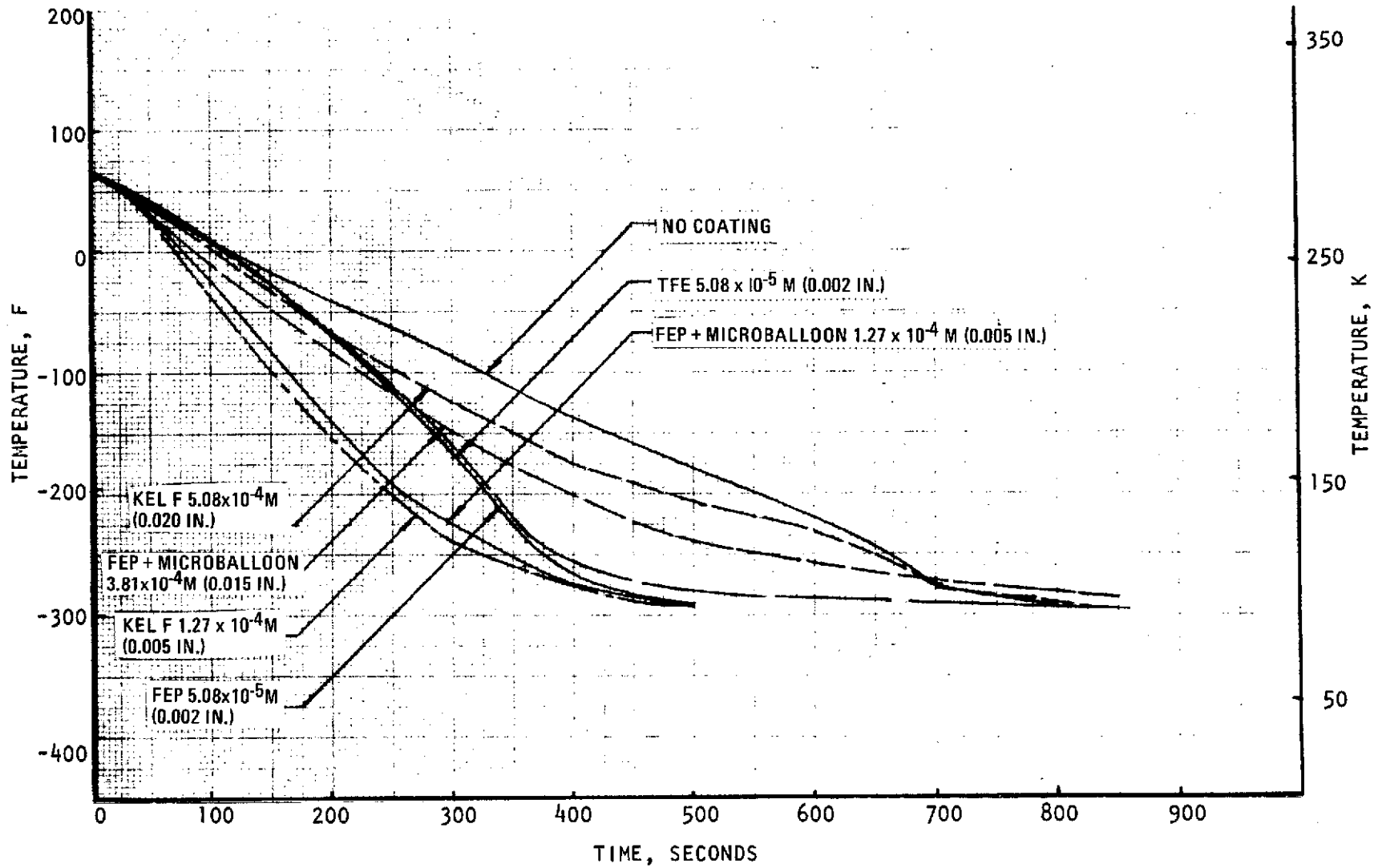

Figure 7. LN_2 Bath Chilldown of Coated CRES Cylinders With Cork Insulators

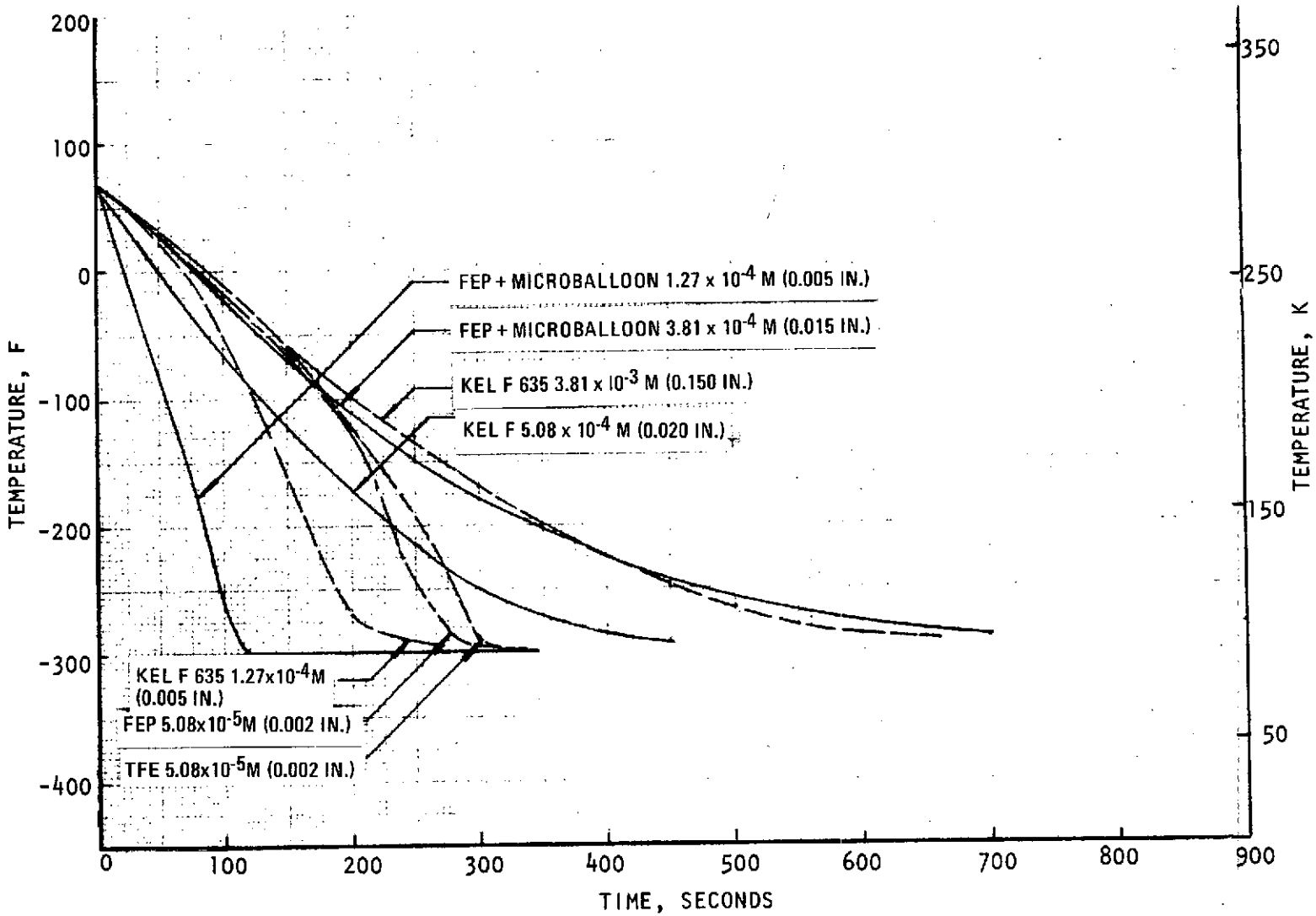

Figure 8. LN_2 Bath Chilldown of Coated Aluminum Cylinders With Cork Insulator

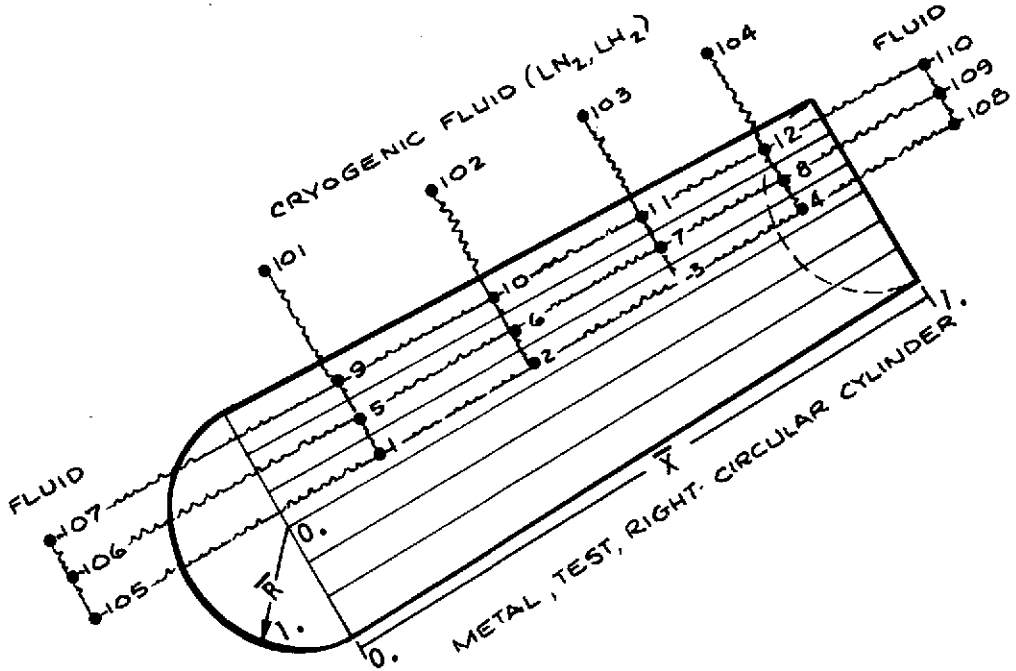

Figure 9. Test Cylinder Analytical Model

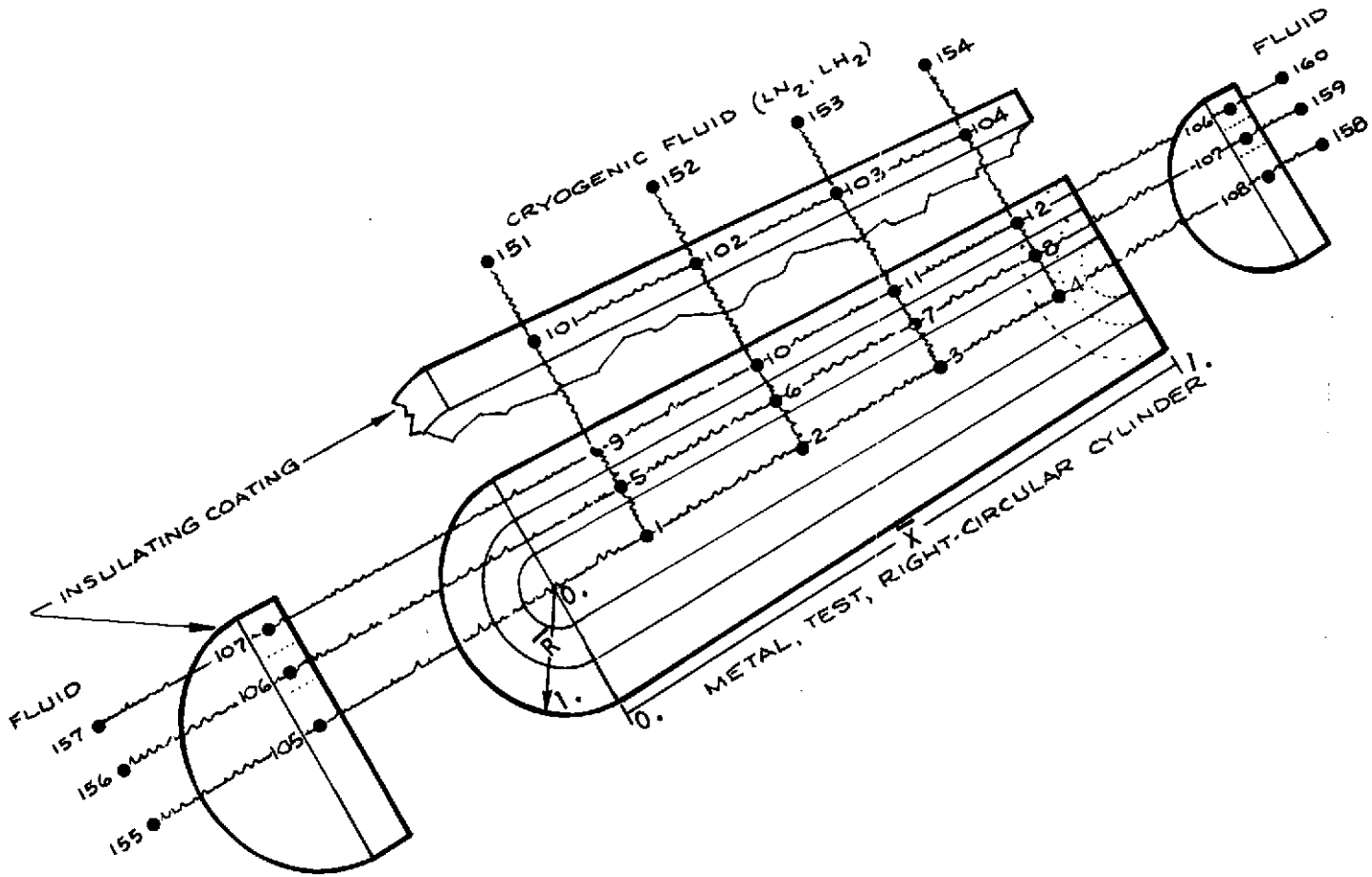

Figure 10. Insulated Test Cylinder Analytical Model

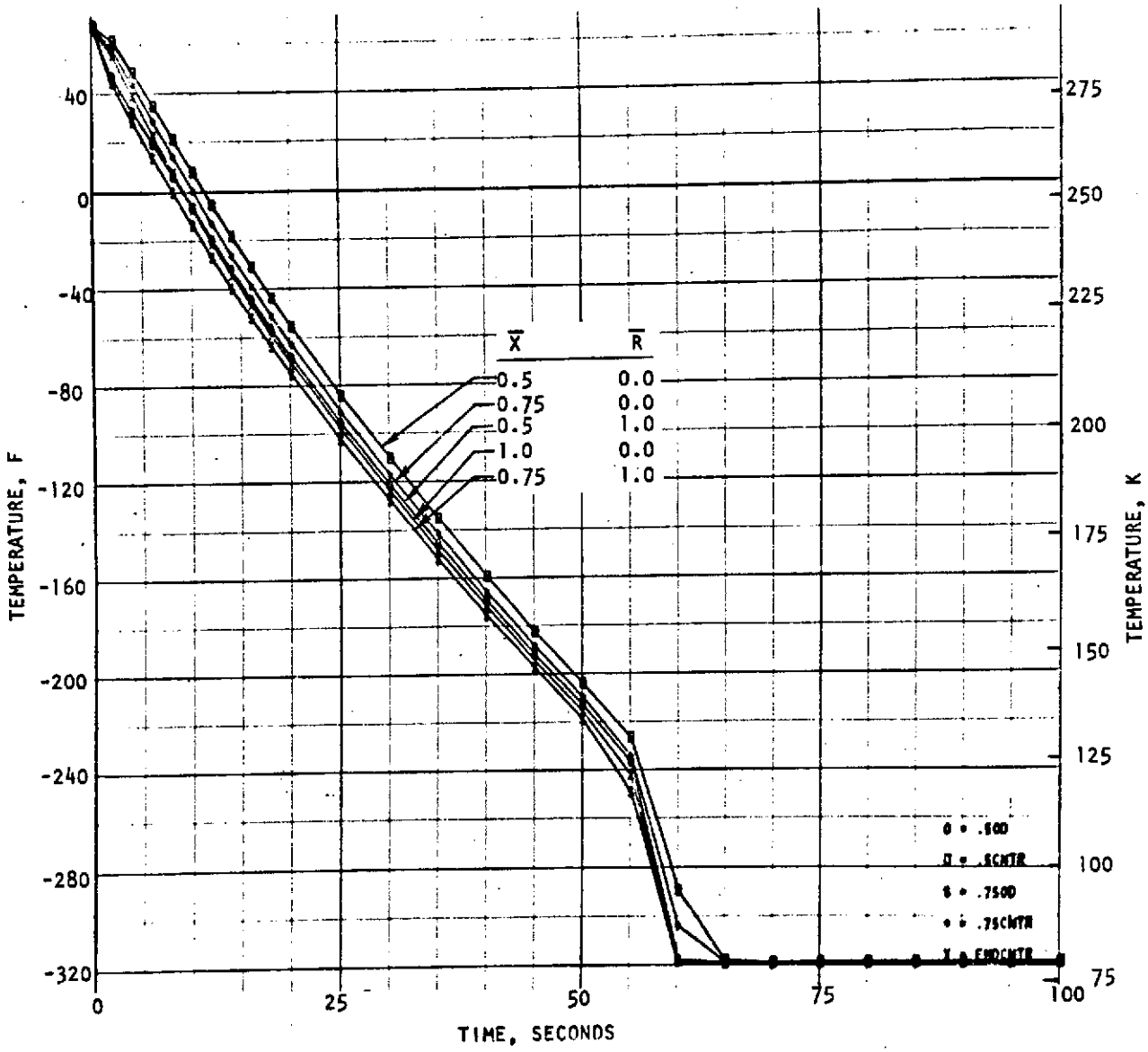

Figure 11. Analytical Chilldown of Bare Titanium Cylinder (LN_2)

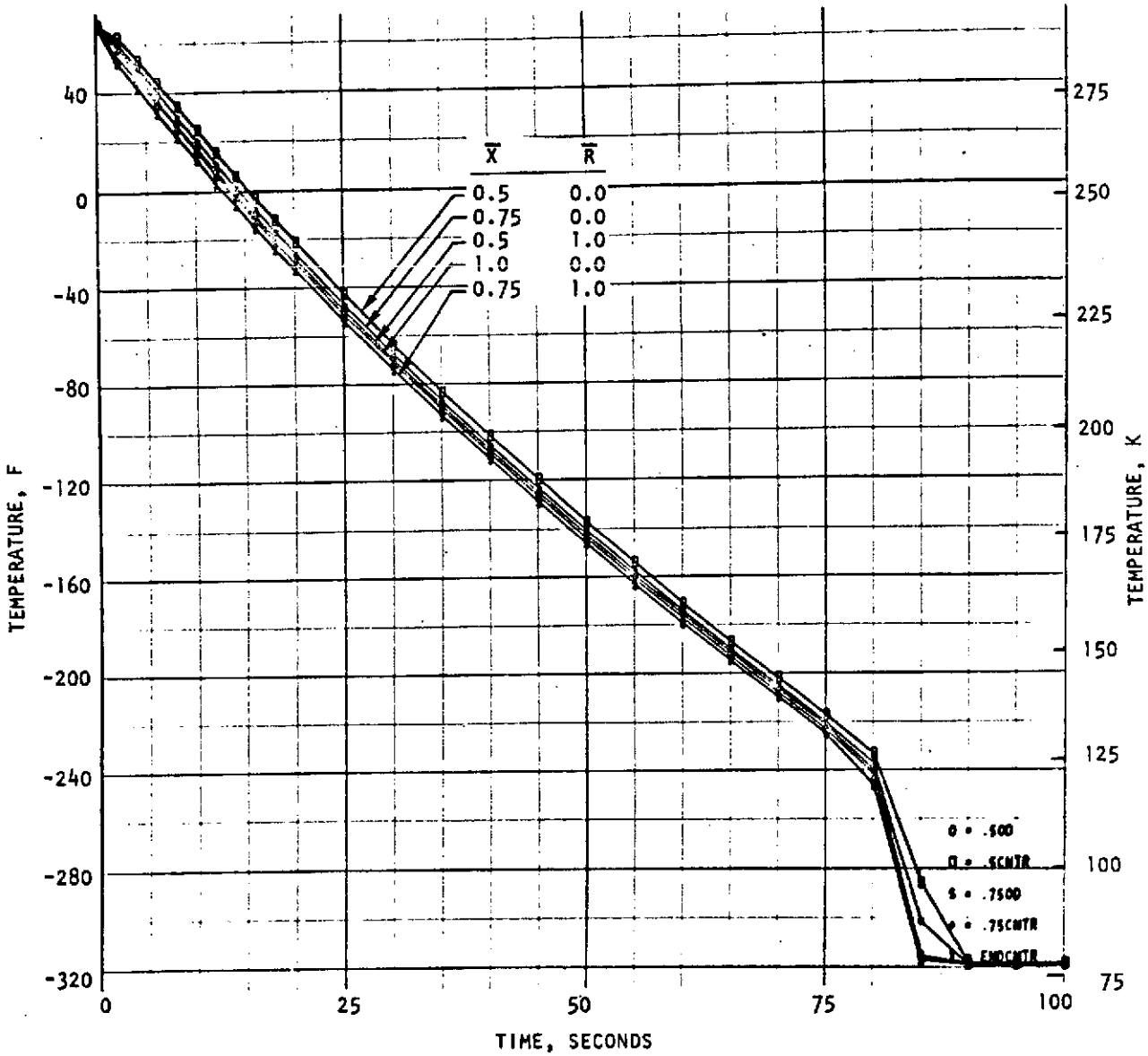

Figure 12. Analytical Chilldown of Bare CRES Cylinder (LN_2)

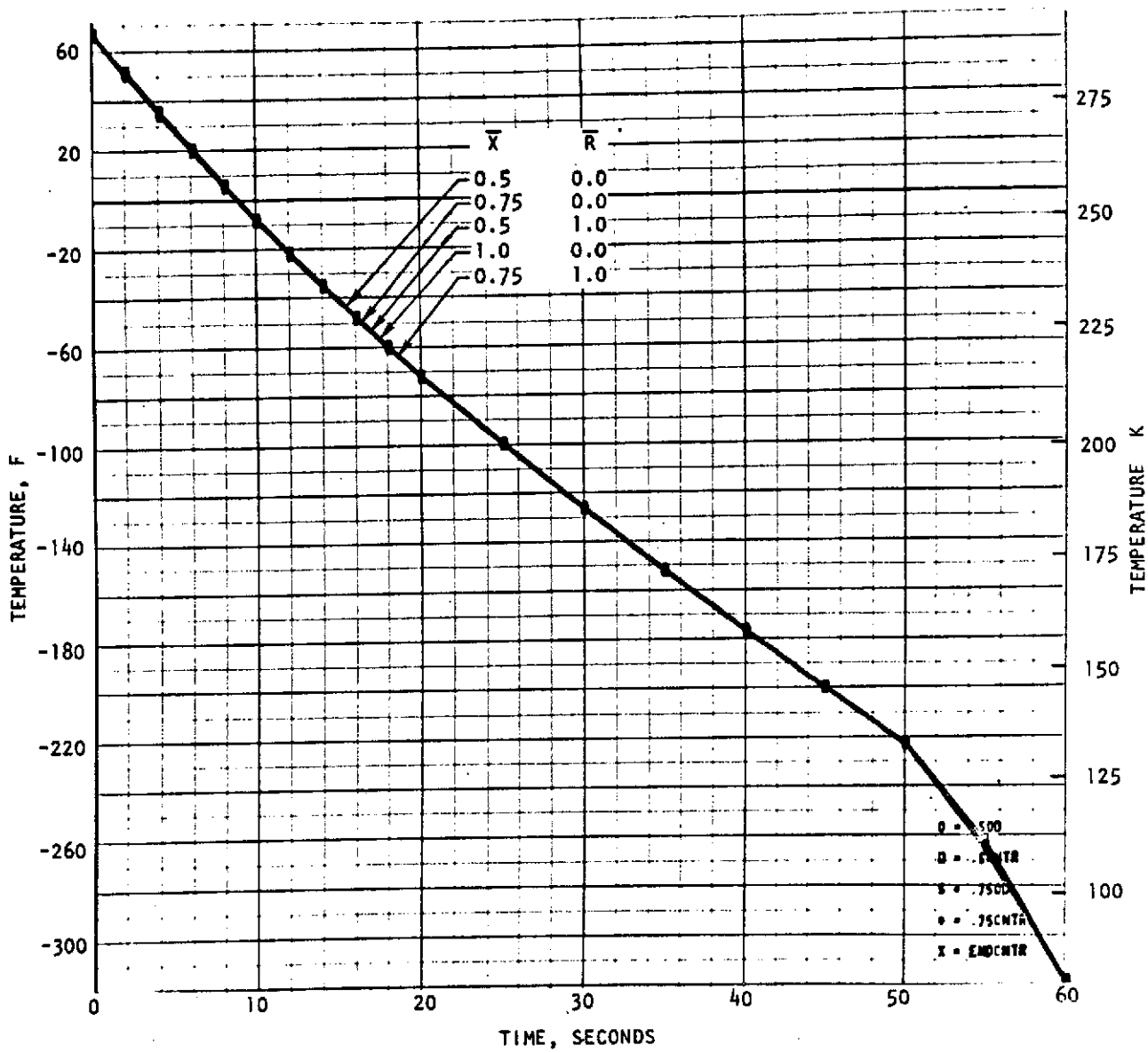

Figure 13. Analytical Chilldown of Bare Aluminum Cylinder (LN_2)

LN_2 Chilldown of Cork Insulated Titanium Cylinder. A substantial increase in the chilldown time for the titanium cylinder with the cork insulator is shown in Fig. 14. Nucleate Boiling onset is shown at 450 seconds with chilldown complete at 700 to 800 seconds.

LN_2 Chilldown of Cork Insulated CRES Cylinder. Figure 15 illustrates similar results for the CRES cylinder. Nucleate boiling onset occurs at 640 seconds with chilldown complete at about 800 seconds.

LN_2 Analytical to Experimental Chilldown Comparison. Reduction of the LN_2 test data on the heat transfer cylinders was completed and a comparison of the experimental and analytical predicted results was made. Figures 6 and 14 illustrate the computer predicted analytical LN_2 chilldown time comparison for titanium with different types of coatings and thicknesses. As illustrated, all coatings except the 3.81×10^{-4} m (0.015 in.) FEP + microballoon coating were shown to speed up the heat removal from the titanium base material with a 2 to 1 time reduction for the best coating which is the FEP 5.08×10^{-5} m (0.002 in.) coating.

Uncoated Cylinder Analytical Model. Based on LN_2 immersion test data, comparative coating thicknesses to enhance the chilldown were compared by defining a simplified chilldown model shown below:

$$\frac{T_w - T_{LN_2}}{T_{wi} - T_{LN_2}} = e - \left(\frac{h_c \beta \tau}{\rho C_p}\right)$$

$$\beta = \left(\frac{2 + \frac{4L}{D}}{L}\right) \quad \text{cylinder without cork insulator}$$

$$\beta = \left(\frac{1}{L}\right) \quad \text{cylinder with cork insulator}$$

For purposes of comparing the time it takes to achieve a nearly complete chill, it was assumed that:

$$\frac{T_w - T_{LN_2}}{T_{wi} - T_{LN_2}} = e^{-2.0} = 0.135$$

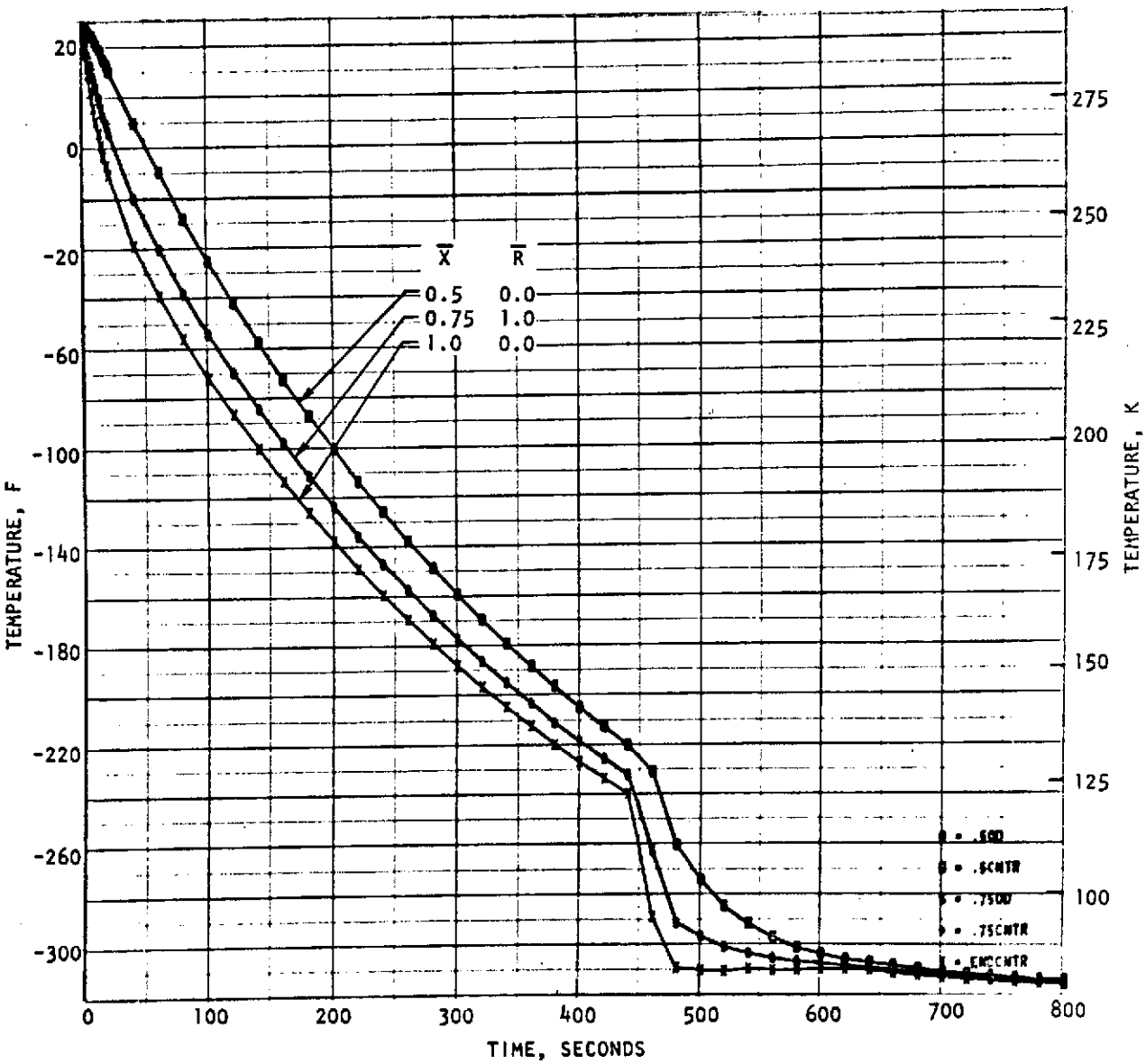

Figure 14. Analytical Chilldown of Cork Insulated Titanium Cylinder (LN_2)

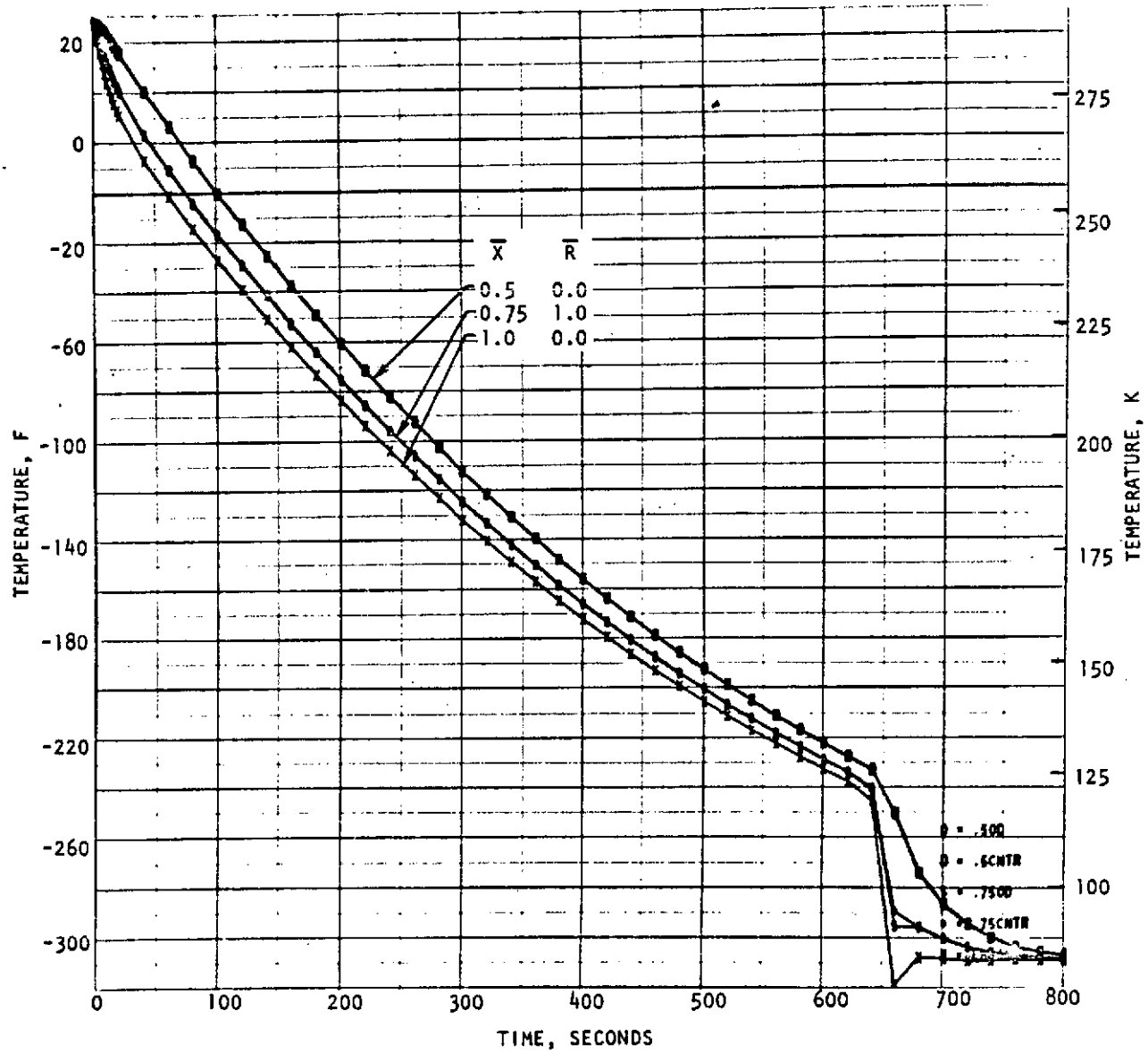

Figure 15. Analytical Chilldown of Cork Insulated CRES Cylinder (LN_2)

This corresponds to a wall temperature of 99.8 K (-280 F) or 87 percent of chill completion. For the simple model, this relates to the critical time, τ_{c_2}, as follows:

$$\tau_{c_2} = \left(\frac{2 \rho C_p}{\overline{h}_c \beta} \right)$$

$\beta = 39.4\ m^{-1}$ (1 $in.^{-1}$) cork insulator
$\beta = 394\ m^{-1}$ (10 $in.^{-1}$) without cork

where the coating effect is lumped into the average chilldown film coefficient, h_c.

Table 2 illustrates the comparative ratings for the various metal base and coating materials used. The uncoated base sample testing indicated titanium to have the shortest chill, and CRES the longest chill. Coatings were found to have the greatest effectiveness in the 5.08×10^{-5} to 1.27×10^{-4} m (0.002 to 0.005 in.) thickness range with 1.27×10^{-4} m (0.005 in.) thickness providing the best chill rate for most materials. On the average, the 1.27×10^{-4} m (0.005 in.) thick Kel-F material proved to be the most advantageous as shown. However, instances are shown where FEP and TFE are better choices for more rapid chills.

Comparison of Analytical and Experimental Chilldown of Kel-F Coated Cylinders in LN_2. Comparisons of the analytical and experimental LN_2 chilldown of the coated cylinders were completed. Typical graphs are shown in Fig. 16 and 17 for aluminum and titanium with a Kel-F 1.27×10^{-4} m (0.005 in.) coating. As shown by the experimental dotted lines, the effective film coefficients in the film boiling ranges are more than 4 times the uncoated values. In addition, for some of the rapid chilldown cases, alteration of the nucleate boiling range to a higher subcooling difference appears to occur.

Thermal Analysis of LH_2 Immersion Chilldown of Coated and Uncoated Metal Cylinders

Figures 18 through 23 illustrate the reduced chilldown data for immersion testing of aluminum, CRES, and titanium instrumented cylinder test samples in an LH_2 bath, as described in Task II.

TABLE 2. COMPARATIVE COATED CYLINDER CHILL TIME (SECONDS) RATED TO 99.8 R (-280 F) IN LN_2

Material of Base	Cork Insulator	(0.000 in.) Base	5.08×10^{-5}m (0.002 in.) FEP	5.08×10^{-5}m (0.002 in.) TFE	1.27×10^{-4}m (0.005 in.) KEL-F	1.27×10^{-4}m (0.005 in.) FEP	3.81×10^{-4}m (0.015 in.) FEP	5.08×10^{-4}m (0.020 in.) KEL-F	3.81×10^{-3}m (0.150 in.) KEL-F
CRES	Yes	710	500	440	*415*	445	775	705	--
Aluminum	Yes	445	275	295	215	*120*	625	375	550
Titanium	Yes	455	*230*	390	425	400	645	330	--
CRES	No	87.5	48	*25*	29.5	39.5	125	62.5	--
Aluminum	No	71.5	37.5	37.5	*14*	--	--	55	--
Titanium	No	46	30.5	23	20.5	*19.5*	54.5	51	--

NOTE: Shortest chill time in italics

LH_2 Analytical Chilldown Study. Cases for the LH_2 chilldown of the test Al, Ti, and CRES cylinders were modeled on the digital computer. Based on preliminary LH_2 film coefficients, comparisons of chilldown for both the corked and uncorked (bare) test cylinders of Ti, Al, and CRES were compared for chilldown times. Figure 24 shows typical samples.

Figures 25 through 27 illustrate the analytical chilldown times for the bare test cylinders. Figures 28 through 30 illustrate the predicted chilldown for the corked test cylinders. Chilldown times to 57 K (-358 F) are shown in Table 3 compared to the experimental test results.

TABLE 3. COMPARATIVE LH_2 UNCOATED CYLINDER CHILLDOWN TIMES

	Experimental Time, seconds	Analytical Time, seconds	Discrepancy, percent
CRES - Corked	480	565	+18
Ti - Corked	340	430	+26
Al - Corked	317	338	+07
CRES - Uncorked	49.5	52.5	+06
Ti - Uncorked	28	37	+32
Al - Uncorked	29.5	33	+12
			Average = 16

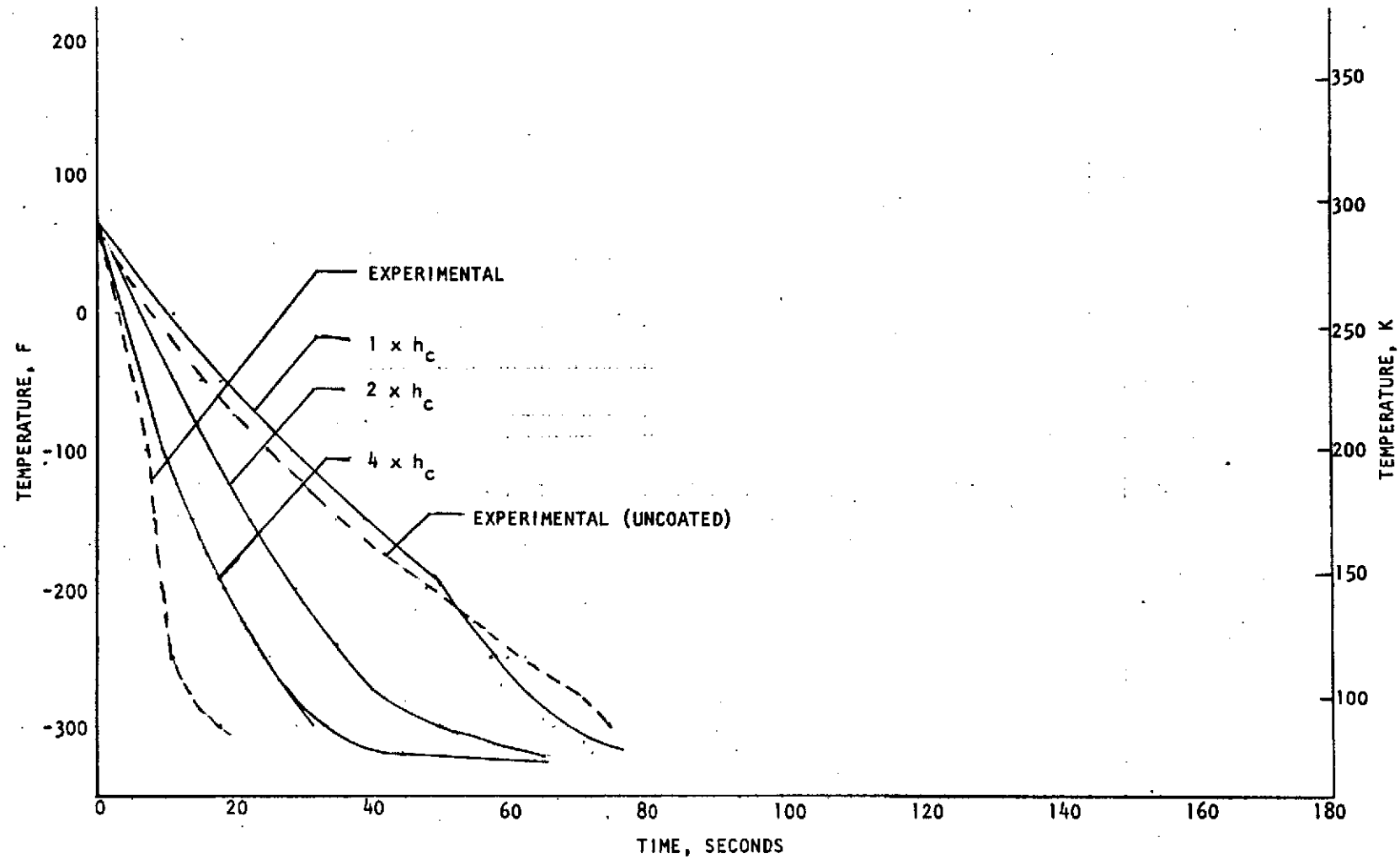

Figure 16. Comparison of Analytical and Experimental LN_2 Chilldown of Kel-F Coated Cylinder Aluminum 1.27×10^{-4} m (0.005 In.)

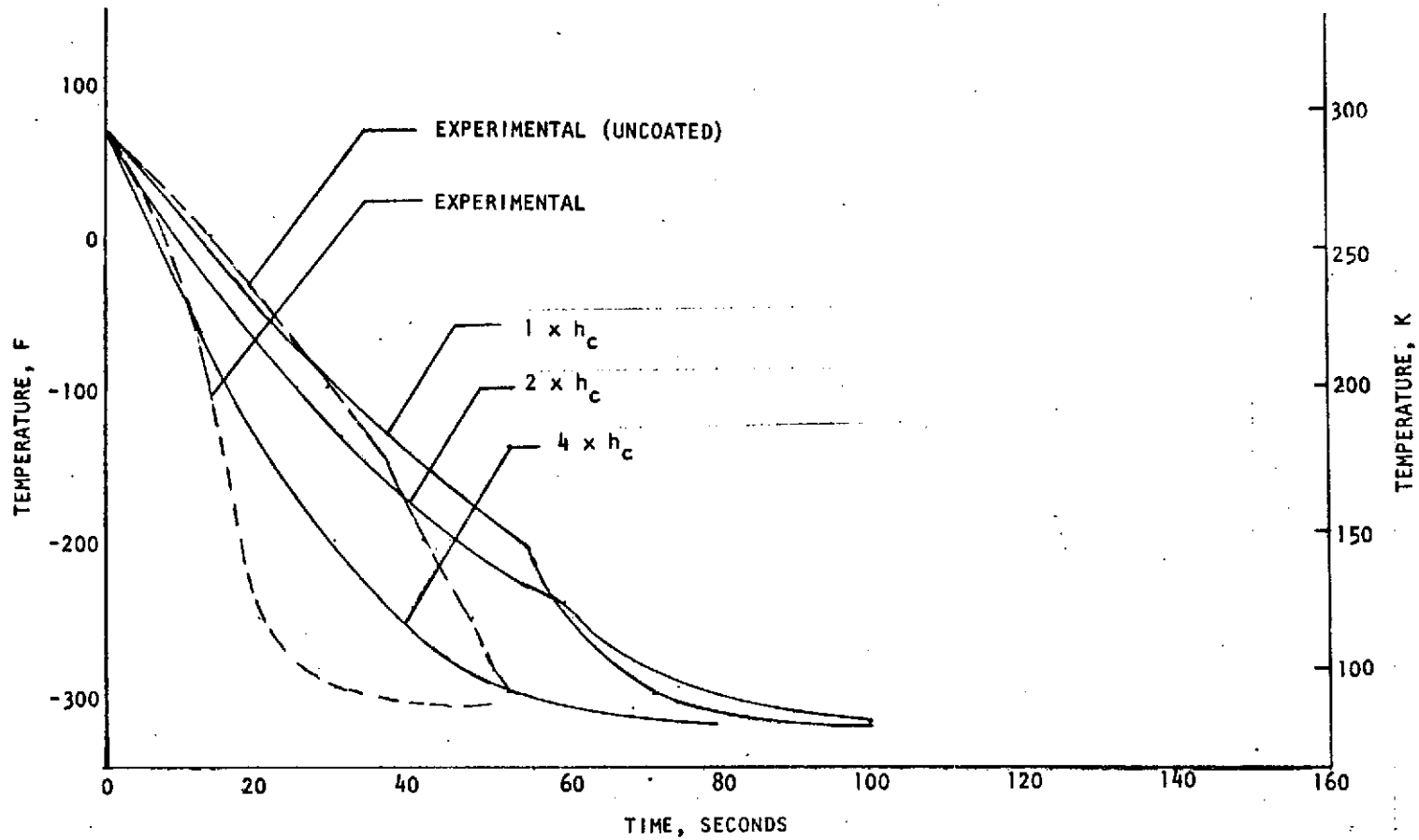

Figure 17. Comparison of Analytical and Experimental LN_2 Chilldown of Kel-F Coated Cylinder Titanium 1.27×10^{-4} m (0.005 In.)

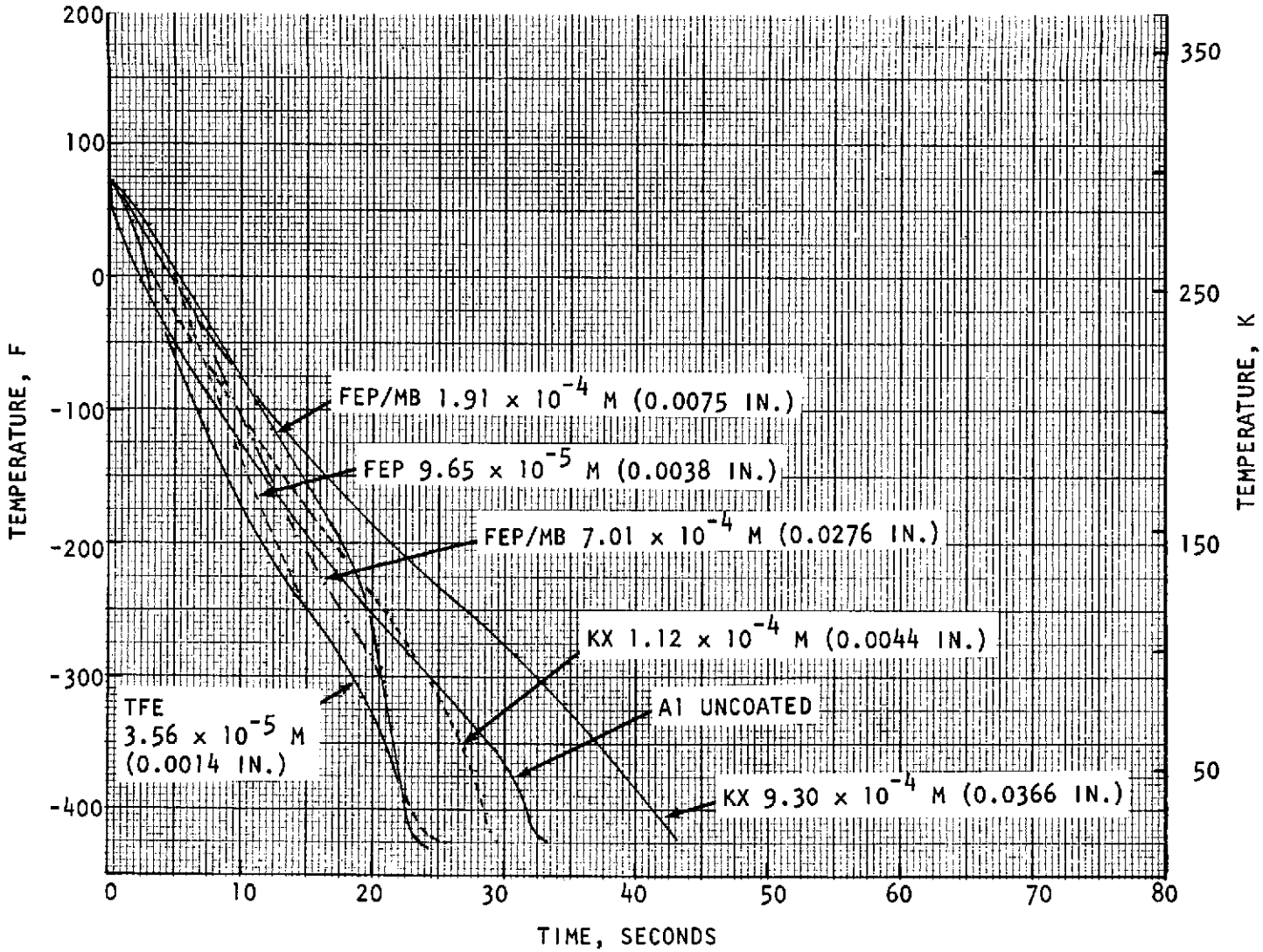

Figure 18. LH_2 Immersion of Aluminum With and Without Coatings (Without Cork Insulator)

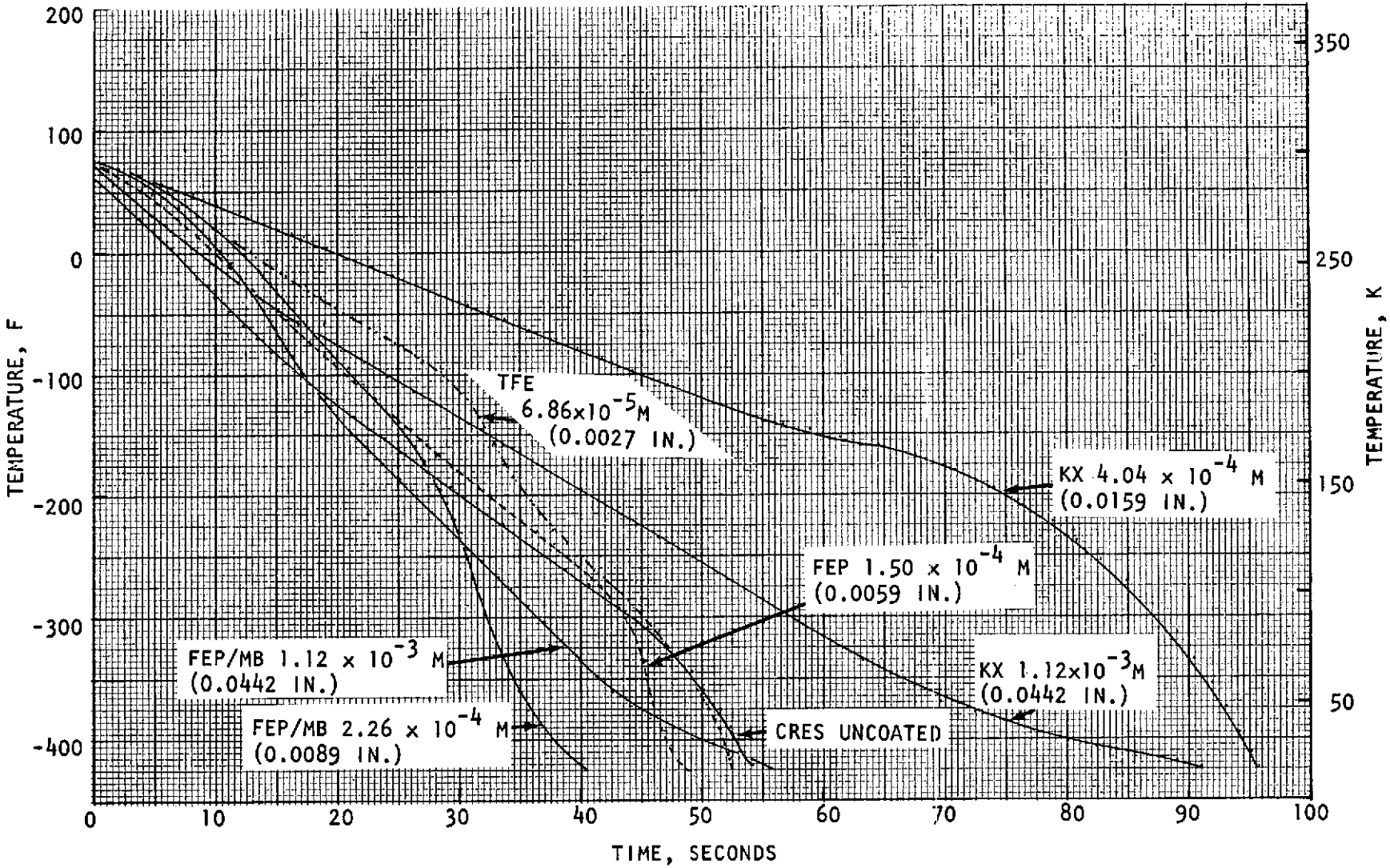

Figure 19. LH_2 Immersion of CRES With and Without Coatings (Without Cork Insulator)

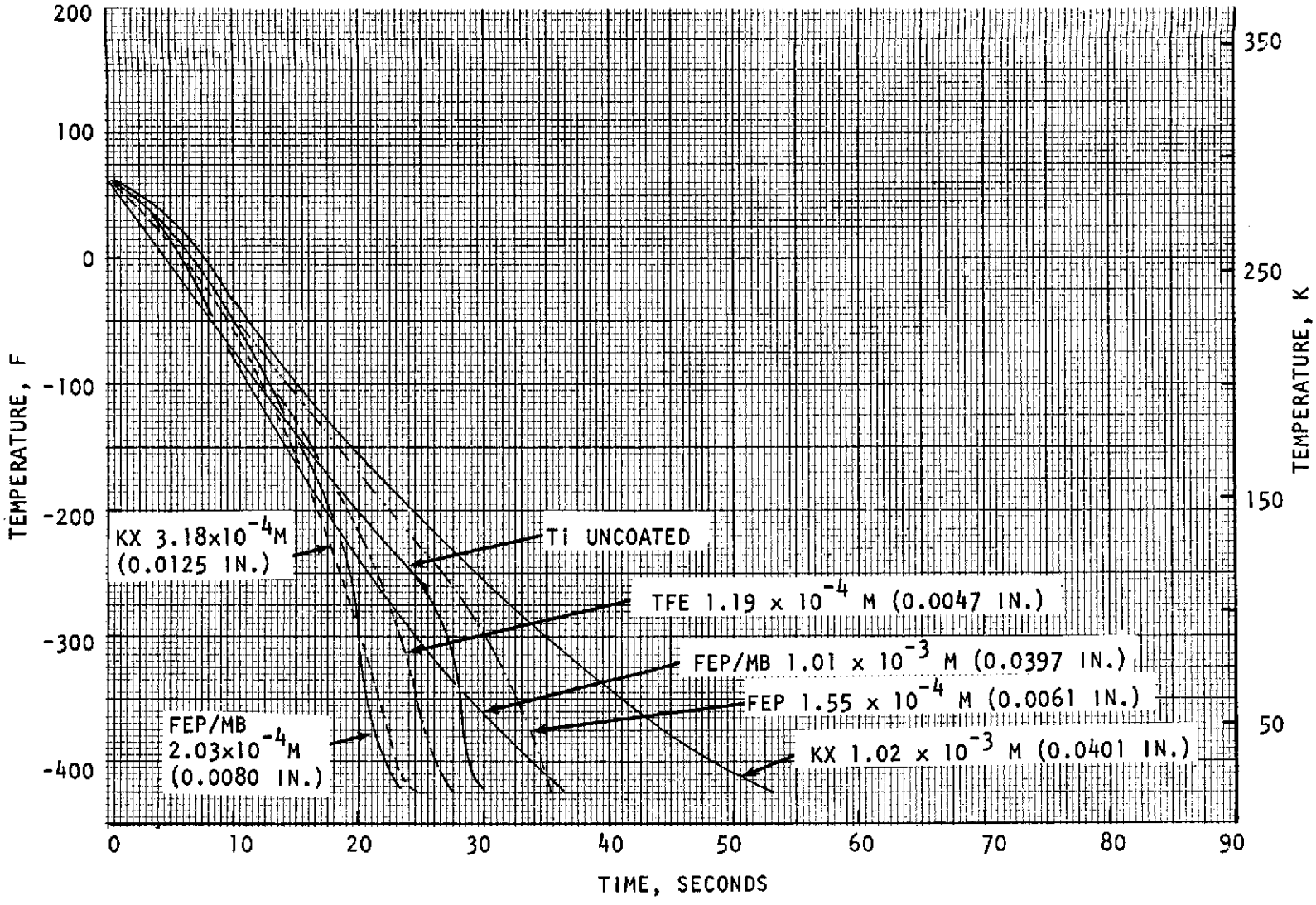

Figure 20. LH_2 Immersion of Titanium With and Without Coatings (Without Cork Insulator)

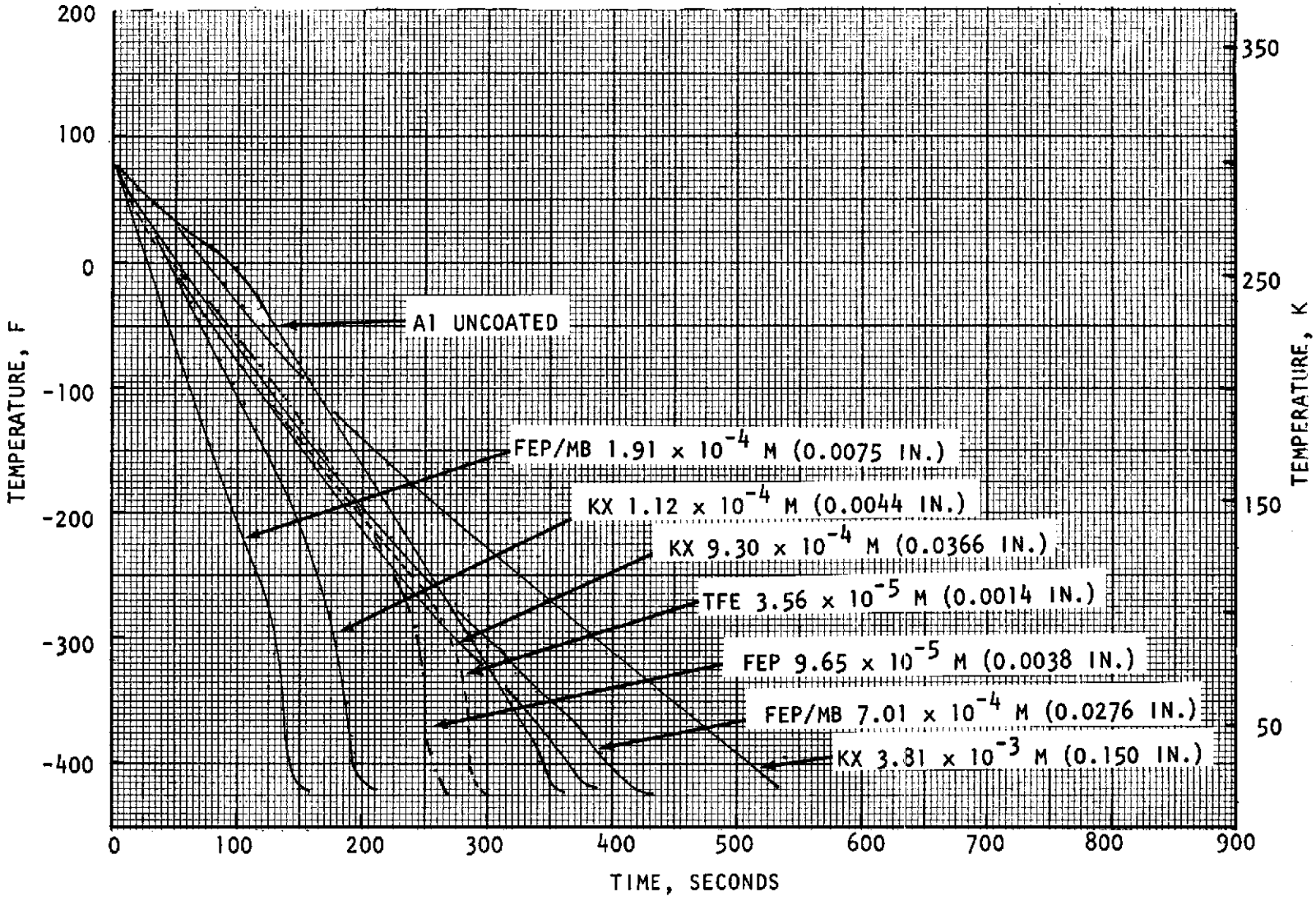

Figure 21. LH_2 Immersion of Aluminum With and Without Coatings (With Cork Insulator)

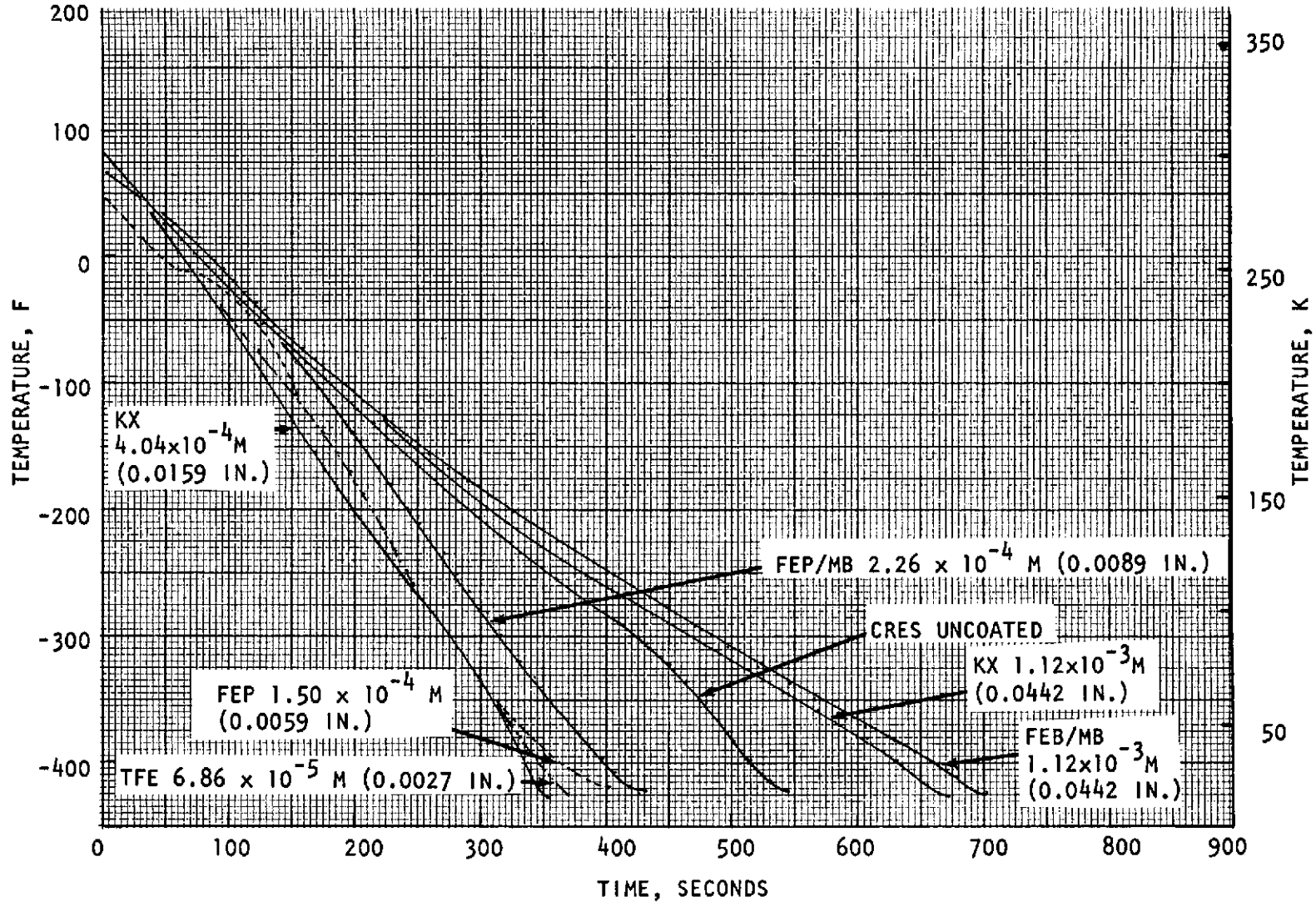

Figure 22. LH_2 Immersion of CRES With and Without Coatings (With Cork Insulator)

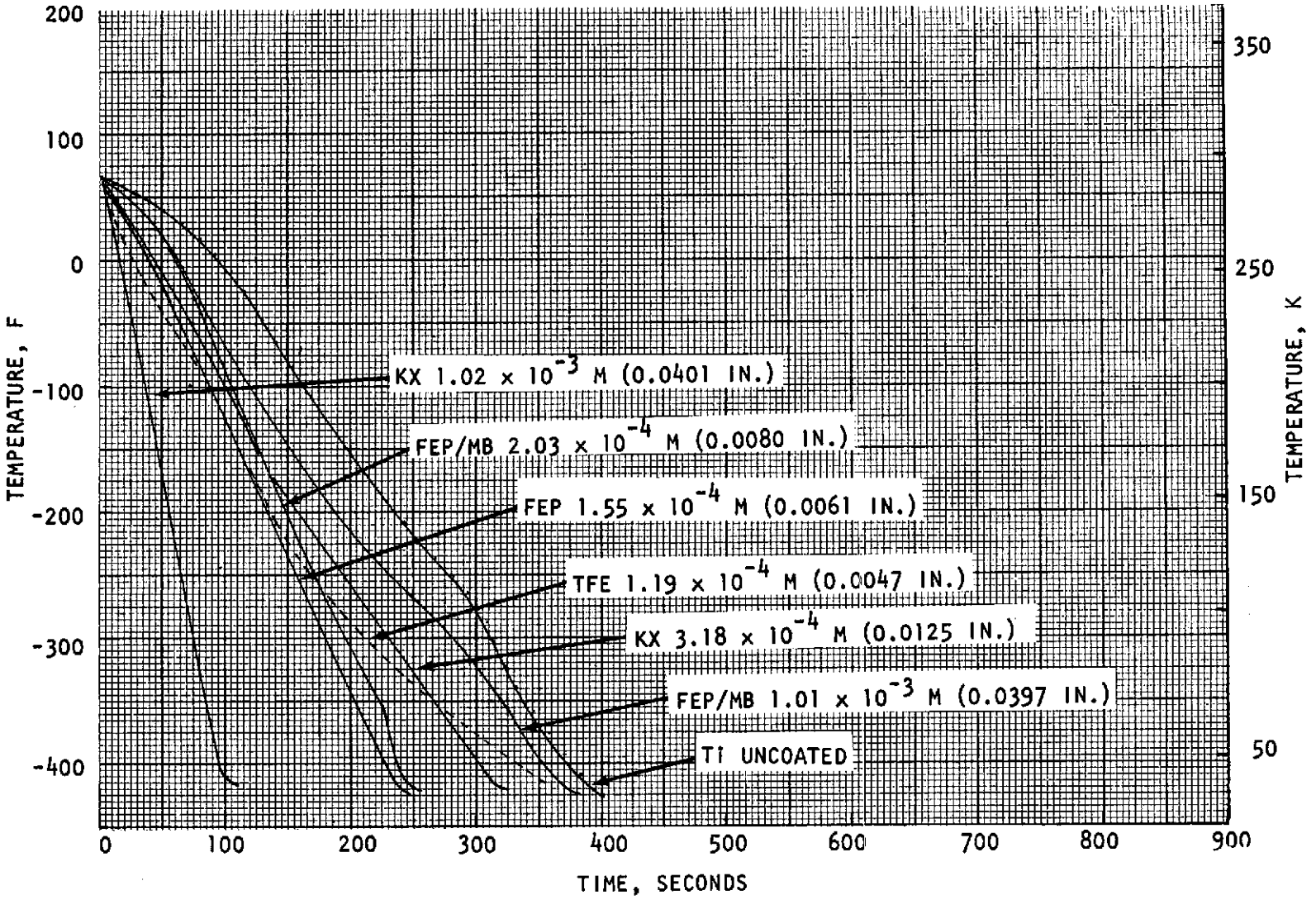

Figure 23. LH_2 Immersion of Titanium With and Without Coatings (With Cork Insulator)

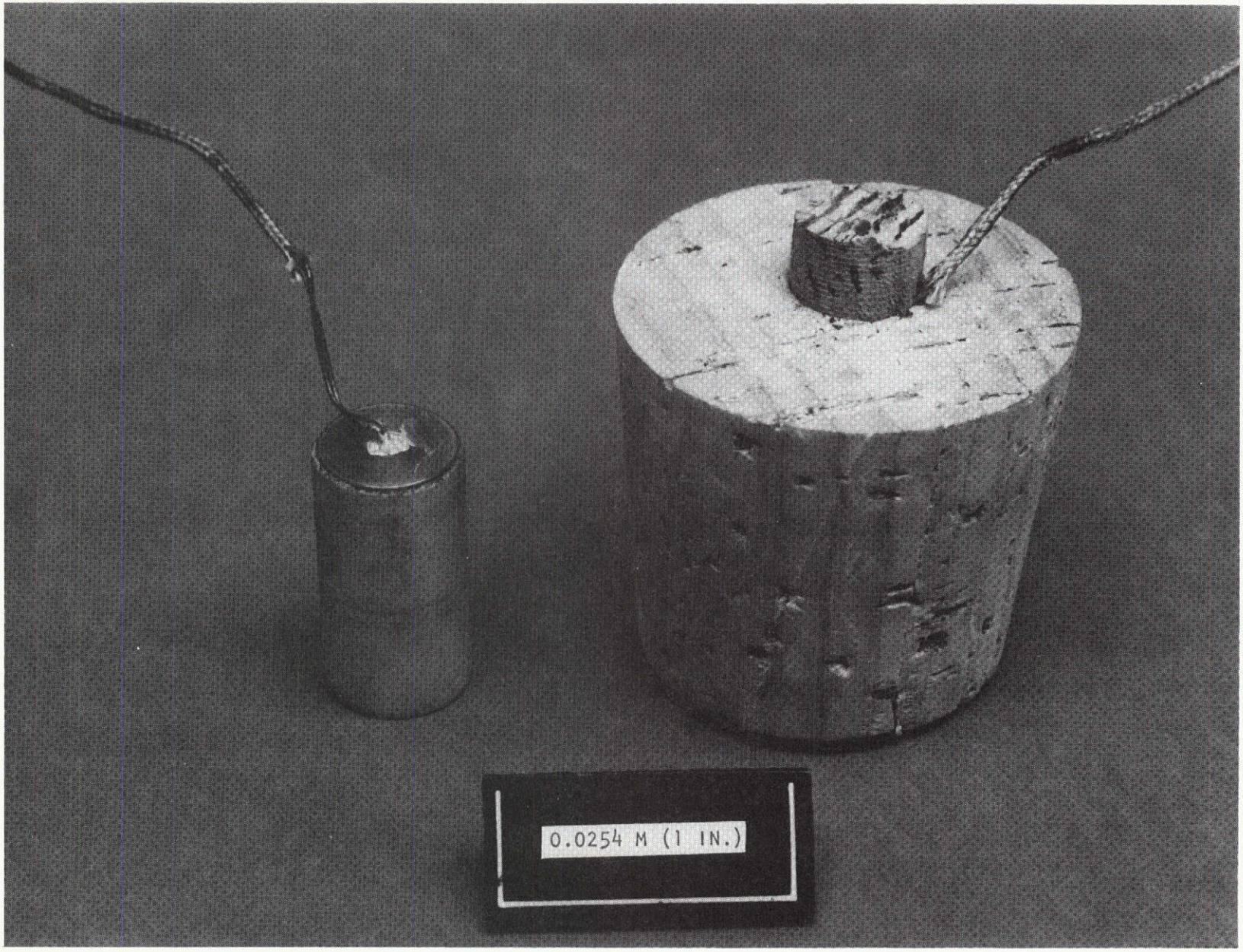

1XZ52-9/27/71-C1

Figure 24. Corked and Uncorked Bare Test Cylinders

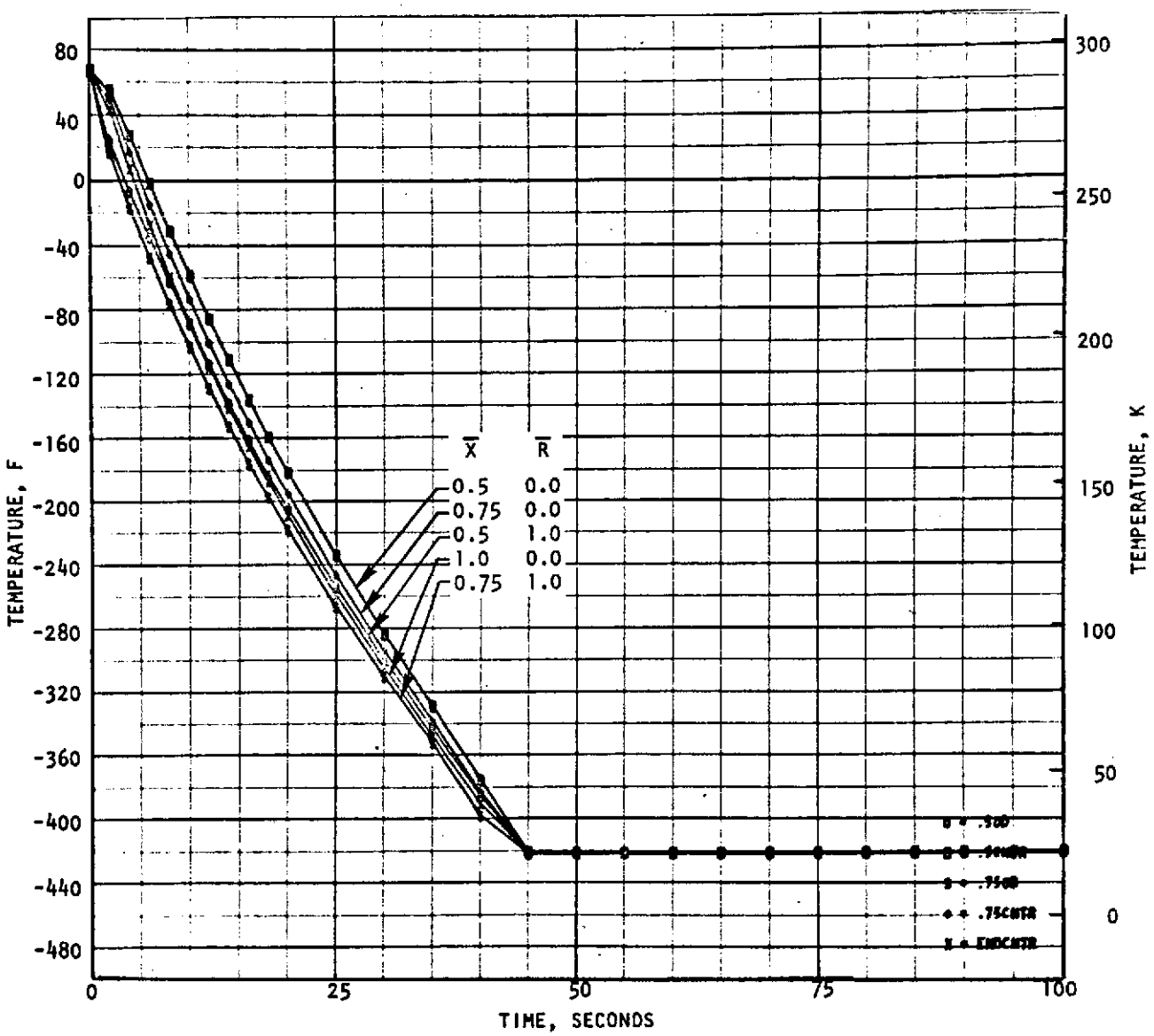

Figure 25. Chilldown of Titanium Cylinder in LH_2 Bath-Analytical Prediction

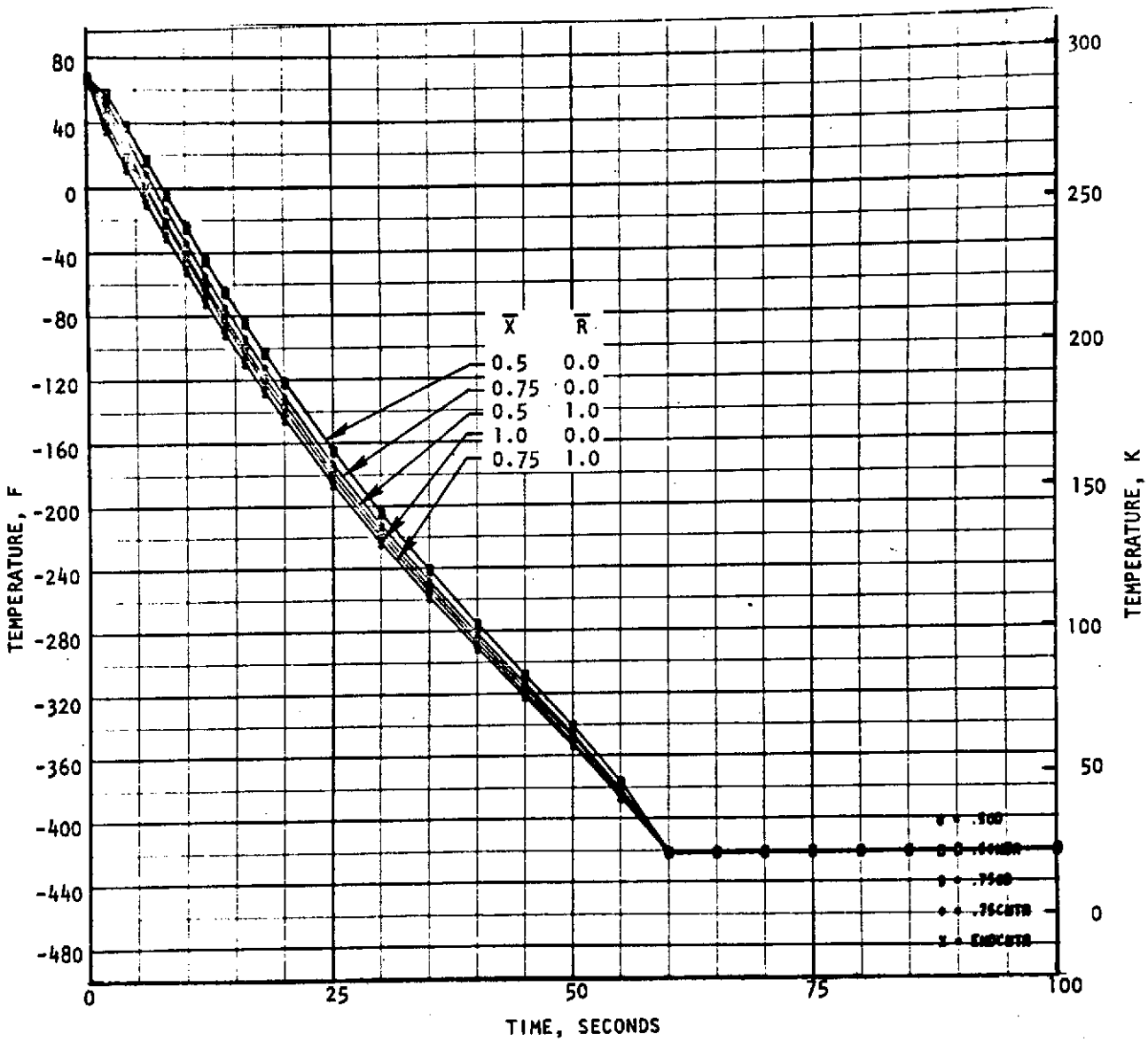

Figure 26. Chilldown of Bare CRES Cylinders in LH_2 Bath

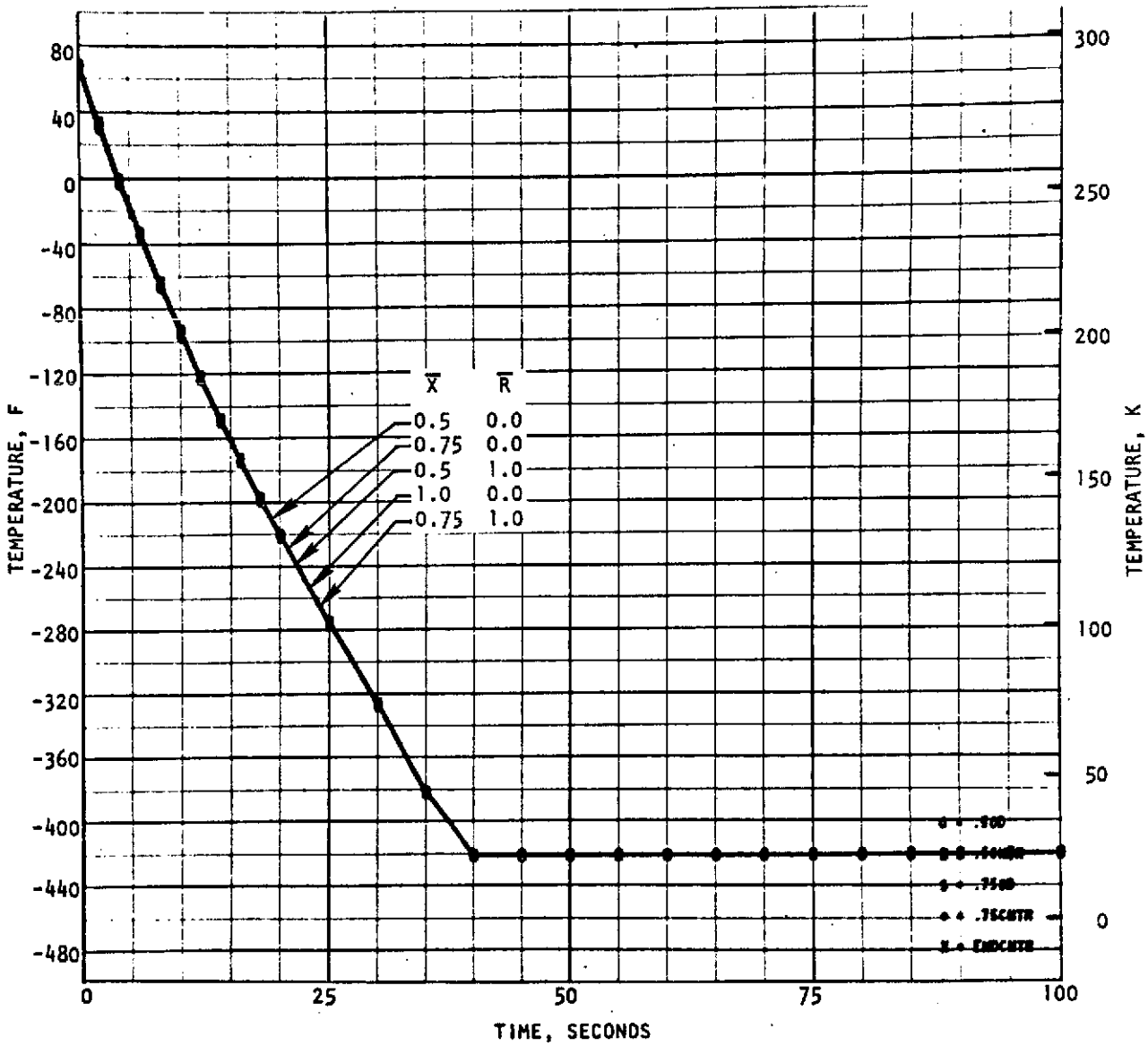

Figure 27. Chilldown of Bare Aluminum Cylinders in LH_2 Bath

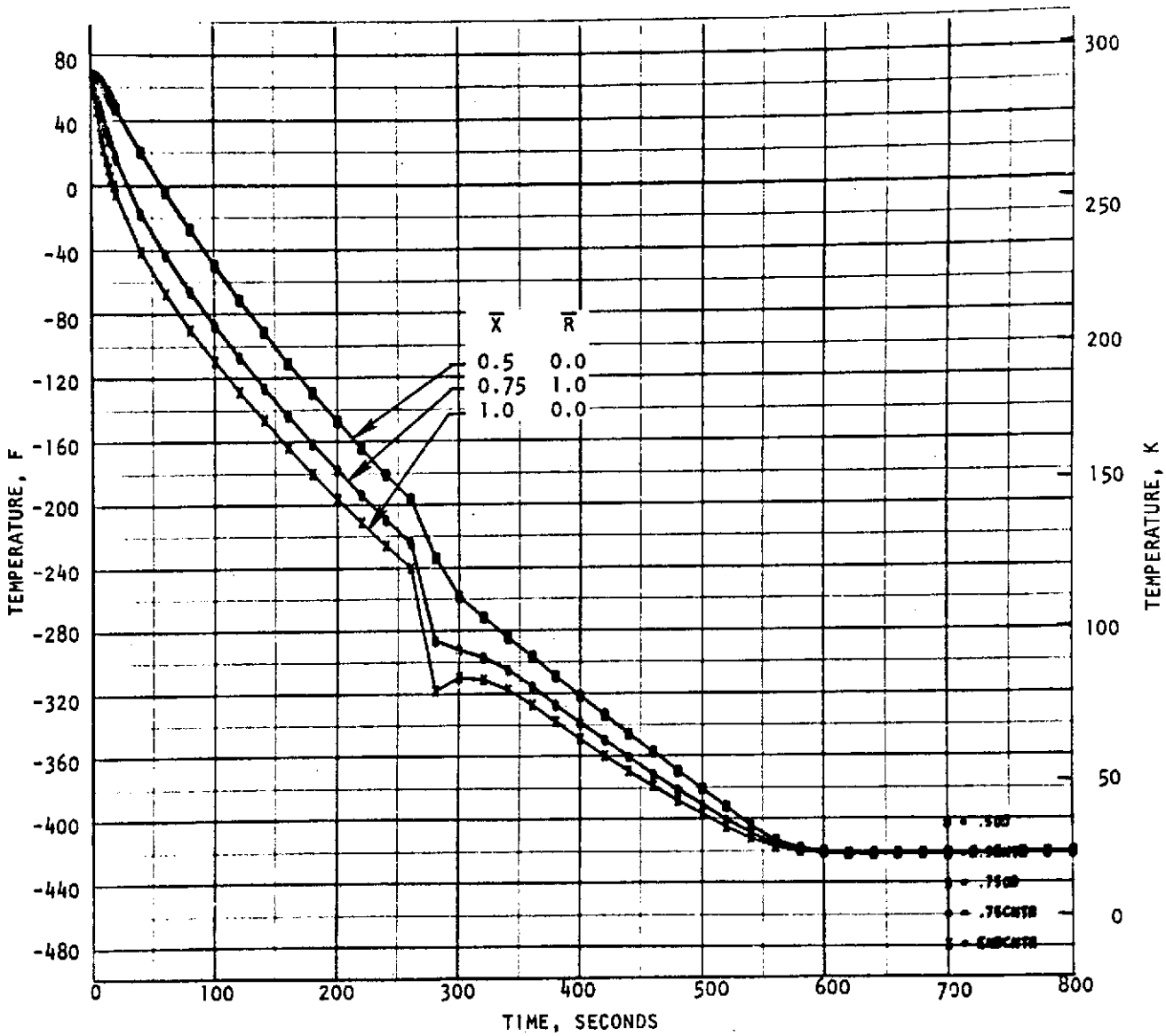

Figure 28. Analysis of Titanium Cylinders in LH_2 Bath

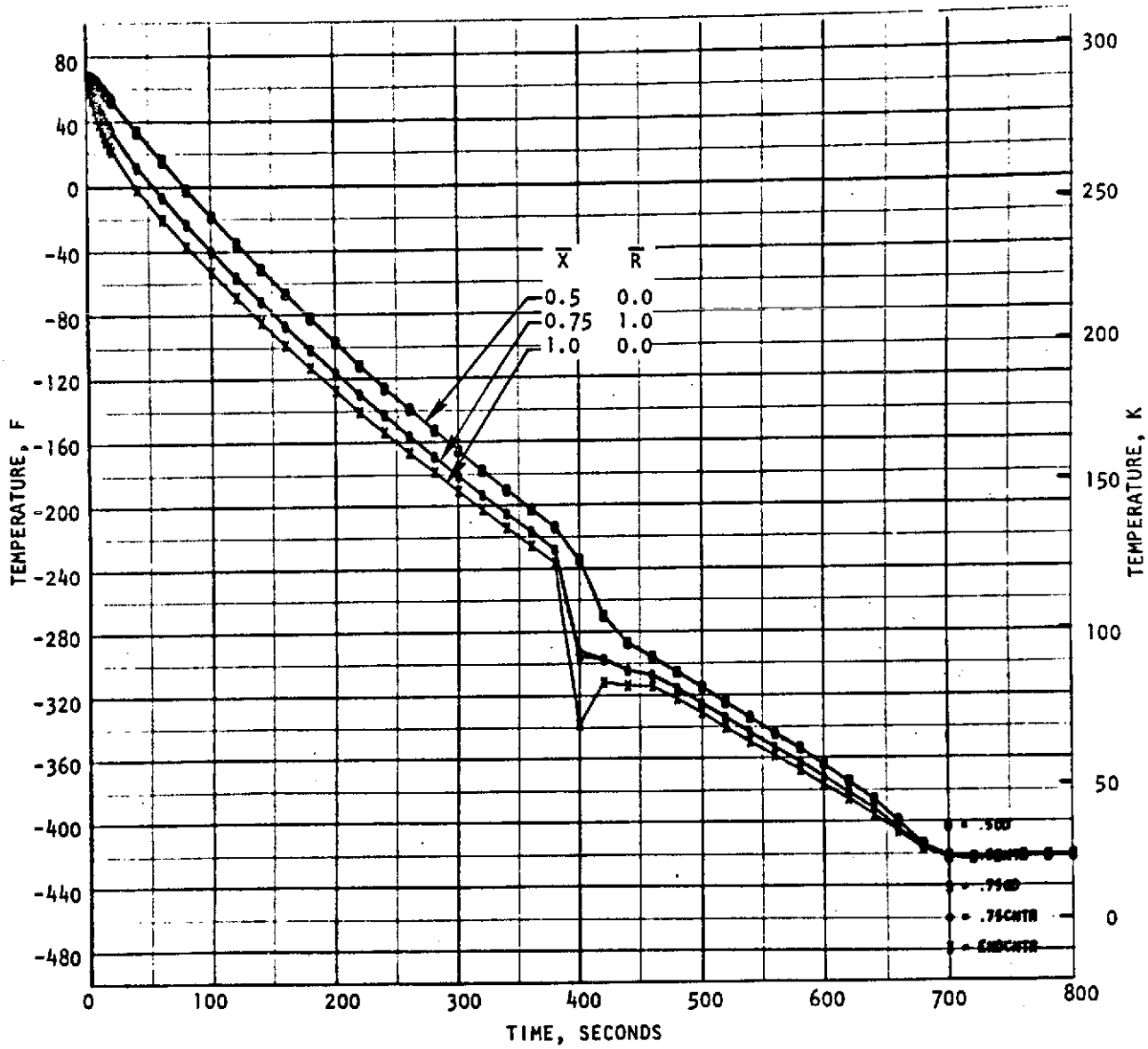

Figure 29. CRES Cylinders Chilled From One End in LH_2 Bath-Analytical Prediction

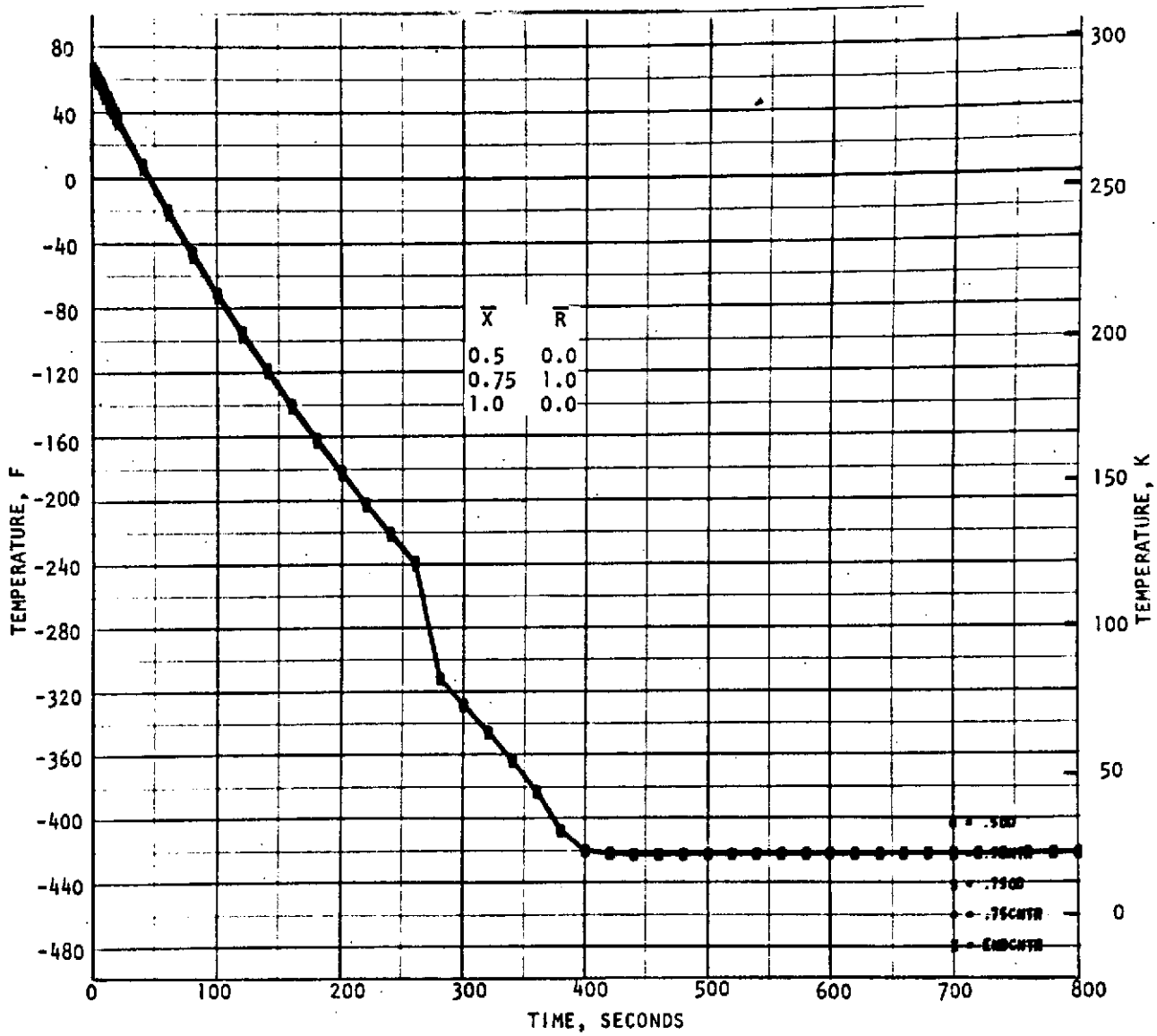

Figure 30. Aluminum Cylinder Chilled From One End in LH_2 Bath-Analytical Prediction

Additional analytical computer cases were run at a 16-percent increased LH_2 film coefficient, which brought the analytical results into close agreement to the experimental test data.

Coated Cylinder Model. Both the simplified analytical model for chilldown and the digital computer exact chilldown model were developed during the previous studies. The simplified model used for the chilldown of the test metal cylinders without coatings (without the chilldown enhancement associated with the coating) was previously expressed as:

$$\left[\frac{T_w - T_{LN_2}}{T_{wi} - T_{LN_2}}\right] = e^{-\left(\frac{h_{c_1}\beta\tau}{\rho C_p}\right)}$$

$\beta = \left(\frac{2 + \frac{4L}{D}}{L}\right)$ cylinder without cork insulator

$\beta = \frac{1}{L}$ cylinder with cork insulator

A similar model developed for the insulated cases with coatings was developed:

$$\left[\frac{T_w - T_{LN_2}}{T_{wi} - T_{LN_2}}\right] = e^{-\left(\frac{h_{c_1}\psi\beta\tau}{\rho C_p}\right)}$$

where ψ is a chilldown enhancement ratio

$$\psi = \left(\frac{1}{\frac{h_{c_1}}{h_{c_2}} + N_{bi_1}}\right)$$

The Biot number of the coating is based on the reference film coefficient h_{c_1} for the uncoated cylinder and the coating thickness to conductivity ratio.

$$B_{bi_1} \equiv \left(\frac{h_{c_1} t}{k_c}\right)$$

Material chilldown enhancement over the uncoated case occurs when $\psi > 1.0$ and chilldown retardation results when $\psi < 1.0$. At the $\psi = 1$ point where chilldown enhancement and retardation are divided:

$$\left(\frac{h_{c_1}}{h_{c_2}}\right) = \left(1 - N_{bi_1}\right)$$

Figure 31 illustrates the effect of coating Biot number versus enhancement factor. As shown, the Biot number of the coating must be in the ≤ 0.5 range in order to provide any appreciable chilldown time enhancement. For large N_{Bi} values the fast chilldown is obviously degraded.

Based on the levels of LN_2 film boiling, LH_2 film boiling, and LH_2 forced convection shown in Fig. 32, for a mean coating conductivity of 0.075 J/m-s-K (1×10^{-6} Btu/in-sec-R) for LN_2 film boiling, a thickness of approximately 2.54×10^{-4}m (0.010 inch) appears optimum. For LH_2 film boiling, shown with the attendant higher film coefficient, an 1.52×10^{-4} m (0.006 inch) coating appears optimum. For the respective higher film coefficient levels for 127, 633, and 1266 kg/m^2-s (0.1, 0.5 and 1.0 lb/in^2-sec) LH_2 forced convection conditions, coating thicknesses required approach the 2.54×10^{-5}m (0.001 inch) range.

Comparison of Coating Effects in LN_2 and LH_2. Based on a chilldown time comparison to $e^{-2.0}$ or chill to within 13.5 percent of the final temperature value, comparisons were made with both the LN_2 and LH_2 bath chills, with enhancement factors for both the corked and uncorked conditions. As shown in Table 4 for the corked samples tested, time enhancements of 1.5 to 2.4 for the LH_2 bath and 1.6 to 3.7 for the LN_2 bath were obtained.

Chilldown enhancement factors for the samples without the cork insulation are shown in Table 5. Coatings with thicknesses in the range of 5.08×10^{-5} to 1.17×10^{-4}m (0.002 to 0.0046 inch) side thickness were found to have the highest chilldown enhancement ψ values for the LH_2 chilldowns.

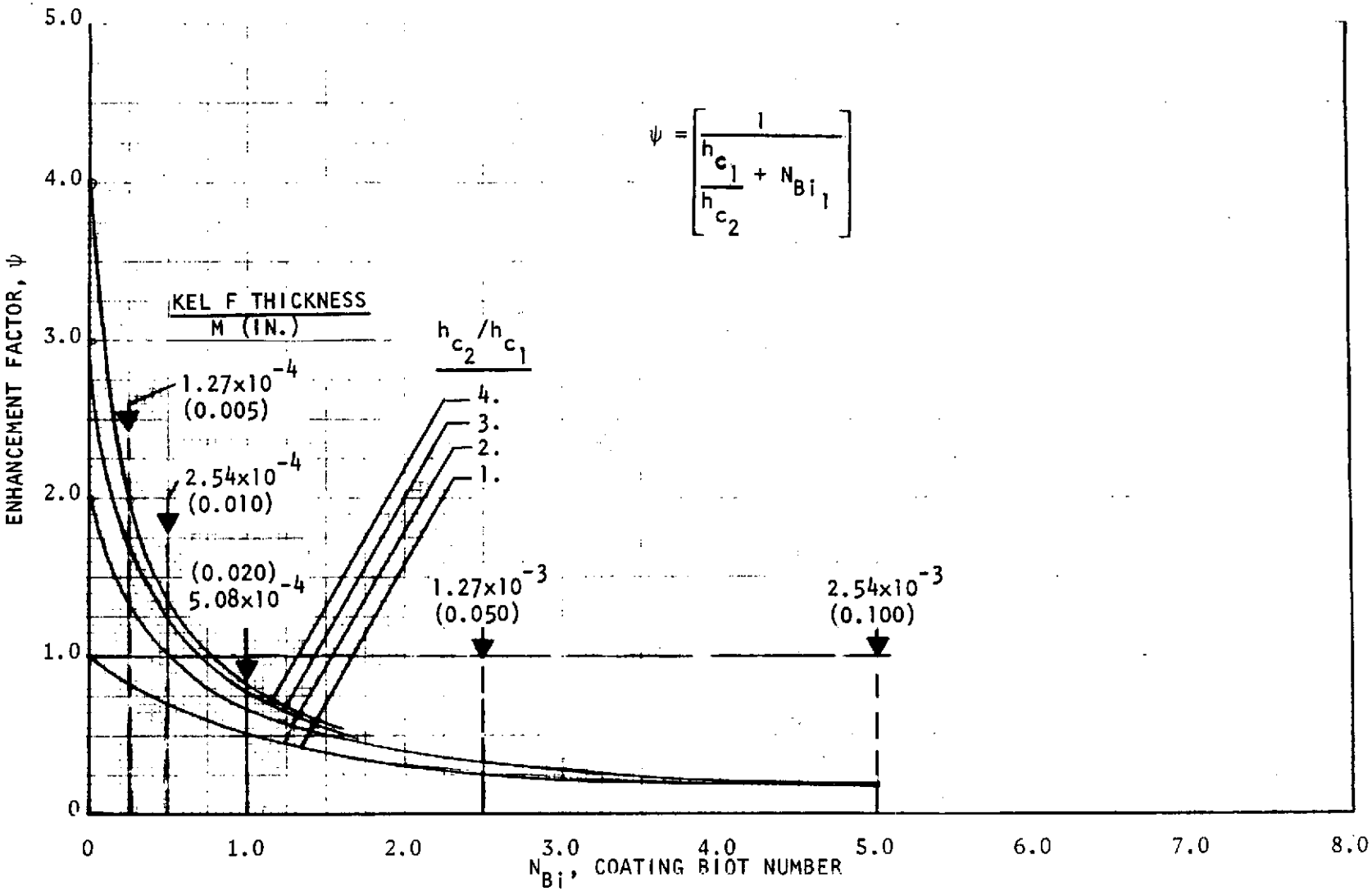

Figure 31. LN_2 Chill Enhancement Factor vs Biot Number

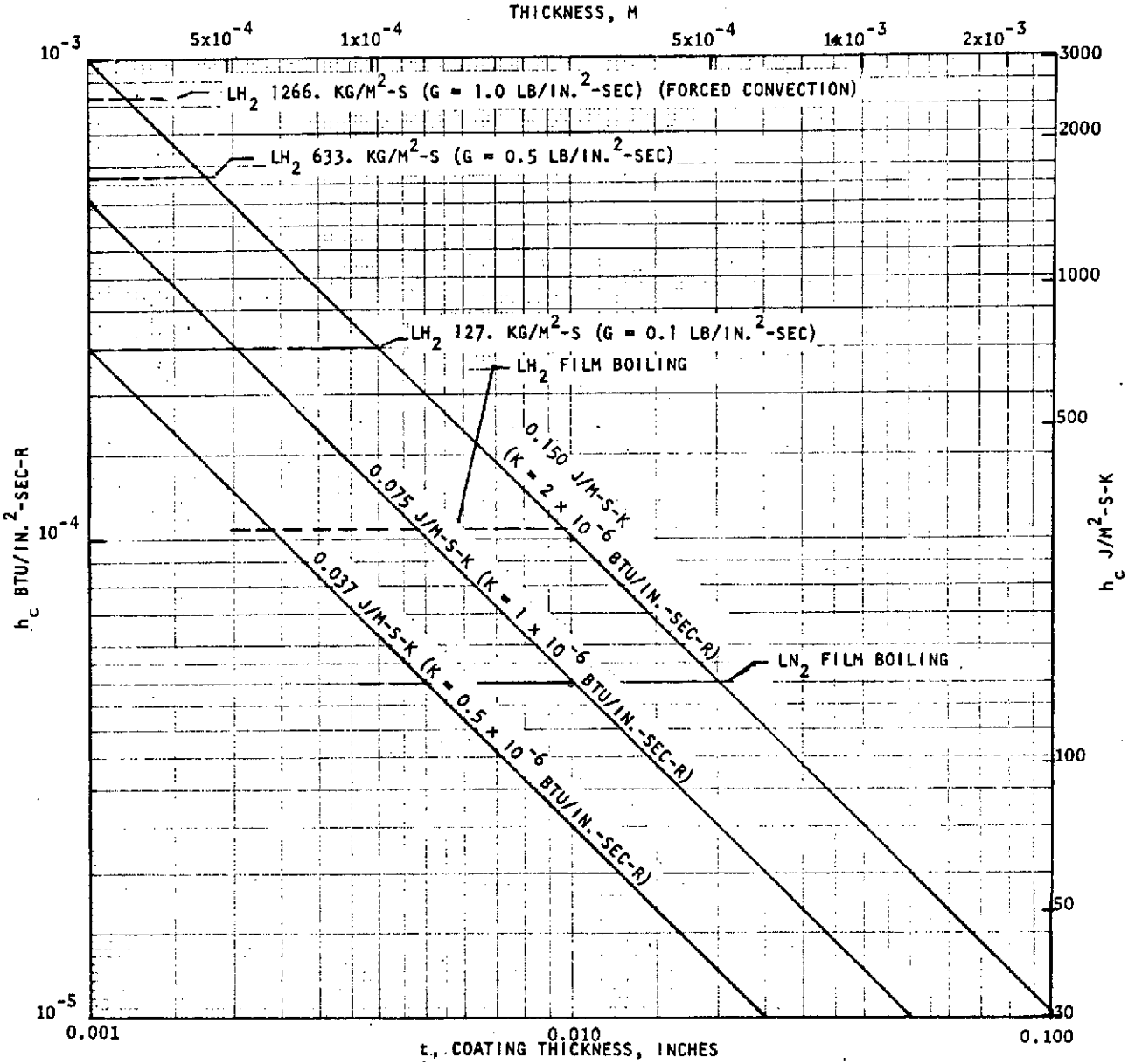

Figure 32. Coating Thickness Requirements vs Applied Film Coefficient (N_{Bi} = 0.5)

TABLE 4. LH_2 AND LN_2 CHILLDOWN COATING ENHANCEMENT FACTORS (CORKED CYLINDER SAMPLES)

Base Material	End Thickness m, (inches)	Coating Material	ψ_{LH_2}	ψ_{LN_2}
Ti	1.55×10^{-4} (0.0061)	FEP	1.64	1.97
	2.03×10^{-4} (0.008)	FEP	1.36	1.13
	3.18×10^{-4} (0.0125)	KEL-F	1.28	1.07
	1.19×10^{-4} (0.0047)	TFE	1.26	1.17
	0 (0)	-	1.0	1.0
	1.01×10^{-3} (0.0397)	FEP	1.04	0.707
	1.02×10^{-3} (0.0401)	KEL-F	4.0*	1.37*
Al	1.91×10^{-4} (0.0075)	FEP	2.35	3.71
	1.12×10^{-4} (0.0044)	KEL-F	1.74	2.07
	9.65×10^{-5} (0.0038)	FEP	1.28	1.62
	3.56×10^{-5} (0.0014)	TFE	1.12	1.51
	0 (0)	-	1.0	1.0
	9.30×10^{-4} (0.0366)	KEL-F	0.912	1.19
	7.01×10^{-4} (0.0276	FEP	0.876	0.712
	3.81×10^{-3} (0.150)	KEL-F	0.768	0.808
CRES	6.86×10^{-5} (0.0027)	TFE	1.53	1.61
	1.50×10^{-4} (0.0059)	FEP	1.53	1.42
	4.04×10^{-4} (0.0159)	KEL-F	1.53*	1.71*
	2.26×10^{-4} (0.0089)	FEP	1.33	1.59
	0 (0)	-	1.0	1.0
	1.12×10^{-3} (0.0442)	KEL-F	0.848	1.01
	1.12×10^{-3} (0.0442)	FEP	0.835	0.917

ψ values >1.0 fast chill

ψ values <1.0 slow chill

*Indicates questionable data due to bad thermocouple or intermittent circuit readings.

TABLE 5. LH_2 AND LN_2 CHILLDOWN COATING ENHANCEMENT FACTORS
(UNCORKED CYLINDER SAMPLES)

	End Thickness m, (inches)	Side Thickness m, (inches)	Coating Material	ψ_{LH_2}	ψ_{LN_2}
Ti	2.03×10^{-4} (0.008)	1.07×10^{-4} (0.0042)	FEP	1.64	1.97
	3.18×10^{-4} (0.0125)	1.17×10^{-4} (0,0046)	KEL-F	1.27	2.25
	1.19×10^{-4} (0.0047)	5.08×10^{-5} (0.002)	TFE	1.12	2.0
	1.55×10^{-4} (0.0061)	5.84×10^{-5} (0.0023)	FEP	0.848*	1.51
	0 (0)	0 (0)	-	1.0	1.0
	1.01×10^{-3} (0.0397)	3.71×10^{-4} (0.0146)	FEP	0.932	0.846
	1.02×10^{-3} (0.0401)	5.11×10^{-4} (0.0201)	KEL-F	0.667	0.902
Al	3.56×10^{-5} (0.0014)	6.10×10^{-5} (0.0024)	TFE	1.41	1.52
	9.65×10^{-5} (0.0038)	5.08×10^{-5} (0.0020)	FEP	1.40	1.52
	1.12×10^{-4} (0.0044)	1.14×10^{-4} (0.0045)	KEL-F	1.09*	4.07*
	1.19×10^{-4} (0.0075)	1.17×10^{-4} (0.0046)	FEP	1.34	--
	7.01×10^{-4} (0.0276)	3.43×10^{-4} (0.0135)	FEP	1.34	--
	0 (0)	0 (0)	-	1.0	1.0
	9.30×10^{-4} (0.0366)	4.72×10^{-4} (0.0186)	KEL-F	0.788	1.03
	3.81×10^{-3} (0.150)	-	KEL-F	---	--
CRES	2.26×10^{-4} (0.0089)	9.65×10^{-5} (0.0038)	FEP	1.43	2.22
	1.50×10^{-4} (0.0059)	5.84×10^{-5} (0.0023)	FEP	1.15*	1.82
	6.86×10^{-5} (0.0027)	5.08×10^{-5} (0.002)	TFE	1.01*	3.5
	4.04×10^{-4} (0.0159)	1.09×10^{-4} (0.0043)	KEL-F	0.544*	2.97
	0 (0)	0 (0)	-	1.0	1.0
	$1.12z10^{-3}$ (0.0442)	$3.51z10^{-4}$ (0.0138)	FEP	1.18	0.70
	1.12×10^{-3} (0.0442)	4.88×10^{-4} (0.0192)	KEL-F	0.744	1.40

ψ values >1.0 fast chill

ψ values <1.0 slow chill

*Indicates questionable data due to bad thermocouple or intermittent circuit readings

It is expected that with the higher LH_2 film coefficients, the optimum coating thickness for enhancement will be in the 2.54×10^{-5} to 7.62×10^{-5}m (0.001 to 0.003 inch) range.

Comparison of LN_2 and LH_2 Coefficients. Based on the chilldown rates obtained for the test cylinders with and without the cork insulators, the film coefficients obtained were compared as shown in Fig. 33. Also shown are the General Dynamics analytical LN_2 boiling curve employed in the inlet line chilldown model. Good agreement is shown in the LN_2 heat flux conditions.

Thermal Analysis of LH_2 Flow Chilldown of Coated and Uncoated Turbular Collars

The data from the experimental LH_2 flow testing of the coated and uncoated tubular collars (made from aluminum, titanium, and stainless steel) at the three flowrates of 1.89×10^{-3}, 5.05×10^{-3}, and 1.26×10^{-2}m 3/s (30, 80, and 200 gpm) were analyzed. The flow data for the series of seven tests ranging from 211 to 1230 kg/m^2-s (0.3 to 1.75 lb/in^2-sec) mass velocity is illustrated in Fig. 34 through 40. Oscillations in flow about a mean level are seen as characteristic of chilldowns with large vapor percentages formed. The chilldown temperatures vs time for the aluminum, CRES, and titanium collars may be seen illustrated in Fig. 41 through 46 for the $1.89 \times 10^{-3} m^3/s$ (30 gpm) flowrate. Figures 47 through 52 illustrate the 5.05×10^{-3} m^3/s (80 gpm) flowrate conditions and Fig. 53 through 58, the $1.26 \times 10^{-2} m^3/s$ (200 gpm) flow condition.

Data Interpretation. The heat transfer data were reduced in terms of the time taken to achieve chilldown temperatures to within $1/e^2$ (13.5 percent) of the final value of 20K (-423 F). In addition, the rating factor ψ which compares the equivalent enhancement on the hydrogen film coefficient over the chill period was developed for the coated and uncoated samples. Tables 6 through 8 illustrate the summary results for the aluminum, titanium, and CRES wall materials respectively.

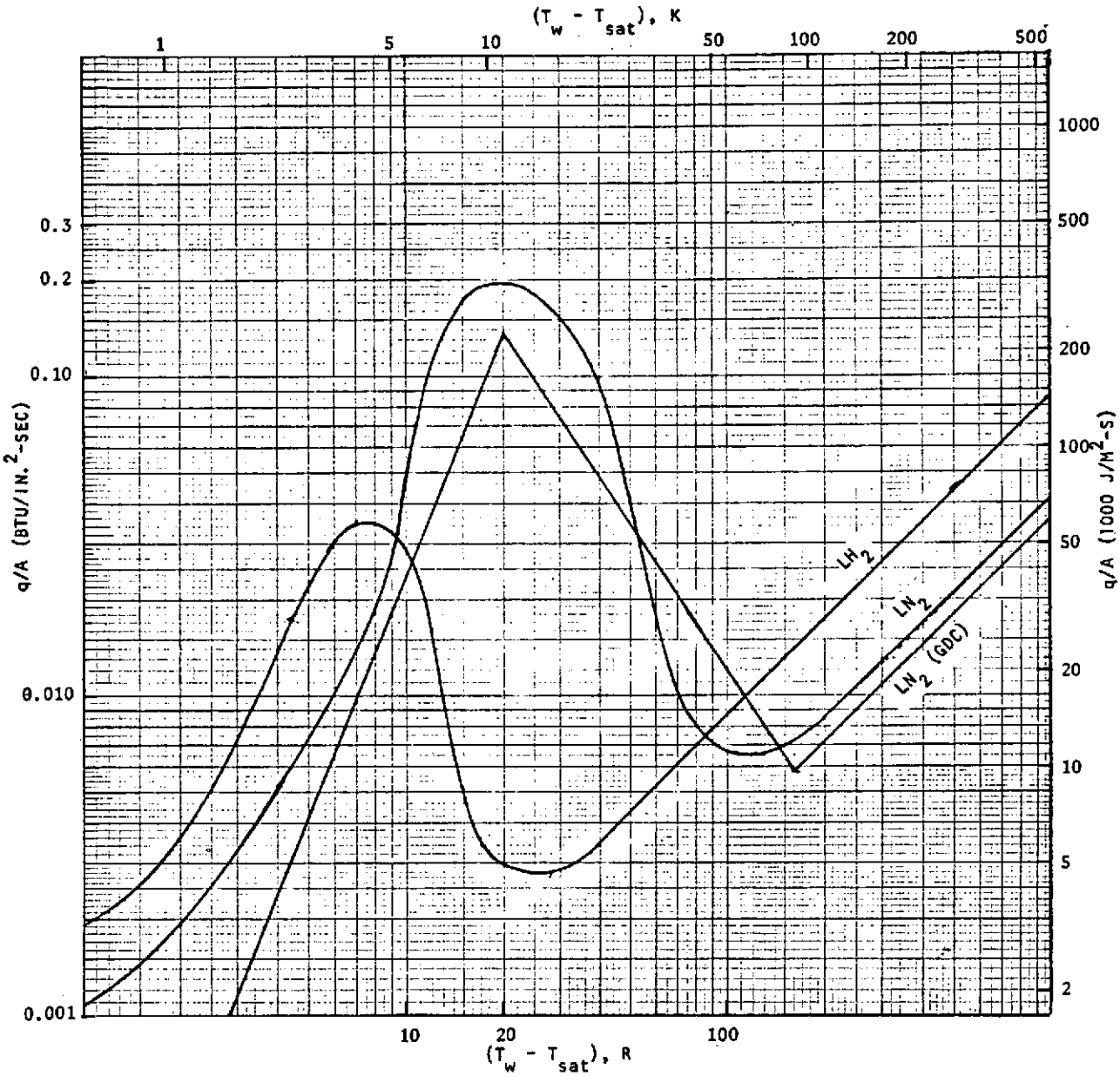

Figure 33. LH_2 and LN_2 Boiling Heat Transfer Rates vs ΔT

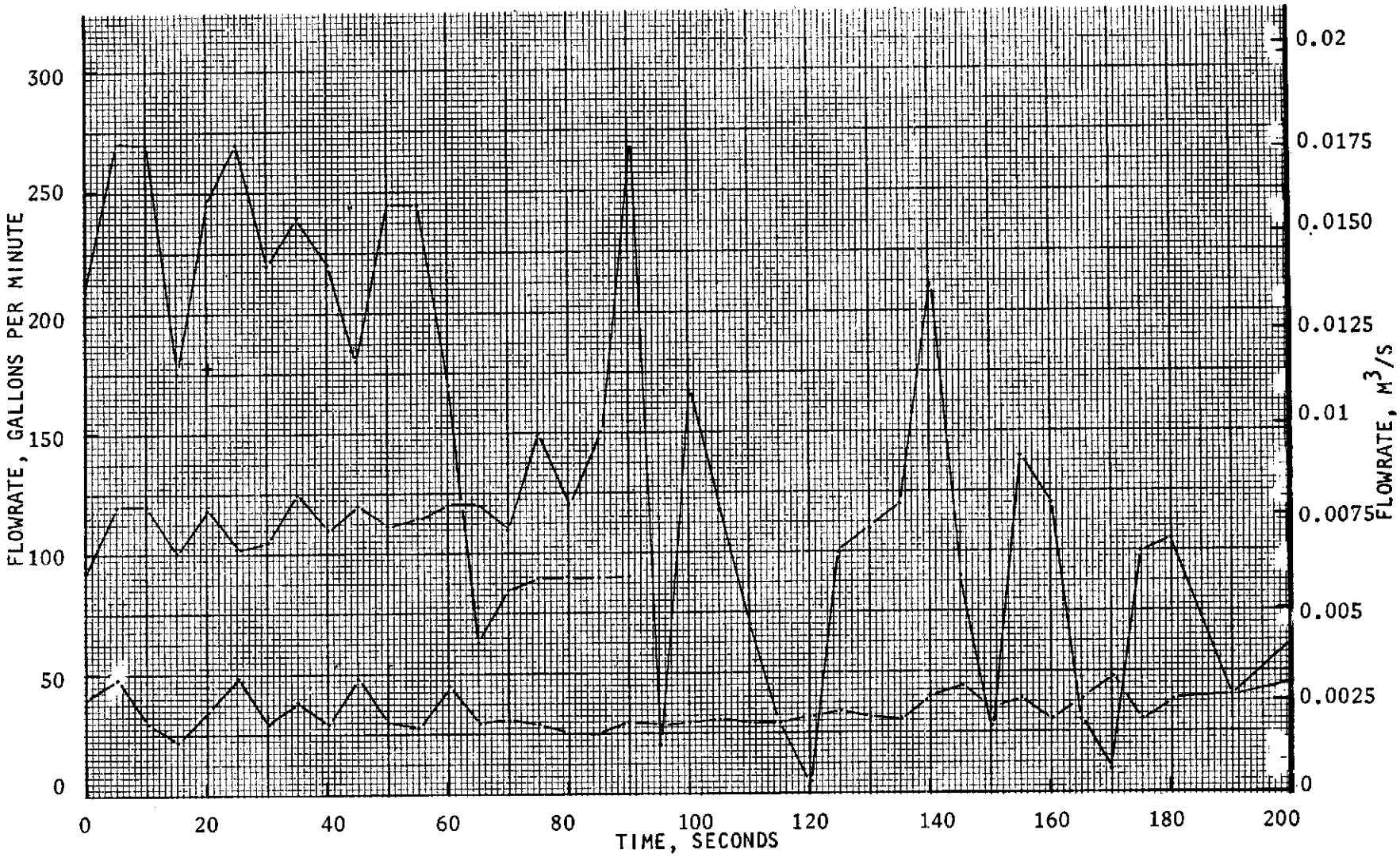

Figure 34. Liquid Hydrogen Flowrate for Test 1

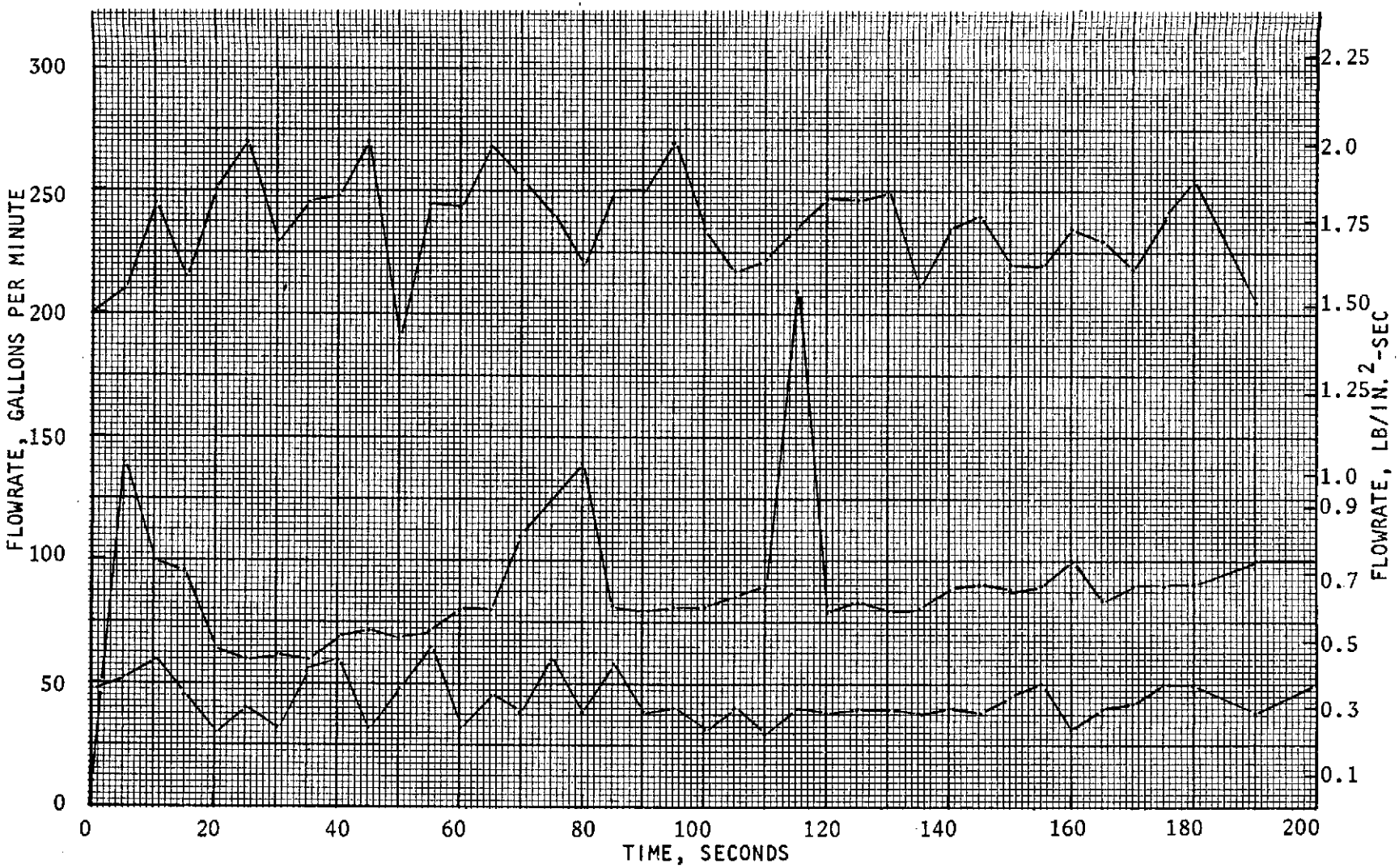

Figure 35. Liquid Hydrogen Flowrate for Test 2

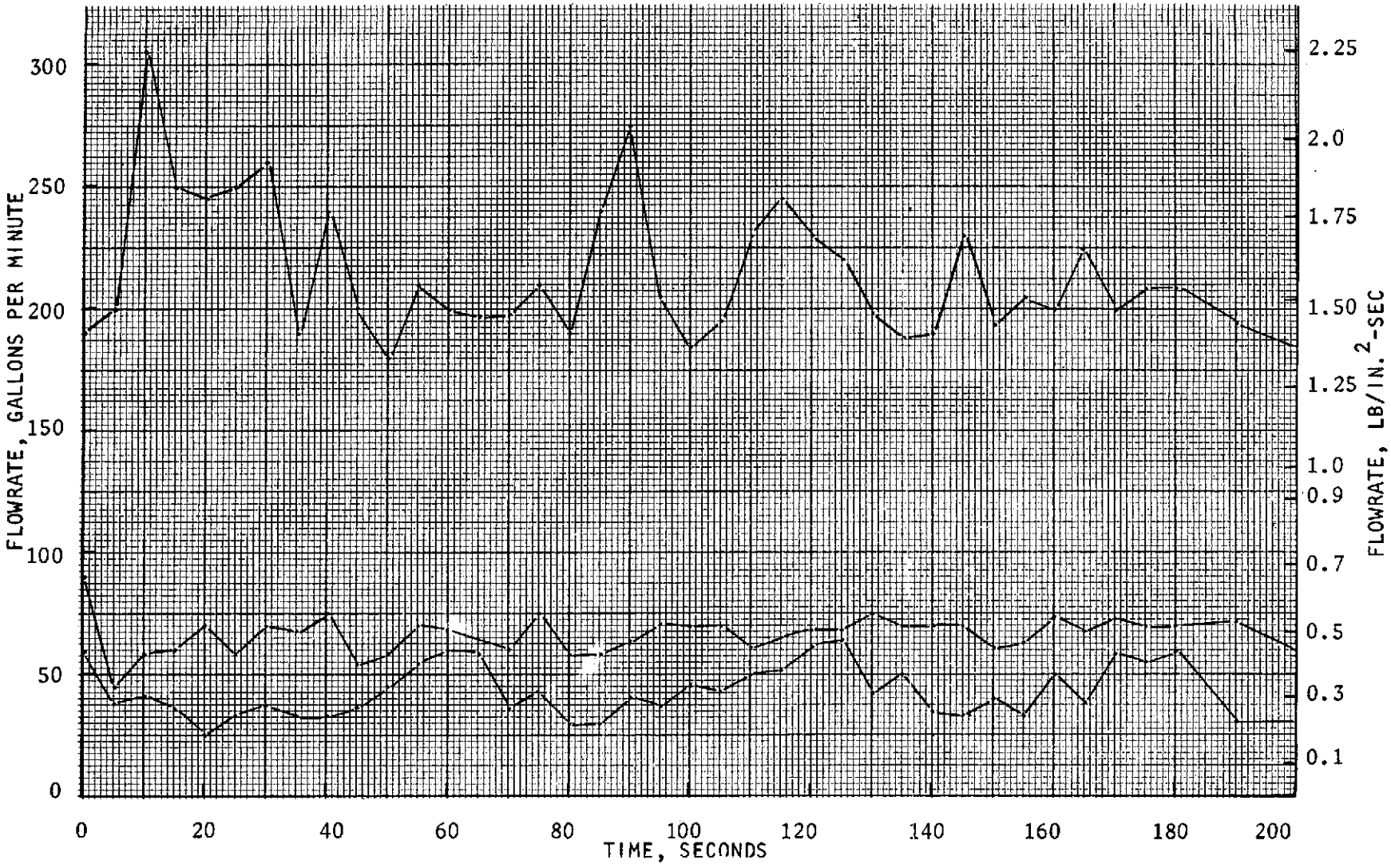

Figure 36. Liquid Hydrogen Flowrate for Test 3

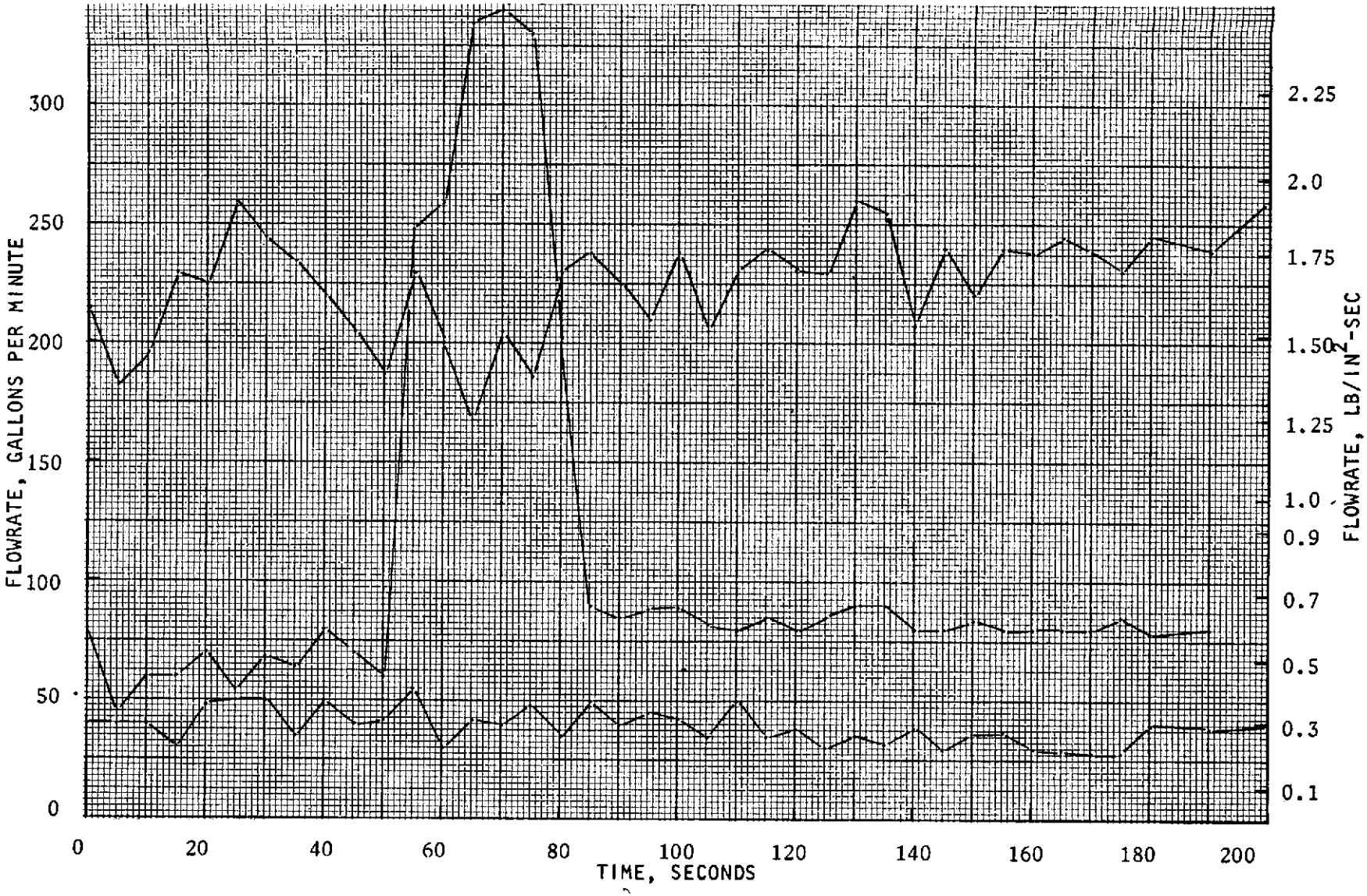

Figure 37. Liquid Hydrogen Flowrate for Test 4

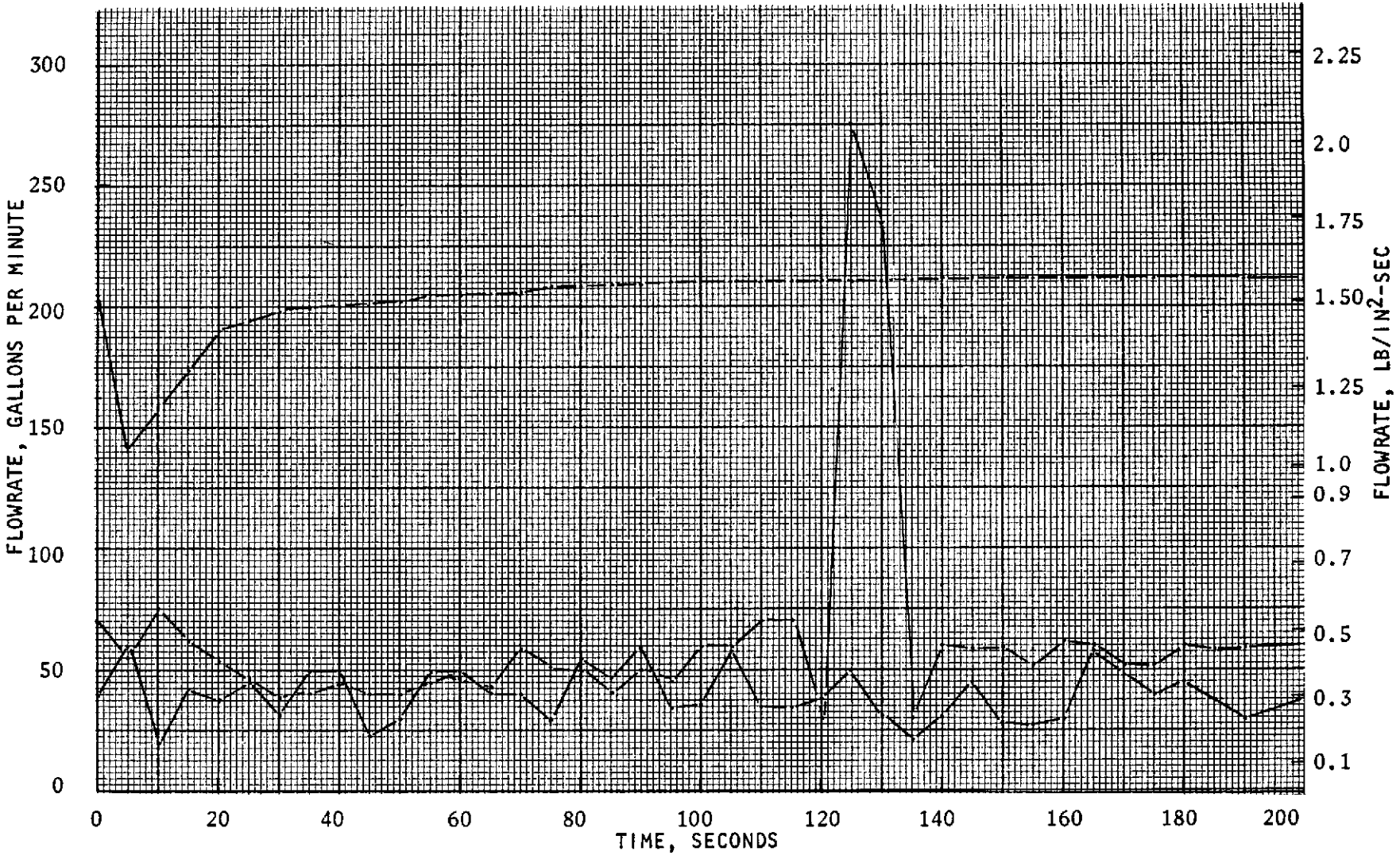

Figure 38. Liquid Hydrogen Flowrate for Test 5

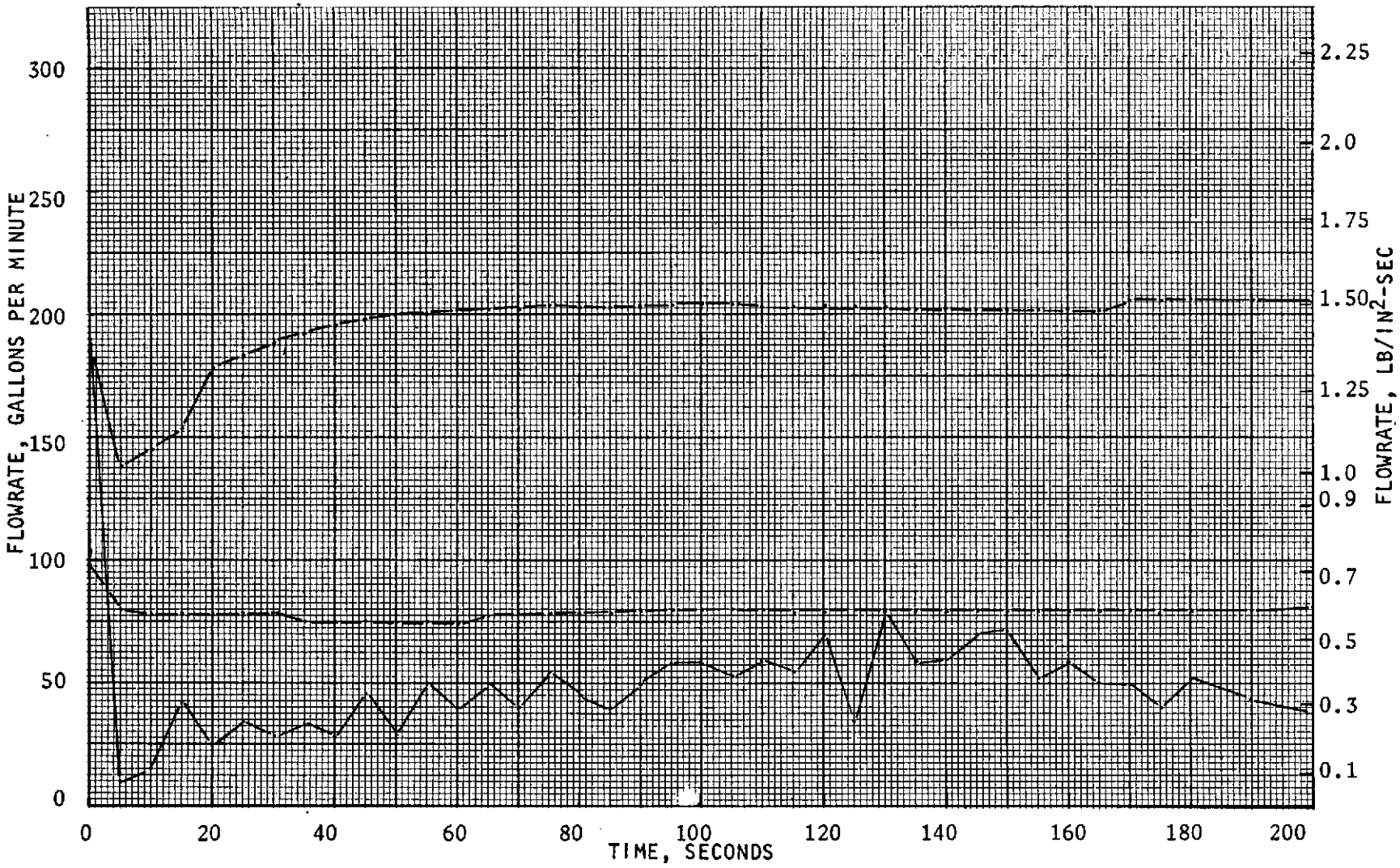

Figure 39. Liquid Hydrogen Flowrate for Test 6

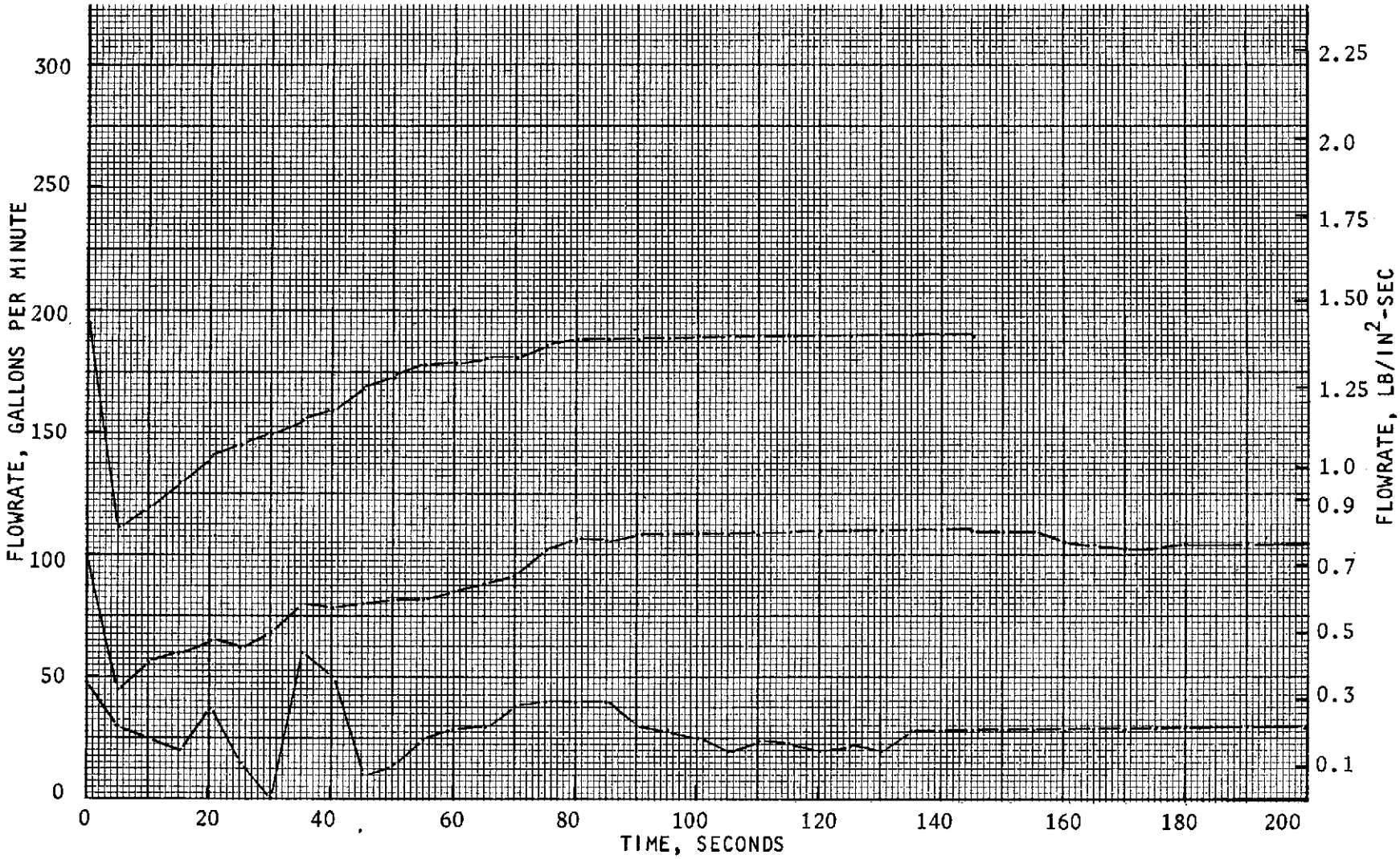

Figure 40. Liquid Hydrogen Flowrate for Test 7

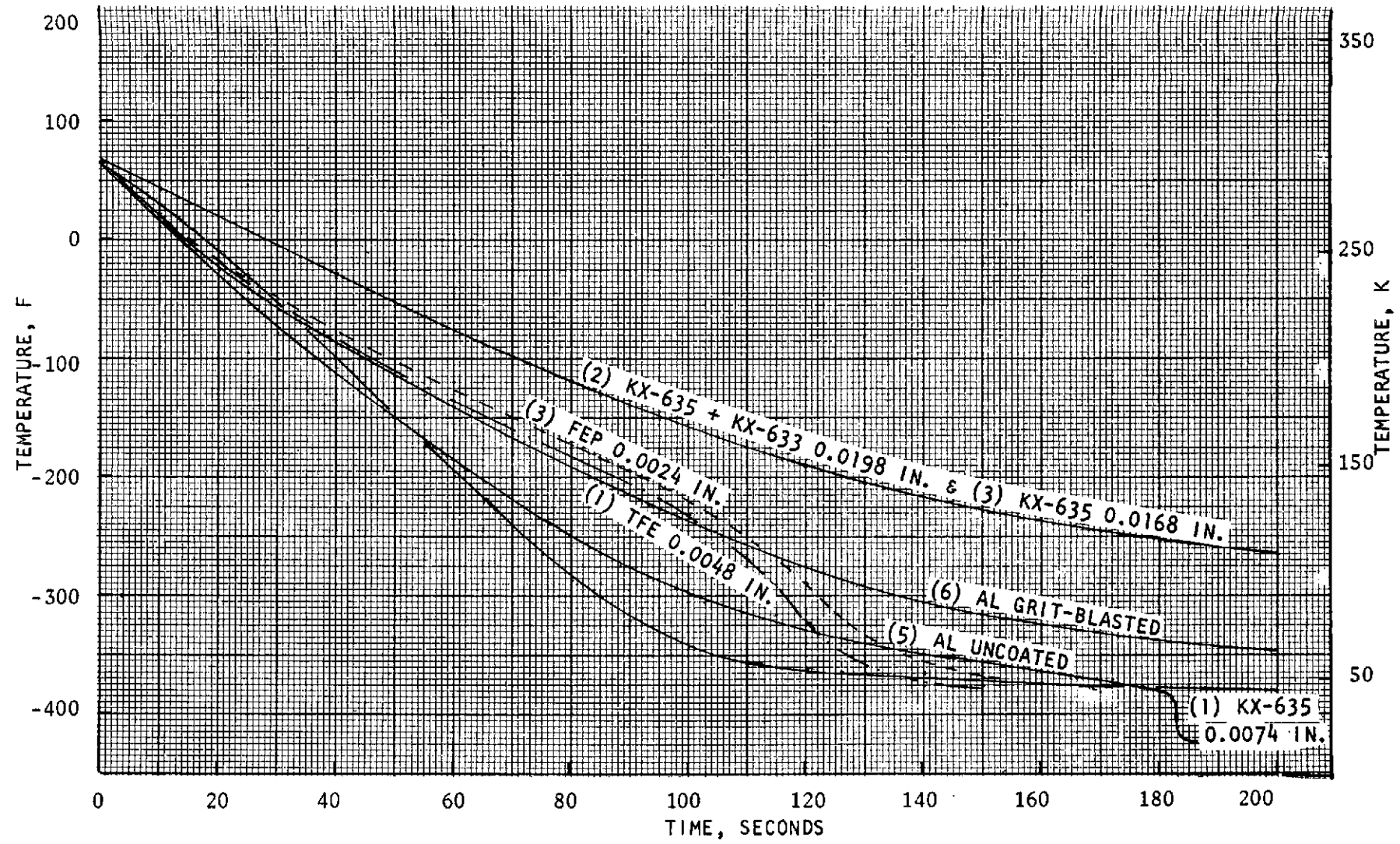

Figure 41. LH_2 Flow at 30 gpm Aluminum Collars with Sprayed Coatings

R-9273

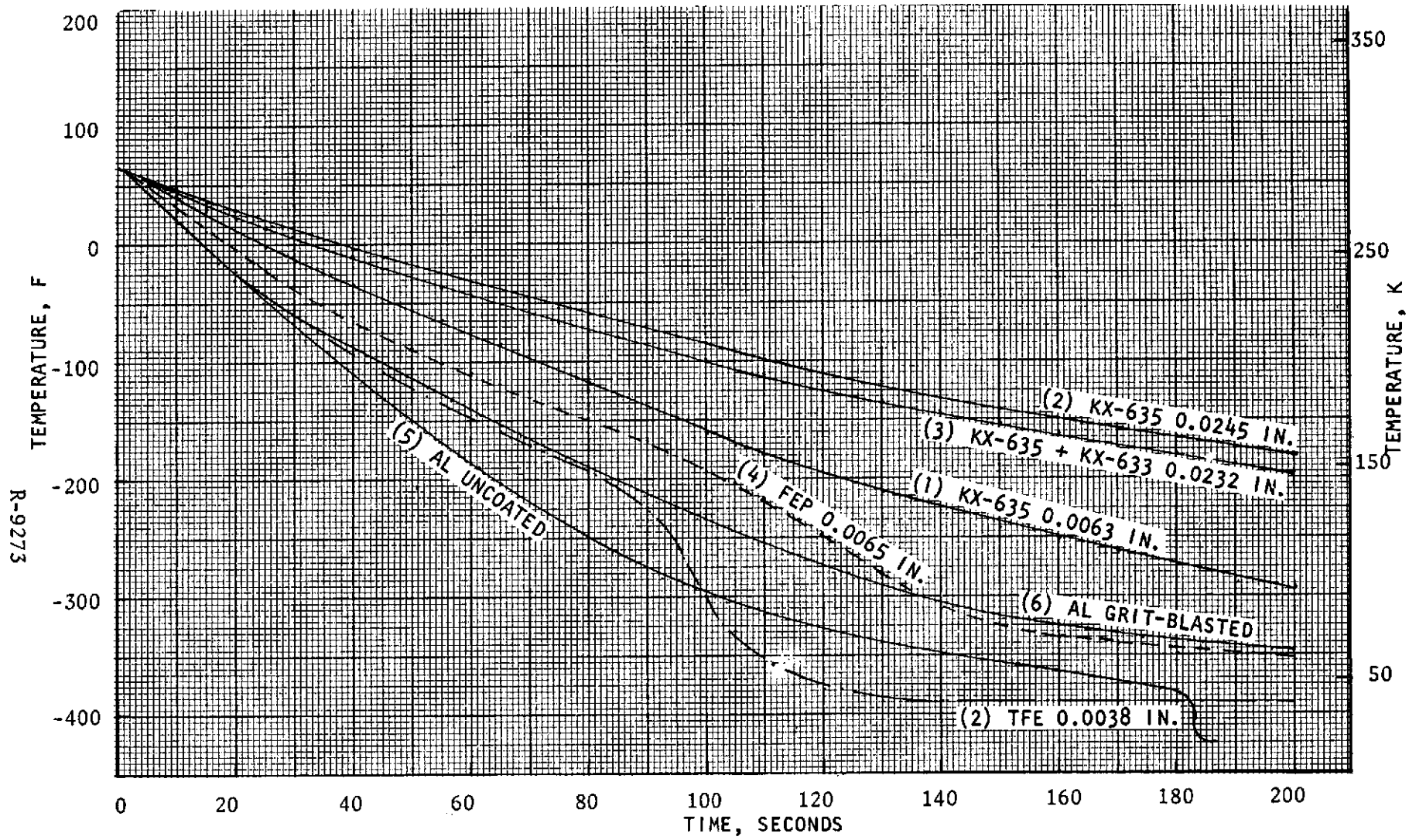

Figure 42. LH_2 Flow at 30 gpm Aluminum Collars with Fill & Drain Coatings

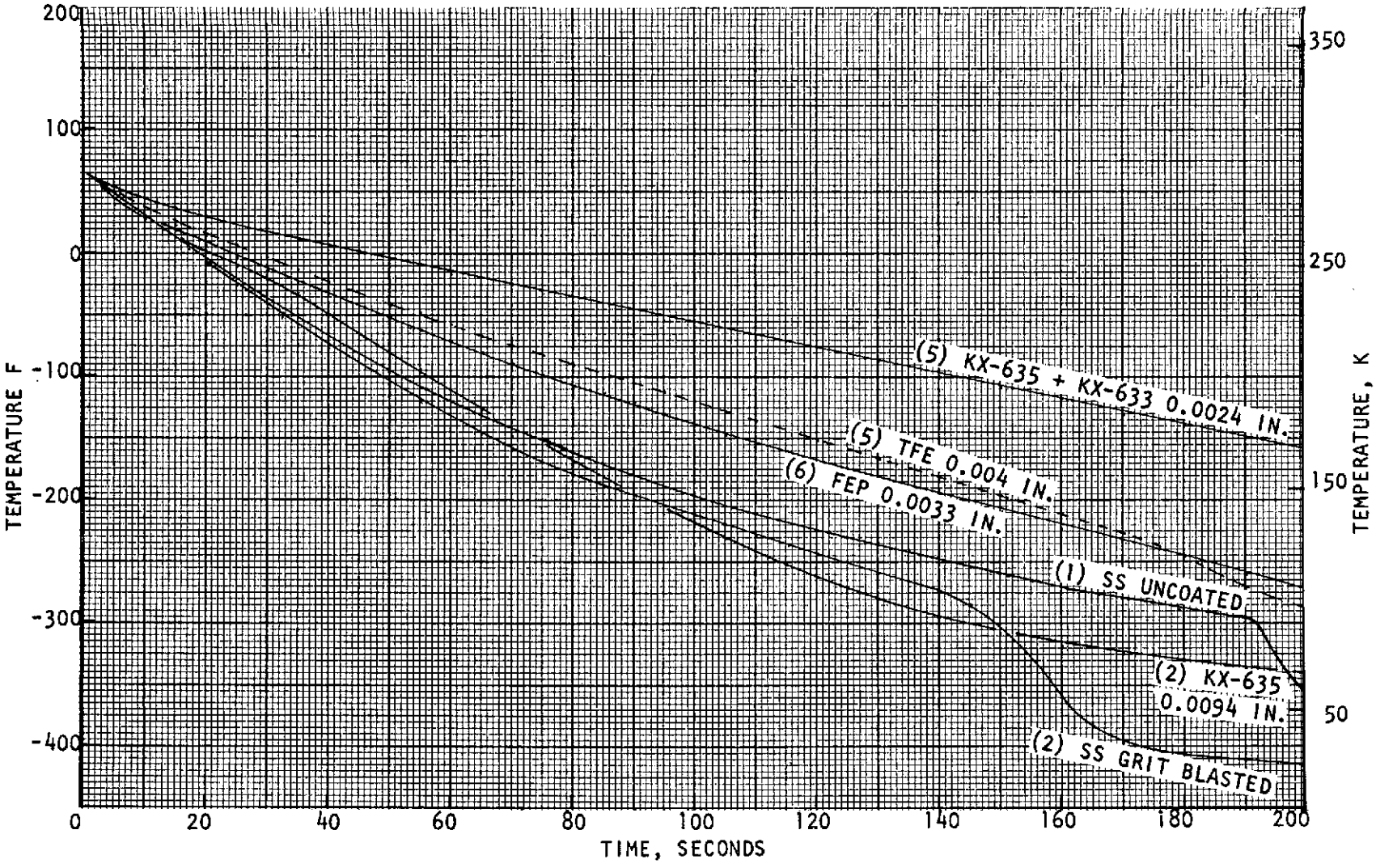

Figure 43. LH_2 Flow at 30 gpm Stainless Steel Collars with Sprayed Coatings

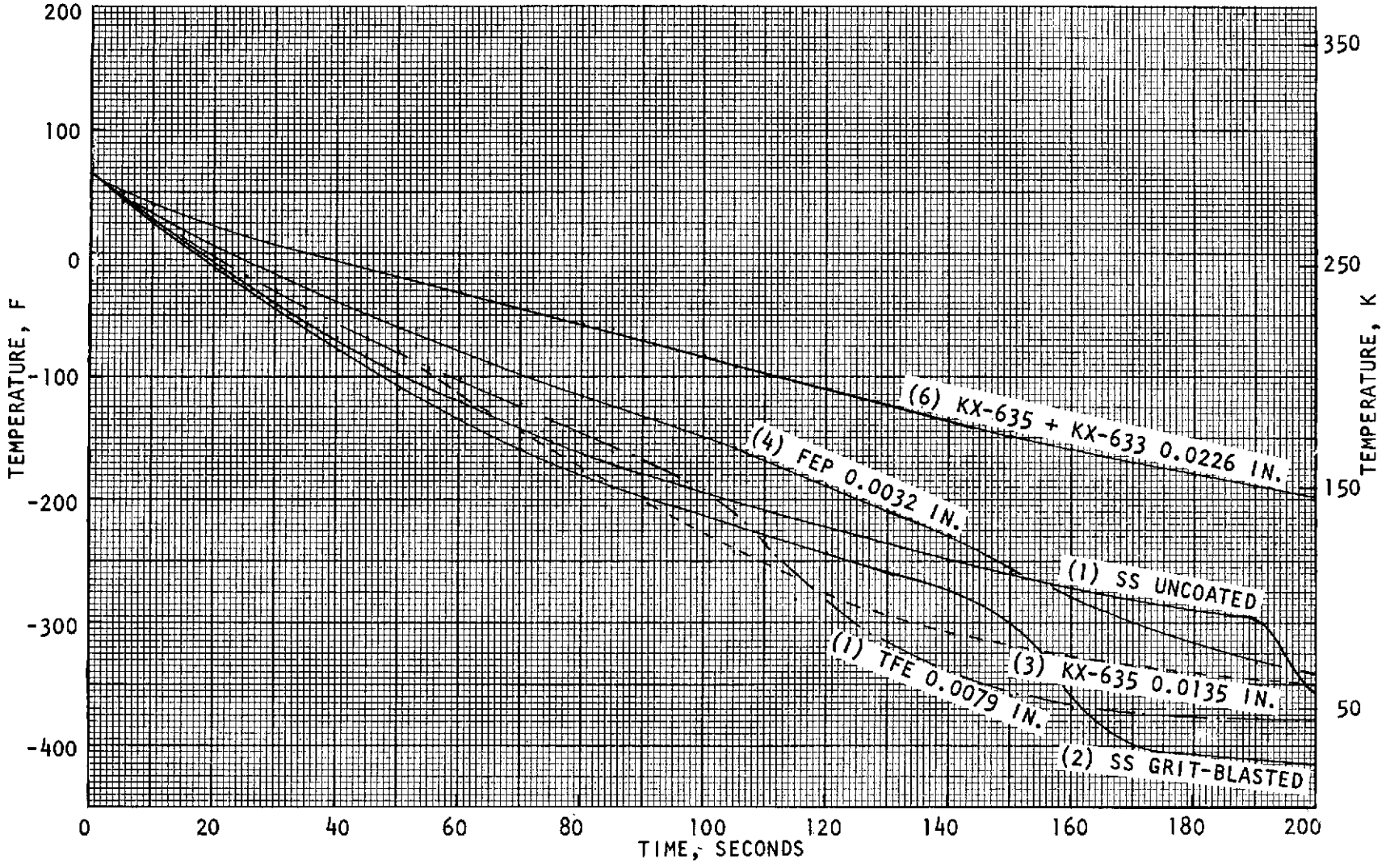

R-9273
62

Figure 44. LH_2 Flow at 30 gpm Stainless Steel Collars with Filled & Drained Coatings

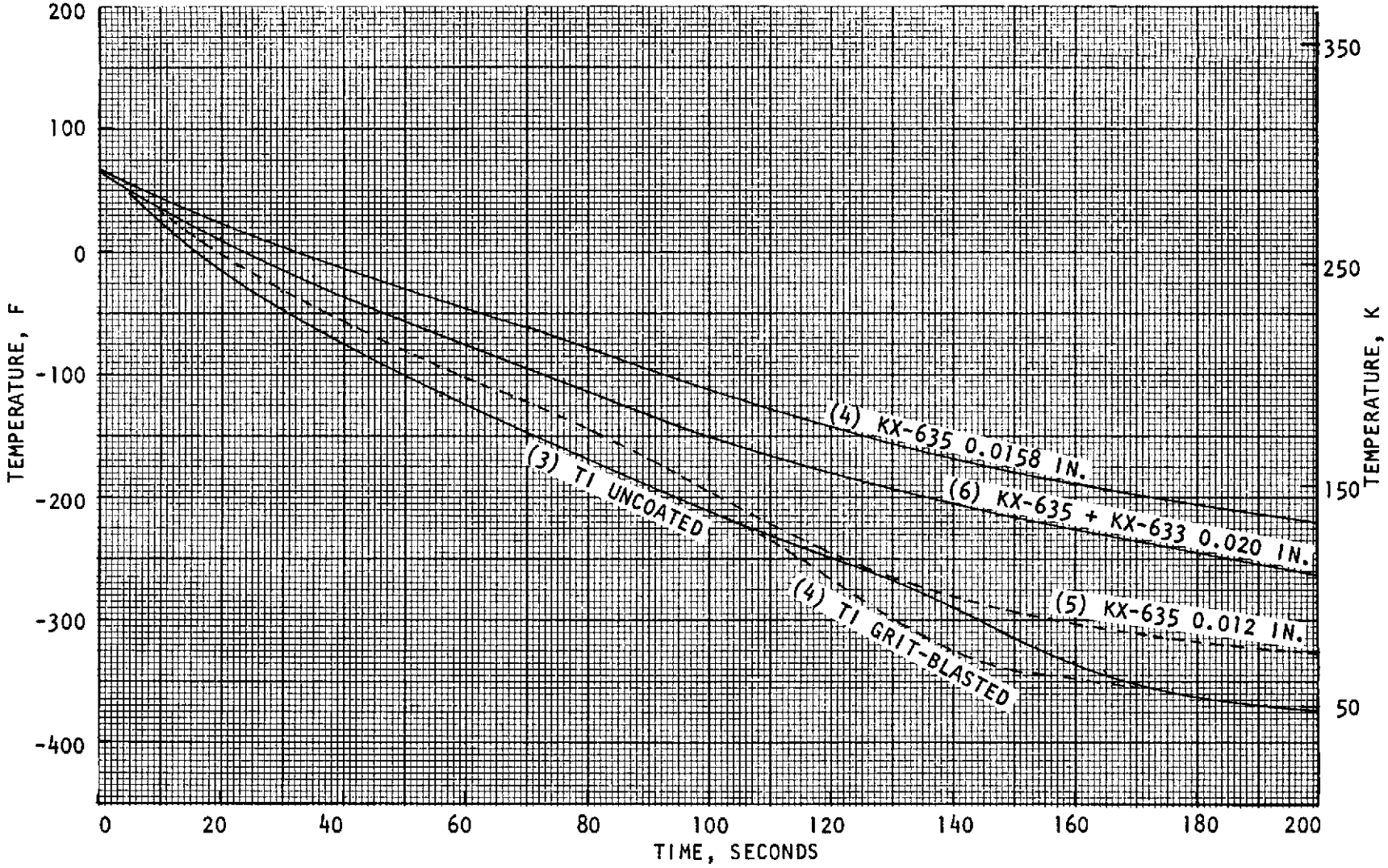

R-9273

Figure 45. LH_2 Flow at 30 gpm Titanium Collars with Sprayed Coatings

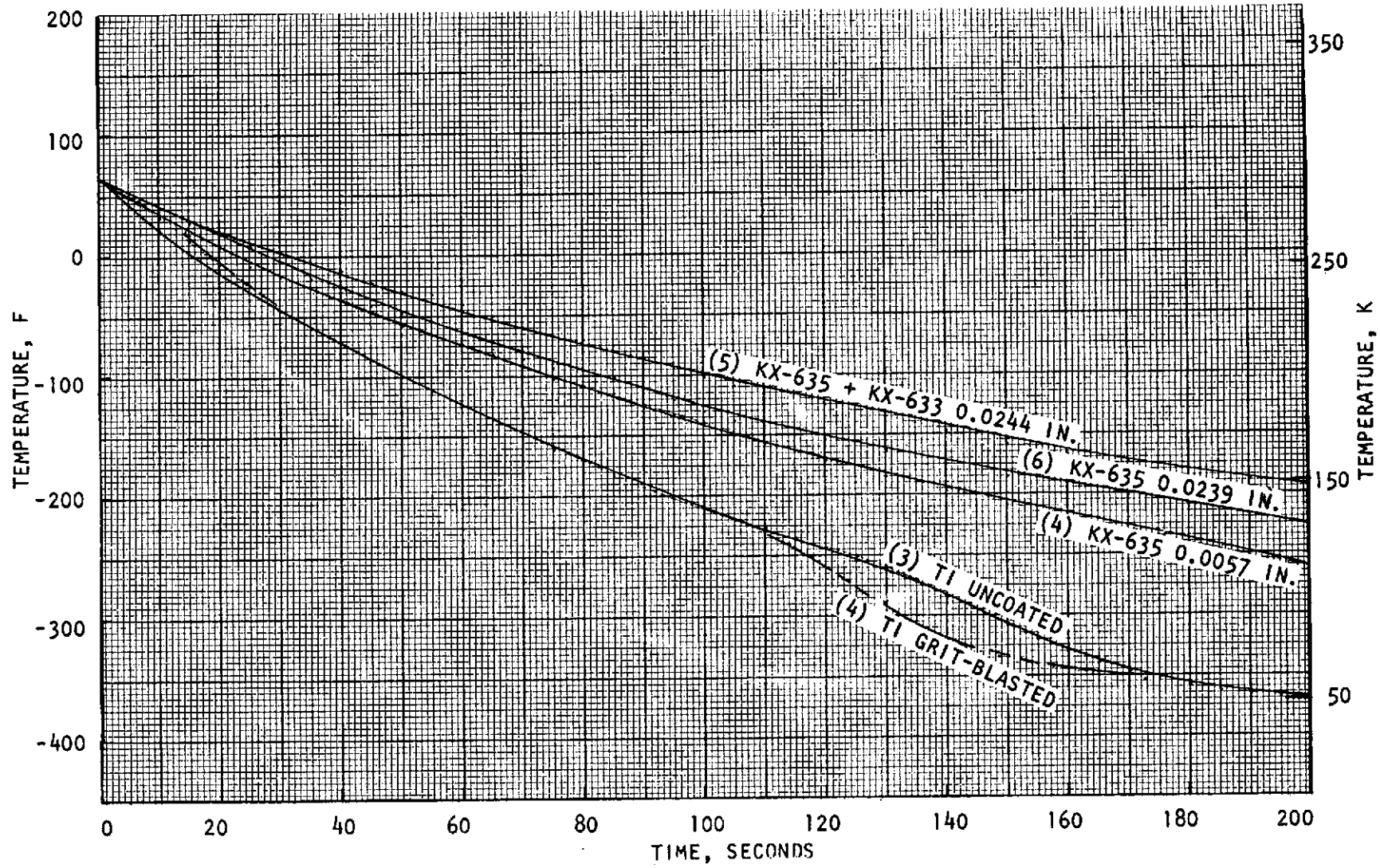

Figure 46. LH_2 Flow at 30 gpm Titanium Collars with Filled & Drained Coatings

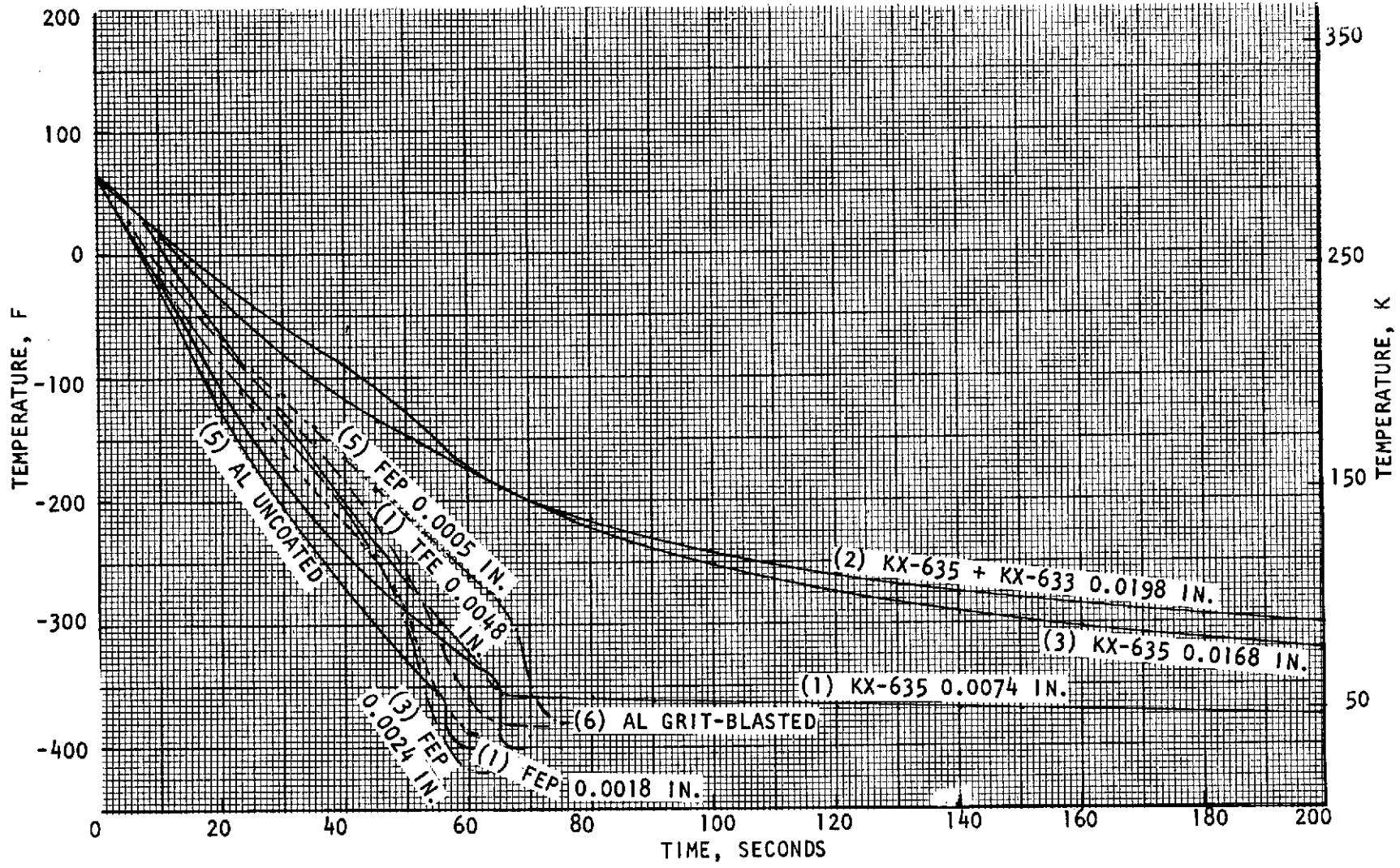

R-9273

Figure 47. LH_2 Flow at 80 gpm Aluminum Collars with Sprayed Coatings

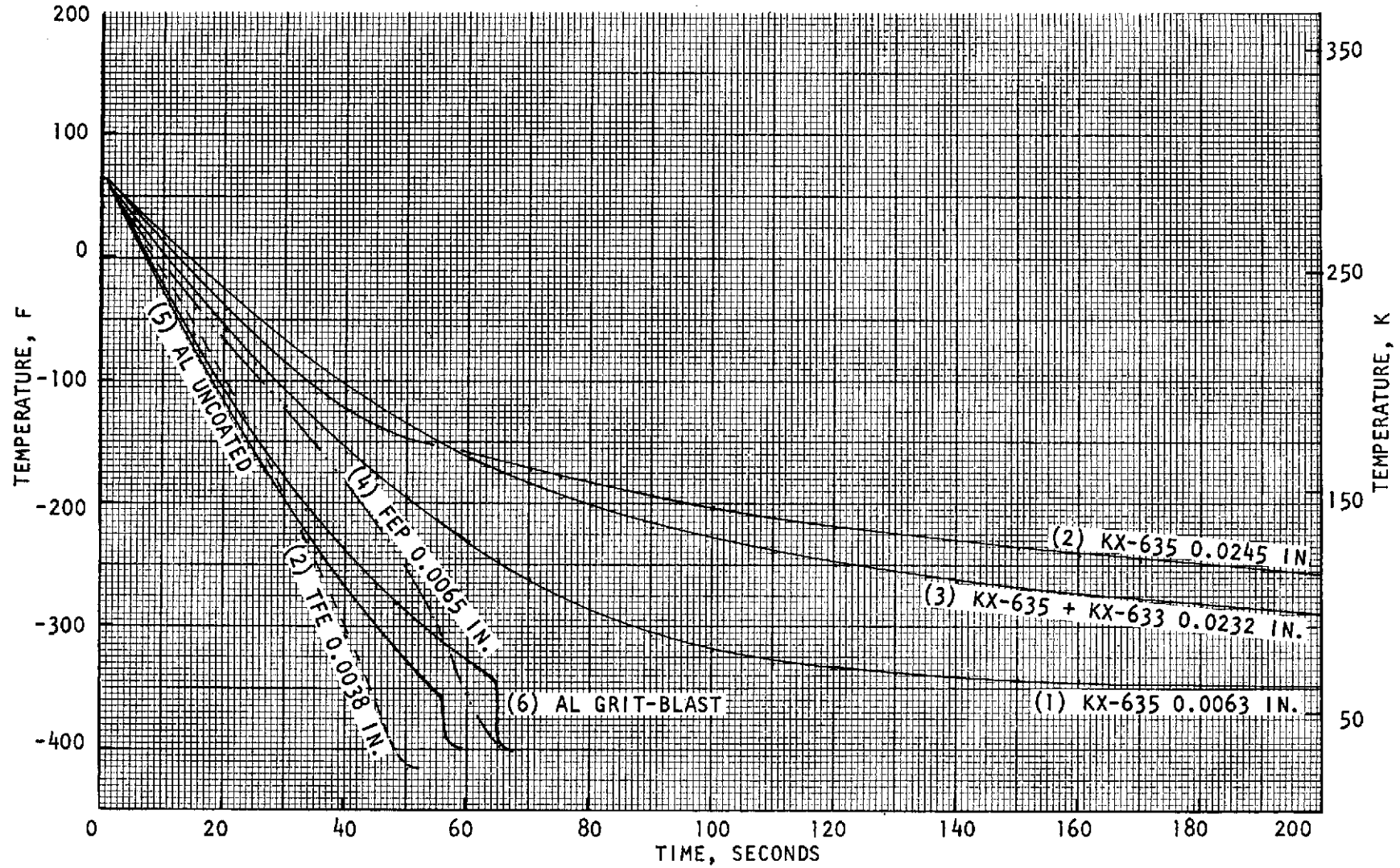

Figure 48. LH_2 Flow at 80 gpm Aluminum Collars with Fill & Drain Coatings

R-9273

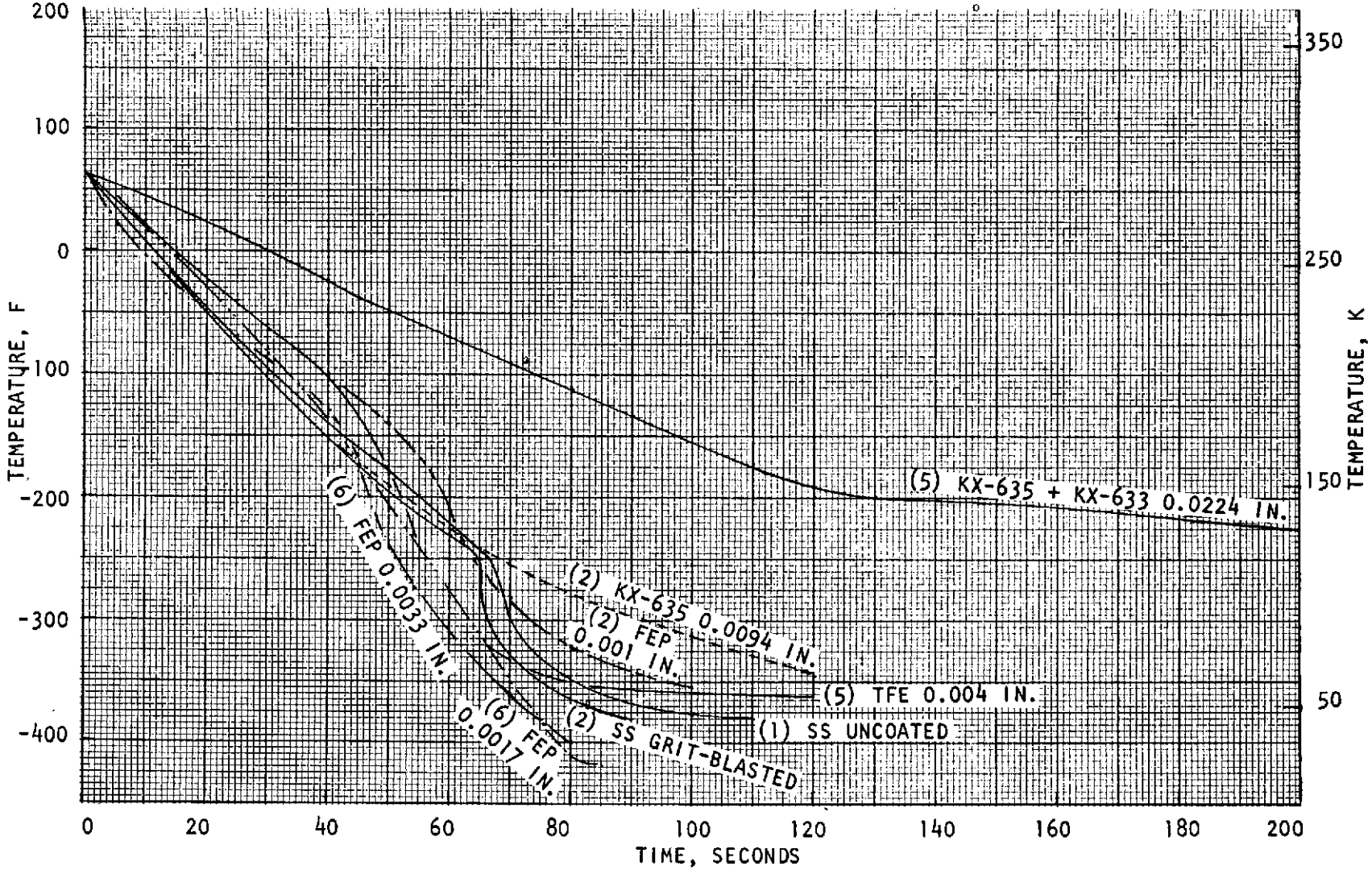

R-9273

Figure 49. LH_2 Flow at 80 gpm Stainless Steel Collars with Sprayed Coatings

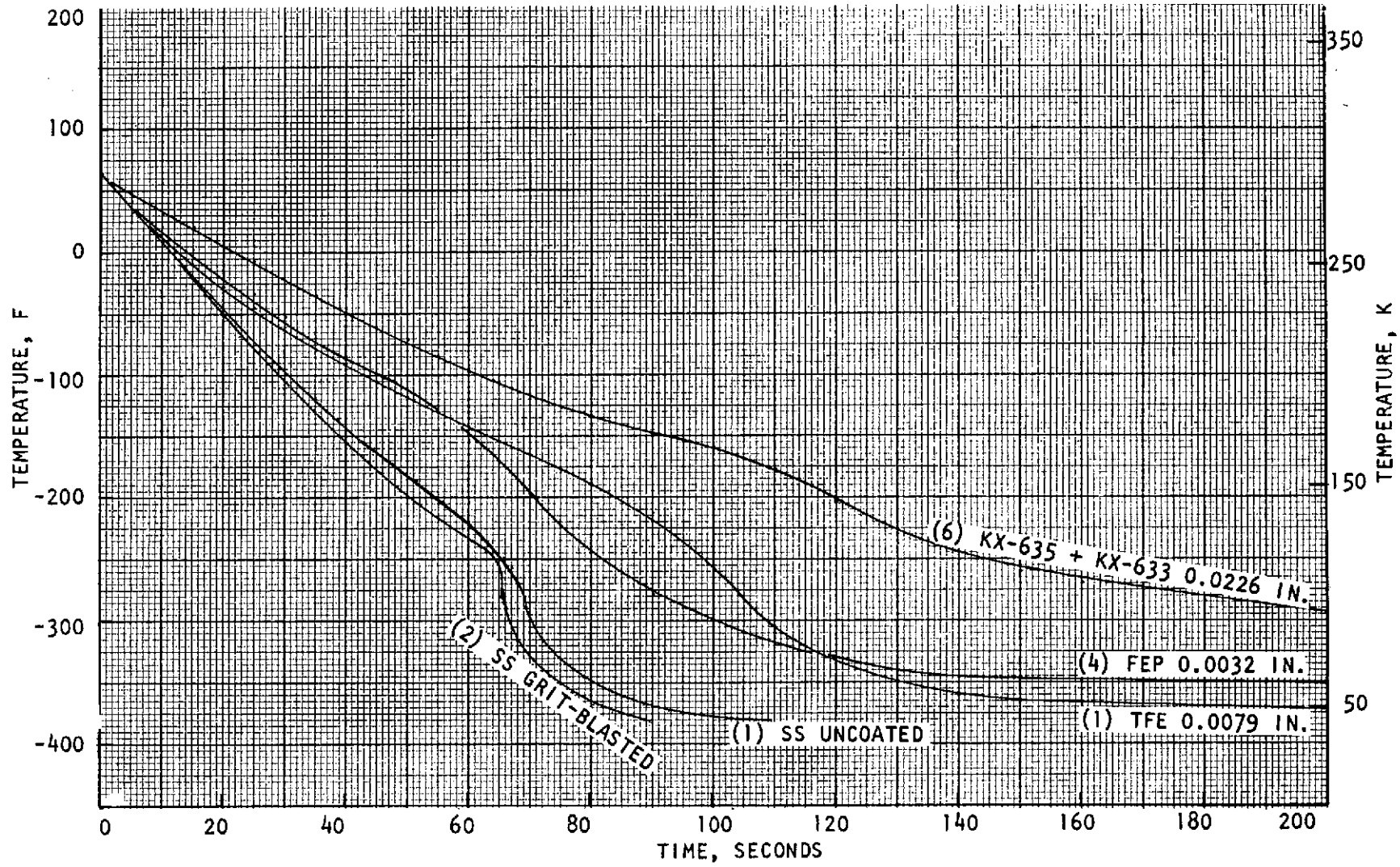

Figure 50. LH_2 Flow at 80 gpm Stainless Steel Collars with Filled & Drained Coatings

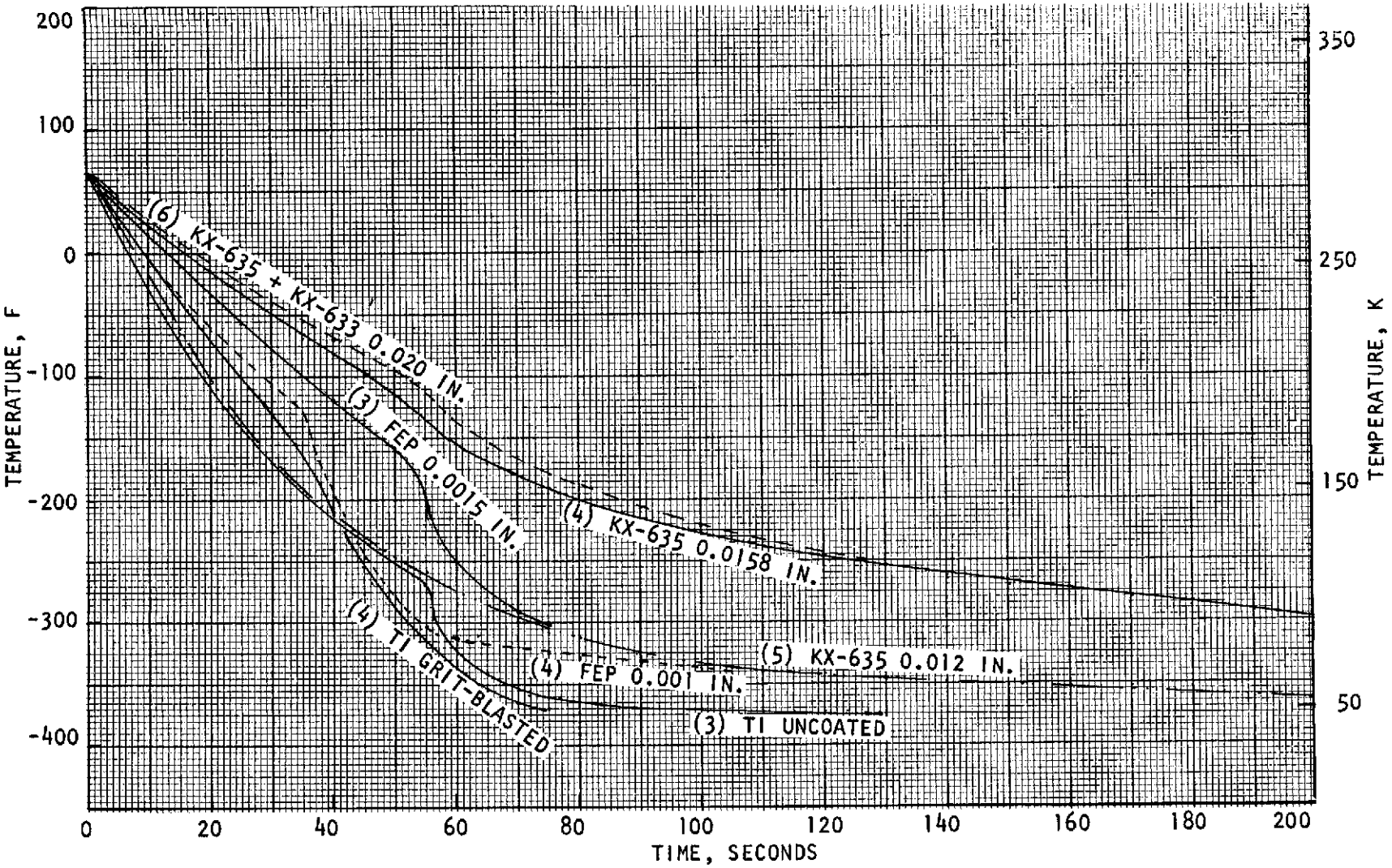

R-9273

Figure 51. LH_2 Flow at 80 gpm Titanium Collars with Sprayed Coatings

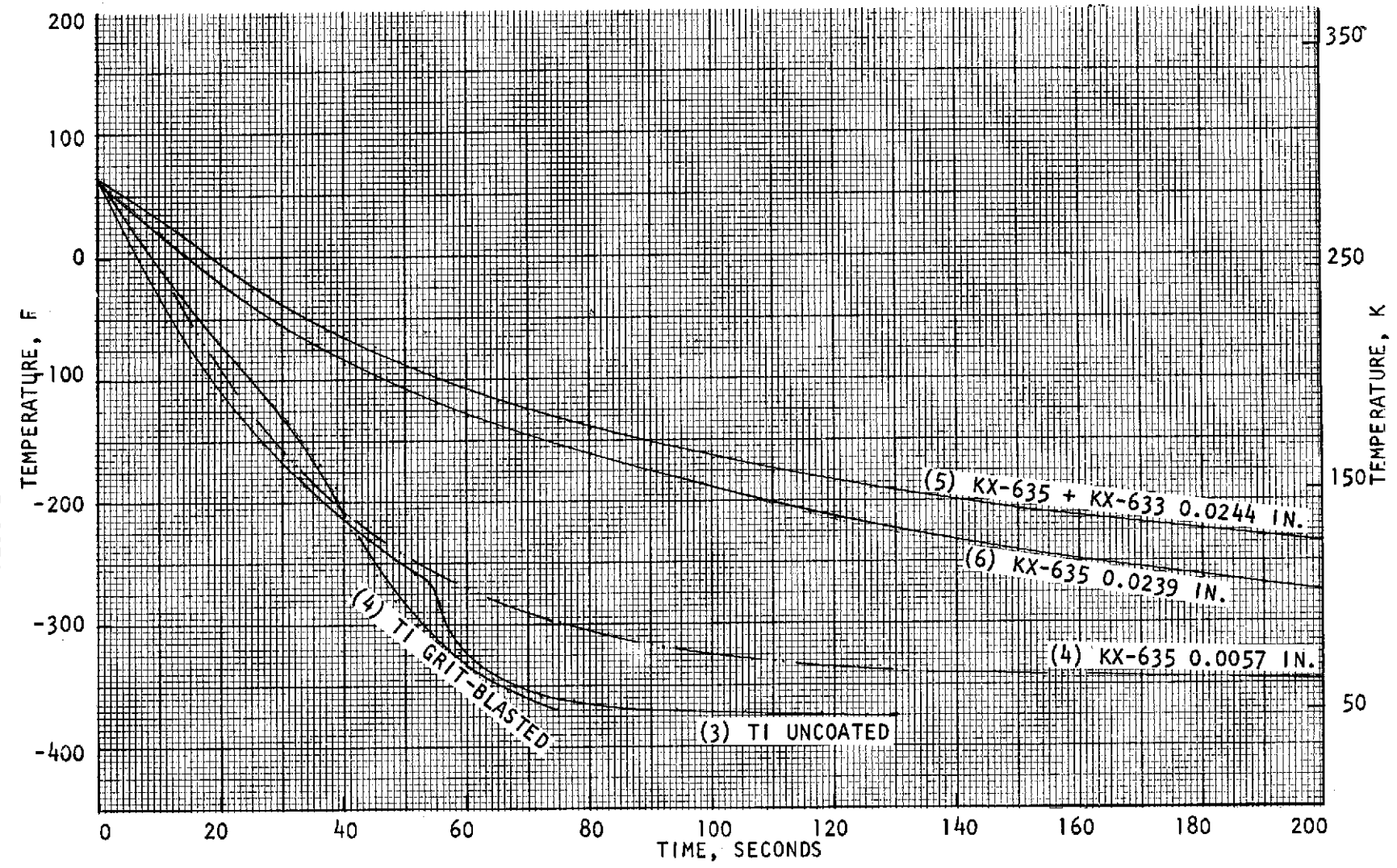

Figure 52. LH_2 Flow at 80 gpm Titanium Collars with Filled & Drained Coatings

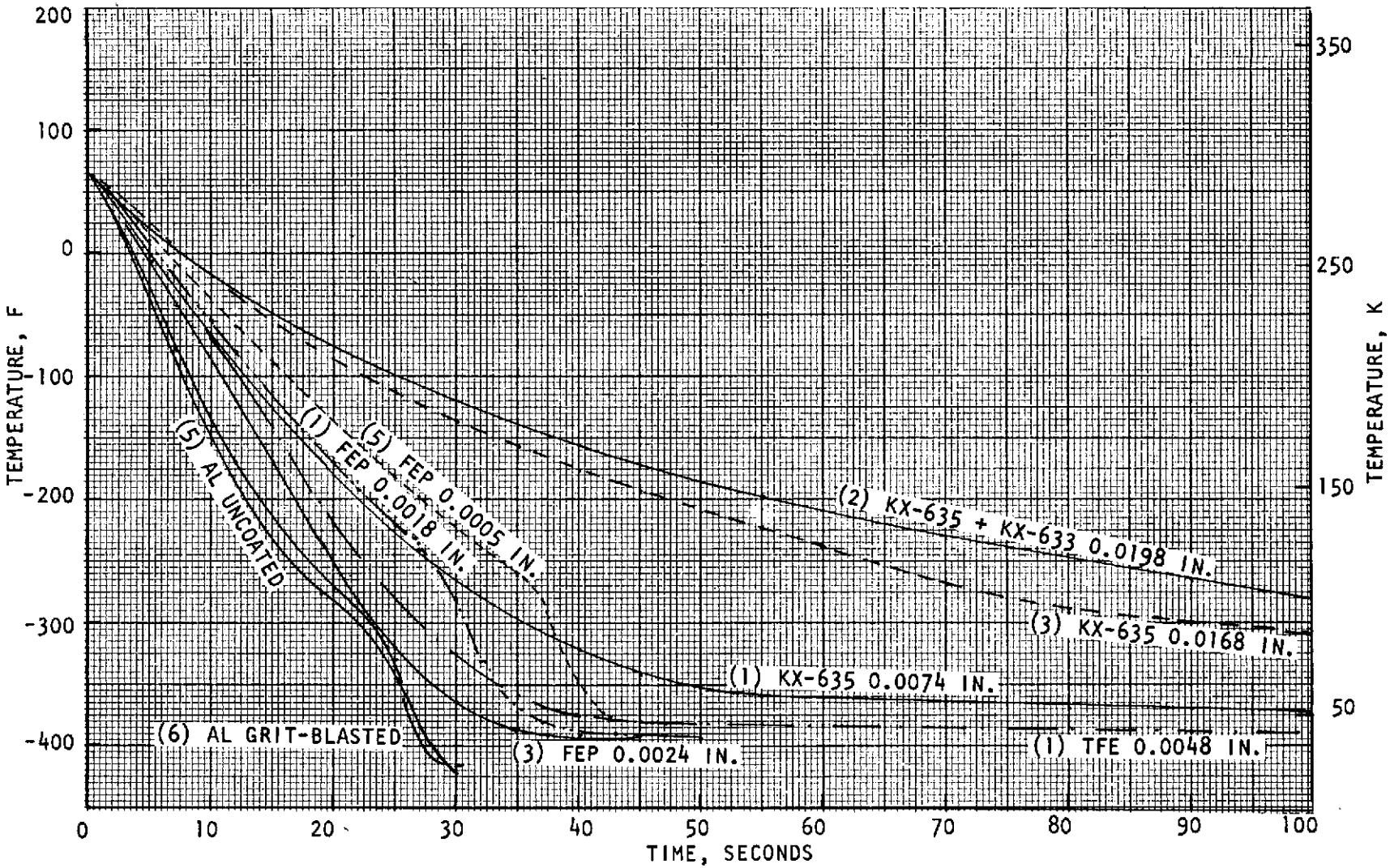

Figure 53. LH_2 Flow at 200 gpm Aluminum Collars with Sprayed Coatings.

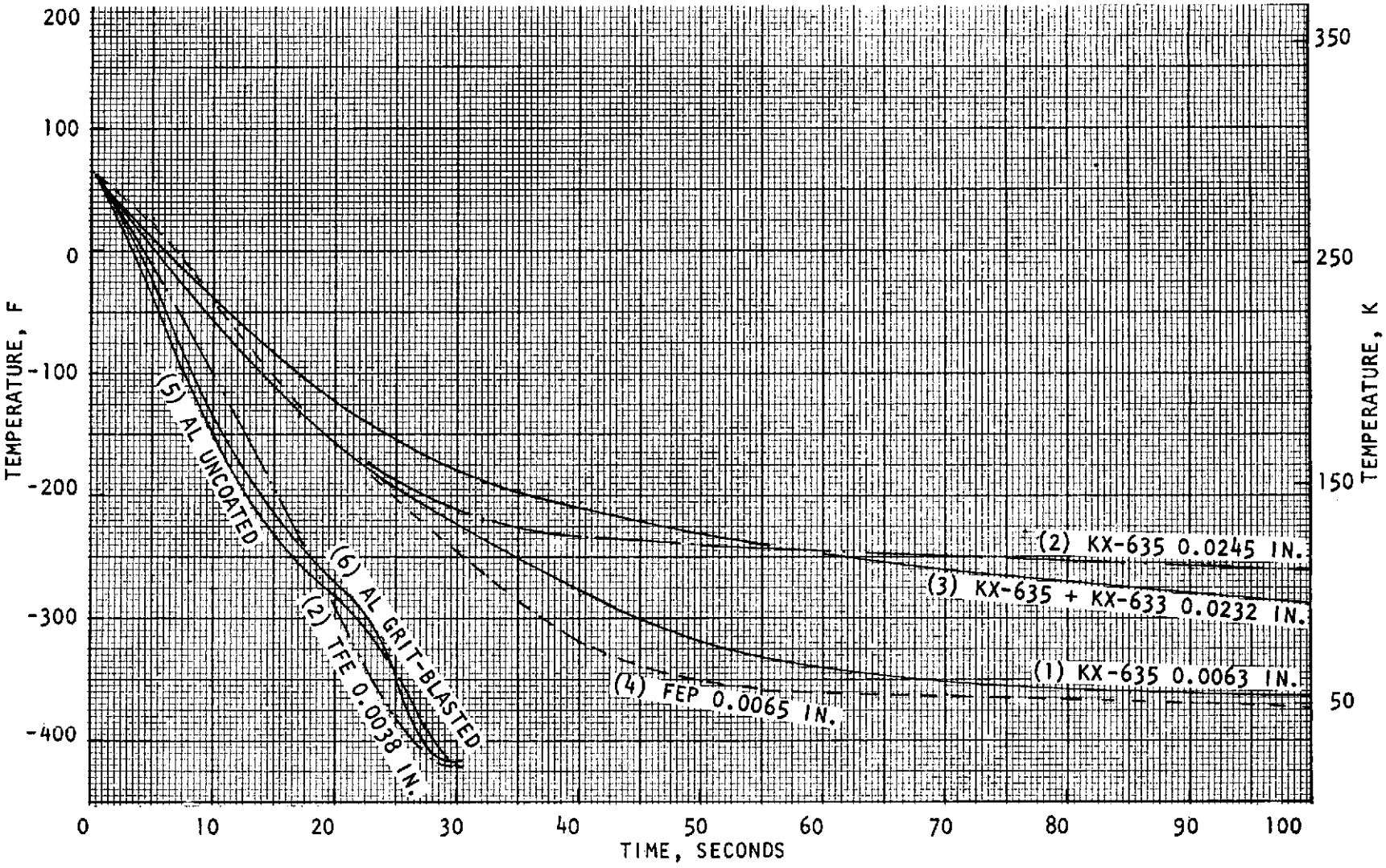

Figure 54. LH_2 Flow at 200 gpm Aluminum Collars with Fill & Drain Coatings

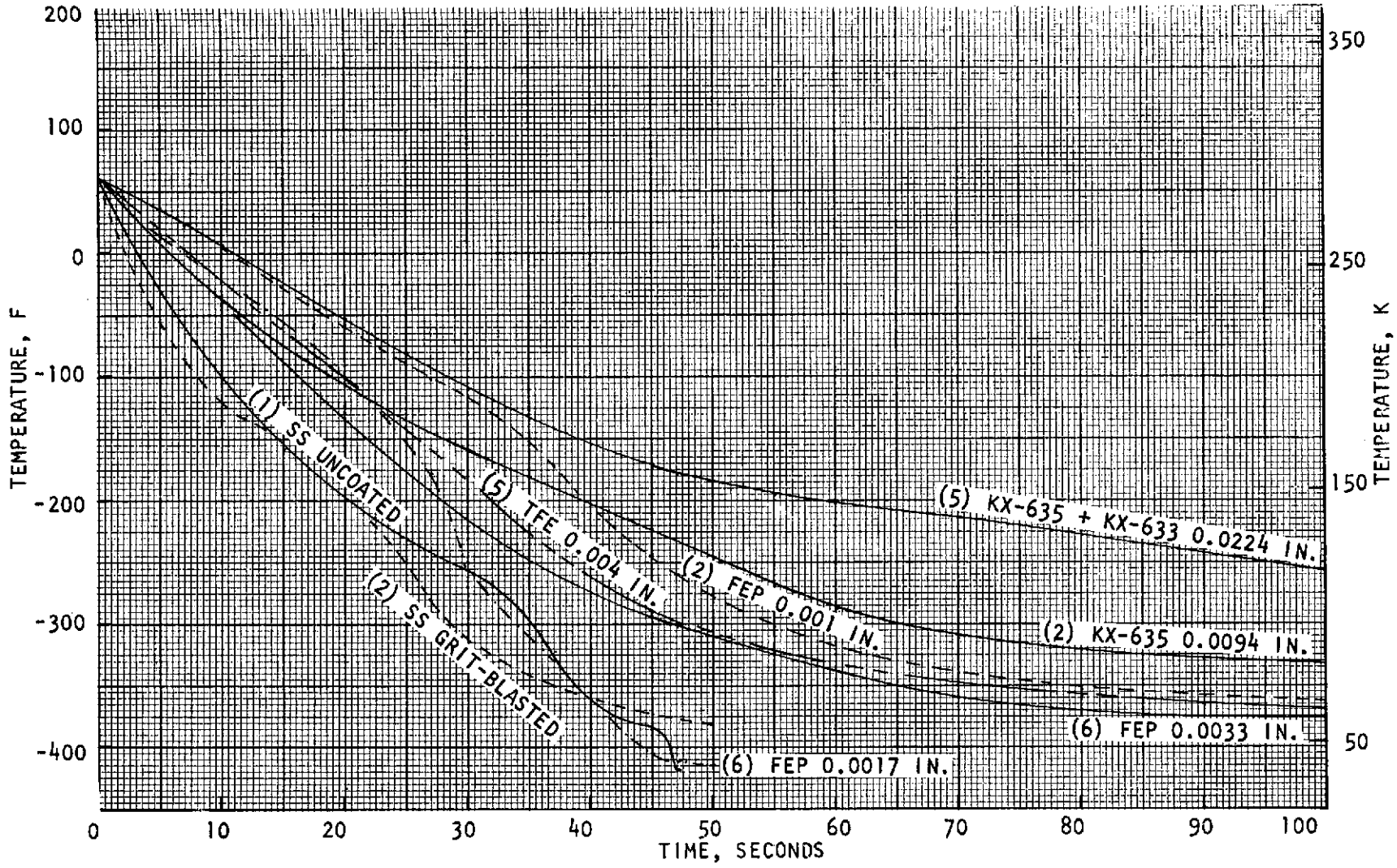

Figure 55. LH_2 Flow at 200 gpm Stainless Steel Collars with Sprayed Coatings

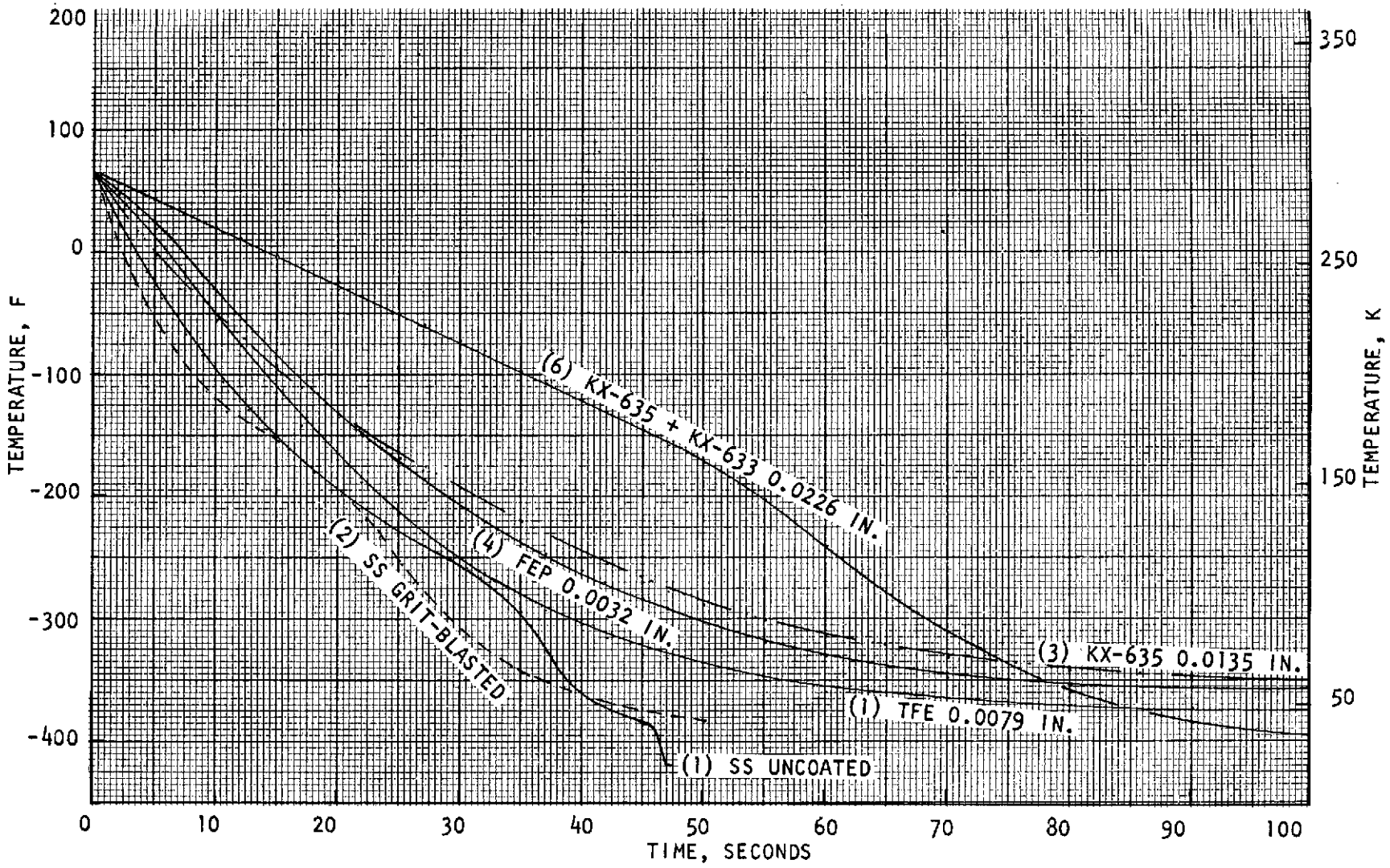

Figure 56. LH_2 Flow at 200 gpm Stainless Steel Collars with Filled & Drained Coatings

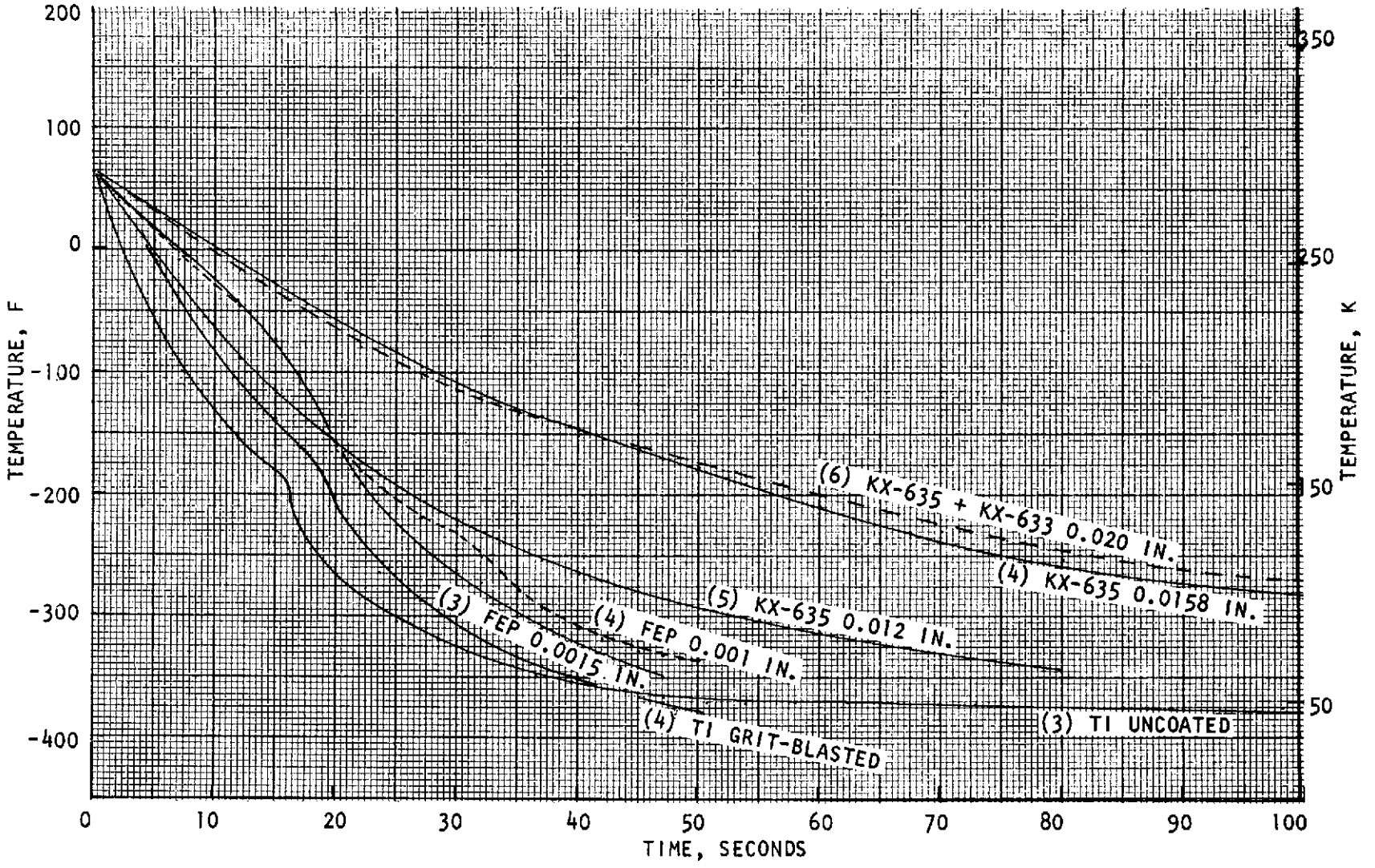

Figure 57. LH_2 Flow at 200 gpm Titanium Collars with Sprayed Coatings

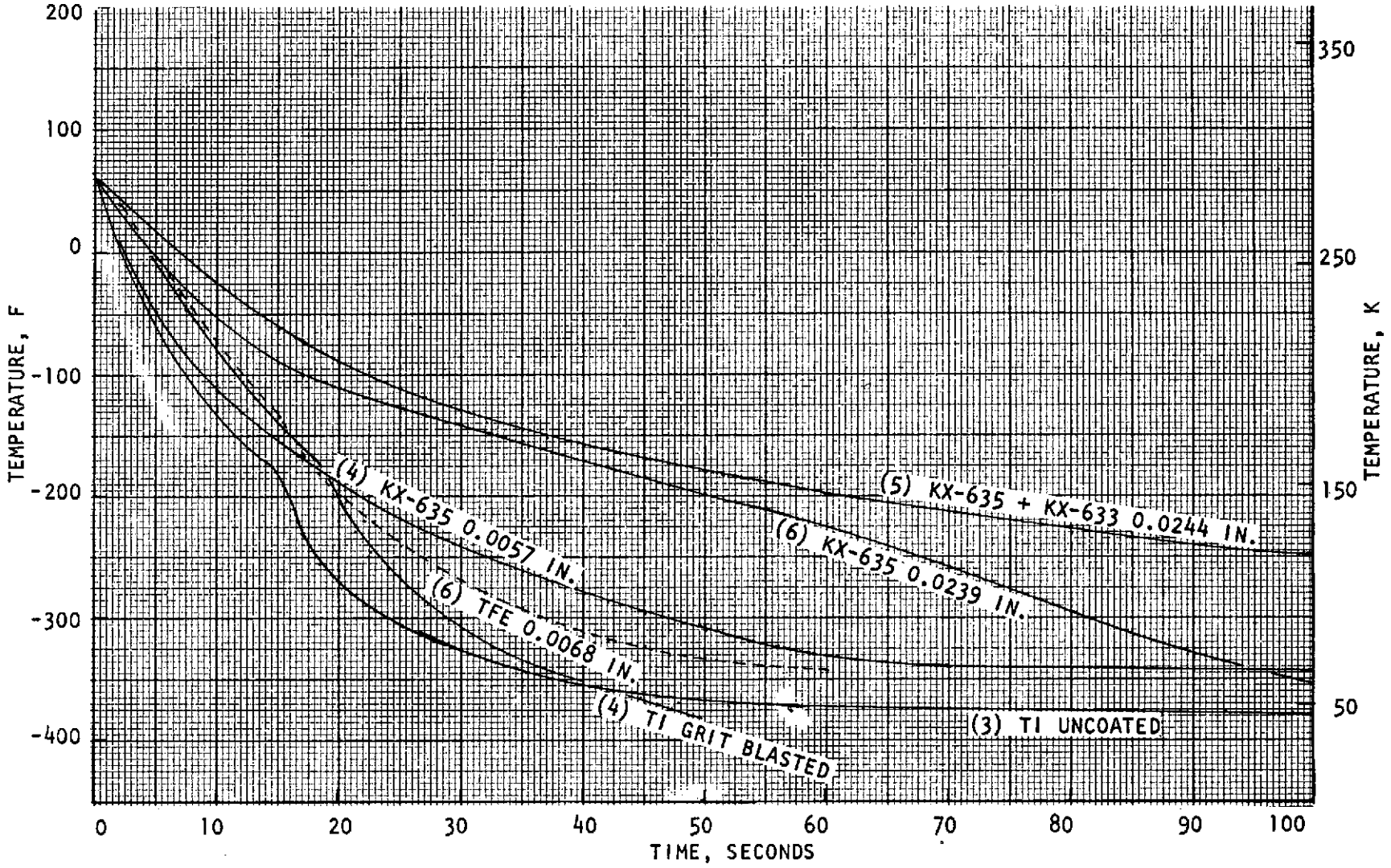

R-9273

Figure 58. LH_2 Flow at 200 gpm Titanium Collars with Filled & Drained Coatings

C-8

TABLE 6. COMPARISON OF CHILLDOWN TIMES* AND LH_2 HEAT TRANSFER COEFFICIENT ENHANCEMENT FACTORS FOR COATED AND UNCOATED SAMPLES

Aluminum Chilldown

Coating	Coating Method	tm (in.)	$0.0019 m^3/s$ (30 gpm)		$0.0050 m^3/s$ (80 gpm)		$0.013 m^3/s$ (200 gpm)	
			τ(sec)	ψ	τ(sec)	ψ	τ(sec)	ψ
Uncoated	--	0. (0.0000)	153	1.0	56	1.0	26	1.0
Grit Blasted	--	0. (0.0000)	230	0.665	65	0.862	26	1.0
FEP	Sprayed	1.27×10^{-5} (0.0018)	-	--	71	0.788	41	0.634
FEP	Sprayed	4.57×10^{-5} (0.0018)	-	--	56	1.0	34	0.764
FEP	Sprayed	6.10×10^{-5} (0.0024)	142	1.07	53	1.06	29	0.896
TFE	Fill/Drain	9.65×10^{-5} (0.0038)	112	1.37	45	1.24	23.5	1.11
TFE	Sprayed	1.22×10^{-4} (0.0048)	130	1.18	60	0.933	35	0.743
KX-635	Fill/Drain	1.60×10^{-4} (0.0063)	300	0.51	225	0.249	80	0.325
FEP	Fill/Drain	1.65×10^{-4} (0.0065)	210	0.73	60	0.933	55	0.473
KX-635	Sprayed	1.88×10^{-4} (0.0074)	113	1.35	70	0.800	55	0.473
KX-635	Sprayed	4.27×10^{-4} (0.0168)	407	0.376	250	0.224	157	0.165
KX-635/633	Sprayed	5.03×10^{-4} (0.0198)	407	0.376	280	0.200	209	0.124
KX-635/633	Fill/Drain	5.89×10^{-4} (0.0232)	600	0.255	320	0.175	167	0.156
KX-635	Fill/Drain	6.22×10^{-4} (0.0245)	500	0.304	300	0.187	232	0.112

*Chilldown time to within $1/e^2$ of final values. Nominal sample inside diameter 0.034m (1.34 in.), outside diameter 0.051 (2.0 in.).

TABLE 7. COMPARISON OF CHILLDOWN TIMES* AND LH_2 HEAT TRANSFER COEFFICIENT ENHANCEMENT FACTORS FOR COATED AND UNCOATED SAMPLES

Titanium Chilldown

Coating	Coating Method	tm (in.)	$0.0019 m^3/s$ (30 gpm)		$0.005 m^3/s$ (80 gpm)		$0.013 m^3/s$ (200 gpm)	
			τ(sec)	ψ	τ(sec)	ψ	τ(sec)	ψ
Uncoated	--	0. (0.0000)	175	1.0	72	1.0	41.5	1.0
Grit Blasted	--	0. (0.0000)	175	1.0	67	1.07	41.0	1.01
FEP	Sprayed	2.54×10^{-5} (0.0010)	-	-	180	0.40	67	0.62
FEP	Sprayed	3.81x10-5 (0.0015)	-	-	130	0.554	49	0.847
KX-635	Fill/Drain	1.45×10^{-4} (0.0057)	269	0.65	230	0.313	100	0.415
TFE	Fill/Drain	1.73×10^{-4} (0.0068)	-	--	-	--	70	0.594
KX-635	Sprayed	3.05×10^{-4} (0.0120)	233	0.75	180	0.400	95	0.437
KX-635	Sprayed	4.01×10^{-4} (0.0158)	271	0.645	240	0.300	193	0.215
KX-635/633	Sprayed	5.08×10^{-4} (0.0200)	333	0.525	235	0.307	202	0.205
KX-635	Sprayed	6.07x10-4 (0.0239)	324	0.540	294	0.245	101	0.411
KX-635/633	Fill/Drain	6.20×10^{-4} (0.0244)	376	0.465	320	0.225	227	0.183

*Chilldown time to within $1/e^2$ of final values. Nominal sample inside diameter 0.034m (1.34 in.), outside diameter 0.051 (2.0 in.).

TABLE 8. COMPARISON OF CHILLDOWN TIMES* AND LH_2 HEAT TRANSFER COEFFICIENT ENHANCEMENT FACTORS FOR COATED AND UNCOATED SAMPLES

CRES Chilldown

Coating	Coating Method	tm (in.)	$0.0019 m^3/s$ (30 gpm)		$0.0050 m^3/s$ (80 gpm)		$0.013 m^3/s$ (200 gpm)	
			τ (sec)	ψ	τ (sec)	ψ	τ (sec)	ψ
Uncoated	--	0. (0.0000)	201	1.0	82	1.0	39.5	1.0
Grit Blasted	---	0. (0.0000)	160	1.26	79	1.04	39.5	1.0
FEP	Sprayed	2.54×10^{-5} (0.0010)	-	--	105	0.78	90	0.438
FEP	Sprayed	4.32×10^{-5} (0.0017)	-	--	71	1.15	39	1.010
FEP	Fill/Drain	8.13×10^{-5} (0.0032)	220	0.914	210	0.39	90	0.438
FEP	Sprayed	8.38×10^{-5} (0.0033)	251	0.800	70	1.17	69.5	0.569
TFE	Sprayed	1.02×10^{-4} (0.0040)	217	0.926	90	0.91	80	0.494
TFE	Fill/Drain	2.01×10^{-4} (0.0079)	151	1.330	140	0.586	65	0.607
KX-635	Sprayed	2.39×10^{-4} (0.0094)	230	0.873	135	0.607	135	0.293
KX-635	Fill/Drain	3.43×10^{-4} (0.0135)	215	0.935	-	--	125	0.316
KX-635	Sprayed	5.69×10^{-4} (0.0224)	502	0.400	271	0.303	160	0.247
KX-635	Fill/Drain	5.74×10^{-4} (0.0226)	352	0.571	259	0.233	80	0.494

*Chilldown time to within $1/e^2$ of final values. Nominal sample inside diameter 0.034m (1.34 in.), outside diameter 0.051m (2.0 in.).

The test results show that chilldown of the aluminum collars (Table 6) was achieved in the shortest time at the highest flowrate of 0.013 m^3/s (200 gpm). Moreover, a decreasing enhancement ψ on the heat transfer coefficient due to coating effect is shown with increased heat transfer coefficient levels. As illustrated, a peak ψ of 1.37 was illustrated at 0.0019 m^3/s (30 gpm) and only 1.11 at the 0.013 m^3/s (200 gpm) for aluminum. Comparable values for titanium (Table 7) were shown to result in degraded chilldown times with coating; the uncoated samples show the best chilldown time.

For CRES material (Table 8), a peak improvement was noted for the coated surfaces of 1.33 with 0.0019 m^3/s (30 gpm) and only 1.01 for the 0.013 m^3/s (200 gpm) high flowrate. In the cases shown, both the chill enhancement level shown and the coating thickness to induce this speedier chill were small. This indicates the effect of forced convection with the LH_2 dominating the boiling at the high flowrates. In addition, the coating acts as a significant thermal resistance at the higher coolant mass velocities, thereby insulating the wall heat from the chill flow.

Immersion Chill and Flow Chill Comparison. A comparison for the three base materials was made for the LN_2-immersion chill, LH_2-immersion chill, and the 0.0019, 0.0050, and 0.013 m^3/s (30, 80, and 200 gpm) LH_2-flow chill results. The heat transfer coefficient enhancement factors (ψ) compared to the uncoated cases (ψ = 1.0) was used for common comparison base. Table 9 illustrates these results for the peak measured values of ψ. As shown, the peak ψ values were noted at reduced values of heat transfer coefficients (LN_2-immersion chill).

Moreover, the effect of the material substrate conductivity is such that lower base wall thermal conductivity (Al → CRES → Ti) resulted in lower levels of enhancement values.

Final graphical correlation charts based on the enhancement as a function of heat transfer coefficient, coating, and base Biot numbers are shown in the summary of coating results below.

TABLE 9. COMPARISON OF PEAK ENHANCEMENT COEFFICIENTS AND MATERIAL THICKNESS VALUES

Material	Coating	Thickness m(in.)	Peak ψ	Coolant Condition
Al	TFE	9.65×10^{-5} (0.0038)	1.11	LH_2 $0.013 m^3/s$ (200 gpm)
Al	TFE	9.65×10^{-5} (0.0038)	1.24	LH_2 $0.0050 m^3/s$ (80 gpm)
Al	TFE	9.65×10^{-5} (0.0038)	1.37	LH_2 $0.0019 m^3/s$ (30 gpm)
Al	TFE	6.10×10^{-5} (0.0024)	1.41	LH_2 Uncorked
Al	TFE	6.10×10^{-5} (0.0024)	1.52	LN_2 Uncorked
Al	FEP	1.91×10^{-4} (0.0075)	2.35	LH_2 Corked
Al	FEP	1.91×10^{-4} (0.0075)	3.71	LN_2 Corked
CRES	FEP	4.32×10^{-5} (0.0017)	1.01	LH_2 $0.013 m^3/s$ (200 gpm)
CRES	FEP	8.38×10^{-5} (0.0033)	1.17	LH_2 $0.0050 m^3/s$ (80 gpm)
CRES	TFE	2.01×10^{-4} (0.0079)	1.33	LH_2 $0.0019 m^3/s$ (30 gpm)
CRES	FEP	9.65×10^{-5} (0.0038)	1.43	LH_2 Uncorked
CRES	TFE	6.86×10^{-5} (0.0027)	1.53	LH_2 Corked
CRES	TFE	6.86×10^{-5} (0.0027	1.53	LH_2 Corked
CRES	TFE	6.86×10^{-5} (0.0027)	1.61	LN_2 Corked
CRES	FEP	9.65×10^{-5} (0.0038)	2.22	LN_2 Uncorked
Ti	Grit Blasted	0. (0.0000)	1.01	LH_2 $0.013 m^3/s$ (200 gpm)
Ti	Grit Blasted	0. (0.0000)	1.07	LH_2 $0.0050 m^3/s$ (80 gpm)
Ti	Grit Blasted	0. (0.0000)	1.0	LH_2 $0.0019 m^3/s$ (30 gpm)
Ti	FEP	1.07×10^{-4} (0.0042)	1.33	LH_2 Uncorked
Ti	FEP	1.55×10^{-4} (0.0061)	1.64	LH_2 Corked
Ti	FEP	1.55×10^{-4} (0.0061)	1.97	LN_2 Corked
Ti	FEP	1.07×10^{-4} (0.0042)	2.36	LN_2 Uncorked

Rapid Start Chill Application. Based on the results of the experimental and analytical studies, it is apparent that at the high LH_2-velocity condition, a substantial insulation benefit is obtained from thick coatings, and the most rapid start will be achieved with a quick coating-surface chill without a complete base-wall chill. Low wall thermal conductivity (Ti, CRES) was shown to reduce the level of enhancements and lengthen chilldown times. This aspect would be beneficial for high LH_2 velocity, coated surface-chill start applications. However, at low LH_2-velocity conditions, the base wall will chill more quickly with a coating and a rapid pump start can be obtained with an optimum coating thickness, provided that the system can absorb the rapid generation of vapor.

Summary of Coating Results

The cylinder and the collar chilldown data summary of the enhancement coating thickness effects on chilldown for the three materials tested (Al, CRES, and Ti) is indicated in Fig. 59 through 67.

Comparisons of the influence of base material and coating thickness for varying levels of applied heat transfer coefficient (i.e., pool boiling, low, medium, and high forced convection) show the applied coating thicknesses to be a strong variable. An increased level of convection reduces the enhancement benefit to be derived from the coating in terms of chilldown time reduction. Similarly, the optimum coating thickness was shown to vary from 2.03×10^{-4} m (0.008 in.) at low heat transfer coefficients to $\leq 5.08 \times 10^{-5}$ m (0.002 in.) at the 0.013 m^3/s (200 gpm) flowrate condition. A coating Biot number based on the unenhanced film coefficient and coating thickness-to-conductivity ratio showed an optimum at $N_{Bi} \approx 0.4$.

RL-10 Pump Thermal Analysis

The analytical heat transfer model of the RL-10 LH_2-turbopump that was used in the thermal analysis of the feed system was set up using the differential

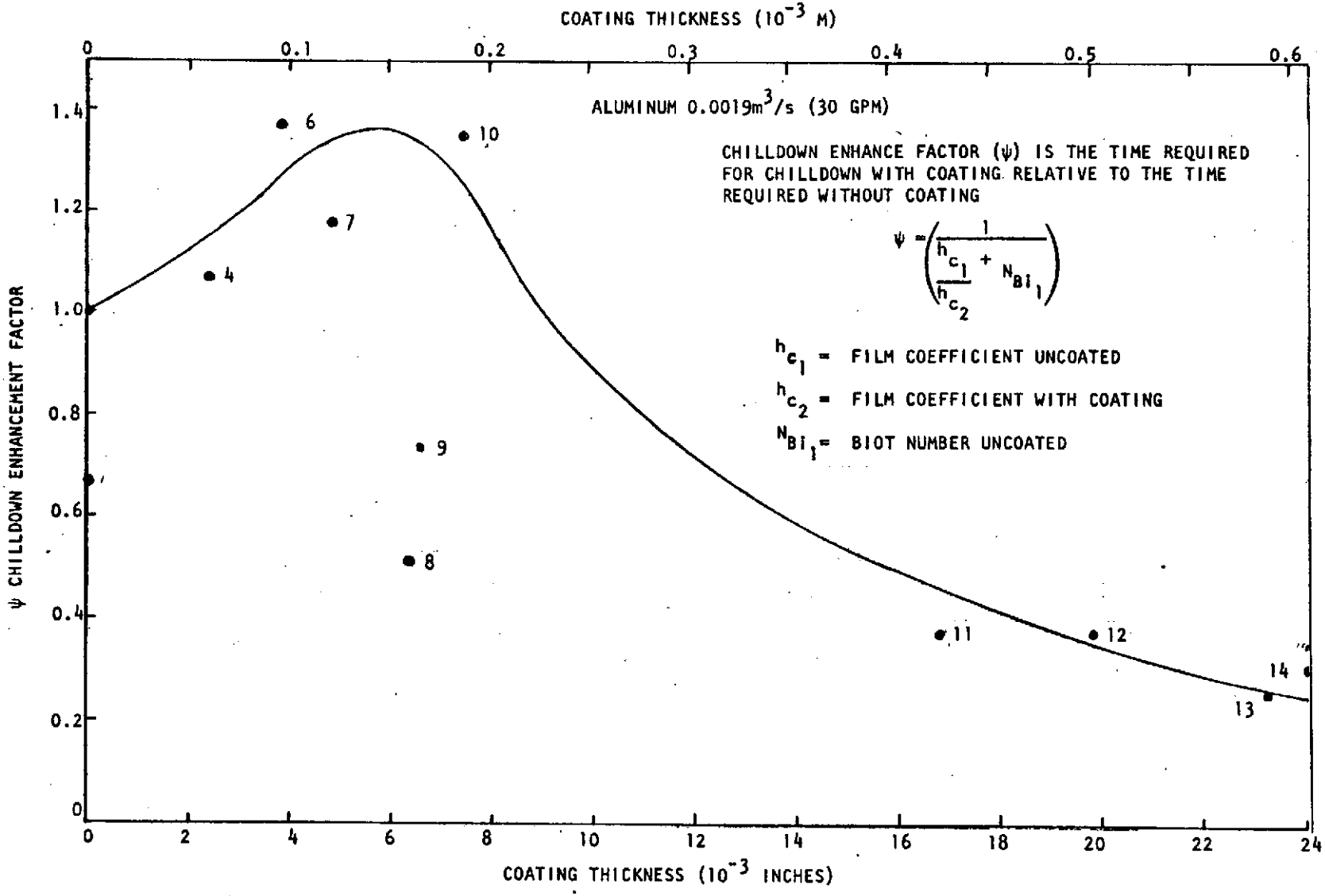

Figure 59. LH_2 Collar Chilldown Enhancement Factor Versus Coating Thickness

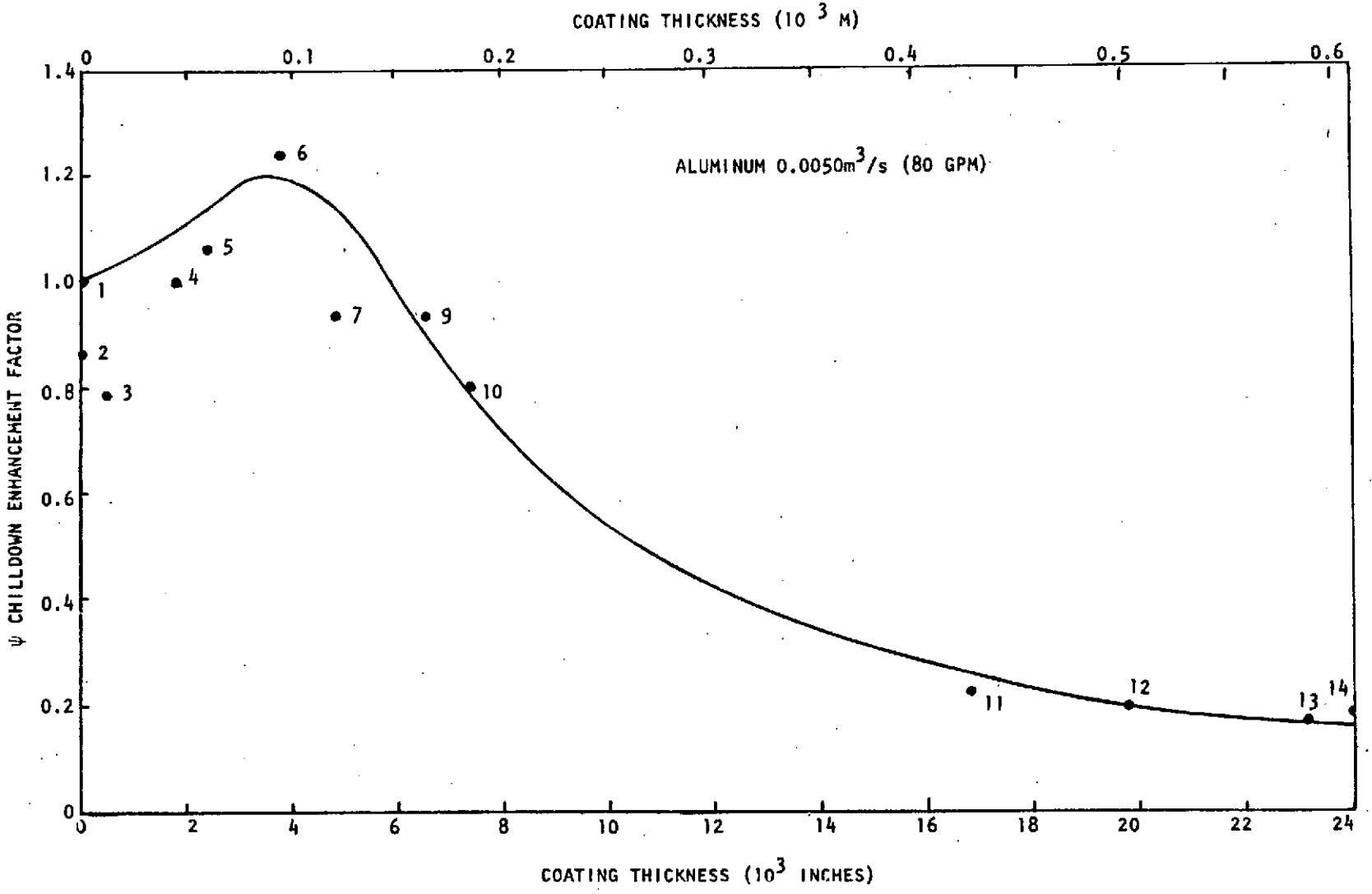

Figure 60. LH_2 Collar Chilldown Enhancement Factor Versus Coating Thickness

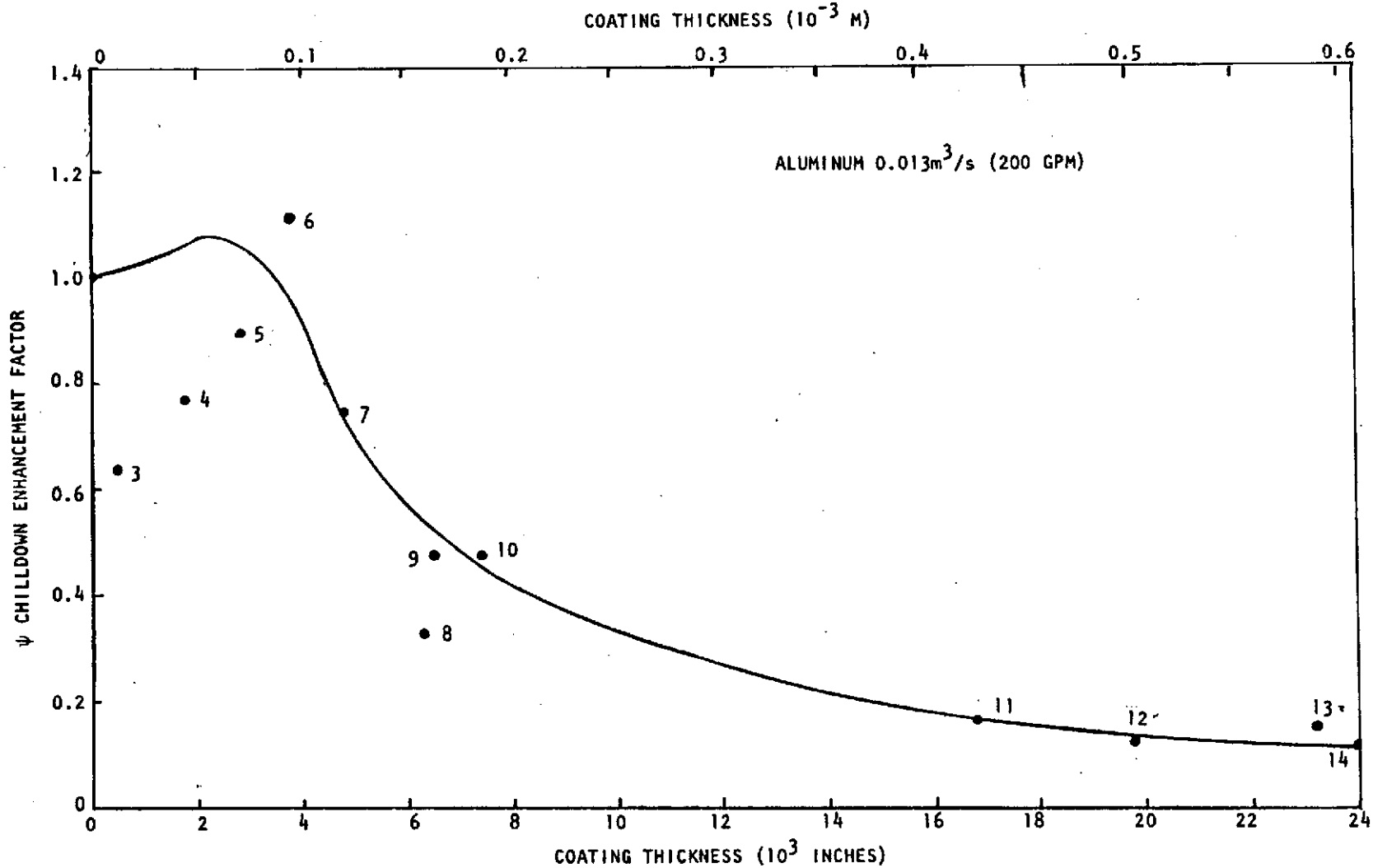

Figure 61. LH_2 Collar Chilldown Enhancement Factor Versus Coating Thickness

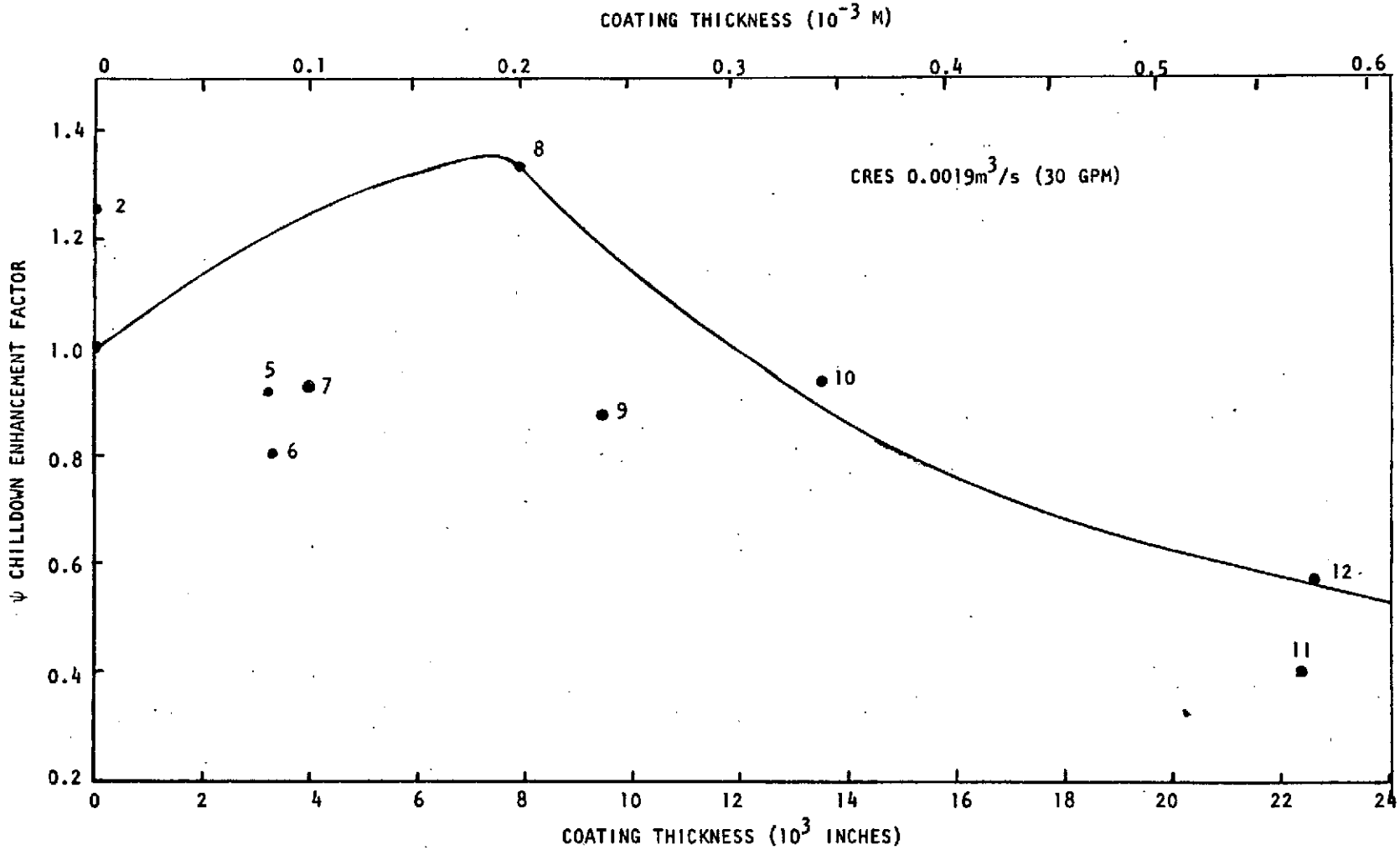

Figure 62. LH_2 Collar Chilldown Enhancement Factor Versus Coating Thickness

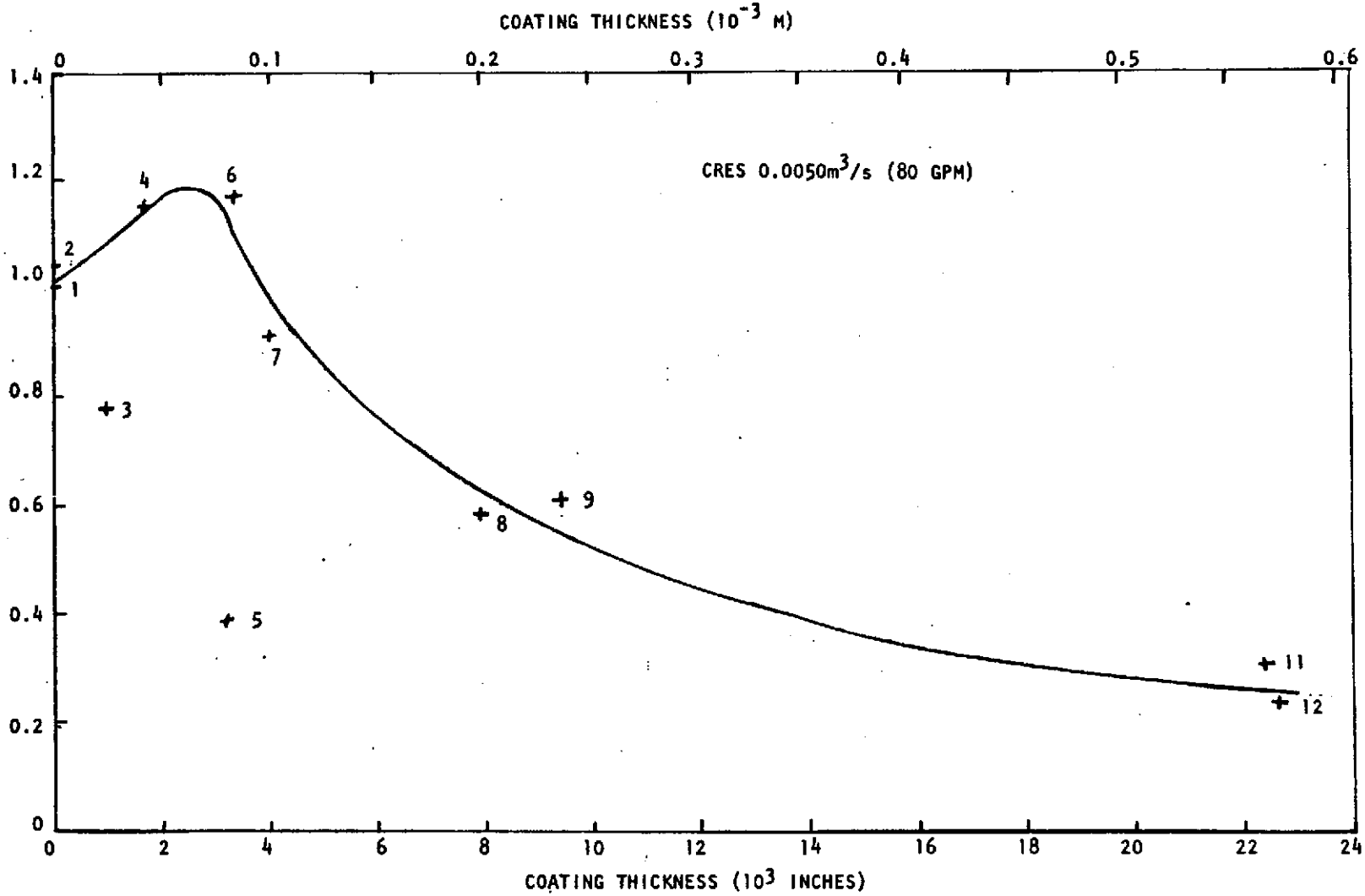

Figure 63. LH_2 Collar Chilldown Enhancement Factor Versus Coating Thickness

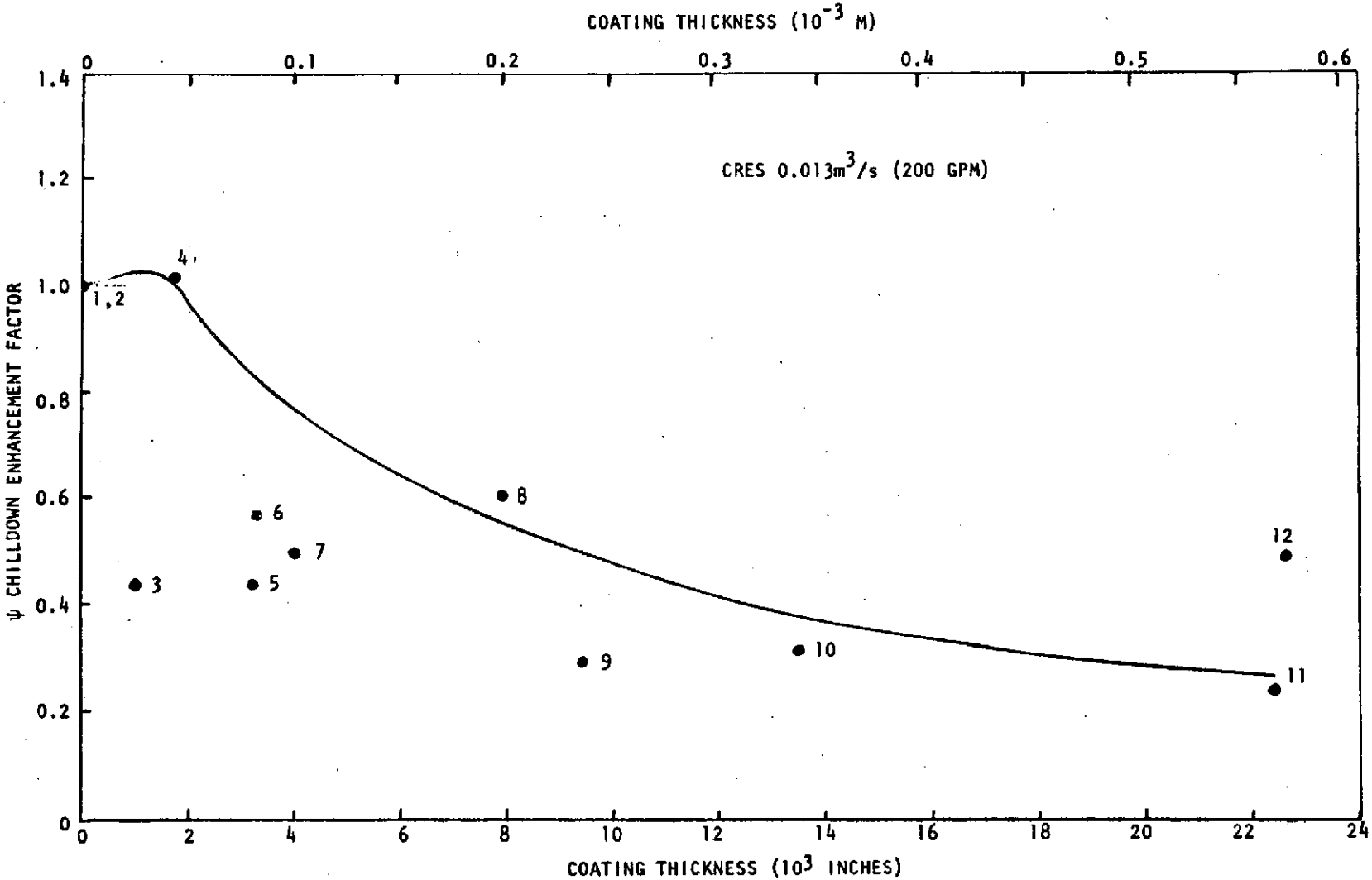

Figure 64. LH_2 Collar Chilldown Enhancement Factor Versus Coating Thickness

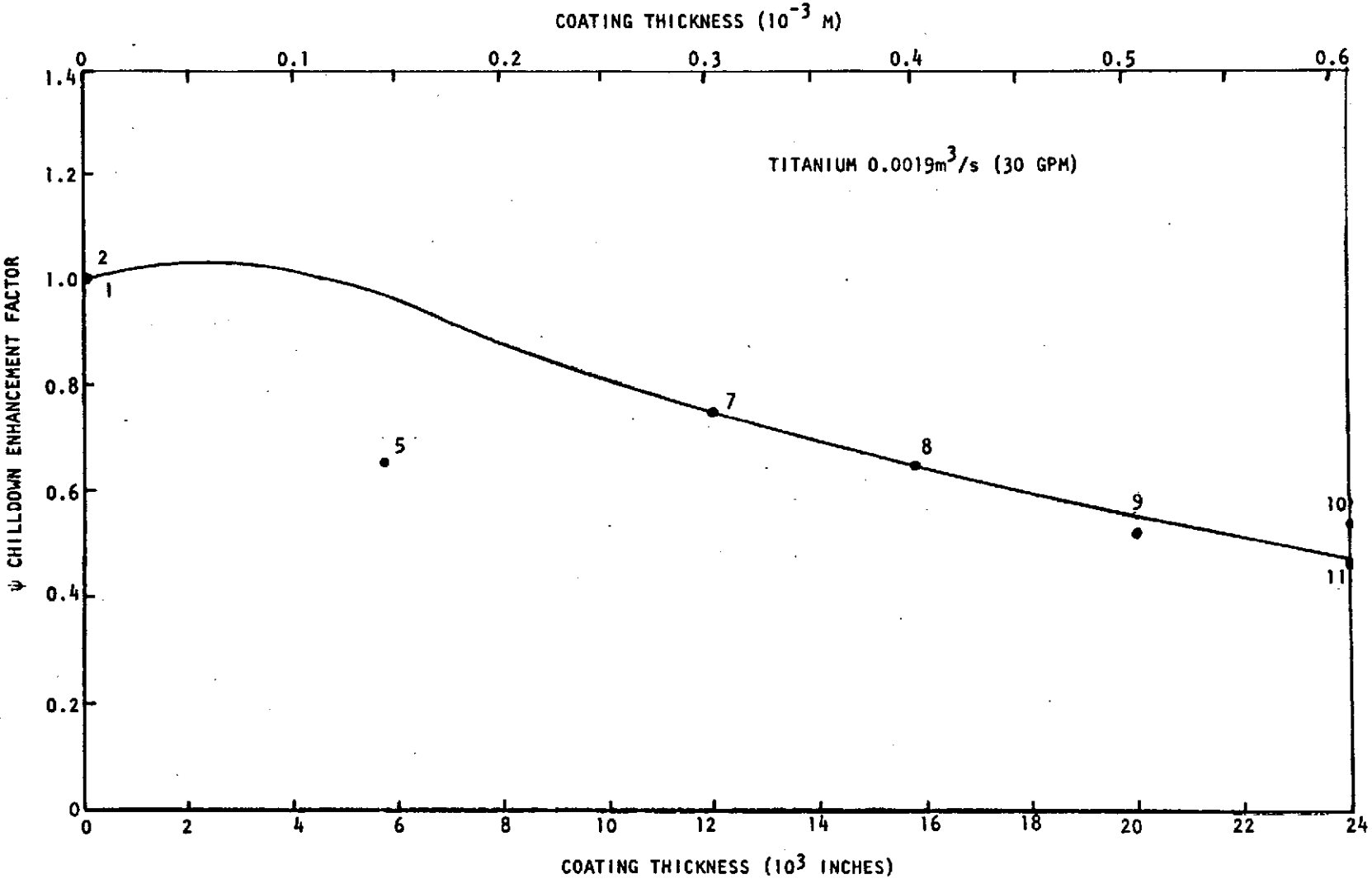

Figure 65. LH_2 Collar Chilldown Enhancement Factor Versus Coating Thickness

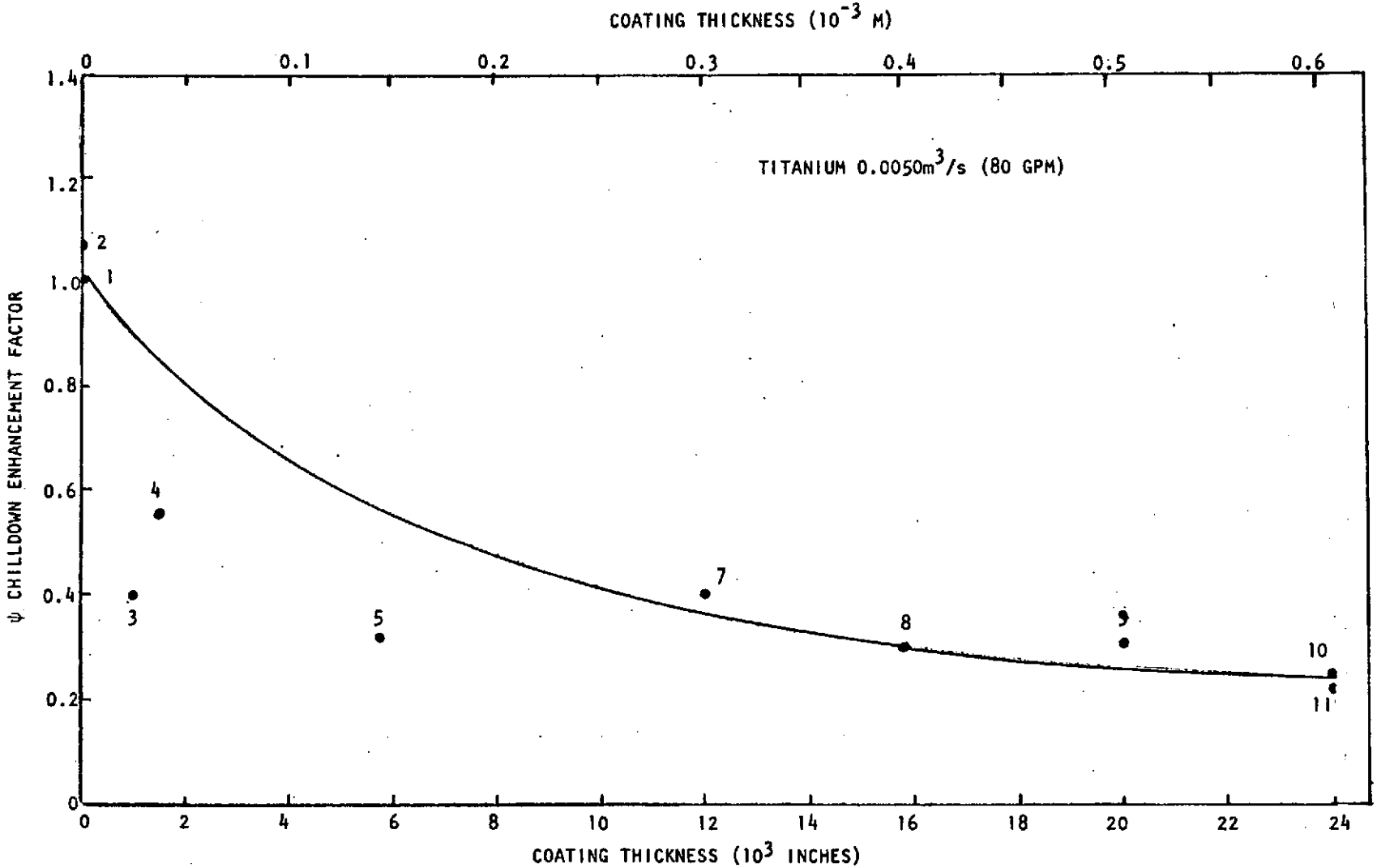

Figure 66. LH_2 Collar Chilldown Enhancement Factor Versus Coating Thickness

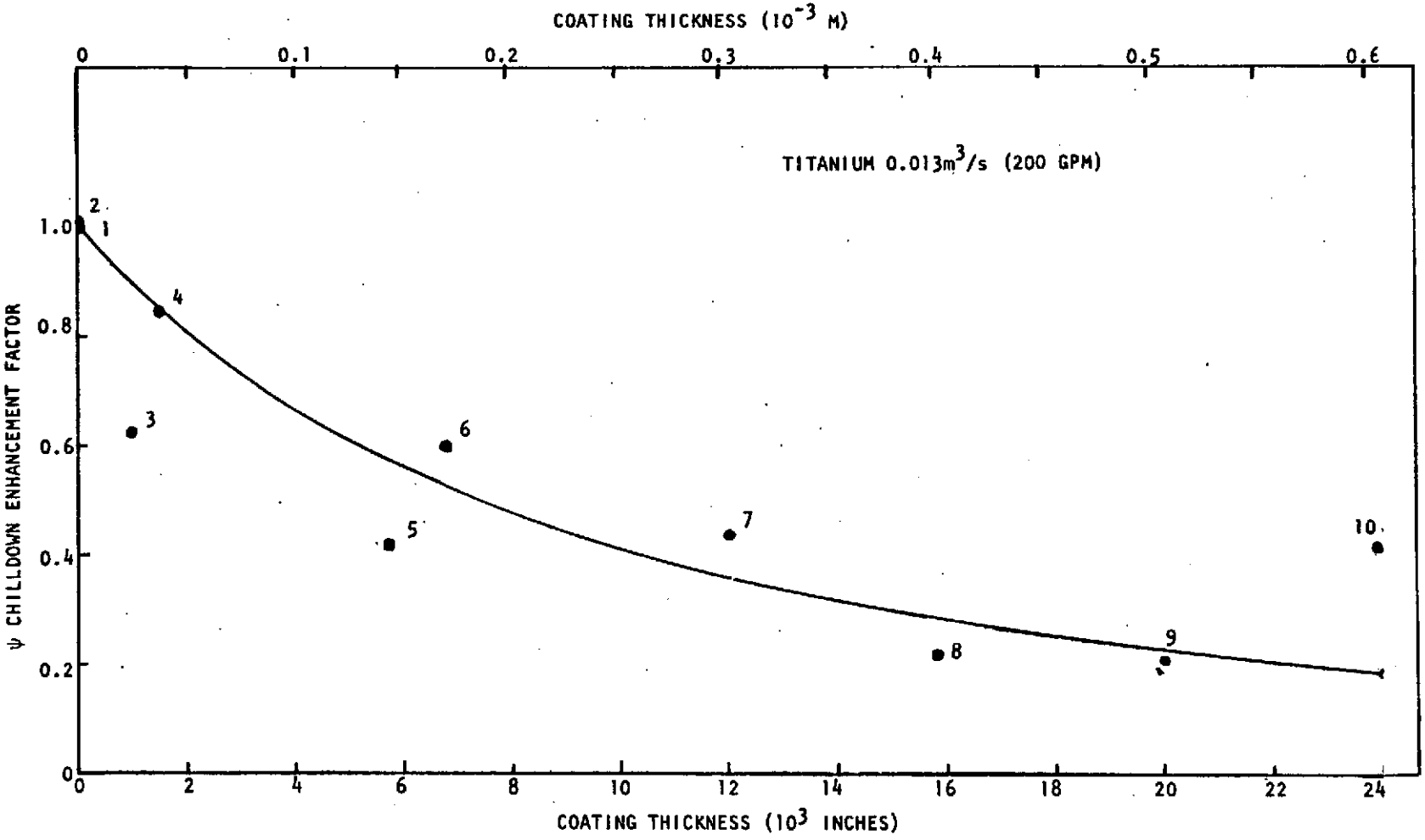

Figure 67. LH_2 Collar Chilldown Enhancement Factor Versus Coating Thickness

equation analyzer digital computer program (DEAP-1). More than 200 lumped parameter nodes were incorporated into the model to simulate analytically internal conduction, liquid hydrogen convection, external conduction, and radiation. The model had the capability of predicting transient wall and fluid temperatures corresponding to the test program matrix. Figure 68 is a sketch of the RL-10 LH_2-turbopump and indicates the nodal distribution of the corresponding analytical model.

The differential equation analyzer program (DEAP-1) was modified to predict internal, external, and fluid temperatures for the entire RL-10 hydrogen turbopump. The digital computer program solves, in finite difference form, the following second-order partial differential equation:

$$\nabla \cdot (k \nabla\phi) + \vec{W} \cdot \nabla\phi + S\,\phi + q = \lambda \frac{\partial^2 \phi}{\partial t} + \rho\, C \frac{\partial \phi}{\partial t}$$

The enthalpy change of the liquid hydrogen due to sensible heating and vaporization are represented by the path through the fluid node points 401-500. Bearing, seal, and interstage fluid flow are included in the comprehensive system. Inlet and outlet lines, casing, and stator wetted path are included in the nodes 1-150 with convection and/or radiation at each surface node. The rotor components are simulated in nodes 301-399. The environmental nodes are the 600-699 and the insulation nodes when used are 700-799.

LH2 Pump Thermal RL-10 Analyses Results. The input of the liquid hydrogen chill flowrate resulted in predicted transient temperatures during chilldown and start for the pump. Results were used as described in the Task III and IV result summaries.

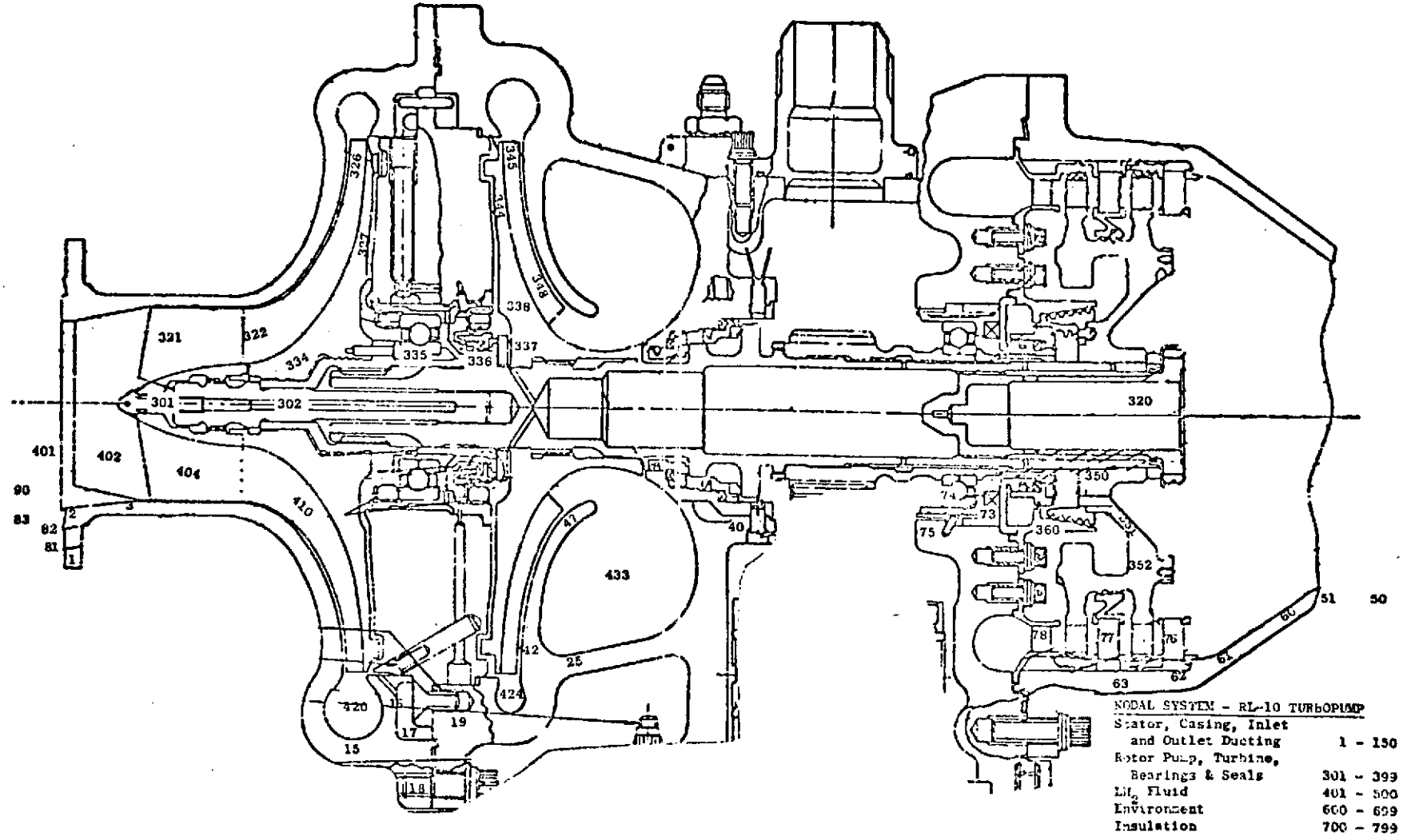

Figure 68. RL-10 Turbopump Heat Transfer Model

TURBOMACHINERY ANALYSIS

An analysis was made to study turbopump startup under a deadhead (no flow) condition with turbine power transmitted to the pump during the start transient. The starting characteristics of the RL-10 hydrogen turbopump were estimated for constant normalized pump flow coefficients (ϕ/ϕ_{design}) between 0.0 (deadhead) and 1.2 using data obtained from Ref. 2, which is shown normalized in Fig. 69.

The turbopump speed transient was predicted by integrating the excess turbine torque as shown in the following equation:

$$\frac{d}{dt}\ (N/N_{des}) = t_c \left(\frac{\tau_{turbine}}{\tau_{des}} - \frac{\tau_{pump}}{\tau_{des}} \right)$$

where

$$t_c = \frac{2\pi\ N_{des}\ I}{60\ \tau_{des}}$$

and I is the rotating inertia. The following design values were used:

Speed, N	=	3142 rad/s (30,000 rpm)
Flowrate, Q	=	0.0386 m^3/s (612 gpm)
Headrise, ΔH	=	10,409 m (34,150 ft)
Efficiency, η	=	65 percent
Power, HP	=	424,300 W (569 HP)

The speed transients are shown in Fig. 70. As shown, increasing the pump flow coefficient increases the start time. This is because horsepower ratio (Fig. 69) and, therefore, pump torque ratio increases with flow coefficient, thereby causing the net torque for acceleration to decrease. The corresponding pump headrises were predicted by the following equation and are shown in Fig. 71:

$$\Delta H = \Delta H_{des} \left(\frac{\psi}{\psi_{des}} \right) \left(N/N_{des} \right)^2$$

The headrise at flow coefficient ratios greater than 1.0 does not reach the design value because the pump horsepower exceeds the design value, while the horsepower delivered by the turbine was assumed to equal the design value. The corresponding propellant heating in the pump during the start transients was predicted by the following equation and is shown in Fig. 72:

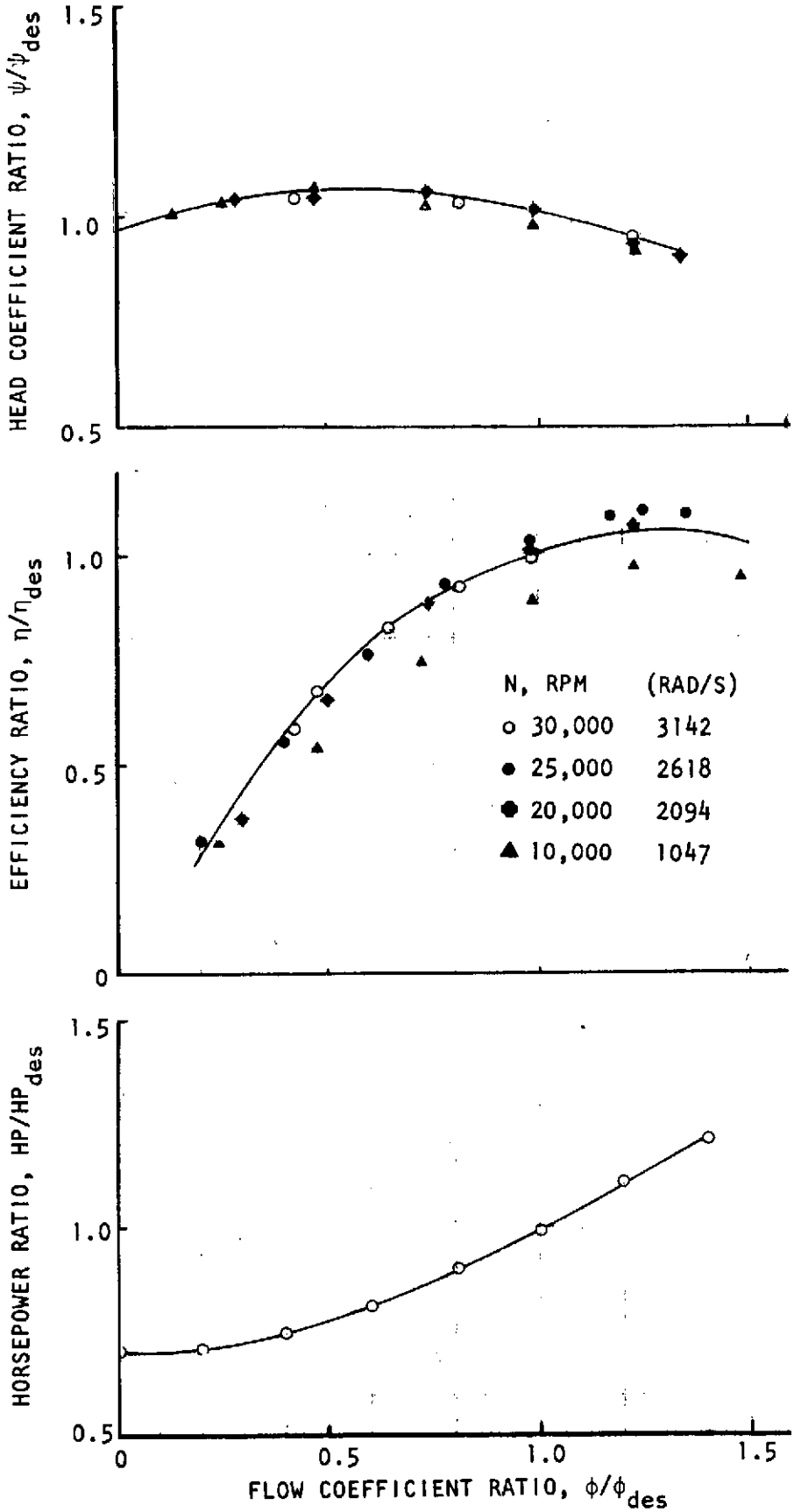

Figure 69. Normalized RL-10 H_2 Pump Characteristics

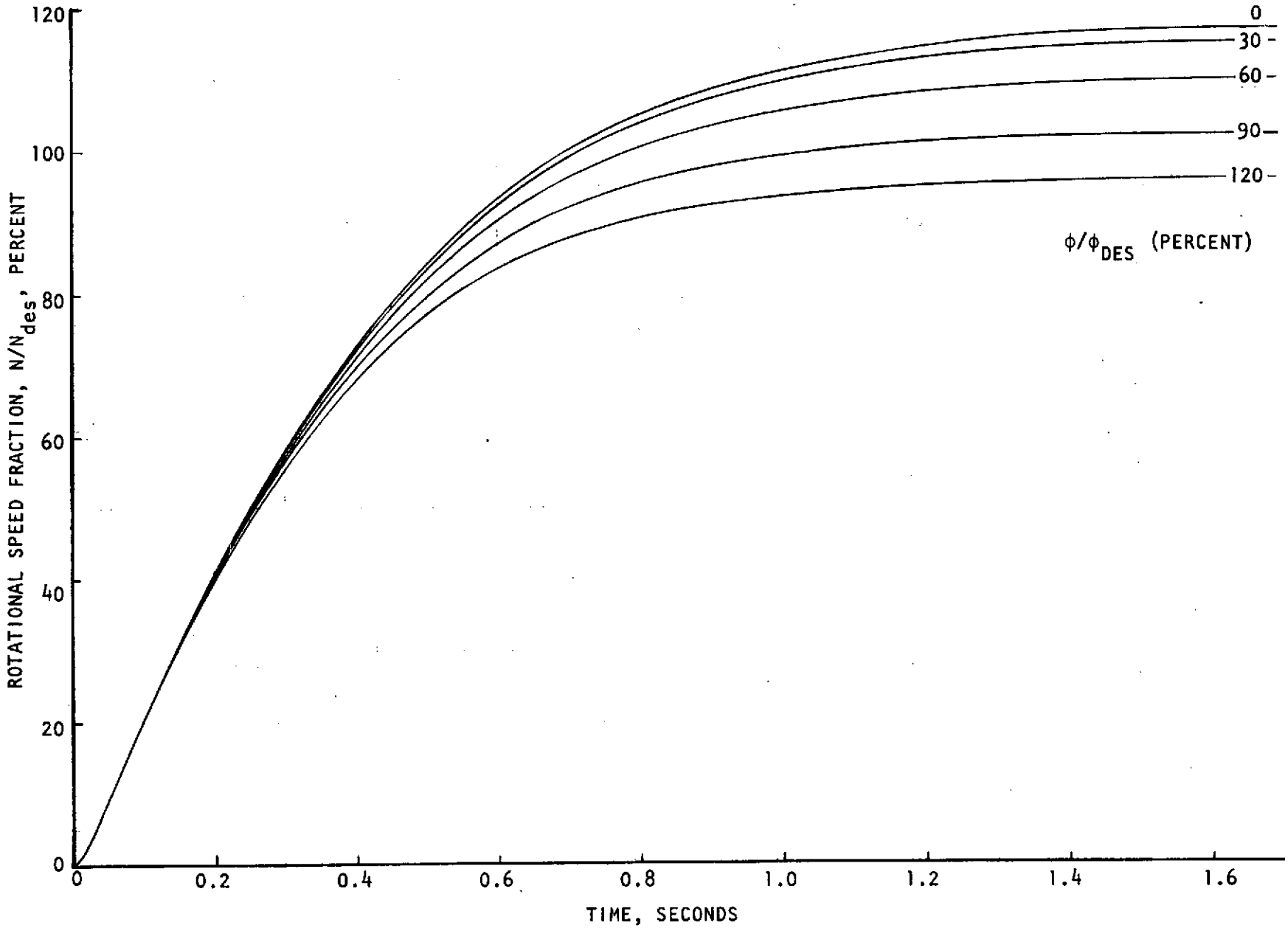

Figure 70. Predicted Start Transients for the RL-10 Hydrogen Pump

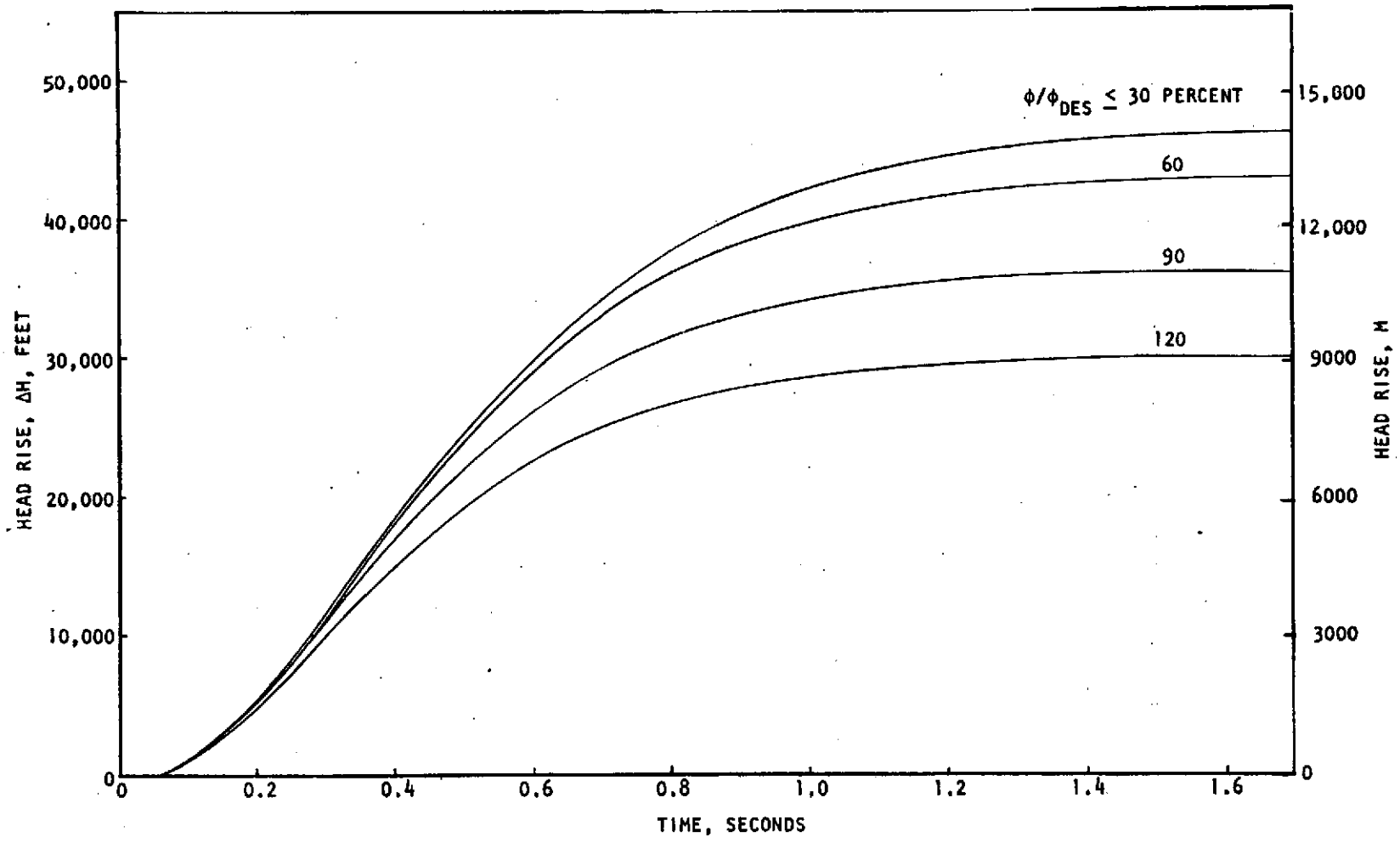

Figure 71. Predicted RL-10 Hydrogen Pump Head Rise for Various Start Transients

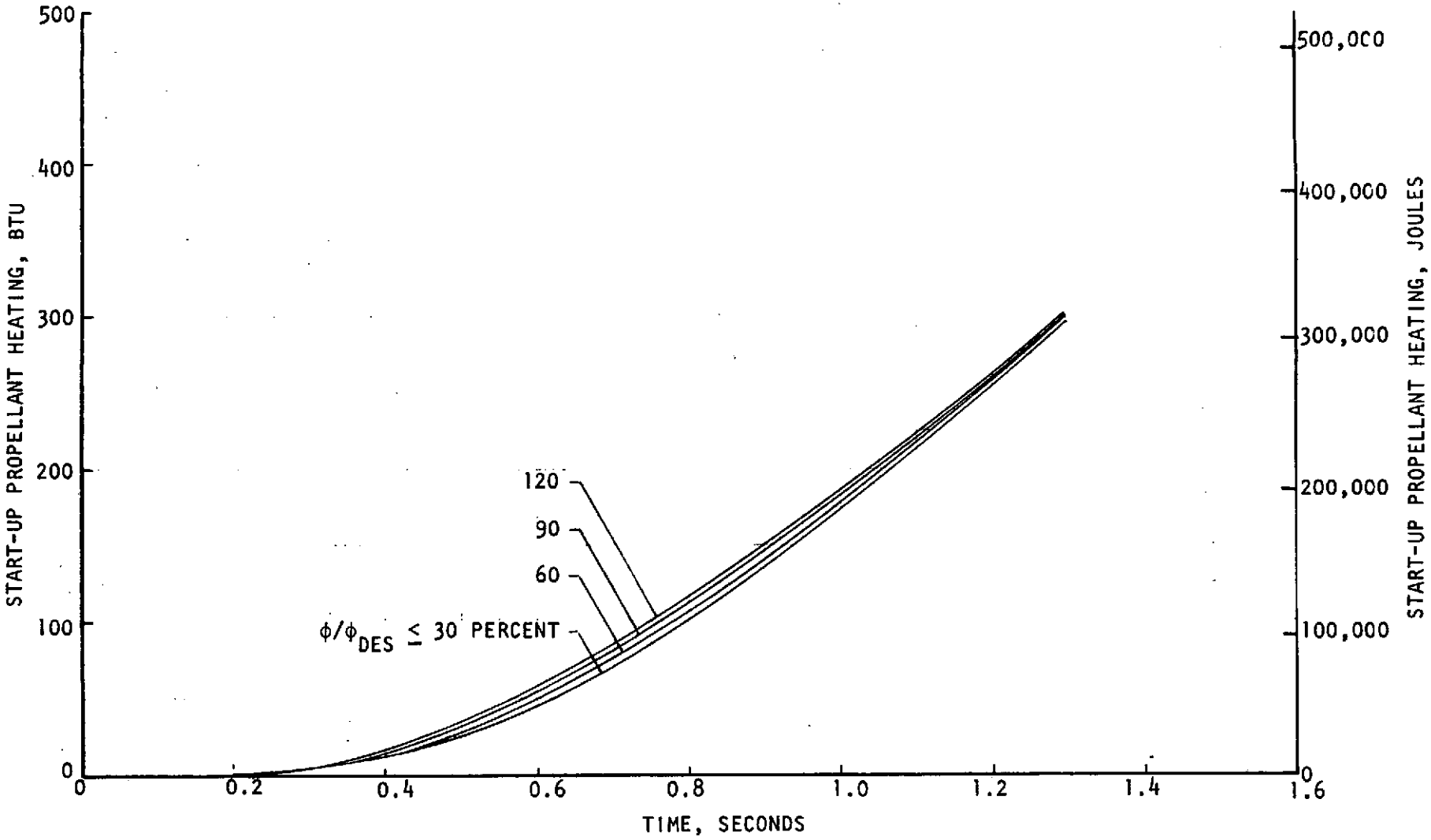

Figure 72. Propellant Heating in RL-10 Hydrogen Pump for Various Start Transients

$$Q = K\, HP_{des}\, t_c \int_0^{N/N_{des}} \frac{(N/N_{des})^3}{\frac{\tau_t}{\tau_{des}} - \frac{\tau_p}{\tau_{des}}}\, d\,(N/N_{des})$$

where:

$$K = \frac{HP}{HP_{des}} \text{ or } \frac{550}{778}\ \frac{HP}{HP_{des}}\ \left(\frac{Btu}{hp}\right)$$

and HP_{des} is in units of watts or horsepower.

It can be seen from Fig. 72 that the ϕ/ϕ_{des} at which the pump accelerates has little effect on the total heat input by the pump.

During deadhead pump starts ($\phi/\phi_{des} = 0$), propellant heating can become a problem because the heat input is rejected only to the propellant trapped within the pump and, therefore, causes a rather large heat input per unit mass of propellant. The pump discharge pressure developed during a deadheaded pump start transient was predicted using the following assumptions: (1) a chilled pump, (2) a constant mass of trapped propellant, and (3) a propellant density that is equal to the discharge value. The temperature-entropy chart for hydrogen, the following equation, and the start transient predictions of speed, head and propellant heating (Fig. 70, 71, and 72) were also used. The predicted pressure developed during the deadheaded start transient is shown in Fig. 73 and 74.

$$\Delta P = \Delta P_{des} \left(\frac{\psi}{\psi_{des}}\right) \left(\frac{\rho_2}{\rho_{2_{des}}}\right) \left(\frac{N}{N_{des}}\right)^2$$

As shown, the deadheaded pump discharge pressure reaches a peak value of 4.55 x 10^6 N/m^2 (660 psia), 60 percent of design, at 85 percent of design speed. At higher speeds, the accumulated heating decreases the propellant density enough to cause the pump discharge pressure to drop. Thus, a system with this pump would be unable to start if the system pressure downstream of the pump was equal or greater than 4.55 x 10^6 N/m^2 (660 psia).

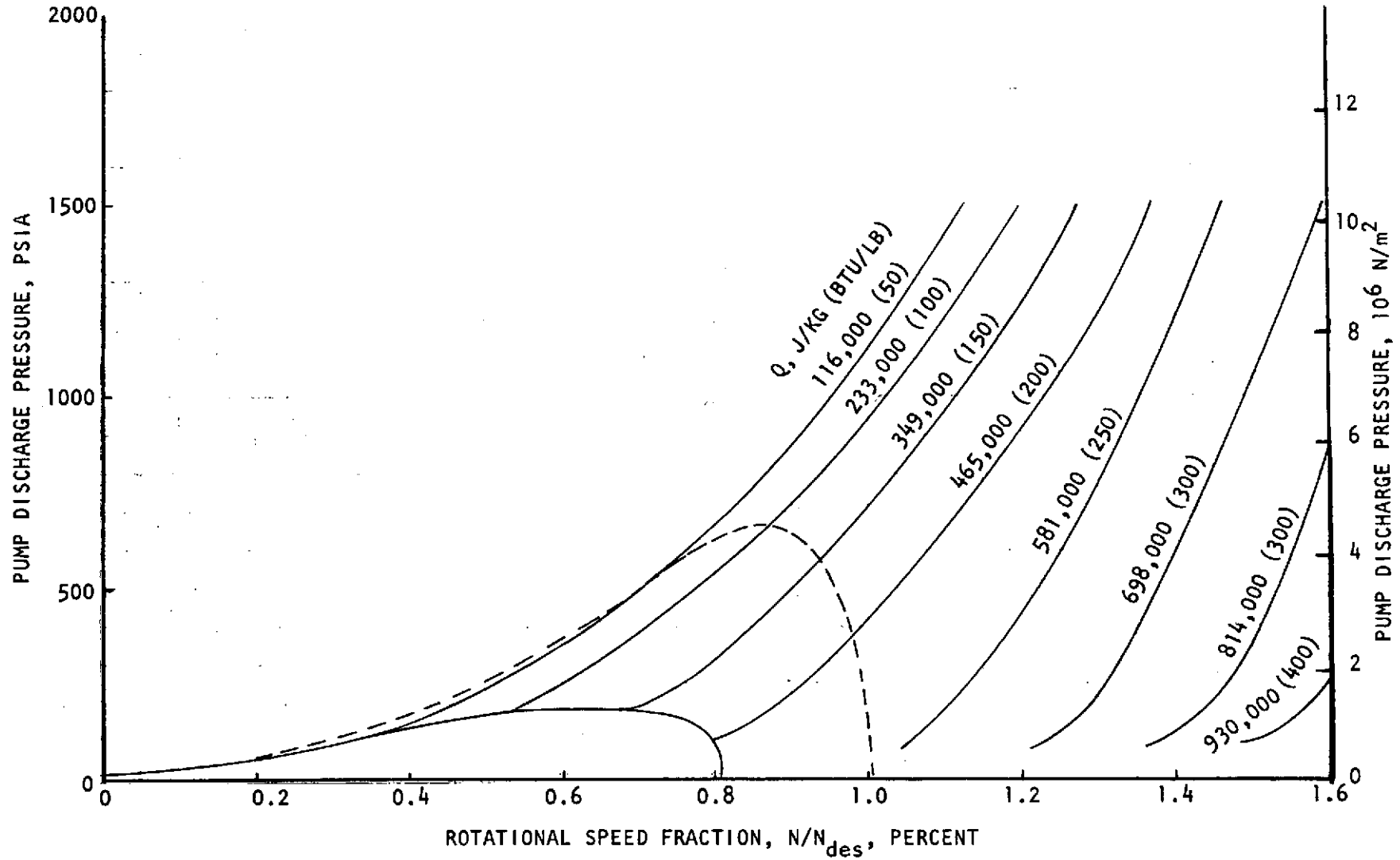

Figure 73. Predicted RL-10 Hydrogen Pump Discharge Pressure During Deadhead Start

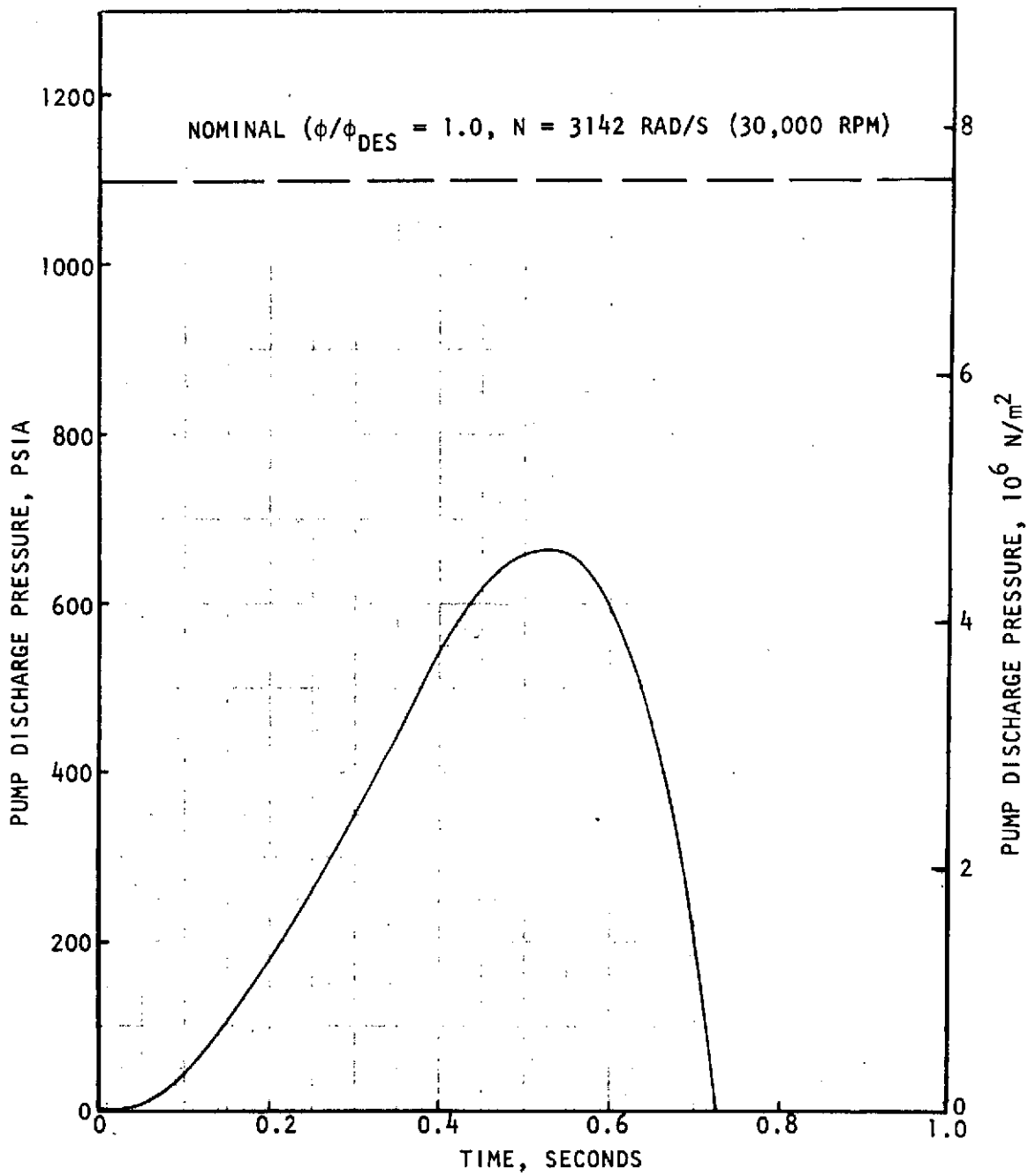

Figure 74. Predicted RL-10 Hydrogen Pump Discharge Pressure Transient for Deadhead Start

SYSTEM EVALUATION

An analytical model of the experimental feed system was developed for use with the IBM 360 digital computer. The model was used to determine the effects of chilldown heat transfer on turbopump deadhead start. Both preconditioned and warm feed systems with various downstream reservoir volumes and back pressures were analyzed. The primary utilization of the model was to establish a start sequence and specify the volume of the ducting downstream of the pump that will permit a deadhead start.

Model Description

An existing dynamic model, where the turbopump acceleration is governed by the excess turbine torque and the rotating moment of inertia, was modified for this program. This model is capable of determining the low-frequency dynamic response of system components. Each component is described mathematically by relating its geometric, hydrodynamic, and thermal characteristics to calculate flowrates and pressures throughout the system. Resistance, inertia, and compressibility effects are included in the lumped-parameter modeling of the ducts. The heat transferred into the hydrogen from the inlet duct and pump, and the discharge pressure required to initiate opening of the discharge valve were varied parametrically. The heat transferred into the hydrogen from the warm pump was assumed to be on the order of 40 times the amount transferred from the inlet duct. This heat transfer was programmed proportional to the square root of propellant flowrate.

Components simulated in the model include a General Dynamics inlet line, an RL-10 hydrogen turbopump, a discharge line and valve, a pump discharge reservoir, and a turbine inlet valve. These components are shown schematically in Fig. 75.

Pressures and flows through the system are calculated as a function of time by numerical integration using lumped-parameter modeling. Each component is described mathematically by relating its geometric, hydrodynamic, and thermal characteristics; and assuming the fluid properties, i.e., resistance, inertia, and compressibility to be independent of each other.

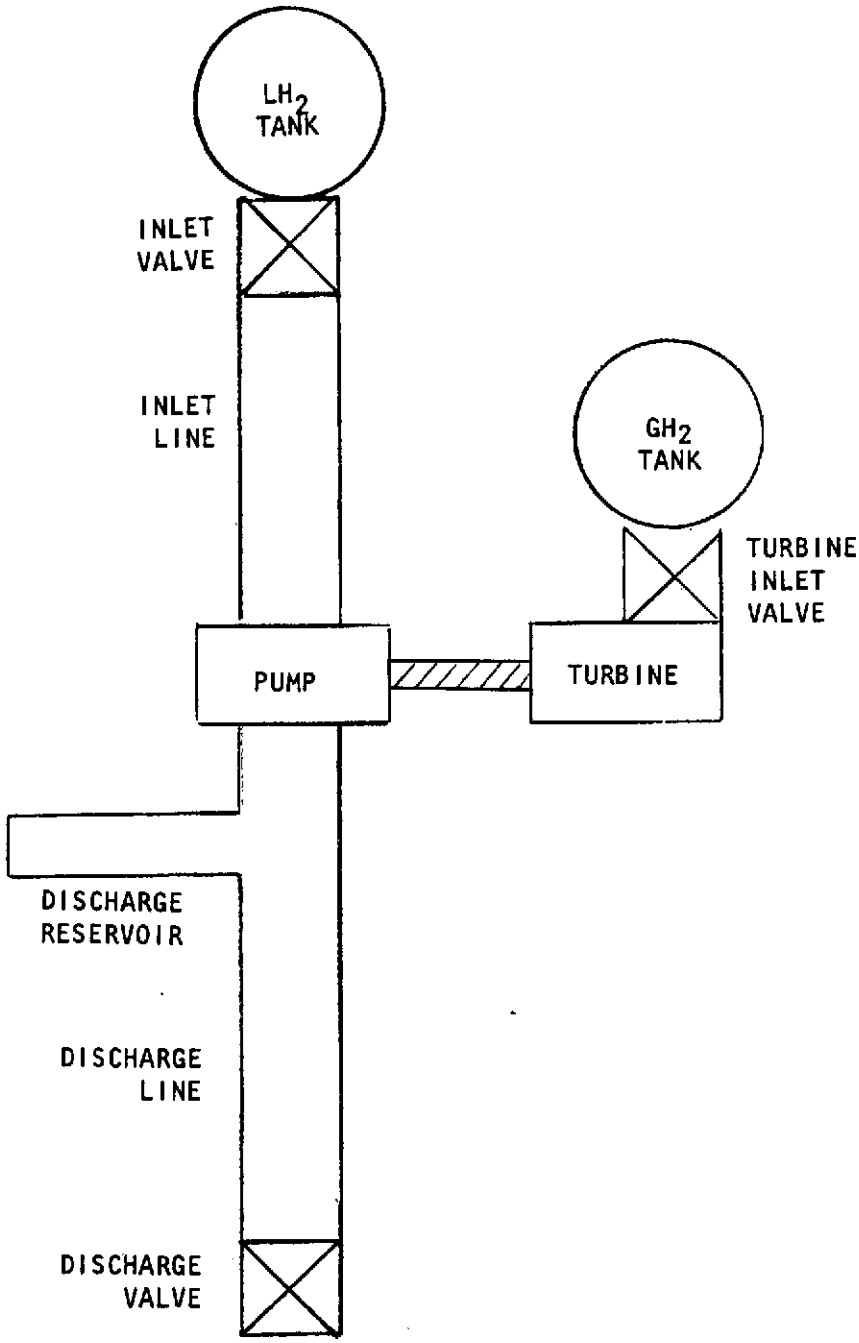

Figure 75. Schematic of Components Included in Model

Pressures in the ducts are calculated using:

$$P_{t2} = P_{t1} + (C^2/(V\ g_o))\ (\int_{t1}^{t2} (\dot{W}_i - \dot{W}_o)\ dt)$$

whereas, flowrates are determined using:

$$P_{x2} = P_{x1} - (R\dot{W}^2)/\rho + (L\ddot{W})/(Ag_o)$$

where:

A	=	flow area
C	=	sonic velocity
g_o	=	gravitational constant
i	=	inch
L	=	length
o	=	out
P	=	pressure
R	=	flow resistance
t1	=	initial time
t2	=	final time
V	=	volume
$\dot{W}$	=	flowrate
$\ddot{W}$	=	flow acceleration
x1	=	upstream station
x2	=	downstream station
ρ	=	density

The propellant density and sonic velocity used by these equations are functions of pressure and enthalpy. Pressure losses are assumed to occur at constant enthalpy, but the enthalpy is changed as the hydrogen flows through the system; first, by heat transfer during chilldown of the components, and then, by energy addition during the pumping process.

The groupings of parameters $C^2/(Vg_o)$ and $L/(Ag_o)$ simulate fluid compressibility and inertia, respectively. These terms, plus the flow resistance, define a component's dynamic-flow characteristics and are collectively called a lump. The inlet and discharge ducts and the discharge reservoir are each modeled with three lumps. Dynamic modeling of the pump is accomplished with a single lump.

The equations used to define the steady-state pump performance were derived by curve-fitting the data presented in Ref. 2. Figure 76 shows a graphic representation of these equations. Turbopump acceleration, and hence speed, is governed by the excess torque developed by the turbine and the moment of inertia, i.e.,

$$I\dot{N} = T_T - T_P - T_f$$

where:

I = moment of inertia
$\dot{N}$ = acceleration
T_f = friction torque
T_P = pump torque
T_T = turbine torque

The turbine performance map (Fig. 77) was derived from the plot of turbine efficiency presented in Ref. 2 and the inlet conditions specified by Rocketdyne for the experimental program.

Turbopump Start Transient

The initial analyses assumed the components to be thermally preconditioned to tank-propellant temperatures. The first case investigated included a reservoir with a volume of 0.056 m^3 (1.96 ft^3). The back pressure on the pump discharge duct was 1.01 x 10^5 N/m^2 (14.7 psia). The valve sequence (Fig. 78) is initiated by opening the inlet valve to prime the system. A relatively slow opening of the

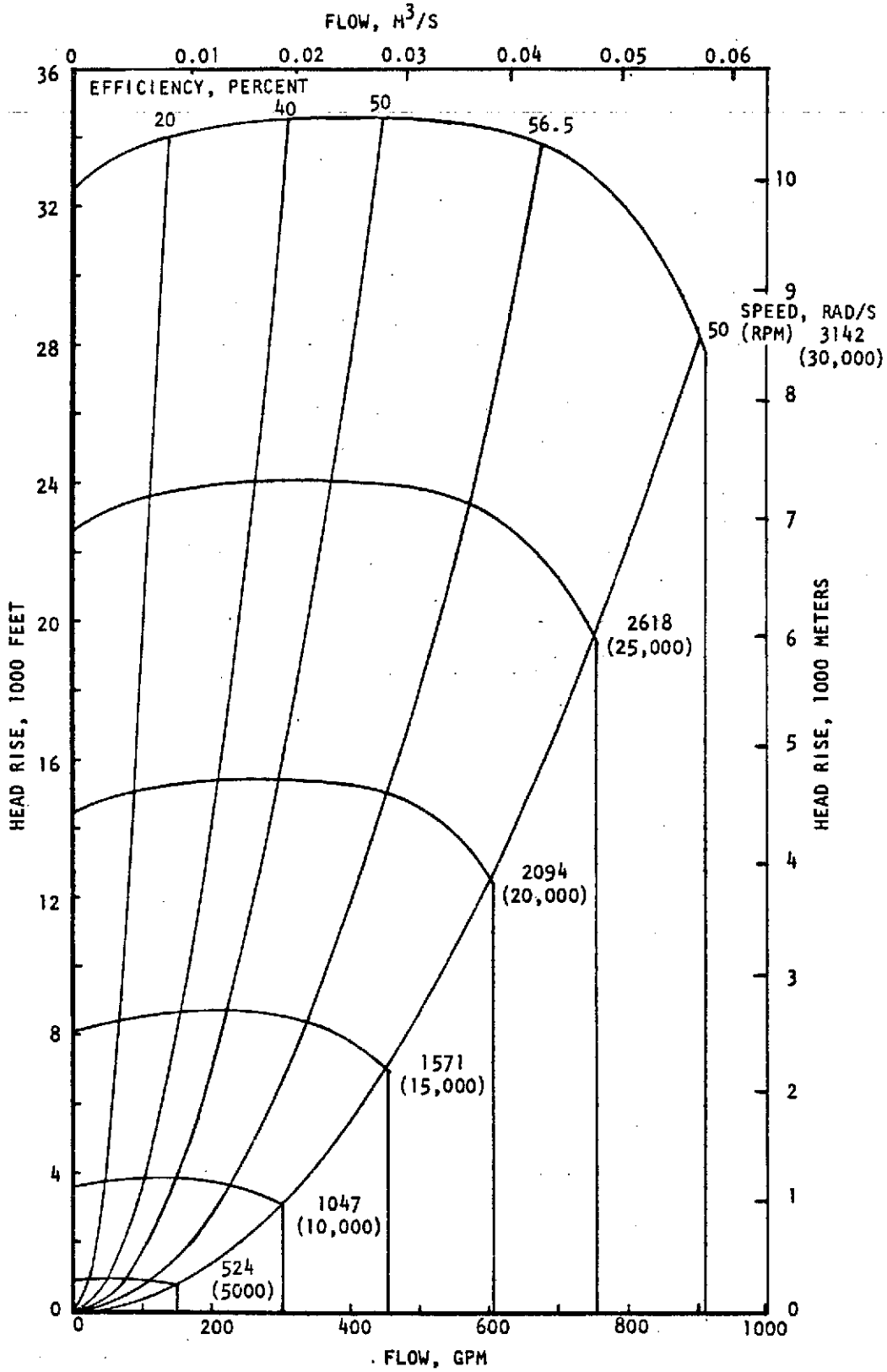

Figure 76. Pump Performance

N = SPEED, RAD/SEC

MW = MOLECULAR WEIGHT

T_1 = INLET TEMPERATURE

T = TORQUE

P_1 = INLET PRESSURE

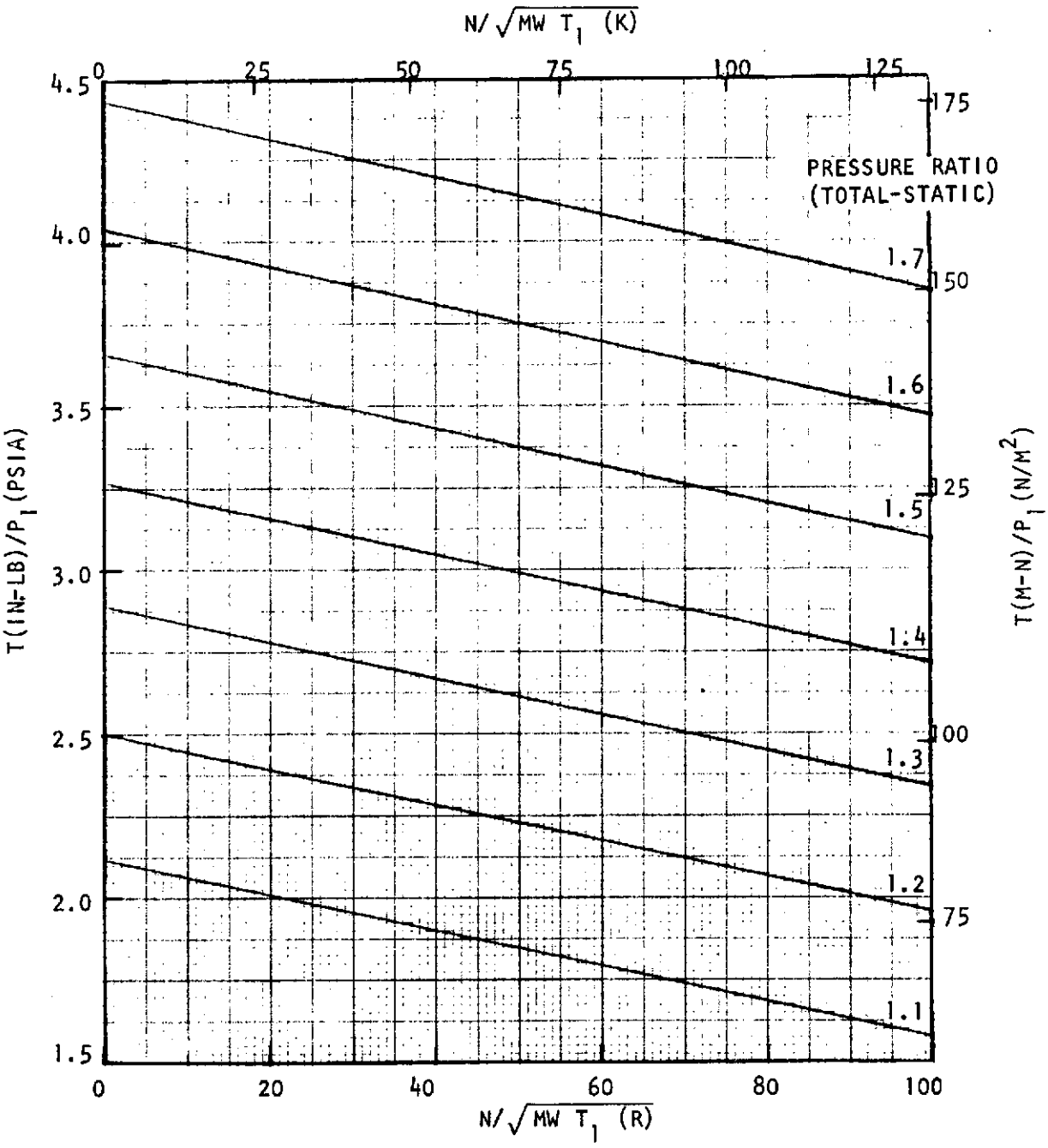

Figure 77. Turbine Performance

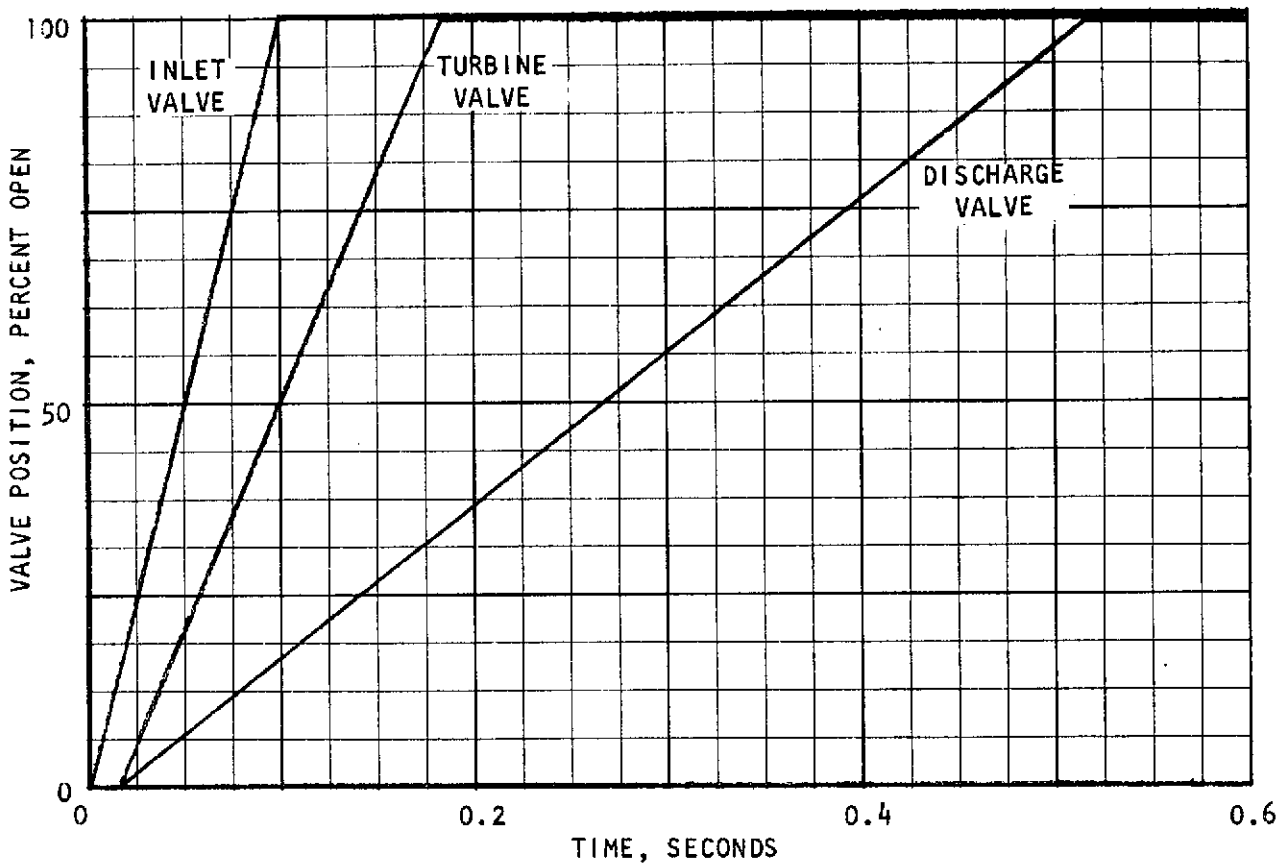

Figure 78. Valve Sequence

discharge valve is required to restrict the pump flow and prevent excessive flow coefficients during the acceleration transient. The pump performance during the start transient is shown graphically in Fig. 79.

A series of cases were run to determine the effect of the discharge-reservoir volume on the start transient for a discharge back pressure of 3.45×10^6 N/m^2 (500 psia). The range of volumes considered was 0.02 to 0.11 m^3 (0.71 to 3.90 ft^3). To this, the volume of the discharge duct, 0.006 m^3 (0.22 ft^3) was added. For each of these cases, the discharge valve was ramped open in 0.2 seconds from the time the valve inlet pressure reached 3.45×10^6 N/m^2 (500 psia).

The start transient of the turbopump for a reservoir volume of 0.02 m^3 (0.71 ft^3) is shown in Fig. 80. As shown, the flow oscillations are severe and periods of backflow through the pump are evident. The start transient for a reservoir volume of 0.035 m^3 (1.23 ft^3) is shown in Fig. 81. The increased volume damped the flow oscillations and shifted the head-flow transient to the right. Although no reverse flow is indicated, it should be noted that propellant properties within any model lump are assumed to be uniform, and localized regions of reverse vapor flow probably occurs through the pump. The most critical period indicated by Fig. 82 is at a speed of approximately 2304 rad/s (22,000 rpm), when the developed head is relatively high and the efficiency is only 31 percent. Propellant heating is very high under these conditions because of the low flowrate. Increasing the reservoir volume to 0.056 m^3 (1.96 ft^3) further reduces the flow oscillations as shown in Fig. 82. This volume results in the most "acceptable" start transient of the cases investigated. A reservoir volume of 0.11 m^3 (3.9 ft^3) causes the start transient to shift to the extreme right side of the performance map as indicated in Fig. 83. Intermittent breakdowns in the developed head were encountered for speeds up to approximately 628 rad/s (6000 rpm).

The back pressure that initiates the opening of the discharge valve was also varied parametrically. The results for a range between 2.76×10^6 and 4.14×10^6 N/m^2 (400 and 600 psia) are in Fig. 82. As the required back pressure was increased, thus delaying the opening of the discharge valve, the head-flow transient shifted

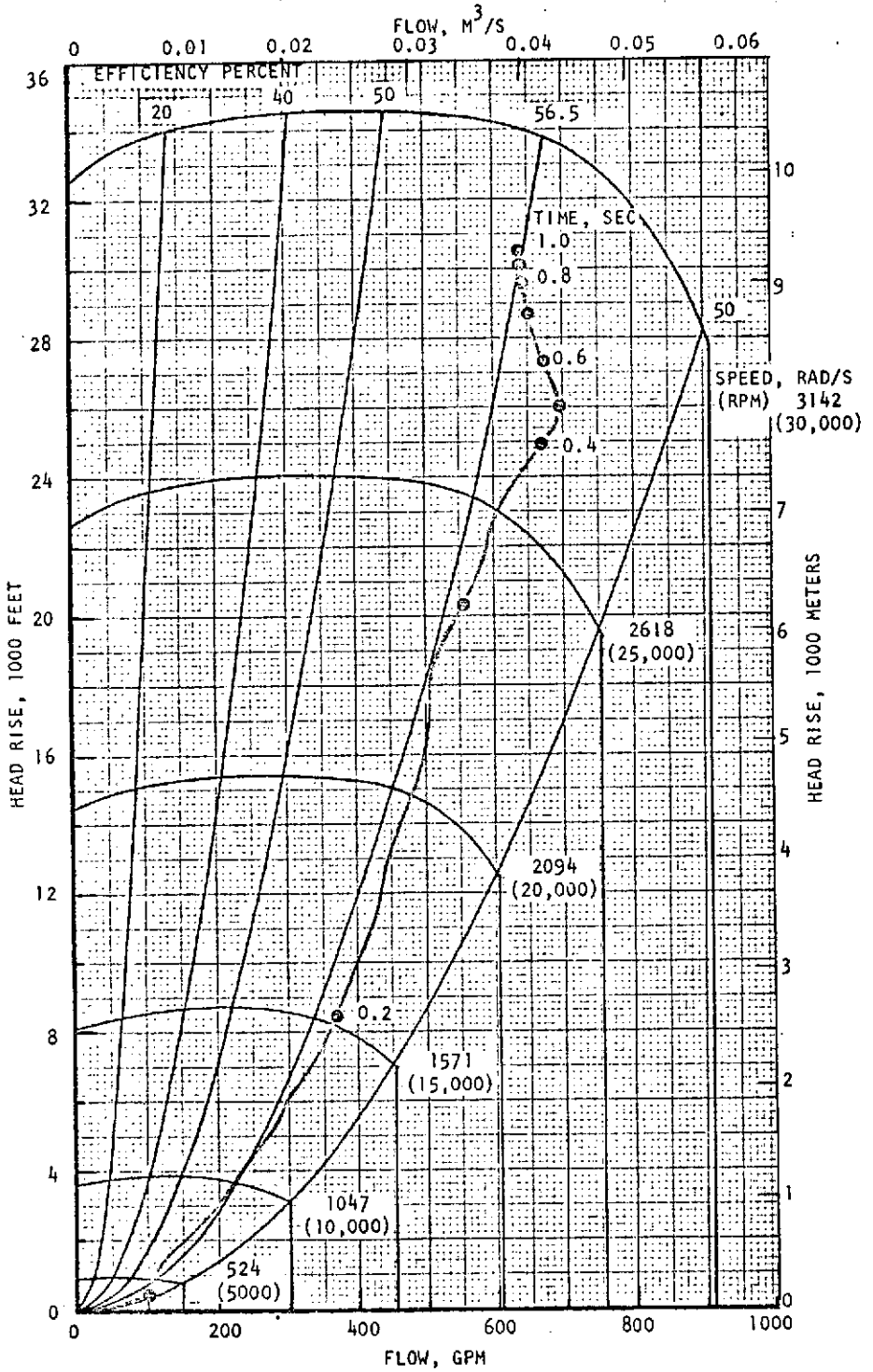

Figure 79. Start Transient with $0.056m^3$ (1.96 ft^3) Reservoir and $1.01x10^{-5}N/m^2$ (14.7 psia) Back Pressure

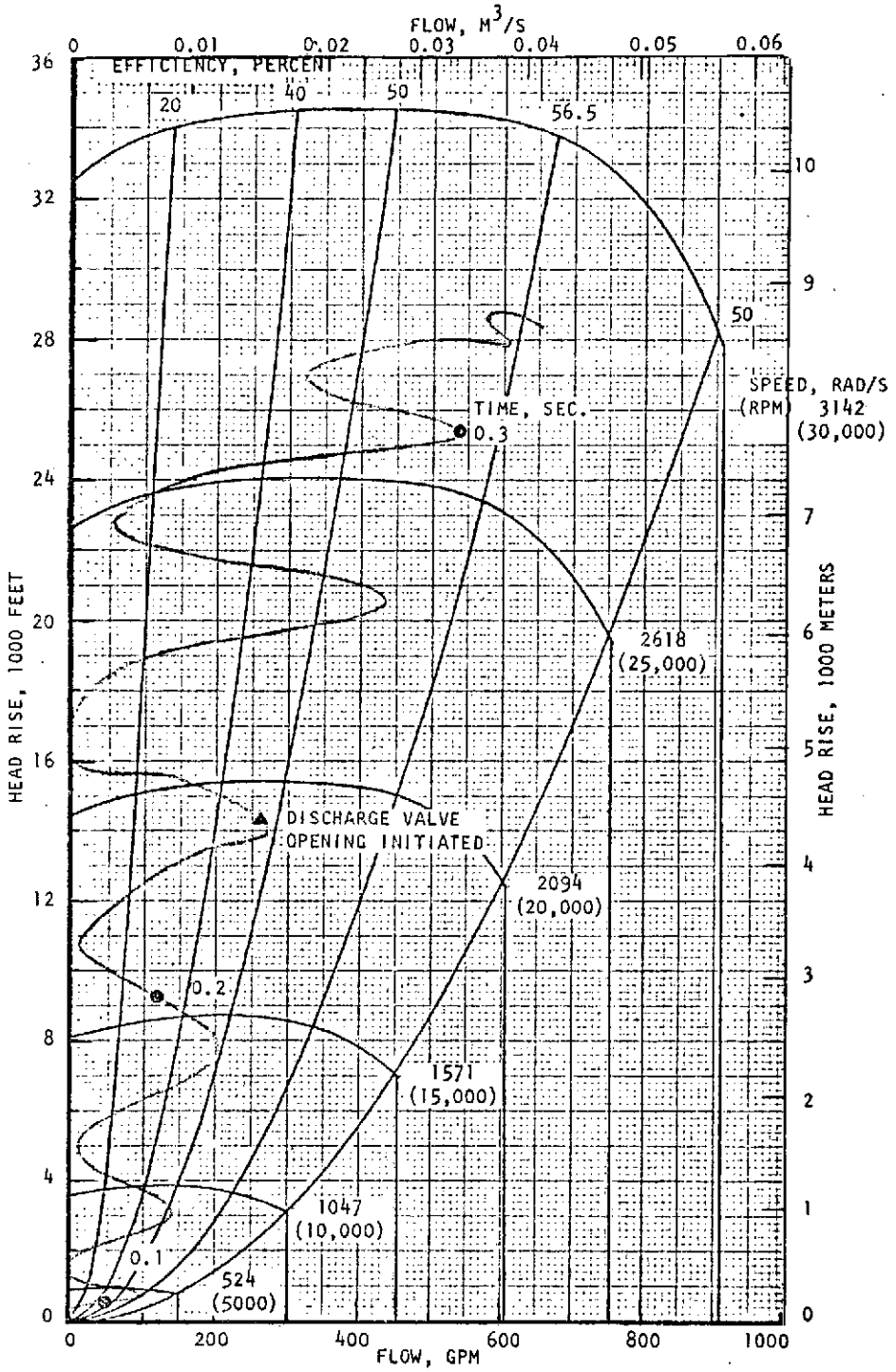

Figure 80. Start Transient with 0.02 M^3 (0.71 ft^3) Reservoir and 3.45×10^{-6} N/M^2 (500 psia) Back Pressure

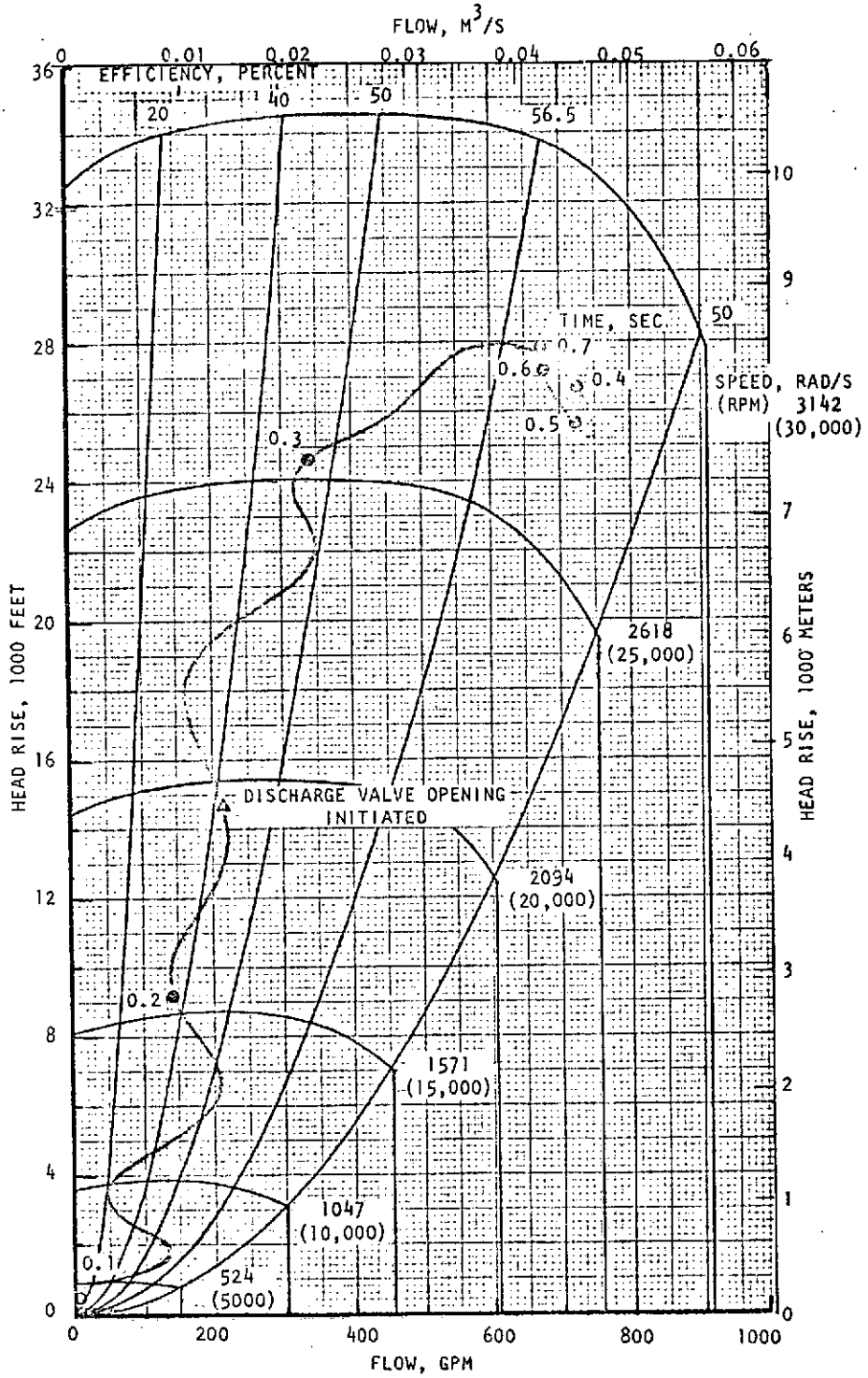

Figure 81. Start Transient with 0.035 M^3 (1.23 ft^3) Reservoir and 3.45×10^{-6} N/M^2 (500 psia) Back Pressure

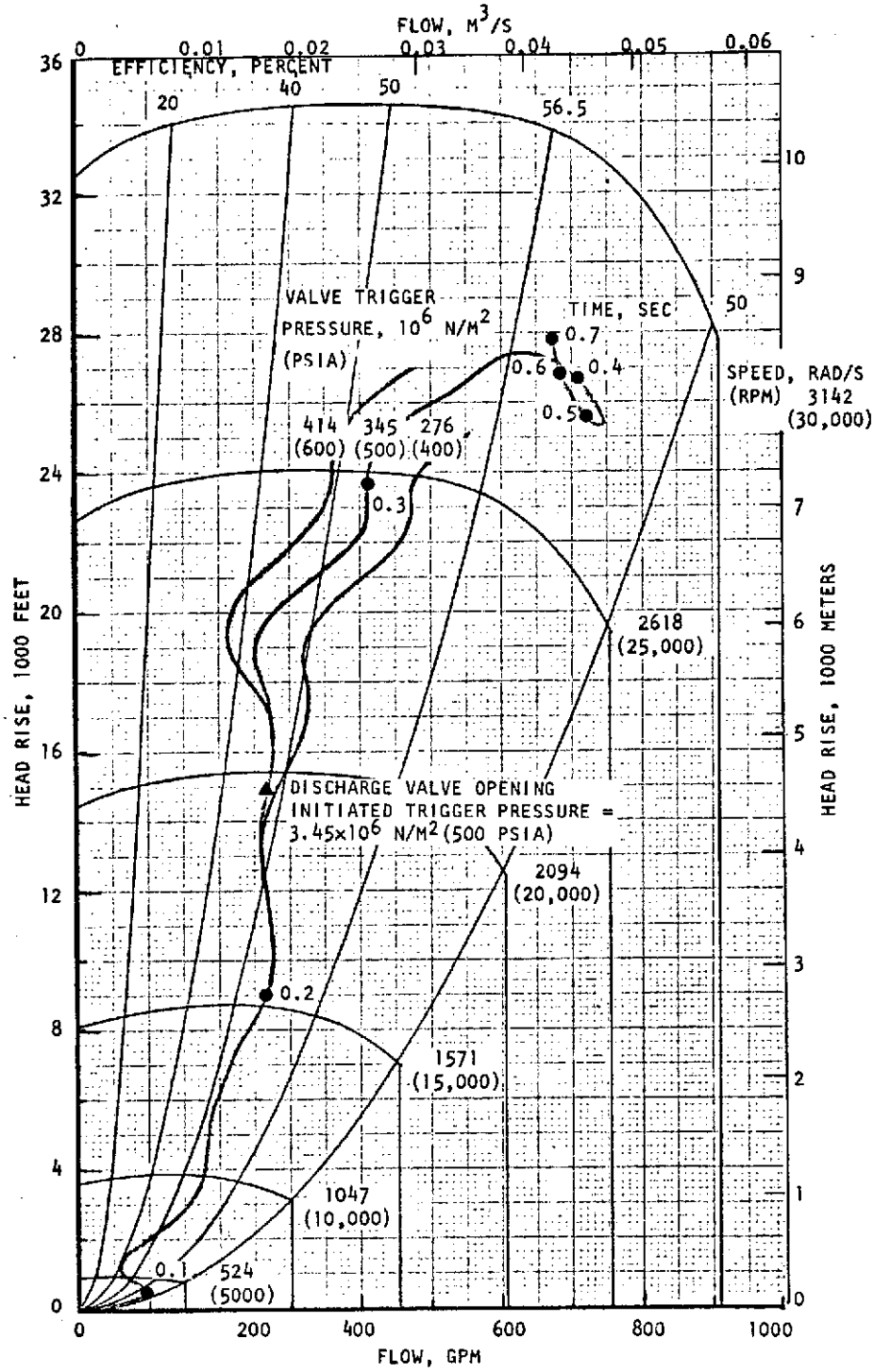

Figure 82. Start Transients with 0.056 M^3 (1.96 ft^3) Reservoir

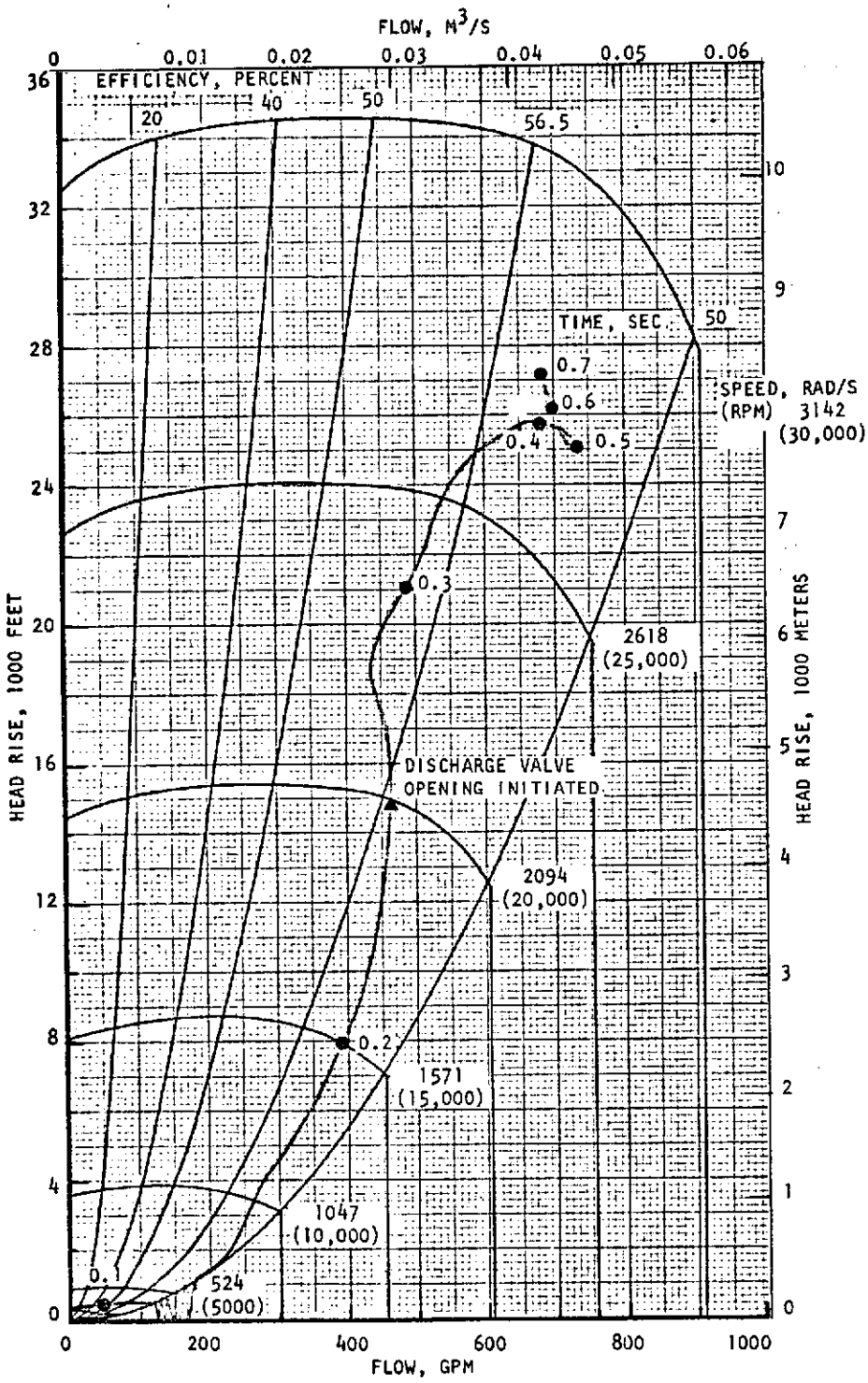

Figure 83. Start Transient with 0.11 M^3 (3.9 ft^3) Reservoir and 3.45×10^{-6} N/M^2 (500 psia) Back Pressure.

to the left and resulted in increased propellant heating due to the low efficiency and flowrate. At a pump discharge pressure of 4.48×10^6 N/m^2 (650 psia), the variation in enthalpy at the pump discharge, between the extreme cases shown, was 4.07×10^4 J/kg (17.5 Btu/lb).

The model was modified before determining the influence of heat transfer on the start transient. Predicted vapor-pumping limits, resulting from inducer-blade blockage and sonic-flow limits within the pump were included. Steady-state modeling of pump performance was divided into two lumps, inducer and first-stage impeller and second-stage impeller, to allow the influence of heat transfer on pump performance to be modeled more accurately.

The first set of cases run with the modified model were for a fully-chilled system. The results for discharge-valve openings initiated at 4.48×10^6, 4.14×10^6, and 3.45×10^6 N/m^2 (650, 600, and 500 psia) are shown in Fig. 84. The downstream-reservoir volume was 0.056 m^3 (1.96 ft^3) and the discharge duct volume was 0.006 in.^{3} (0.22 ft^3). The runs were terminated before reaching steady-state conditions to conserve computer time. The flow oscillations and the effect of back pressure on the pump-start transient are more pronounced than those produced with the initial model (Fig. 82). Backflow through the pump occurs, if the discharge valve is scheduled to open at a pressure greater than approximately 4.14×10^6 N/m^2 (600 psia). The pump does not recover after reverse flow occurs, because the propellant at the pump discharge (which is at a relatively high enthalpy) vaporizes as it flows to the pump inlet and its pressure decreases.

Figure 85 shows the pump transients for three cases with heat transferred to the propellant from the inlet duct and pump. The total heat-transfer at the design flowrate is 1.62×10^5 J/s (154 Btu/sec) and is programmed proportional to the square root of flowrate. This is the maximum heat-transfer rate that can be tolerated without cavitation breakdown occurring in the developed head. As shown, backflow through the pump occurs if the discharge valve is scheduled to open at a pressure greater than approximately 4.83×10^6 N/m^2 (700 psia). More careful analysis was required, because this pressure was unexpectedly higher than the corresponding value for a completely prechilled system.

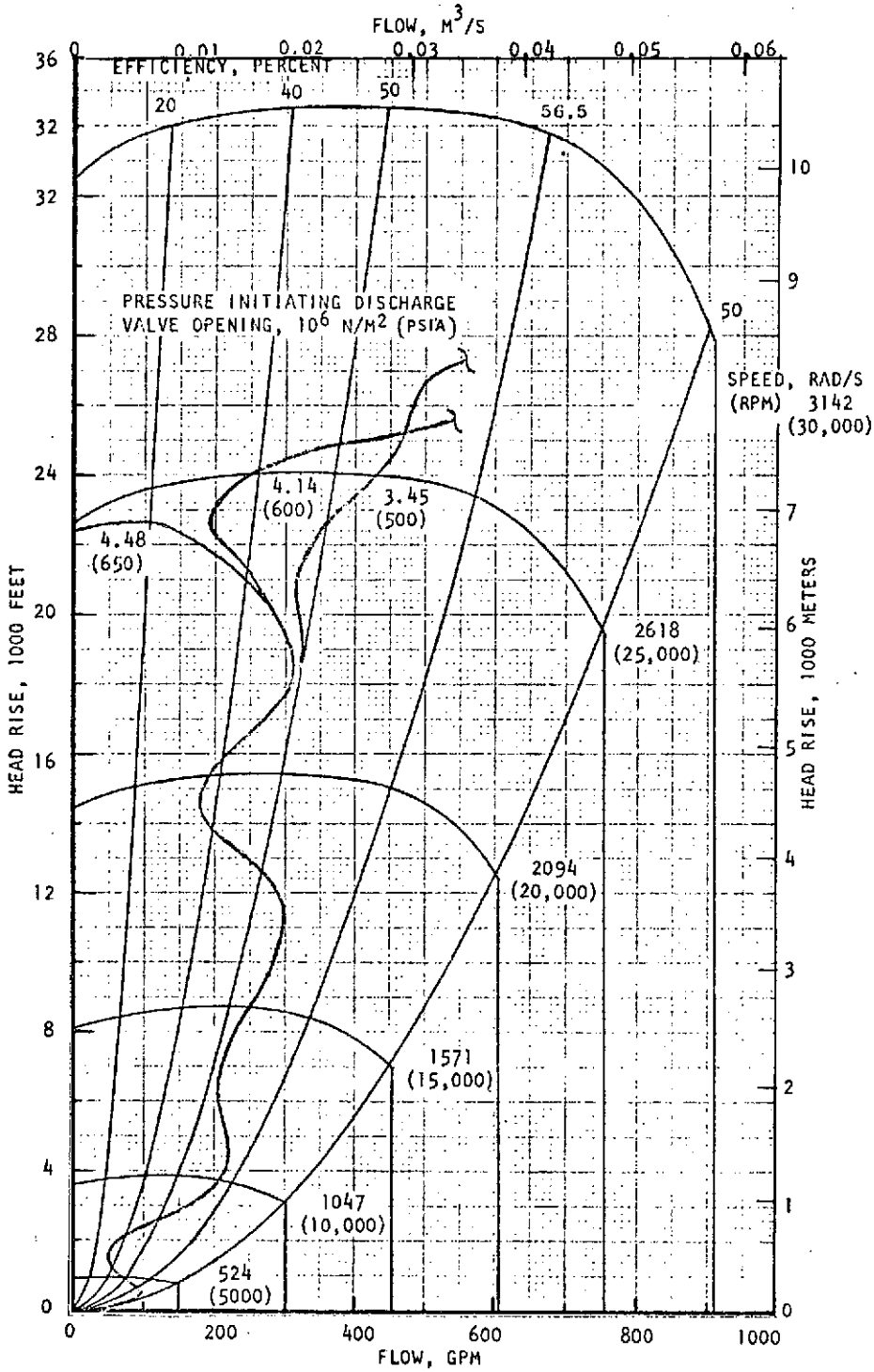

Figure 84. Effect of Discharge Valve Opening on Pump Performance for Chilled System.

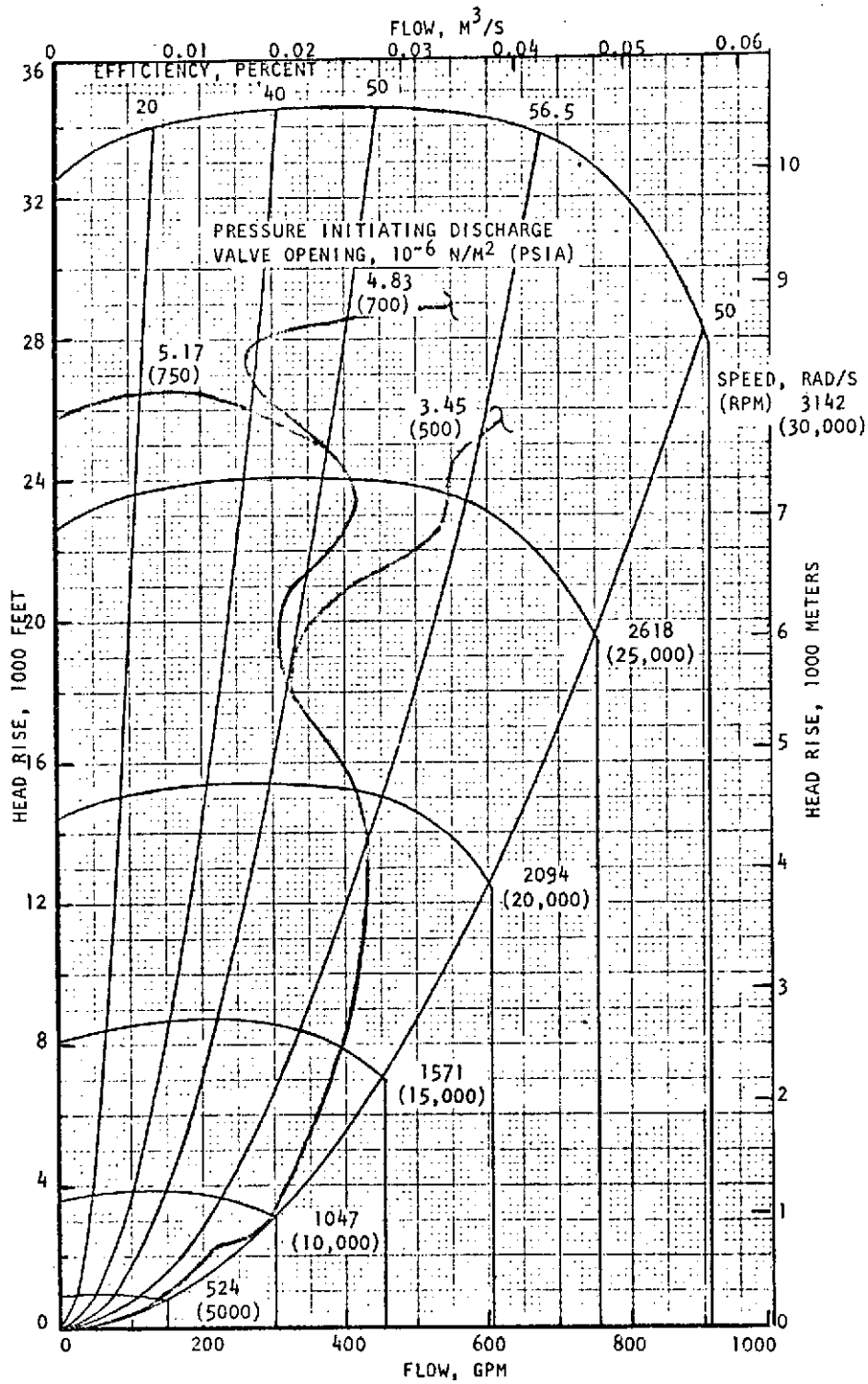

Figure 85. Effect of Discharge Valve Opening on Pump Performance for Warm System

For the conditions considered, the propellant heating due to pump inefficiency is at least as important as the chilldown heat transfer. The amount of pump heat transfer used in this study was 1.58×10^5 J/s (150 Btu/sec) at the design flowrate, and was selected because it shifts the pump transient to the extreme right-hand side of the operating envelope. It is this shift to the right on the performance map that is responsible for the unchilled pump being able to operate with higher back pressures.

Flow oscillations (Fig. 84) for the prechilled case result in relatively low flowrates and pump efficiencies. It should be noted that pump efficiency decreases very rapidly with decreasing flowrate. It is this combination of lower efficiency and flowrate (both of which increase propellant heating on a per-mass of propellant basis) that results in a decrease in pump discharge pressure and reverse flow at a lower back pressure for the prechilled pump. For a head rise of 6706 m (22,000 ft), heating due to pump inefficiency is approximately 10-percent greater than that resulting from heat transfer for a pump efficiency of 40 percent, and approximately 90-percent greater for a pump efficiency of 20 percent.

GENERAL DYNAMICS INLET LINE ANALYSIS

The thermal-analyzer program from the Knolls Atomic Power Laboratory was modified by Convair Aerospace Division of General Dynamics and used for the inlet line analysis. The baseline inlet line modeled was the one used in the experimental feed system tests conducted under Tasks III and IV. The inlet line thermal analysis included the following effects on line chilldown: (1) line material, (2) line diameters, (3) coatings, (4) coating thickness, (5) line pressure drops, and (6) fluid flowrates.

The thermodynamic models for both the uncoated and coated baseline configurations were completed and a number of runs conducted to determine the effect of variations in the major parameters. In the following sections, detailed discussions are presented on the coated line analysis and on examples of results obtained from the computer program for both uncoated and coated line conditions. The heat transfer coefficients used in the film boiling regime for liquid hydrogen cooldown are given.

Chilldown of Coated Lines

A literature survey was conducted to determine the current data relative to chilldown of cryogenic fluids and the application of insulative coatings to reduce chilldown times. Selected, applicable literature was summarized and presented in Appendix A. Applicable reports were used in the modification of the thermal-analyzer program.

Chilldown times of metals in liquid N_2, O_2, and H_2 can be dramatically decreased by the use of thin-insulative coatings (Ref. 3, 4, and 5) approximately 2.54×10^{-4} m (0.010 in.) thick. This phenomena is explained by a large temperature differential obtained between the base metal and the surface adjacent to the cooling fluid. This allows the transition to nucleate boiling (higher heat transfer rate) to occur earlier in the cooldown process. The experimental evidence with liquid nitrogen in Ref. 6 supports this hypothesis; the coating surface may

undergo a rapid and large-temperature drop early in the chilldown process and promote early attainment of liquid contact and large heat removal rates. The experiments of Ref. 4 and 5 indicate that a thin-insulative coating of 2.54×10^{-4} m (0.010 in.) Kel-F is sufficient to insure nitrogen wetting of the coating surface of the base metal at near room temperatures. The transition to nucleate boiling in hydrogen also appears to occur at much higher temperatures (Ref. 4 and 7) with coated, as compared to uncoated, metals; although it is not so clear that nucleate boiling occurs at base metal temperatures as high as room temperature. The nitrogen cases may be clearer because of both pool-boiling experiments and for the relatively high Reynold's number forced-convection experiments. The peak nucleate-boiling fluxes would be considerably higher than the film-boiling peak fluxes (e.g., $\sim$5 to 8 times). In hydrogen pool boiling, the ratio is not so high ($\sim$2 times) and in forced-convection flow, the maximum film-boiling heat flux may be higher than for the peak nucleate-boiling flux.

Maddox (Ref. 6) suggested that the rapid drop in surface temperature can occur as the result of vapor-liquid interfacial fluctuations during film boiling, which can produce large temperature changes in the coating due to its low thermal diffusity (with relatively negligible fluctuations in temperature for an uncoated metal). Analog simulation results were presented in support of this concept. An explanation for the phenomena was given in Ref. 4 based on a nucleate boiling, micro-layer evaporation theory. It was concluded that liquid nitrogen wetting of a teflon surface occurred at superheat; well in excess of that at the minimum heat flux point determined from liquid nitrogen boiling on conventional surfaces.

The analysis of the effect of coating on the base metal chilldown has assumed that transition to nucleate boiling occurs at the earliest time in the chilldown process, consistent with stabilization of the heat-flux solution in the nucleate-boiling (wetted surface) region. It is assumed that transition occurs by an instantaneous change in temperature of the coating surface. It is, therefore, implied that the heat capacitance of the thin coating is small, relative to the base metal.

The following brief examination of the simple heat flux equation follows previous observations in Ref. 4, 7, and 8. The resistance to heat flow from the base metal to the fluid is the sum of the resistance of the coating and the fluid-boundary layer, assuming the base metal resistance is negligible in comparison. The heat flow per unit surface area (q/A) is given by:

$$q/A = \frac{T_m - T_B}{t_c/k_c + 1/h}$$

where:

T_m = base metal temperature
T_B = bulk fluid temperature
t_c = coating thickness
k_c = coating conductivity
h = surface heat transfer coefficient

For the hydrogen case, of primary interest here, 1/h is larger in the film-boiling regime than in the nucleate-boiling regime for pool boiling or low-speed convection with boiling.

It can be noted that the resistance due to the coating controls the heat flow when

$$t_c/k_c >> 1/h$$

Typical values with Kel-F for pool boiling, or low-speed flows in liquid hydrogen, are as follows:

$h_f \approx 284$ J/m^{2}s K (50 Btu/ft^2 hr R) (film boiling regime)

$h_n \approx$ 28,400-56,800 J/m^{2}s K (5000-10,000 Btu/ft^2 hr R) [maximum nucleate boiling, $\rho = 1.01 \times 10^5 - 2.02 \times 10^5$ N/m^2 (1-2 atm)]

$k_c \approx 0.087$ J/m^{2}s K (0.05 Btu/ft^2 hr R)

The heat-flux (q/A) equation indicates that for a shortened cooldown time with Kel-F coating when early transition to nucleate boiling occurs

$$1/\bar{h}_f > t_c/\bar{k}_c + 1/\bar{h}_n$$

or

$$t_c < 3.05 \times 10^{-4} \text{ m (0.012 in.) approximately}$$

The above is of course approximate, and optimization of t_c requires a complete computation of the chilldown process to account for the variation of properties with temperature, consideration of partial cooldown initially by film boiling in the coated case, and variation in the heat transfer coefficients. However, it can be seen that for the case considered, slower chilldown is inevitable for coated (compared to the uncoated) case for coatings thicker than 3.05×10^{-4} m (0.012 in.). A particular coating thickness exists between zero and 3.05×10^{-4} m (0.012 in.) which results in a minimum chilldown time.

Heat Transfer Coefficient for LH_2

The heat transfer coefficients used in this study have been previously discussed. In the nucleate-boiling regime, the pool-boiling data of Kutateladze were used and this assumption will be retained together with the method used previously for the transition region. A further examination of the film-boiling region has been undertaken. Previously, a superposition method was used in the film-boiling region. Figure 86 shows a comparison of the heat-transfer coefficients computed by various correlations for the case of a 0.089 m (3.5 in.) diameter line, having a flowrate of 0.27 kg/s (0.6 lb/sec), and a presentative quality of 0.55 at 1.01×10^5 N/m^2 (1 atm). Curve D represents the superposition technique previously utilized and can be seen to give a relatively high value for the heat-transfer coefficient which is generally regarded as resulting in an overestimate. Curve E was obtained from a correlation of experiments with hydrogen flowing in tubes at Reynolds number similar to the present cases (Eq. 25, Ref. 9; and Eq. 9, Ref. 10).

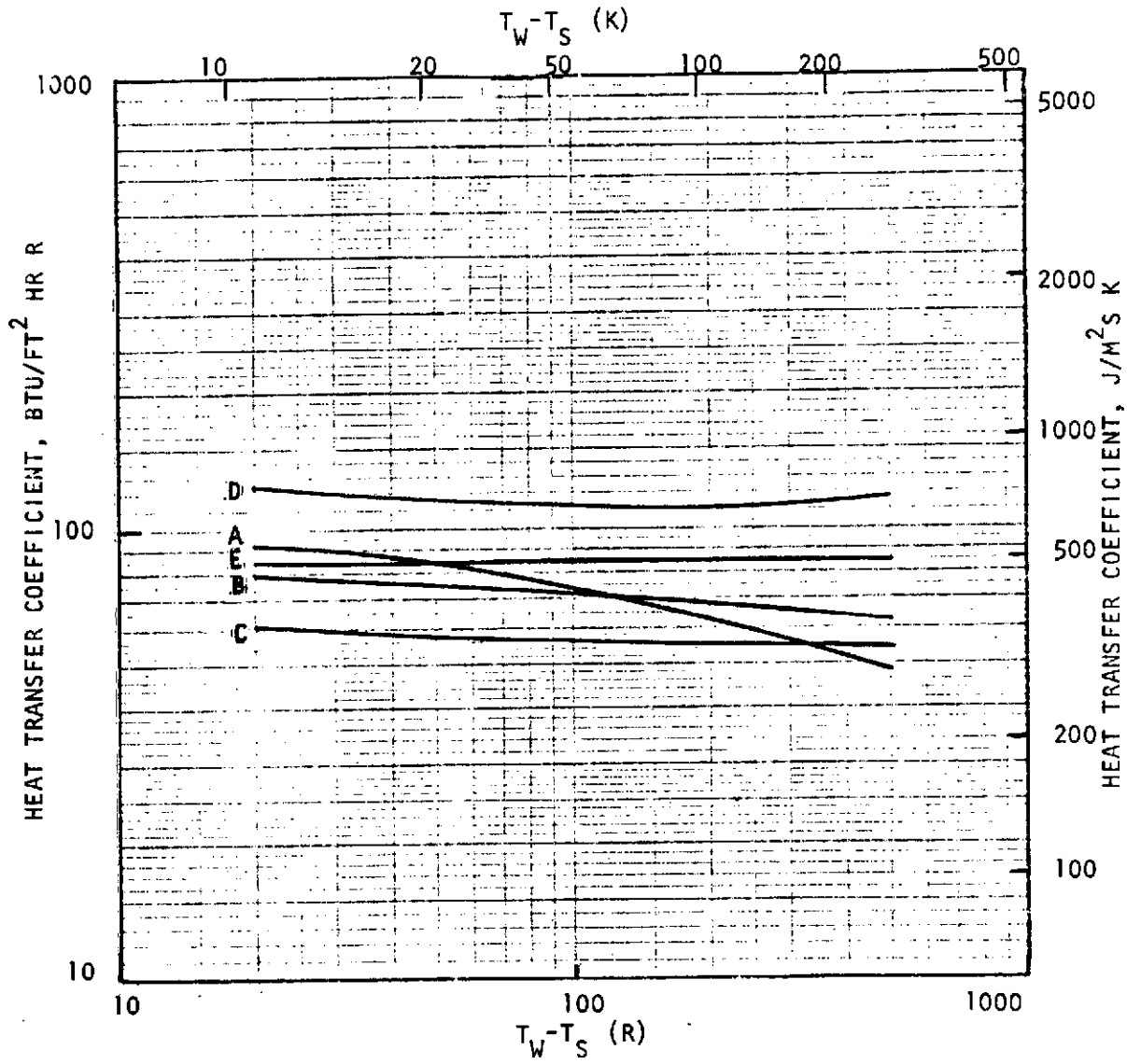

Figure 86. Film Boiling Heat Transfer Coefficients

Figure 86 indicates that this correlation, shown below, gives reasonable values of h_f for the conditions considered when compared to the other predictions

$$h = 72.2\ G^{0.5}\ J/m^2 s\ K \text{ or } 337.0\ G^{0.5}\ Btu/ft^2\ hr\ R$$

where G is in $kg/m^2 s$ or $lb/in.^2$ sec.

It has to be noted that the equation above is an approximate correlation over a limited range of Reynolds numbers. It is assumed that a minimum value of h will be given for a flowrate corresponding to G = 14.8 $kg/m^2 s$ (0.021 $lb/in.^2$ sec), i.e., $h_{(min)}$ = 276 $J/m^2 s$ K (48.6 Btu/ft^2 hr R), and this value will remain constant for lower Reynolds numbers and pool boiling.

Computer Results

Results from the initial computer runs were made using the model for the baseline configuration that is shown schematically in Fig. 87. The effect of a variation in flowrate is shown in Fig. 88 where temperature versus time plots are given for node 39. The mass flowrates shown represent 3 to 10 percent of the design flowrate of the pump.

Table 10 shows the computer run schedule that was designed to provide the information necessary to determine the influence of the major parameters and system performance with respect to chilldown. The heat-transfer coefficients have been modified over those used for the data of Fig. 88, and the modified data were used in the remainder of the computations.

Results used to check the computer modifications for the coated conditions were obtained. Input data were prepared for runs in which flowrates and coating thicknesses were varied. Figure 89 shows comparative data obtained for a flowrate of 0.18 kg/s (0.4 lb/sec) for both the uncoated line and a 2.54×10^{-4} m (0.010 in.) Kel-F coated line. Node 22 is typical of the thin-wall 4.06×10^{-4} m (0.016 in.) tubing that makes up the major portion of the heat-transfer surface in contact

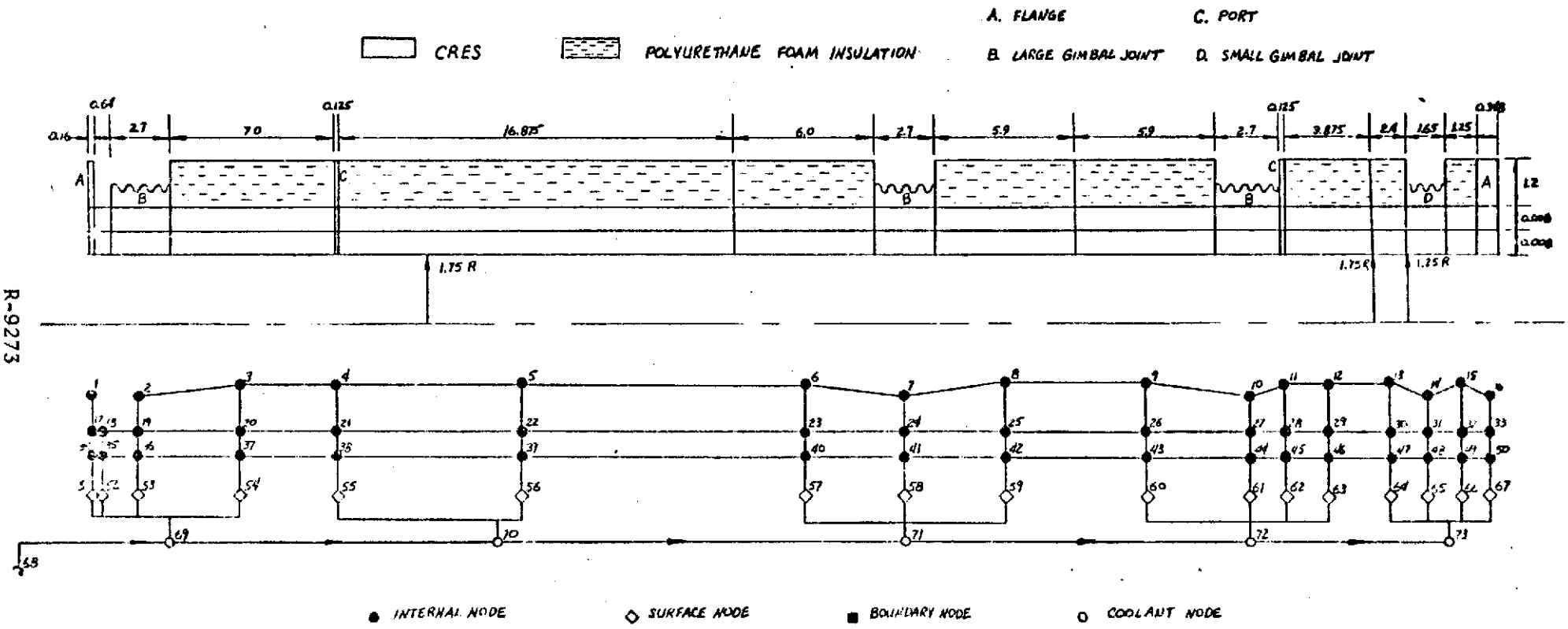

Figure 87. Suction Line Thermodynamic Model

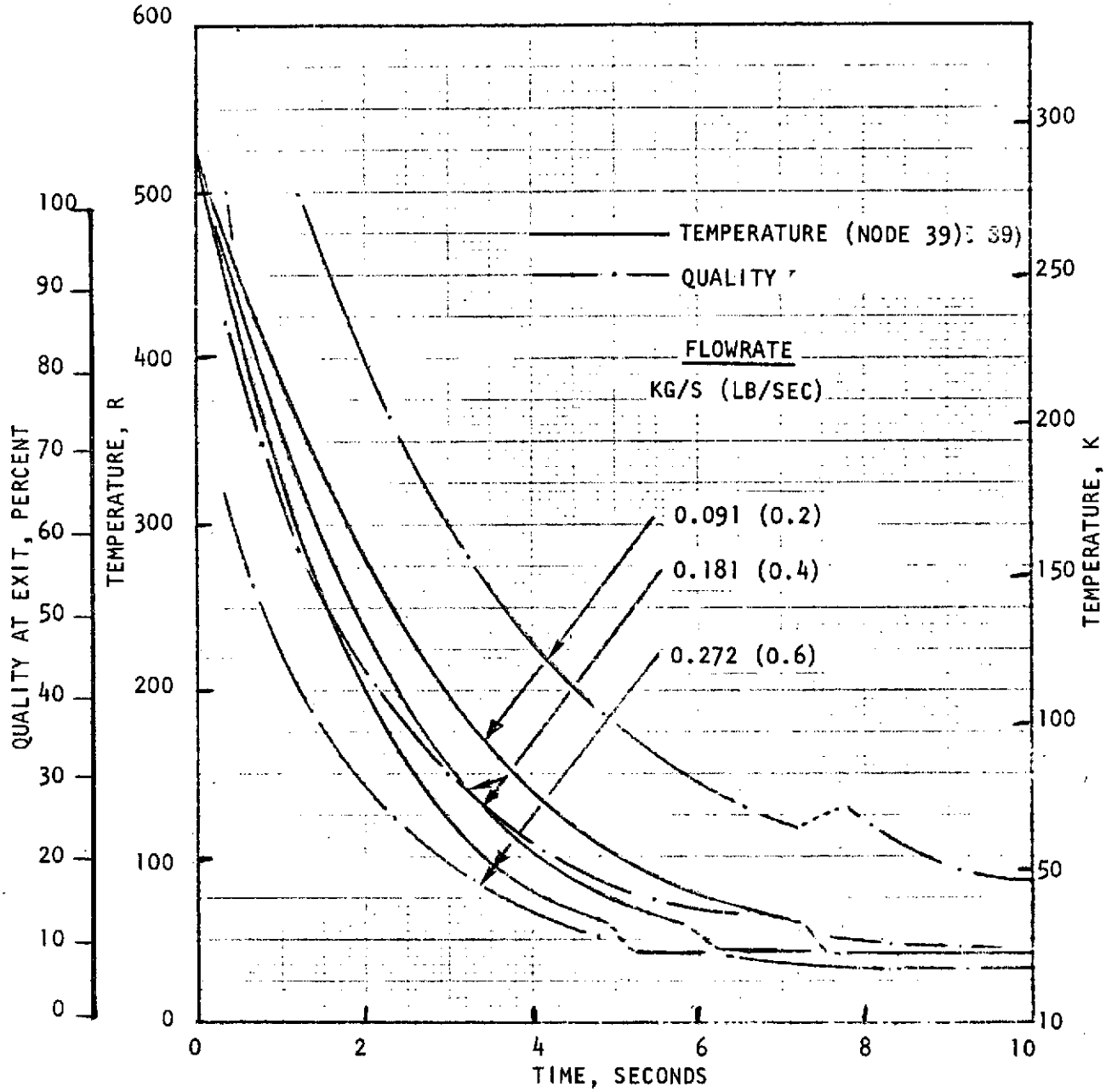

Figure 88. LH_2 Cooldown Temperatures and Fluid Quality for Uncoated Line, Node No. 39

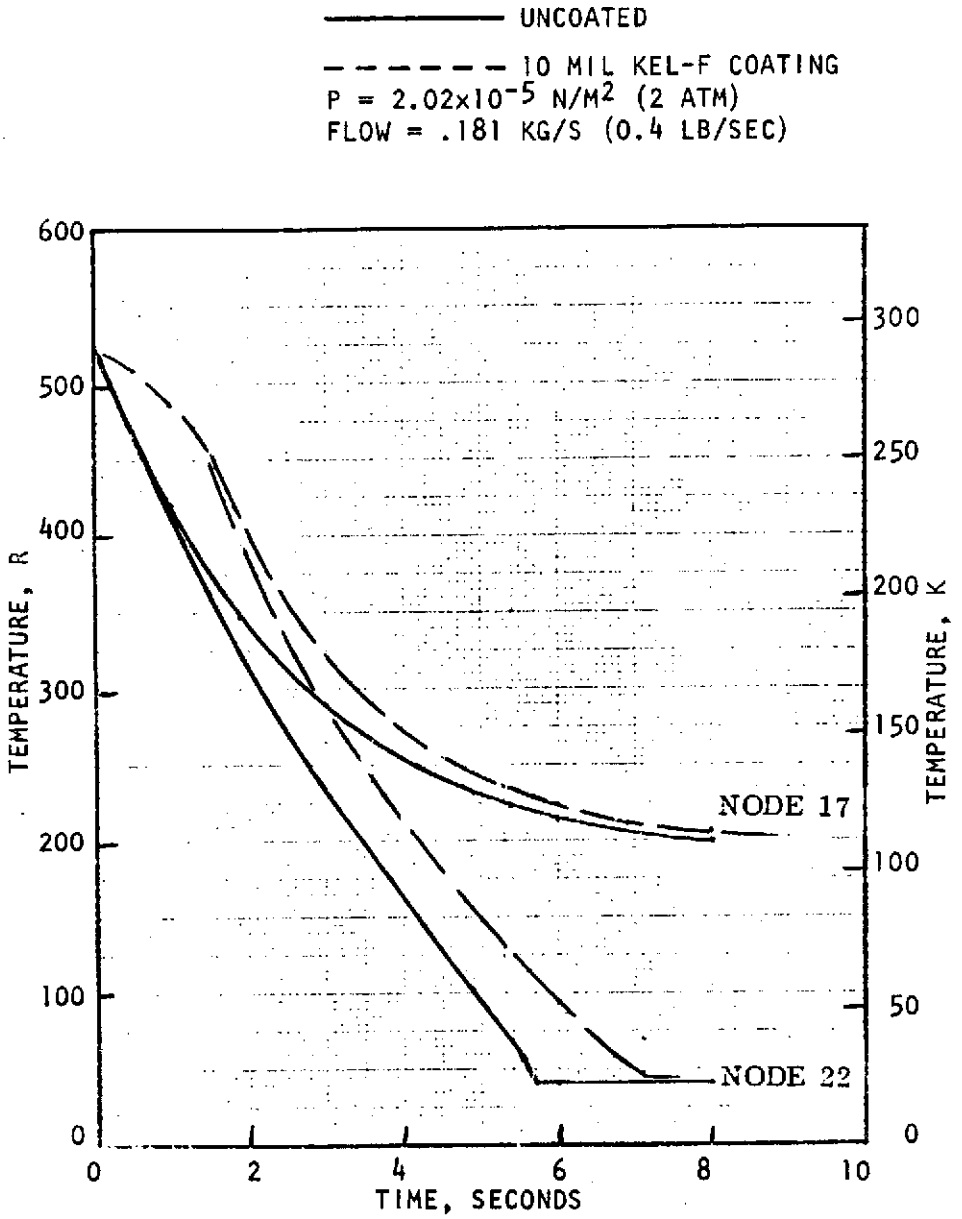

Figure 89. LH_2 Cooldown of Uncoated and $2.54x10^{-4}$M(0.010 IN.) Kel-F Coated Line

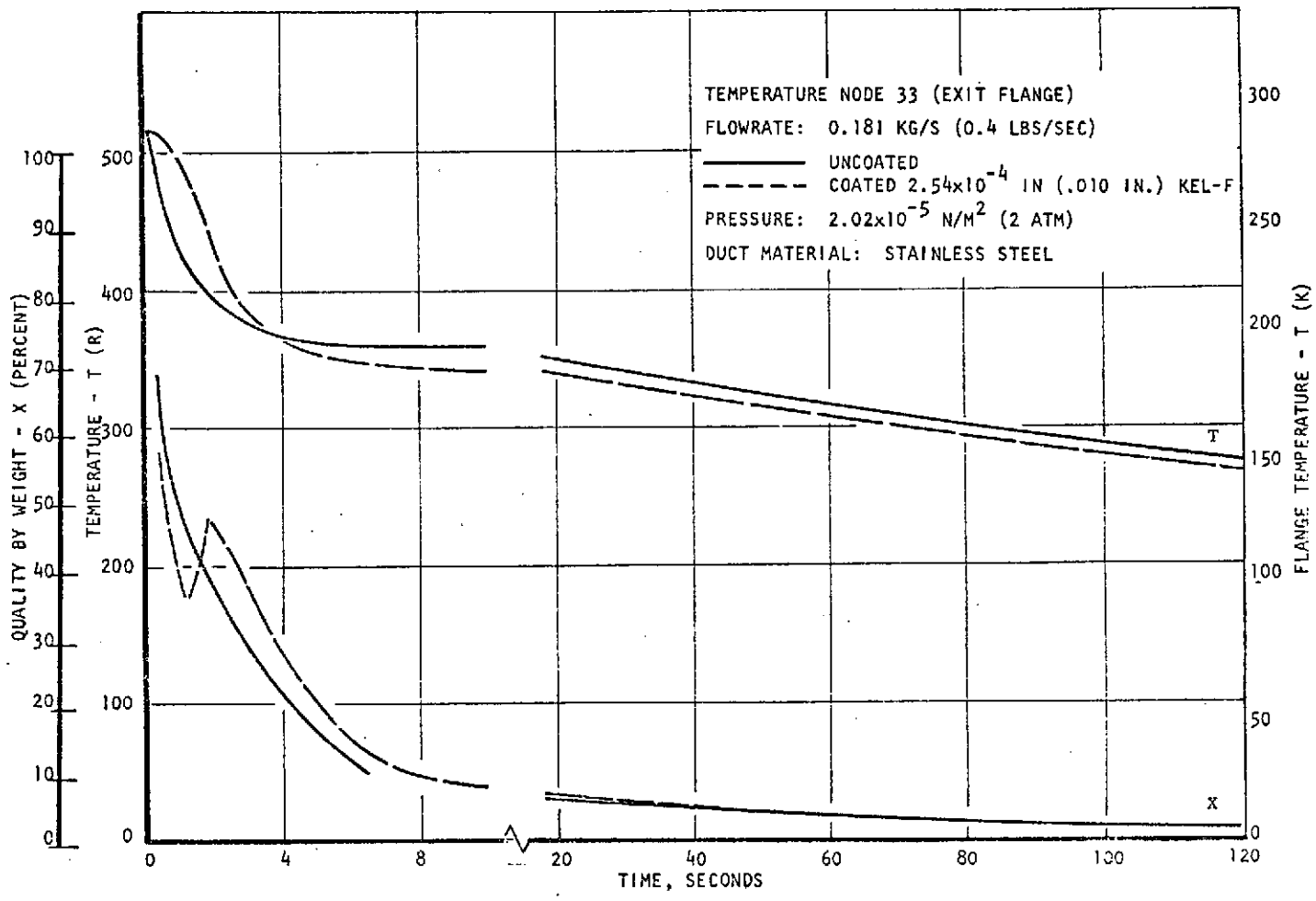

Figure 90. Fluid Quality and Exit Flange Temperature Versus Cooldown Time for a Coated and Uncoated Duct

TABLE 10. COMPUTER PROGRAM RUN SCHEDULE FOR LIQUID HYDROGEN SUCTION LINE COOLDOWN DATA

Run No.	Suction Line Configuration and Comments
H2-1 to -4	Baseline* configuration with coating thicknesses of 0.0, 7.62×10^{-5}, 2.54×10^{-4} and 5.08×10^{-4}M (0.0, 0.003, 0.010 and 0.020 inches).
-5 to -7	Baseline configuration, except alternate coating material (three coating thicknesses).
-8 and -9	Baseline configuration, except alternate flow rate (coating thickness of zero and one other).
-10	Baseline configuration with ΔP effects included.
-11 and -12	Baseline configuration, except alternate diameter line (coating thickness of zero and one other).
-13	Baseline configuration, except with external superinsulation.
-14 to -17	Predict performance for 6 test conditions (coated and uncoated) of Tasks III and IV.
-18 to -23	Refinement of parametric studies: study further variation as required in flowrates, pressure effects, line materials, line diameter and superinsulation.
-24 to -25	Vehicle flight simulation with and without coating.
-28 to -30	Computations for Task III test data analysis.
-31 to -33	Computations for Task IV test data.

*Baseline Configuration: 0.089M (3.5 In.) diameter stainless steel (as shown in drawing GDC-65-21007), with KEL-F internal line coating.

with the coolant. Node 17 is the wall temperature at a flange. It is seen that the chilldown of the thin-wall tubing, node 22, is completed rapidly, although node 17 is still at a relatively high temperature. This is true for other nodes with large metal mass, such as those at gimbal joints. The chilldown occurs in two phases for this configuration. The initial phase is from 5 to 10 seconds, during which a large portion of the thin-wall surface areas in direct contact with the coolant are chilled more slowly. Since at the beginning of this second phase, the quality of the fluid at the exit is from about 4 to 8 percent by weight, it may be desirable to continue the chilldown calculations to as low as 0.5 to 1-percent quality to provide data for pump performance.

For the case shown in Fig. 89, it appears that the chilldown is not beneficially affected over the range shown. This is not too surprising in view of the discussion of coated lines. It appears that a coating thickness of approximately 7.62 x 10^{-5} m (0.003 in.) Kel-F will provide more rapid chilldown. Thicker coatings may also be of interest in that the rate of heat flux to the fluid can be considerably reduced, resulting in a small addition of heat to the fluid over a long period of time.

The chilldown computer program was revised to provide for automatic transition in the fundamental heat-transfer mechanism as determined by insulative coating. In addition, modifications were made to the stability criteria for the coated-line base. Very thin nodes, with associated small masses and heat capacities, can drive the computer calculations to unacceptable small calculation times steps; hence, modifications were incorporated into the program for the coated cases to avoid this problem. This was done by neglecting the coating nodes in obtaining the calculation-time interval. It is noted, however, that the coating resistance is completely accounted for in the computations.

Runs were made for the uncoated and coated baseline configurations to determine the effect of variations in the major parameters. The studies were based on liquid hydrogen as the cooling fluid, flowrates of 0.091, 0.181, 0.272, and 0.635 kg/s (0.2, 0.4, 0.6, and 1.4 lb/sec), stainless steel material, two coating materials

(Kel-F and Teflon), and thicknesses of 7.62×10^{-5}, 2.54×10^{-4}, and 5.08×10^{-4}m (0.003, 0.010, and 0.020 in.). The physical properties used in the computer calculations are shown in Table 11.

The thermal-analyzer program was used to predict chilldown time for the heavy sections of the inlet suction line at an LH_2 flowrate of 0.181 kg/s (0.4 lb/sec), as shown in Fig. 90 for an uncoated and a 2.54×10^{-4} m (0.010 in.) Kel-F coated line. Percent quality by weight, as a function of time, is superimposed on the transient-temperature graph in Fig. 90.

The thin 4.04×10^{-4} m (0.016 in.) wall sections of the inlet line were found to approach LH_2-saturated-vapor temperature within 10 seconds. But the heavy sections of the duct, flanges, bellows, and gimbal remained relatively warm and more than 120 seconds were required to reduce the quality to less than 1.5 percent at the duct exit. This quality corresponds to approximately 30-percent vapor by volume at 2.02×10^5 N/m^2 (2 atm).

Preliminary results indicate that with a 5.08×10^{-4} m (0.020 in.) coating of the inlet duct, chilldown can be reduced to less than 20 seconds for inlet pressures of approximately 4.14×10^5 N/m^2 (60 psia), based upon the complete experimental feed system chilldown analysis.

To use the results of the Convair inlet-line thermal analysis in the total-system analysis being conducted by Rocketdyne, a technical discussion between Convair and Rocketdyne personnel was held at Rocketdyne on 20 January 1972. The chilldown results shown in Fig. 90 and 91, the analytical model, and the practical difficulties associated with analytical prediction of fluid quality were discussed. Because a more rapid line chilldown would be desirable, Convair was requested to extend the LH_2 flowrates used in the analysis from the current maximum of 0.272 kg/s (0.6 lb/sec) to 0.635 kg/s (1.4 lb/sec) with coatings up to a thickness of 5.08×10^{-4} m (0.020 in.).

TABLE 11. PHYSICAL PROPERTIES USED IN COMPUTER CALCULATIONS

CRES ρ = 7849 KG/M^3 (490 LB/FT^3)

Temperature K (R)	Specific Heat J/KG K (Btu/lb-R)
97 (175)	234 (0.056)
148 (266)	352 (0.084)
198 (356)	410 (0.098)
298 (536)	477 (0.114)
333 (600)	490 (0.117)

Temperature K (R)	Thermal Conductivity J/S MK (Btu/hr-ft-R)
22 (40)	2.42 (1.40)
56 (100)	6.06 (3.50)
100 (180)	9.17 (5.30)
200 (360)	12.30 (7.10)
300 (540)	15.00 (8.66)

Foam ρ = 32 KG/M^3 (2.0 lb/ft^3)

Temperature K (R)	Specific Heat J/KG K (Btu/lb-R)
61 (110)	419 (0.1)
256 (460)	1256 (0.3)
450 (810)	2093 (0.5)

Temperature K (R)	Thermal Conductivity J/S MK (Btu/hr-ft-R)
22 (40)	0.005 (0.003)
222 (400)	0.024 (0.014)
444 (800)	0.035 (0.020)

TABLE 11. (Concluded)

KEL-F ρ = 2002 KG/M^3 (125 lb/ft^3)

Temperature K (R)	Specific Heat J/KG K (Btu/lb-R)
28 (50)	159 (0.038)
56 (100)	260 (0.062)
111 (200)	473 (0.113)
222 (400)	808 (0.193)
306 (550)	913 (0.218)

Temperature K (R)	Thermal Conductivity J/S MK (Btu/hr-ft-R)
28 (50)	0.047 (0.027)
56 (100)	0.071 (0.041)
111 (200)	0.112 (0.065)
167 (300)	0.121 (0.070)
306 (550)	0.128 (0.074)

Tefloa ρ = 2082 KG/M^3 (130 lb/ft^3)

Temperature K (R)	Specific Heat J/KG K (Btu/lb-R)
28 (50)	154.5 (0.0369)
56 (100)	257.5 (0.0615)
111 (200)	465.1 (0.1111)
167 (300)	665.7 (0.1590)
222 (400)	796.7 (0.1903)
278 (500)	887.6 (0.2120)
333 (600)	925.2 (0.2210)

Temperature K (R)	Thermal Conductivity J/S MK (Btu/hr-ft-R)
28 (50)	0.1869 (0.1080)
56 (100)	0.2139 (0.1236)
111 (200)	0.2336 (0.1350)
167 (300)	0.2423 (0.1400)
222 (400)	0.2509 (0.1450)
278 (500)	0.2544 (0.1470)
333 (600)	0.2572 (0.1486)

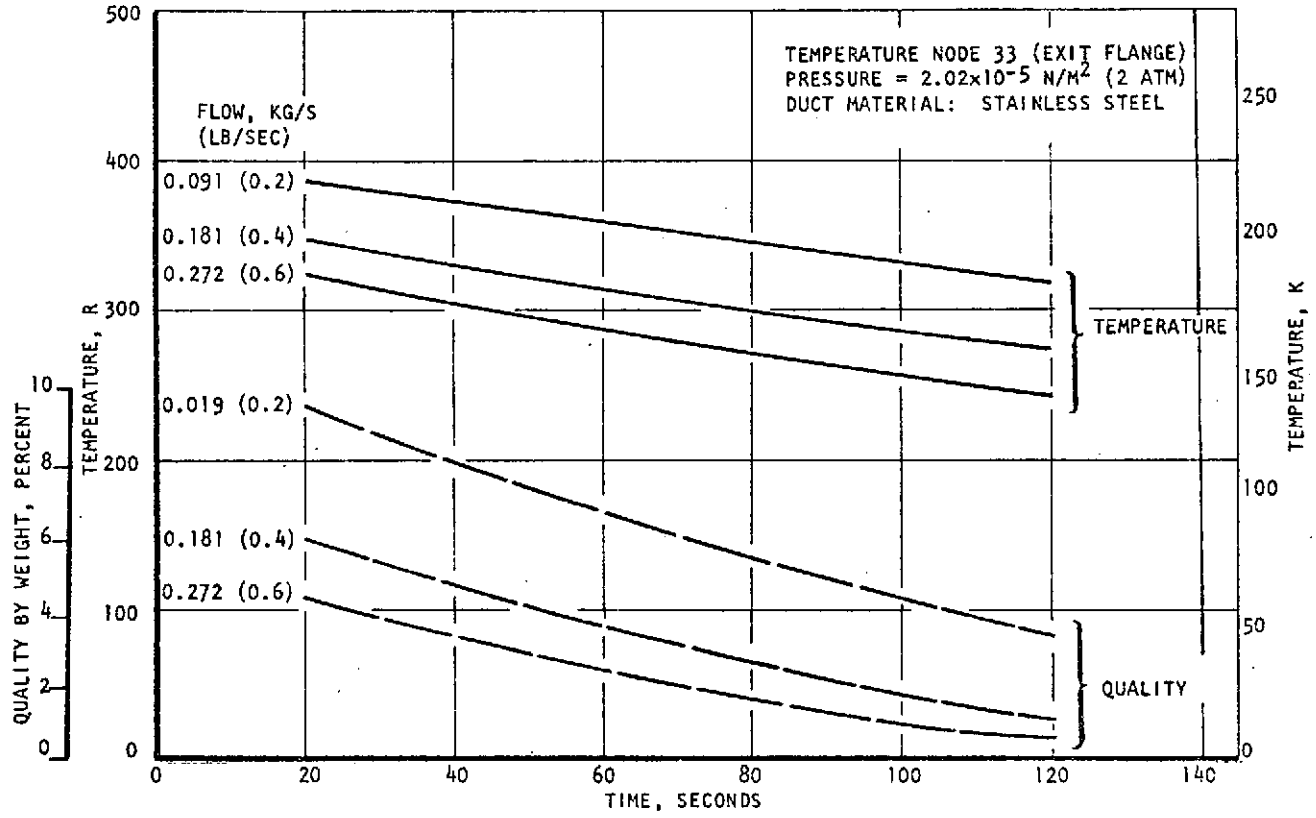

Figure 91. Effect of Flowrates on Duct Cooling for Uncoated Lines

A simplified 27-node computer model was constructed and used in the case requiring long chilldown calculations in the low-fluid-quality range. The simplified model (Fig. 92) neglects all nodes but those of large mass being cooled, such as flanges and gimbal joints. Figure 93 shows the results of computer runs utilizing a flowrate of 0.635 kg/s (1.4 lb/sec) with uncoated and 5.08×10^{-4} m (0.020 in.) Kel-F coated LH_2 lines. Table 12 and 13 present exact computer values for the exit quality and temperature versus cooldown time. It can be seen that for the 5.08×10^{-4} m (0.020 in.) Kel-F coated LH_2 line, the desired quality of 1.5 percent by weight was achieved after approximately 13 seconds.

Results of the parametric computer studies show the following:

1. Chilldown time is beneficially reduced by increasing the flowrates over the range of 0.091 to 0.635 kg/s (0.2 to 1.4 lb/sec).
2. At a flowrate of 0.181 kg/s (0.4 lb/sec), the 2.54×10^{-4} m (0.010 in.) Kel-F coating does not have a significant effect on line cooldown time to the 1.5-percent fluid quality desired for rapid pump start.
3. The behavior of Teflon-coated lines is similar to that of Kel-F coated lines; the major difference being that the higher thermal conductivity of the Teflon requires approximately twice the coating thickness of Kel-F for the same cooldown time.
4. Kel-F coated lines, at a flowrate of 0.635 kg/s (1.4 lb/sec), require approximately 13 seconds to achieve the desired exit quality of 1.5 percent by weight.

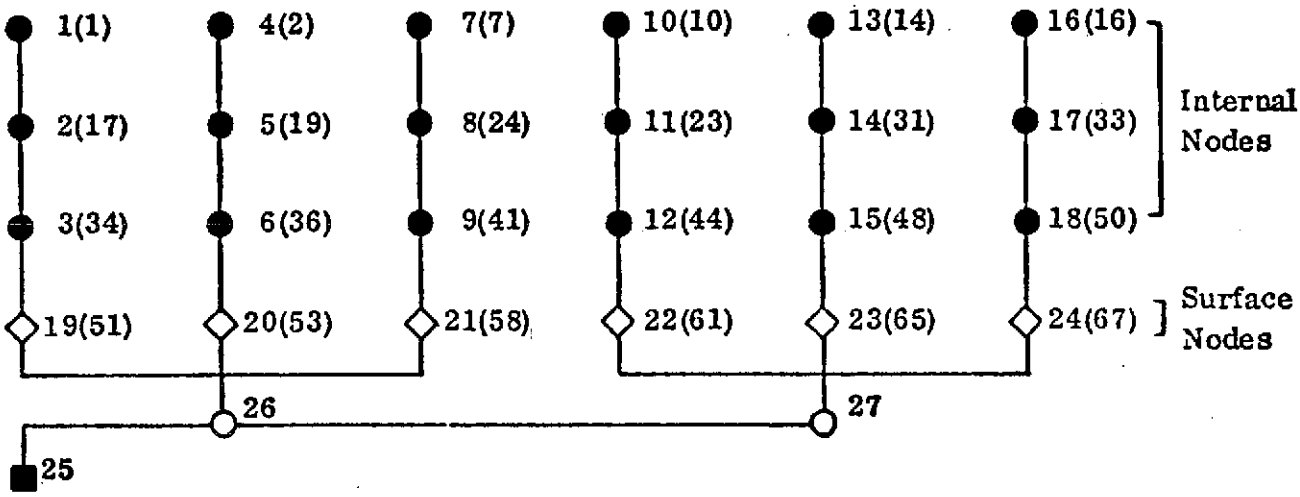

NOTE:

1. The model consists of 18 internal nodes, 6 surface nodes, 1 boundary node and 2 coolant nodes.
2. The numbers in brackets are the corresponding 73 model numbers.
3. ● Internal Node
   ◇ Surface Node
   ■ Boundary Node
   ○ Coolant Node

Figure 92. Simplified LH_2 Suction Line Thermal Model (27 Node Model)

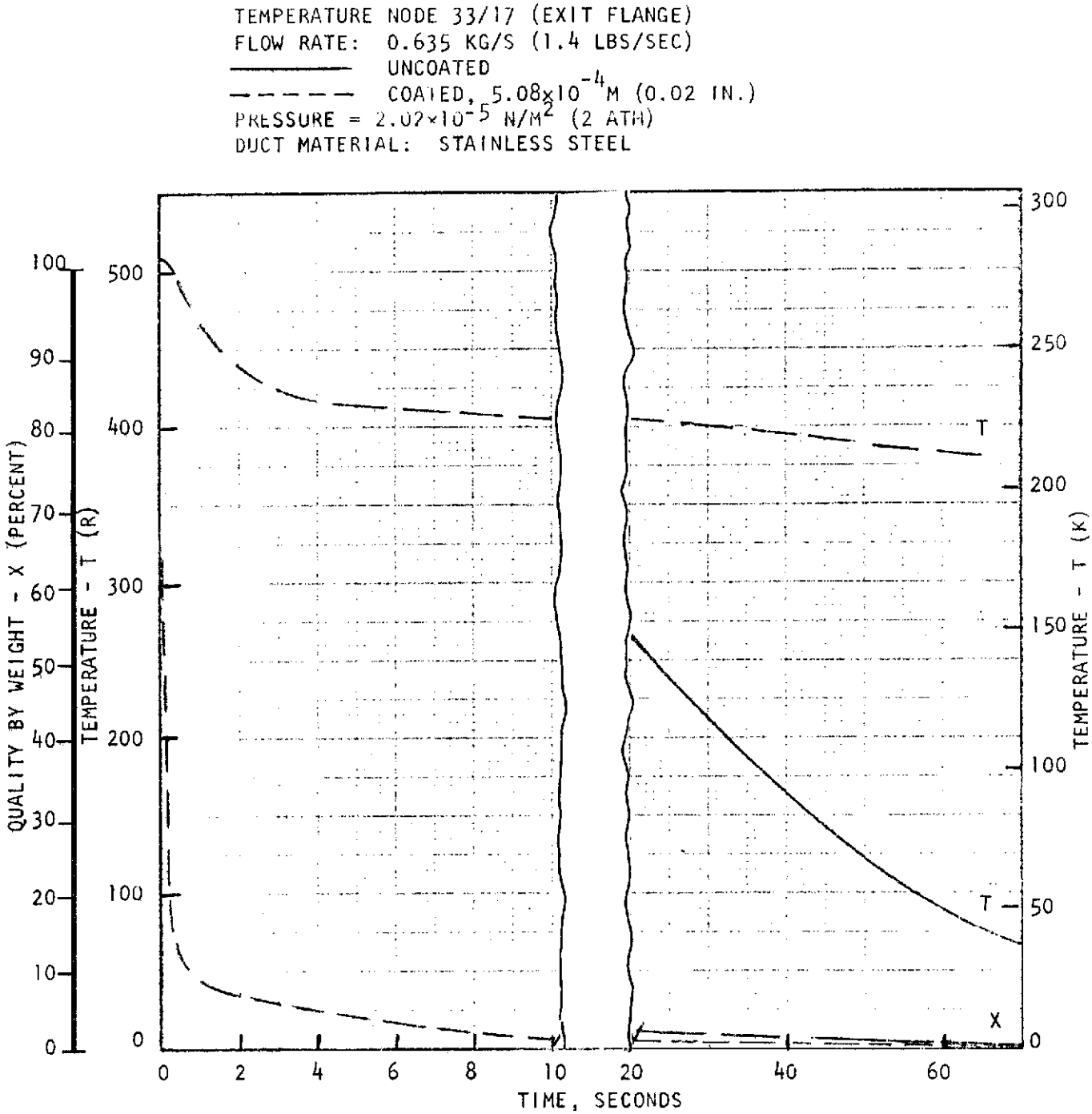

Figure 93. Fluid Quality and Exit Flange Temperature Versus Cooldown Time for a Coated and Uncoated LH_2 Duct for 0.635 KG/S (1.4 lb/sec) Flowrate

TABLE 12. TWENTY-SEVEN NODE COMPUTER RUN: 0.635 KG/S (1.4 LBS/SEC) FLOWRATE WITH AN UNCOATED LH_2 LINE

Cooldown Time Seconds	Exit Quality, Percent By Weight	Temperature K (F) at Exit Flange Node 17
18.00	2.36	410.6 (279.36)
21.04	2.22	400.9 (261.84)
24.02	2.09	391.7 (245.42)
27.02	1.96	383.0 (229.71)
30.02	1.84	374.6 (214.64)
36.02	1.62	358.8 (186.19)
39.02	1.51	351.4 (172.74)
42.02	1.41	344.1 (159.76)
45.00	1.31	337.2 (147.27)
46.80	1.25	333.1 (139.89)
48.05	1.21	330.4 (135.02)
49.21	1.17	327.9 (130.44)
50.45	1.13	325.2 (125.67)
54.04	1.02	317.8 (112.42)
57.04	0.94	312.0 (101.96)
60.04	0.85	306.6 (92.26)
66.03	0.70	297.3 (75.46)
71.64	0.57	290.6 (63.45)

TABLE 13. 73/27 NODE COMPUTER RUN: 1.4 LBS/SEC FLOWRATE WITH A 5.08×10^{-4}M (0.020 IN.) KEL-F COATED LH_2 LINE

	Cooldown Time Seconds	Exit Quality, Percent By Weight	Temperature K (F) at Exit Flange Node 17
27 Node Model	0.06	63.00	544.5 (520.35)
	0.19	23.00	539.4 (511.26)
	0.37	13.53	532.9 (499.48)
	1.08	8.60	514.3 (465.96)
	2.06	7.28	500.0 (440.35)
	3.00	6.27	492.9 (427.51)
	5.18	4.45	486.0 (415.18)
	7.23	3.20	483.4 (410.46)
	10.80	1.83	480.8 (405.67)
	12.00	1.59	480.1 (404.46)
	15.03	1.33	478.7 (401.90)
	18.04	1.26	477.5 (399.72)
	23.10	1.20	475.5 (396.28)
73 Node Model	18.00	1.19	482.0 (407.81)
	21.02	1.16	480.9 (405.86)
	24.01	1.13	479.8 (403.94)
	27.00	1.10	478.7 (402.03)
	30.02	1.07	477.7 (400.12)
	36.03	1.02	475.6 (396.35)
	39.02	0.99	474.6 (394.49)
	42.03	0.97	473.5 (392.63)
	45.05	0.94	472.5 (390.77)
	49.26	0.91	471.1 (388.21)
	51.02	0.89	470.5 (387.15)
	60.05	0.83	467.5 (381.73)
	65.48	0.79	470.7 (378.53)

TASK II: LABORATORY SAMPLE TESTS

The laboratory sample testing was designed to determine the optimum coating material and method of application prior to use on the experimental feed system. This was accomplished by a "process-of-elimination" type of procedure based on: (1) the insulative characteristics of the candidate coating materials, (2) LOX compatibility, (3) coating adhesion to metal substrates, and (4) the erosion resistance under dynamic flow of the proposed coating materials. Also, the methods of coating application and cure schedules were developed during this phase of the program.

MATERIAL SCREENING

Thermal contraction data had indicated that the addition of glass microballoons to the coating materials would bring the contraction of the coating closer to that of the metal substrates, as shown in Fig. 94. Thus, the microballoons would improve the coatings' adhesion to the metal substrates at cryogenic temperatures. Several of the materials selected for testing were modified with glass microballoons to take advantage of this characteristic.

KX-635 (chlorotrifluoroethylene with glass microballoons) was developed during a previous coating program (NAS8-20324). KX-635 was applied over a light coat of Kel-F 630 Clear and Kel-F Primer 640 (3-M products). This material was used as a comparison standard for the other coating candidates. Previous data ruled out the possibility of a KX-635 coating in LOX systems, but it was still a candidate for LH_2 systems.

Glass-filled FEP (fluorinated ethylene-propylene) dispersion was a candidate for LOX and LH_2 systems since preliminary LOX impact data had indicated compatibility with LOX. The FEP microballoon mixture was applied over a light coat of Dupont FEP-120 and either Dupont Primer 850-201 for stainless steel or Dupont Primer 850-202 for aluminum.

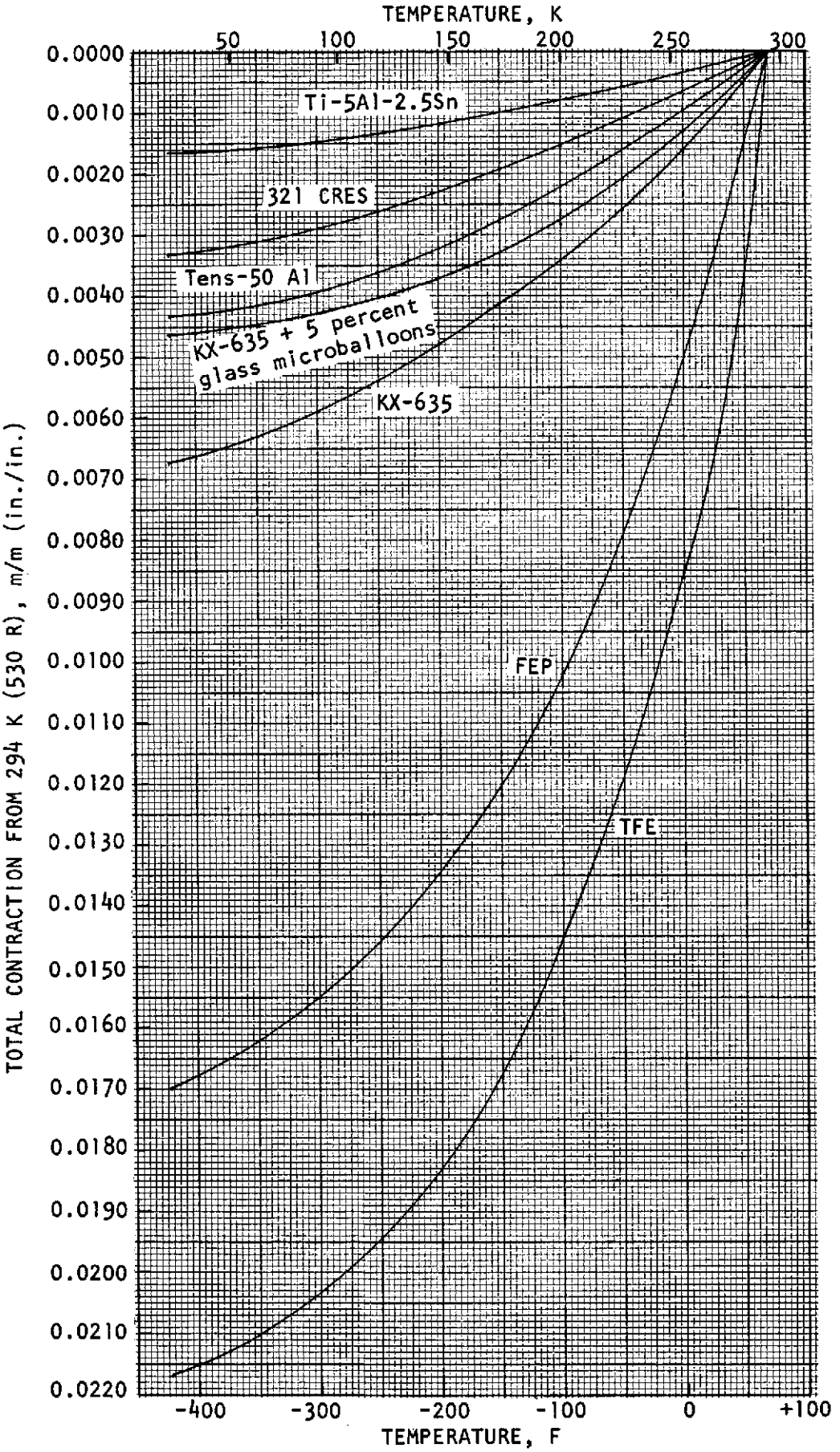

Figure 94. Thermal Contraction

R-9273

Glass-filled FEP, with Lithafrax (Carborundum Company) added to provide a negative coefficient of expansion, was also a candidate coating material for LOX and LH_2 systems.

TFE (tetrafluoroethylene) plain dispersion was a candidate for LOX and LH_2 systems, since this material has been used for cryogenic-Naflex seals and has passed previous LOX-compatibility tests. Dupont TFE 851-245 was applied over a light coat of Dupont 850-204 primer.

FEP plain dispersion was a candidate for LOX and LH_2 systems, since this material also has been used for cryogenic-Naflex seals and has passed previous LOX-compatibility tests. Dupont FEP 856-204 was applied over a light coat of Dupont 850-201 primer.

COATING FACILITIES

Thermech Engineering was chosen to apply the candidate coatings because of their overall familiarity with the problems associated with the coating of internal surfaces of cryogenic-feed systems. The company specializes in this type of business and had worked with Rocketdyne during the previous coating program directed toward the development of "quick-start" cryogenic turbopumps.

MATERIAL TESTING

The coating materials were subjected to four types of tests. These included LOX impact, static immersion in LN_2 and LH_2, adhesion to metal under tensile stress, and LH_2 flow in cylindrical sections.

LOX Impact Tests

LOX compatibility was determined by the use of impact tests at the 98 m-N (72 ft-lb) level per MSFC-SPEC-106B. The criterion for acceptability by this test method was that there be no reactions in 20 tests at the specified level or, alternately, that there be not more than one reaction in 60 tests at the

same level. The samples were 0.0159 m (0.625-in.) stainless-steel discs coated with TFE, FEP, FEP + glass microballons, FEP + glass microballoons + Lithafrax as shown in Table 13 and Fig. 95. A photograph of the test apparatus is shown in Fig. 96.

TABLE 14. LOX IMPACT BUTTONS

Coating Material	Samples Fabricated
1. TFE Dupont 851-245 over Dupont 850-204 5.08×10^{-5} m (0.002 in.) thick	60
2. FEP DuPont 856-204 over DuPont 850-201 5.08×10^{-5} m (0.002 in.) thick	60
3. FEP-120 + 25-percent glass microballoons 5.08×10^{-4} m (0.020 in.)	60
4. FEP-120 + 25-percent glass microballoons + 10-percent Lithafrax 5.08×10^{-4} m (0.020 in.) thick	60
Total	240

TFE and FEP coatings, both 5.08×10^{-5} m (0.002 in.) thick, passed the LOX-impact test at the 98 m-N (72 ft-lb) level, and photographs are shown in Fig. 97. In each case, there were no reactions in 20 tests. At a thickness of 5.08×10^{-4} m (0.020 in.), FEP + 25-percent by weight glass microballoons (both with and without 10-percent by weight Lithafrax) failed this test. FEP + glass-microballoon discs had two reactions in 10 tests. FEP + glass microballoons + Lithafrax discs had two reactions in three tests. Additional testing yielded a threshold level of 27 m-N (20 ft-lbs) for FEP + glass microballoons and 14 m-N (10 ft-lbs) for FEP + glass microballoons + Lithafrax, as shown in Table 15.

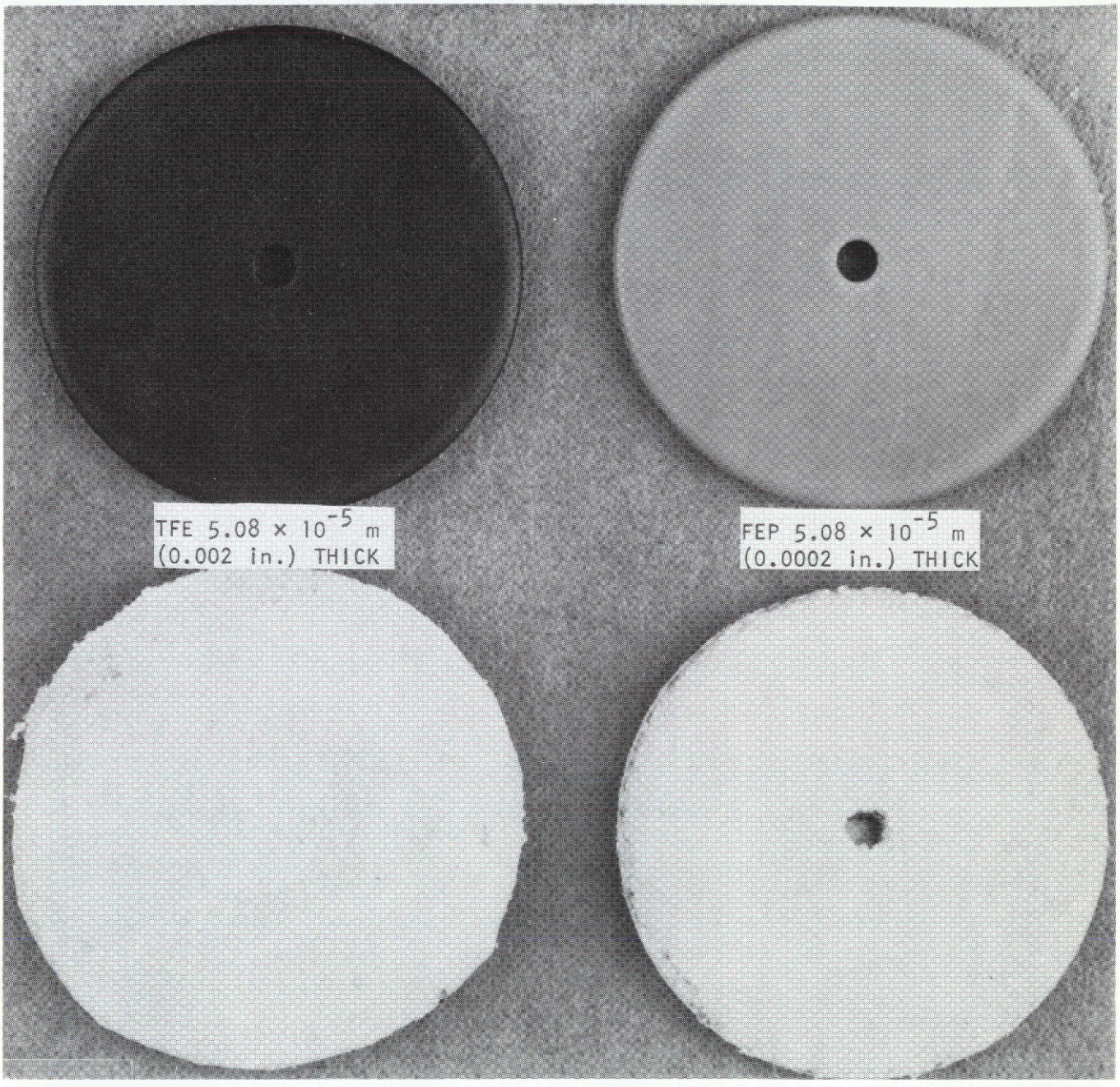

FEP-120 + GLASS MICROBALLOONS
5.08×10^{-4} m (0.020 in.) THICK

FEP-120 + GLASS MICROBALLOONS
+ LITHAFRAX 5.08×10^{-4} m
(0.020 in.) THICK

1XZ65-9/9/71-C2A*

Figure 95. LOX Impact Discs, Pretest

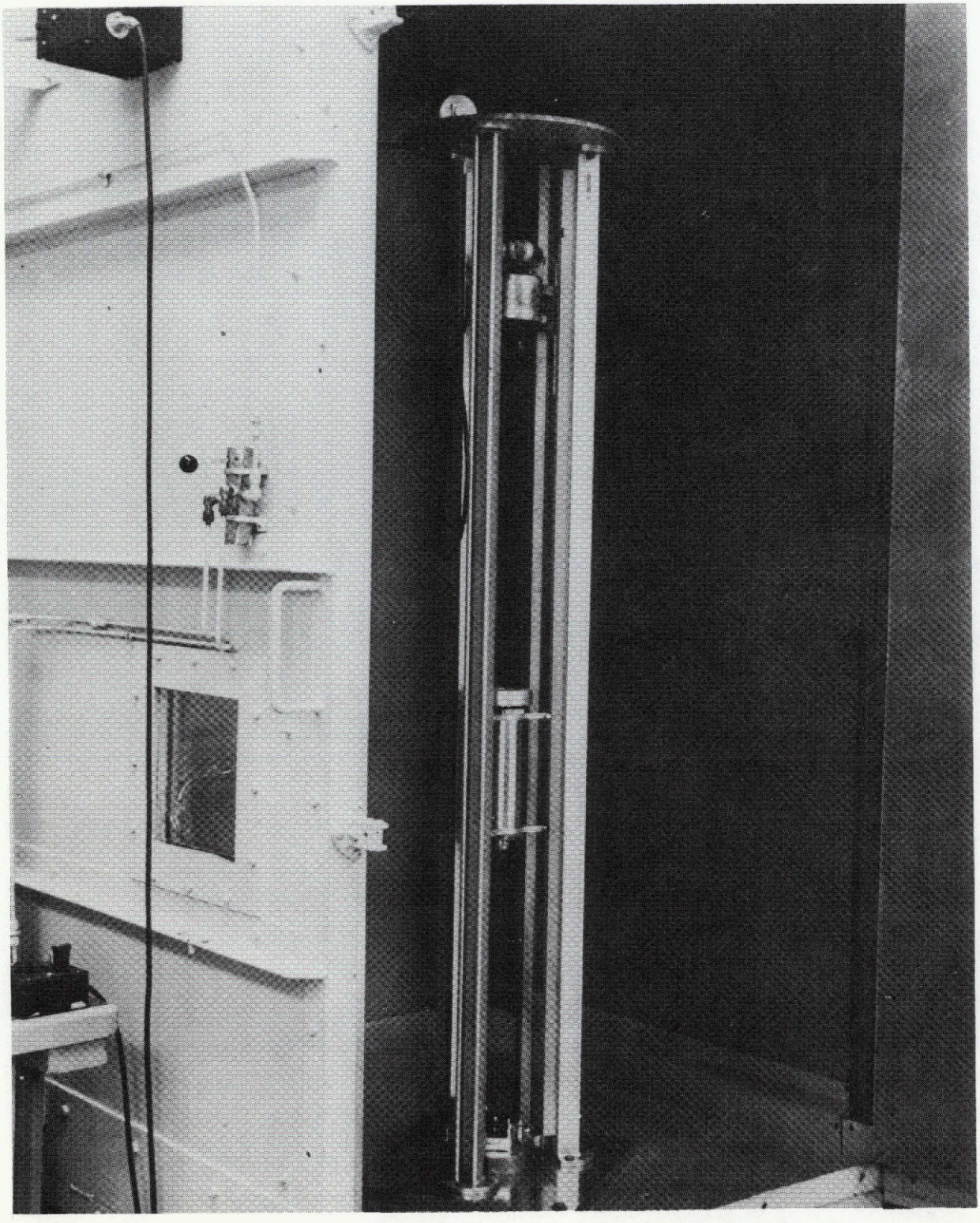

Figure 96. Dropweight Impact Tester

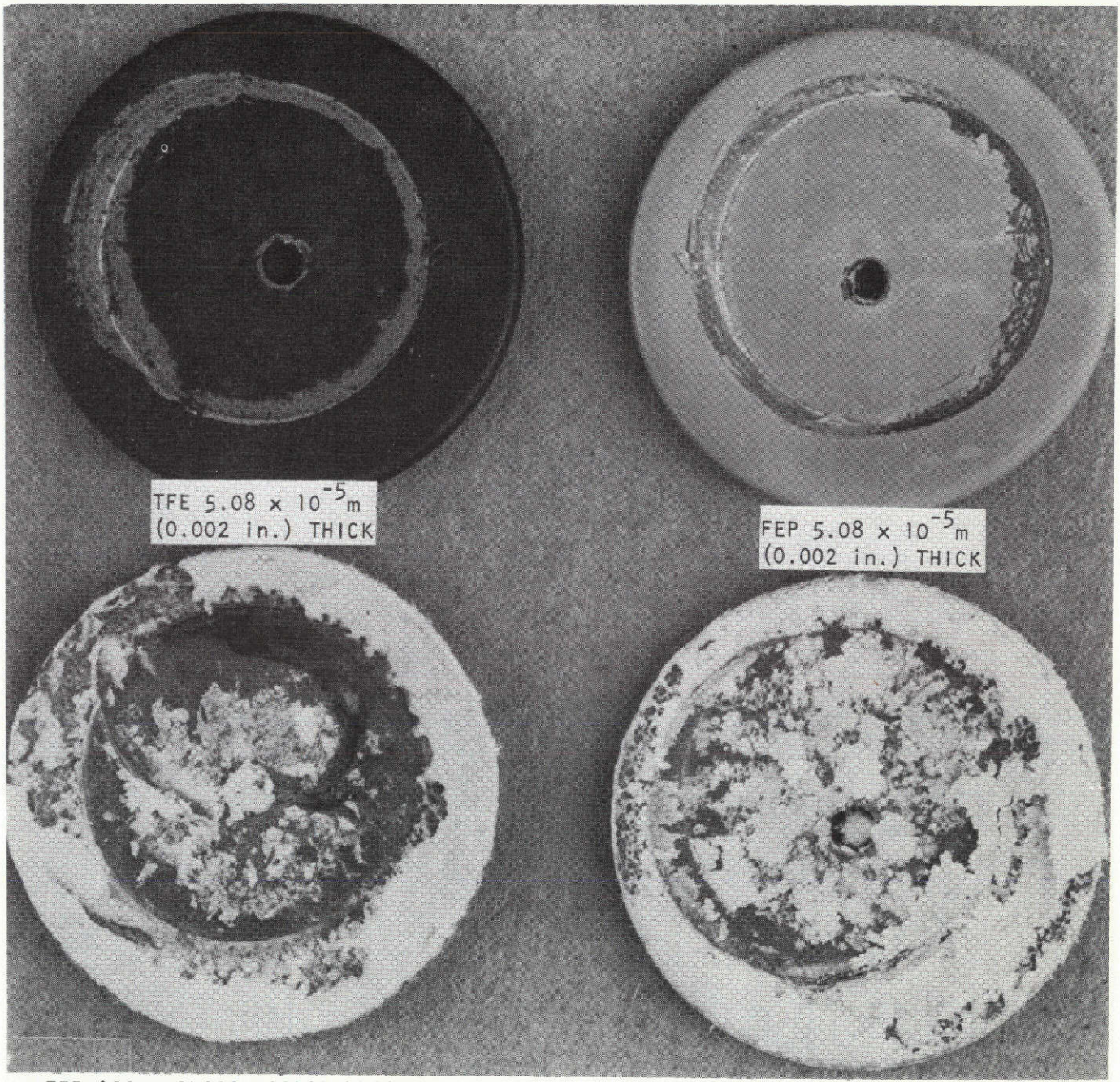

1XZ65-9/9/71-C1

Figure 97. LOX Impact Discs, Posttest

TABLE 15. LOX IMPACT TESTS

Coating Material	Samples Tested	Test Results at 98 m-N (72 ft-lbs)
1. TFE DuPont 851-245 over DuPont 850-204 5.08×10^{-5} m (0.002 in.) thick	20	0/20
2. FEP DuPont 856-204 over DuPont 850-201 5.08×10^{-5} m (0.002 in.) thick	20	0/20
3. FEP-120 + 25-percent glass microballoons 5.08×10^{-4} m (0.020 in.) thick	10	2/10
4. FEP-120 + 25-percent glass microballoons + 10-percent Lithafrax 5.08×10^{-4} m (0.020 in.) thick	3	2/3

LOX Impact Threshold Level Determination

	Height	m-N (ft-lbs)	Samples Tested	Test Results
1. FEP-120 + 25-percent glass microballoons + 10-percent Lithafrax				
	0.61 m (24 in.)	54 (40)	6	4/6
	0.46 m (18 in.)	41 (30)	3	2/3
	0.30 m (12 in.)	27 (20)	3	2/3
	0.15 m (6 in.)	14 (10)	20	0/20
2. FEP-120 + 25-percent glass microballoons				
	0.61 (24 in.)	54 (40)	4	2/4
	0.46 (18 in.)	41 (30)	7	2/7
	0.30 (12 in.)	27 (20)	20	1/20

Static Immersion Tests

Static-insulative characteristics were determined by immersing coated specimens in LN_2 and LH_2 and analyzing the thermal data obtained from copper-constantan thermocouples embedded in the samples. Test samples for immersion testing (Fig. 98) were 0.013 by 0.025 m (0.5 in. by 1.0 in.) cylindrical stock made from aluminum, stainless steel, and titanium. These samples were coated with KX-635, FEP + glass microballoons, TFE, and FEP as indicated in Table 16.

TABLE 16. HEAT TRANSFER RODS

Material	Thickness	Al	Ti	SS	Total
1. KX-635	1.27×10^{-4} m (0.005 in.)	1	1	1	3
2. KX-635	5.08×10^{-4} m (0.020 in.)	1	1	1	3
3. FEP-120 + 25-percent glass microballoons	1.27×10^{-4} m (0.005 in.)	1	1	1	3
4. FEP-120 + 25-percent glass microballoons	3.81×10^{-4} m (0.015 in.)	1	1	1	3
5. TFE (DuPont 851-245 over DuPont 850-204)	5.08×10^{-5} m (0.002 in.)	1	1	1	3
6. FEP (DuPont 856-204 over DePont 850-201)	5.08×10^{-5} m (0.002 in.)	1	1	1	3
					18

The immersion testing in LN_2, shown in Fig. 99, was conducted at the Materials and Processes Laboratory at Rocketdyne. The samples were first tested with all coated surfaces exposed and then with one coated surface exposed. All other surfaces were thermally isolated with approximately 0.019 m (0.75-in.) cork insulation (Fig. 100). A Brush recorder was used to obtain data to compare the effects of

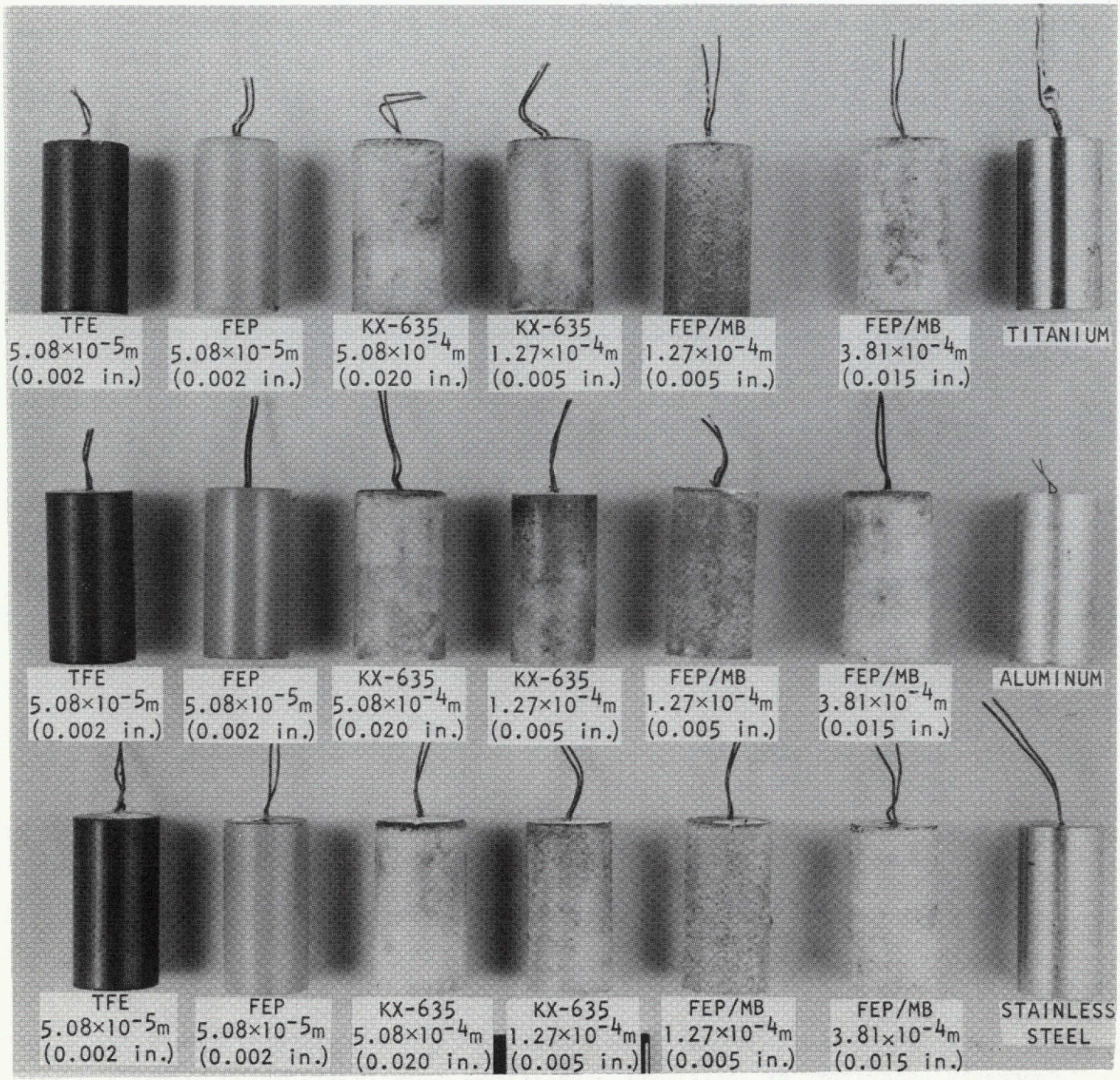

Figure 98. Specimens for Static Immersion Tests

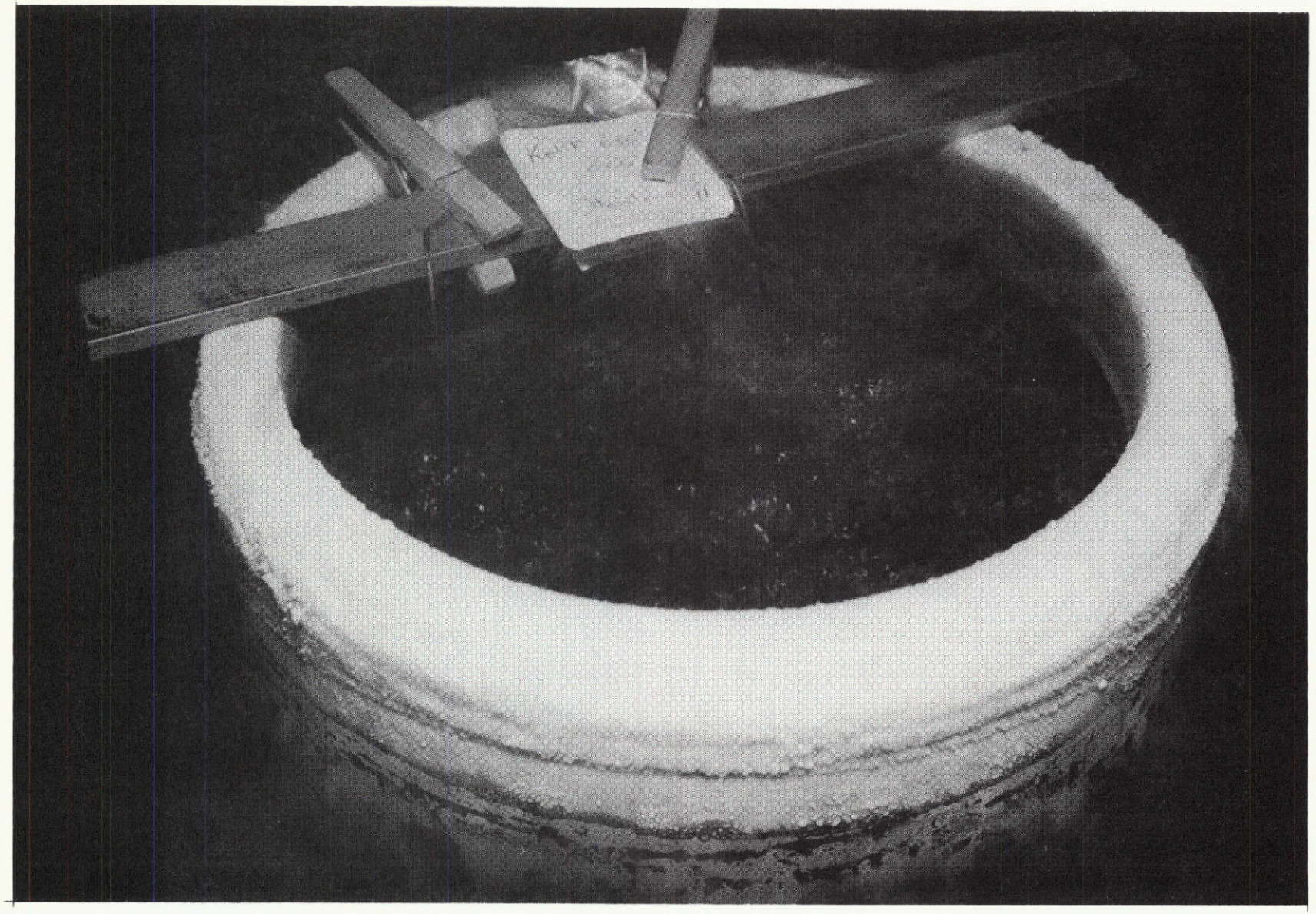

1XZ54-9/13/71-C1A

Figure 99. Immersion Test in Liquid Nitrogen

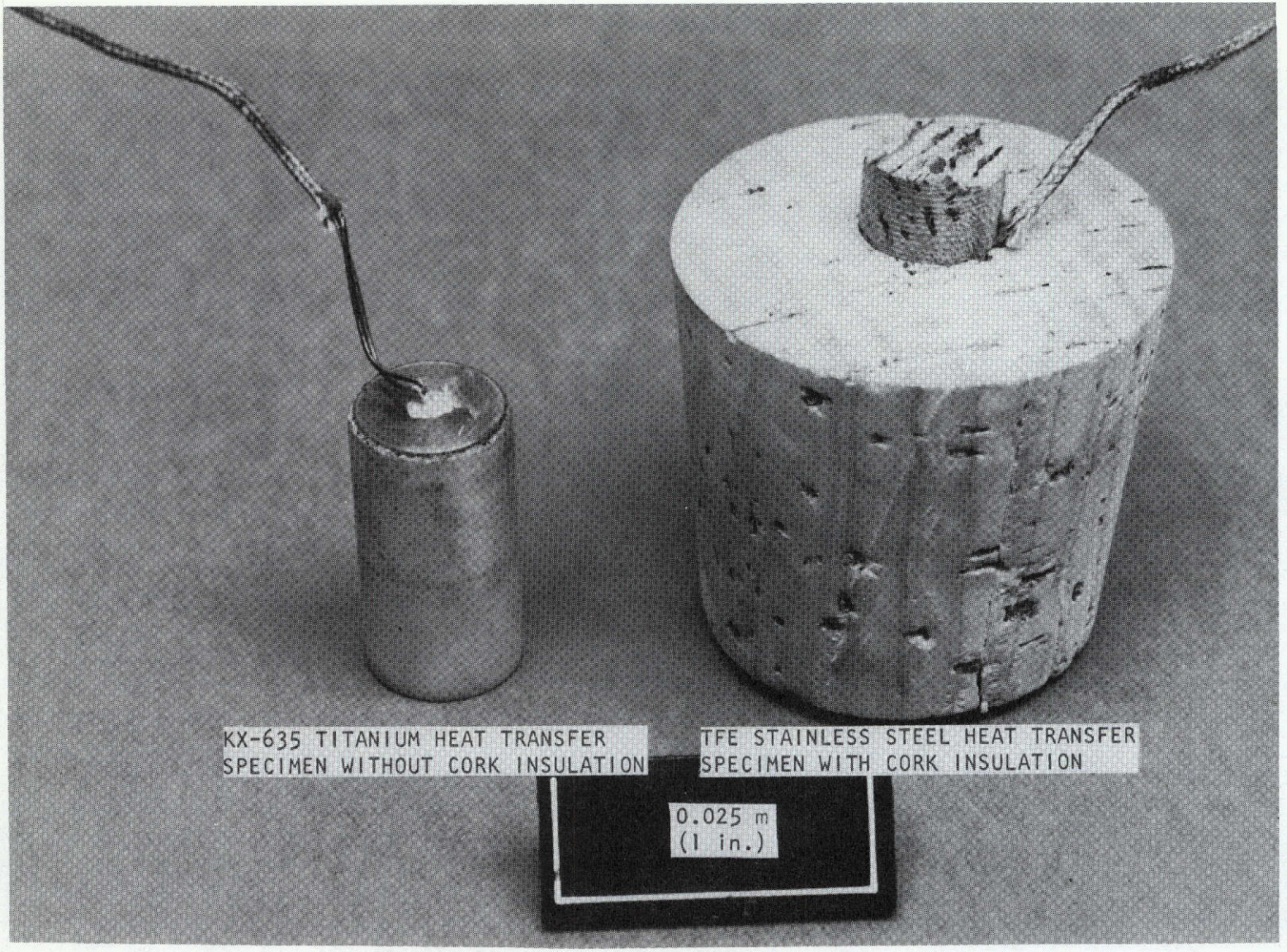

1XZ52-9/27/71-C1

Figure 100. Heat Transfer Specimens With and Without Cork Insulation

thin and thick insulative coating on chilldown rates in LN_2. A photograph of the laboratory equipment is shown in Fig. 101.

Immersion testing in LH_2 was conducted at Wyle Laboratories. Again the samples were tested, first with all coated surfaces exposed and then with one coated surface exposed. Figure 102 presents a photograph of the test apparatus. Moseley recorders were used to obtain thermal data and are shown in Fig. 103.

Thermech Engineering reported difficulty in obtaining a uniform coating of 5.08×10^{-4} m ((0.020 in.) when applying FEP + glass-microballoon material to the immersion samples. It was decided to obtain a uniform coating by machining to a thickness of 3.81×10^{-4} m (0.015 in.). Surface roughness and irregularities were intrinsic characteristics of this coating throughout Task II.

Adherence Tests

Stainless-steel tensile samples were tested for adhesion at room temperature and at 78 K (-320 F). At both temperatures, the samples were tested beyond the yield point of stainless steel. This criterion was based on the assumption that pump parts will not be strained beyond the yield point, and that coatings meeting this criterion will not undergo strain-induced failure. The samples were coated with TFE, FEP, FEP + glass microballoons, and FEP + glass microballoons + Lithafrax (Table 17 and Fig. 104).

All coatings tested exhibited no irregularities when tested beyond the yield point of stainless steel, except for thick 5.08×10^{-4} m (0.020 in.) FEP + glass microballoons + Lithafrax. Photographs of these samples are shown in Fig. 105 and 106. Photomacrographs of the cross-sectioned 5.08×10^{-4} m (0.020-in.) thick coating that cracked during the tensile tests were taken to determine the extent of coating separation from the metal substrate. Photographs in Fig. 107 show that cracking was due to failure of the material and not of the adhesion between the coating and metal.

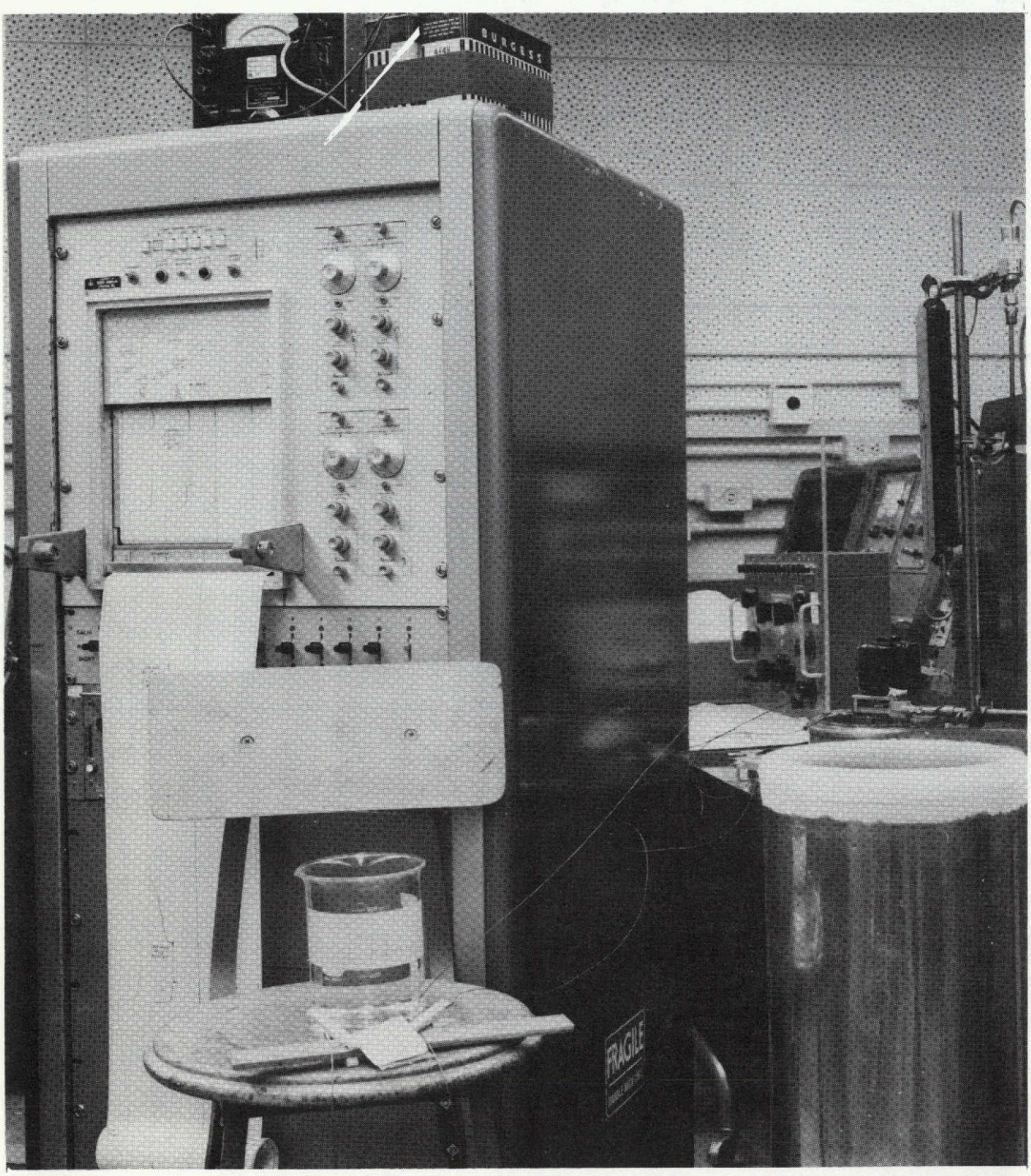

1XZ54-9/13/71-C1C

Figure 101. Brush Recorder for Immersion Testing in Liquid Nitrogen

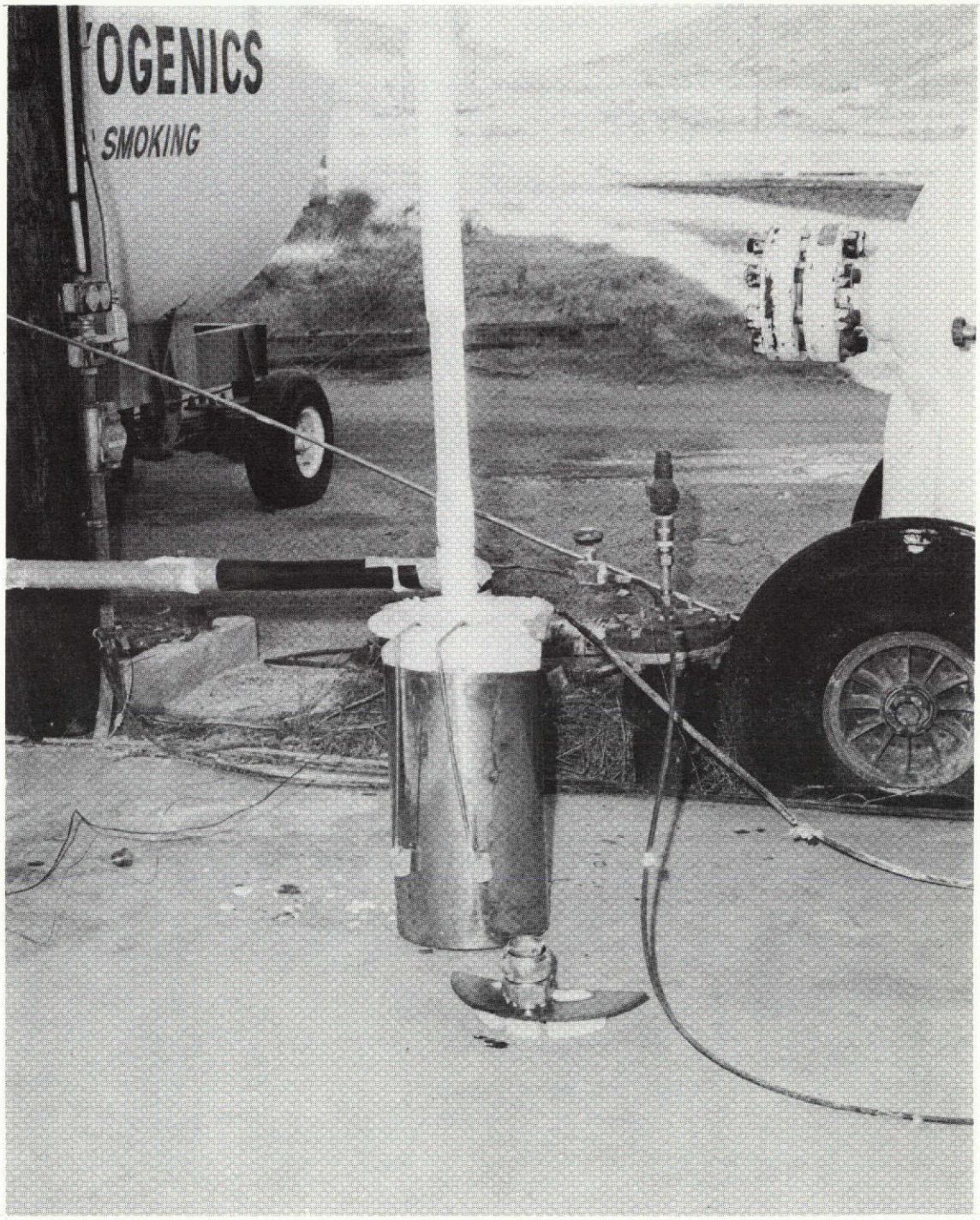

Figure 102. Test Dewar for Immersion Testing in Liquid Hydrogen

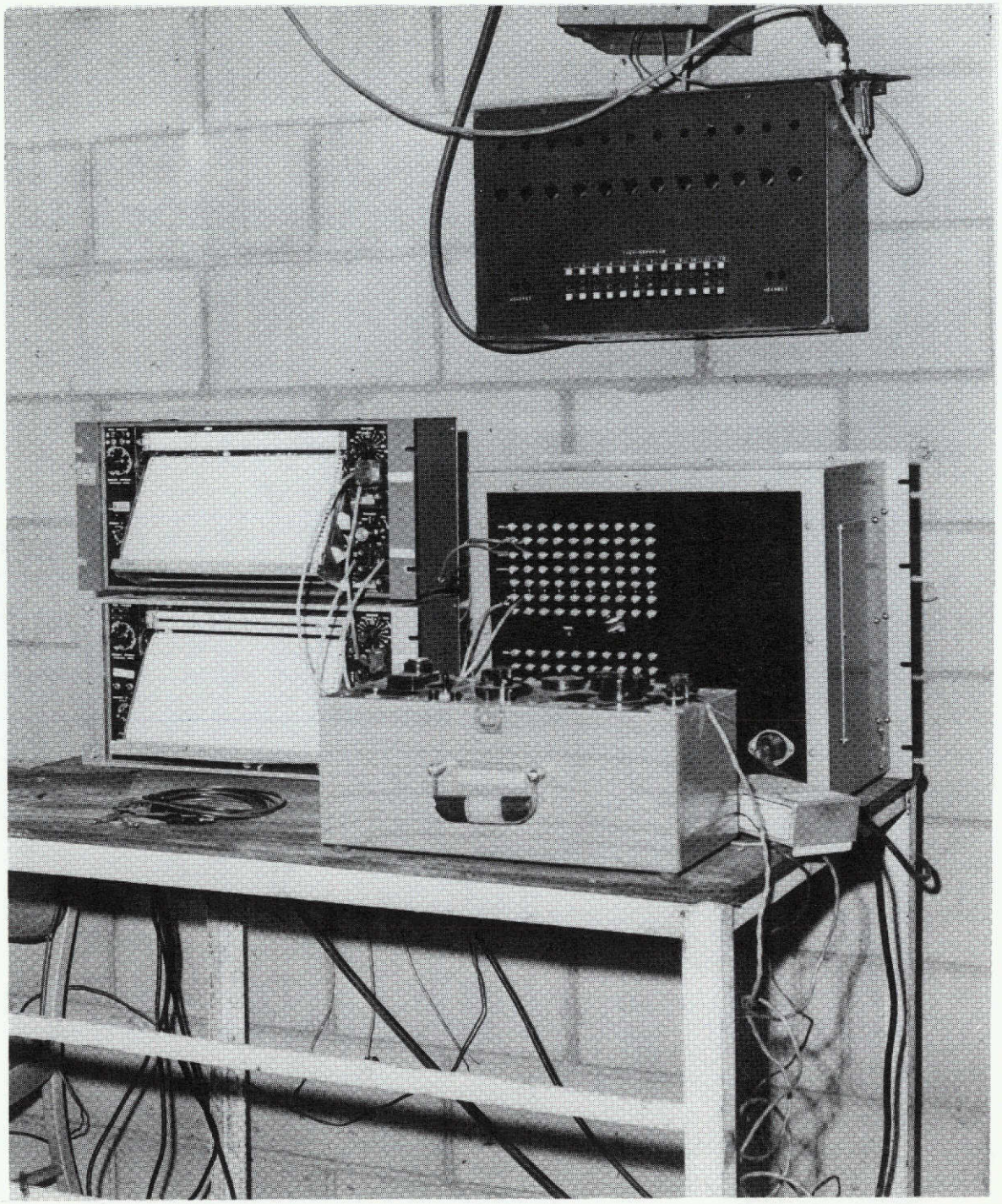

Figure 103. Moseley Temperature Recorders

TABLE 17. STAINLESS STEEL TENSILE SAMPLES

Coating Material	Thickness	Test at Ambient	Test at -320 F
1. TFE (DuPont 851-245 over DuPont 850-204)	1.27×10^{-4} m (0.005 in.)	3	3
2. FEP (DuPont 856-204 over DuPont 850-201)	1.27×10^{-4} m (0.005 in.)	3	3
3. FEP + 25-percent glass microballoons	1.27×10^{-4} m (0.005 in.)	3	3
4. FEP + 25-percent glass microballoons	5.08×10^{-4} m (0.020 in.)	3	3
5. FEP + 25-percent glass microballoons + 10-percent Lithafrax	1.27×10^{-4} m (0.005 in.)	3	3
6. FEP + 25-percent glass microballoons + 10-percent Lithafrax	5.08×10^{-4} m (0.020 in.)	3	3
		18	18

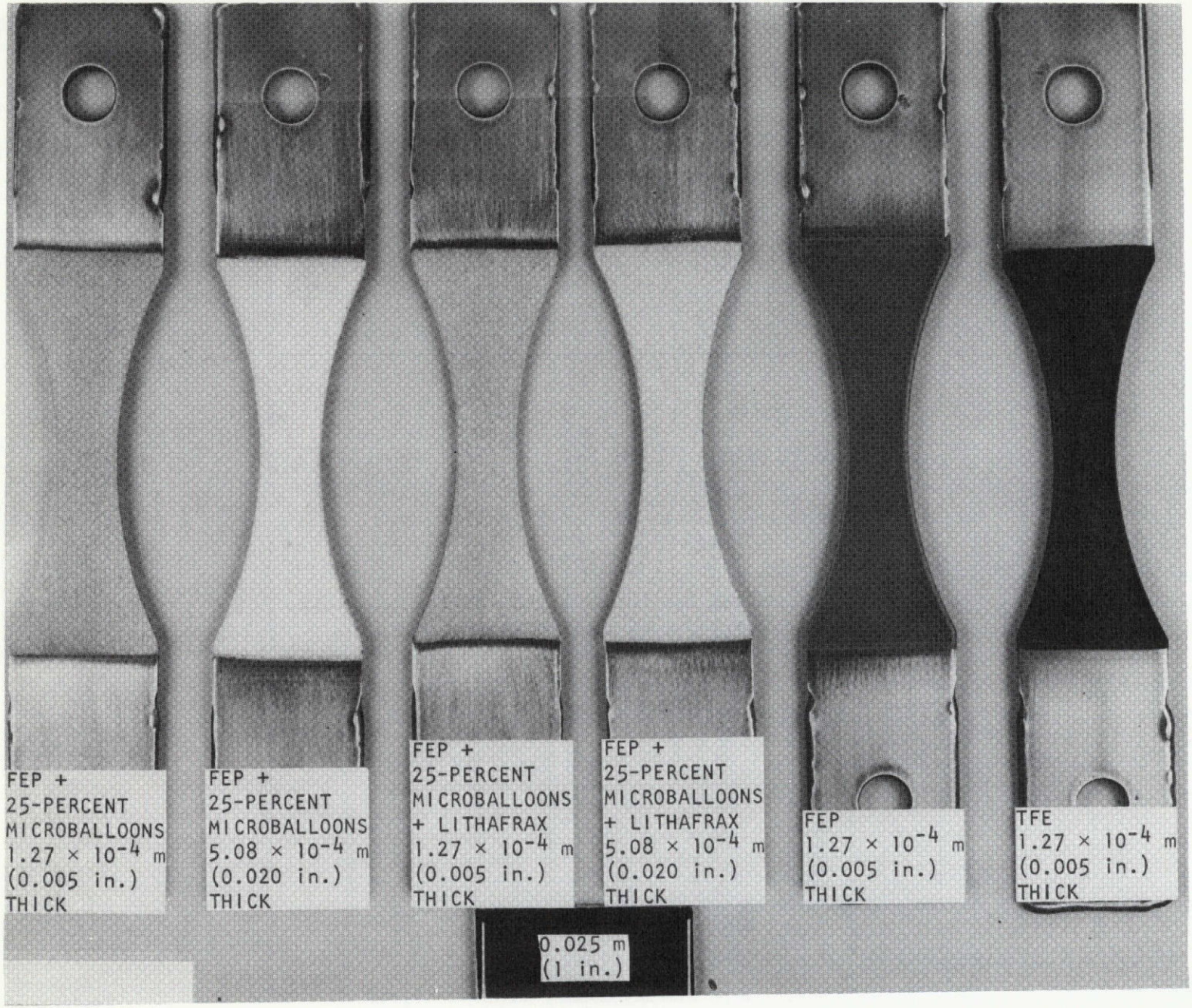

5AG46-1-/28/71-C1A

Figure 104. Tensile Samples for Adhesion Test, Pretest

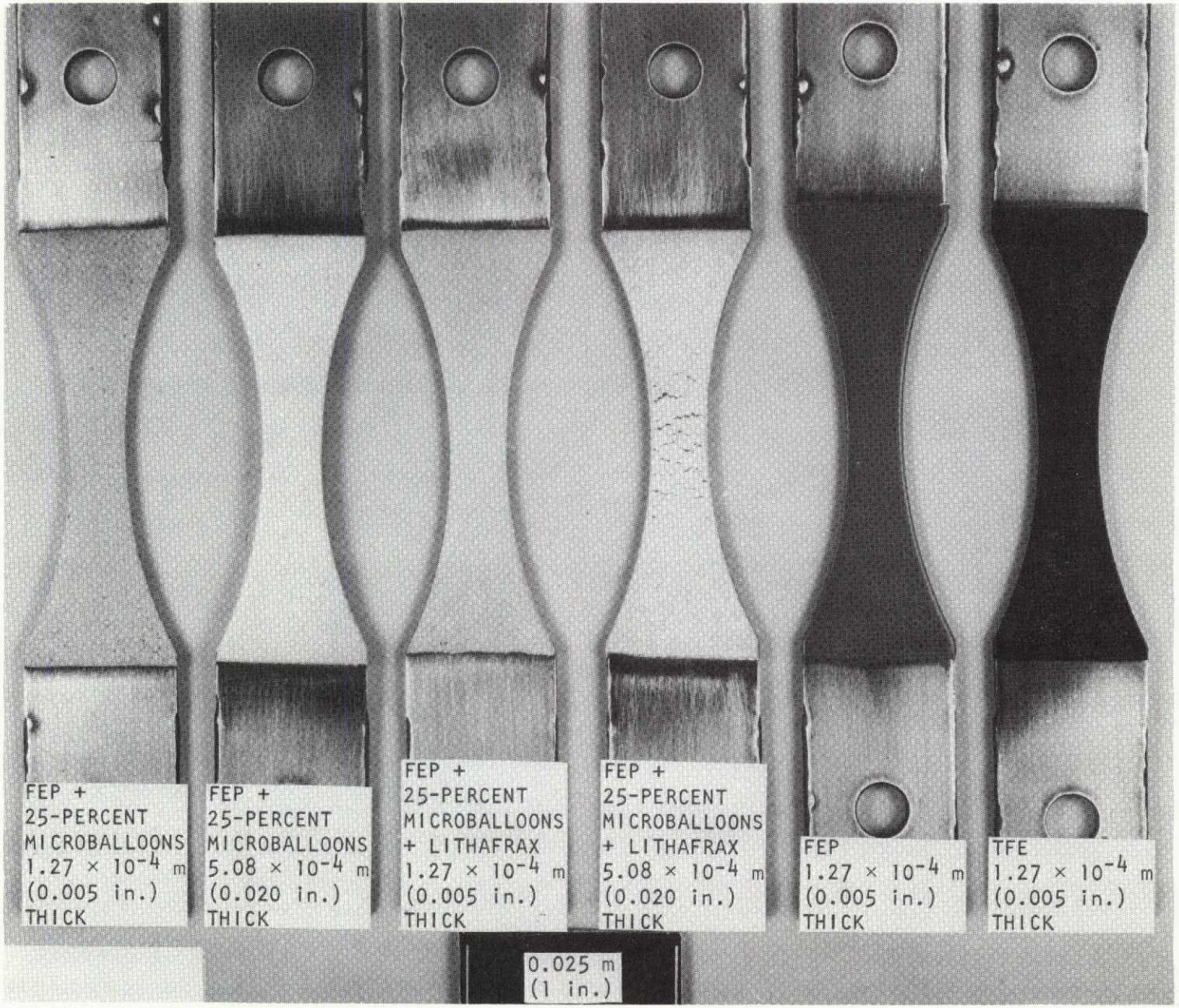

5AG46-10/28/71-C1B

Figure 105. Tensile Samples After Testing at 297 K (75 F)

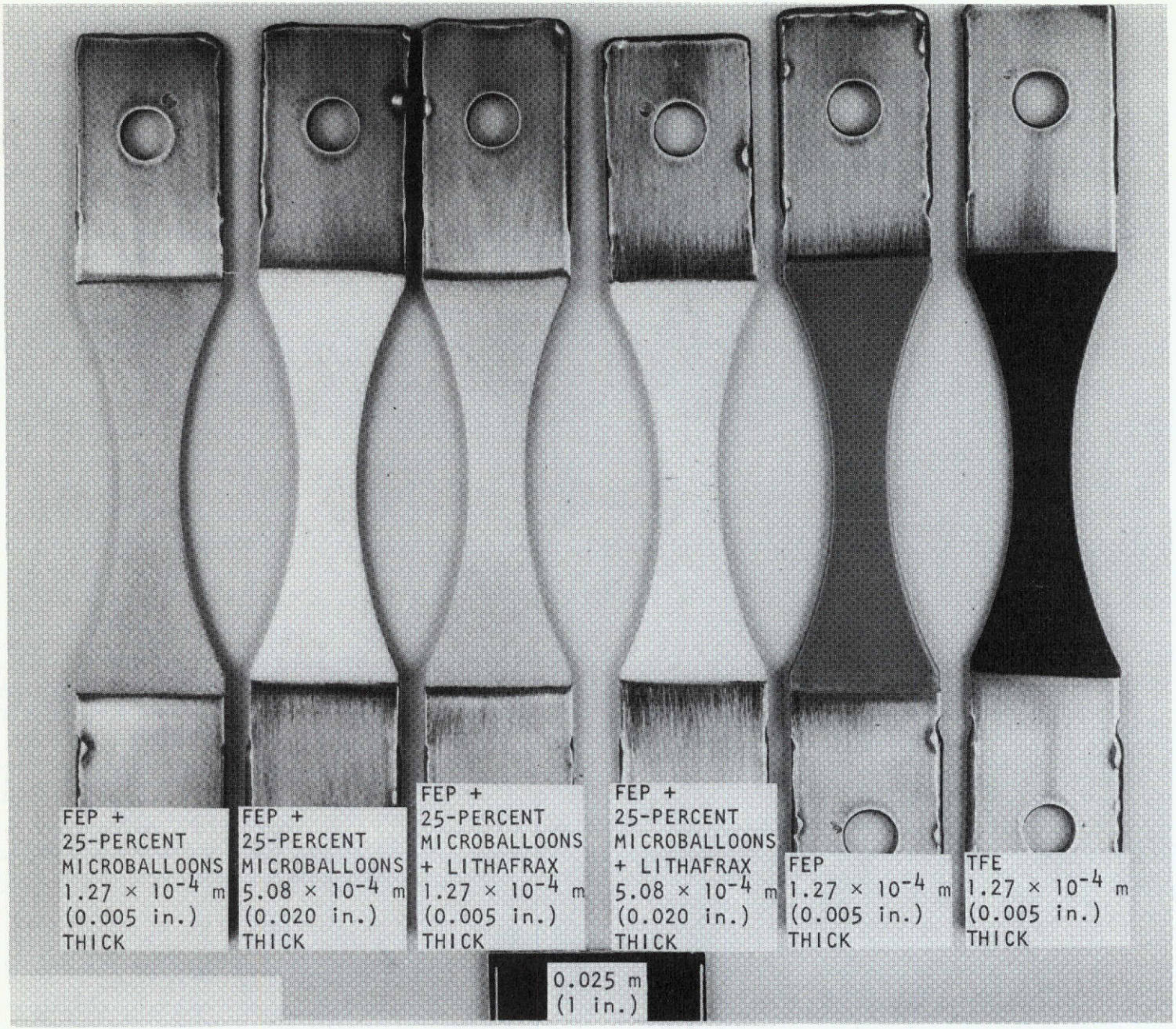

5AG46-10/29/71-C1

Figure 106. Tensile Samples After Testing At 78 K (-320 F)

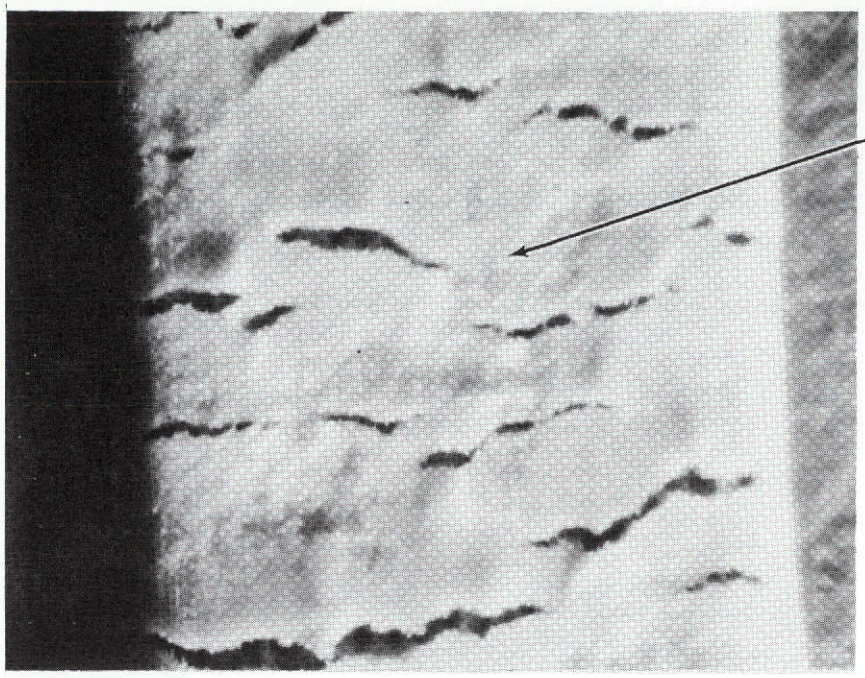

TOP VIEW

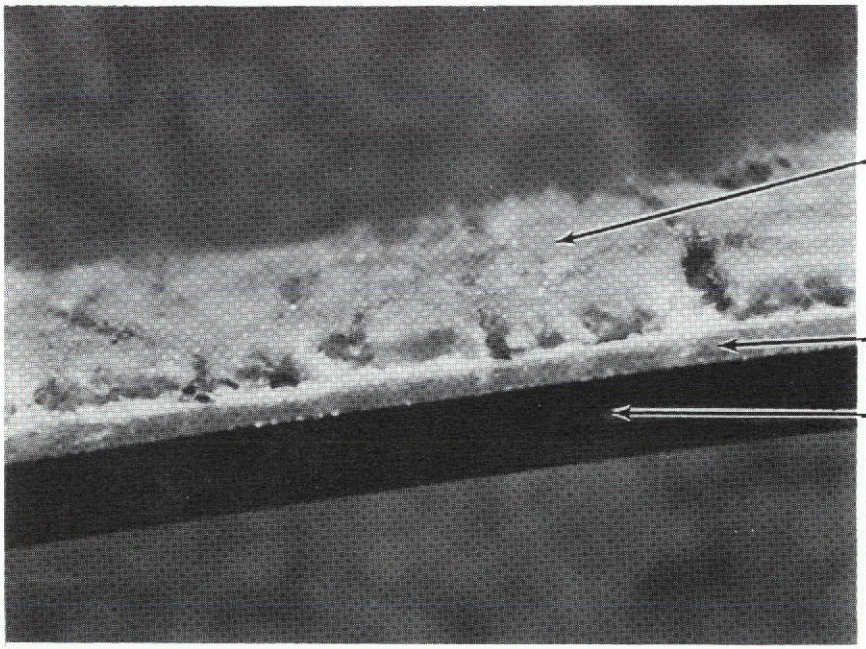

CROSS-SECTIONED

Figure 107. Posttest Tensile Specimen, 10X

LH_2 Flow Tests

Tubular samples, with coatings applied to the inside diameter and with thermocouples attached, were used to determine the insulative and erosion characteristics of the coatings under flow conditions. Samples with an 0.051 m (2.0 in.) OD, 0.033 m (1.3 in.) ID, and 0.038 m (1.5 in.) length were fabricated from aluminum, stainless steel, and titanium. The various coatings, thicknesses, and methods of application are presented in Table 18.

TABLE 18. TUBULAR COLLARS

Coating Material	Thickness	Base Material*			Total
		Al	Ti	SS	
1. TFE (DuPont 851-245 over DuPont 850-204)	1.27×10^{-4} m (o.005 in.)	2	2	2	6
2. KX-635	1.27×10^{-4} m (0.005 in.)	2	2	2	6
3. FEP (DuPont 856-204 over DuPont 850-201)	1.27×10^{-4} m (0.005 in.)	2	-	2	4
4. FEP + 25-percent glass microballoons	1.27×10^{-4} m (0.005 in.)	2	-	2	4
5. KX-635 + KX-633	5.08×10^{-4} m (0.020 in.)	2	2	2	6
6. KX-635	5.08×10^{-4} m (0.020 in.)	2	2	2	6
7. FEP + 25-percent glass microballoons	5.08×10^{-4} m (0.020 in.)	2	-	2	4
8 No Coating		1	1	1	3
					39

*One set of collars spray-coated while the other set coated via fill and drain techniques

A test fixture 0.91 m (36 in.) long was fabricated to accommodate six samples per test. Each sample had a cotton-phenolic spacer between it and the adjacent samples to ensure valid data. The fixture and samples are shown in Fig. 108, 109, and 110. The flow tests were conducted at Wyle Laborabories. Photographs of the facility are shown in Fig. 111, 112, and 113. The test matrix is shown in Table 19. Thin-FEP coatings were substituted for the flass-filled FEP coatings in Test 7 to provide more quick-chill data. Each run consisted of six collars tested at three different flowrates to determine erosion, coating adhesion, and chilldown characteristics of the metals with various coatings.

Thermech Engineering expressed difficulty in coating the aluminum samples with the FEP + glass-microballoon material. When the material was machined to proper thickness, bare metal began to show. The aluminum had received no previous heat treat, causing it to lose concentricity during the curing cycle. The stainless-steel and titanium samples did not exhibit this loss of concentricity. The coatings were exposed to an average of 15 minutes of LH_2 flow and visual examinations revealed no erosion and no coating separation from the metals.

MATERIAL AND APPLICATION SELECTION

The results of the Task II laboratory tests are summarized in Table 20. A discussion of each coating is presented in the following sections.

TFE

TFE is recommended for both LOX and LH_2 systems in thin, less than 1.27×10^{-4} m (0.005 in.), coatings. It passed the LOX-impact and adherence tests and showed no erosion during the flow tests. It exhibited good uniformity when applied by either conventional-spray techniques or by fill-and-drain techniques. This material is susceptible to mud cracking at coatings thicker than 1.27×10^{-4} m (0.005 in.).

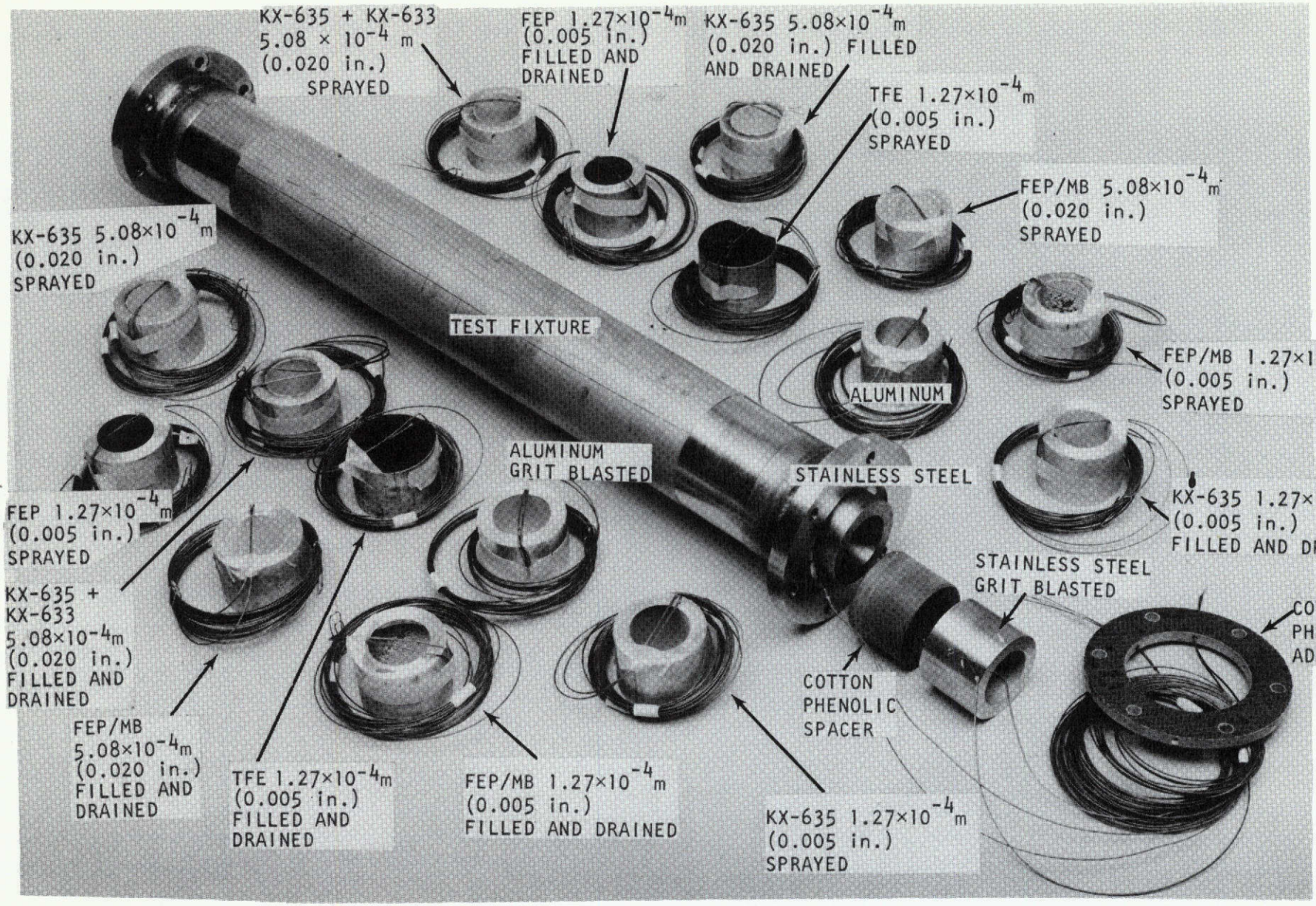

1XY54-12/8/71-C2

Figure 108. Coated Aluminum Tubular Collars and Test Fixture for Liquid Hydrogen Dynamic Flow Tests

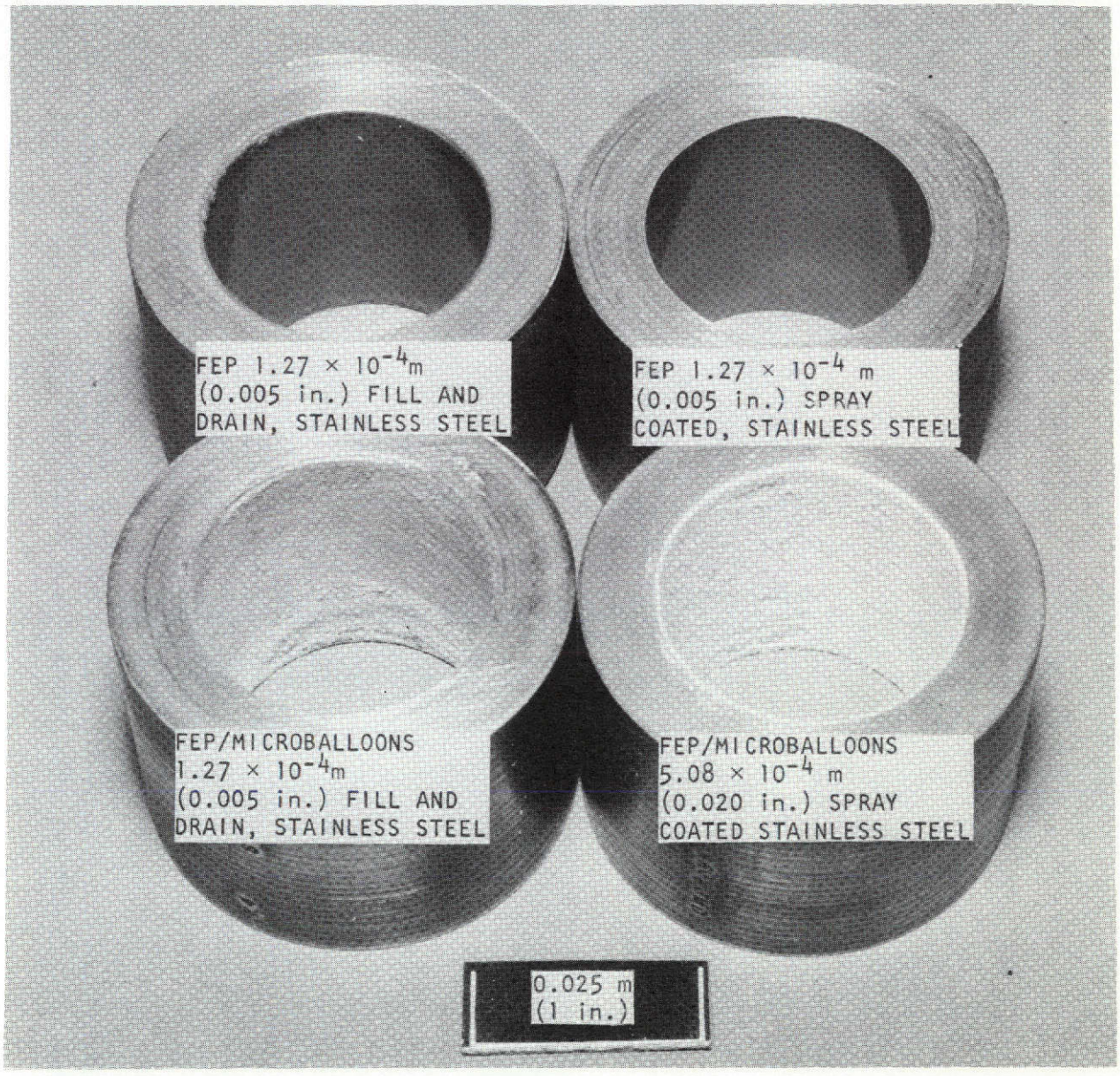

1XY62-11/15/71-C1

Figure 109. Typical Coated Tubular Collars for Liquid Hydrogen Dynamic Flow Testing

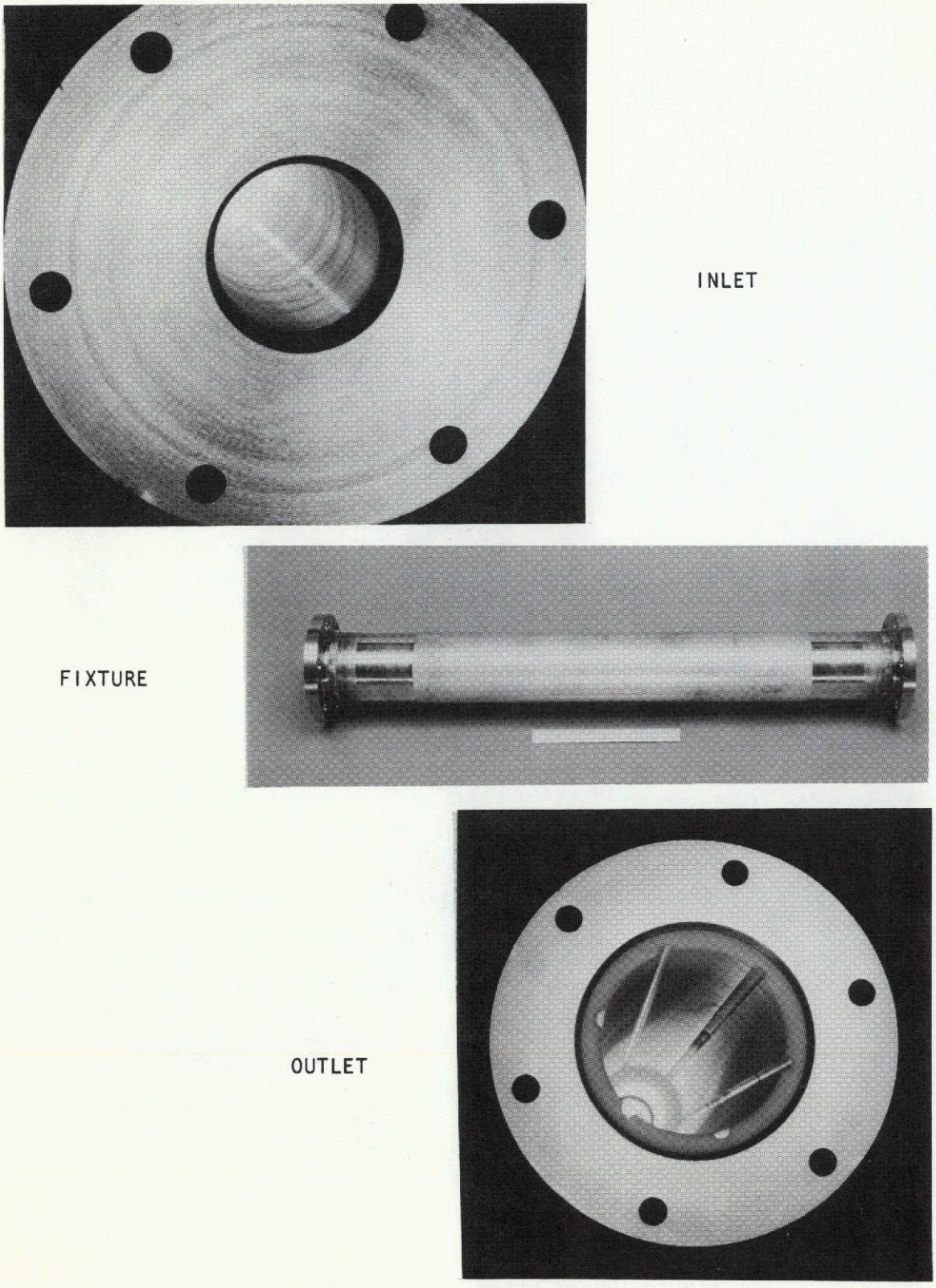

Figure 110. Tubular Collar Test Fixture For LH_2 Flow Tests

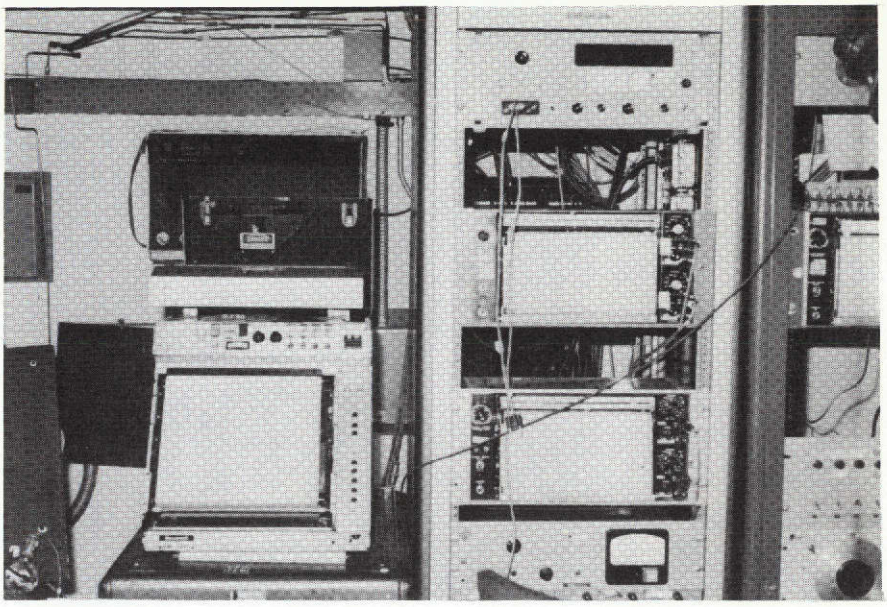

HONEYWELL VISICORDER MOSELEY TEMPERATURE RECORDERS

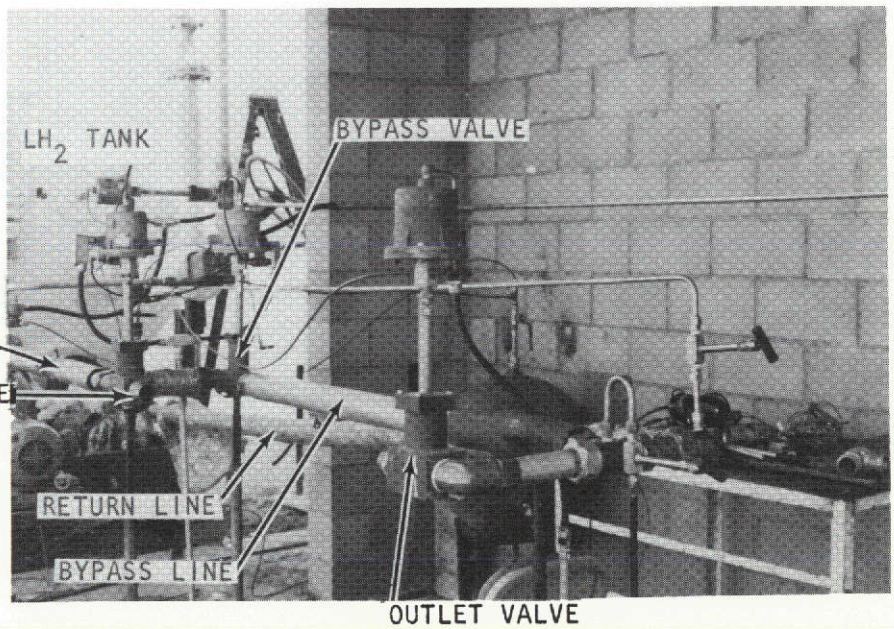

Figure 111. Flow Test Facility and Instrumentation

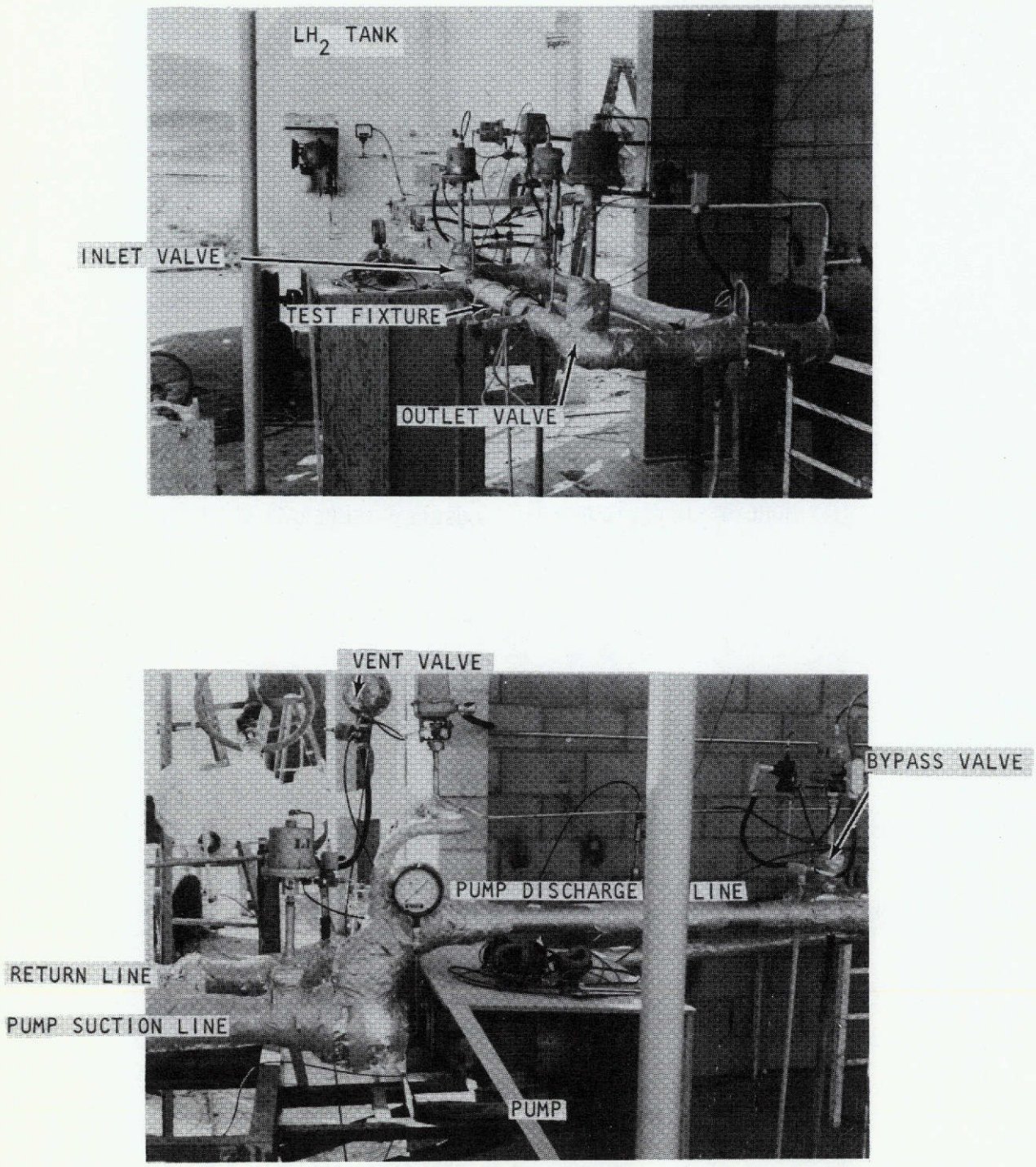

Figure 112. Flow Test Facility for Liquid Hydrogen Dynamic Flow Testing

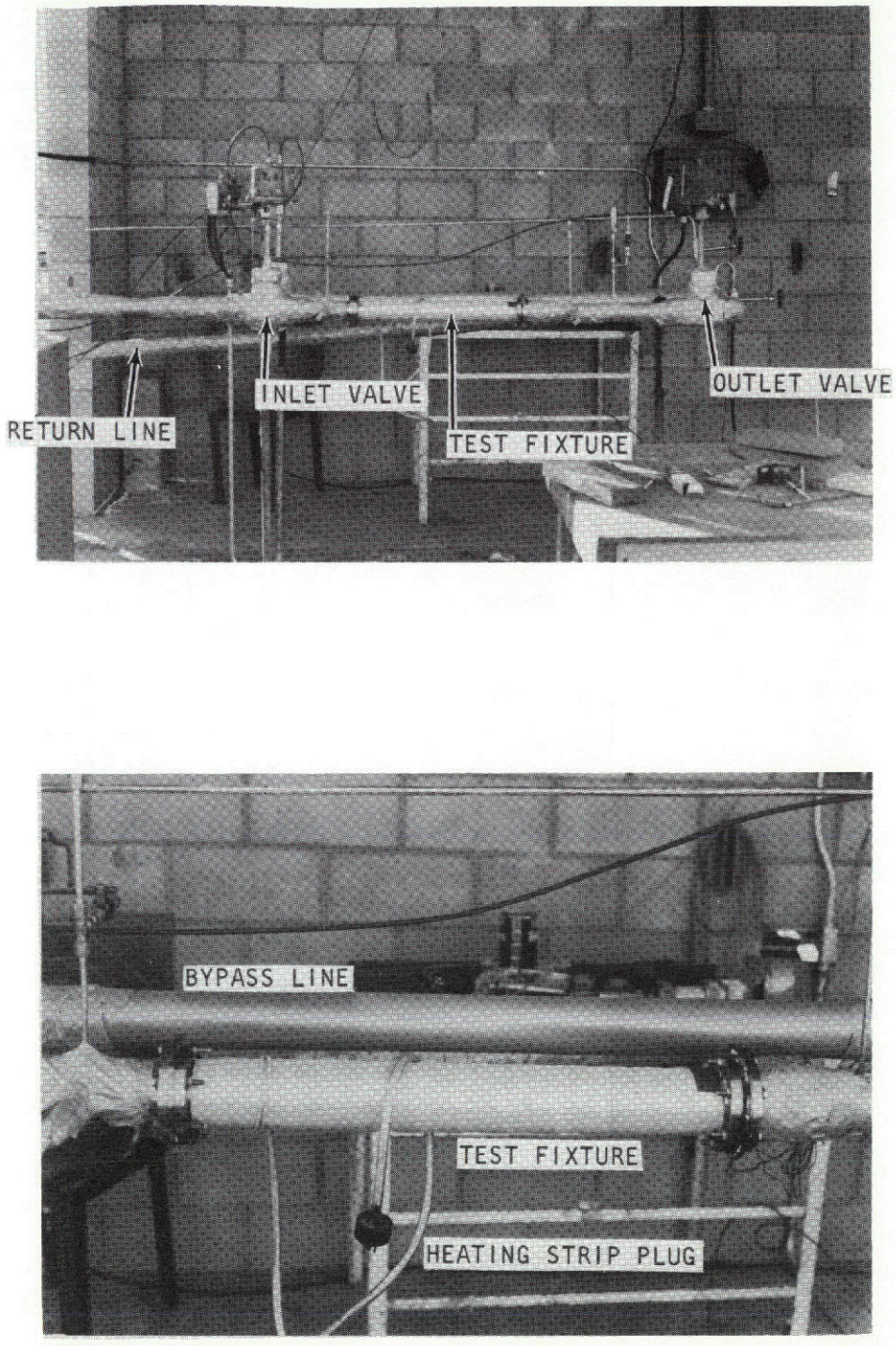

Figure 113. Flow Test Facility Showing Test Section For Tubular Collars

TABLE 19. TEST MATRIX FOR TUBULAR COLLARS

Test	Metal	Coating	Application	Nominal Thickness	Actual Thickness
1	SS (1)	None	-	-	-
	SS (2)	Grit-blasted	-	-	-
	Ti (3)	None	-	-	-
	Ti (4)	Grit-blasted	-	-	-
	Al (5)	None	-	-	-
	Al (6)	Grit-blasted	-	-	-
2	Al (1)	KX-635	Sprayed	1.27×10^{-4} m (0.005 in.)	1.88×10^{-4} m (0.0074 in.)
	Al (2)	KX-635 + KX-633	Sprayed	5.08×10^{-4} m (0.020 in.)	5.03×10^{-4} m (0.0198 in.)
	Al (3)	KX-635	Sprayed	5.08×10^{-4} m (0.020 in.)	4.27×10^{-4} m (0.0168 in.)
	Ti (4)	KX-635	Sprayed	5.08×10^{-4} m (0.020 in.)	4.01×10^{-4} m (0.0158 in.)
	Ti (5)	KX-635	Sprayed	1.27×10^{-4} m (0.005 in.)	3.05×10^{-4} m (0.012 in.)
	Ti (6)	KX-635 + KX-633	Sprayed	5.08×10^{-4} m (0.020 in.)	5.08×10^{-4} m (0.020 in.)
3	Al (1)	KX-635	Filled & Drained	1.27×10^{-4} m (0.005 in.)	1.60×10^{-4} m (0.0063 in.)
	Al (2)	KX-635	Filled & Drained	5.08×10^{-4} m (0.020 in.)	6.22×10^{-4} m (0.0245 in.)

Continues on next page

( ) Indicates collar position in fixture, (1) being closest to the inlet and (6) being farthest

TABLE 19. (Continued)

Test	Metal	Coating	Application	Nominal Thickness	Actual Thickness
	Al (3)	KX-635 + KX-633	Filled & Drained	5.08×10^{-4} m (0.020 in.)	5.89×10^{-4} m (0.0232 in.)
	Ti (4)	KX-635	Filled & Drained	1.27×10^{-4} m (0.005 in.)	1.45×10^{-4} m (0.0057 in.)
	Ti (5)	KX-635 + KX-633	Filled & Drained	5.08×10^{-4} m (0.020 in.)	6.20×10^{-4} m (0.0244 in.)
	Ti (6)	KX-635	Filled & Drained	5.08×10^{-4} m (0.020 in.)	6.07×10^{-4} m (0.0239 in.)
4	Al (1)	TFE	Sprayed	1.27×10^{-4} m (0.005 in.)	1.22×10^{-4} m (0.0048 in.)
	Al (2)	TFE	Filled & Drained	1.27×10^{-4} m (0.005 in.)	9.65×10^{-5} m (0.0038 in.)
	Al (3)	FEP	Sprayed	1.27×10^{-4} m (0.005 in.)	6.10×10^{-5} m (0.0024 in.)
	Al (4)	FEP	Filled & Drained	1.27×10^{-4} m (0.005 in.)	1.65×10^{-4} m (0.0065 in.)
	SS (5)	TFE	Sprayed	1.27×10^{-4} m (0.005 in.)	1.02×10^{-4} m (0.004 in.)
	SS (6)	FEP	Sprayed	1.27×10^{-4} m (0.005 in.)	8.38×10^{-5} m (0.0033 in.)
5	SS (1)	TFE	Filled & Drained	1.27×10^{-4} m (0.005 in.)	2.01×10^{-4} m (0.0079 in.)
	SS (2)	KX-635	Sprayed	1.27×10^{-4} m (0.005 in.)	2.39×10^{-4} m (0.0094 in.)
	SS (3)	KX-635	Filled & Drained	1.27×10^{-4} m (0.005 in.)	3.43×10^{-4} m (0.0135 in.)
	SS (4)	FEP	Filled & Drained	1.27×10^{-4} m (0.005 in.)	8.13×10^{-5} m (0.0032 in.)

Continues on next page

( ) Indicates collar position in fixture, (1) being closest to the inlet and (6) being farthest.

TABLE 19. (Concluded)

Test	Metal	Coating	Application	Nominal Thickness	Actual Thickness
	SS (5)	KX-635 + KX-633	Sprayed	5.08×10^{-4} m (0.020 in.)	5.69×10^{-4} m (0.0224 in.)
	SS (6)	KX-635 + KX-633	Filled & Drained	5.08×10^{-4} m (0.020 in.)	5.74×10^{-4} m (0.0226 in.)
6	Al (1)	FEP + Microballoons	Sprayed	1.27×10^{-4} m (0.005 in.)	7.62×10^{-5} m (0.003 in.)
	Al (2)	FEP + Microballoons	Sprayed	5.08×10^{-4} m (0.020 in.)	5.74×10^{-4} m (0.0226 in.)
	SS (3)	KX-635	Sprayed	5.08×10^{-4} m (0.020 in.)	5.41×10^{-4} m (0.0213 in.)
	SS (4)	KX-635	Filled & Drained	5.08×10^{-4} m (0.020 in.)	4.93×10^{-4} m (0.0194 in.)
	Ti (5)	TFE	Sprayed	1.27×10^{-4} m (0.005 in.)	8.64×10^{-5} m (0.0034 in.)
	Ti (6)	TFE	Filled & Drained	1.27×10^{-4} m (0.005 in.)	1.73×10^{-4} m (0.0068 in.)
7	Al (1)	FEP	Sprayed	3.81×10^{-5} m (0.0015 in.)	4.57×10^{-5} m (0.0018 in.)
	SS (2)	FEP	Sprayed	3.81×10^{-5} m (0.0015 in.)	2.54×10^{-5} m (0.0010 in.)
	Ti (3)	FEP	Sprayed	3.81×10^{-5} m (0.0015 in.)	3.81×10^{-5} m (0.0015 in.)
	Ti (4)	FEP	Sprayed	1.27×10^{-5} m (0.0005 in.)	2.54×10^{-5} m (0.0010 in.)
	Al (5)	FEP	Sprayed	1.27×10^{-5} m (0.0005 in.)	1.27×10^{-5} m (0.0005 in.)
	SS (6)	FEP	Sprayed	1.27×10^{-5} m (0.0005 in.)	4.32×10^{-5} m (0.0017 in.)

( ) Indicates collar position in fixture, (1) being closest to the inlet and (6) being farthest.

TABLE 20. RESULTS OF THE TASK II LABORATORY TESTS

Coating	LOX Impact Tests	Adherence Tests	Erosion Under LH_2 Flow	Coating Uniformity	Thickness Less Than 1.27×10^{-4}m (0.005 in.)	Thickness Greater Than 1.27×10^{-4}m (0.005 in.)
TFE	*	*	*	*	*	X
FEP	*	*	*	*	*	X
KX-635	X	*	*	*	*	*
FEP + glass microballoons	X	*	*	X	*	*
FEP + glass microballoons + Lithafrax	X	X	*	X	*	*

* - coating passed

X - coating failed

FEP

FEP is recommended for both LOX and LH_2 systems in thin, less than 1.27×10^{-4} m (0.005 in.), coatings. It displayed the same results as TFE in the Task II tests. FEP is easier to process than TFE.

KX-635

KX-635 is recommended for LH_2 systems. It is not recommended for LOX systems because it did not pass the LOX-impact tests. It can be applied in thick or thin coatings and exhibited good adherence and no erosion during the flow tests. There were no problems in obtaining a uniform coating when applied by either spray or fill-and-drain techniques.

FEP + Glass Microballoons

FEP + glass microballoons is not recommended for either LOX or LH_2 systems. It did not pass the LOX-impact tests and exhibited poor uniformity when applied to the test samples. Controlling the coating thickness was extremely difficult due to this lack of uniformity.

FEP + Glass Microballoons + Lithafrax

FEP + glass microballoons + Lithafrax is also not recommended for either LOX or LH_2 systems. It not only displayed the same results as the FEP + glass microballoon material in the Task II tests, but also failed the adhesion tests.

Metal Substrates

Stainless-steel and titanium samples exhibited no adverse effects due to the coating-cure cycles. However, the aluminum flow samples did lose their concentricity. The heat-treat condition of aluminum parts must be known prior to coating to ensure that the parts will not be damaged during the cure cycles.

EXPERIMENTAL COATED FEED SYSTEM APPLICATION
AND POSTTEST INSPECTION

An inlet duct and an RL-10 hydrogen pump were coated with the selected material (KX-635) and tested during Task IV: Coated Feed System Tests. This section of the report summarizes the coating applications and posttest inspection.

Description of Coated Pump

Table 21 and Fig. 114 show the turbopump parts that were coated and the nominal thickness of the coatings. The surfaces presented different degrees of accessibility, which required changes in coating application methods (spray and fill-and-drain).

TABLE 21. KX-635 COATING OF RL-10 LH_2 TURBOPUMP

Part Name	Part Number	Thickness, m (in.)
Convair Inlet Line	1004	5.08×10^{-4} (0.020)
Crossover Line	RGFP 1005	5.08×10^{-4} (0.020)
First Stage Impeller	2072363	1.27×10^{-4} (0.005)
Second Stage Impeller	2029676	1.27×10^{-4} (0.005)
Front Housing	2052318	5.08×10^{-4} (0.020)
Rear Housing	2057560	5.08×10^{-4} (0.020)

The microballoons in KX-635 resulted in a surface texture that was coarse when compared to TFE or FEP. Except for LOX compatibility, this coating material had passed every requirement specified in Task II. Requirements were no loss of adhesion and no erosion when tested with flowing LH_2. The surfaces of the impellers were hand-smoothed with #600 grit sandpaper.

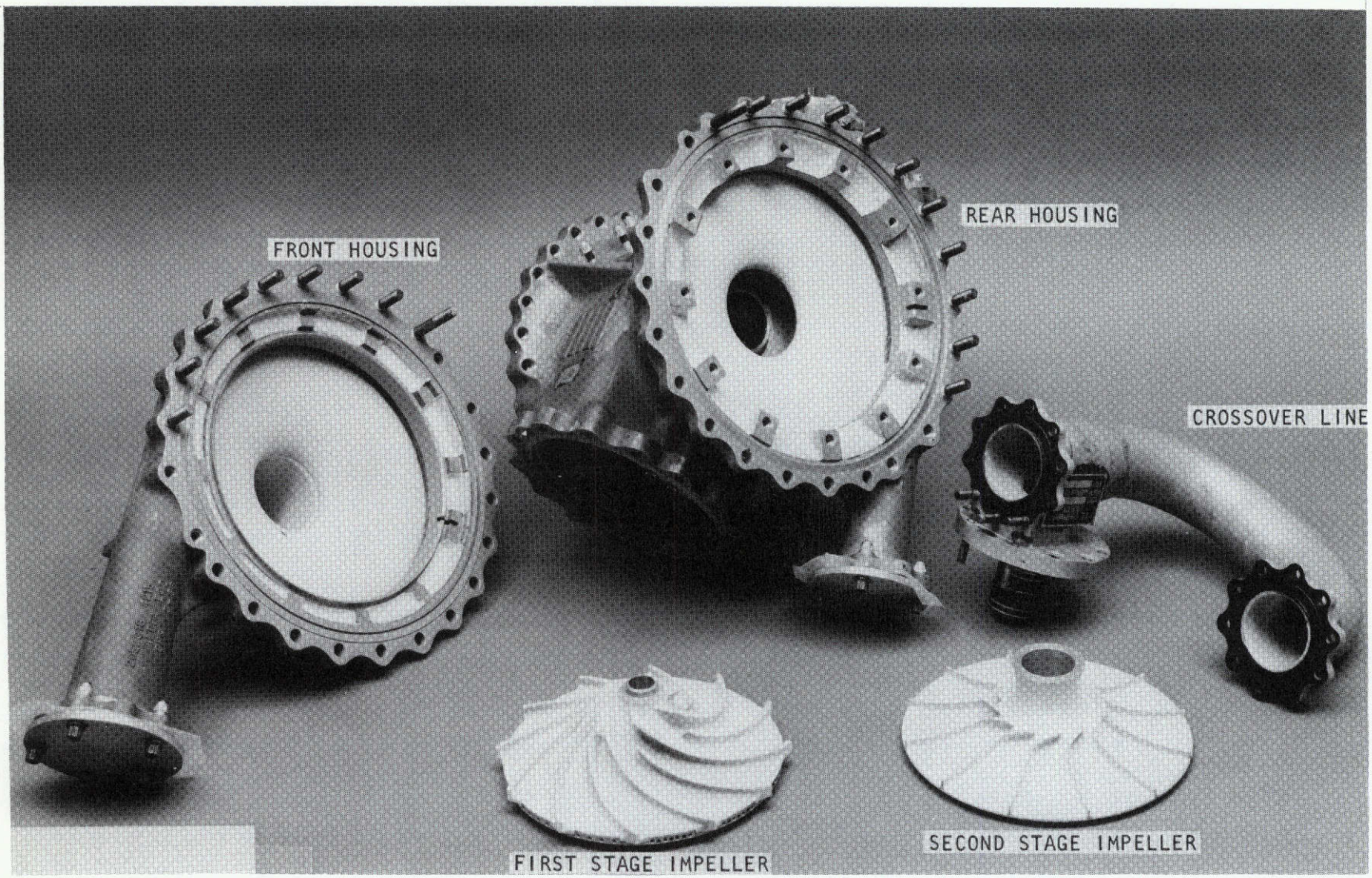

1XY52-11/16/72-C1

Figure 114. RL-10 Turbopump With KX-635 Coating, Pretest

Convair Inlet Line. The inlet line, shown in Fig. 115, was coated to a nominal thickness of 5.08×10^{-4} m (0.020 in.) using fill-and-drain techniques. The design of this line made it most difficult to control the coating thickness, particularly in the areas of the flexible bellows. The areas near the inlet and outlet of the line were of uniform thickness, but it was not possible to determine the degree of coating uniformity and thickness in the bellows sections. The cured coating imparted extra rigidity to the line and flexing of the bellows would crack the coating. There was no evidence of loss of coating adhesion during the pretest inspection.

Crossover Line. The pump crossover duct, Fig. 116, was also coated to a nominal thickness of 5.08×10^{-4} m (0.020) using fill-and-drain techniques. Unlike the Convair line, this line contained no bellows and was less bulky, thus facilitating handling. There were no sharp turns at different angles involved, which made for a smoother coating with a more controllable thickness.

Impellers. The easy accessibility permitted the surfaces of the impellers to be spray-coated to a nominal thickness of 1.27×10^{-4} m (0.005 in.). The coating was very iniform and the thickness moderately controllable. A photograph is presented in Fig. 117.

Turbopump Housings. The front and rear housings were coated to a nominal thickness of 5.08×10^{-4} m (0.020) using a combination of spray and fill-and-drain techniques. The technique used depended upon accessibility. The parts were not bulky, and there were no sharp bends in the areas to be coated. This provided reasonable thickness control and resulted in a uniform coating. The housings are shown in Fig. 118 and 119.

Posttest Inspection

Examination of the coated turbopump parts revealed excellent coating adhesion after approximately seven and a half minutes of operation. These parts are shown in Fig. 120. The surfaces that provided easy coating accessibility and handling

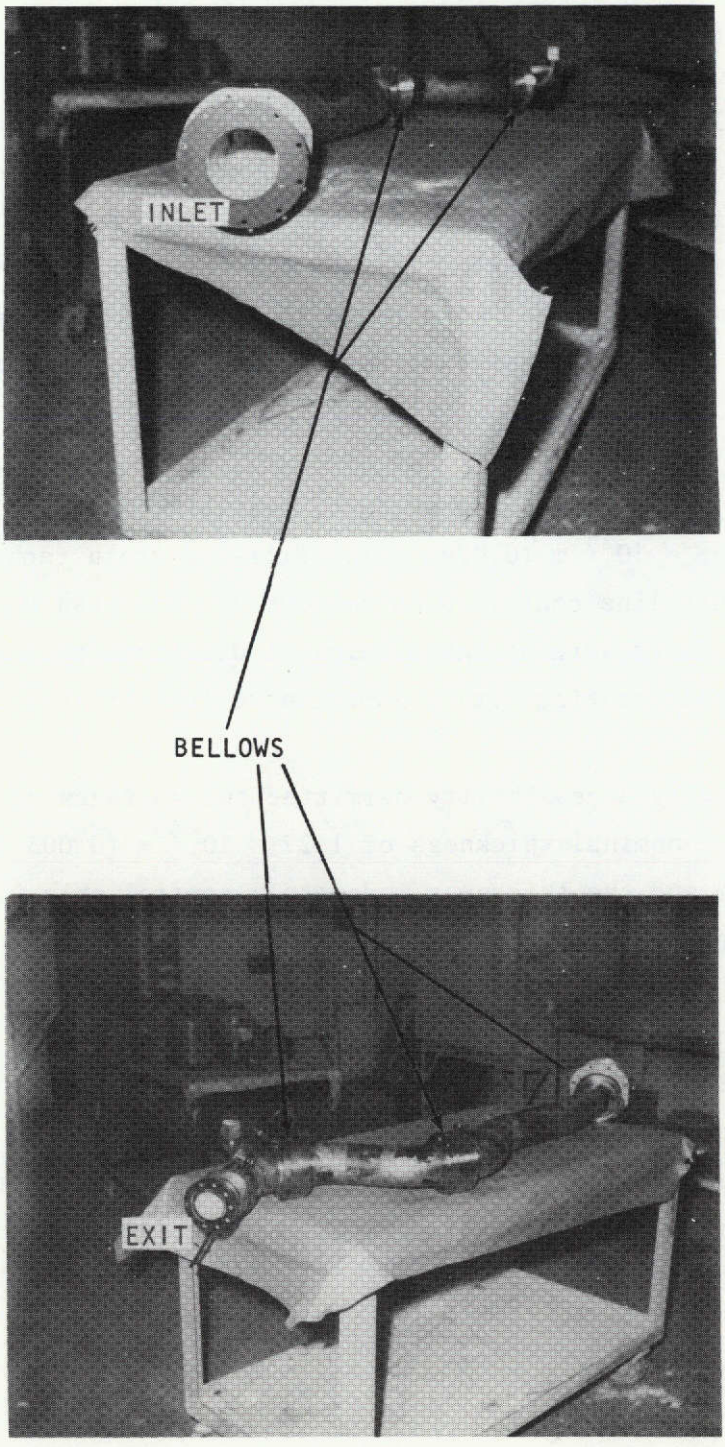

Figure 115. Convair Inlet Line With KX-635 Coating, Pretest

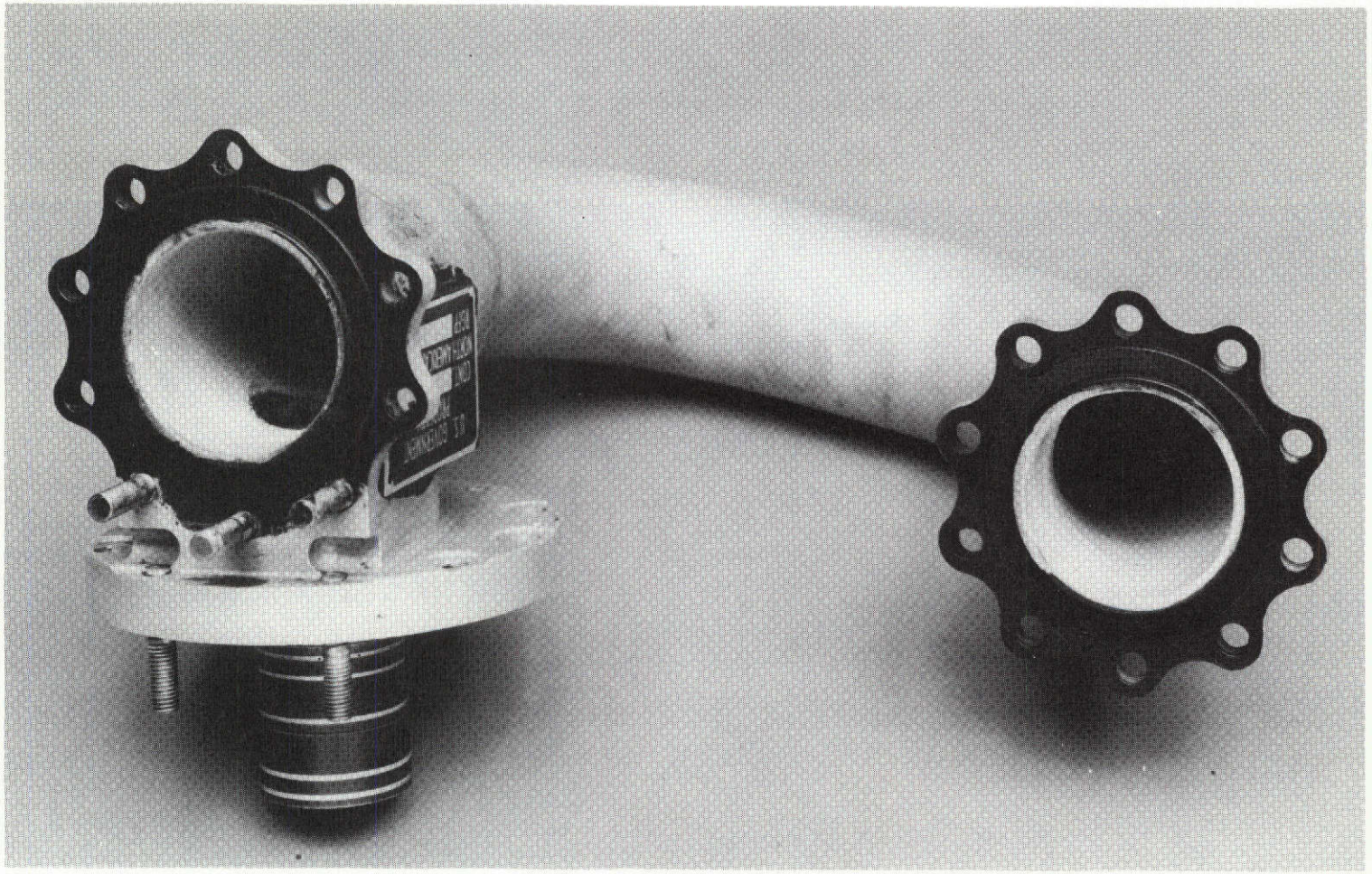

1XY52-11/15/72-C1C

Figure 116. Turbopump Crossover Line With KX-635 Coating, Pretest

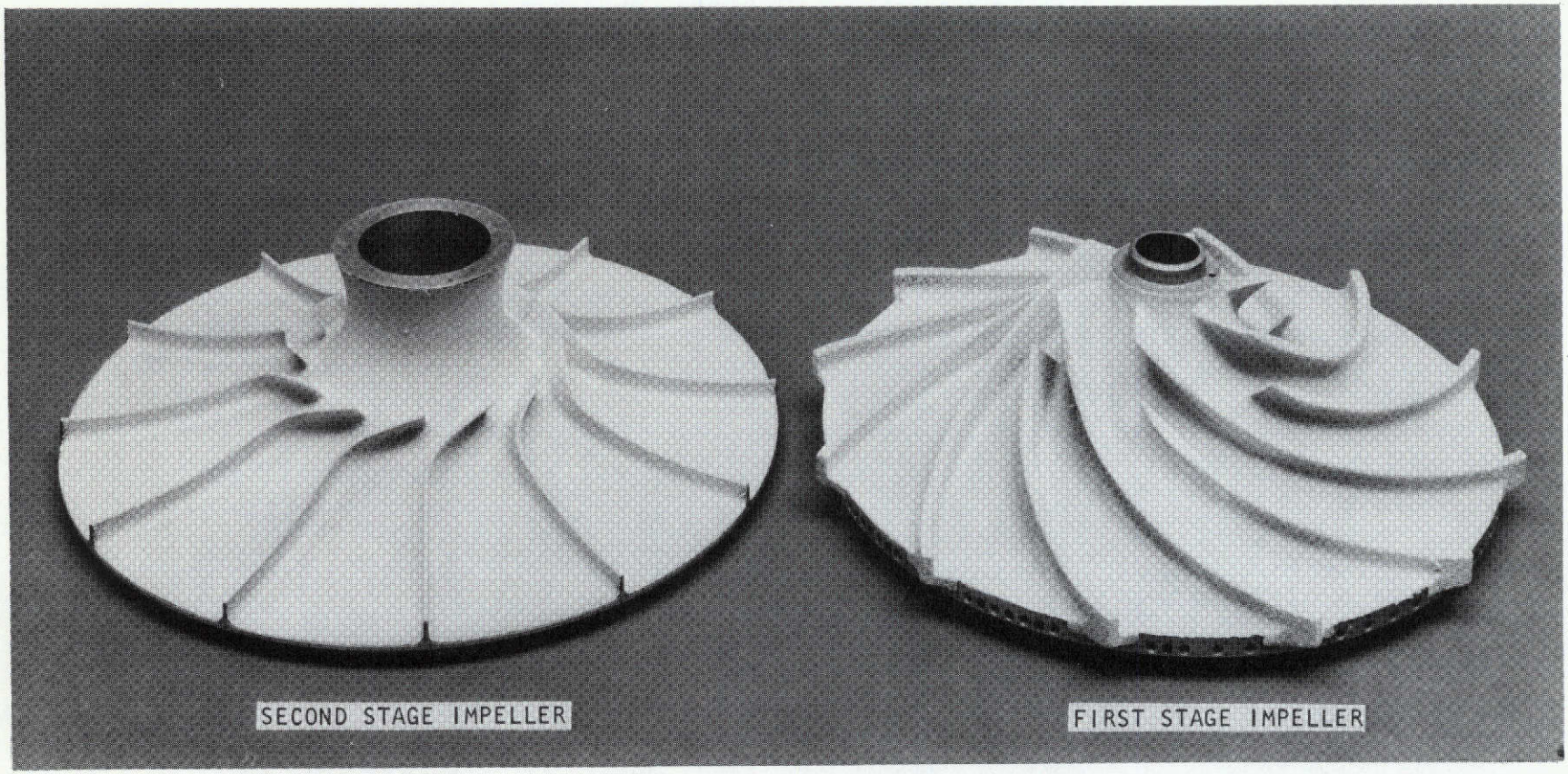

1XY52-11/15/72-C1D

Figure 117. Turbopump Impellers With KX-635 Coating, Pretest

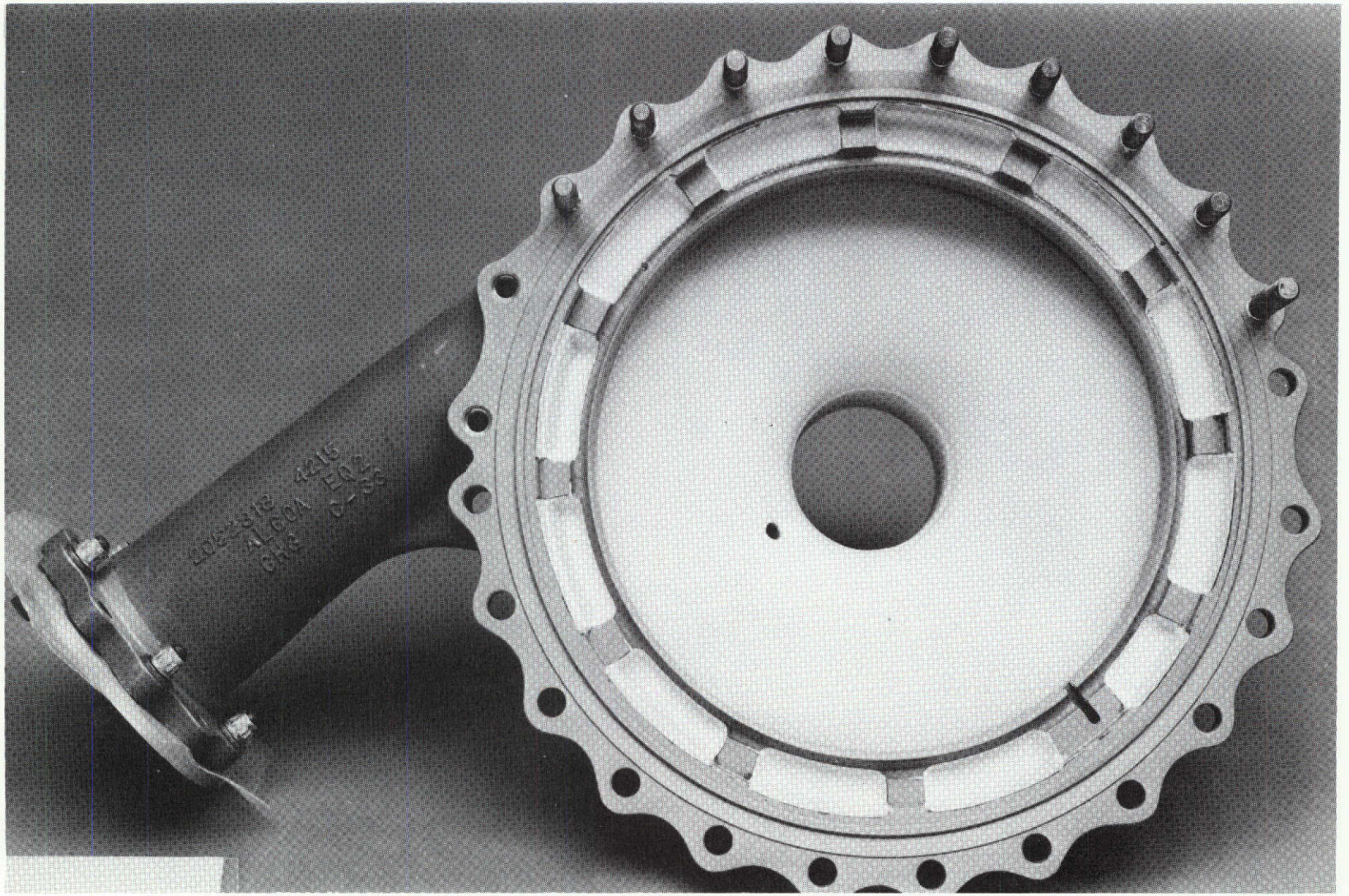

1XY52-11/15/72-C1A

Figure 118. Turbopump Front Housing With KX-635 Coating, Pretest

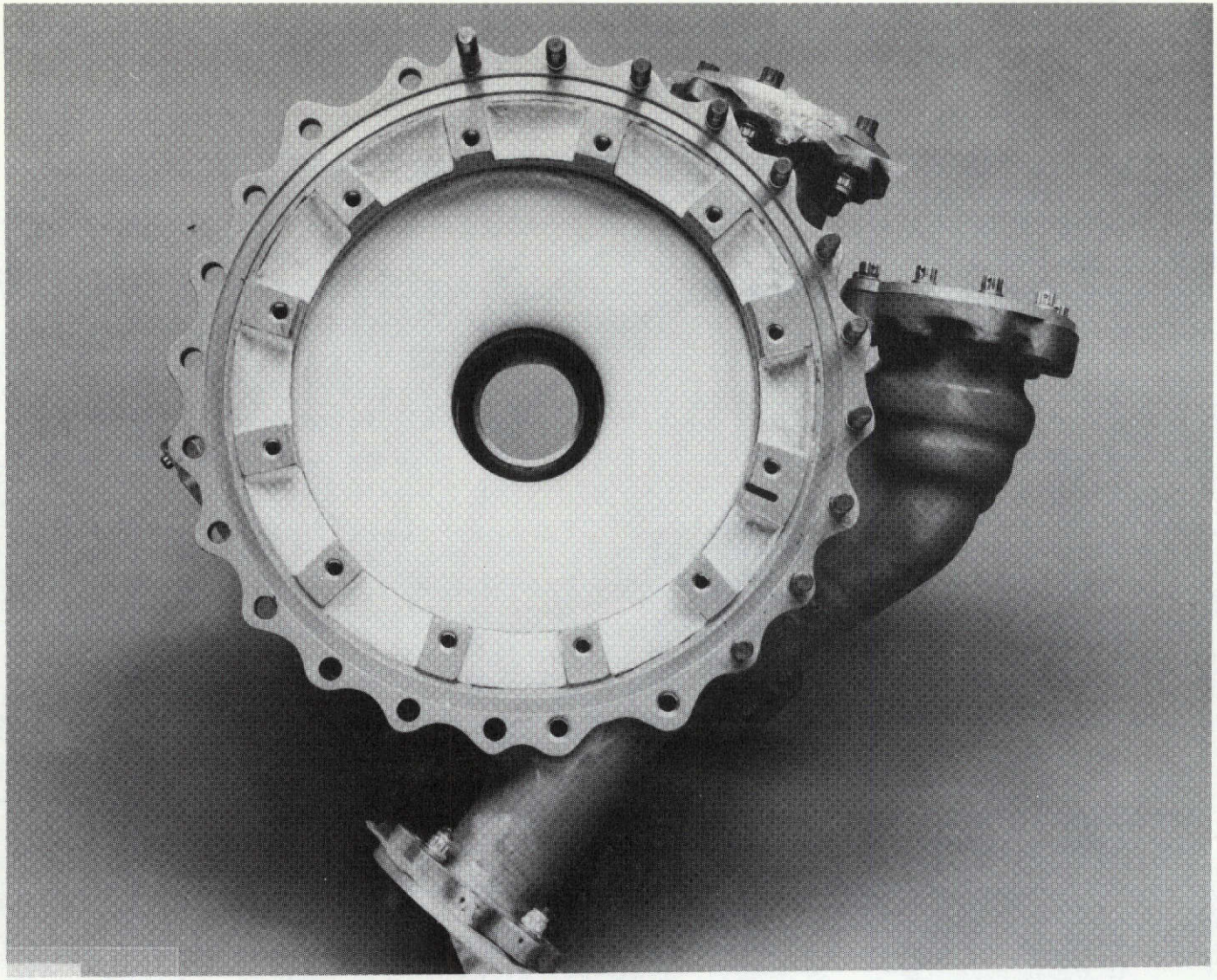

1XY52-11/15/72-C1B

Figure 119. Turbopump Rear Housing With KX-635 Coating, Pretest

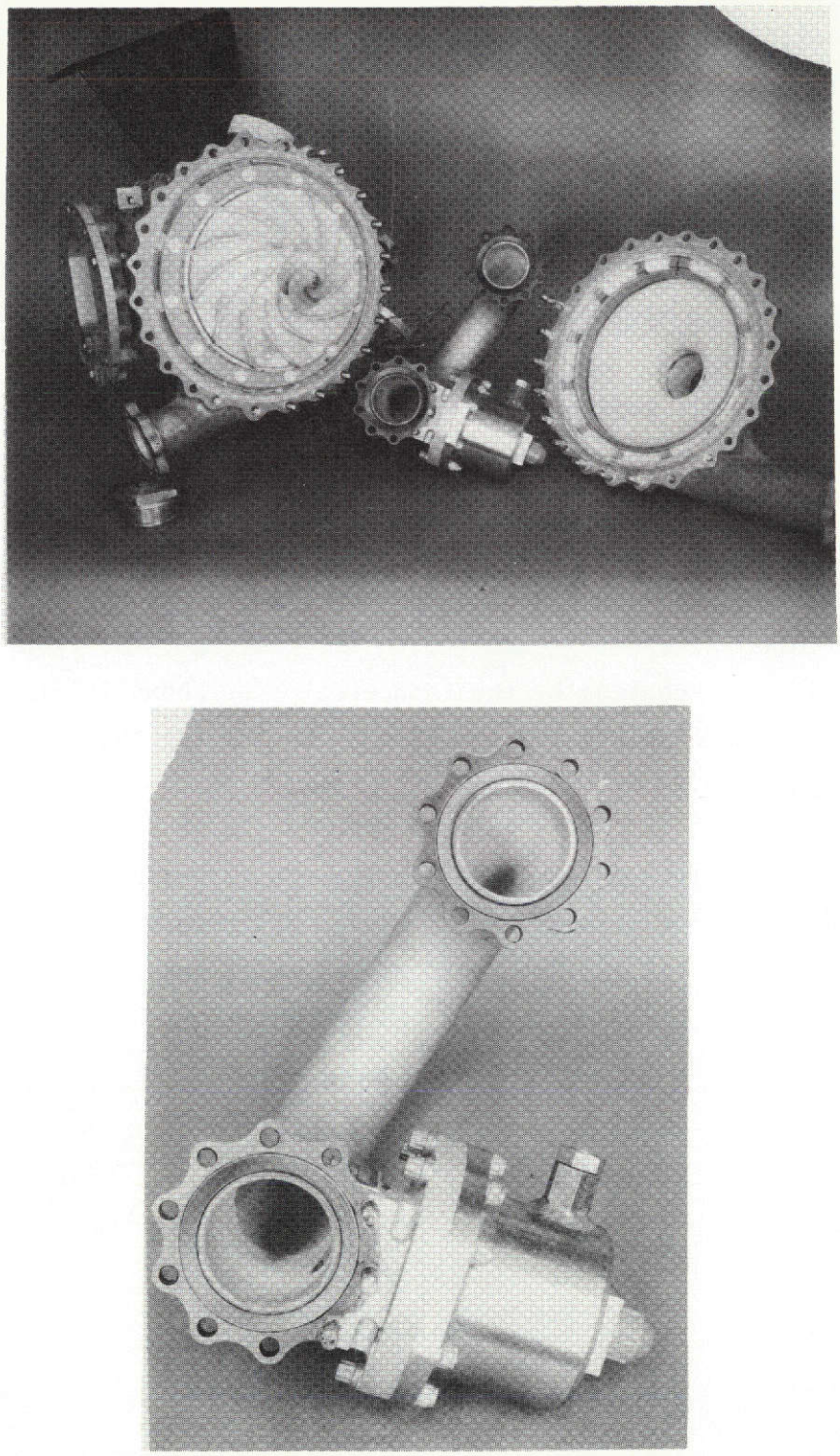

Figure 120. RL-10 Turbopump and Crossover Line With KX-635 Coating, Posttest

had the best coating adhesion. The few places where the coating did erode and lost adhesion were in the bellows of the inlet line and the blade tips of the first-stage impeller. Flakes of coating that were loose from the inlet line had a thickness of 0.013 m (0.5 in.). The shape of the flakes indicated that the coating did not flow between the bellows grooves and stagnated in the bellows sections during the fill-and-drain operation. The straight portions of the line showed no evidence of coating-adhesion loss.

The blade tips of the first-stage impeller exhibited evidence of erosion, as shown in Fig. 121. This erosion appears to be caused by cavitation. This is not surprising since two-phase flow and a breakdown in developed head occurred during five of the start tests at speeds in excess of 3140 rad/s (30,000 rpm). Some of the aluminum anodizing was also removed from the blade tips by erosion. The face of the impeller showed no damage to the coating. The front housing exhibited rubbing of the coating by the inducer tip, as shown in Fig. 122. Inspection of the inducer-blade tip showed that one of the three blades had rubbed with the coating.

The ability of a properly-applied KX-635 coating to withstand the rigors of LH_2-turbopump service has been demonstrated. Designing parts with no sharp bends or unusual configurations will facilitate coating application, adhesion, and thickness control.

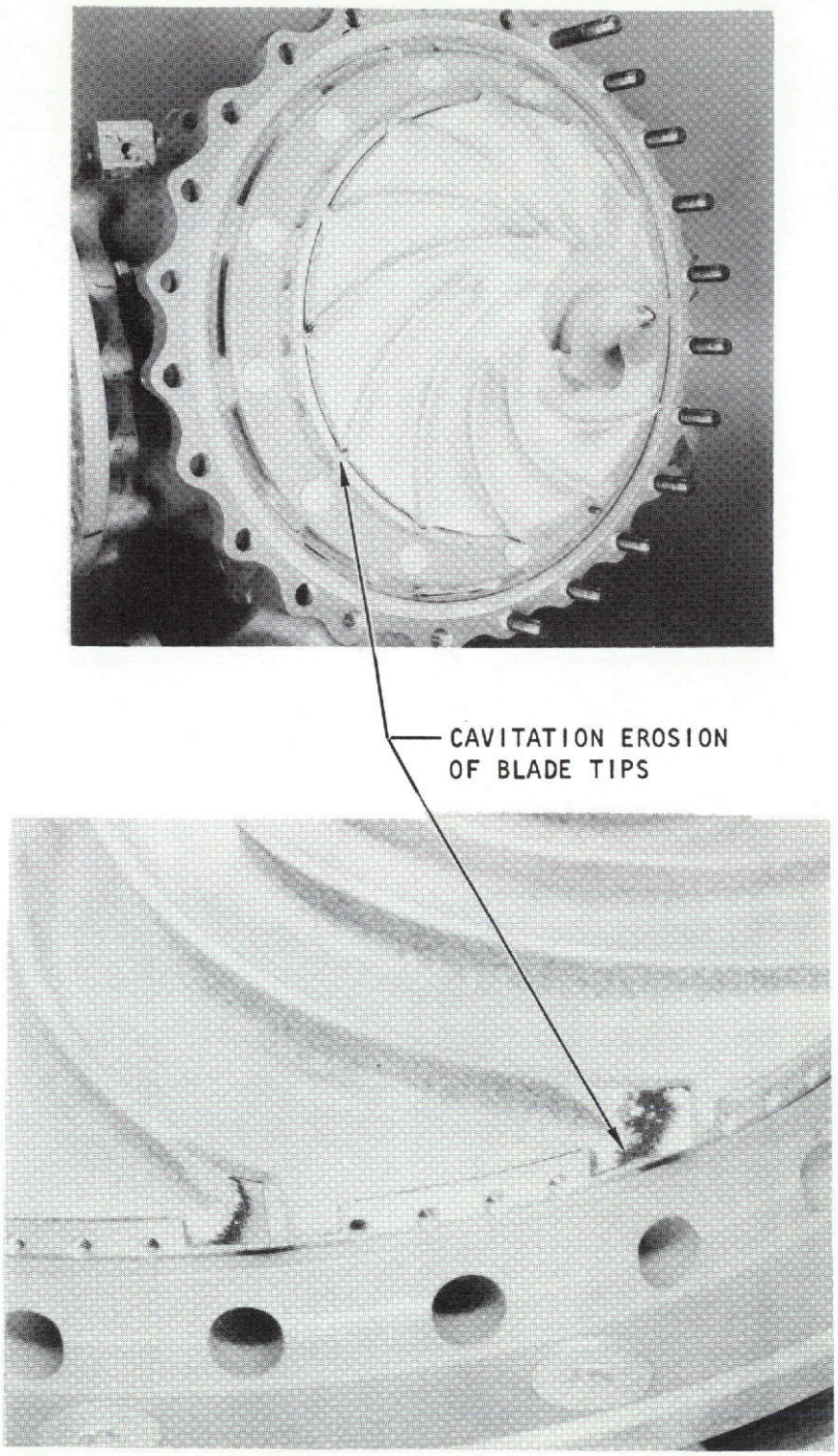

Figure 121. First Stage Impeller With KX-635 Coating, Posttest

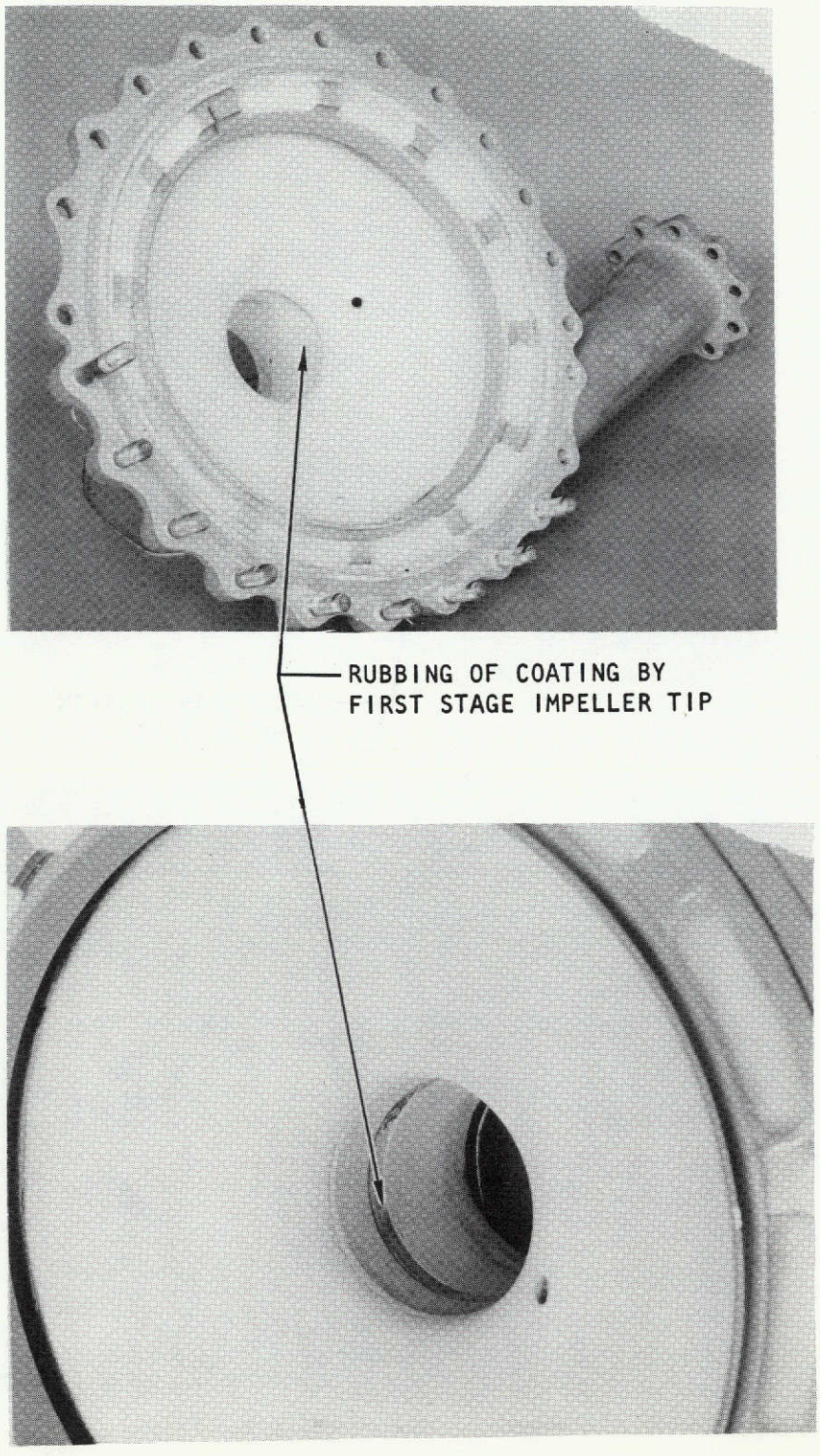

Figure 122. Front Housing With KX-635 Coating, Posttest

TASK III: UNCOATED FEED SYSTEM TESTS

A test facility was constructed for testing an experimental hydrogen feed system. Twenty-three tests were conducted with the uncoated feed system, which consisted of an inlet duct and turbopump. Feed system chill and turbopump start tests were included.

FACILITY AND EXPERIMENTAL FEED SYSTEM PREPARATION

Before testing it was necessary to build the facility test stand, complete with appropriate controls and instrumentation. The test stand was constructed and instrumented to test both the uncoated and coated experimental feed systems under conditions of low flow during chill and high flow during turbopump start. Parallel efforts were also conducted to prepare the uncoated experimental inlet duct and turbopump for installation in the test stand. All of these tasks will be described in the following sections.

Test Facility

The test facility was built in Cell 26C of the CTL-IV area at Rocketdyne's Santa Susana Field Laboratory. The test stand consists of three subsystems. Their functions are: (1) storage and delivery of liquid hydrogen to the experimental feed system, (2) ducting of liquid hydrogen from the pump discharge to the burn stack, and (3) providing gaseous hydrogen for turbine drive power. A schematic of the facility and experimental feed system is shown in Fig. 123.

The storage and delivery subsystem includes a 53 m^3 (14,000 gallons) tank and a duct with a diameter of approximately 0.15 m (6 inches). This duct is connected to three separate flow circuits. One provides a bypass directly to the burn stack and the other two are used for turbopump start and chill tests. Separate ducts are provided for these tests to acquire accurate measurements during high and low flow conditions. Immediately downstream of the facility inlet ducting is a bypass to the burn stack. This circuit is necessary to allow chilling of

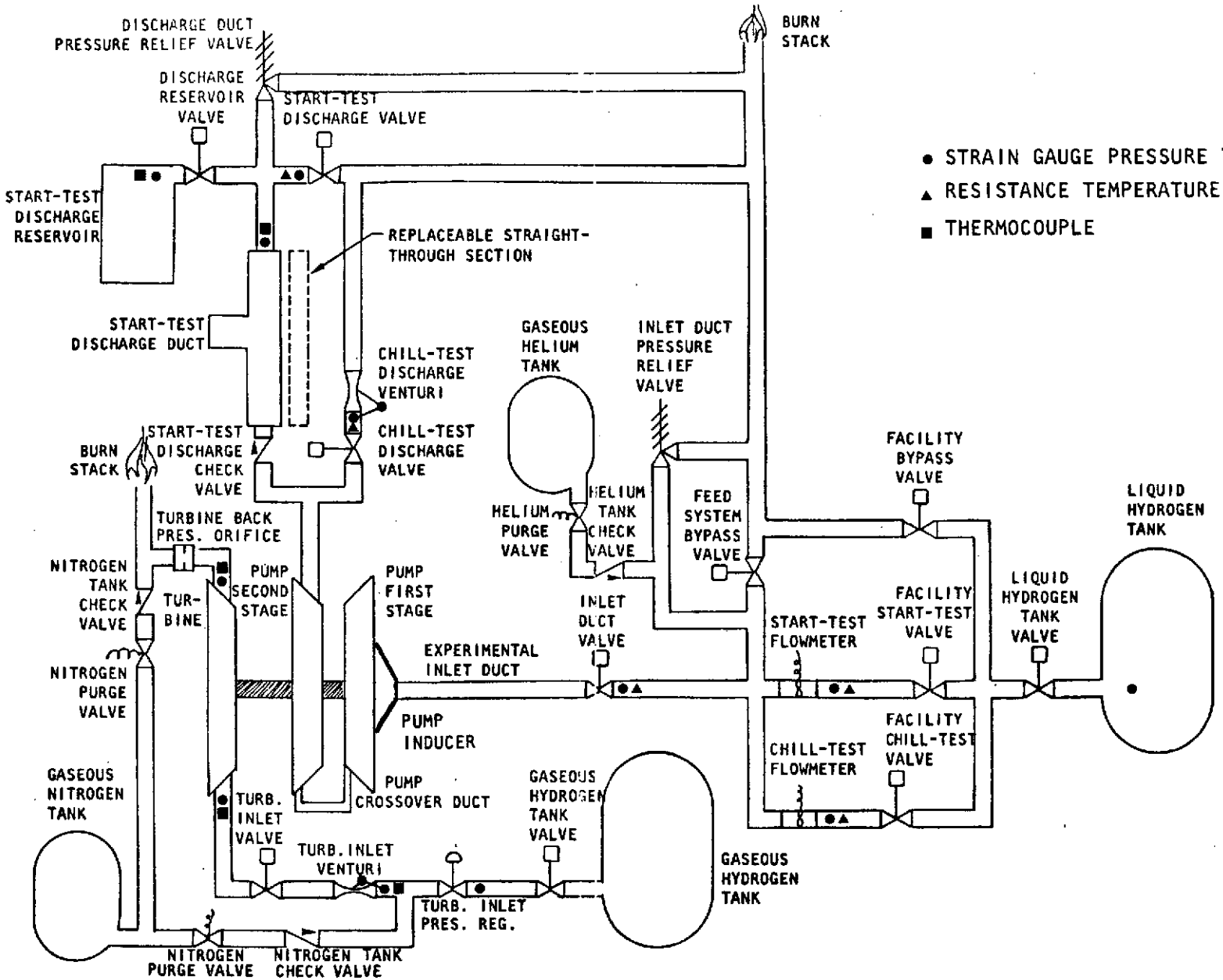

Figure 123. Schematic of Facility and Experimental Feed System

the facility inlet ducting before turbopump start and chill tests are conducted. The approximate diameters of the bypass, chill-test, and start-test ducts are 0.025, 0.051, and 0.10 m (1, 2, and 4 inches), respectively. The burn stack is approximately 0.15 m (6 inches) in diameter.

Instrumentation of the storage and delivery subsystem consists of four strain gage pressure transducers to measure propellant pressures, three resistance temperature bulbs to measure fluid temperatures, and two turbine-type flowmeters to measure liquid flowrates. The locations of these devices are also shown in Fig. 123.

Initially, the start-test liquid hydrogen flowmeter had a redline value of 0.044 m^3/s (700 gpm). The test would be terminated by closing the turbine inlet valve when this volume was exceeded. The redline value was increased during testing, however, because cutoffs were initiated by spikes in the indicated flowrate during rapid-flow acceleration. These spikes were presumably caused by the presence of vapor.

Two parallel ducts are provided between the pump discharge and the burn stack for turbopump start and chill tests. Separate ducts are required to acquire accurate flow data for these two types of tests. The ducting used for the start tests consists of two interchangeable ducts and a reservoir that are used to vary the discharge volume. The duct with a dead-ended branch immediately downstream of the pump is replaceable with a smaller diameter straight-through section, and the discharge reservoir can be closed off with a valve. With this valve closed, the volume between the pump and the start-test discharge valve is 0.0014 or 0.024 m^3 (0.05 or 0.85 ft^3), depending on which of the interchangeable ducts is used. The volume with the discharge reservoir valve open and the stright-through section installed is 0.098 m^3 (3.45 ft^3). The approximate diameters of the straight-through section, the replaceable branched duct, and the reservoir are 0.025, 0.10, and 0.25 m (1, 4, and 10 inches). The final component in the start-test discharge ducting is the discharge valve. This valve is used to vary the discharge resistance and therefore pump operating conditions, and to provide a flow shutoff for deadhead starts.

The discharge ducting used during chill tests has a valve at the entrance, and a venturi for determining vapor flowrates. This ducting is approximately 0.10 m (4 inches) in diameter.

Instrumentation in the start-test ducting includes two thermocouples, a resistance temperature bulb, and three strain gage pressure transducers for determining propellant conditions. The chill-test ducting includes a resistance temperature bulb and two strain gage pressure transducers, one of which measures the venturi differential pressure.

The turbine drive system includes a supply of gaseous hydrogen, a pressure regulator, and a flow-measuring venturi. The turbine exhausts to near ambient pressure and the flow is ducted to the burn stack. The inlet and discharge ducts are approximately 0.051 and 0.15 m (2 and 6 inches) in diameter. The turbine inlet ducting is instrumented with two thermocouples to determine fluid temperatures. Pressures are determined with four strain gage transducers, one of which measures the venturi differential pressure. The turbine discharge is instrumented with a thermocouple and a strain gage pressure transducer to determine fluid conditions. The redline value on turbine inlet pressure is 4.2×10^6 N/m^2 (615 psia). If this value is exceeded, the turbine inlet valve is closed and the test terminated.

Experimental Inlet Duct

The inlet duct used in the uncoated experimental feed system was supplied by NASA, and was manufactured by Convair Aerospace Division of General Dynamics for the Centaur stage. This duct is approximately 0.089 m (3.5 inches) in diameter and 1.7 m (5.5 feet) long. In order to install wall-temperature instrumentation, it was necessary to remove the external insulation (Fig. 124). Seven copper-constantan thermocouples were then mounted on the external surface of the duct to measure thermal transients during chill tests. The precise locations of these thermocouples are also shown in Fig. 124. When the duct was positioned in the test facility, the thermocouples were on the underneath side. Before installation, the duct was covered with 0.025 m (1 inch) polyurethane foam and a layer of aluminum tape.

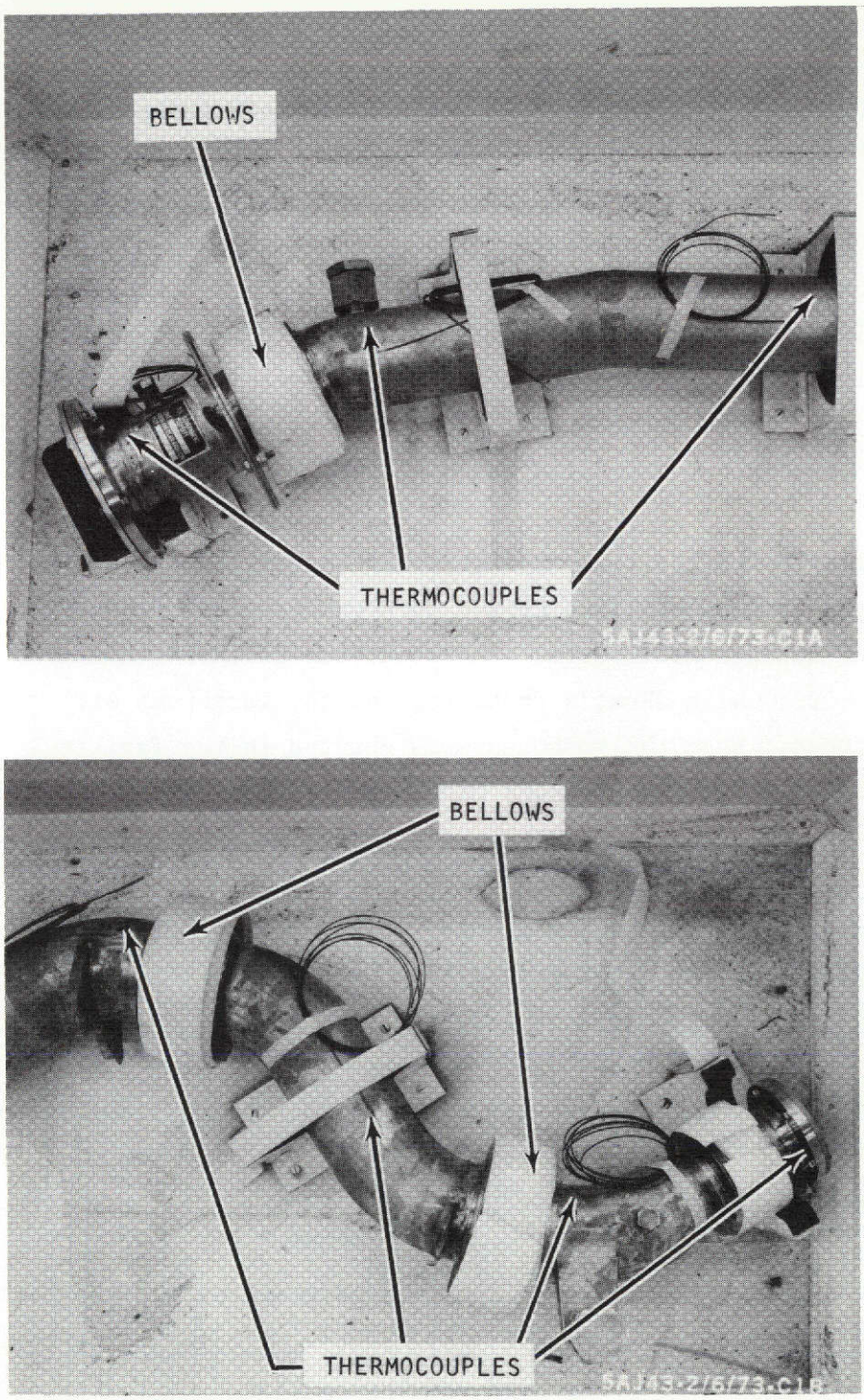

Figure 124. Locations of Surface Thermocouples on Experimental Inlet Ducts

Experimental Turbopump

The turbopump used in the experimental feed system was supplied by NASA and manufactured by Pratt and Whitney Division of United Aircraft for the RL-10 rocket engine. The turbopump includes hydrogen and oxygen pumps and a turbine that uses gaseous hydrogen as the drive fluid. The hydrogen pump is powered directly, but the oxygen pump operates at lower speeds and is powered through a set of gears. Since the oxidizer pump was not to be used during testing, NASA removed it along with the gears. A cover plate was fitted to the resultant opening in the turbopump housing, and the hydrogen pump and turbine assembly was dynamically balanced by NASA. The turbine bypass valve was also removed.

Before installation in the test facility, six copper-constantan thermocouples were attached to the external surface of the turbopump to measure thermal transients of the housing during chill tests. The locations of these thermocouples are indicated in Fig. 125, which shows a photograph of the turbopump with the crossover duct disconnected. When the turbopump was mounted in the facility, the thermocouples were on the lower right-hand side, when viewed from a position facing the pump inlet.

A strain gage pressure transducer is used to measure the pump inlet pressure near the inlet flange (Fig. 126). The pump inlet resistance temperature bulb, used to measure inlet hydrogen temperature, is inserted in the coupling between the inlet duct and the pump. Pump interstage propellant conditions are made in the adapter near the crossover duct flange at the inlet to the second stage of the pump. This location corresponds to where the bleed valve is normally located. The bleed valve had been removed by NASA for this contract.

The pump discharge propellant conditions are also measured with a resistance temperature bulb and strain gage pressure transducer. These measurements are made in the short adapter between the pump and the discharge duct (Fig. 127). The pump pressure rise is determined with a strain gage pressure transducer that measures the difference between the inlet and discharge pressures. Turbopump

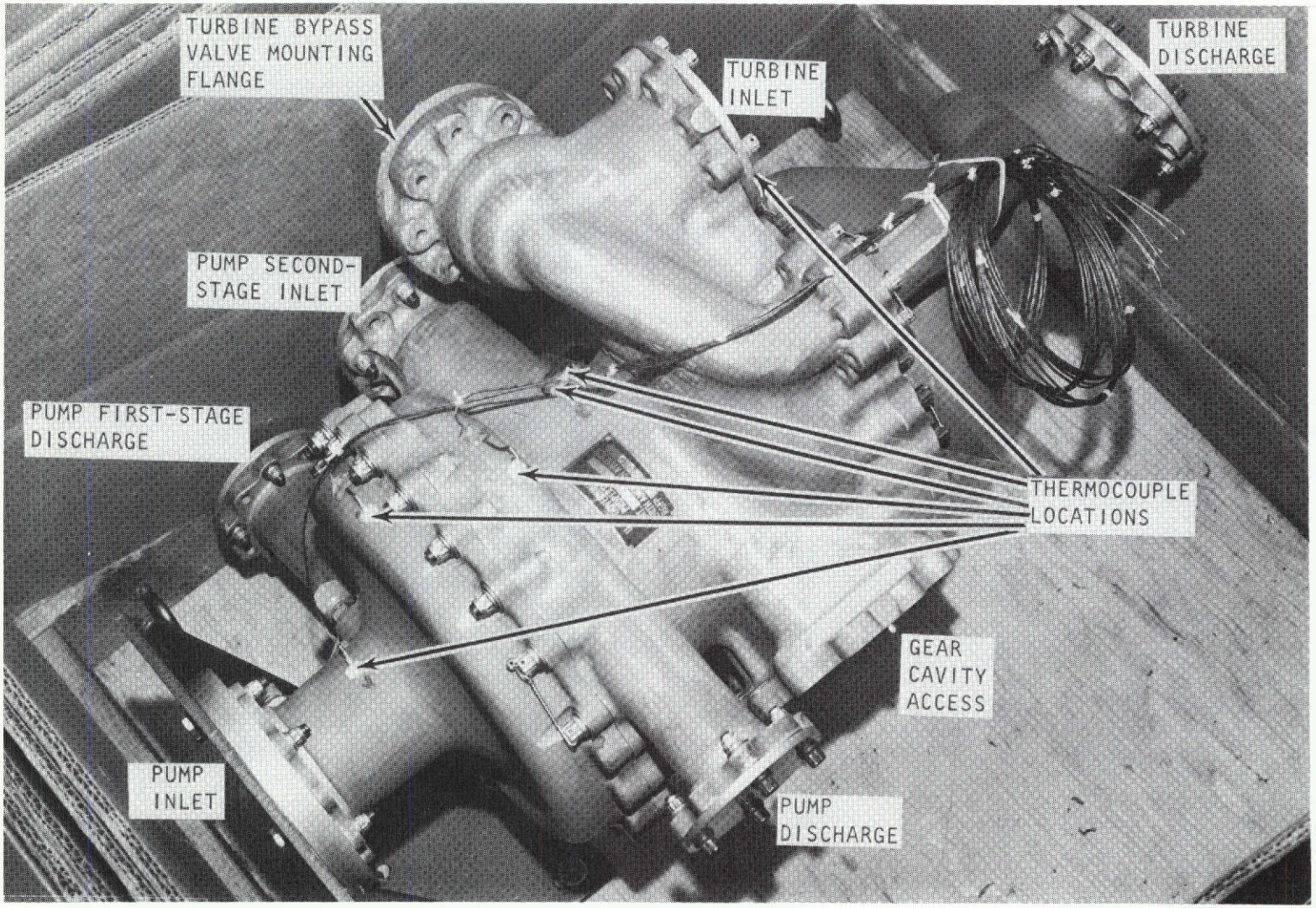

5AJ48-2/6/73-C1C

Figure 125. Locations of Surface Thermocouples on Experimental Turbopumps

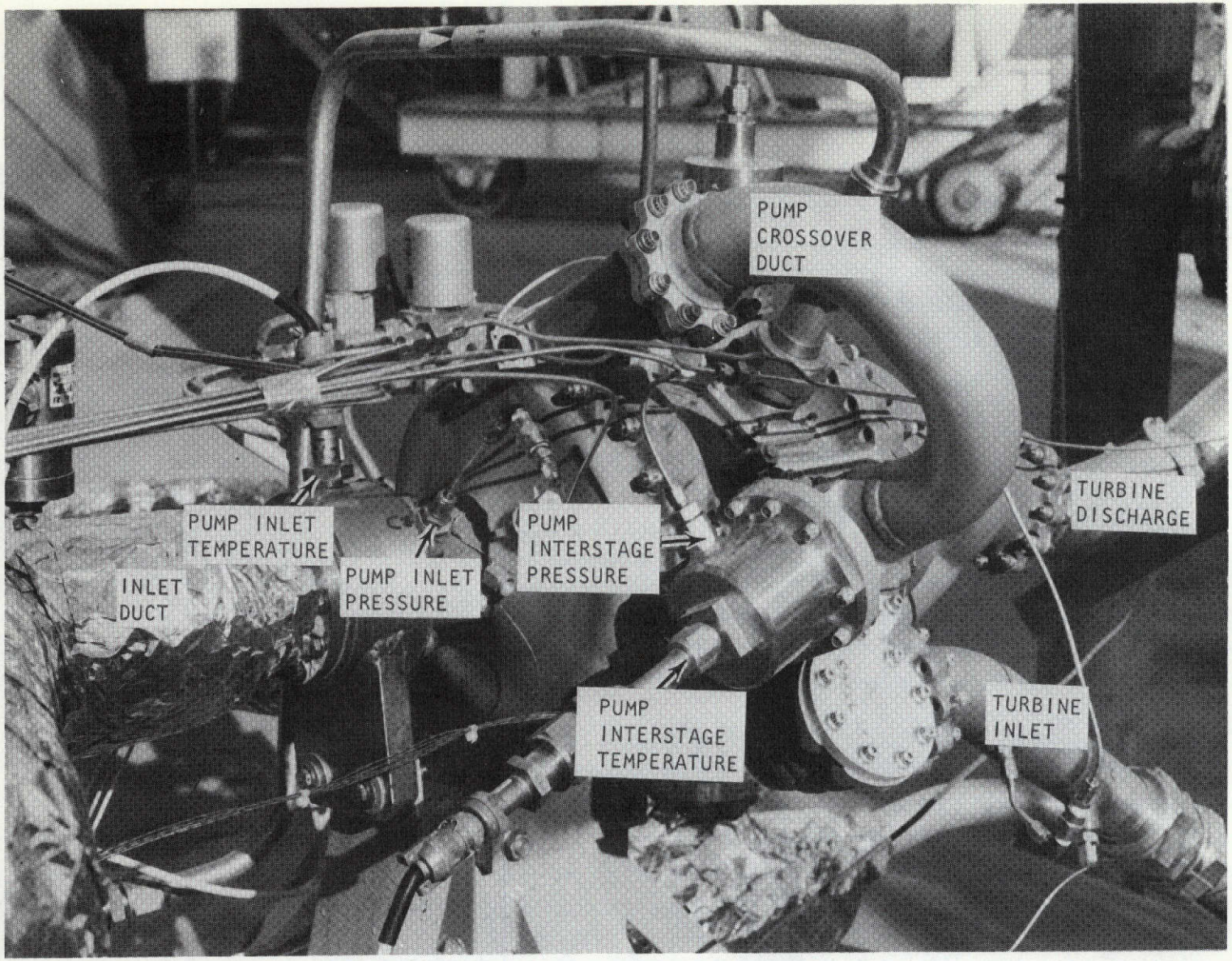

1XY53-4/10/73-S2A

Figure 126. Locations of Pump Inlet and Interstage Propellant Measurements

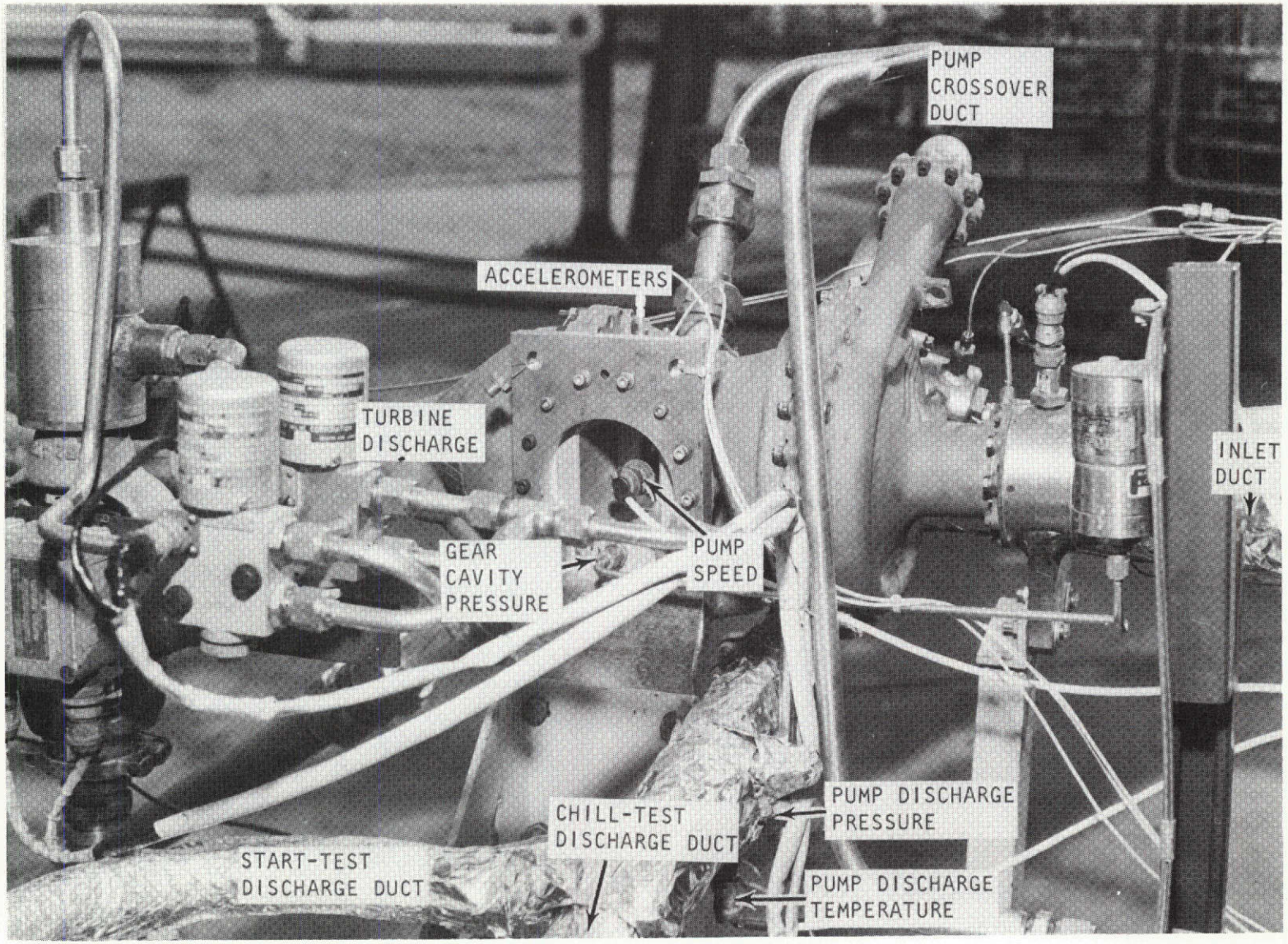

1XY53-4/10/73-S1D*

Figure 127. Locations of Turbopump Measurements

vibrations are measured with accelerometers mounted in all three spatial directions on a fixture near the cover plate where the oxygen pump was removed. Pressure within the gear cavity was measured with a strain gage pressure transducer. The final sensor mounted on the turbopump is a magnetic pickup to indicate rotational speed by counting the gear teeth on the rotating drive shaft.

In addition to the previously mentioned redline values on inlet duct flow and turbine inlet pressure, six redlines were established on other turbopump parameters. All of these limits activate closing of the turbine inlet valve to prevent hardware damage during turbopump rotation tests. Initially, maximum limits of 7.9 x 10^5 N/m^2 (115 psia) on pump inlet pressure, 7.0 x 10^6 N/m^2 (1015 psia) on pump discharge pressure, 3.1 x 10^5 N/m^2 (45 psia) on gear cavity pressure, 3140 rad/s (30,000 rpm) on turbopump speed, 23 K (41 R) on pump inlet temperature, and 98 m/s^2 (10 g) on turbopump vibration were established. In addition, the pump inlet pressure had a minimum redline value of 3.8 x 10^5 N/m^2 (55 psia). The limit on gear cavity pressure was increased during testing for reasons discussed later.

Two views of the completed facility with the experimental feed system installed are shown in Fig. 128 and 129. Major components are identified in these photographs.

TEST PROCEDURES

Two basic test procedures were used depending on whether the purpose of the test being conducted was to obtain feed system chill or turbopump start data. These two sequences are described in the following sections.

Feed System Chill Tests

The chill-test procedure is initiated with pressurization of the liquid hydrogen storage tank. Before any hydrogen is allowed to flow through the experimental feed system during a chill test, it is necessary to chill the facility ducting between the liquid hydrogen tank and the inlet duct valve. Except for one of the

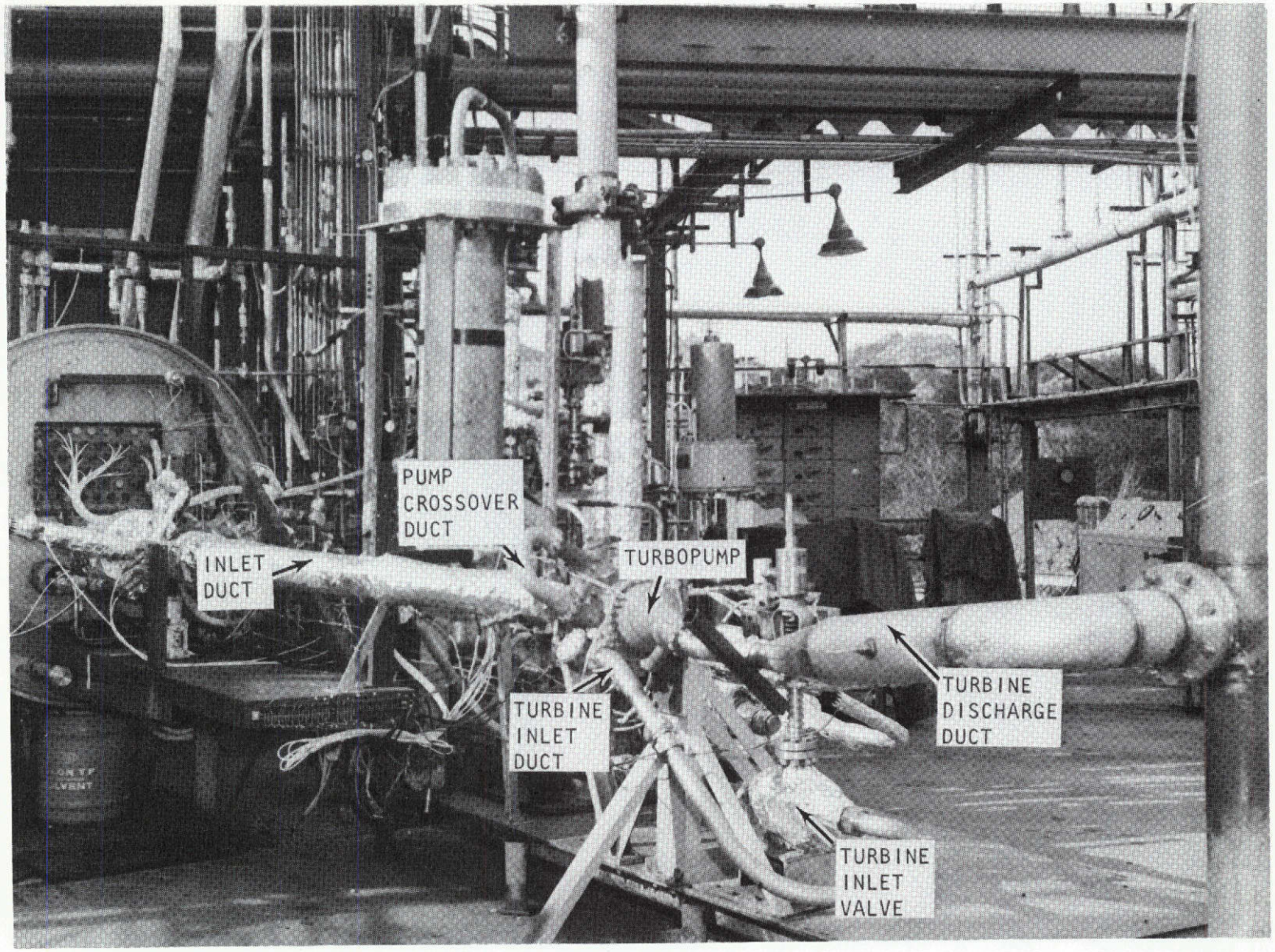

1XY53-4/10/73-S1C*

Figure 128. Left View of Facility and Experimental Feed System

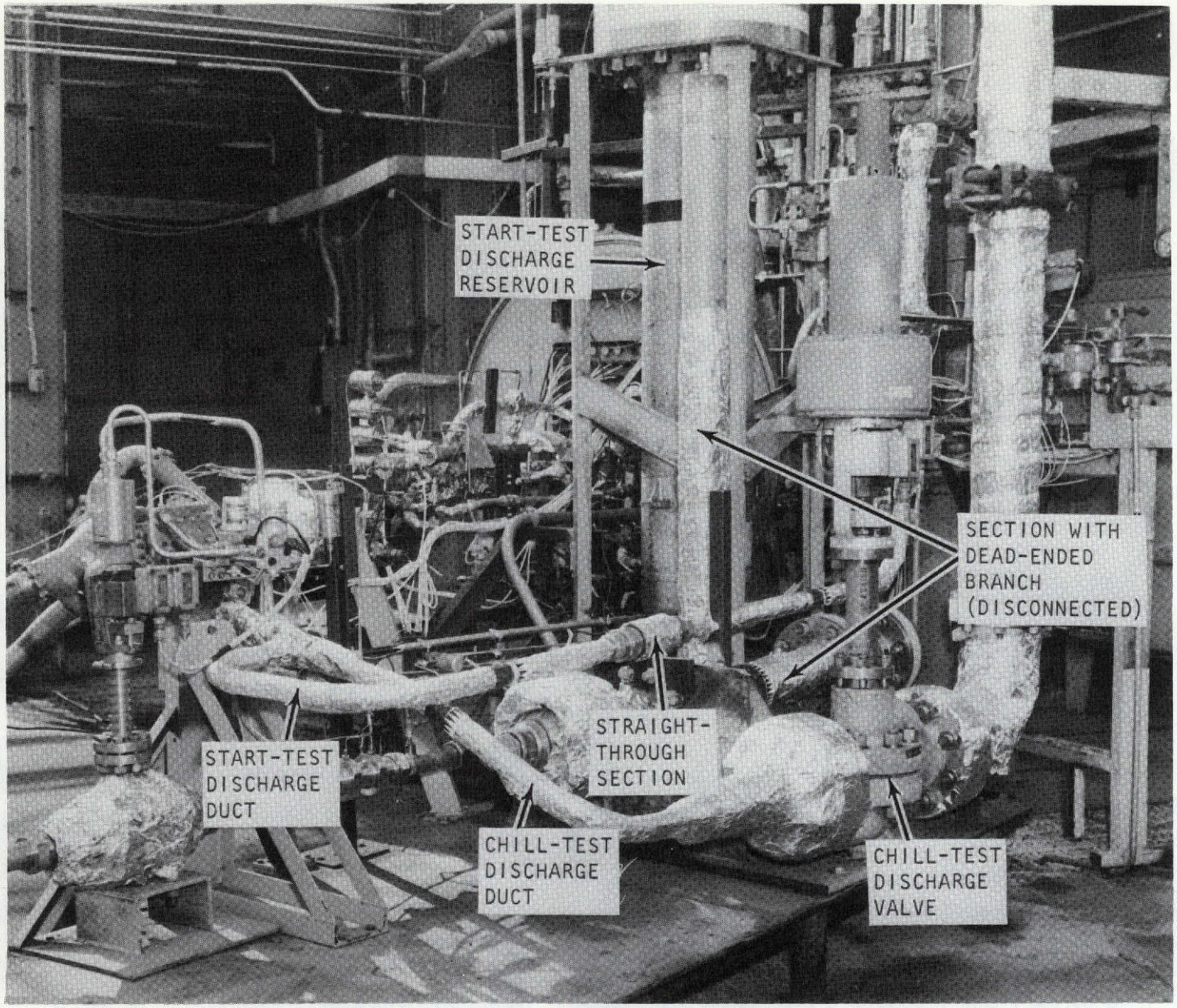

1XY53-4/10/73-S1B*

Figure 129. Right View of Facility and Experimental Feed System

chill tests, this was accomplished by opening the appropriate facility valves to allow flow (Fig. 130). After chilling the facility ducting, the chill-test discharge valve and the inlet duct valve are opened and the feed system bypass valve is closed. Hydrogen then flows through the inlet duct and pump (Fig. 131) and transient data is recorded.

The exception noted in the previous paragraph, with respect to chilling the facility ducting, was required for a special chill test. One of the deadhead turbopump-start tests was to follow a partial chill. Rather than conduct the chill portion of this test with the chill-test ducting and then modulate the appropriate valves in the middle of the test to divert the flow through the start-test ducting, the start-test ducting was used for the chill portion of the test. In order to determine the relative degree of partial chill at initiation of turbopump rotation for this test, a fully-chilled baseline test was conducted. The facility inlet ducting was chilled as shown in Fig. 132. Figure 133 shows the flow schematic for chilling the experimental feed system.

Turbopump Start and Steady-State Performance

Prior to turbopump rotation, the liquid hydrogen storage tank was set at the desired pressure and the facility ducting and experimental feed system were chilled by flowing through the circuit shown in Fig. 134 (with appropriate start-test discharge ducting). The turbine drive system was then pressurized with gaseous hydrogen up to the turbine inlet valve (Fig. 134). If the purpose of the test was a deadhead start, the start-test discharge valve was then closed (otherwise, it is left open at a preset position) and the turbine-inlet valve opened to provide power for turbopump acceleration. During the deadhead start transients, the discharge valve opens automatically when the pump discharge pressure reaches a prescribed value. The flow schematic with the turbopump operating at nominal conditions is shown in Fig. 135. When investigating steady-state pump performance, the discharge valve position was varied to obtain a range of pump operating conditions.

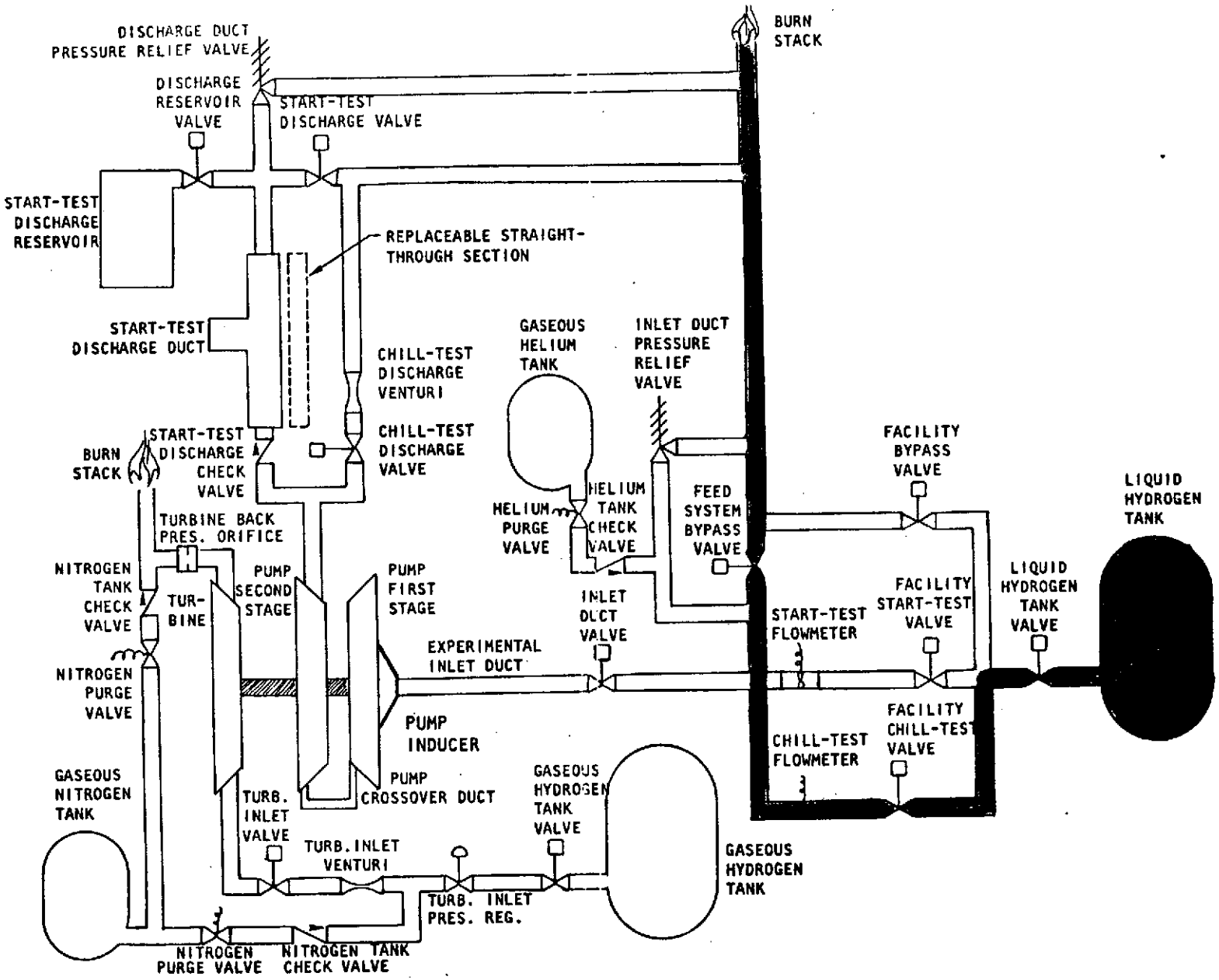

Figure 130. Flow Schematic for Chilling Facility Inlet Ducting Prior to Chill Test

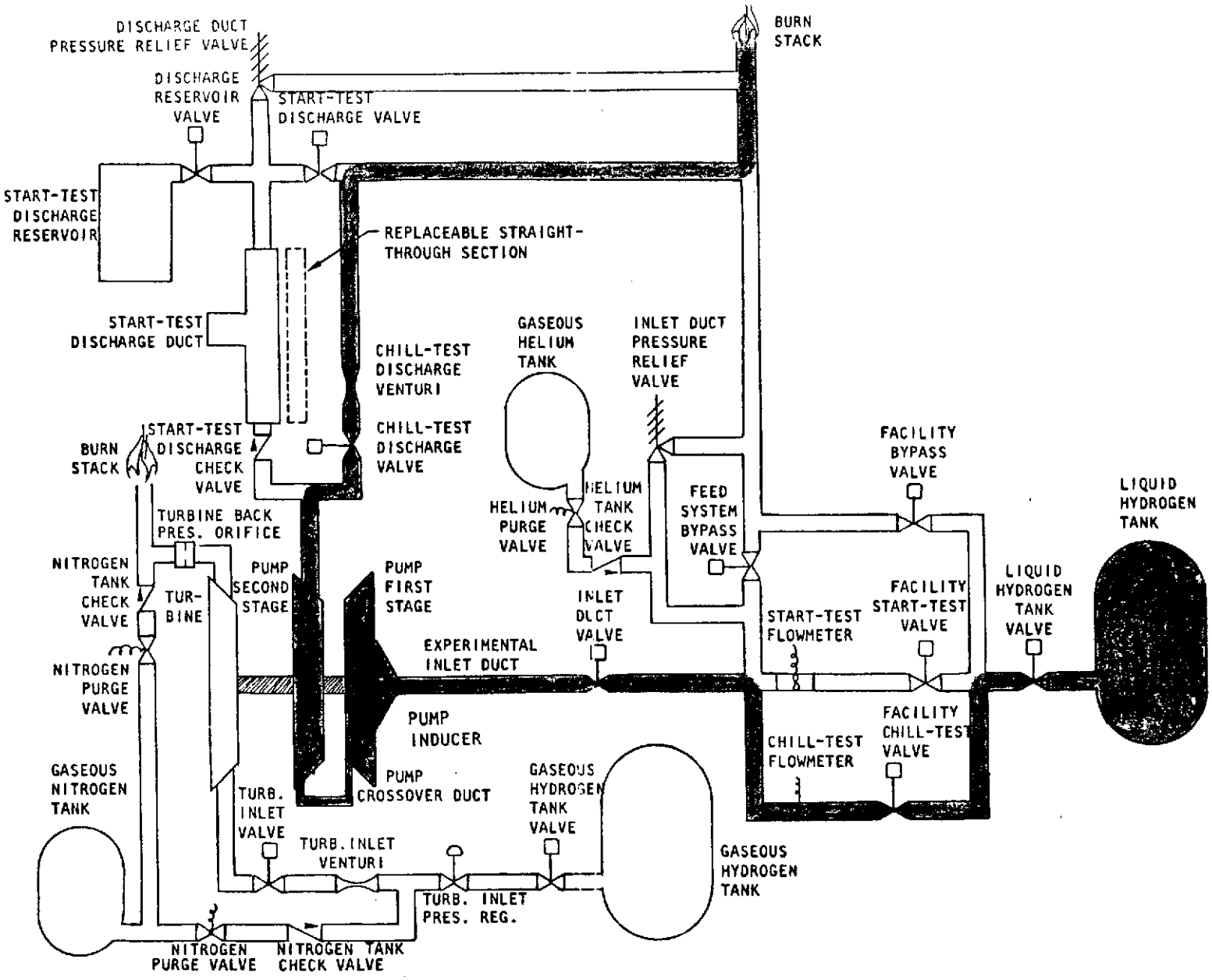

Figure 131. Flow Schematic for Chilling Experimental Feed System During Chill Test

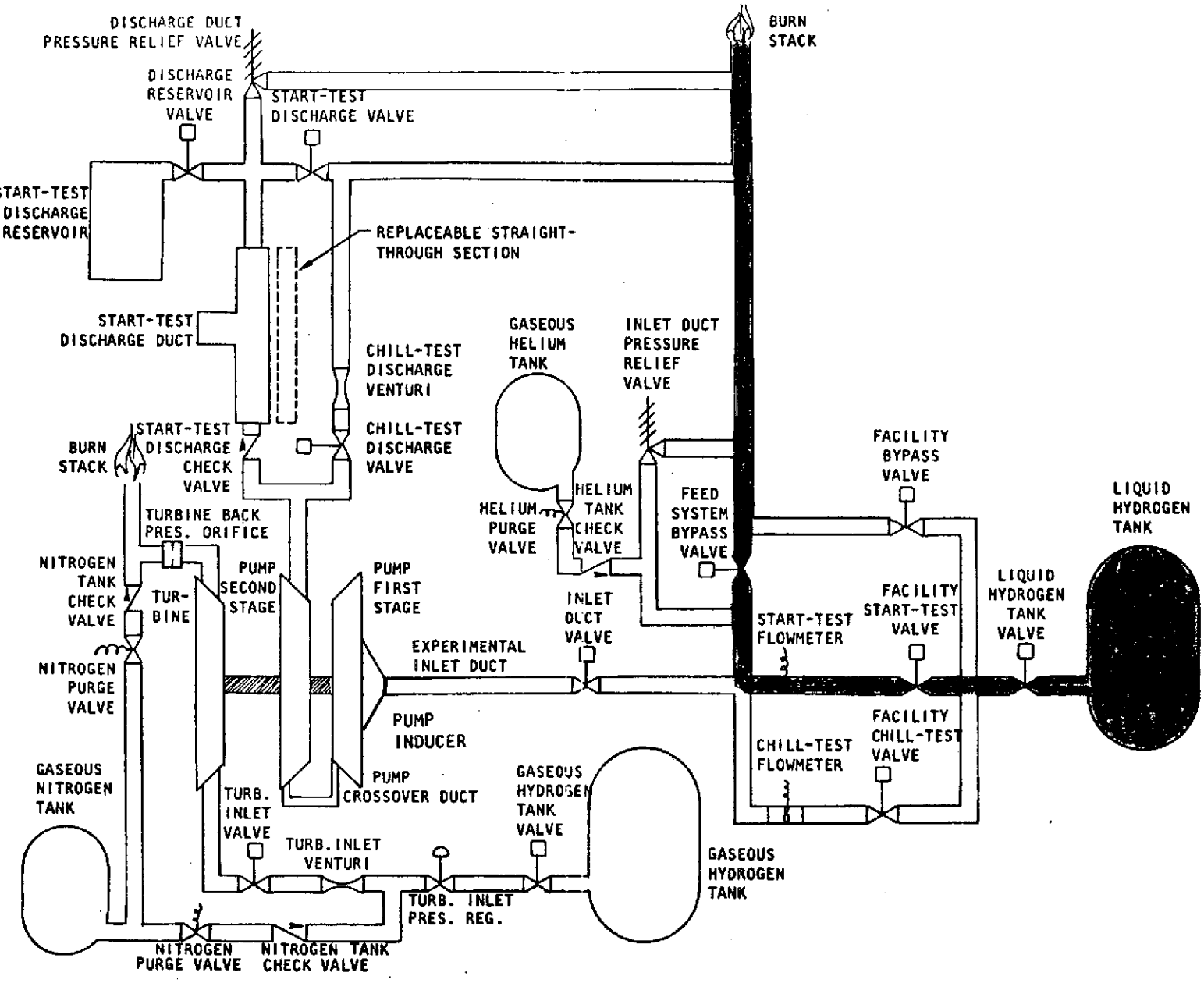

Figure 132. Flow Schematic for Chilling Facility Inlet Ducting Prior to Partially Chilled Deadhead Start Test

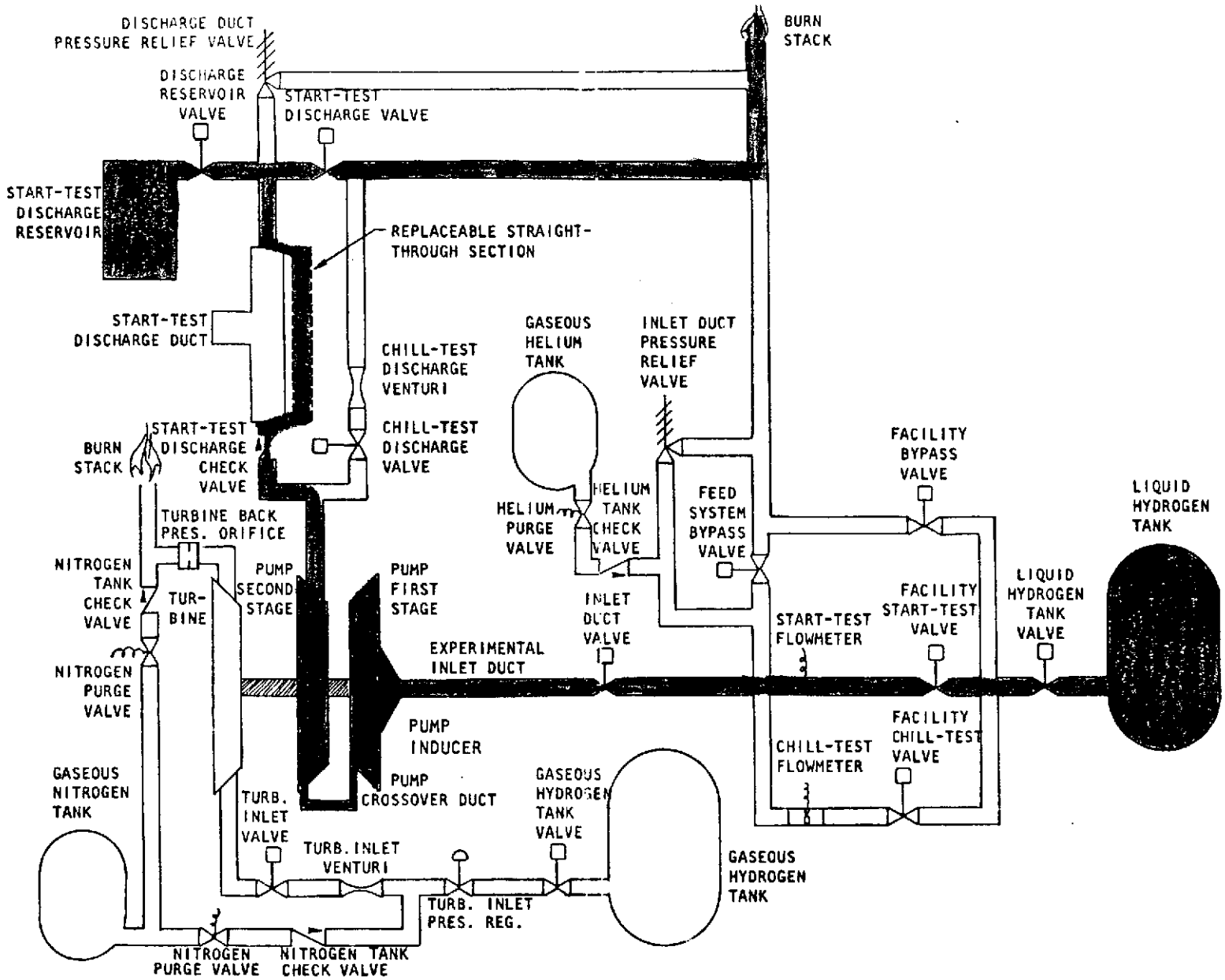

Figure 133. Flow Schematic for Partially Chilling Experimental Feed System Prior to Deadhead Start Test

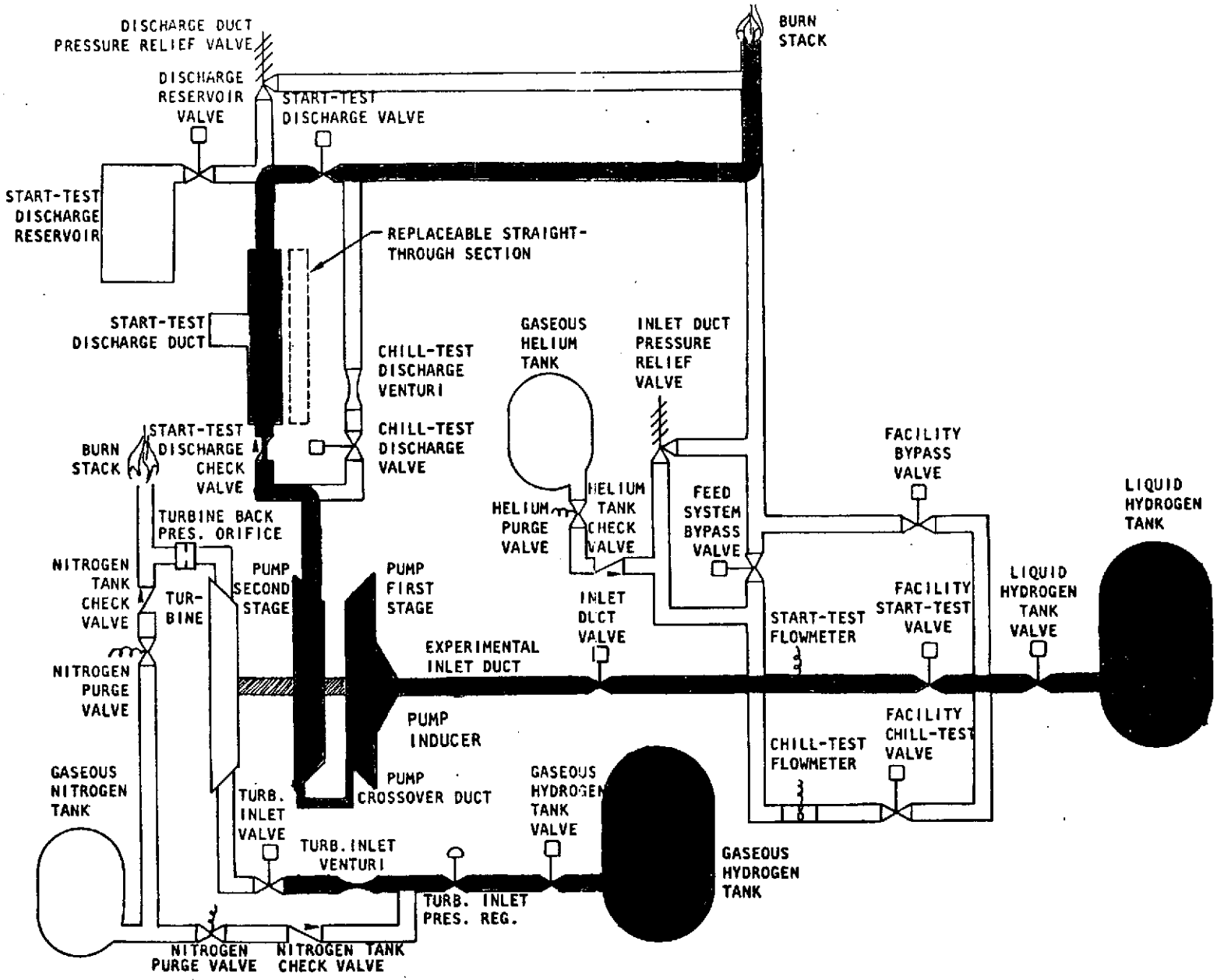

Figure 134. Flow Schematic for Chilling Facility and Experimental Feed System, and Pressurizing Turbine Drive System Prior to Turbopump Start Test

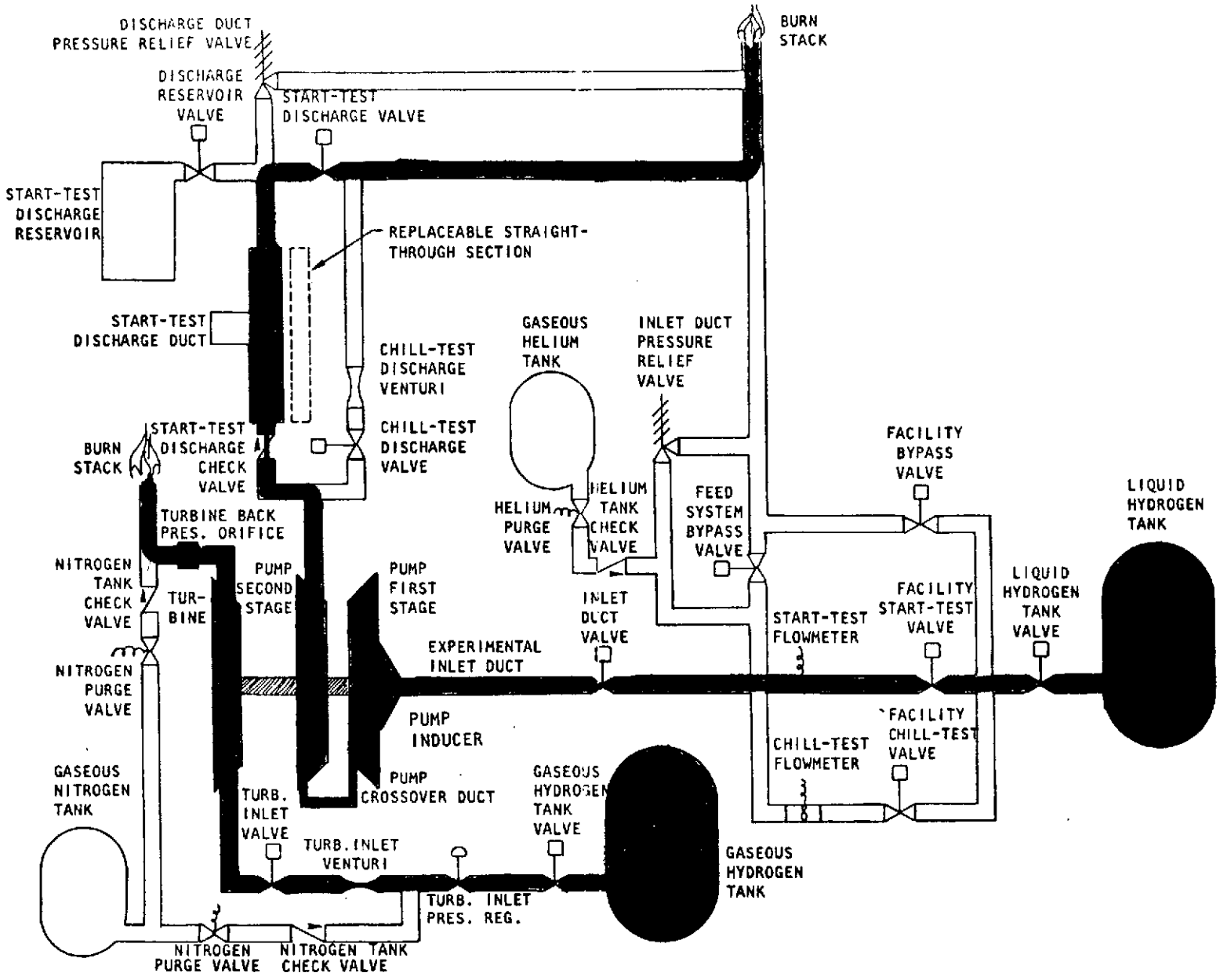

Figure 135. Flow Schematic With Turbopump Operating

DISCUSSION OF RESULTS

Twenty-three tests were conducted with the experimental uncoated feed system. The objectives of these tests were to obtain data on thermal conditioning and deadhead-turbopump start. A list of the tests run is presented in Table 22.

Feed System Chill

In an effort to obtain empirical data that could be used to design and develop liquid cryogen turbomachinery capable of rapid start with minimum thermal preconditioning, a series of chill tests was conducted. The objective of the chill tests was to develop the parametric relationship between chill time and total fluid flow as a function of chill flowrate and fluid pressure.

Analysis of Test Data. Evaluation of the uncoated feed system chill characteristics was accomplished based upon test data from six chill tests; 1, 2, 4, 7, 9, and 13. Four of these tests; 2, 4, 7, and 9 were conducted at constant inlet pressures of 1.93×10^5, 3.38×10^5, 5.17×10^5, and 2.14×10^5 N/m^2 gage (28, 47, 75, and 31 psig) through the chill-test discharge venturi and the chill-test discharge duct. Tests 1 and 13 were conducted under conditions not consistent with the other tests.

Test 1 was the initial system test and was used for checkout of the facility and feed system. The pump inlet pressure was allowed to vary as a function of time from 7.9 N/m^2 to 2.41×10^5 N/m^2 gage (0.11 to 35 psig) over a chill time of 80 seconds to make certain that system pressure limits were not exceeded. The time required to deliver liquid hydrogen to the pump exit was 70 seconds and the total chill weight of hydrogen was 15 kg (33 pounds), which is consistent with the constant inlet pressure tests 2, 4, 7, and 9 in the same facility.

Test 13 was conducted at constant inlet pressure of 4.69×10^5 N/m^2 gage (68 psig), but the chill flow exited through the start-test discharge duct, which included a flow restriction less than 0.2 times the minimum pump area restriction. Chill time continued beyond 200 seconds and data was not complete for the entire chill.

TABLE 22. SUMMARY OF UNCOATED FEED SYSTEM TESTS

Purpose	Test Number	Pump Inlet Pressure, 10^5 N/m^2 (psia)	Start-Test Discharge Valve Trigger Pressure, 10^5 N/ ^{2} (psia)	Discharge Volume, m^3 (ft^3)	Comments
Chill to 100 percent	1	3.4 (50)	NA	NA	Unacceptable data, inlet pressure varied
	2	3.0 (44)			Acceptable data
	4	4.4 (64)			Acceptable data
	7	6.3 (91)			Acceptable data
	9	3.2 (46)			Acceptable data; check repeatability of test No. 2
	13	5.7 (83)	Valve open	0.024 (0.85)	Acceptable data; baseline chill for start test with partial chill
Pump Performance	3	5.5 (80)			Gear cavity pressure cut (conservative redline)
	5	4.8 (70)			Flowrate cut (conservative redline)
	6	4.8 (70)			Inlet pressure cut due to pressure oscillations
	8	5.5 (80)			Acceptable data; low turbine pressure at end of test
Nominal Start Conditions and Overspeed Cutoff Sequence	10	5.5 (80)			Acceptable data; timer cut (set too low)
Nominal Start Conditions	16	5.5 (80)			New turbine gas supply system
Overspeed Cutoff Sequence	11	5.5 (80)			Accelerometer cut
Overspeed Cutoff Sequence	12	5.5 (80)			Discharge pressure cut
Deadhead Start with 100-percent Chill	14	5.5 (80)	3.6 (515)		Breakdown in developed head; overspeed cut
	15		2.9 (415)		
	17		2.2 (315)		
	18		2.2 (315)	0.0014 (0.05)	
	19		2.2 (315)	0.098 (3.45)	Acceptable start
	20		3.6 (515)		Acceptable start
	21		4.2 (615)		Flow cut (conservative redline
	23		4.2 (615)		Acceptable start
Deadhead Start with Partial Chill	22		3.6 (515)		Was 100 percent chilled (did not reach thermal equilibrium before test); flow cut (conservative redline

NA--Not applicable (flowing through chill-test discharge duct)

Because of the variation of inlet pressure during Test 1, and the lack of complete data, and the severe flow restriction of Test 13, chill characteristics of an uncoated feed system were based upon data from Tests 2, 4, 7, and 9.

Schematics of the chill-test system are shown in Fig. 130 and 131 for facility chill before test, and for chill testing for Tests 1, 2, 4, 7, and 9. Test 13 was conducted with the system shown in Fig. 133.

Inlet pressures for Tests 2, 4, 7, and 9 are shown in Fig. 136 and 137 as raw data in the form of reproductions of the actual dynalog charts. Raw flow data for these same tests are presented in Fig. 138 and 139. Reproductions of dynalog charts recorded by the LH_2 chill-test flowmeter are presented in these figures, which are calibrated to indicate a percentage of 0.0158 m^3/s (250 gpm) LH_2 full scale. Conversion to kg/sec (lb/sec) requires m^3/s (gpm) be multiplied by the factor $2.86\ 10^{-7}$ (0.010). The incoming liquid hydrogen at approximately 25 K (-415 F) contacts the inlet duct, pump, and facility discharge hardware at temperatures up to 294.4 K (70 F), resulting in violent vaporization, fluid pressure oscillations, and flow reversal. Inlet pressure oscillations can be readily seen in Fig. 136 and 137. The extreme oscillations indicated by the flow dynalog charts of Fig. 138 and 139 obscure the actual chill flow during these chill tests. Pump fluid inlet and outlet temperatures and flow Brush recording data are reproduced as Fig. 140 through 144 for Tests 2, 4, 7, 9, and 24. Chill flow for these tests as a function of time are shown in Fig. 145, based upon an estimated average of the mean of oscillations recorded on the dynalog charts shown in Fig. 138 and 139. System hardware temperatures and fluid flow, temperature, and pressure data for Tests 1, 2, 4, 7, 9, and 24 are listed in Tables 23 and 24. Hardware and fluid temperatures versus time are presented graphically in Fig. 146 through150 for these same tests. These chilldown test data were analyzed in detail for the purpose of determining the uncoated pump system chilldown characteristics as a function of system inlet pressure and corresponding LH_2 chill flow.

Chill Flow Measurement. Flow and pressure oscillations were observed in all of the tests, especially test 2. Severe pressure and flow oscillations have been

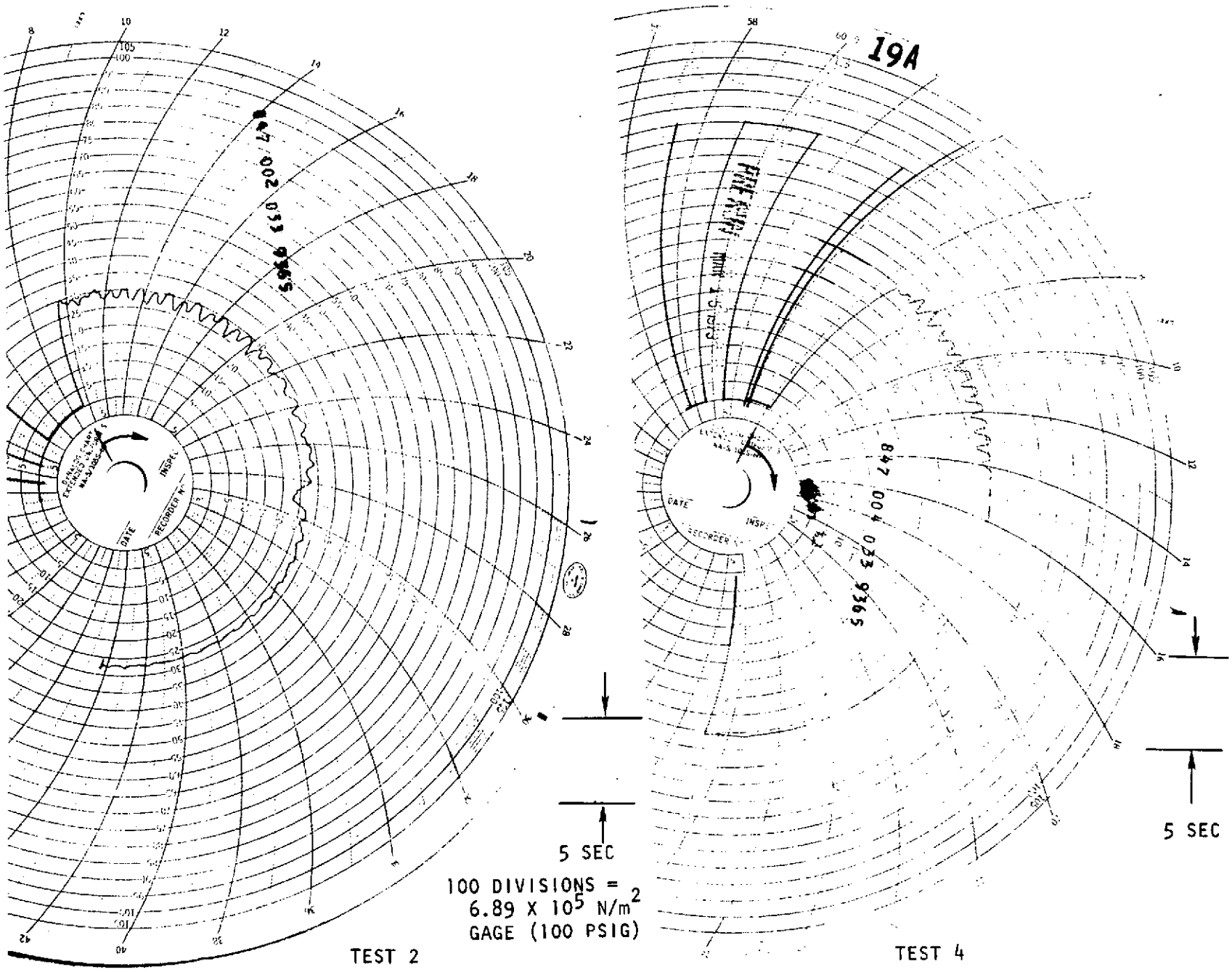

Figure 136. Uncoated System Pump Inlet Pressure Dynalog Data, Tests 2 and 4

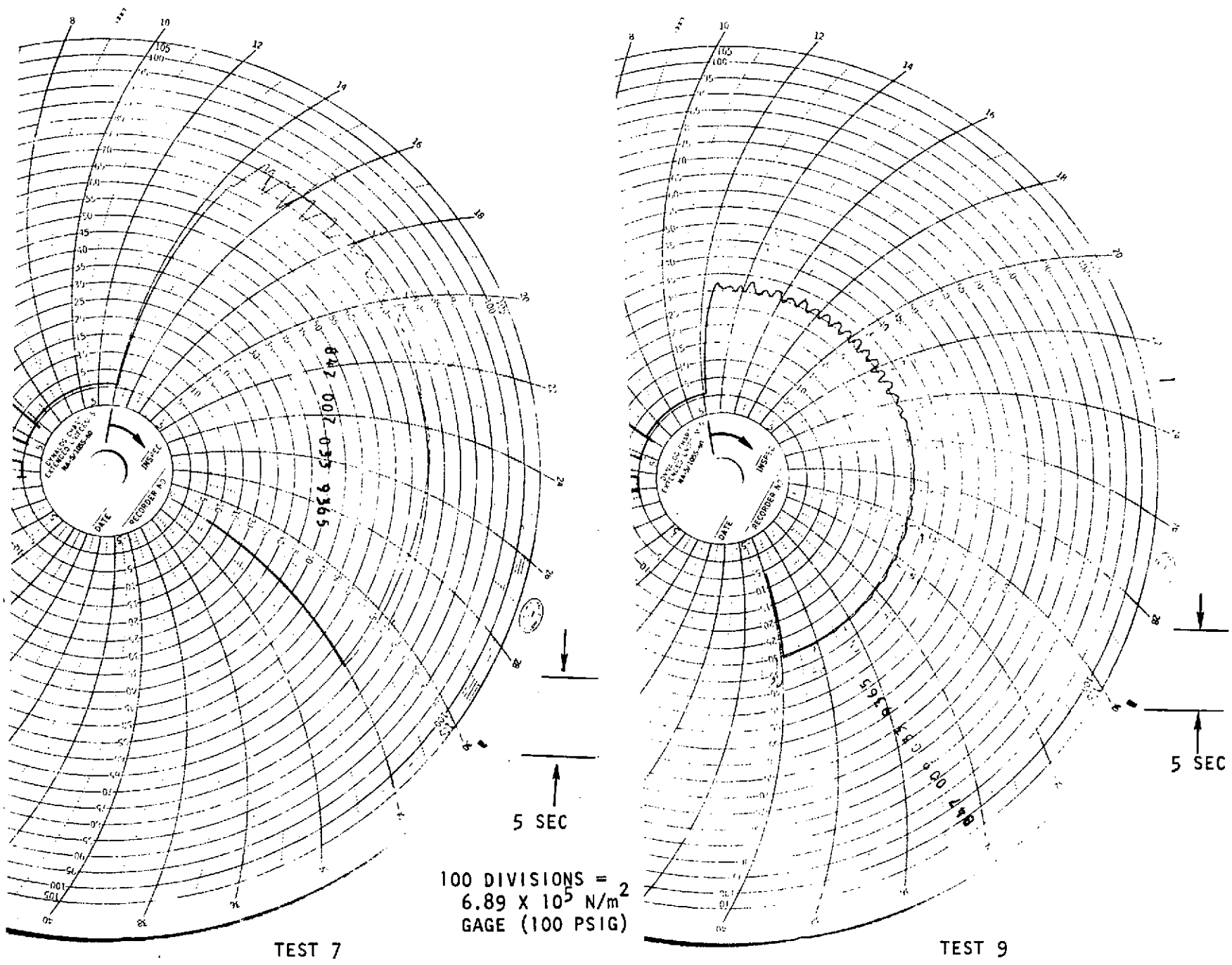

Figure 137. Uncoated System Pump Inlet Pressure Dynalog Data Tests 7 and 9

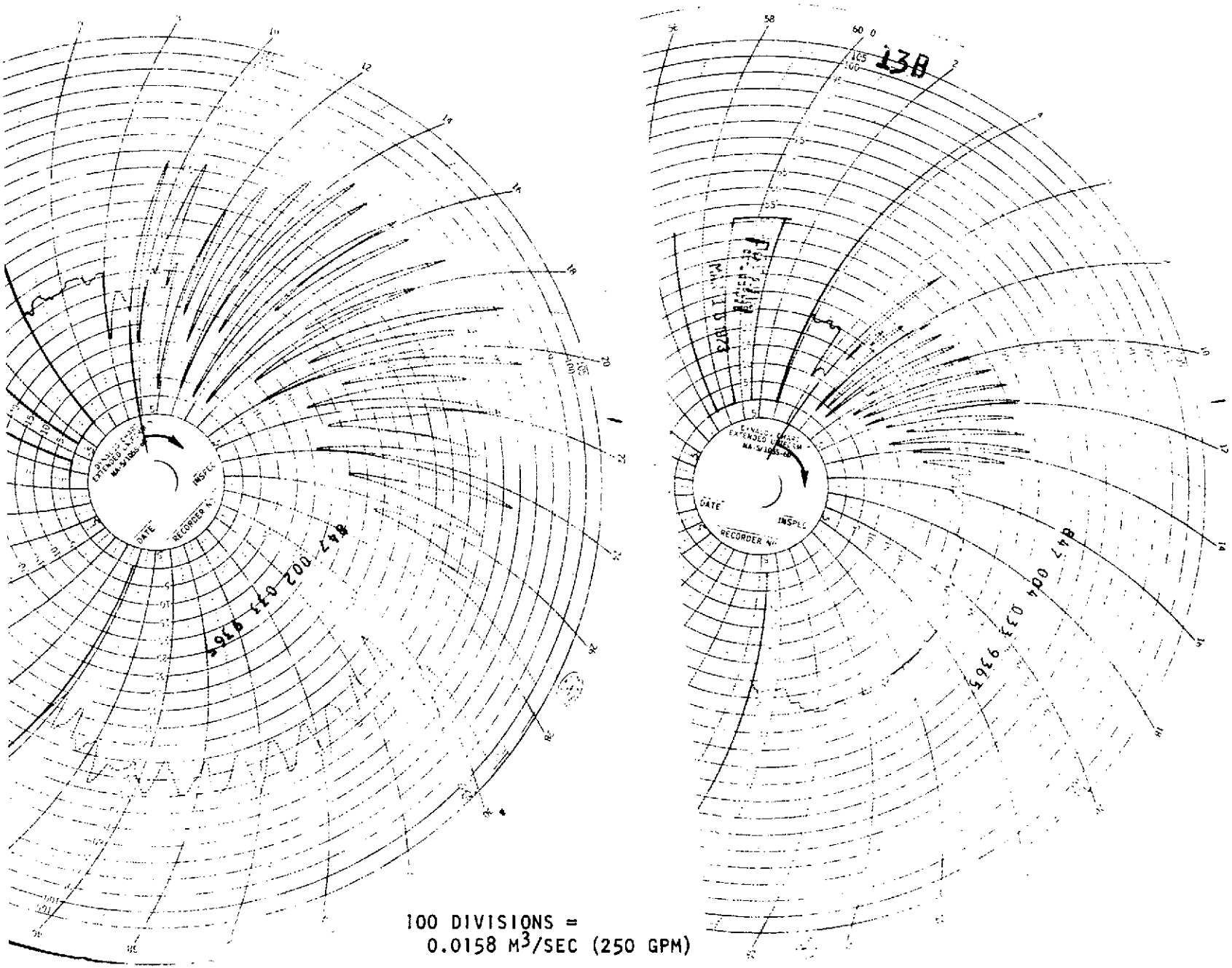

Figure 138. Uncoated System Turbine Flowmeter Flowrate Dynalog Data Tests 2 and 4

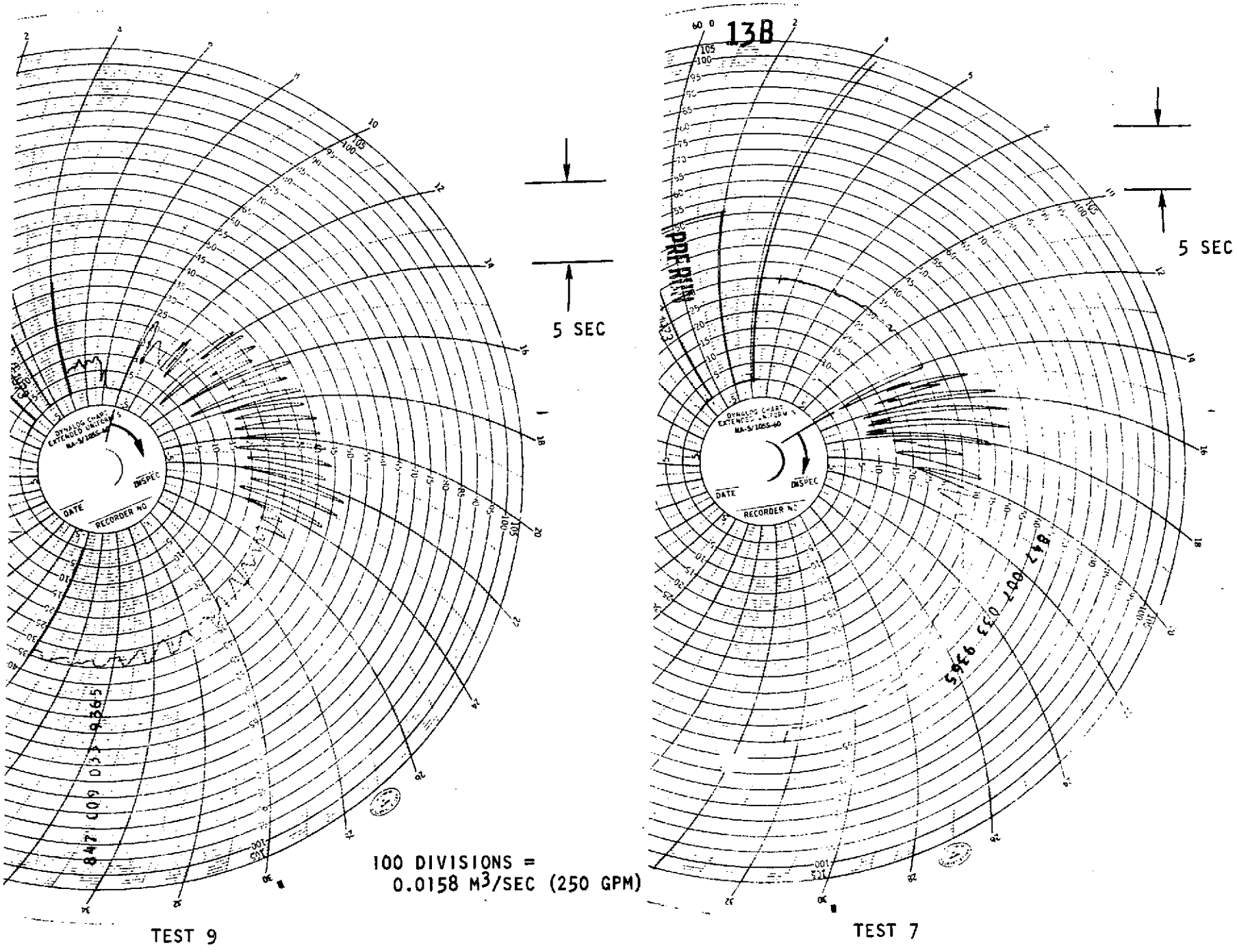

Figure 139. Uncoated System Turbine Flowmeter Flowrate Dynalog Data Tests 7 and 9

Page intentionally left blank

Page intentionally left blank

FOLDOUT FRAME

T_{IN} (FLUID TEMPERATURE AT PUMP INLET)

1 SEC

306 K (550 R)

NONLINEAR

0

FOLDOUT FRAME 2

T_{OUT} (FLUID TEMPERATURE AT PUMP EXIT)

1 SEC

306 K (550 R)

NONLINEAR

0

FLOW (TURBINE FLOWMETER FLOWRATE)

1 SEC

100 DIVISIONS = 0.0158 M^3/S (250 GPM)

Figure 141. Uncoated Pump System Brush Recorded Data, Test 4

FOLDOUT FRAME

FOLDOUT FRAME 2

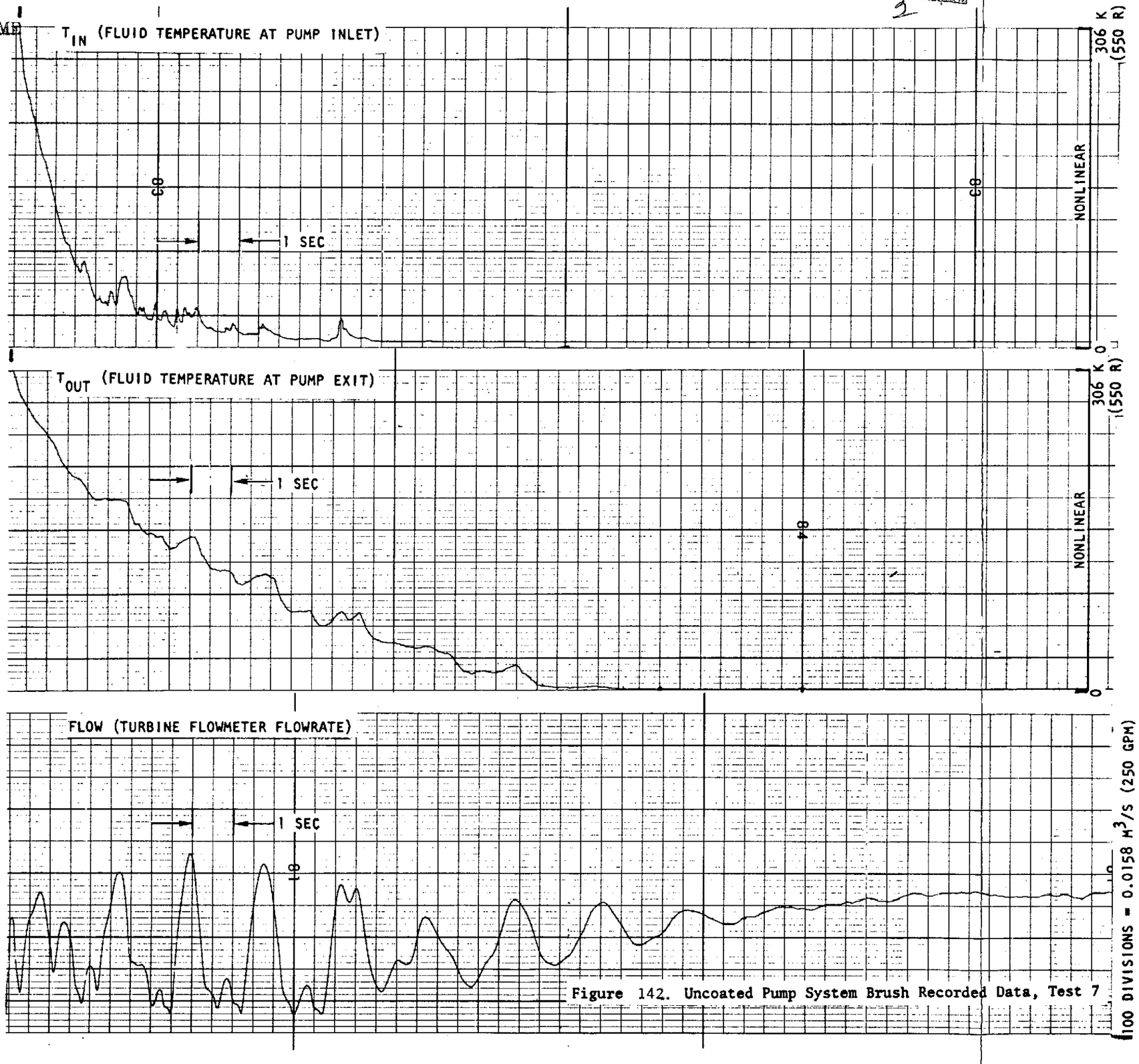

Figure 142. Uncoated Pump System Brush Recorded Data, Test 7

Figure 143. Uncoated Pump System, Brush Recorded Data, Test 9

FOLDOUT FRAME 1

FOLDOUT FRAME 2

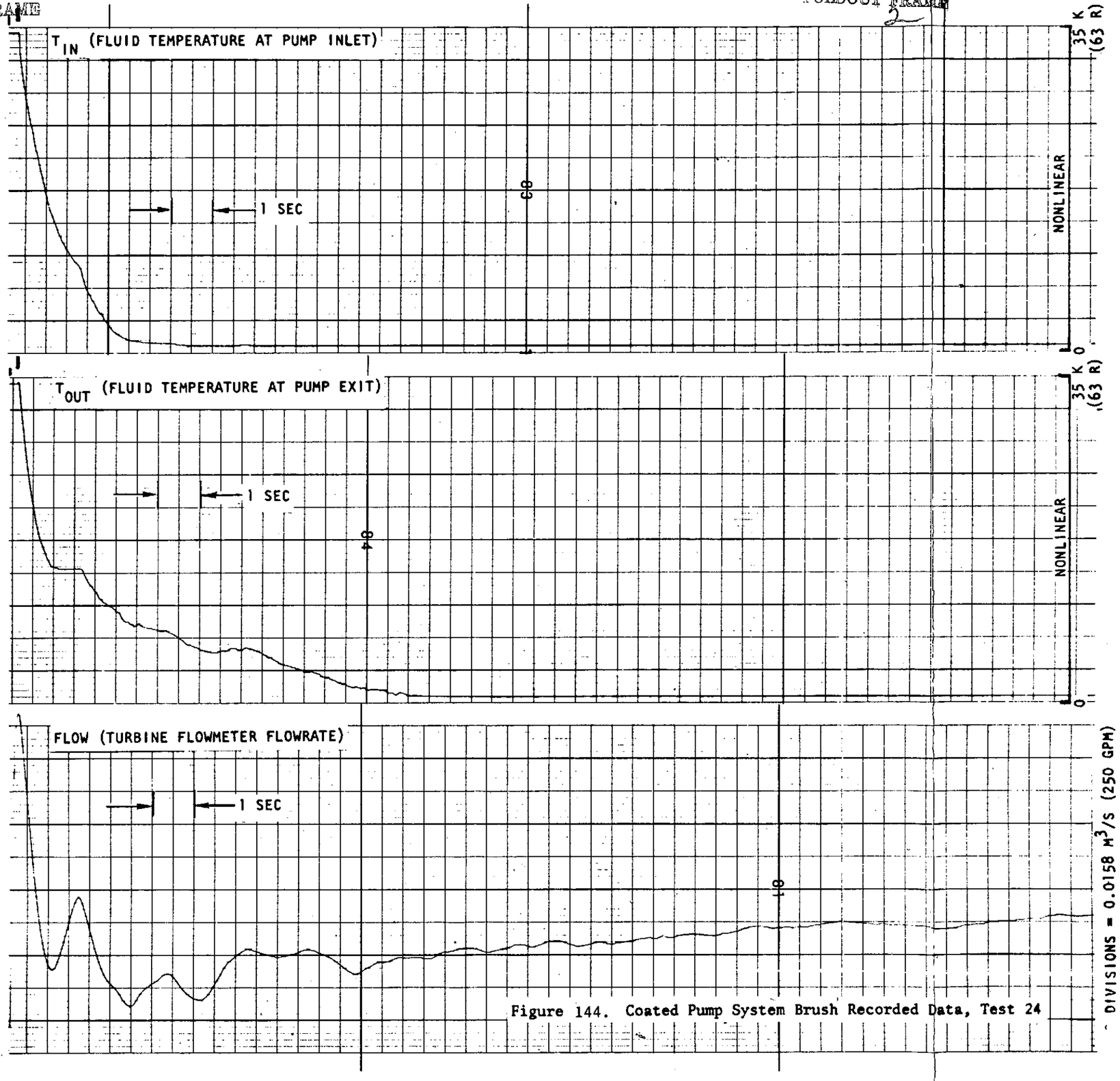

Figure 144. Coated Pump System Brush Recorded Data, Test 24

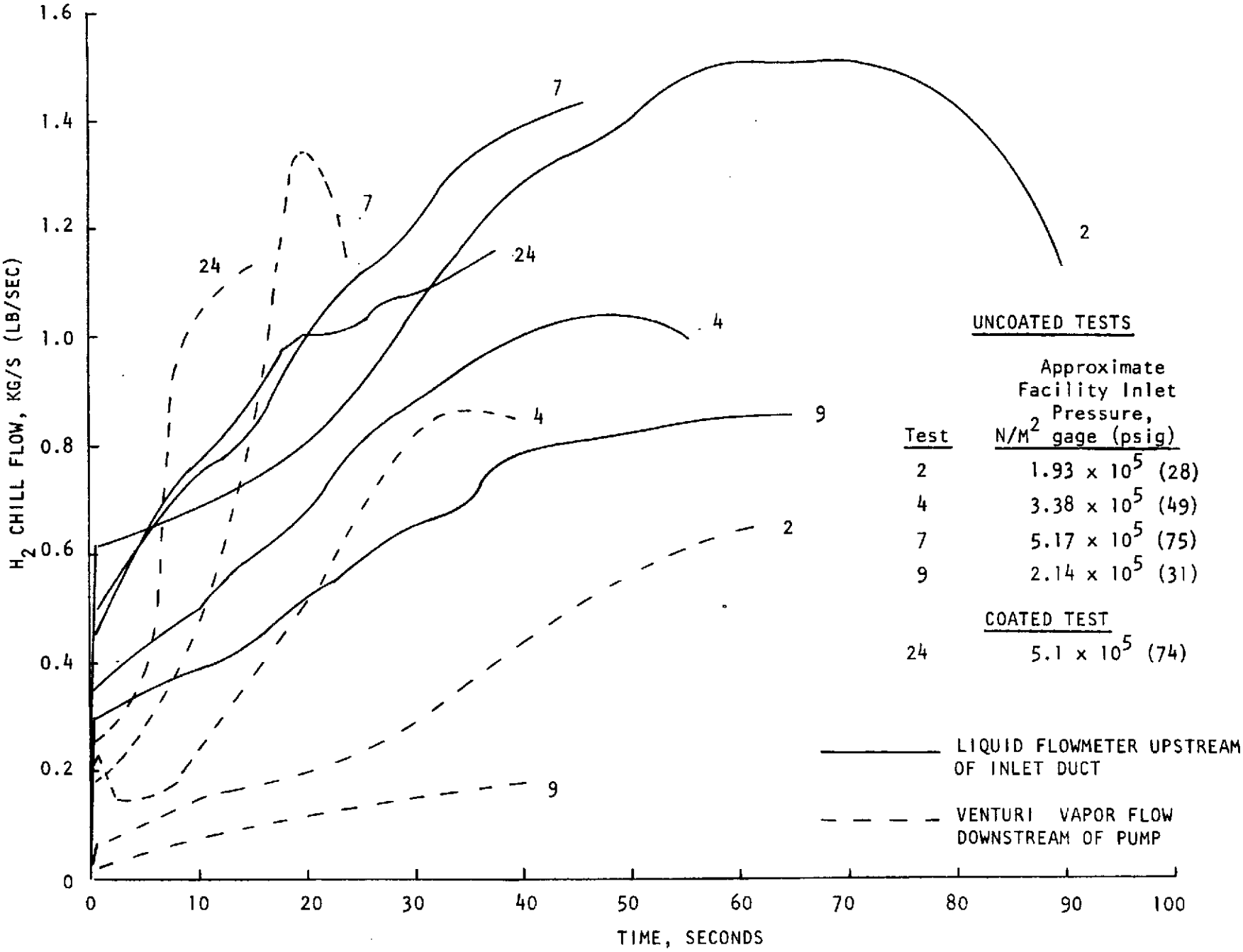

Figure 145. Pump Flowrate History During Chill Tests

TABLE 23. CHILL TEST DATA METRIC UNITS

Test	Time Sec.	System Inlet Pressure N/M^2 Gage $\times 10^{-5}$	Pump Fluid			Liquid Flowrate Facility Inlet $M^3/Sec \times 10^{-3}$	Chill Test Venturi			Pump Wall Temperature, K				Inlet Line Temperature, K				
			Inlet Temp. K	Interstage Temp. K	Outlet Temp. K		Pressure N/M^2 Gage $\times 10^{-4}$	Temp. K	ΔP N/M^2 $\times 10^{-4}$	Thermocouple Number				Thermocouple Number				
										1	2	3	5	1	2	3	4	7
1	0	6.57	281.4	281.6	281.1	3.2	-0.0014	283.1	0.006	282	282	282	282	114.3	176	236	280	280
	10	1.21	78	125	209	7.1	0.0028	260	0.0048	210	269	259	271	62	61	105	120	234
	20	1.12	84	69	144	3.25	0.0034	198	0.0055	138	233	192	237	22	OS*	OS	OS	170
	30	1.01	66	66	122	11.6	0.0028	160	0.0048	93	193	139	203	54	OS	OS	OS	126
	40	0.89	59	38	87	5.4	0.0069	128	0.0069	67	157	103	175	OS	OS	OS	OS	101
	50	1.38	41	24	46	4.4	0.021	88	0.012	OS	119	46	133	OS	OS	OS	OS	79
	60	1.93	25	25	21	2.3	0.053	52	0.018	OS	48	17	89	OS	OS	OS	OS	72
	70	2.28	25	25	21	5.3	0.071	22	0.021	OS	OS	OS	72	OS	OS	OS	OS	65
	90	2.28	25	25	21	5.4	0.046	21	0.014	OS	OS	OS	58	OS	OS	OS	OS	42
	110	2.14	25	25	21	5.2	0.034	21	0.013	OS	OS	OS	54	OS	OS	OS	OS	33
2	0	2.03	291	291	289	4.1	-0.114	292	-0.0076	292	292	292	293	139	210	278	291	289
	5	1.99	78	130	208	5.6	-0.04	262	0.03	221	278	268	282	63	87	137	144	247
	10	1.96	46	79	154	2.7	0.009	216	0.052	158	253	222	259	62	59	61	69	198
	15	2.14	45	52	122	9.97	0.066	180	0.056	118	226	179	235	OS	37	OS	OS	160
	20	1.82	60	49	101	4.6	0.032	145	0.061	89	198	140	211	OS	OS	OS	OS	133
	30	2.01	25	24	59	9.8	0.172	107	0.083	17	140	73	164	OS	OS	OS	OS	84
	40	1.99	25	24	22	5.0	0.354	73	0.096	OS	89	18	104	OS	OS	OS	OS	70
	45	1.99	25	24	21	9.4	0.350	64	0.090	OS	34	OS	85	OS	OS	OS	OS	69
	49	1.67	25	24	21	26.2	0.113	77	0.057	OS	OS	OS	OS	OS	OS	OS	OS	OS
	51	1.86	25	24	21	17.2	0.212	74	0.064	OS	OS	OS	OS	OS	OS	OS	OS	OS
	53	1.81	25	24	21	13.8	0.162	60	0.056	OS	OS	OS	OS	OS	OS	OS	OS	OS
	57	1.92	25	24	21	9.3	0.315	43	0.092	OS	OS	OS	OS	OS	OS	OS	OS	OS
4	0	3.65	205	193	261	6.4	0.215	293	0.165	289	300	298	302	115	206	256	243	292
	3	3.31	76	128	203	6.2	0.123	256	0.063	220	291	270	290	57	109	148	131	250
	6	3.31	58	90	159	5.2	0.166	212	0.070	165	275	228	270	54	63	74	73	207
	12	3.45	40	39	93	2.4	0.397	145	0.155	94	234	154	228	54	32	29	OS	141
	18	3.47	28	27	59	3.2	0.613	104	0.197	29	191	95	188	OS	OS	OS	OS	91
	24	3.38	27	27	33	5.3	0.671	75	0.176	OS	146	28	137	OS	OS	OS	OS	64
	27	3.38	27	27	22	5.4	0.754	63	0.181	OS	125	OS	113	OS	OS	OS	OS	63

* = Off Scale

TABLE 23. (Continued)

Test	Time Sec.	System Inlet Pressure N/M^2 Gage $\times 10^{-5}$	Pump Fluid			Liquid Flowrate Facility Inlet $M^3/Sec \times 10^{-3}$	Chill Test Venturi			Pump Wall Temperature, K				Inlet Line Temperature, K				
			Inlet Temp. K	Interstage Temp. K	Outlet Temp. K		Pressure N/M^2 Gage $\times 10^{-4}$	Temp. K	ΔP N/M^2 $\times 10^{-4}$	Thermocouple Number				Thermocouple Number				
										1	2	3	5	1	2	3	4	7
4	30	3.31	27	27	22	5.6	0.78	53	0.174	OS*	103	OS	98	OS	OS	OS	OS	62
	33	3.31	27	27	22	5.9	0.759	48	0.165	OS	74	OS	88	OS	OS	OS	OS	62
	39	3.24	27	27	22	6.4	0.746	37	0.142	OS	OS	OS	58	OS	OS	OS	OS	58
7	0	5.10	306	312	304	4.0	0.390	308	0.004	307	309	308	311	116	189	260	301	301
	2	5.17	144	154	243	6.1	0.424	292	0.127	283	305	302	310	54	60	178	195	290
	4	5.24	65	95	180	6.6	0.448	254	0.170	219	290	268	296	51	69	117	117	247
	6	5.31	43	61	135	3.3	0.771	218	0.273	174	273	227	279	51	45	67	68	207
	8	5.17	333	333	98	1.5	0.885	190	0.363	138	251	185	259	52	36	57	56	173
	10	5.24	29	28	76	3.7	1.171	145	0.405	110	230	150	240	OS	36	47	51	147
	12	5.17	28	28	57	4.0	1.167	114	0.358	85	208	117	220	OS	23	36	OS	243
	14	5.17	28	28	32	5.0	1.47	89	0.376	65	191	79	190	OS	OS	OS	OS	240
	16	5.03	28	28	22	6.0	1.66	69	0.367	42	179	41	171	OS	OS	OS	OS	94
	18	4.96	28	28	22	6.2	1.88	53	0.396	25	165	22	152	OS	OS	OS	OS	86
	20	4.96	28	28	22	6.4	2.08	42	0.374	OS	151	OS	137	OS	OS	OS	OS	75
	24	4.90	28	28	22	7.1	2.30	20	0.352	OS	123	OS	115	OS	OS	OS	OS	59
	28	4.90	28	28	22	7.2	1.922	OS	0.298	OS	97	OS	103	OS	OS	OS	OS	50
9	0	2.21	287	289	285	2.3	0.02	292	0.02	287	287	287	287	184	246	285	285	285
	2	2.21	287	289	285	1.6	0.02	292	0.02	287	287	287	287	189	246	285	285	285
	4	2.07	142	162	234	1.3	0.085	281	0.02	257	285	281	286	114	176	216	196	271
	6	2.21	90	137	210	5.2	0.085	264	0.02	223	280	268	279	71	126	157	151	254
	8	2.14	76	105	181	0.35	0.085	244	0.02	195	273	250	271	65	88	115	110	231
	10	2.14	63	99	58	4.2	0.085	226	0.02	170	260	232	263	63	62	82	87	211
	14	2.00	44	71	141	5.8	0.085	194	0.02	132	298	196	243	59	38	65	62	175
	18	2.14	41	44	109	3.0	0.117	164	0.02	103	228	163	224	59	197	63	49	148
	22	2.00	43	51	102	6.8	0.147	142	0.02	80	208	135	205	OS	OS	54	OS	125
	26	2.21	30	26	69	3.3	0.230	121	0.02	56	186	110	187	OS	OS	OS	OS	108
	30	2.00	41	34	65	5.3	0.312	106	0.02	OS	165	87	168	OS	OS	OS	OS	93
	34	2.14	25	25	49	4.8	0.271	94	0.02	OS	144	60	146	OS	OS	OS	OS	84
	36	2.14	25	25	42	4.2	0.300	88	0.02	OS	133	46	133	OS	OS	OS	OS	82

* = Off Scale

TABLE 23. (Concluded)

Test	Time Sec.	System Inlet Pressure N/M^2 Gage $\times 10^{-5}$	Pump Fluid			Liquid Flowrate Facility Inlet $M^3/Sec \times 10^{-3}$	Chill Test Venturi			Pump Wall Temperature, K				Inlet Line Temperature, K				
			Inlet Temp. K	Interstage Temp. K	Outlet Temp. K		Pressure N/M^2 Gage $\times 10^{-4}$	Temp. K	ΔP N/M^2 $\times 10^{-4}$	Thermocouple Number				Thermocouple Number				
										1	2	3	5	1	2	3	4	7
9	38	2.14	25	25	36	4.4	0.320	82	0.02	OS*	122	32	119	OS	OS	OS	OS	82
	40	2.19	25	25	27	4.2	0.344	74	0.02	OS	109	17	108	OS	OS	OS	OS	82
24	0	5.17	298	300	295	1.4	0.002	296	-0.008	298	297	296	299	188	246	292	291	294
	0.5	4.62	237	202	238	17.0	0.919	292	0.189	298	297	296	299	188	241	288	287	294
	1	5.10	157	87	150	6.4	0.341	260	0.135	296	297	296	299	182	227	267	269	294
	1.5	4.96	114	73	138	4.9	0.323	243	0.146	294	296	296	299	175	214	244	256	293
	2	4.96	76	61	127	7.1	0.375	224	0.146	292	295	296	299	167	199	218	238	292
	2.5	5.10	50	44	108	4.0	0.52	204	0.20	290	293	295	299	160	188	196	221	291
	3.5	5.10	33	34	88	3.5	0.569	187	0.236	284	286	292	299	147	162	152	187	288
	4.5	5.17	29	29	75	3.0	0.696	167	0.27	280	281	290	299	134	149	130	170	286
	5.5	5.03	29	29	74	4.4	0.653	145	0.25	276	275	286	297	123	133	105	152	284
	6.5	5.03	29	29	64	4.9	0.754	130	0.265	273	269	281	297	115	118	84	135	281
	7.5	4.96	29	29	52	5.1	0.863	117	0.291	269	261	276	295	107	105	66	122	278
	8.5	5.03	29	29	39	4.0	1.12	101	0.332	265	255	271	294	99	94	50	111	276
	9.5	5.03	29	29	29	4.6	1.18	89	0.334	261	248	265	292	92	84	37	102	273
	10.5	5.03	29	29	23	4.8	1.27	79	0.340	258	241	259	290	84	74	26	93	270
	11.5	5.05	29	29	22	5.1	1.34	71	0.333	254	234	252	288	81	65	OS	85	268
	12.5	5.03	29	29	22	5.4	1.46	64	0.342	250	226	245	286	78	57	OS	79	265
	13.5	5.03	29	29	22	5.6	1.54	56	0.341	247	220	238	284	74	50	OS	74	263
	14.5	4.96	29	29	22	5.5	1.67	51	0.345	244	213	231	281	75	44	OS	71	260

* OS = Off Scale

TABLE 24. CHILL TEST DATA AS RECORDED IN ENGLISH UNITS

Test	Time sec.	System Inlet Press. psig	Pump Fluid			Liquid Flowrate Facility Inlet GPM	Prechill Venturi Vapor Flowrate			Pump Wall Temperature (F)				Inlet Line Temperature (F)				
										Thermocouple				Thermocouple				
			Inlet Temp. F	Inter-stage Temp. F	Outlet Temp. F		Press. psig	Temp. F	ΔP psid	1	2	3	5	1	2	3	4	7
1	0	95.227	46.6	46.9	46.0	50.739	-0.002	49.6	0.009	47.8	47.8	47.7	48.2	-254	-142	-35	44	45.3
	10	17.6	-320	-235	-84	112.8	0.004	7.7	0.007	-81	24	6	28	-349	-350	-270	-244	-39
	20	16.3	-308	-335	-200	51.5	0.005	-103	0.008	-212	-40	-114	-33	-421	(MV)	(MV)	(MV)	-153
	30	14.6	-341	-340	-241	184.0	0.004	-172	0.007	-292	-113	-210	-95	-362				-233
	40	12.9	-353	-391	-304	85.0	0.01	-230	0.01	-340	-177	-274	-144	(MV)				-278
	50	20	-386	-416	-378	70.5	0.03	-301	0.017	*(MV)	-246	-378	-220					-318
	60	28	-415	-416	-423	36.6	0.077	-367	0.026		-374	-430	-299					-331
	70	33				83.3	0.103	-420	0.03		(MV)	(MV)	-330					-342
	90	33				85.2	0.067	-423	0.021				-356					-385
1	110	31	-415	-416	-423	82.4	0.049	-423	0.019	(MV)	(MV)	(MV)	-362	(MV)	(MV)	(MV)	(MV)	-400
2	0	29.5	65.5	66.3	60.7	65	0.165	66	-0.011	66	67	67	68.6	-209	-81	40	63.5	61
	5	28.9	-320	-226	-86	89	0.064	12	0.043	-62	40	23	48.5	-346	-303	-213	-200	-15
	10	28.4	-377	-317	-183	43	0.013	-70	0.076	-175	-4.6	-60	7.3	-348	-354	-350	-335	-104
	15	30.97	-379	-367	-240	158	0.096	-135	0.082	-247	-52.5	-137	-36	(MV)	-393	(MV)	(MV)	-171
	20	26.4	-352	-372	-278	73	0.046	-198	0.089	-300	-103	-208	-79		(MV)			-220
	30	29.2	-415	-416	-354	156	0.250	-267	0.12	-429	-197	-328	-164					-309
	40	28.8			-420	80	0.514	-329	0.139	(MV)	-299	-428	-272					-333
	45	28.7			-422	149	0.508	-345	0.131		-399	(MV)	-306					-336
	49	24.2				415	0.164	-322	0.083		(MV)		(MV)					(MV)
	51	27.0				273	0.307	-327	0.093									
	53	26.2				218	0.235	-352	0.082									
2	57	27.8	-415	-416	-422	148	0.5	-382	0.133	(MV)	(MV)	(MV)	(MV)	(MV)	(MV)	(MV)	(MV)	(MV)

*Off Scale Reading is designated by (MV)

TABLE 24. (Continued)

Test	Time sec.	System Inlet Press. psig	Pump Fluid			Liquid Flowrate Facility Inlet GPM	Prechill Venturi Vapor Flowrate			Pump Wall Temperature (F)				Inlet Line Temperature (F)				
			Inlet Temp. F	Inter-stage Temp. F	Outlet Temp. F		Press. psig	Temp. F	ΔP psid	Thermocouple				Thermocouple				
										1	2	3	5	1	2	3	4	7
4	0	53	-91	-113	10	102	0.312	68	0.239	61	80	78	84	-253	-89	2	-22	67
	3	48	-323	-229	-95	99	0.178	2	0.092	-64	64	26	62	-358	-264	-194	-224	-10
	6	48	-355	-298	-174	83	0.241	-78	0.102	-163	36	-49	26	-363	-346	-327	-329	-87
	12	50	-388	-390	-292	38	0.576	-199	0.225	-290	-38	-183	-49	-363	-403	-408	(MV)	-206
	18	50.4	-410	-412	-353	50	0.889	-272	0.285	-407	-116	-288	-122	(MV)	(MV)	(MV)	(MV)	-296
	24	49	-412		-400	84	0.973	-324	0.255	*(MV)	-197	-410	-213					-344
	27	49			-421	85	1.094	-347	0.262		-235	(MV)	-256					-346
	30	48		-412	-422	88	1.132	-364	0.253		-275		-283					-348
	33	48	-412	-413	-422	94	1.101	-374	0.240		-327		-302					-348
4	39	47	-412	-413	-422	101	1.082	-394	0.206	(MV)	(MV)	(MV)	-355	(MV)	(MV)	(MV)	(MV)	-355
7	0	74	91	103	87	64	0.566	95	0.006	94	96	95	100	-251	-119	8.4	82	83
	2	75	-200	-182	-23	96	0.615	66	0.184	50	89	85	98	-362	-352	-139	-109	63
	4	76	-342	-288	-136	104	0.650	-2	0.246	-65	63	22	74	-369	-335	-250	-251	-15
	6	77	-382	-350	-217	52	1.118	-67	0.396	-147	31	-51	42	-369	-379	-339	-337	-87
	8	75	-400	-399	-284	24	1.284	-117	0.526	-212	-7	-126	7	-366	-396	-358	-360	-149
	10	76	-408	-409	-323	58	1.698	-198	0.588	-262	-46	-190	-27	(MV)	-396	-375	-369	-195
	12	75	-409	-410	-357	63	1.693	-254	0.519	-307	-85	-250	-64		-419	-395	(MV)	-23
	14	75	-409		-403	79	2.132	-300	0.545	-342	-115	-317	-118		(MV)	(MV)		-27
	16	73			-420	95	2.414	-336	0.532	-385	-138	-387	-152					-290
	18	72				98	2.733	-364	0.575	-415	-162	-421	-186					-305
	20	72				101	3.013	-385	0.542	(MV)	-187	(MV)	-213					-325
	24	71				113	3.330	-424	0.511	(MV)	-238	(MV)	-252					-354
7	28	71	-409	-410	-420	114	2.788	0	0.432	(MV)	-286	(MV)	-275	(MV)	(MV)	(MV)	(MV)	-370

*Off-scale reading is designated by (MV)

TABLE 24. (Concluded)

Test	Time sec.	Pump Fluid: System Inlet Press. psig	Pump Fluid: Inlet Temp. F	Pump Fluid: Inter-stage Temp. F	Pump Fluid: Outlet Temp. F	Liquid Flowrate Facility Inlet GPM	Prechill Venturi Vapor Flowrate: Press. psig	Prechill Venturi Vapor Flowrate: Temp. F	Prechill Venturi Vapor Flowrate: ΔP psid	Pump Wall Temperature (F) Thermocouple: 1	2	3	5	Inlet Line Temperature (F) Thermocouple: 1	2	3	4	7
9	0	32	58	60	53	37	0.025	66	0.022	57	57	57	58	-129	-17	53	54	53
	2	32	58	60	53	26	0.024	66	0.022	57	57	57	58	-129	-17	53	54	53
	4	30	-205	-168	-38	21	0.124	47	0.022	2.5	53	46	55	-255	-142	-71	-107	29
	6	32	-298	-214	-82	82	0.123	16	0.022	-58	44	22	43	-332	-233	-177	-188	-3
	8	31	-323	-271	-133	5.5	0.124	-20	0.022	-108	32	-9	29	-342	-302	-252	-262	-44
	10	30	-346	-282	-155	67	0.124	-52	0.0225	-153	19	-42	13	-347	-348	-312	-304	-80
	14	31	-380	-332	-206	92	0.125	-110		-222	-13	-107	-22	-353	-392	-342	-348	-144
	18	31	-386	-380	-264	47	0.162	-165		-275	-50	-166	-57	-353	-105	-347	-371	-194
	22	29	-382	-369	-277	108	0.213	-205		-316	-86	-217	-91	(MV)	(MV)	-362	(MV)	-234
	26	32	-406	-414	-336	52	0.333	-242		-359	-124	-261	-123			(MV)		-266
	30	29	-386	-398	-343	84	0.453	-269		*(MV)	-162	-303	-157					-292
	34	31	-415	-415	-371	76	0.393	-290			-200	-352	-197					-308
	36	31			-385	66	0.435	-302			-220	-377	-220					-312
	38	31			-395	69	0.464	-313			-241	-403	-245					-313
9	40	31	-415	-415	-411	66	0.499	-327	0.0225	(MV)	-264	-429	-265	(MV)	(MV)	(MV)	(MV)	-313
24	.0	75	77	80	72	22	0.003	74	-0.011	77	75	74	79	-122	-17	66	65	69
	0.5	67	-33	-96	-31	270	1.333	67	0.274	77	75	74	79	-122	-25	59	58	69
	1.0	74	-178	-304	-189	102	0.494	20	0.196	74	75	74	79	-132	-51	21	25	69
	1.5	72	-255	-329	-211	77	0.469	-23	0.212	70	74	74	79	-145	-75	-21	1	68
	2.0	72	-323	-350	-232	113	0.544	-56	0.212	66	71	73	79	-160	-101	-68	-31	67
	2.5	74	-370	-380	-266	63	0.754	-92	0.290	62	68	71	79	-172	-122	-107	-61	65
	3.5	74	-401	-398	-301	56	0.825	-123	0.343	51	56	66	78	-196	-168	-186	-123	59
	4.5	75	-408	-407	-324	47	1.009	-160	0.391	45	47	62	78	-219	-192	-226	-153	56
	5.5	73			-327	70	0.947	-198	0.362	38	36	55	76	-238	-221	-271	-187	51
	6.5	73			-345	77	1.093	-225	0.384	31	24	47	75	-252	-247	-309	-216	46
	7.5	72			-367	81	1.252	-250	0.422	24	11	38	72	-267	-270	-341	-240	41
	8.5	73		-407	-390	63	1.62	-278	0.481	17	-1	28	70	-281	-290	-370	-260	37
	9.5	73		-410	-407	73	1.715	-300	0.485	10	-14	18	66	-294	-309	-393	-277	32
	10.5	73			-418	76	1.843	-317	0.493	4	-26	6	63	-308	-326	-413	-293	27
	11.5	73			-420	81	1.946	-332	0.483	-3	-39	-6	59	-314	-348	(MV)	-307	22
	12.5	73				86	2.113	-345	0.496	-9	-52	-18	55	-320	-357		-318	18
	13.5	73				88	2.234	-360	0.495	-15	-64	-31	51	-326	-370		-326	13
24	14.5	72	-408	-410	-420	87	2.420	-368	0.501	-21	-76	-43	47	-325	-381	(MV)	-332	9

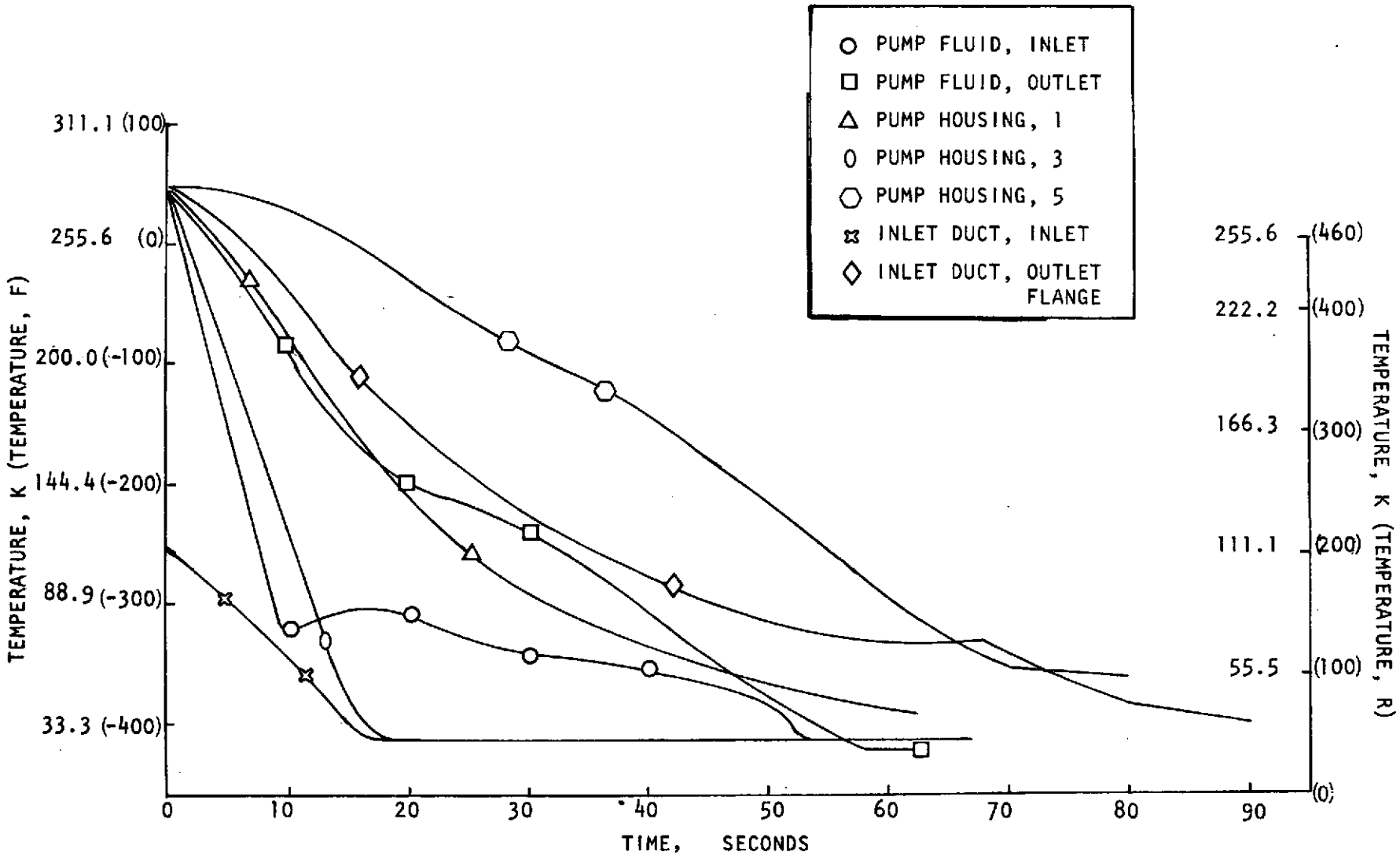

Figure 146, Uncoated Pump System Chill Fluid and Hardware Temperature History, Test 1

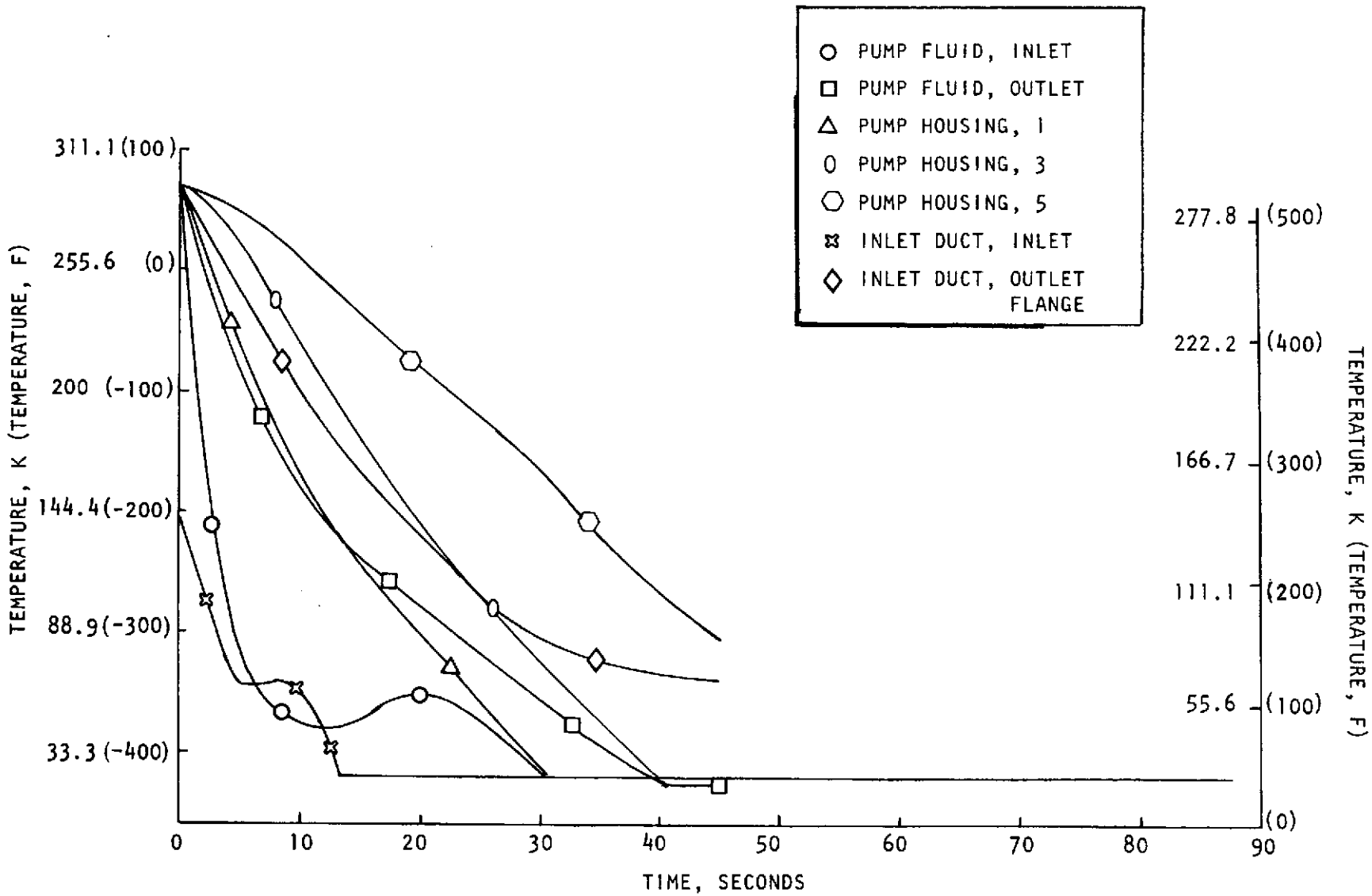

Figure 147. Uncoated Pump System Chill Fluid and Hardware Temperature History, Test 2

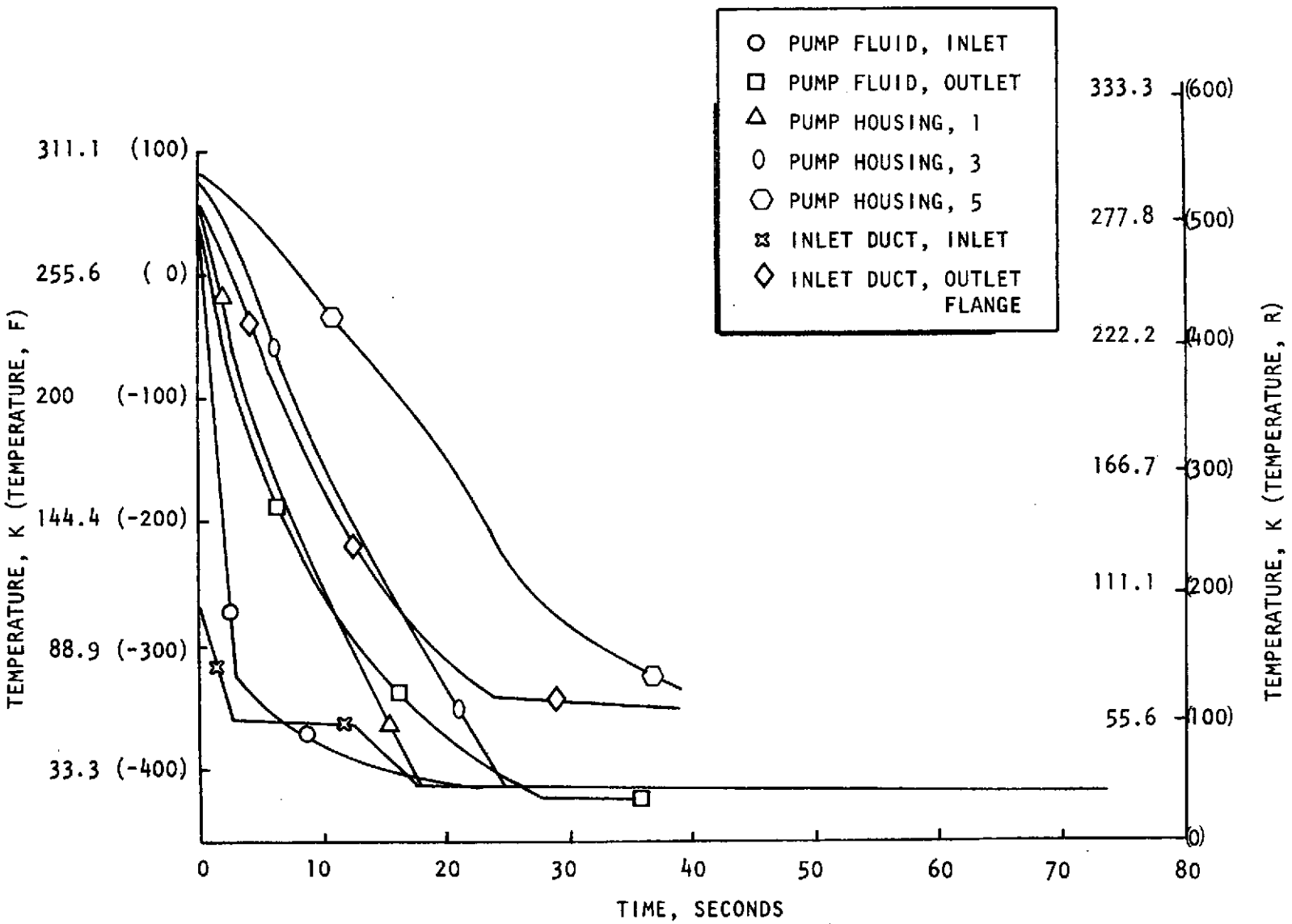

Figure 148. Uncoated Pump System Chill Fluid and Hardware Temperature History, Test 4

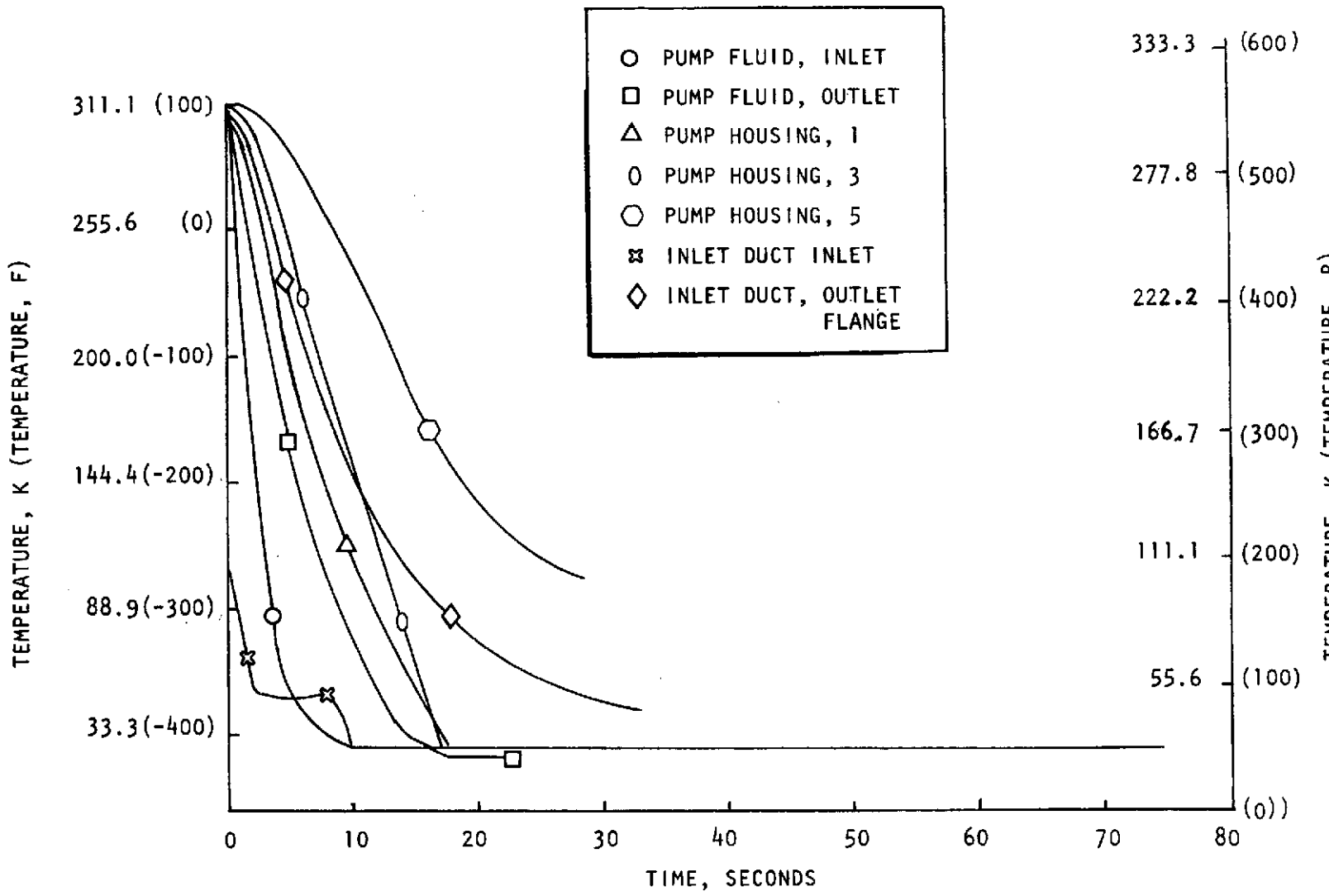

Figure 149. Uncoated Pump System Chill Fluid and Hardware Temperature History for Test 7

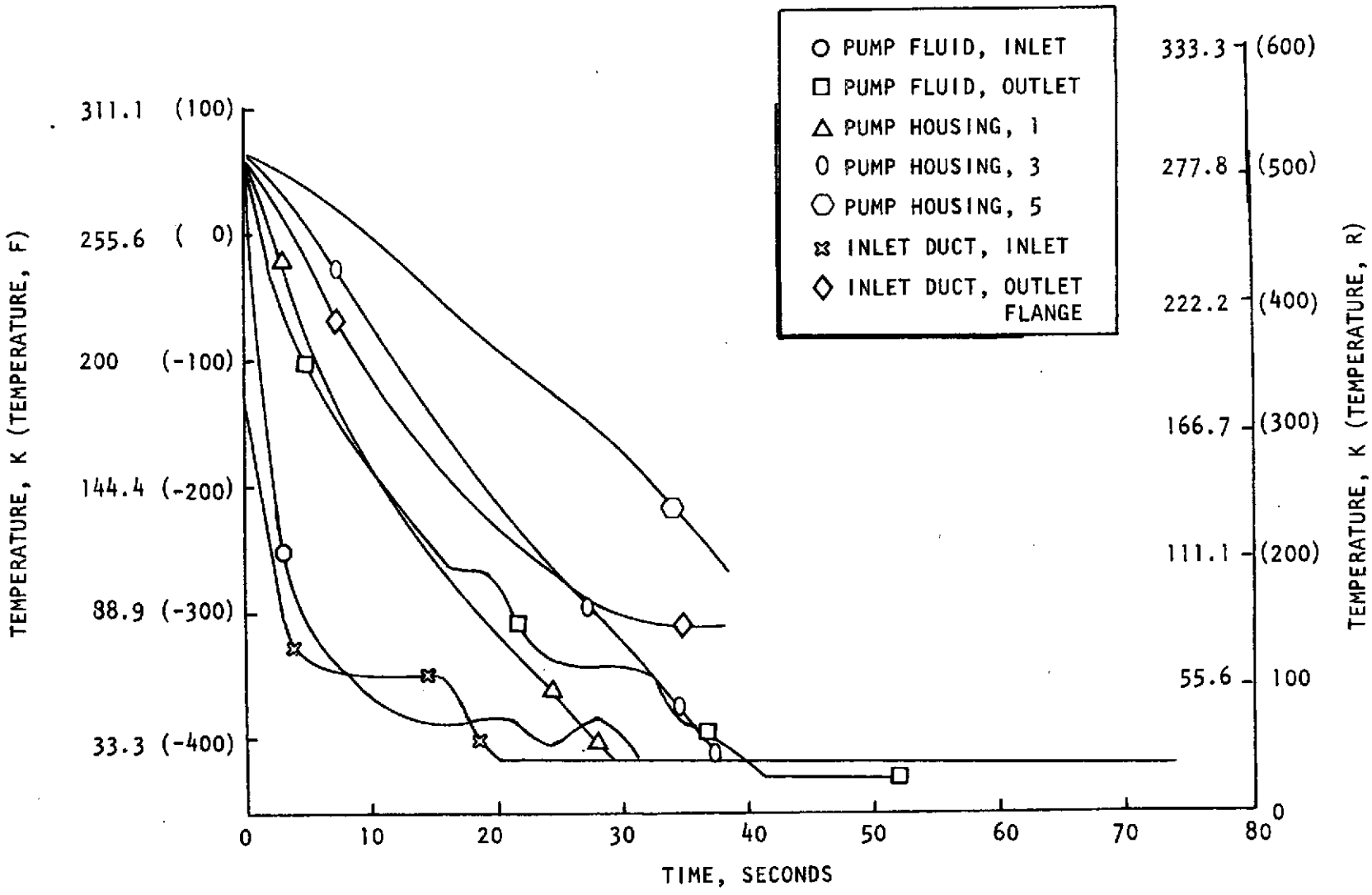

Figure 150. Uncoated Pump System Chill Fluid and Hardware Temperature History Test 9

observed in experiments carried out with various fluids in the two-phase thermodynamic region, and were anticipated for this series of tests.

There are many mechanisms that can induce thermohydraulic oscillations in the two-phase regime and under certain conditions into the near-critical and super-critical pressures. Some of these mechanisms are as follows:

1. Variation of the heat-transfer coefficient through the phase change region
2. The effect of large compressibility in the phase change region
3. Variation of flow characteristics brought about by variations of fluid density during the heat process
4. Flow oscillations due to low or high inlet subcooling.

It is, however, generally agreed that the oscillations are caused by the large variations of the thermodynamic and transport properties of the fluid as it passes through the phase change region. These oscillations and the associated heat transfer mechanism are boiling or "boiling-like" phenomena associated with nonequilibrium conditions. In the vicinity of the boiling temperature, the density gradient and the specific heat reach maximum values giving an indication of the energy required to overcome the mutual attraction between the molecules. The fluid in the immediate vicinity of the heated wall is in a gas-like state; whereas, the bulk fluid may still be in the liquid-like state. If by means of turbulent fluctuations the liquid-like fluid is brought into contact with the heating surface, a large amount of energy will flow from the surface to the fluid because of the large temperature difference and because of the high conductivity of the liquid-like fluid. This energy is large enough to rapidly change the liquid-like state to a gas-like state. The boiling region is where rapid expansion of liquid-like fluid into gas-like state takes place.

For this feed system, the liquid hydrogen is subcritical and goes through the two-phase phase boiling dome. The severe fluid oscillations resulted in flow reversal through the turbine-type liquid flowmeter in the facility chill-test duct, with an associated erroneous flowrate recorded. This effect appears more pronounced as chill nears completion at the low pressures near 2.07×10^5 N/m^2 gage (30 psi) in Tests 1, 2, and 9 (Fig. 140 and 143) and at lower amplitude during Tests 4 and 7 at increased pressures of 3.44×10^5 and 5.17×10^5 N/m^2 gage (50 and 75 psig), respectively (Fig. 141 and 142). The pressure oscillations in the feed-system hardware, which can be achieved more easily with low supply pressures, are limited by the vapor pressure of hydrogen.

In anticipation of the difficulty in chill-flow measurement, a hydrogen vapor venturi flow-measurement device was installed in the chill-test discharge duct to allow flow-measurement redundancy. To reduce the flow resistance and minimize pressure spike amplitude, the venturi was oversized for the anticipated chill flowrates. This resulted in a low venturi differential pressure and a large potential measurement error. For example, during Test 9, with an inlet pressure of 2.14×10^5 N/m^2 gage (31 psig), the recorded venturi differential pressure was at a constant 155 N/m^2 (0.0225 psid) throughout the test, as listed in Table 23 (Table 24). The inlet diameter of the venturi is 0.124 m (4.897 inches), and the minimum diameter is 0.085 m (3.349 inches). Vapor flowrate was calculated from the venturi inlet pressure, ambient pressure, differential pressure, upstream vapor temperature, and hardware geometry based upon the isentropic, compressible flow relationship:

$$\dot{W} = \frac{A_2}{\sqrt{1 - \left(\frac{P_2}{P_1}\right)^{\frac{2}{\gamma}} \left(\frac{A_2}{A_1}\right)^2}} \sqrt{\frac{2\,g\,\gamma}{\gamma - 1}\; P_1\; \rho_1 \left[\left(\frac{P_2}{P_1}\right)^{\frac{2}{\gamma}} - \left(\frac{P_2}{P_1}\right)^{\frac{\gamma+1}{\gamma}}\right]}$$

A_1 = Upstream area, (in.^{2}) m^2 x 0.0007236
A_2 = Minimum area, (in.^{2}) m^2 x 0.0007236
g = Acceleration of gravity, (in./sec^2) m/sec^2 x 0.0254

P_1 = Upstream pressure, (psia) $N/m^2 \div 6894.8$

P_2 = Minimum area pressure, (psia) $N/m^2 \div 6894.8$

γ = Ratio of specific heats

ρ = Hydrogen vapor density, $(lb/in.^3)$ $kg/m^3 \times 3.6\times10^{-5}$, at the upstream pressure and temperature

$\dot{W}$ = Flowrate, (lb/sec) kg/s × 2.2

Density and specific heat ratio were corrected to reflect the non-perfect gas characteristics of the very low temperature hydrogen. Venturi flow measurement accuracy decreases significantly in late stages of system chill as near liquid fluid temperature approaches.

Flow measurement for Tests 2, 4, 7, and 9 were shown in Fig. 145, which superimposes an average value of the turbine-type flowmeter data on the venturi calculated flowrates. The pump inlet pressure and exit temperature were correlated with turbine-flowmeter flow data of Test 7 to determine the constant K of the following flow equation:

$$\dot{W} = K \frac{P_{in}}{\sqrt{T_{out}}}$$

K = Flowrate constant

P_{in} = Pump inlet fluid pressure, (psia) $N/m^2 \div 6894.8$

T_{out} = Pump exit fluid temperature, (R) K × 1.8

$\dot{W}$ = (lb/sec) kg/s × 2.2

Based upon the data of Table 23 (Table 24), flowrate versus time was calculated using K = 0.115 and the equation above. Results are presented graphically in Fig. 151. Chill flowrate was integrated over the chill time for Tests 2, 4, 7, and 9 and results are presented in Fig. 152. Chill flow varies from 13.2 to 15.9 Kg (29 to 35 lb) as inlet pressure increases from 1.9×10^5 to 5.2×10^5 N/m^2 gage (28 to 75 psig). Approximately 15 Kg (33 lb) of LH_2 is required to chill the uncoated inlet duct and RL-10 pump system, independent of the wide variation in

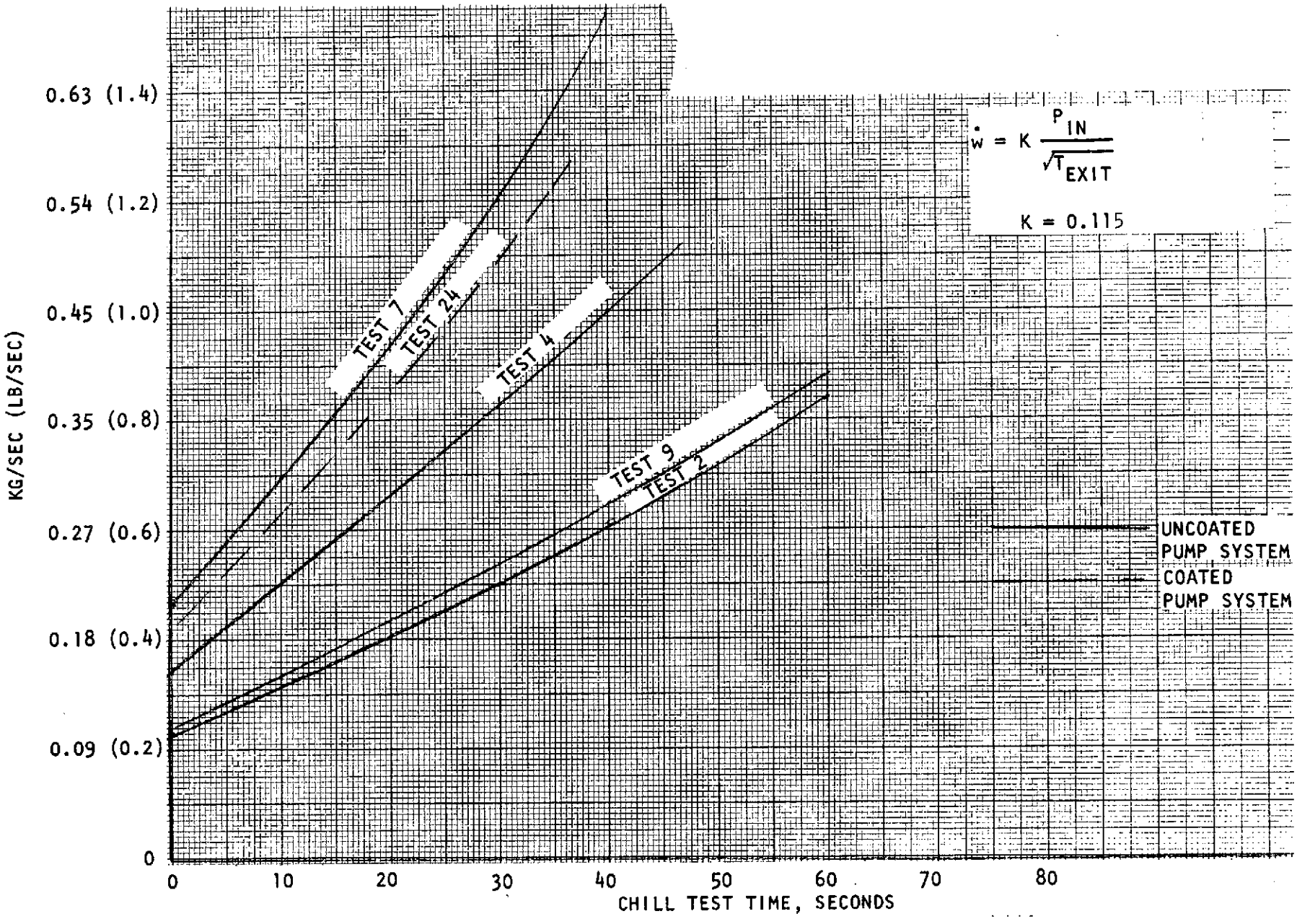

Figure 151. Chill Flowrate Based on Chocked Flow Through Pump

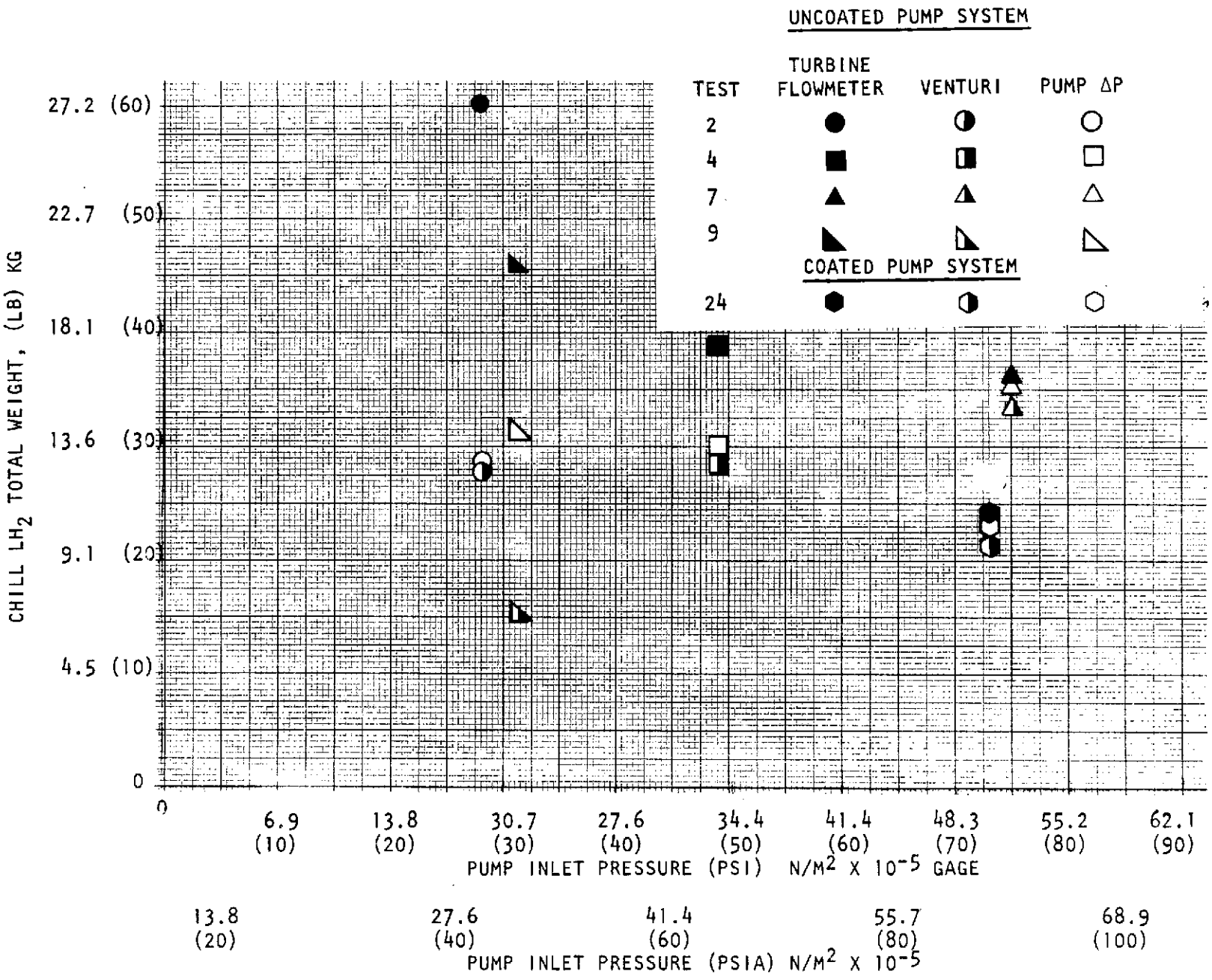

Figure 152. Total Weight of LH_2 Required to Chill Pump Resulting in 100-Percent Liquid at Pump Outlet

inlet pressure and associated chill flowrate. The above equation is valid to correlate flow, since the crossover duct pressure data indicate a pressure drop of 0.34×10^5 to 0.41×10^5 N/m^2 (5 to 6 psid) through the first impeller and crossover duct during tests 2 and 9. Projecting another 0.34×10^5 to 0.41×10^5 N/m^2 (5 to 6 psid) through the second impeller results in at least 1.1×10^5 N/m^2 gage (16 psig) just upstream of system minimum area in the pump exit. The flow is therefore choked and a simplified equation is justified to compare flowrate from test to test. The low-pressure tests 2 and 9 were selected since the pressure ratio across the minimum area is a minimum for these tests, and is approximately 2.0 during chill, which is greater than the choking pressure ratio for hydrogen vapor of 1.9. The factor K for each test as a function of time was determined from the following equation:

$$K = \frac{\dot{W} \sqrt{T_{out}}}{P_{in} A_{min}}$$

where

A_{min} = pump system minimum area, m^2 x 6.45×10^{-4} (in.^{2})

P_{in} = pump fluid inlet pressure, N/m^2 ÷ 6894.8 (psia)

T_{out} = fluid temperature at pump exit, K x 1.8 (R)

$\dot{W}$ = turbine flowmeter averaged flowrate, kg/s x 2.2 (lb/sec)

Figure 153 presents K vs time based upon turbine flowmeter averaged data as shown in Fig. 144, test parameters of Table 23, (Table 24), and a minimum area of 6.1×10^{-4} m^2 (0.95 in.^{2}).

Test 7 appeared to have the least error due to fluid-pressure oscillations and K was assumed to be the average of the 11.5 seconds of chill time for this test. The value of K is 0.1165 from this average, and although large variations in flow data occurred, this value was assumed constant for all tests for comparison purposes.

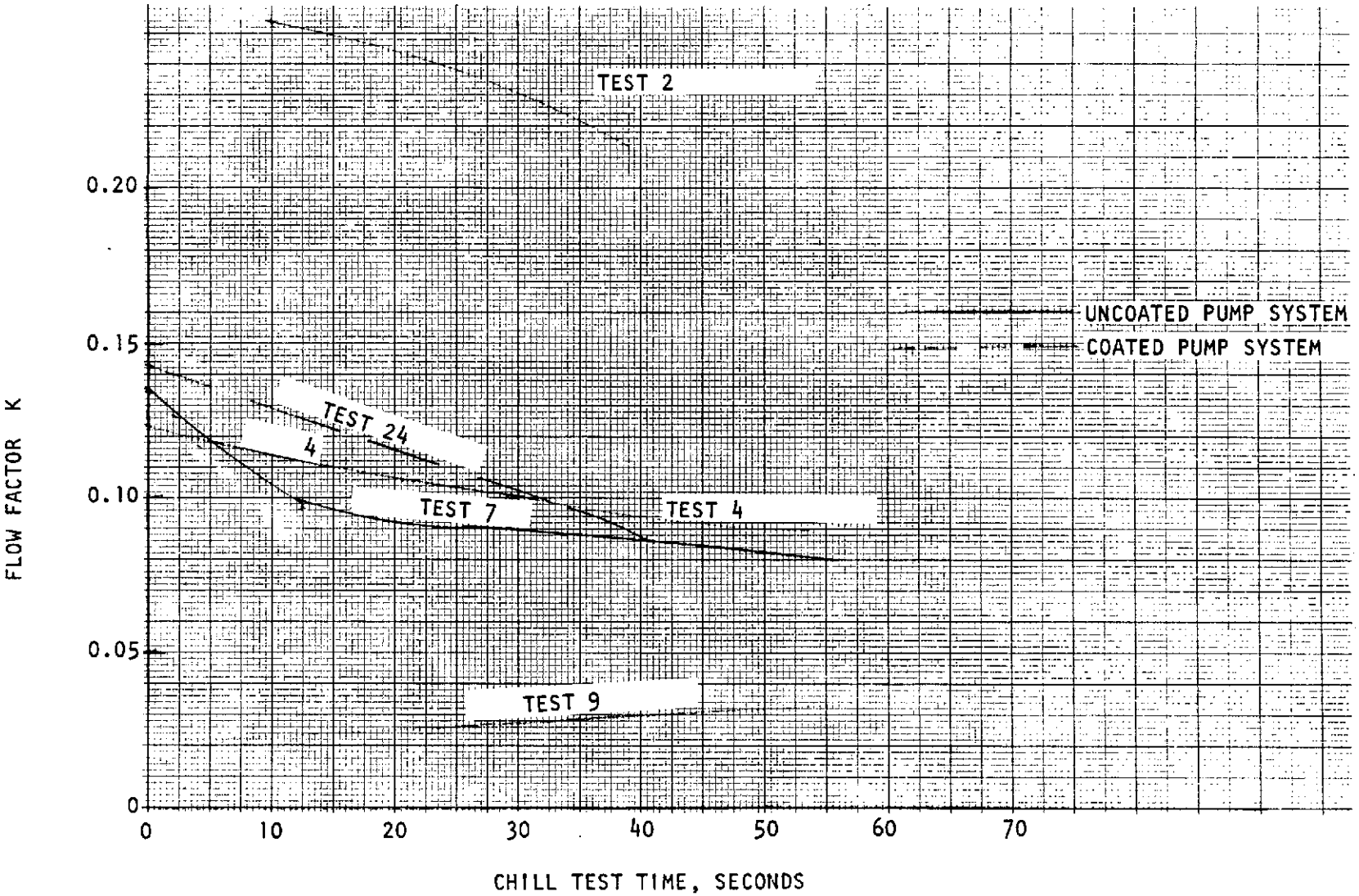

Figure 153. Flow Factor K, Based Upon Flowrate From Turbine Flowmeter, Fluid Pressure at Pump Inlet, and Fluid Temperature at Pump Exit

Inlet Duct Hardware Temperature. Duct-wall temperatures were recorded at seven locations along the inlet duct. The thermocouple stations were numbered consecutively, 1 to 7, with increasing station numbers downstream. Thermocouple data, temperature in Kelvin (Fahrenheit), were recorded for all stations for all chill tests. The data for stations 1, 2, 3, 4, and 7 for the chill tests are listed in Table 23 (Table 24). The thermocouple at station 7 is attached to the outer surface of the base of the inlet duct exit flange and was the highest duct temperature during all the chill tests as predicted. Thermocouple No. 1 was attached a few inches from the duct inlet and experienced chill to temperatures of 200 K (-100 F) or lower, during the chill of the upstream facility sections. Before each chill test, liquid hydrogen was circulated through the facility sections up to the inlet duct valve, and was exhausted through the feed system bypass valve. This facility chill before start accomplished some chill of the upstream section of the inlet duct due to conduction through the inlet duct valve. Thus, thermocouple No. 1 was 139 K (-209 F) at the start of testing, thermocouple No. 2 was 211 K (-80 F), thermocouple No. 3 was 278 K (40 F), and the downstream sections of the duct approached ambient. These data are from test 2 and were typical for all tests, in that some prechill of the inlet duct due to conduction from the facility was always present. The amount of prechill was dependent upon facility chill duration and was greater for tests 4 and 7, and less prior to test 9, as shown in Fig. 147 through 150.

During Task I of this program, inlet duct wall temperatures were predicted at constant chill flowrates. Figure 154 compares the wall temperatures at 0.27 kg/sec (0.6 lb/sec) chill flow with the chill-flow data from tests 2, 4, 7, and 9. Although the flowrate varied during the testing, the chill flow was bracketed near 0.27 kg/sec (0.6 lb/sec) during the initial few seconds of these tests. Initial chill flowrate was approximately 0.14 kg/sec (0.3 lb/sec) during tests 2 and 9, 0.20 kg/sec (0.45 lb/sec) during test 4, and 0.23 kg/sec (0.5 lb/sec) during test 7. Inlet duct wall chill characteristics are in reasonable agreement with those predicted. The inlet duct wall temperature data from thermocouple No. 1 reflect the hydrogen flow oscillation and flow reversals of relatively warm

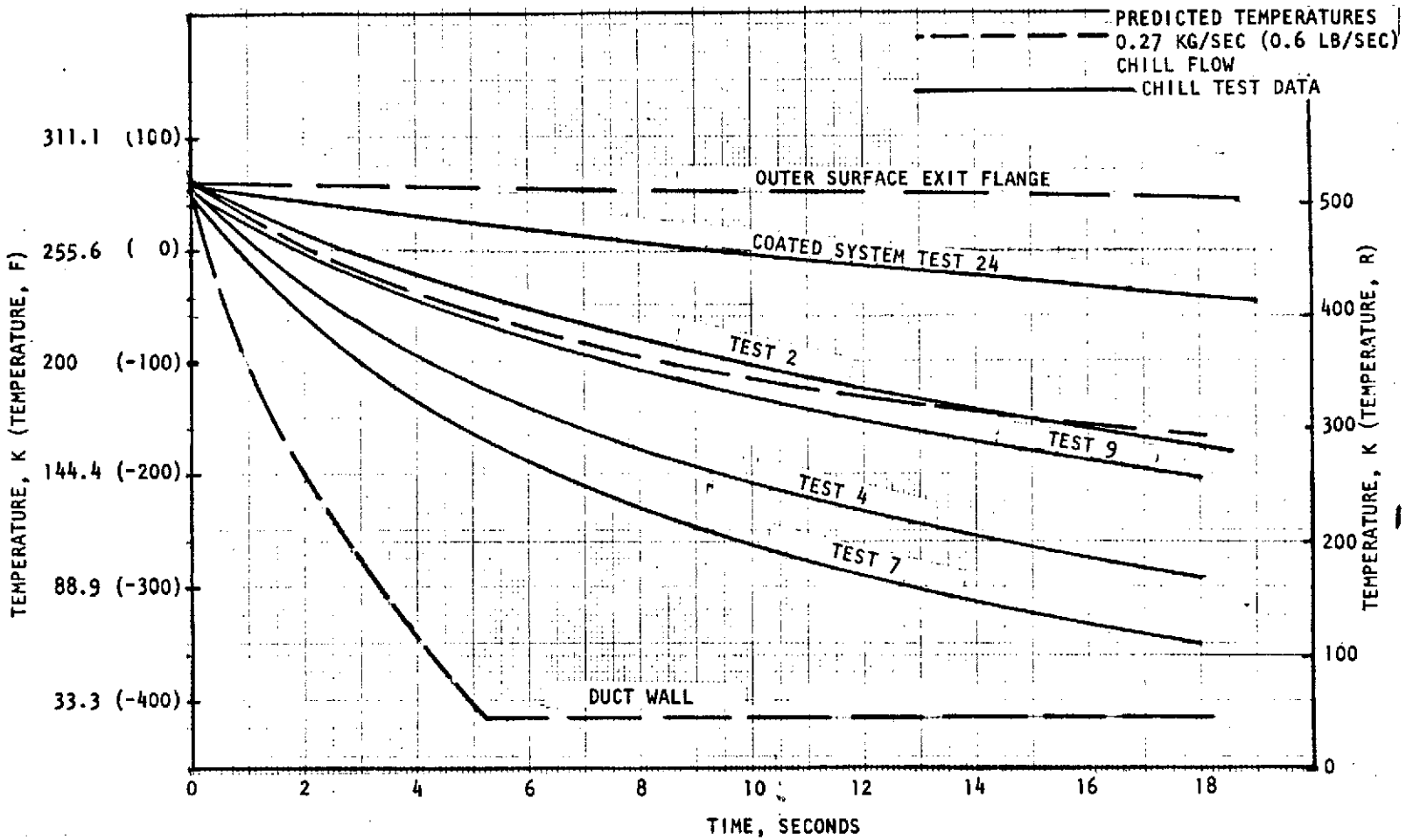

Figure 154. Inlet Duct Hardware Temperatures Test Data at Base of Exit Flange

vapor, which appears as a plateau in the temperature data history just following start of testing during Tests 2, 4, 7, and 9. The exit flange (thermocouple No. 7) was the last section of the inlet duct to be chilled as predicted, and always remained much warmer than the cryogen liquid. This fact appeared to predict reduced chill fluid and time requirements, if the flow path boundary conduction resistance could be incresed.

Pump Housing Temperatures. Pump housing temperatures were recorded by using five thermocouples placed on the external surface. Thermocouples were placed on the inlet housing around the inducer (thermocouple No. 1), the first impeller (thermocouple No. 2), the second impeller (thermocouple No. 3), on the surface of the exit volute (thermocouple No. 4), and on the housing connecting to the turbine (thermocouple No. 5). The temperature histories of thermocouples 1, 2, 3, and 5 are listed in Table 23 (Table 24) for Tests 1, 2, 4, 7, and 9.

Temperature histories of thermocouples 1, 3, and 5 are presented graphically for these tests in Fig. 146 through 149. Significantly, the housing temperature of the inlet section of the pump approaches the temperature of the liquid hydrogen and appears to be completely chilled almost simultaneously with the onset of inlet two-phase flow.

The pump exit fluid approaches 100-percent liquid long before the exit pump housing and turbine connect housing are completely chilled, as shown in Fig. 147 through 150. The resistance to conduction through the pump hardware, from the warm sections to the flow path boundary, is obviously a critical factor in determining the chill duration and the amount of fluid required in prestart-chilldown conditioning of cryogen turbomachinery. An increase in conduction resistance of the flow path in the boundary hardware was therefore predicted to reduce chill time and prestart thermal conditioning fluid weight.

A second pump with the flow path coated to increase the thermal resistance between the bulk of the pump system hardware and the cryogen fluid, was subjected to chill testing and results are reported under the Task IV section of this report.

Nominal Turbopump Start and Steady-State Performance

A total of eight rotating turbopump tests were conducted for the purposes of facility checkout, determination of a nominal start sequence, verification of pump performance, and checkout of the turbine-overspeed cutoff sequence. The experimental feed system was completely chilled before all of these tests. Extreme care was exercised during the initial turbopump rotation tests to preclude hardware damage that would be critical to the accomplishment of test objectives. Conservative redlines were established for certain parameters that, if exceeded, would terminate the test. These redlines were relaxed only when required to meet specific test objectives after facility operation experience had been acquired.

The first three turbopump rotation tests, while they did not yield steady-state pump performance data, resulted in the establishment of realistic redlines and valuable facility operation experience. During the first of these tests (test No. 3), the turbopump was initially accelerated to approximately 1550 rad/s (14,800 rpm), and then gradually stepped to approximately 2530 rad/s (24,200 rpm). When the gear cavity pressure reached the redline value of 3.1×10^5 N/m^2 (45 psia), the test was automatically terminated. After consulting with the contract monitor concerning this redline, the pump-inlet pressure was reduced from approximately 5.5×10^5 N/m^2 (80 psia) to approximately 4.8×10^5 N/m^2 (70 psia) for the next test.

The second turbopump rotation test (test No. 5) was terminated due to a flowrate cut during the initial acceleration. After increasing the flowrate redline, the third turbopump rotation test (test No. 6) was attempted. During this test the turbopump was accelerated to approximately 2220 rad/s (21,200 rpm), but an automatic cut was encountered after 3.5 seconds due to a low pump-inlet pressure. During the initial rapid flow acceleration the pump-inlet pressure was perturbed and pressure and flow oscillations were sustained throughout the test. The peak-to-peak pressure oscillation was nearly constant at 1.9×10^5 N/m^2 (28 psi) with a frequency of approximately 4.5 Hz (4.5 cps). It is probable that the oscillations were sustained by the generation of vapor in the inlet line. This conclusion

is supported by the observance of pump inlet pressures equal to the vapor pressure during the oscillations. Since these oscillations damped out within 0.7 second in the first test of this series, it was decided to revert back to the original pump inlet pressure of approximately 5.5 x 10^5 N/m^2 (80 psia) and to increase the gear-cavity redline pressure to 3.4 x 10^5 N/m^2 (50 psia) for all subsequent start tests.

The fourth test (test No. 8) in this series resulted in extensive pump performance data. The turbopump was initially accelerated to approximately 2050 rad/s (19,600 rpm) and steady-state performance was determined for combinations of speeds between 1680 and 2680 rad/s (16,000 and 25,600 rpm), flows between 0.024 and 0.037 m^3/s (380 and 585 gpm), and discharge valve areas between 41 and 69 percent of the full-open value. The duration of this test was over 7 minutes and was cut due to a declining turbine supply pressure.

Seven steady-state operating conditions were selected from this run to verify the pump performance characteristics. Pressure measurements at the pump inlet (pump mounted) and pump discharge (mounted in the adapter between pump flange and discharge duct) were used for this purpose. Resistance temperature bulbs within an inch of these same locations were used with the measured pressures to determine the average density within the pump. The developed heads calculated from these measurements were all between 95 and 98 percent of the corresponding values interpolated from Fig. 155. The rotational speeds for the seven operating conditions were between 2090 and 2600 rad/s (20,000 and 24,800 rpm) and the flow coefficients were between 81 and 114 percent of the "design point" value shown in Fig. 155.

The fifth turbopump rotation test (test No. 10) was conducted to define the nominal start transient, i.e., a start to the nominal run conditions selected for this test program. The turbopump was accelerated to 2560 rad/s (24,400 rpm) with the dishcarge valve area preset to 55 percent of its full-open value. The steady-state flow was 0.033 m^3/s (530 gpm). The pump speed, flowrate, inlet pressure, and pressure rise for this baseline start are shown in Fig. 156 and 157. During the initial acceleration the indicated flow spikes to a very high value. It is

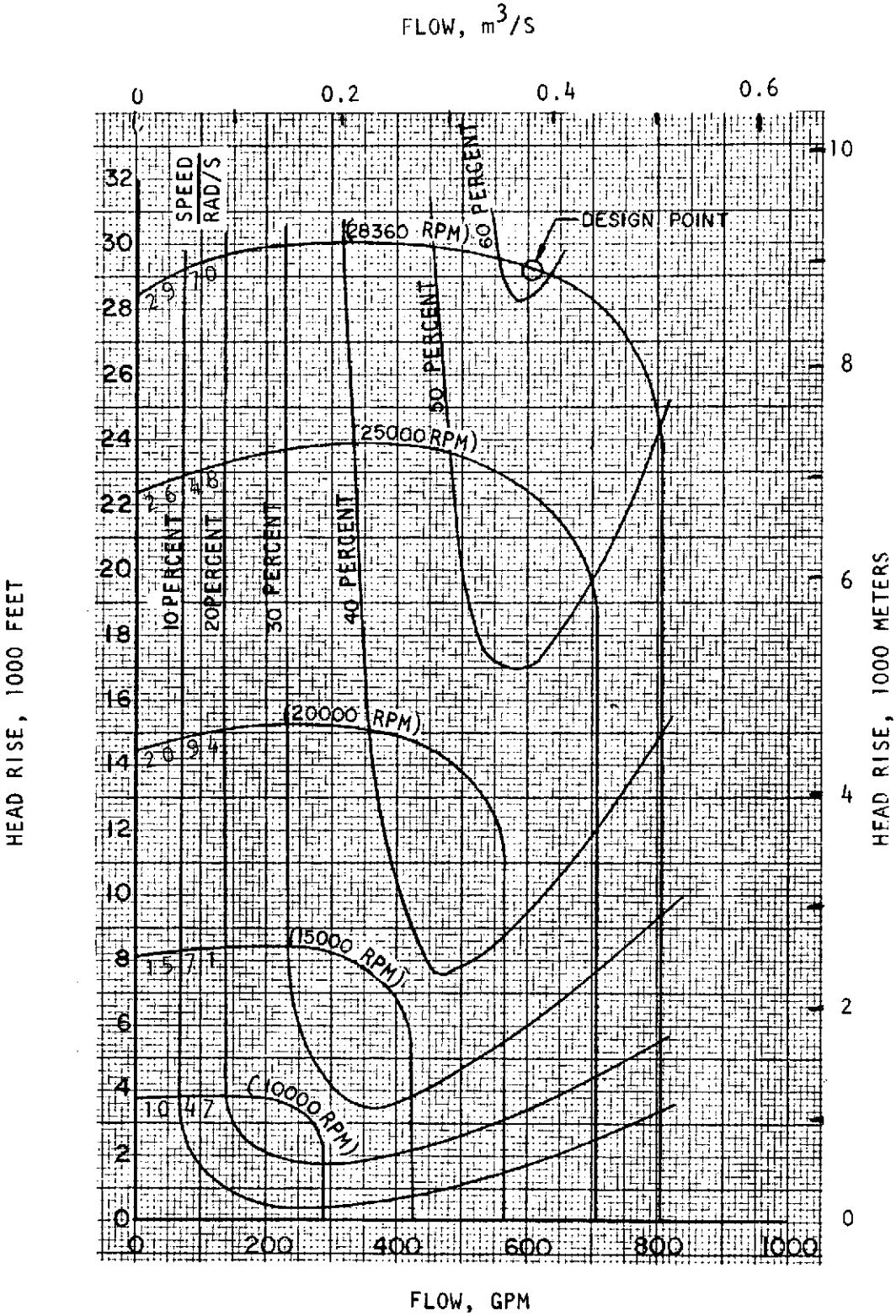

Figure 155. RL10A-3-1 Fuel Pump Predicted Performance (Ref. 2)

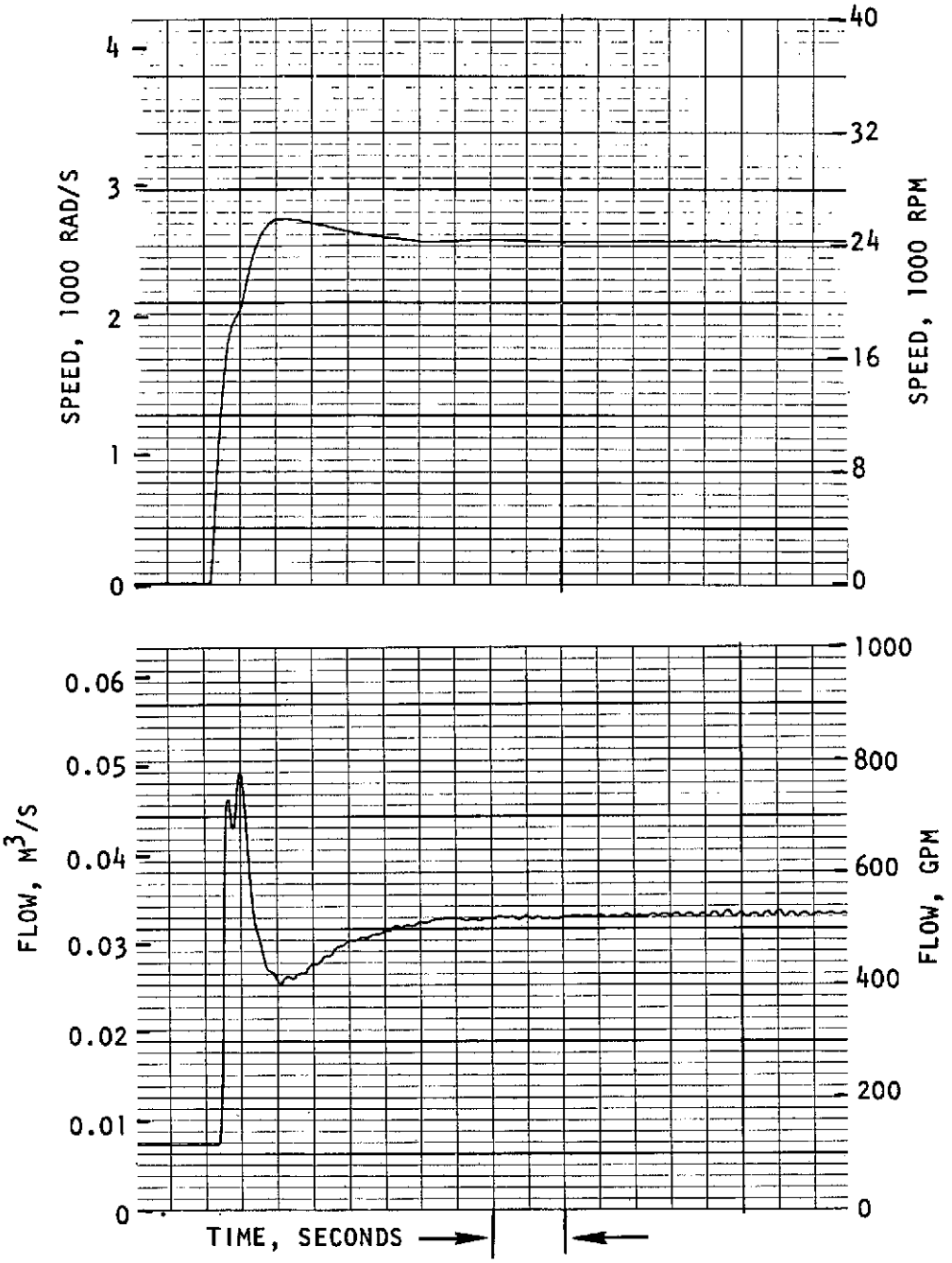

Figure 156. Turbopump Speed and Inlet Duct Flow Transients for Baseline Start

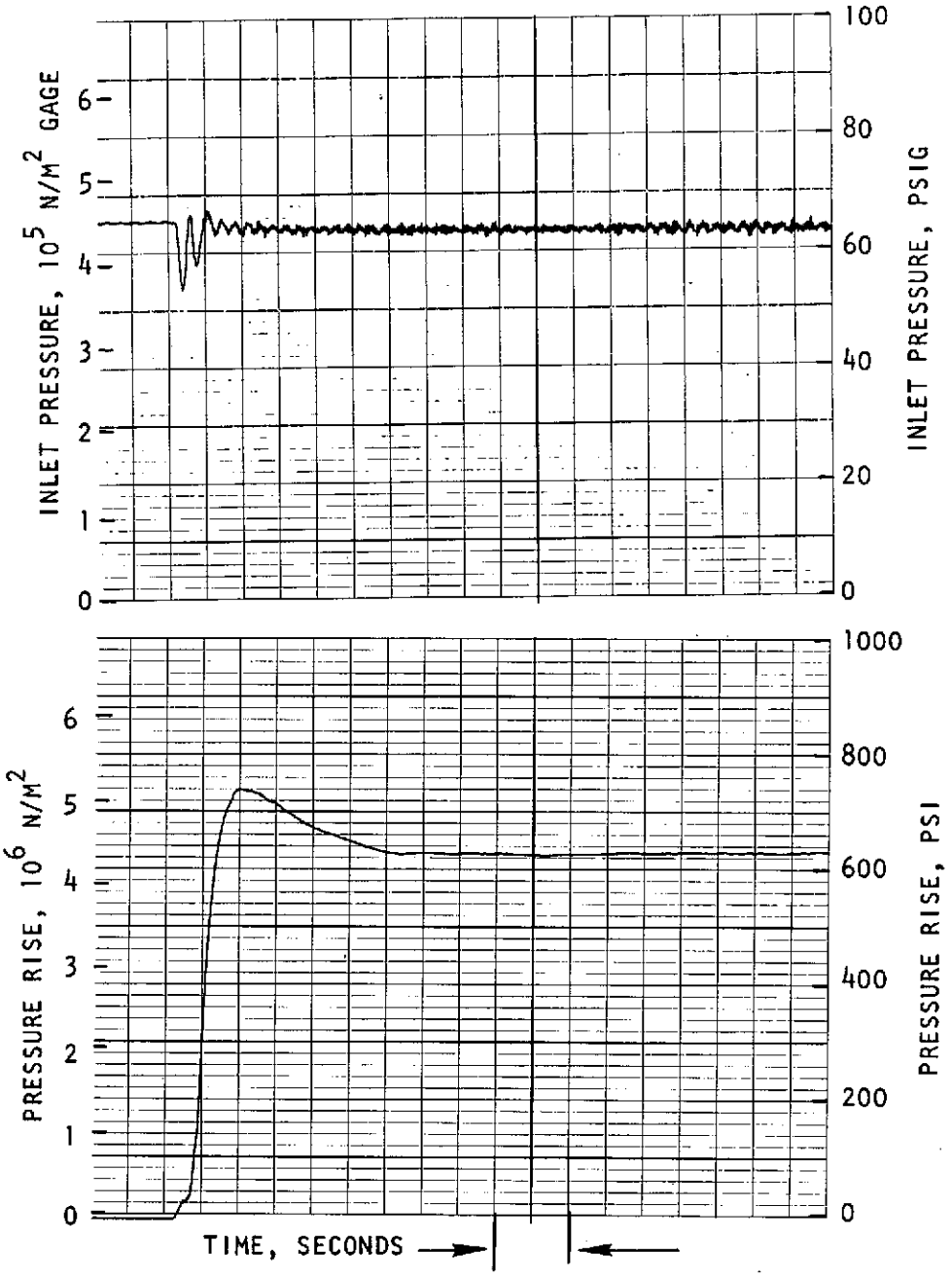

Figure 157. Pump Inlet Pressure and Pressure Rise for Baseline Start

questionable that such high flows are attained for two reasons. First, the available pump performance map (Fig. 155) indicates a breakdown in developed head during operation at these conditions, but there is no evidence that this occurs. Secondly, increases in propellant temperature and pressure, indicating the presence of vapor, are observed near the liquid flowmeter during this time period. The vapor may be generated in the feed system bypass duct after the bypass valve is closed. Assuming vapor to be present, higher-than-actual flow measurements would be indicated. This test was terminated by an automatic timer before the turbine overspeed cutoff sequence could be investigated and, therefore, the next two tests (tests No. 11 and 12) were conducted for this purpose.

Neither of the turbopump overspeed tests were successful in demonstrating that the precautionary cutoff was operating satisfactorily. The first of these tests was terminated at 2.5 seconds into the run due to an accelerometer cut. During the second of these tests the turbopump was accelerated to 2600 rad/s (24,800 rpm) and then gradually stepped to 3020 rad/s (28,800 rpm). At this point, a pump discharge pressure cut was initiated at 7.0×10^6 N/m^2 (1015 psia) before reaching the rotational speed redline of 3140 rad/s (30,000 rpm). Due to the limited amount of testing remaining, it was decided to suspend any further investigation of this cutoff sequence.

An additional rotating turbopump test (test No. 16) was conducted during the series of deadhead-start tests to re-establish nominal steady-state operating conditions. This was necessary because the turbine inlet pressure regulator was replaced because of frequent damage to the seat.

Deadhead Turbopump Start

Nine tests were conducted with the start-test discharge valve closed, i.e., under deadhead conditions, to determine the start characteristics for this mode of operation. The effects due to the size of the discharge volume and the pressure used to initiate opening of the discharge valve were investigated for a fully chilled system. One attempt was made to start with a partially chilled feed system but posttest analysis indicated that the system was actually fully chilled.

The first test in this series (test No. 14) had a downstream volume of approximately 0.024 m^3 (0.85 ft^3) and the discharge valve was set to open at a pressure of 3.6 x 10^6 N/m^2 (515 psia). When turbine power was applied, the pump accelerated very rapidly to 3140 rad/s (30,000 rpm) and the overspeed redline initiated cutoff. The rotational speed peaked at 3900 rad/s (37,200 rpm). The overspeed resulted from a breakdown in developed head that occurred before the discharge valve could open and before through-flow could be established. The discharge valve trigger pressure was then lowered to 2.9 x 10^6 N/m^2 (415 psia) for the next test (test No. 15). The transients were essentially the same as the preceding test and the trigger pressure was therefore lowered to 2.2 x 10^6 N/m^2 (315 psia) for the next.

Again, the lower trigger pressure did not have any noticeable effect on the start transient. The pump speed transient for this test (Test No. 17) is presented in Fig. 158. Sequence numbers on this figure refer to the following events: (1) close start-test discharge valve, (2) open turbine inlet valve, (3) open start-test discharge valve, and (4) turbopump overspeed cut initiated. As shown, the pump accelerated very rapidly to 3140 rad/s (30,000 rpm) and the overspeed redline initiated cutoff. The rotational speed peaked at 3770 rad/s (36,000 rpm). Figure 158 also shows the discharge valve position transient and indicates it started opening almost simultaneously with power cutoff. The pump inlet pressure and pressure rise are shown in Fig. 159. The discharge pressure increased to 4.5 x 10^6 N/m^2 (655 psia) before the breakdown in developed head occurred. The inlet duct flowrate is shown in Fig. 160, but it is not extremely useful in analyzing the start transient. Initially, the flow starts to decrease when the discharge valve is closed, but then increases when the turbopump starts to rotate. The double-humped peak is an erroneous indication of flow and is due to vapor generated near the turbine-type liquid flowmeter. Before a reliable reading is established, cutoff is initiated.

The best supporting evidence for an explanation of the failure to start under the deadhead conditions imposed is obtained by examining the propellant temperature transients. Temperatures measured at the pump discharge and pump inlet are shown in Fig. 161. The transients indicate that the propellant temperature at the pump discharge heats up first, followed by the temperature at the pump inlet. The pump

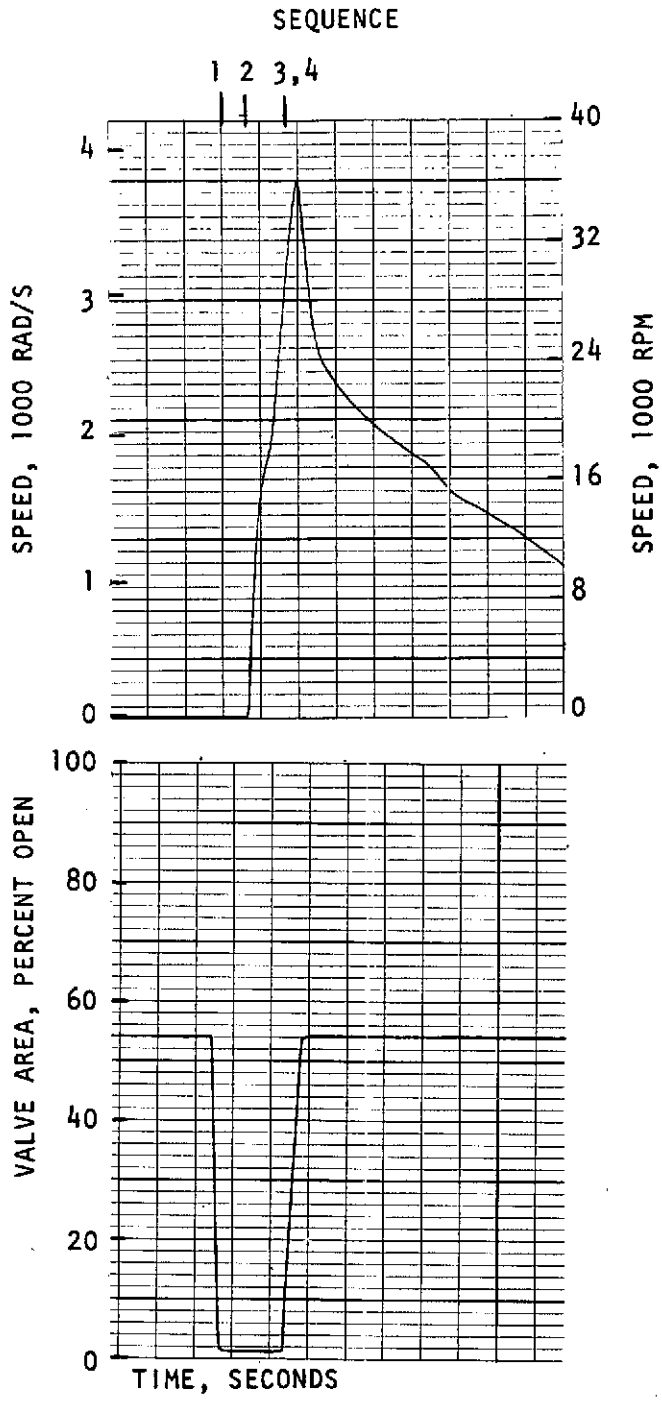

Figure 158. Turbopump Speed and Discharge Valve Area Transients for Deadhead Start Test With 0.024 m^3 (0.85 ft^3) Discharge Volume and 2.2 x 10^6 N/m^2 (315 psia) Trigger Pressure

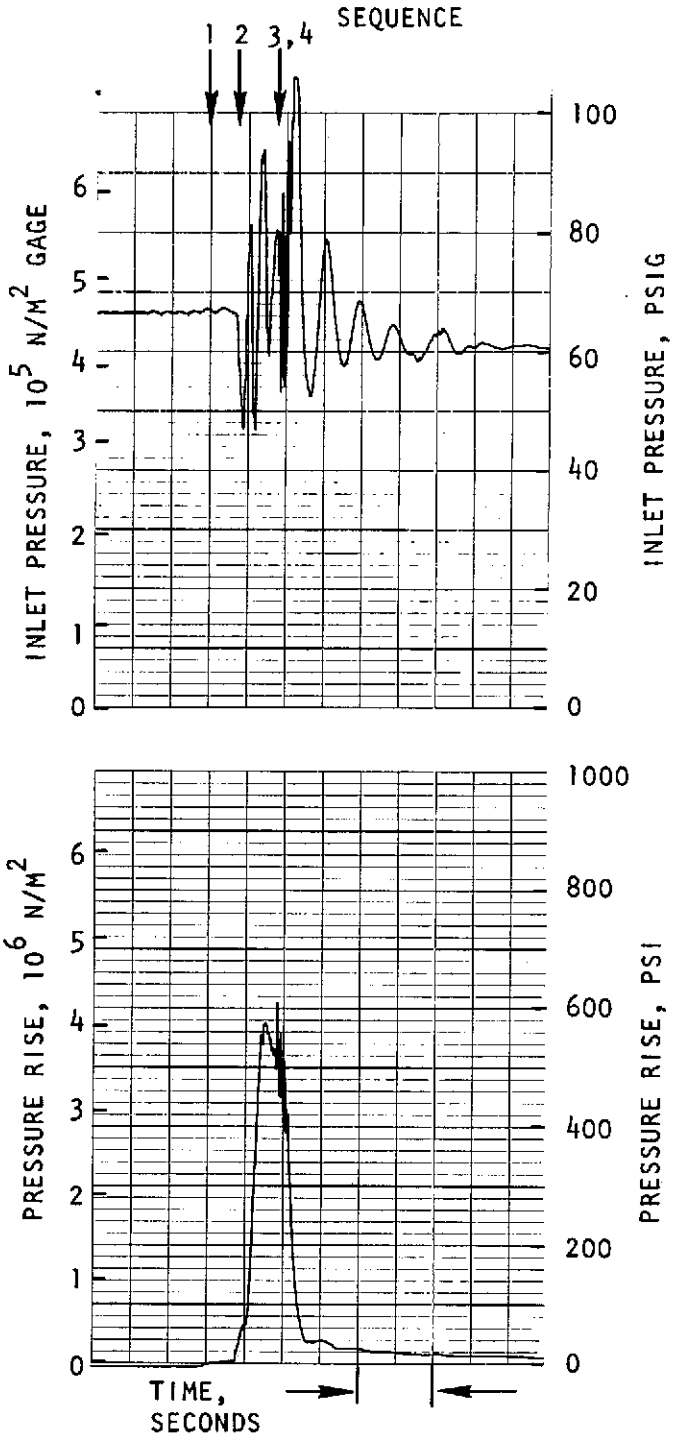

Figure 159. Pump Inlet Pressure and Pressure Rise Transients For Deadhead Start Test With 0.024 m^3 (0.85 ft^3) Discharge Volume and 2.2 x 10^6 N/m^2 (315 psia) Trigger Pressure

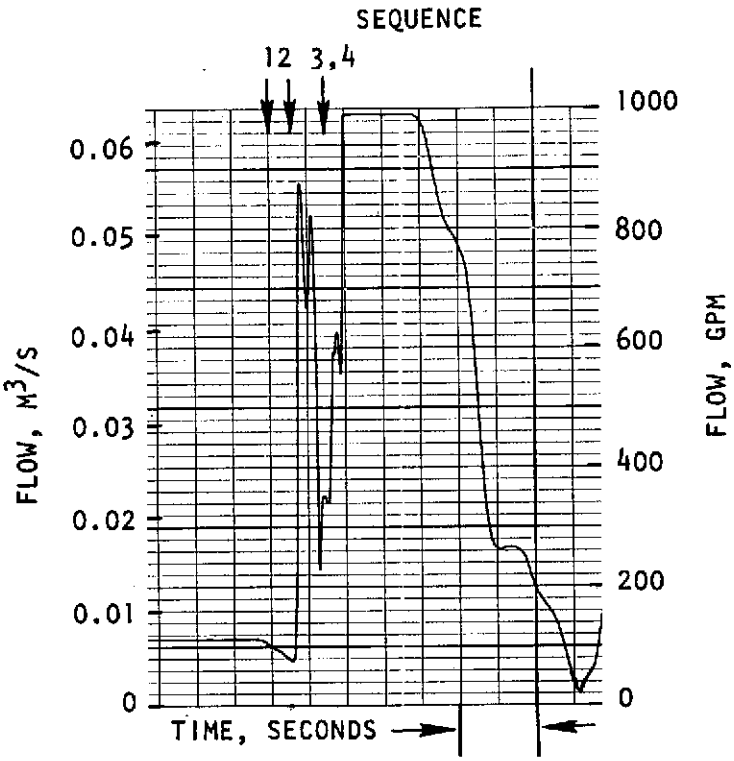

Figure 160. Inlet Duct Flow Transient for Deadhead Start Test With 0.024 m^3 (0.85 ft^3) Discharge Volume and 2.2 x 10^6 N/m^2 (315 psia) Trigger Pressure

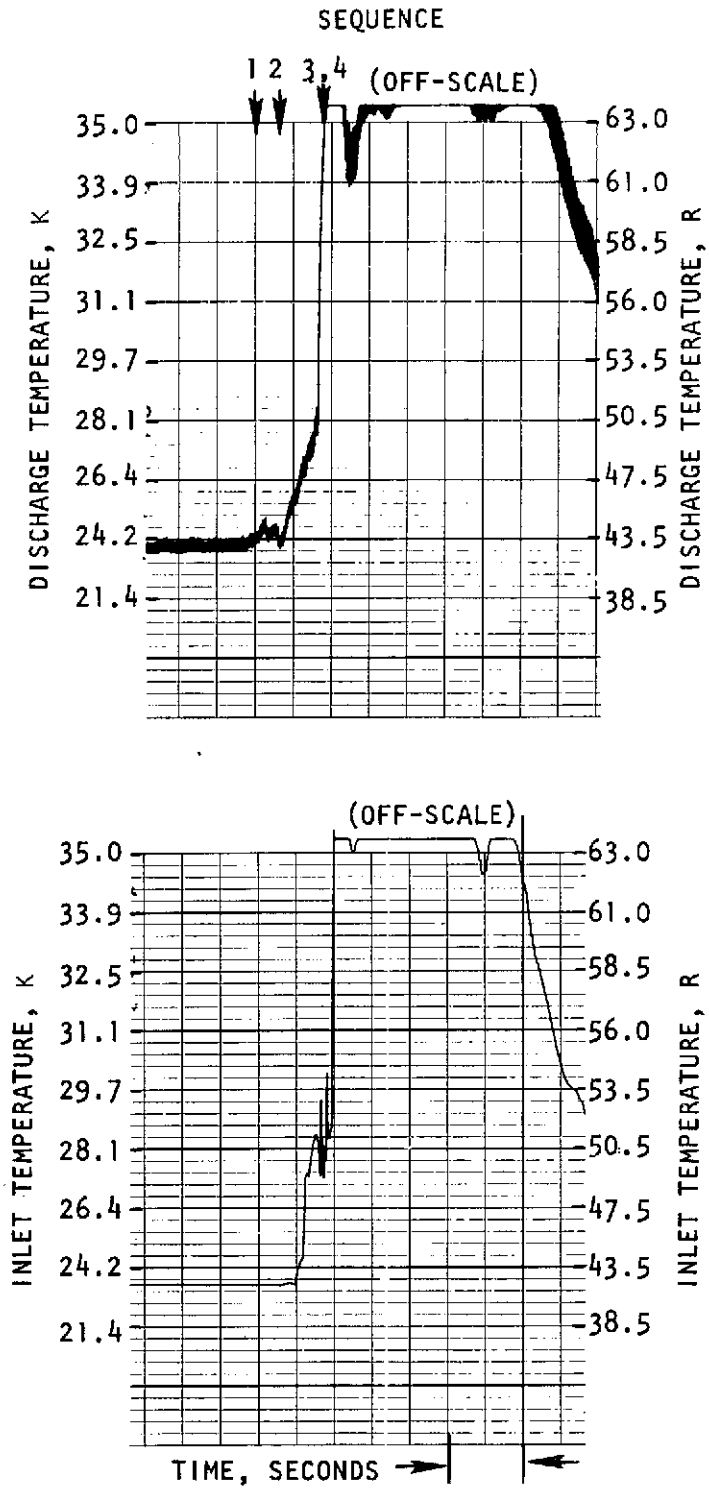

Figure 161. Pump Discharge and Inlet Hydrogen Temperature Transients for Deadhead Start Test With 0.024 m^3 (0.85 ft^3) Discharge Volume and 2.2 x 10^6 N/m^2 (315 psia) Trigger Pressure

discharge temperature is affected by heat transfer from the pump discharge housing and flange adapter to the stagnated fluid, and by the large amount of energy absorbed by the very low pump flow at high rotational speeds. Since the discharge pressure peaks before the peak in pump speed, head breakdown and reverse flow through the pump probably occur and account for the turbopump overspeed and subsequent decrease in discharge pressure. If reverse flow exists, it would explain the observed temperature increase, first at the pump discharge and then at the pump inlet. Expansion of the high-energy fluid at the pump discharge to the low pressures in the inlet duct would result in vaporization of the hydrogen and in very high temperatures.

Rather than lower the trigger pressure below 2.2×10^6 N/m^2 (315 psia) or improve the response of the discharge valve from 0.23 seconds, the volume between the pump and discharge valve was varied. Since the pump flowrate during the initial part of the start transient is not known due to inaccurate flowmeter readings, a smaller volume was used for the next test (test No. 18). A larger volume would increase the flow and, since the pump transient operating conditions are not known accurately, might result in cavitation damage. However, reducing the volume to approximately 0.014 m^3 (0.05 ft^3) with a trigger pressure of 2.2×10^6 N/m^3 (315 psia) yielded similar transients to the unsuccessful tests with the 0.024 m^3 (0.85 ft^3) volume.

The downstream volume was therefore increased to 0.098 m^3 (3.45 ft^3) for the next test (test No. 19). This test, with a trigger pressure of 2.2×10^6 N/m^2 (315 psia) started successfully. Successful starts with trigger pressures of 3.6×10^6 N/m^2 (515 psia) and 4.2×10^6 N/m^2 (615 psia) were also accomplished (these two tests were No. 20 and 23, respectively). The first attempt with the higher of these two trigger pressures (test No. 21) was unsuccessful because of a cutoff initiated by the redline on flowrate. The redline was exceeded during the initial peak in flow indicated by the flowmeter. The redline was increased for the successful test.

Transients for the successful test with a downstream volume of 0.098 m^3 (3.45 ft^3) and a trigger pressure of 4.2×10^6 N/m^2 (615 psia) are presented in Fig. 162 through 165. The pump acceleration transient is shown in Fig. and is similar

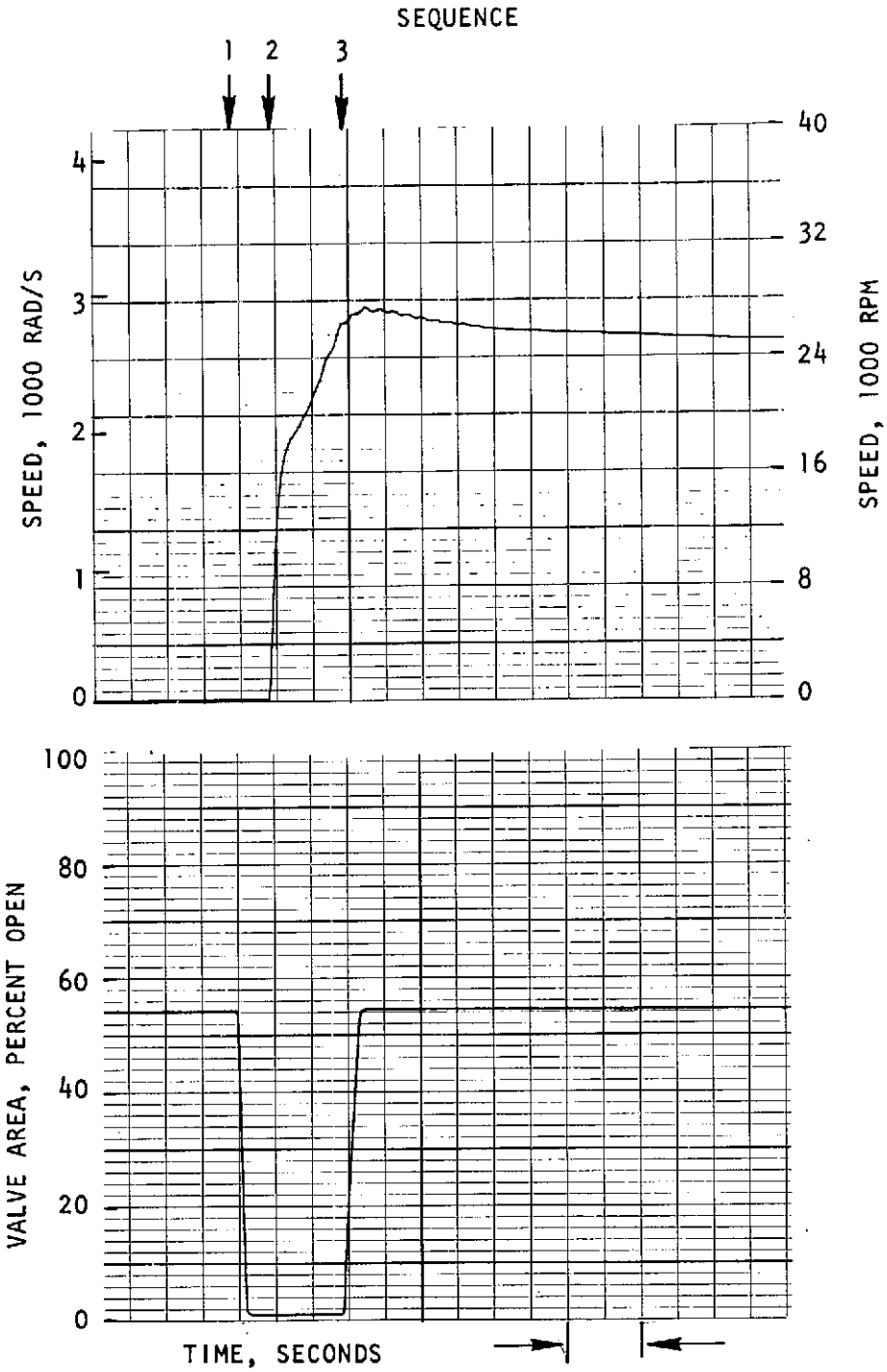

Figure 162. Turbopump Speed and Discharge Valve Area Transients for Deadhead Start Test With 0.098 m^3 (3.45 ft^3) and Discharge Volume and 4.2 x 10^6 N/m^2 (615 psia) Trigger Pressure

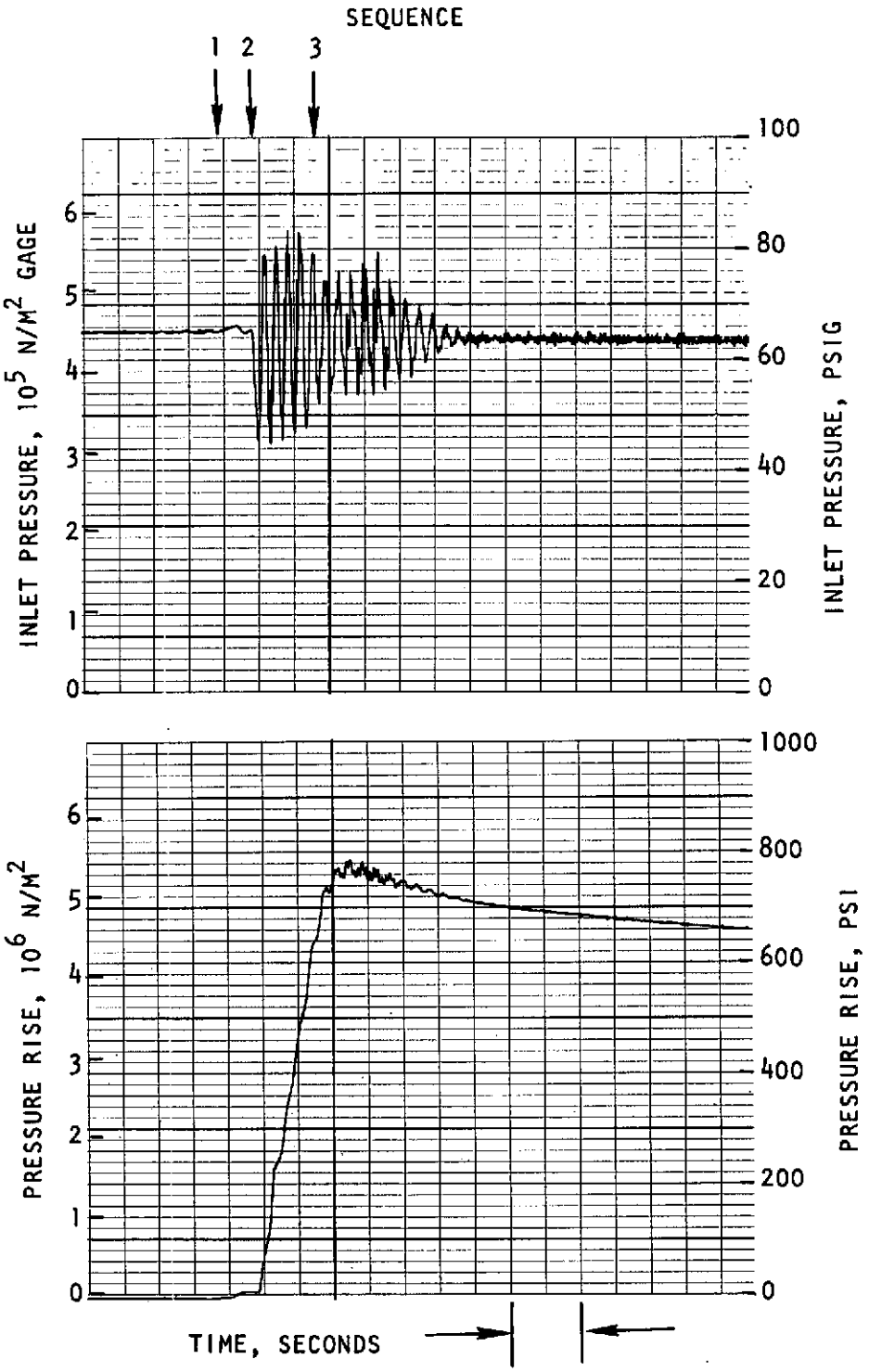

Figure 163. Pump Inlet Pressure and Pressure Rise Transients for Deadhead Start Test With 0.098 m^3 (3.45 ft^3) Discharge Volume and 4.2 x 10^6 N/m^2 (615 psia) Trigger Pressure

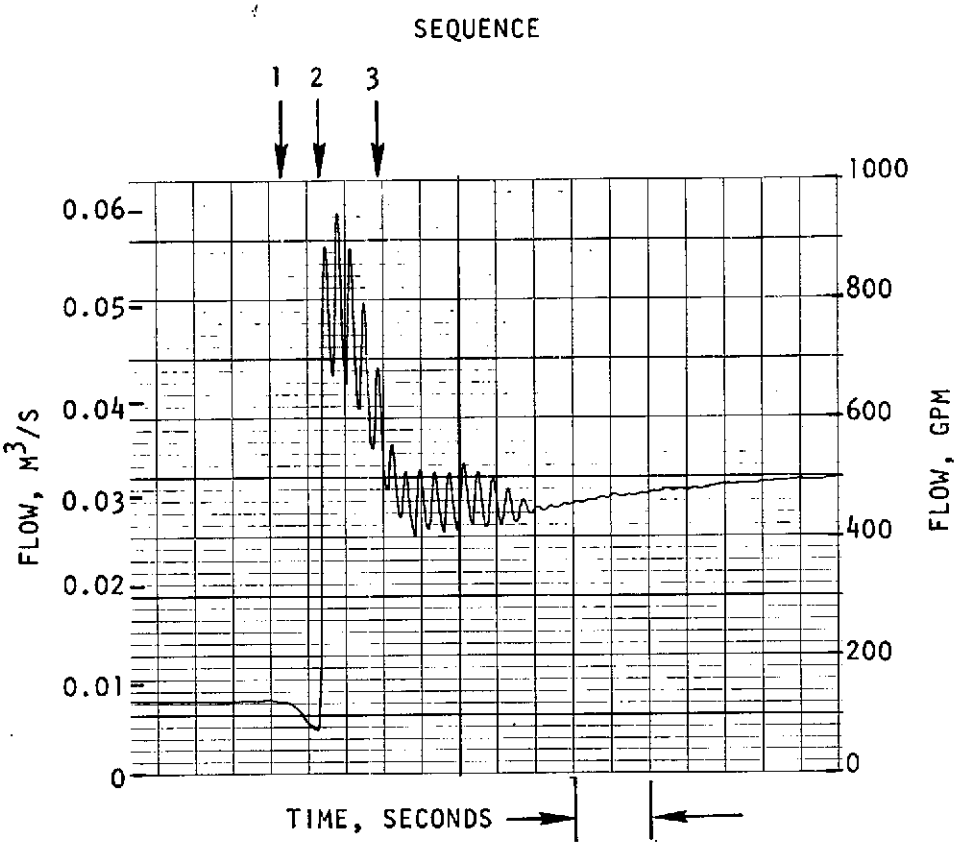

Figure 164. Inlet Duct Flow Transient for Deadhead Start Test With 0.098 m^3 (3.45 ft^3) Discharge Volume and 4.2 x 10^6 N/m^2 (615 psia) Trigger Pressure

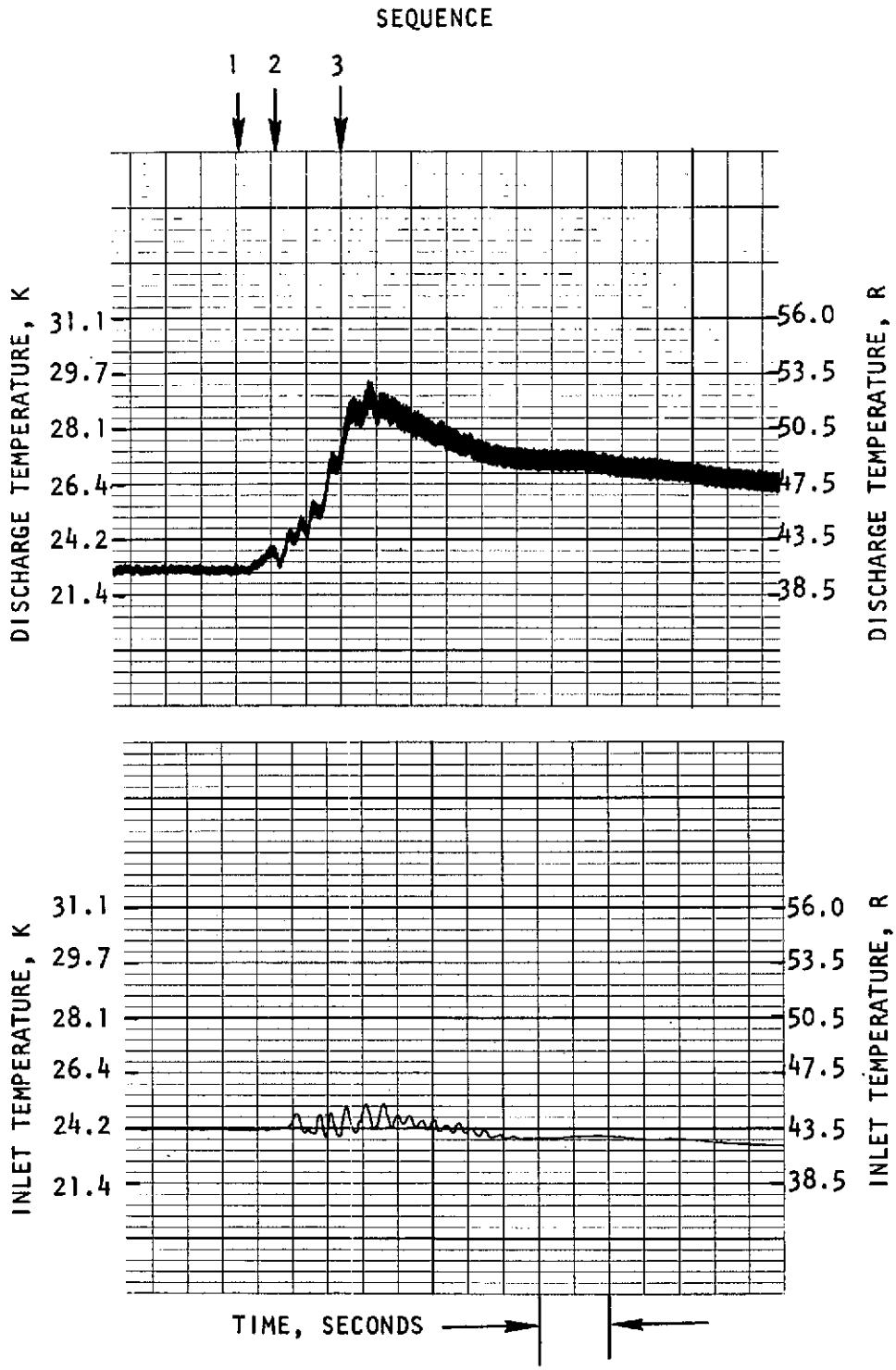

Figure 165. Pump Discharge and Inlet Hydrogen Temperature Transients for Deadhead Start Test With 0.098 m^3 (3.45 ft^3) Discharge Volume and 4.2 x 10^6 N/m^2 (615 psia) Trigger Pressure

to the one presented for the nominal test with the start-test discharge valve open (Fig. 156). The throttle valve position transient is also shown in Fig. 162. The pump inlet pressure and pressure rise are presented in Fig. 163. Figure shows the flowrate at the interface between the facility and inlet duct. The oscillations in pump inlet pressure and flowrate were present in all three successful deadhead starts. They were thought to be set up by the rapid acceleration of the high-pressure fluid in the discharge duct when the discharge valve is ramped open, however, later testing disproved this speculation. Temperature transients are shown in Fig. 165 for comparison with those presented for the previously discussed unsuccessful deadhead start (Fig. 161). One additional deadhead start was attempted (test No. 22) following what was to have been a partial chill. Since this test followed a previous test, rather than having ambient initial conditions, there was no accurate method of establishing the proper duration of chill and the system was actually fully chilled when turbopump rotation was initiated.

TASK IV: COATED FEED SYSTEM TESTS

The test facility built in Task III: Uncoated Feed System Tests was used to test the experimental coated feed system. The wetted surfaces of the inlet duct and pump were coated and 11 tests were run. These tests were conducted to obtain data on thermal conditioning and turbopump start under partial chill conditions. The results of these tests were used to evaluate the effectiveness of the coatings.

EXPERIMENTAL FEED SYSTEM PREPARATION

Since the inlet ducts and turbopumps used in the two experimental feed systems are identical, except for applied coatings, it was not necessary to make any facility modifications prior to testing the coated system. Instrumentation was also mounted at identical locations to facilitate comparative analyses. Descriptions of the test facility, inlet duct, and turbopump were presented in the section on Task III: Uncoated Feed System Tests. Coating materials, application techniques, and thicknesses were discussed in the section on Task II: Laboratory Sample Tests.

TEST PROCEDURES

Except for the coated turbopumps start tests that were attempted with only partially chilled hardware, the test procedures for coated and uncoated systems tests were identical. These procedures were presented in the section on Task III: Uncoated Feed System Tests.

Before testing the coated feed system, discussions with the contract monitor resulted in a decision to emphasize starting the turbopump in the shortest possible time from the initiation of pre-chill flow. It was therefore decided to alter the start sequence and flow through the chill-test discharge ducting during pre-chill because of its lower resistance. Since turbopump operating conditions, i.e., head, flow and speed, were unknown with this discharge ducting, and it had not

previously been used at high pressure, it was necessary to close the chill-test discharge valve before turbopump rotation. Rather than simultaneously open the valve in the start-test discharge ducting, it was opened at the start of pre-chill. Sequencing of the chill-test discharge valve and the turbine-inlet valve was done manually during this series of tests. A flow schematic showing this method of chilling the system is presented in Fig. 166.

DISCUSSION OF RESULTS

Eleven tests were conducted with the experimental coated feed system. The objectives of these tests were to obtain thermal-conditioning and turbopump start data to compare with the results of the uncoated feed system tests and to evaluate the effectiveness of the coatings. A list of the tests is shown in Table 25.

Feed System Chill

To obtain empirical data that would verify the predicted improvement in rapid start of cryogen turbomachinery, and verify the predicted reduction of required thermal preconditioning with increased thermal resistance at the fluid path boundary, the flow path boundary hardware of the inlet duct and pump were coated with a low thermal conductance material, KX-635, and the coated pump system was subjected to a prestart chill test.

The inlet duct was coated internally over the entire fluid boundary with approximately 0.0005 m (0.020 in.) KX-635. The stationary portion of the pump housing along the fluid flow path was also coated with approximately 0.0005 m (0.020 in.) KX-635. This coating thickness was applied to the housing around the inducer and the first- and second-stage impellers, and inside the crossover duct and the entrance and exit volutes.

To develop a valid comparison between the coated and uncoated pump systems, test 24 was conducted in the same upstream and downstream facility and at the same inlet pressure as for the uncoated system during test 7. The upstream facility was prechilled down to the inlet-duct valve in the same manner as for test 7, and

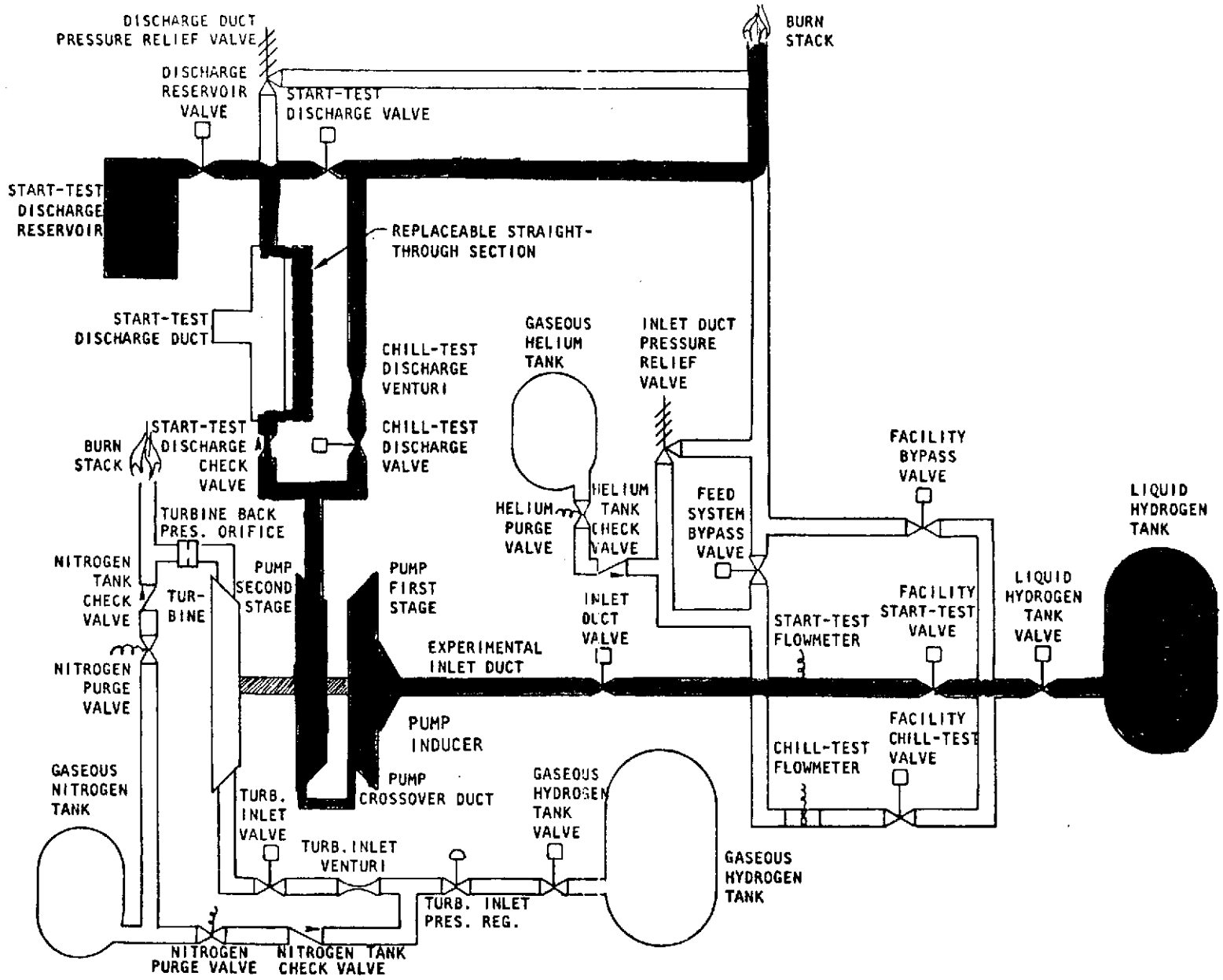

Figure 166. Flow Schematic for Partially Chilling Experimental Feed System Prior to Turbopump Start

TABLE 25. SUMMARY OF COATED FEED SYSTEM TESTS

Purpose	Test No.	Pump Inlet Pressure 10^5 N/m^2 (psia)	Start-Test Discharge Valve Trigger Pressure 10^6 N/m^3 (psia)	Discharge Volume m^3(ft^3)	Comments
Chill to 100 Percent	24	6.1 (88)	NA	NA	Acceptable data
Pump Performance	25	5.5 (80)	Valve Open	0.098 (3.45)	Acceptable data, double rpm indicated (wrong number of gear teeth assumed)
Pump Performance	26	5.5 (80)	Valve Open	0.098 (3.45)	Acceptable data
Nominal Start Conditions	27	5.5 (80)	Valve Open	0.098 (3.45)	Acceptable data
Start With Partial Chill	28a	5.5 (80)	Valve Open*	0.098 (3.45)	Pre-start cut (incorrect valve position detect)
Start With Partial Chill (Intermediate Chill)	28b	5.5 (80)	Valve Open*	0.098 (3.45)	Breakdown in developed head, overspeed cut
Start With Partial Chill (Least Chilled)	30	5.5 (80)	Valve Open*	0.098 (3.45)	Breakdown in developed head, overspeed cut
Start With Partial Chill (Most Chilled)	31	5.5 (80)	Valve Open*	0.098 (3.45)	Acceptable start
Deadhead Start With 100 Percent Chill	29	5.5 (80)	4.2 (615)	0.098 (3.45)	Breakdown in developed head (trigger pressure set higher than nominal discharge pressure), overspeed cut
Deadhead Start With 100 Percent Chill	32	5.5 (80)	4.2 (615)	0.098 (3.45)	Breakdown in developed head (trigger pressure set higher than nominal discharge pressure), overspeed cut
Deadhead Start With 100 Percent Chill	33	5.5 (80)	3.6 (515)	0.098 (3.45)	Breakdown in developed head (trigger pressure set higher than nominal discharge pressure), overspeed cut
Deadhead Start With 100 Percent Chill	34	5.5 (80)	2.9 (415)	0.098 (3.45)	Acceptable start

NA - Not Applicable (flowing through chill test discharge duct)

* Chill-test discharge valve also open during chill

within practical limits test 24 was a duplicate of test 7, except that the uncoated pump system was replaced by a coated pump system. Both the coated and uncoated pump systems during tests 24 and 7, respectively, were initially at ambient temperature except for the conduction to the inlet of the inlet duct through the inlet duct valve from the prechilled facility as discussed in the Task III section of this report.

Analysis of Coated Pump System Test Data. System hardware temperatures and fluid flow temperature, and pressure data as a function of time are listed for test 24 in Table 23 (Table 24). These are the same data as listed for the uncoated pump systems in the same table and are directly comparable. The pump inlet pressure was 5.03×10^5 N/m^2 gage (73 psig), purposely close to the inlet pressure of 5.17 10^5 N/m^2 gage (75 psig) during chill test 7 with the uncoated system.

Fluid temperatures, inlet duct temperatures and pump housing temperatures are presented graphically in Fig. 167 for the coated pump system during test 24. Dynalog pump inlet pressure and turbine flowmeter flowrate time histories are presented in Fig. 168 and 169.

Figure 170 superimposes the fluid temperatures into and exiting the pump on selected inlet duct and pump housing temperatures, comparing the coated pump test 24 data and the uncoated pump test 7 data. The fluid flow path coating insulation blocks the heat transfer from the hot inlet duct and pump hardware as reflected by the higher hardware temperatures during test 24 and evidenced by comparing tests 24 and 7 in Fig.167 and 149 or in Table 23 (Table 24).

The hydrogen fluid begins liquefying at the pump inlet (inlet duct exit) in 5 seconds and the pump exit in 11 seconds. The fluid approaches 100-percent liquid at the pump inlet in 14.5 seconds and through the entire pump at the exit in 20 seconds. These data indicate a significant reduction in required thermal preconditioning for the coated pump compared to the uncoated pump, comparing data from test 24 and 7 .

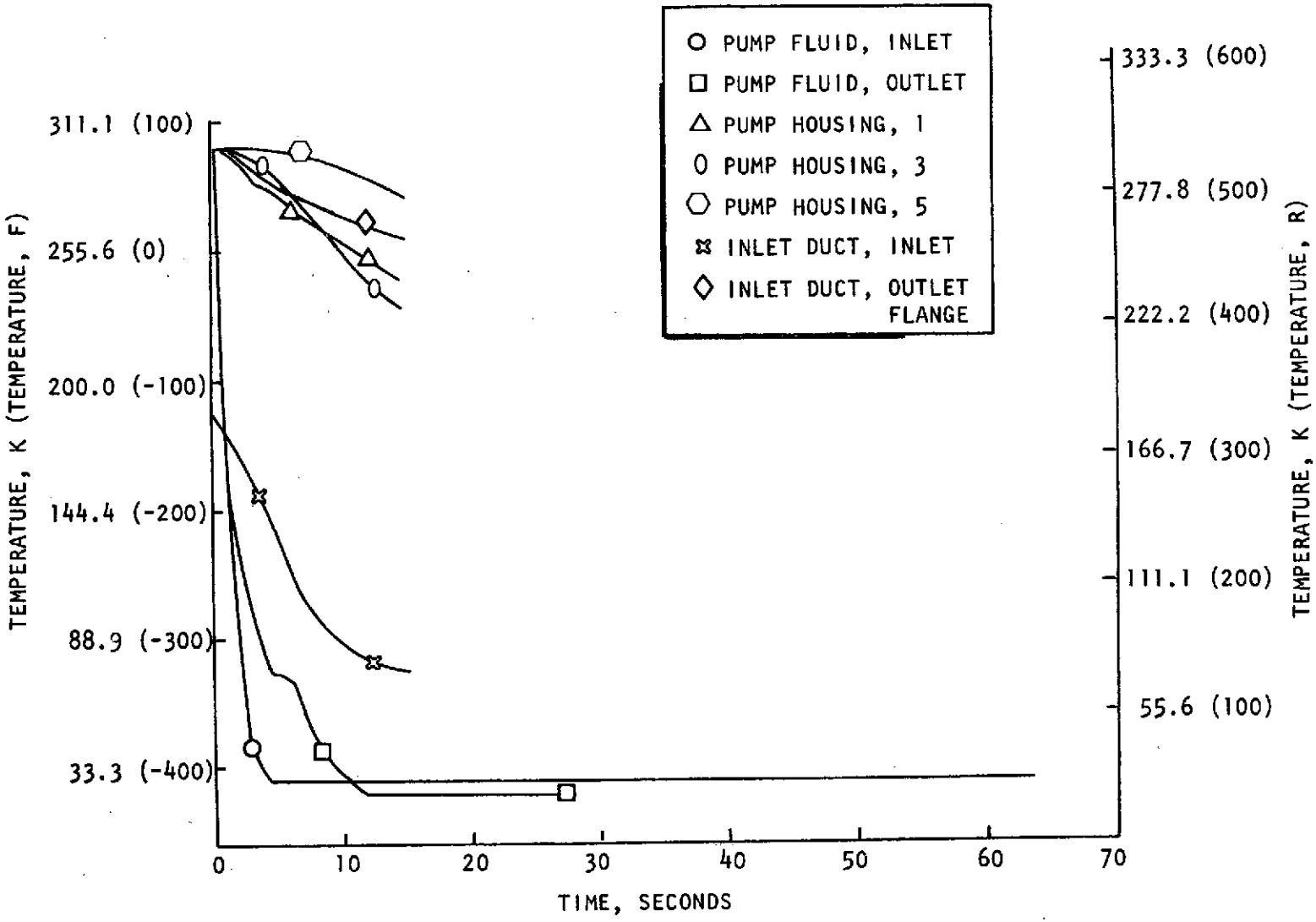

Figure 167. Coated Pump System Chill Fluid and Hardware Temperature History Test 24

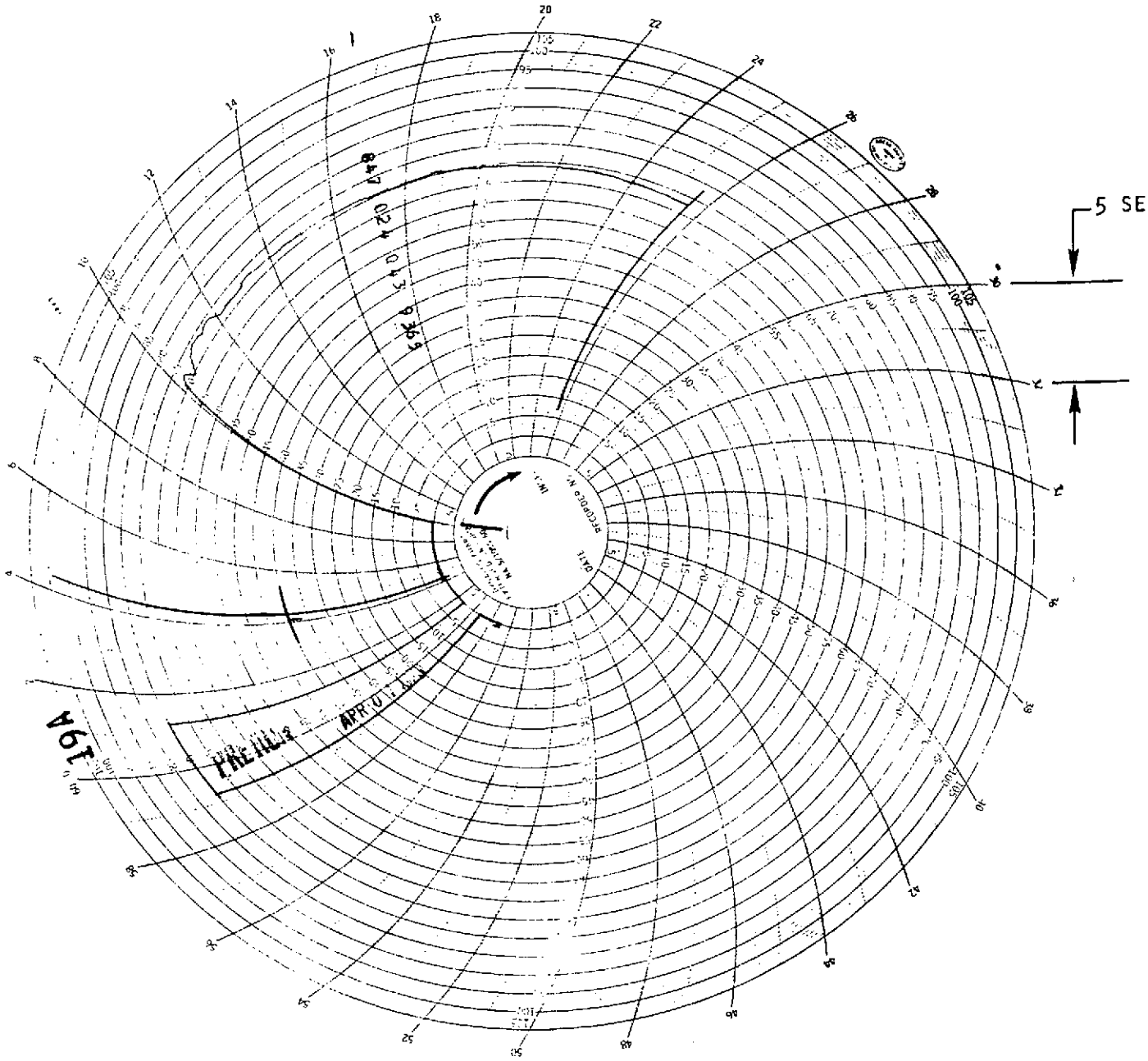

Figure 168. Coated System Pump Inlet Pressure Dynalog Data Test 24

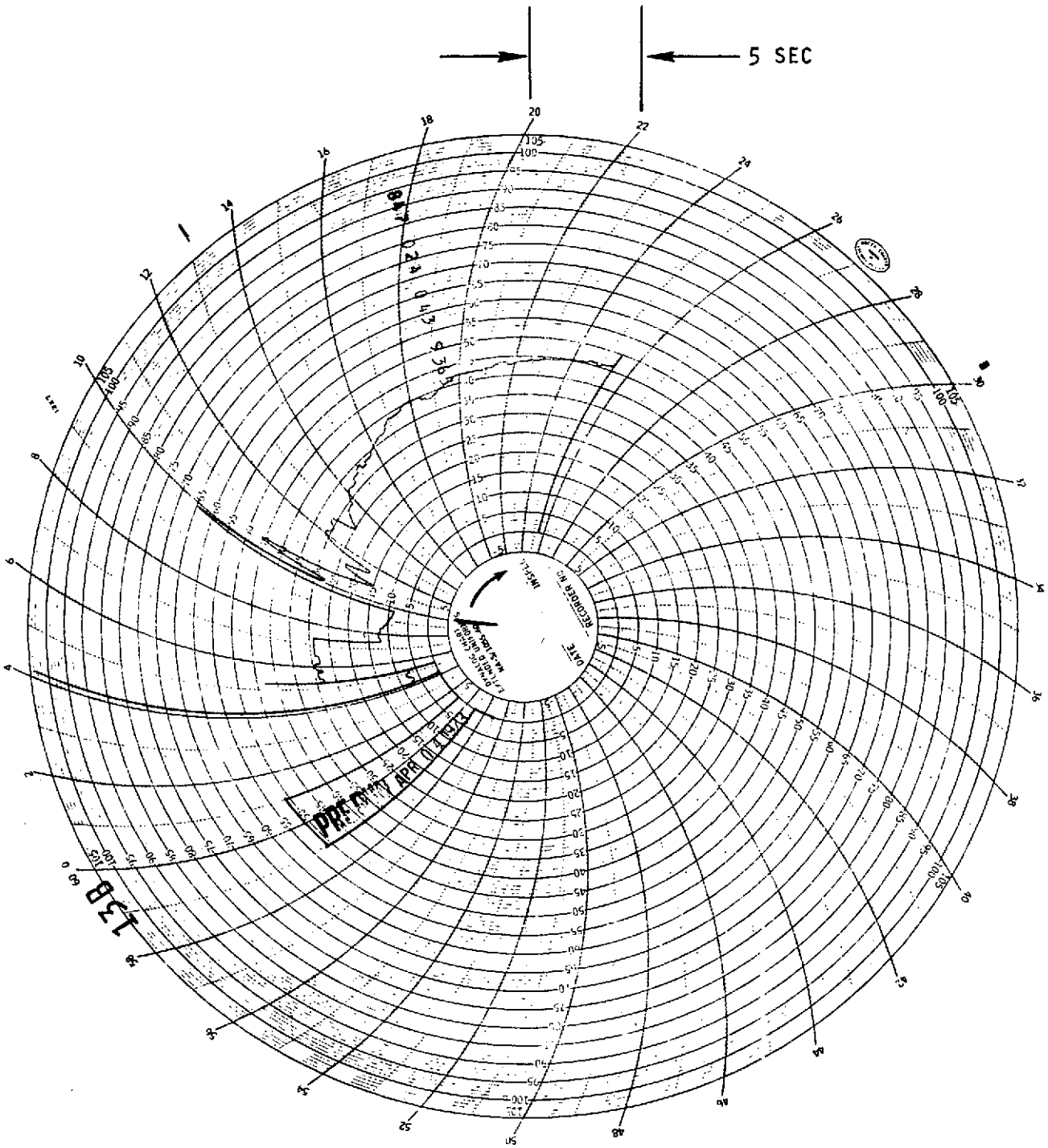

Figure 169. Coated System Turbine Flowmeter Flowrate Dynalog Data Test 24

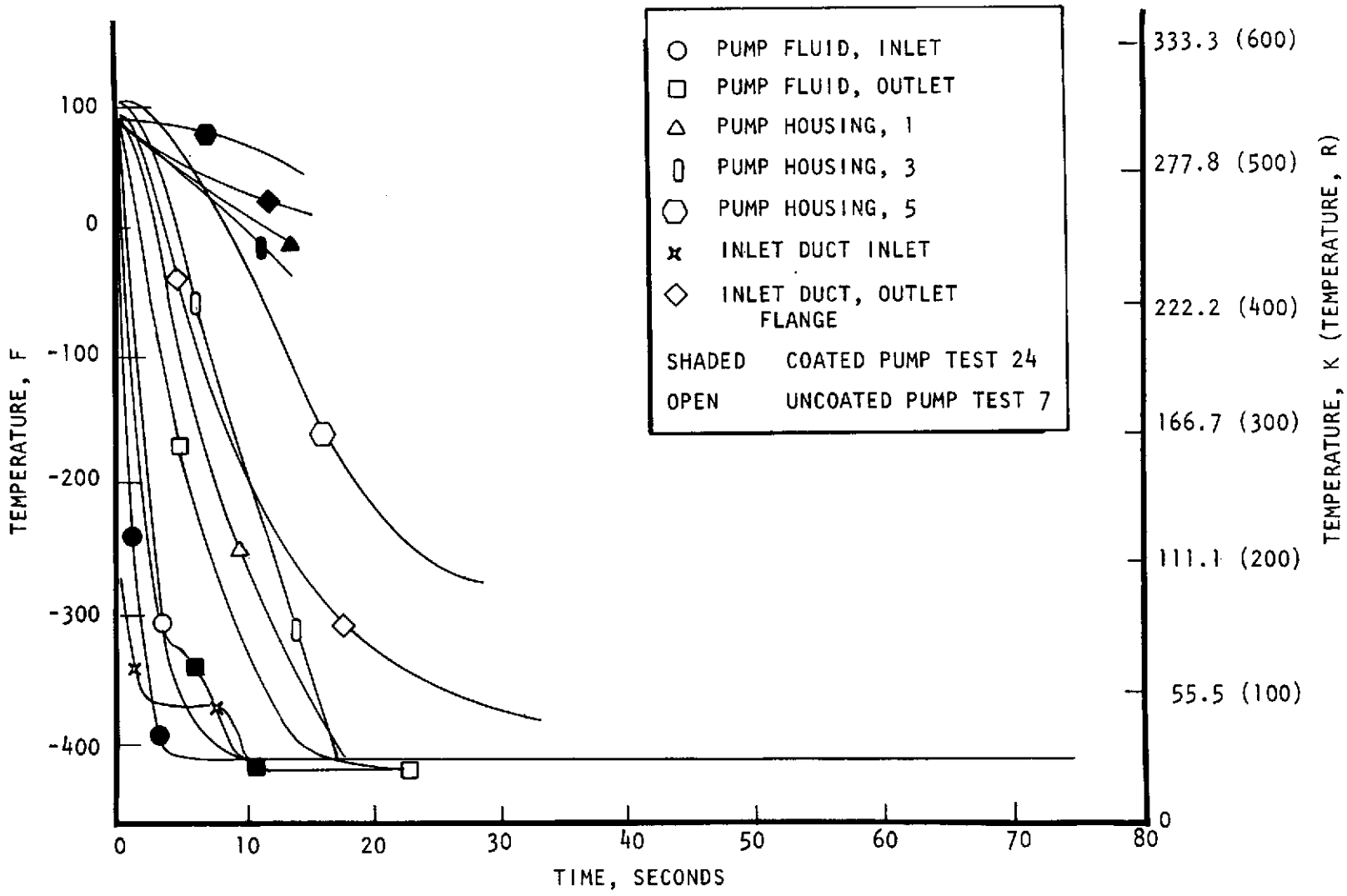

Figure 170. Coated and Uncoated Pump Systems Comparison of Chill Fluid and Hardware Temperature Histories of Tests 7 and 24

Partially chilled hardware temperatures were predicted for the uncoated pump system are presented graphically in Fig. 171. Data for partial chill of an uncoated and a coated feed system, from start tests 22 and 31, are superimposed on this same figure for comparison. The coated pump hardware is chilled at a reduced temperature gradient indicating significantly reduced heat flux from the hardware to the cryogen as anticipated.

Nominal Turbopump Start and Steady-State Performance. Three tests were conducted to determine steady-state pump performance and the nominal start transient. The first test conducted for pump performance data (test No. 25) was inadvertantly run at speeds below 1360 rad/s (13,000 rpm). The number of gear teeth on the turbopump drive shaft was incorrectly assumed and resulted in an indicated speed equal to twice the actual value. The duration of this test was 2-1/2 minutes.

The second pump performance test (test No. 26) resulted in extensive data. The turbopump was initially accelerated to approximately 590 rad/s (5600 rpm) and gradually increased to 1590 rad/s (15,200 rpm). Steady-state operating conditions were then varied for combinations of speeds between 1590 and 2600 rad/s (15,200 and 24,800 rpm), flows between 0.019 and 0.03 m^3/s (300 and 470 gpm), and discharge valve areas between 50 and 75 percent of the full open value. The duration of this test was over 3-1/2 minutes.

Seven steady-state operating conditions were selected from this run to determine the effect of the coatings on pump performance. The rotational speeds for these seven conditions were between 1590 and 2560 rad/s (15,200 and 24,400 rpm) and the flow coefficients were between 78 and 108 percent of the "design point" value shown in Fig. 155. The heads developed by the pump were calculated in the same manner as described for the uncoated pump. The calculated values for all seven conditions were between 75 and 82 percent of the corresponding developed heads interpolated from Fig. 155. This performance is significantly less than the 95 to 98 percent reported for the uncoated pump. A part of this performance reduction is caused by the thick coating on the pump discharge. The discharge flow area is significantly reduced by the coating which alters the velocity vectors within the pump. This is not a problem, since it can be precluded by allowing for coating thicknesses during pump design.

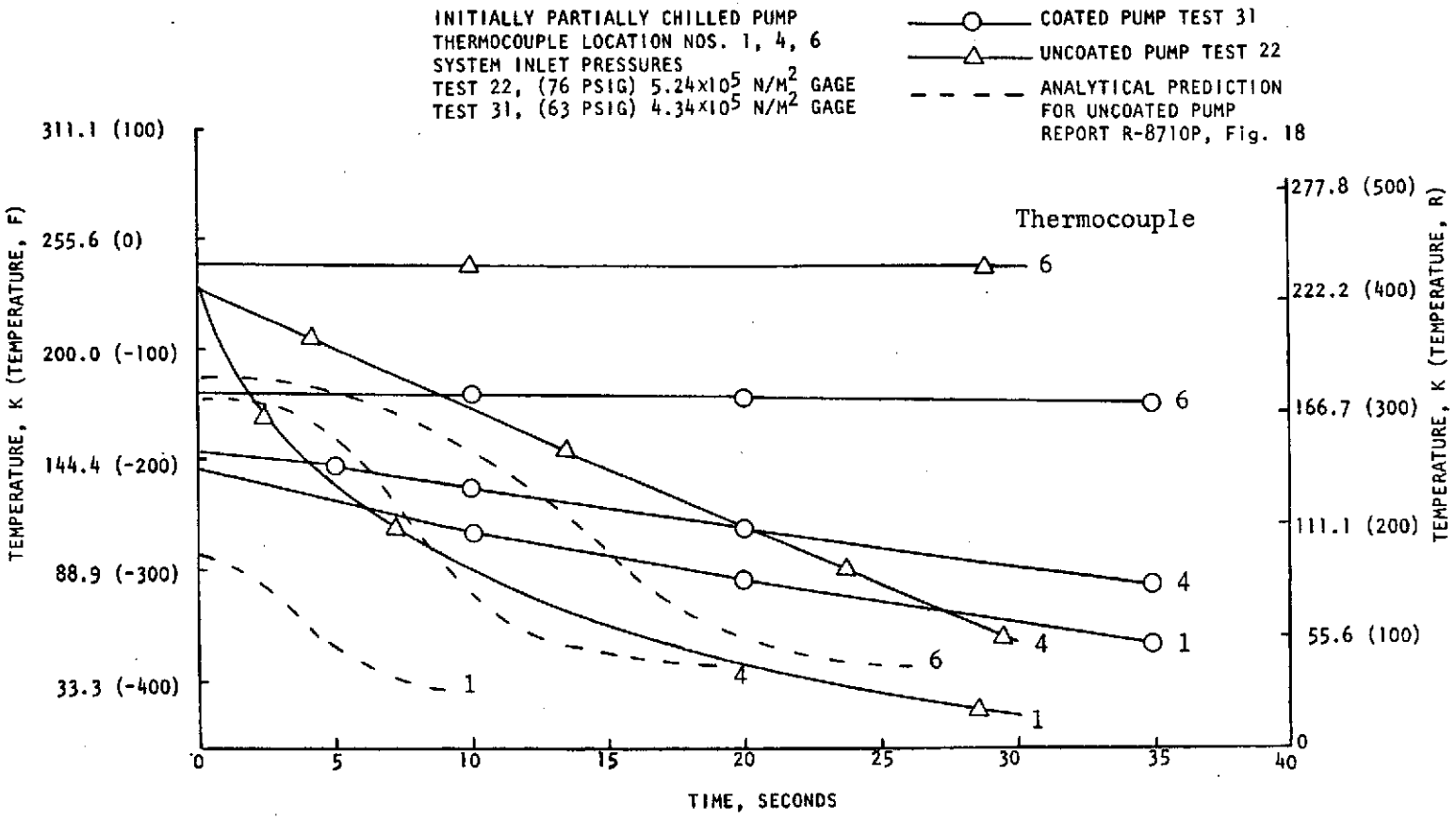

Figure 171. Partial Chill Pump Housing Temperatures History

During the test conducted to define the nominal start transient for the coated feed system (test No. 27), pressure and flow oscillations were experienced in the inlet duct as shown in Fig. 172. These oscillations are similar to those present in the successful deadhead starts conducted with the uncoated feed system. During testing of the uncoated feed system, it was thought the oscillations were precipitated by deadhead-start conditions since they were the only tests in which the oscillations occurred when the pump inlet pressure was approximately 5.5×10^5 N/m^2 (80 psia), and they occurred in all three tests that started successfully. However, the nominal start test with the coated system was conducted with the discharge valve open. The oscillations cannot be attributed, in total, to the inlet-propellant conditions either. For example, oscillations existed in this coated system test with pump inlet propellant conditions of 5.6×10^5 N/m^2 (80.5 psia) and 24 K (43 R), but not in a subsequent coated system start test with corresponding conditions of 5.4×10^5 N/m^2 (79 psia) and 27.5 K (49.5 R). If the oscillations were due to the generation of vapor in the inlet duct during high flow acceleration, it is expected that the latter of these two tests would have experienced oscillations since the hydrogen was at saturated conditions, and in the other one the hydrogen was subcooled at the initiation of turbopump rotation.

Turbopump Start With Partially Chilled System. Three turbopump start tests were conducted with different degrees of prechill. The test that was least chilled at the initiation of turbopump rotation (test No. 30) was chilled from ambient initial conditions. The results of this test are presented in Fig. 173 and 174. Sequence numbers on these figures refer to the following events:

1. Open inlet duct valve
2. Close chill-test discharge valve
3. Open turbine inlet valve
4. Turbopump overspeed cut initiated

When turbine power was applied, the turbopump accelerated very rapidly to 3140 rad/s (30,000 rpm) and an automatic cut was initiated (Fig. 173). The pump

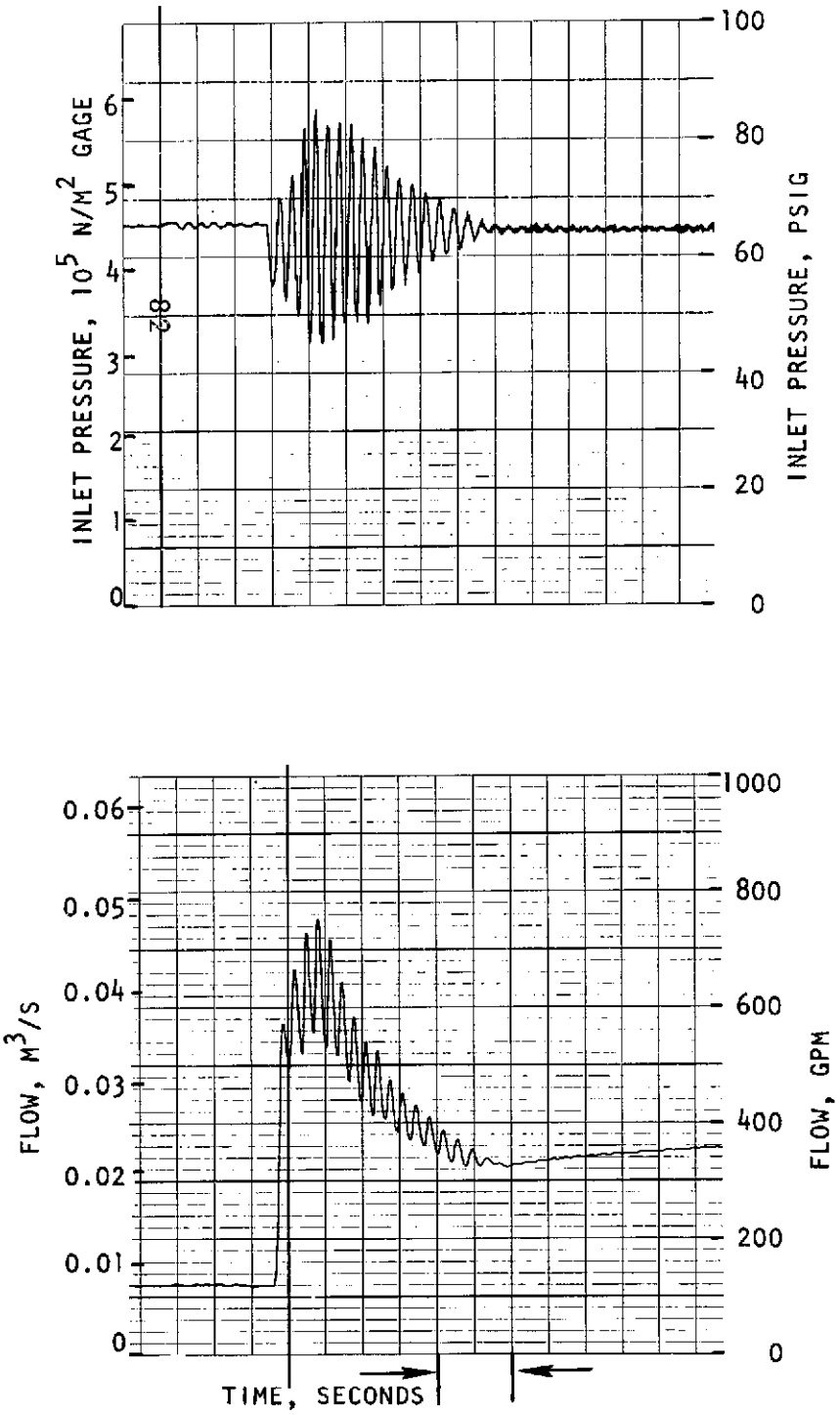

Figure 172. Pump Inlet Pressure and Inlet Duct Flow Transients for Baseline Start

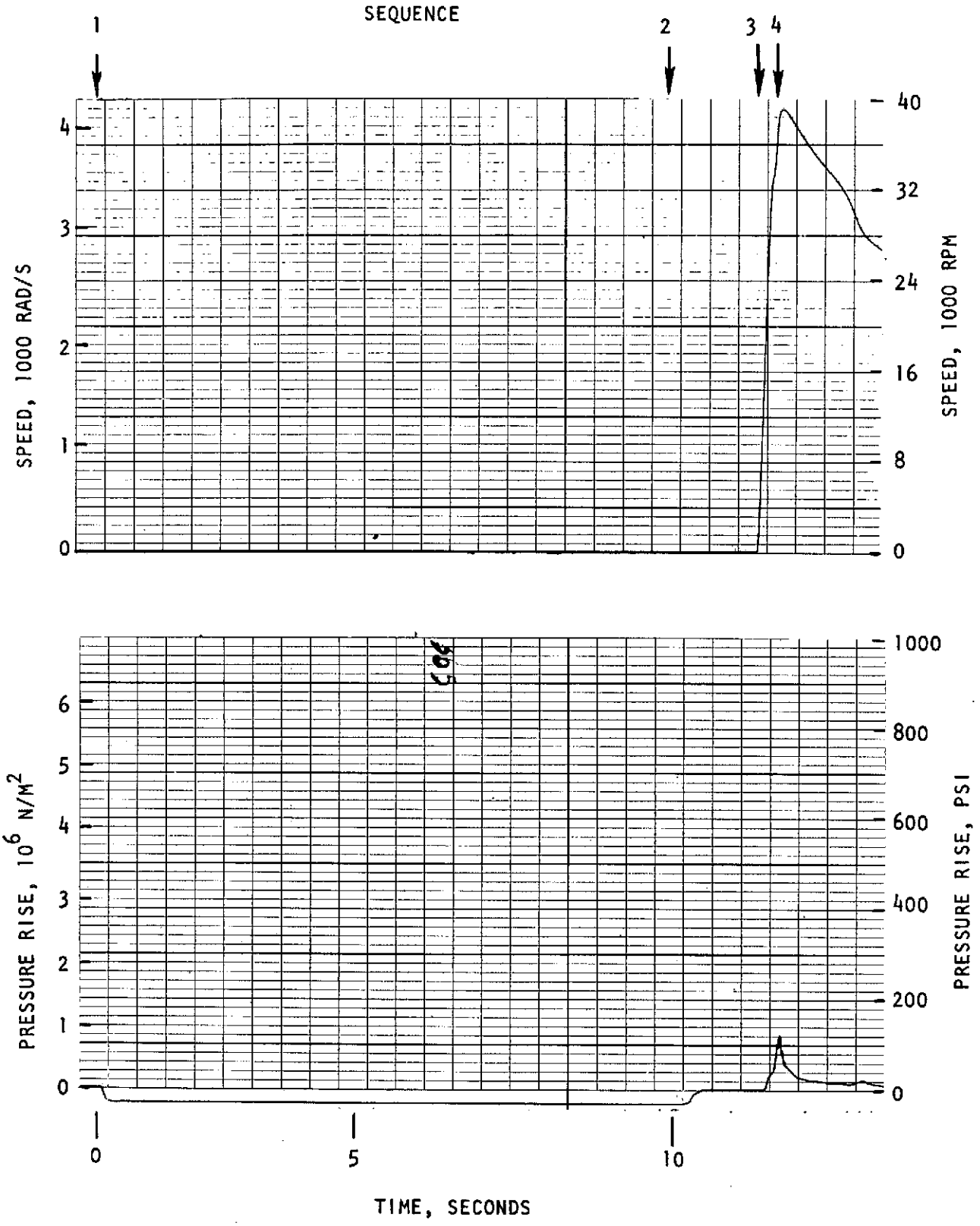

Figure 173. Pump Speed and Pressure Rise Transients for Least Chilled Start Test

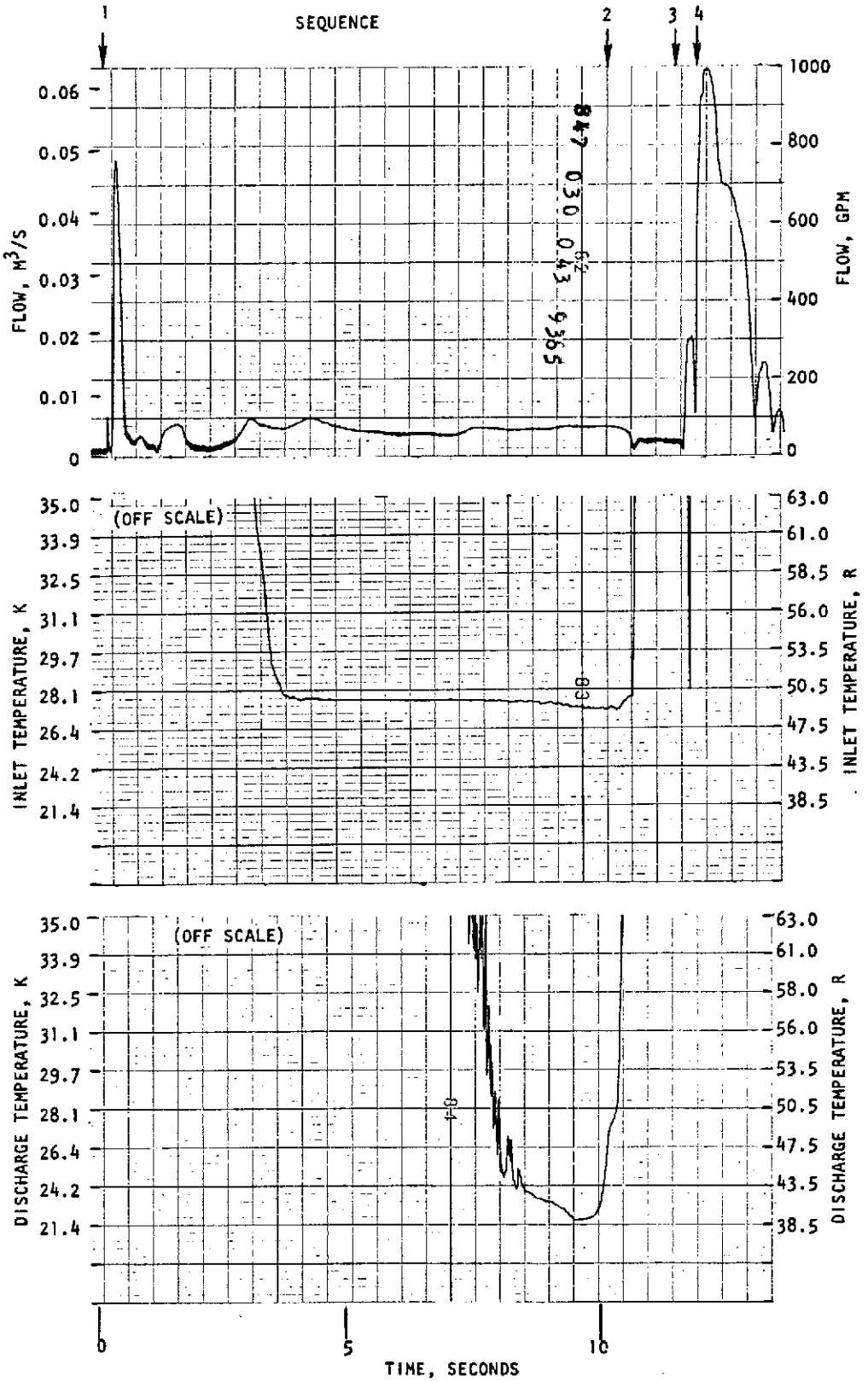

Figure 174. Inlet Duct Flow, Pump Inlet Hydrogen Temperature and Pump Discharge Hydrogen Temperature Transients for Least-Chilled Start Test

pressure rise was negative prior to rotation due to friction losses (Fig. 173). At approximately 10 seconds the pressure rise approached zero, however, when the chill-test discharge valve was closed, the chill flow decreased. The start-test discharge valve remained open as discussed previously. During rotation the pump pressure rise peaked at approximately 8.3×10^5 N/m^2 (120 psi) when head breakdown occurred. A chill flowrate of approximately 0.005 m^3/s (80 gpm) was established before the chill-test discharge valve was closed; but afterwards, the flow was cut to half this value (Fig. 174). The pump-inlet hydrogen temperature decreased to 27 K (49 R) before the chill-test discharge valve was closed, but heated vapor was generated after closing the valve (Fig. 174). Heated vapor was present at the pump inlet when rotation was initiated. The pump exit hydrogen temperature followed a similar transient. The temperature decreased to 22 K (39 R), but heated vapor was generated when the prechill flow was reduced. During prechill, a lower temperature was achieved at the pump discharge than at the inlet, due to the lower pressure at the discharge.

Results from the test with an intermediate degree of prechill (test No. 28b) are presented in Fig.175 and 176. The portion of the test shown in these figures did not have ambient initial conditions, however, and absolute times should not be compared with the previously discussed partial-chill test. During prechill from ambient conditions (test No. 28a) an automatic cut was initiated due to detection of an incorrect valve position that required the test to be rerun.

The pump accelerated to approximately 2300 rad/sec (22,000 rpm) and leveled off for one second before a breakdown in developed head occurred (Fig. 175). A pump pressure rise of nearly 2.8×10^6 N/m^2 (400 psi) was developed before breakdown (Fig. 175). After a steady prechill flow of 0.005 m^3/s (80 gpm), the flow decreased (after an initial oscillation) when the chill-test discharge valve was closed (Fig. 176). Hydrogen temperature at the pump inlet was 27 K (49 R) before the discharge valve was closed; but afterwards, the lower chill flow caused the inlet temperature to spike to over 34 K (61 R), and undoubtedly pockets of vapor were generated in the inlet duct (Fig. 176). This was a less-severe condition than observed in the previously discussed test and indicates a more fully-chilled system. The pump discharge temperature was 23 K (41 R) before the chill-test

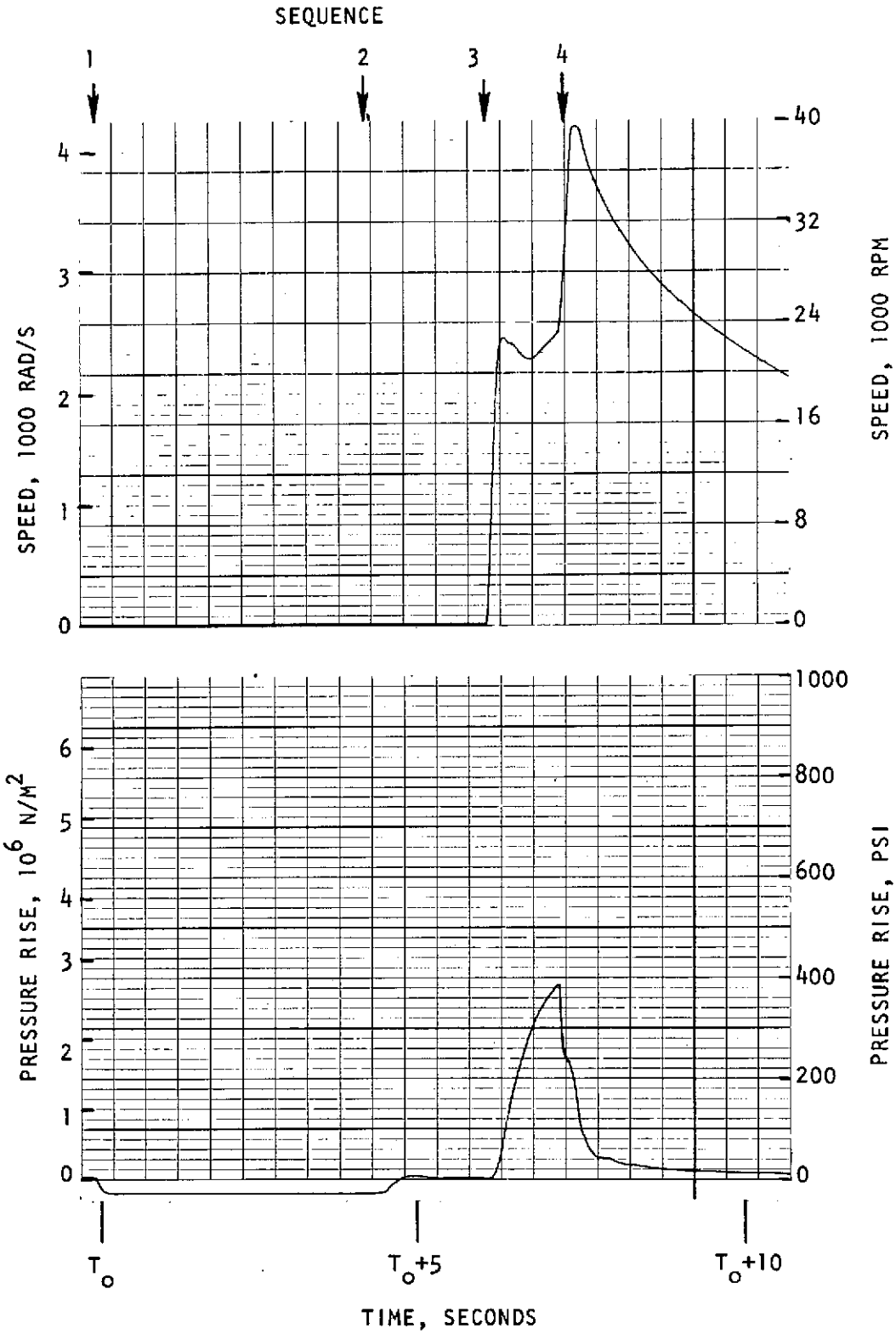

Figure 175. Pump Speed and Pressure Rise Transients for Intermediate Chilled Start Test

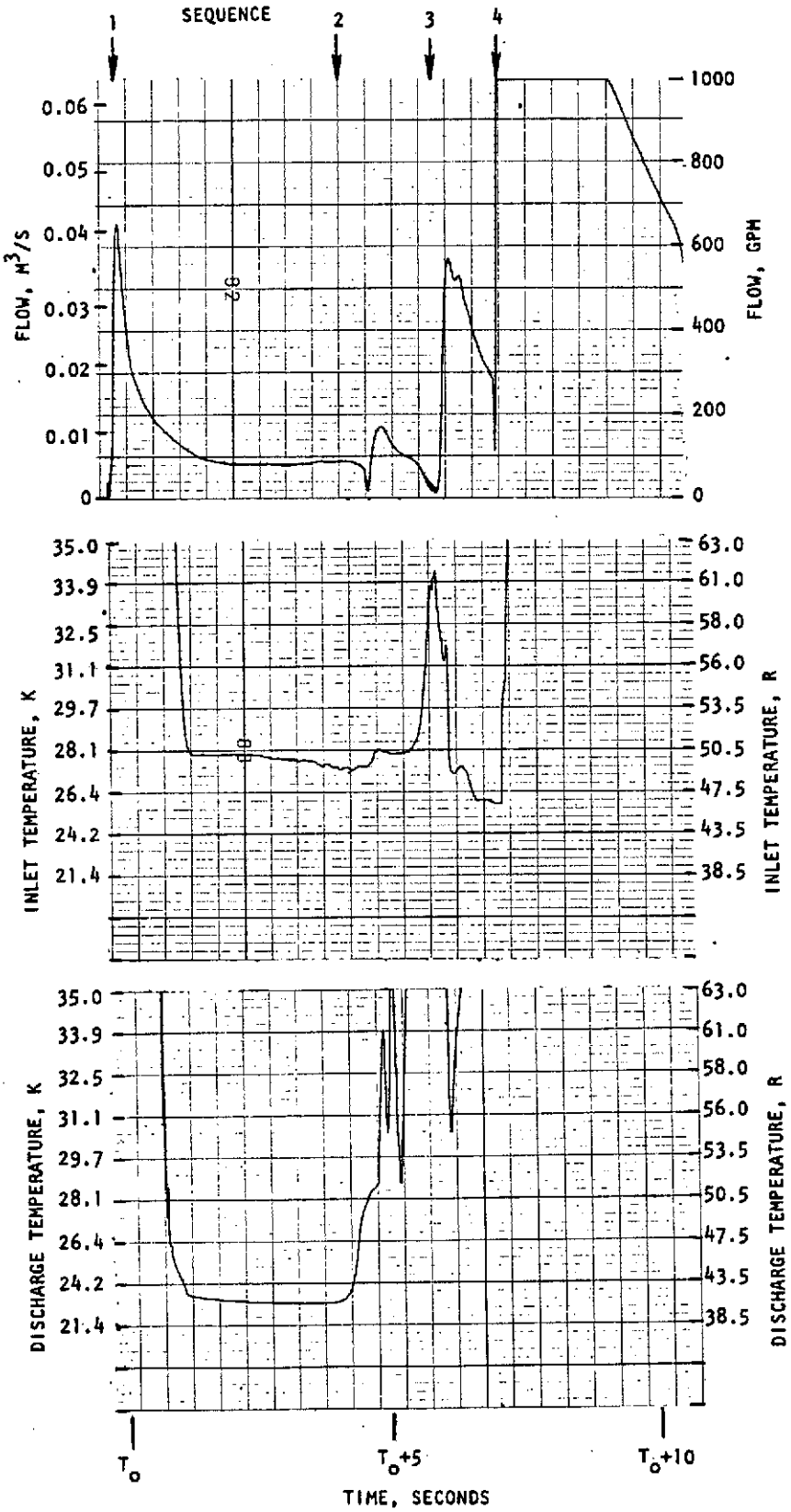

Figure 176. Inlet Duct Flow, Pump Inlet Hydrogen Temperature and Pump Discharge Hydrogen Temperature for Intermediate Chilled Start Test

discharge valve was closed; but, after oscillating, went off scale after the valve was closed (Fig. 176). Heated vapor was present at the discharge when the pump was initially accelerated, but the temperature indicator did come back on-scale for approximately 0.25 seconds.

The most chilled of the three partially-chilled start tests (test No. 31) was conducted the same day after the test just described and, likewise, was not prechilled from ambient initial conditions. The results of this successful start test are presented in Fig. 177 and 178.

The pump speed transient (Fig. 177) was very smooth and settled out at 2300 rad/s (22,000 rpm). The pump pressure rise was 3.1×10^6 N/m^2 (450 psi) at this speed (Fig. 177). The prechill flow gradually increased from 5.5×10^5 to 1.2×10^6 m^3/sec (80 to 180 gpm) before the chill-test discharge valve was closed (Fig. 178). Afterwards, the prechill flow decreased to 2.8×10^5 m^3/sec (40 gpm). A normal flow transient was then indicated during turbopump start. The pump inlet temperature decreased to 24 K (44 R) before the discharge valve was closed, but then increased to only 28 K (50 R) after it was closed (Fig. 178). This transient indicates this test was the most chilled of the three in this series. After pump rotation was initiated the inlet temperature decreased again. The pump exit temperature decreased to 22 K (40 R) before the chill-test valve was closed, but increased to 28 K (50 R), afterwards (Fig. 178). Upon initiation of pump rotation, the exit temperature increases due to pump inefficiency.

It is conceivable that the first two partially chilled tests were unsuccessful because of propellant conditions that resulted from closing the chill-test discharge valve, rather than being the result of lesser degrees of prechill. It is significant to note that the third test started successfully with an inlet temperature of 28 K (50 R), the temperature that existed after the chill-test discharge valve was closed. Figure 174 shows that this temperature can be achieved in less than ten seconds with ambient initial conditions and a prechill flow of 5.5×10^5 m^3/s (80 gpm). Figure 174 shows that very low hydrogen temperatures

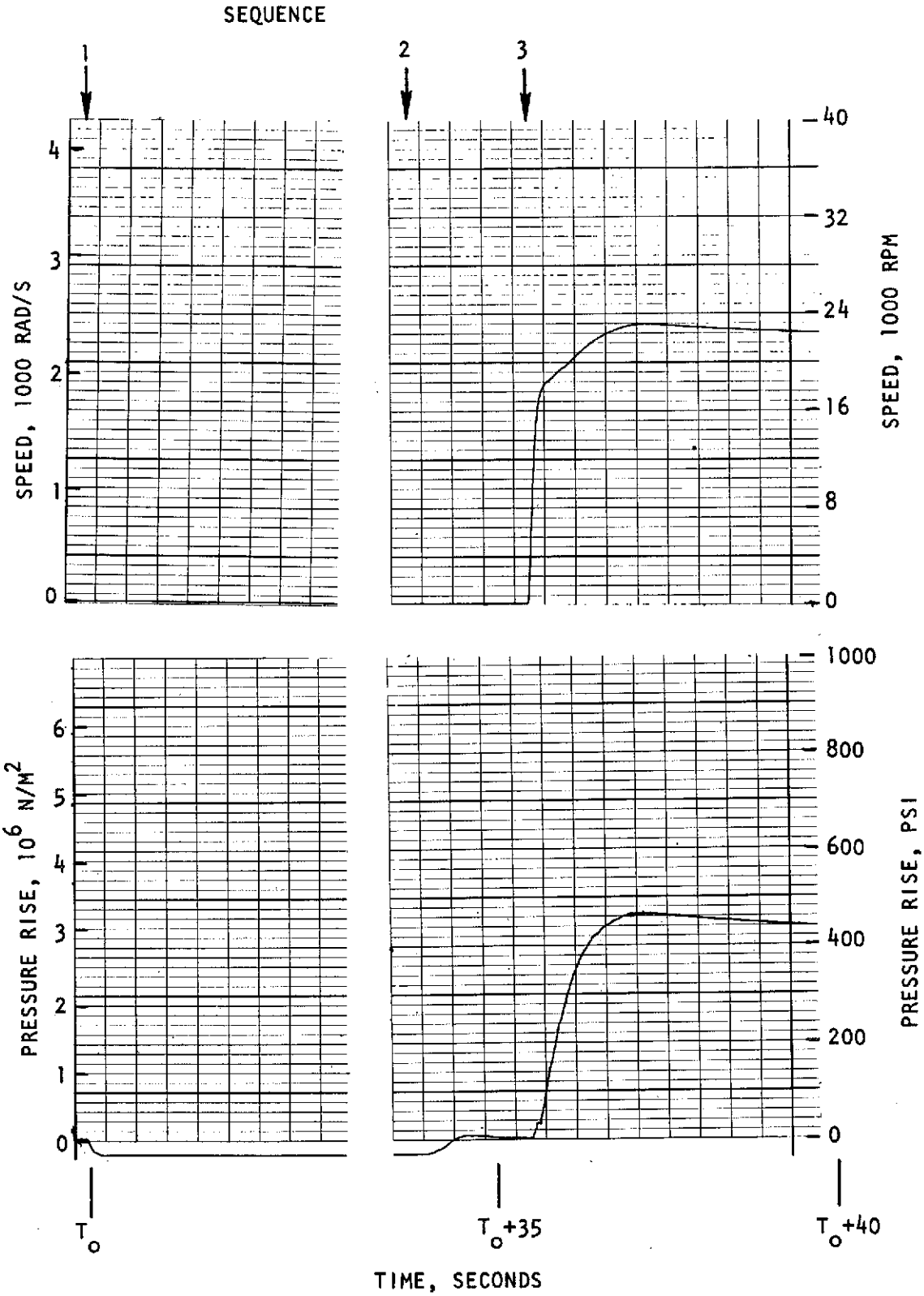

Figure 177. Pump Speed and Pressure Rise Transients for Most Chilled Start Test

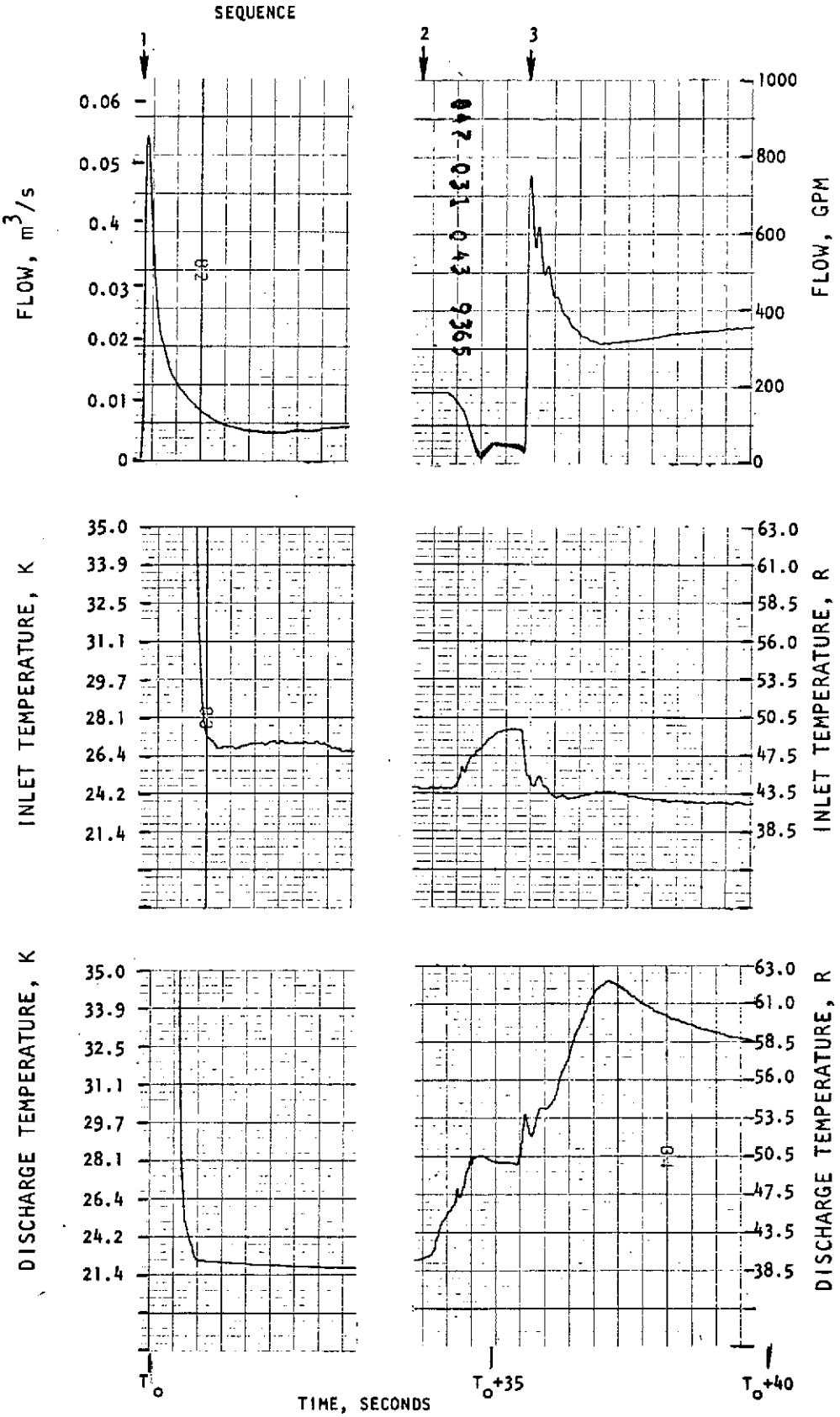

Figure 178. Inlet Duct Flow, Pump Inlet Hydrogen Temperature and Pump Discharge Hydrogen Temperature for Least Chilled Start Test

R-9273

can also be obtained at the pump discharge in less than 10 seconds. It is speculated that with a modified start sequence to prevent the reduction in prechill flow immediately preceding pump rotation, the coated pump could be started in less than 10 seconds.

Deadhead Turbopump Start. Four coated feed system start tests were conducted under deadhead conditions with a fully-chilled system on the two days that partial-chill tests were run. Since it takes several hours for the feed system to warm up sufficiently to run partial-chill tests, no more than two could be run on any day. Rather than conclude testing in the early afternoon after the second test, deadhead-start tests were conducted. Unfortunately, the results cannot be directly related to the uncoated system tests because the coated pump develops significantly less head. The downstream volume used in the coated system deadhead starts was 0.098 m^3 (3.45 ft^3), the same as used in the successful uncoated system tests.

The first two tests in this series of deadhead starts (tests No. 29 and 32) required a pump discharge pressure of 4.2×10^6 N/m^2 (615 psia) to initiate opening of the start-test discharge valve. This trigger pressure exceeded the pressures developed by the pump during the transients and, therefore, the discharge valve did not open in either test. A breakdown in developed head occurred in both tests and cutoffs were initiated by the overspeed redline. The transient data and sequence of events resulting from these two tests is very similar to the data presented for the unsuccessful uncoated system deadhead starts and will not be reiterated in this section.

The discharge valve trigger pressure was lowered to 3.6×10^6 N/m^2 (515 psia) for the next test (test No. 33), but it had little effect on the start transient. Although the discharge valve opened, sufficient through-flow was not established soon enough to prevent a breakdown in developed head.

The final test in this series (test No. 34) had a trigger pressure of 2.9×10^6 N/m^2 (415 psia) and started successfully. The transient data for this test, presented in Fig. 179 through 182, is similar to the successful uncoated system test data, except the pressure and flow oscillations in the inlet duct were not evident. The data is presented in this section for that reason and further explanation of the transients is not considered necessary.

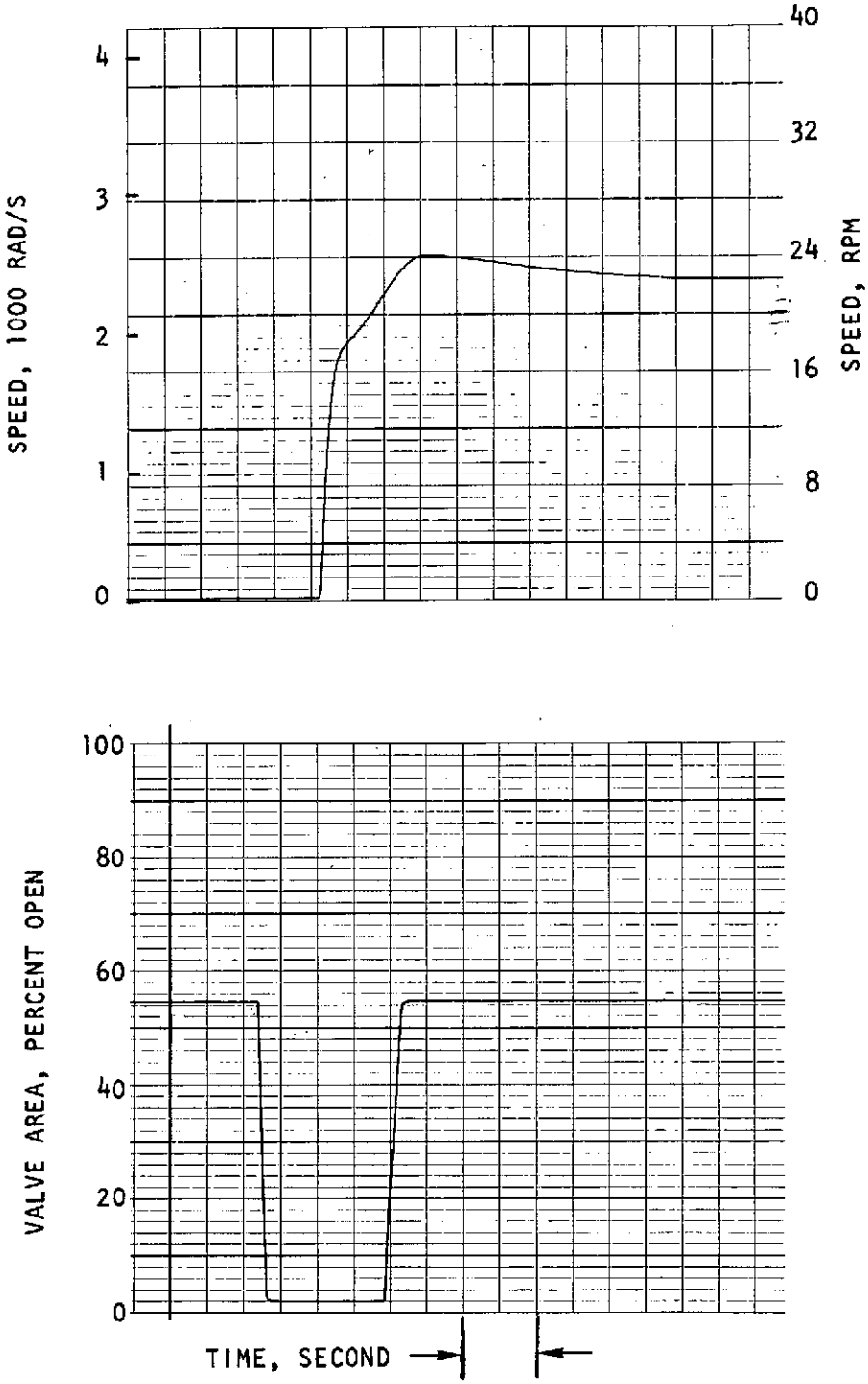

Figure 179. Turbopump Speed and Discharge Valve Area Transients for Deadhead Start Test With 0.098 m^3 (3.45 ft^3) Discharge Volume and 2.9×10^6 N/m^2 (415 psia) Trigger Pressure

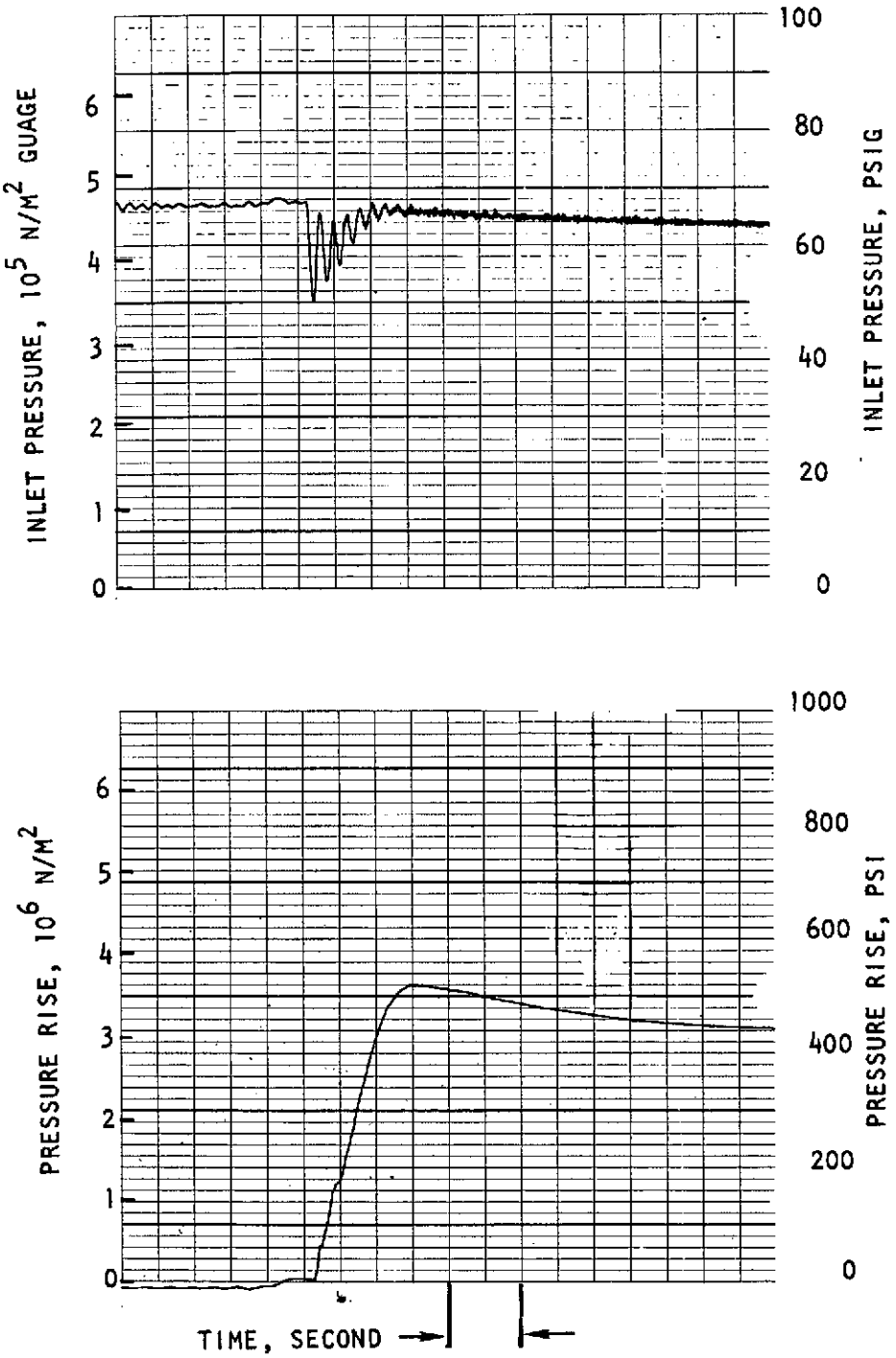

Figure 180. Pump Inlet Pressure and Pressure Rise Transients for Deadhead Start Test with 0.098 m^3 (3.45 ft^3) Discharge Volume and 2.9 × 10^6 N/m^3 (415 psia) Trigger Pressure

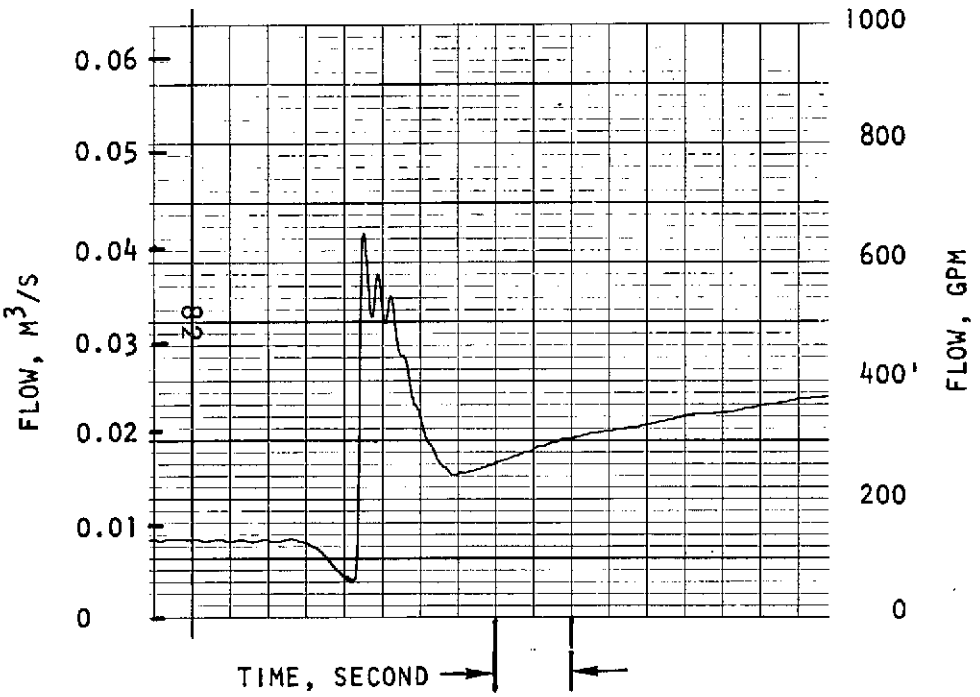

Figure 181. Inlet Duct Flow Transient for Deadhead Start Test with 0.098 m^3 (3.45 ft^3) Discharge Volume and 2.9 × 10^6 N/m^2 (415 psia) Trigger Pressure

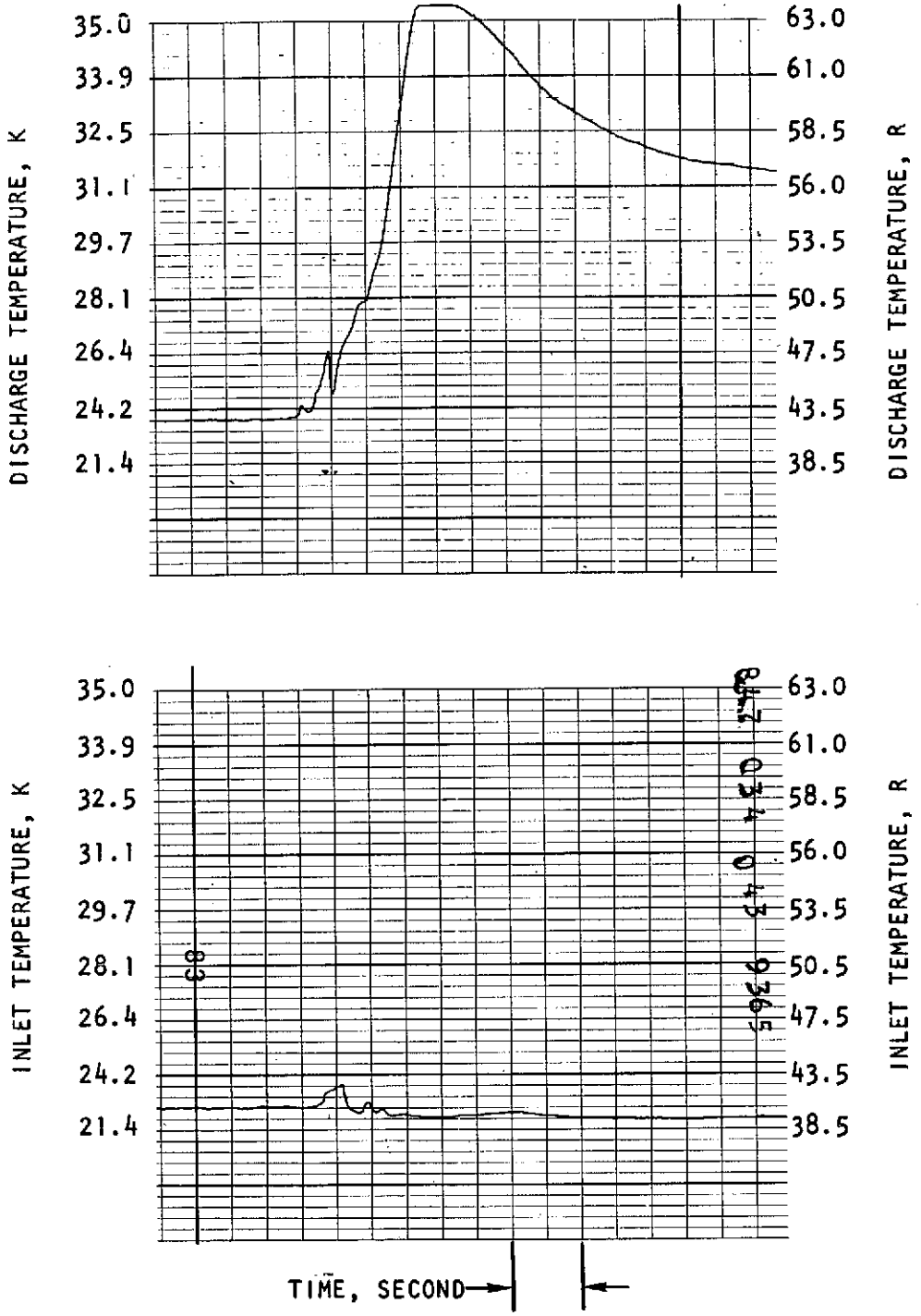

Figure 182. Pump Discharge and Inlet Hydrogen Temperature Transients for Deadhead Start Test With 0.098 m^3 (3.45 ft^3) Discharge Volume and 2.9×10^6 N/m^2 (415 psia) Trigger Pressure

REFERENCES

1. McFarland, B. L., and H. A. Friedman, "An Explicit Three Time Level Method for Thermal Analyzer Programs", prepared for publication at the 1970 International Heat Transfer Conference, Paris, France.

2. PWA FR-1042, Design Report for RL10A-3-1 Rocket Engines, Contract NAS8-5623, Florida Research and Development Center, Pratt and Whitney Aircraft, July 1964.

3. Cowley, C. W., W. J. Timson, and J. A. Sawdye, "A Method for Improving Heat Transfer to a Cryogenic Fluid", Advances in Cryogenic Engineering, Vol. 7, Plenum Press, New York (1961), p 385.

4. Manson, L., and J. D. Seader, "Study of Boiling Heat Transfer With LOX, LH_2 and LN_2", Report R-6259, Contract No. NAS8-11367, Rocketdyne, July 1965.

5. Leonhard, K. E., R. C. Getty, and D. E. Franks, Convair General Dynamics, "A Comparison of Cooldown Time Between Internally Coated and Uncoated Propellant Lines", Advances in Cryogenic Engineering, Vol. 12, (1966).

6. Maddox, J. P., "Cooldown of Insulated Metals Quenched in Liquid Nitrogen", M.S. Thesis, U.C.L.A. (1966).

7. Manson, L. and W. S. Miller, "A Study of Cooldown of Metals, Flow Instability, and Heat Transfer in Two-Phase Flow of Hydrogen", R.N. 68-4, Rocketdyne, 1968.

8. Frederking, T. H. K., and R. C. Chapman, "Optimization of Cooldown of Solids in Low Boiling Point Liquid". International Institute of Refrigeration, Commission I meeting, Grenoble (1965).

9. Wong, G. S., and W. R. Wagner, "Thermodynamic Improvements in Liquid Hydrogen Turbopumps," Second Interim Report Contract No. NAS8-20324, Rocketdyne Report R-7585, September 1968.

10. Wagner, W. R. and G. S. Wong, "Thermodynamic Improvement in Liquid Hydrogen Turbopumps", Final Report, Contract NAS8-20324, Rocketdyne Report R-8083, December 1969.

APPENDIX A

APPLICABLE LITERATURE REVIEW SUMMARIES

AUTHOR: Maddox, P. J. and T. H. K. Frederking

REPORT TITLE & DATE: Cooldown of Insulated Metal Tubes to Cryogenic Temperatures, August 1965

JOURNAL/ IDENTIFYING NO. Advances in Cryogenic Engineering. Vol. 11, 1965

AGENCY/COMPANY: U.C.L.A.

SUMMARY: The paper considers some theoretical aspects of the vapor film formation process and reports on experiments using metal tubes (copper and stainless) and immersing in a test liquid of nitrogen. The tubes were 0.30 m (12 in.) length, 0.025 m (1 in.) dia with 0.0012 m (0.049 in.) walls. Coating materials used in the experiments were Teflon, KEL-F, Rokide Z (zirconium oxide) and aluminized mylar.

The paper indicates that insulative coatings on good conductors provide rapid lowering in surface temperature which, in turn, provides rapid attainment of liquid-solid contact with good heat removal rates. Also, it was concluded that film boiling heat transfer during transient heat removal from the coated metals can only be approximately evaluated using the quasi-steady assumption.

AUTHOR: Leonhard, K. E., R. C. Getty, and D. E. Frankcs

REPORT TITLE & DATE: A Comparison of Cooldown Time Between Internally Coated and Uncoated Propellant Lines, 1966

JOURNAL/ IDENTIFYING NO. Advances in Cryogenic Engineering, Vol. 12, 1966

AGENCY/COMPANY General Dynamics/Convair Aerospace

SUMMARY: Chilldown tests were conducted on a 0.91 m (three-foot) section of 0.051 m (2 in.) dia stainless steel line. Both uncoated and internally Kel-F coated lines were tested to determine the effect that a thin insulating liner had on the transition point to nucleate boiling. Nitrogen was the test fluid and liquid flow rates varied from 0.0091 to 0.018 m^3/s (145 to 278 gpm). In general the Kel-F pipe cooled faster and was insensitive to change in flow rate. As the distance down the pipe progressed, the Kel-F coated pipe cooled progressively faster than the uncoated one.

COMMENTS: The data described here will be used in the LH_2 Turbopump Rapid Start Program to evaluate and checkout the computer program techniques.

AUTHOR: Manson, Lidia

REPORT TITLE
& DATE: Cooldown of Shrouded Spherical Vessels in Liquid Nitrogen, 1966

JOURNAL/
IDENTIFYING NO. Paper C-1, 1966 Cryogenic Engineering Conference, Colorado

AGENCY/COMPANY Rocketdyne

SUMMARY: The cooldown of 0.10 m (four-inch) diameter hollow copper spheres enclosed in spherical shrouds containing liquid nitrogen were studied. The main purpose of the investigation was to provide information for design of high-pressure liquid N_2-cooled gas storage tanks, particularly on tank-shroud gap requirements. Boiling heat fluxes were obtained at ten locations on the sphere for various shroud sizes.

Results showed that the presence of the shrouds (0.0064 m (1/4 inch) min. gap) did not significantly influence the transfer of heat from the sphere. The sphere surface finish did not influence the total cooldown time. The application of a thin teflon coat reduced the cooldown time by half. Peak nuclear boiling fluxes varied between 63,100 and 189,300 J/m^2 s (20,000 and 60,000 Btu/ft^2 hr). It was shown that in a two-sphere system (with one sphere placed close to and vertically above the other) cooling occurred faster because of increased free connection.

COMMENTS: The experiments indicate clearly that a thin teflon coating reduced cooldown time.

AUTHOR: Brentari, P. J., P. J. Giarratano, and R. V. Smith

REPORT TITLE
& DATE: Boiling Heat Transfer for Oxygen, Nitrogen, Hydrogen and Helium, 20 Sept. 1965

JOURNAL/
IDENTIFYING NO. Technical Note 317

AGENCY/COMPANY: N.B.S.

SUMMARY: An orderly examination of the information relative to boiling heat transfer for the four cryogenic fluids is undertaken. Experimental data are examined with respect to the available predictive correlations. The results are discussed and computational aids in the form of graphs and equations are presented for recommended correlations.

COMMENTS: The report brings together much of the available experimental data and correlations and provides a discussion and evaluation in many areas of boiling heat transfer. The graphical presentations are extremely useful for preliminary studies.

AUTHOR: Schmid, J. R., et al

REPORT TITLE
& DATE: LION Temperature Distributions for Arbitrary Shapes and Complicated Boundary Conditions, 27 July 1966

JOURNAL/
IDENTIFYING NO. Report No. KAPL-M-6532

AGENCY/COMPANY: Knolls Atomic Power Lab

SUMMARY: This report describes the LION digital computer program developed by the General Electric Company. This computer code was used in obtaining the thermal analyzer program used in the chilldown studies.

AUTHOR: Fischer, W. W.

REPORT TITLE
& DATE: LION Tales, A Users' Manual for the LION Thermal-Structural Evaluation Code, July 1967

JOURNAL/
IDENTIFYING NO. KAPL-M-6533 (EC-58), July 1967

AGENCY/COMPANY: Knolls Atomic Power Lab

SUMMARY: This report presents details pertinent to the use of the LION code when applied to transient and steady state, thermal-structural temperatures distribution problems.

AUTHOR: Stark, J. A. and M. H. Blatt

REPORT TITLE
& DATE: Analysis of Zero-Gravity Receiver Tank Vent Systems, July 1969

JOURNAL/
IDENTIFYING NO. Report GDC-DDB69-001 (Contract NAS8-20146)

AGENCY/COMPANY: GDCA

SUMMARY: This study was undertaken to extend the vapor/liquid separation and low-g venting technology to the definition, design and testing of an optimum vent system for an orbital propellant transfer receiver tank.

COMMENTS: During this work the Knolls Atomic Power Lab thermal analyzer program was developed and modified to more readily compute chilldown data for the receiver tank. The modifications included the capability of specifying surface to fluid heat transfer coefficients as a function of wall to fluid temperature difference as well as fluid phase and consideration of material properties as functions of temperature. This computer program development and documentation will assist in adapting and using the computer code in the present study.

AUTHOR: Manson, L. and J. D. Seader.

REPORT TITLE
& DATE: Study of Boiling Heat Transfer with LOX, LH_2 and LN_2, July 1965

JOURNAL/
IDENTIFYING NO. R-6259, Final Report Contract NAS8-11367

AGENCY/COMPANY: Rocketdyne

SUMMARY: The results of experimental and analytical investigations of some special boiling conditions of interest to the SATURN V improvement program are given. Included are heat transfer in shrouded spherical vessels, boiling heat transfer on Teflon-coated surfaces, combined convection and boiling heat transfer to LN_2 from a moving vertical plate, boiling heat transfer in a porous plut heat exchanger, and the effect of thermopheresis on the behavior of hydrogen bubbles in a low gravity field.

The influence of Teflon coatings on the cooldown of copper was measured on the shrouded spheres and on several flat plates and was found to appreciably shorten cooldown time.

COMMENTS: The experiments clearly indicated that a thin Teflon coating reduced cooldown time for the copper spheres.

Some of the work of this report applicable to the chilldown problem is reported elsewhere but more detail is presented here. A discussion is given on the theoretical aspects of coating effects on surface boiling mechanisms. It was found that the existing theories did not provide a satisfactory explanation for these experiments.

AUTHOR: Chi, J. W. H.

REPORT TITLE
& DATE: Cooldown Temperatures and Cooldown Time During Mist Flow, 1964

JOURNAL/
IDENTIFYING NO. Advances in Cryogenic Engineering, pp 332-340, 1964

AGENCY/COMPANY: Westinghouse Electric Corporation

SUMMARY: An experimental program was undertaken to study the cooldown of metal test sections by liquid hydrogen. The data was analyzed to develop an equation for the prediction of temperatures and cooldown time. The test sections were 0.66 m (26-in.) long aluminum tubes, all 0.0048 m (3/16 in.) ID, and 0.003 and 0.051 m (1/2 in. and 2 in.) OD. Temperature versus time records were obtained for different flow rates, around 0.0013 kg/s (10 lb/hr).

The cooldown period was assumed to be dominated by a film boiling phase (90 percent of total cooldown time) and the data indicated that during this time

the lumped parameter ψ was approximately constant (where ψ = constant $\cdot \rho_w^{-1} \cdot C_w^{-1}$ for a given pipe). From the data correlation it was suggested that for conditions similar to the experiments the cooldown times could be readily estimated by the equation developed: the lumped parameter ψ being evaluated at the initial temperatures with the heat transfer coefficient given by

$$\frac{hD}{k_f} = 0.0310 \left(\frac{DG}{\mu_f}\right)^{0.8} \left(\frac{C_p \mu}{k}\right)_f^{0.4} \left(\frac{T_w}{T_L}\right)^{-0.55}$$

where the properties are evaluated at the average film temperature, 1/2 (T_W + T_L), W denotes wall locations and L denotes liquid condition.

COMMENTS: The paper confirms the validity of the assumption that the film boiling period is a large fraction of the total cooldown time for metallic bodies under these conditions. The experimental data adds to useful measurements of hydrogen cooldown and heat transfer coefficient values are inferred.

AUTHOR: Frederking, T. H. K., R. C. Chapman, and S. Wang

REPORT TITLE & DATE: Heat Transfer and Fluid Motion During Cooldown of Single Bodies to Low Temperatures, 1965

JOURNAL/ IDENTIFYING NO. Advances in Cryogenic Engineering (1965)

AGENCY/COMPANY: U.C.L.A.

SUMMARY: Experiments were undertaken to explore phenomena associated with removal of thermal energy from solid bodies (spheres) by saturated liquid helium. The studies were supplemented by nitrogen data. The spheres were 0.0064 and 0.0095 m (1/4 in. and 3 in.) diameter copper. The helium dewar was 0.08 m ID by 1.20 m high.

Cooldown times from 300 K to cryogenic temperatures were measured in N_2 and He_I by recording temperature versus time with a copper-constantan thermocouple. At low solid temperatures because of reduced thermocouple sensitivity, additional qualitative studies were undertaken with resistance thermometers. A time constant expression for the cooldown process was estimated from a first-order film boiling heat removal approximation and compared with the measured cooldown times. Also, heat transfer coefficients for the film boiling phase were obtained for N_2 and He_I and discussed with regard to the transient measurements. Limited data on cooldown in liquid He_{II} is also discussed.

COMMENTS: The paper directs attention on the cooldown of single bodies and the predominant thermal resistance from the Leidenfrost phenomena and adds to the experimental data available on liquid helium.

AUTHOR: Leibenberg, D. H.

REPORT TITLE
& DATE: Cooldown of Cryogenic Transfer Lines, 11/22/65

JOURNAL/
IDENTIFYING NO. University of California Report No. LA-3426-MS, 1965.

AGENCY/COMPANY: Los Alamos Lab (Univ. of California)

SUMMARY: Computational techniques developed to predict the cooldown process in liquid hydrogen lines are described. The transfer lines involved were 8 to 10 inches in diameter and vacuum-jacketed. Two techniques were used in the computations. The first equates the total heat to be removed with the expected average refrigeration available from the fluid. The second method considers the energy balance over short time steps as the cooldown progresses. Comparison of the computations with measurements are made.

COMMENTS: The process here is vent-line-limited. Useful data are presented on temperature versus time during cooldown of large diameter lines with liquid hydrogen.

AUTHOR: Chi, J. W. H.

REPORT TITLE
& DATE: Forced Convection Boiling Heat Transfer to Hydrogen, Jan. 1966

JOURNAL/
IDENTIFYING NO. J. Spacecraft, Jan. 1966

AGENCY/COMPANY: Westinghouse Electric Corp.

SUMMARY: An attempt was made to develop a general correlation for forced convection boiling heat transfer to hydrogen to cover both the nucleate and film boiling regimes. An annular flow model was postulated. This means two-phase flow with a liquid core in film boiling and a vapor core in nucleate boiling. It was further postulated that forced convection film boiling heat flux is the sum of a convective flux and a boiling flux, thus:

$$(q/A) = (q/A)_{conv} + (q/A)_{Bo}$$

where for film boiling $(q/A)_{conv} = h_f (T_w - T_f)$ where T_w is the inside wall temperature and T_f is the arithmetic mean of the wall and liquid temperatures. Heat transfer coefficients for hydrogen gas are given by a modified Dittus-Boelter equation.

For the transition regime either vapor or liquid may be in intermittent contact with the wall. Thus, the heat flux in the transition regime is presented in an equation employing variables representing time fractions for vapor-to-liquid contact, and contributions to the heat flux from both film boiling and nucleate boiling expressions.

A comparison is presented on experimental and calculated heat fluxes for forced convection film boiling and nucleate boiling. The data covered the range from 6.5×10^4 to $9.8 \times 10^6 J/m^{-2}s$ (0.04 to 6.0 Btu/in.^{2}-sec) 0.27 to 0.91 kg/s (0.6 to 2.0 lb/sec), and 1.7×10^5 to 1.1×10^6 N/m^2 (24 to 158 psia). The average deviation between experimental and calculated heat flux was 17 percent.

COMMENTS: The annular flow models assumed in the correlations appear reasonable for situations where the flow is fairly well defined as in nucleate or film boiling regimes and where other types of slug or bubbly flow do not form a major contribution. Transition region correlations were not covered in the data correlations.

AUTHOR: Chi, J. W. H.

REPORT TITLE
& DATE: Slug Flow and Film Boiling of Hydrogen, October 1967

JOURNAL/
IDENTIFYING NO. J. Spacecraft 4, 10, p 1329, October 1967

AGENCY/COMPANY: Westinghouse

SUMMARY: Forced convective, transient boiling heat transfer was studied by the cooldown of a copper test section by liquid hydrogen. From the slopes of the local wall temperature histories, local forced convective boiling heat flux was obtained for a range of conditions. Based on the bulk stream temperature traces and the apparent mechanisms of two-phase flows, a general equation was derived for forced convective film boiling heat flux:

$$q/A = (1 - K_{TP})\, h_v\, (T_{wi} - T_v) + X_{TP}\, h_f\, (T_{wi} - T_i) + X_{TP}\, (q/A)_{Bo}$$

where X_{TP} is the time fraction of two-phase flow, referred to slug flow; h_f and h_v are heat transfer coefficients for gas film and vapor, respectively; T_f and T_{wi} are gas film and inside wall temperatures, respectively; T_w is the average superheated vapor slug temperature; and $(q/A)_{Bo}$ is the boiling flux component. The equation correlated the data with an average deviation of ±21%. A correlation also was developed for X_{TP} which is given as a function of the boiling number, $(q/A)_{Bo}/G\lambda$;

$$X_{TP} = 3.72 \times 10^{-5} [G\lambda/(q/A)_{Bo}]^{1.2}$$

COMMENTS: This approach to forced convection boiling heat transfer attempts to include the various mechanisms including single phase gas, mist flow slug flow and annular flow transfer. All of these regimes may be important in problems connected with chilldown. The correlations are developments of earlier work by the same author. The empirical equation given above to evaluate X_{TP} was obtained from horizontal flow data and does not apply to vertical flow.

AUTHOR: Wagner, W. R., G. S. Wong, and E. B. Monteath

REPORT TITLE
& DATE: Thermodynamic Improvements in Liquid Hydrogen Turbopumps, December 1969.

JOURNAL/
IDENTIFYING NO. R-8083 Final Report, Contract NAS8-20324

AGENCY/COMPANY: Rocketdyne

SUMMARY: Three main tasks were undertaken: (1) to investigate pump chilldown times under reduced gravity, (2) to establish feasibility and effectiveness of coated feed systems to hasten chilldown, and (3) to establish the effect of improved criteria on engine start capability.

The nucleate boiling regime was found to be relatively insensitive to gravity, but the heat transfer coefficients in the transition and film boiling regimes was concluded to be reduced by as much as a factor of 4 in gravity reduction from unity to near zero.

The effect of coatings on the cooldown times of three materials was investigated (Ti, Al and K-monel) and coating techniques for both conventionally applied polymeric materials and plasma spray coatings were developed. Thermal and flexural tests were included in the evaluation of these coatings.

Analyses were performed to investigate engine start for various preconditioning and restart requirements. System preconditioning, two-phase pumping capabilities, coating effects and the analysis of Saturn SIVB stage fuel-lead chilldown were areas emphasized. Using coated feed systems and two-phase flow capability it was concluded that significant system gains are obtainable by reducing chilldown flow loss by 35 to 80 percent.

COMMENTS: The report contains extensive analytical and experimental studies directly related to improvements of LH_2 turbopumps by means of rapid chilldown and start.

AUTHOR: Frederking, T. H. K. and R. C. Chapman

REPORT TITLE
& DATE: Optimization of Cooldown of Solids in Low Boiling Point Liquid, June 1965.

JOURNAL/
IDENTIFYING NO. International Institute of Refrigeration, Commission I Meeting, Grenoble, 1965

AGENCY/COMPANY UCLA

SUMMARY: A theoretical model is proposed to determine optimum conditions and limitations on the applications of insulative coatings on metals to reduce

cooldown times. Copper cylinders of 0.025 m (one-inch) diameter and 0.051 m (two-inch) length were coated with various materials and immersed in liquid He_l or nitrogen.

The chilldown process is described as follows. After immersion at the initial solid excess temperature (over saturation temperature of the liquid) ΔT_i, a vapor forms rapidly and covers the solid. The resulting heat transfer coefficient remains fairly constant for an extended period when film boiling is established on the uncoated copper. At a maximum excess temperature ΔT_m of metastable liquid, solid-liquid contact becomes possible and heat removal rate increases significantly, in particular near the peak flux of nucleate boiling. Thus, a simplified model is introduced which incorporates a thermal resistance-capacitance circuit and constant (average) heat transfer coefficients in the two fundamentally different boiling nodes, i.e., film boiling $\bar{h}_v$ when $\Delta T \geq \Delta T_m$ and solid-liquid contact regime boiling $\bar{h}_L$ when $\Delta T < \Delta T_m$. Time constants are then derived in terms of heat capacity of the solid, surface area, conductivity and average heat transfer coefficients. For a coated body the parameter δ_c/k_c (coating thickness to conductivity ratio) is shown to be important. An expression is derived for cooldown time of a coated body in terms of the uncoated body cooldown time. A minimum in cooldown time was obtained in terms of the dimensionless coating thickness,

$$\Delta = \bar{h}_v \delta_c / k_c, \text{ at } \Delta = \frac{1 - \bar{h}_v \bar{h}_L}{\ell n(\Delta T_i / \Delta T_f)} - \frac{\bar{h}_v}{\bar{h}_L}$$

Quantitative comparison with the derived equations was not possible since the apparent thermal conductivity of the coatings and solid-solid contact resistances were not known. However, all material combinations examined with N_2 gave evidence of a minimum in cooldown time.

It was stated that a complete understanding of chilldown would require a knowledge of transient phenomena during initial vapor build-up. At the instant of immersion the large latent heat of N_2 caused rapid lowering of coating surface temperature. With liquid He_I the absence of a cooldown time reduction would have to be examined by such transient effects.